UNITED STATES DEPARTMENT OF THE INTERIOR

GEOLOGICAL SURVEY

THREE-COMPONENT DIGITAL VELOCITY AND ACCELERATION RECORDINGS MADE IN CONJUNCTION WITH THE PACE REFRACTION EXPERIMENT (NOVEMBER 1985)

edited by

L. Wennerberg
U.S. Geological Survey

OPEN-FILE REPORT 86-387

CONTENTS

INTRODUCTION

As part of the Pacific–Arizona Crustal Experiment (PACE; Howard, 1986), a seismic-refraction experiment was conducted in western Arizona and southeastern California. PACE is a multidisciplinary effort to understand the crust of the southwestern U.S. Cordillera along a transect from the southern California borderland to the Colorado Plateau. The data reported here were collected in conjunction with the first seismic-refraction experiment of PACE, consisting of two perpendicular profiles centered on the Whipple Mountains metamorphic core complex in the Colorado Desert of eastern California. Preliminary results of the seismic-refraction experiment are reported by Fuis and others (1985).

This report describes only the three-component seismic data recorded on portable broadband digital recorders (GEOS; Borcherdt *et al.*, 1985). The vertical-component data recorded on portable analog recorders (Healy and others, 1982) will be described in forthcoming reports. This report provides analog copies of the digital recordings obtained from velocity transducers and accelerometers for each of the sources detonated during these experiments. Complete response curves are provided for each GEOS system for each deployment. Digital copies of the data are available on request.

Scientific objectives for this experiment with GEOS include shear-wave velocity structure and structure of the crust-mantle interface, especially as it can be inferred from near- and post-critical reflection data. A study of near-critical reflection data is stimulated by laboratory evidence and recent theoretical work (Brekhovskikh, 1960; Becker and Richardson; 1969, 1972; Borcherdt and Wennerberg, 1985; Borcherdt, Glassmoyer, and Wennerberg, 1986). This work shows that the characteristics of low-loss anelastic body waves near critical angles are distinct from those that would be predicted on the basis of elasticity or on the basis of one-dimensional anelastic models. These distinctions have proved useful in the laboratory for measurement of material properties, especially intrinsic absorption. The wide-angle three-component reflection data should provide information on the structure of the crust-mantle interface as well as an opportunity to examine recently predicted characteristics of post-critical reflections.

Other objectives for this experiment include: assessment of ground motion severity near shot points and an evaluation of instrument performance characteristics for seismic-

refraction experiments. For locations near shot points the GEOS systems were set as six-channel systems with two sets of three-component transducers. This configuration permitted on-scale strong-motion records to be obtained for all sources at each GEOS location. The experiments also provided an opportunity to evaluate design features of the GEOS in the field. Although the system was designed explicitly for a variety of active and passive seismic experiments, including seismic refraction, these experiments provided the first opportunity to evaluate these features for a complete seismic-refraction experiment using arrays of 11 and 12 systems (66–72 channels).

INSTRUMENTATION

Data presented in this report were recorded, using General Earthquake Observation Systems (GEOS). A detailed description of the systems is provided by Borcherdt *et al.*, 1985. A brief summary is provided of recording and playback system characteristics of interest for this report. Recording system parameters chosen for this experiment are provided in the next chapter.

Recording System

The GEOS recording system was developed by the U.S. Geological Survey for use in a wide variety of active and passive seismic experiments. The digital data acquisition system operates under control of a central microcomputer, which permits simple adaptation of the system in the field to a variety of experiments; including, seismic refraction studies, near-source high-frequency studies of strong motion, teleseismic earth structure studies, studies of earth tidal strains, and free oscillation studies. Versatility in system application is achieved by isolation of the appropriate data acquisition functions on hardware modules controlled with a single microprocessor via a general computer bus. CMOS hardware components are utilized to reduce quiescent power consumption to less than two watts for use of the system as either a portable recorder in remote locations or in an observatory setting with inexpensive backup power sources. The GEOS together with two sets of three-component sensors (force-balance accelerometer, velocity transducer) and ferrite WWVB

antenna was used at the station locations near shot points as shown in Figure 1 (see Borcherdt *et al.*, 1985 for hardware modules comprising the system).

The signal conditioning module for the GEOS has six input channels, selectable under software control, permitting acquisition of seismic signals ranging in amplitude from a few nanometers of seismic background noise to 2 g in acceleration for ground motions near large events. The analog-to-digital conversion module is equipped with a 16-bit CMOS analog-to-digital converter which affords 96 dB of linear dynamic range or signal resolution; this, together with two sets of sensors, implies an effective system dynamic range of about 180 dB. A data buffer with direct memory access capabilities allows for maximum throughput rates of 1200 sps. With sampling rates of any integral quotient of 1200, broad and variable system bandwidth ranging from $(10^{-5} - 6 \times 10^{2}$ Hz) is achieved allowing the use of recorders with a wide variety of sensor types.

Modern high-density (1600–6400 bpi) compact tape cartridges offer large data storage capacities (1.25–25 Mbyte) in ANSI standard format to facilitate data accessibility via minicomputer systems. Read capabilities of cartridge tape recorders are utilized to allow recording parameters and system operational software to be changed automatically. Installation of an expanded data buffer module allows the system to act as a solid-state or a dual-media recorder. Systems equipped with modems can be utilized to transmit data via telecommunications to a central data processing laboratory.

Microprocessor control of time-standard provides the capability to synchronize internal clock via internal receivers (such as WWVB and satellite), external master clock, or conventional digital clocks. Microprocessor control of internal receivers permits systems on command to determine time corrections with respect to external standard. This capability permits especially accurate correction for conventional drift of internal clocks.

Accurate *in situ* calibration of system components improves data accuracy and permits on-site evaluation of potential system performance malfunctions. The calibration module currently implemented in the GEOS permits calibration of three types of sensors and the signal-conditioning module under software control of the CPU. Calibration capabilities for sensors include velocity transducers with and without calibration coils and force-balance accelerometers. In the case of the velocity transducers, a dc voltage, derived under CPU

control for appropriate gain setting from the D/A converter, is applied to either the main or calibration coil of the transducer for a software-selectable time interval. Voltage termination corresponds to an applied step function in acceleration to the sensor mass with the resultant signal determining relative calibration. In the case of force-balance accelerometers ± 12 volts are applied to the damped and undamped control lines. The signal-conditioning module is calibrated using impulse of one sample duration and an alternating dc voltage derived and applied under software control to the amplifiers while the sensors are disconnected via appropriate relays.

Using a 32-character alphanumeric display under control of the microcomputer makes for convenient system set-up and the flexibility to modify the system in the field for a wide variety of applications. English-language messages to the operator, executed in an interactive mode, reduce operator field set-up errors. A complete record of recording system parameters is recorded on each tape together with calibration signals for both the sensor and the recorders. These records assure rapid and accurate interpretation via computer of signals, both in the field and in the laboratory.

Flexibility to modify the system to incorporate future improvements in technology is achieved using a structured software architecture and modular hardware components. Incorporation of new hardware modules is accomplished in a straightforward manner by replacing appropriate modules and corresponding segments of controlling software.

The system response designed for seismic refraction applications was intended to allow broadband signals (1–200 Hz) to be recorded on scale at as high a resolution as permitted by seismic background noise levels. The amplitude response of the recording system, together with that for two types of sensors frequently used is shown in Figure 2. Response curves determined from signals recorded at each station location are described in a subsequent chapter.

Data Playback System

The read and write capabilities of the mass-storage module, together with the D/A conversion module, permits the GEOS to be used as an analog as well as digital (via RS–232) playback system in the field. Visual inspection of digitally recorded data is useful

for determining instrument performance, evaluation of recording parameters, evaluation of environmental factors (*e.g.*, local noise sources, etc.). RS–232 capabilities of data playback unit and ANSI-standard tape cartridges permit playback of digital time series on minicomputer systems in the field or laboratory. Digital playback of data is generally performed using an ANSI-standard serpentine tape reader as a peripheral to minicomputer systems in the laboratory. Deployment of minicomputer digital playback systems in the field is generally most feasible for large-scale high-data volume experiments.

For these experiments only analog playback capability was utilized in the field. Analog playbacks on light-sensitive paper were utilized in the field to identify seismic events, trigger parameters, and evaluate instrument performance. Digital playback of the data was conducted with a Tanberg serpentine tape drive attached to the PDP 11/70 at the National Strong Motion Data Center in Menlo Park, using a variety of software packages, developed in large part by G. Maxwell, E. Cranswick, and C. Mueller.

SITE SELECTION/INSTRUMENT CONFIGURATION AND EVALUATION

Locations for the seismic refraction profiles are shown in Figure 3. Information regarding shot points for the profiles is provided in Table 1. Sites along these profiles were chosen for the GEOS recorders to provide near- and post-critical reflection data from the crust-mantle interface. The instruments were colocated with some of the sites used to record vertical component data on the U.S.G.S. cassette recorders. Portions of the profiles occupied by GEOS also overlapped the near-vertical reflection profiles recorded by U.C. Santa Barbara. The locations for each of the GEOS recorders are shown in Figures 3 and 4. Station coordinates and pertinent recording parameters for each of the three separate deployments of the instrumentation are tabulated (Table 2).

Each of the shots detonated during the experiment were recorded on the GEOS set to record in the pre-set time mode. The systems were programmed to automatically record during time intervals pre-established for detonation of the various shot points. Operation in this mode resulted in all shot points being recorded at each station with no exceptions.

Timing at each of the stations was achieved using the capability of the recorders to synchronize to WWVB. Timing corrections were recorded at selectable intervals during the

24–48 hr. deployment periods to provide a timing accuracy of generally less than 5 ms. A check of ten systems on the first deployment and a spot check of systems thereafter with an external master clock confirmed this accuracy. In comparison, recorders without remote correction capabilities yield timing accuracies of 40–80 ms over a 24–48 hour interval, using comparable clocks. Measurement of clock drift rate and interpolation has been used in some cases to reduce uncertainties encountered when remote correction capabilities are not available, but they are often difficult to implement in large-scale field experiments.

In anticipation of recording a wide range in signal amplitudes ranging from seismic background noise to more than 1 g in acceleration near the shot points, two different types of sensors were used. For those sites near the shot points, the GEOS systems were set as six-channel systems. These systems were used to simultaneously record the output of both force-balance accelerometers and velocity transducers. The gain settings for the accelerometers were estimated at the various sites based on distance and size of the explosion (see Table 2).

For those sites more than 3 km from the shot points, the GEOS were set as three-channel systems to record the output of L–22 velocity transducers. These configurations of the systems permitted the signals from all sources to be recorded on-scale at each site and at maximum signal resolution relative to seismic background noise levels. By recording the output of each of the velocity transducers at 60 dB gain, the minimum level of signal resolution was determined by seismic background noise and the upper limit by a clipping level of the A/D module. This gain setting allowed seismic radiation fields for all shot points at a distance of more than 3 km to be detected and recorded on-scale.

Sampling rates for all but one of the locations were chosen at 200 sps per channel with an anti-aliasing high-cut filter selected at 50 Hz (for a resultant Nyquist frequency of 100 Hz). One location (station 379) was operated at 400 sps and 100 Hz anti-aliasing high-cut filter. The sampling rate of 200 sps/channel resulted in an approximate 45-minute continuous record capacity per cartridge tape for the systems used as three-channel systems.

Automatic self-calibration capabilities of the GEOS permitted calibration signals for both the sensor-recording system and the recording system without sensors to be recorded

at each station location. Calibration signals for the systems set as three-channel systems were recorded at both 36 and 54 dB gain levels. The gain levels used to calibrate the accelerometer channels were those used to record the data (see Table 2). As calibration signals were recorded for each GEOS deployment location, a complete evaluation of sensor and recording system response is feasible for these locations. An evaluation of system response for the cassette recorders and those used by U.C. Santa Barbara can be persued at locations of cosited instrumentation using simultaneously recorded seismic signals.

In regards to an evaluation of seismic refraction design goals for the GEOS, improvements in regard to deployment procedures were recognized, but no fundamental changes in software or hardware were found to be needed for routine use of the system on seismic-refraction experiments. Eleven systems were utilized for each of the first two deployments and twelve systems for the third. For each deployment the systems were required to record a total of 39 channels (see Table 2). Of this total, three of the channels failed on each of the first two profiles. With the exception of these malfunctions all thirty shots were recorded on the remaining channels. The percentage of channels operating correctly throughout the experiment was 95%. The exceptionally high data return for the first field deployment/test of the GEOS for seismic refraction studies confirms the initial design goals of the system for this particular application. In addition to instrument reliability, a large part of the success of the experiment is attributable to the competent execution of a vast array of complicated logistics by an experienced crew coordinated by E. Criley, G. Fuis, and W. Mooney (not necessarily in that order).

Several aspects of the deployment procedures were found to be in need of improvement. These included equipping field vehicles with instrument carrying racks and battery charging capabilities. Implementing these improvements would permit the GEOS to be deployed without external batteries and all record parameters to be preprogrammed at the field office. Significant reductions in size and weight of GEOS carrying cases (shipping boxes) also would facilitate frequent changes in instrument locations often required in refraction studies.

The GEOS architecture represents a general framework from which a variety of special-purpose data acquisition systems can be developed. Configuration of special-purpose or

limited application systems may be practical, provided resources (financial and personnel are available for development, construction and maintenance). As the GEOS was developed for application in a variety of passive and active seismic experiments, it is of interest to consider packaging changes to the GEOS that might improve its usefulness for crustal imaging studies, but decrease applicability for other applications.

Desirable system attributes for crustal imaging are small size and ease in operation. A configuration of GEOS currently being implemented is that of extending the data buffer module to near 1 Mbyte. This extension, which is easily implemented by adding memory to the data buffer module and changes in corresponding software modules, would allow the system to be used without the tape cartridge and corresponding controller modules. This configuration would allow reductions in size and weight of the system. Further reductions can be achieved easily by reducing the number of input channels by simply removing corresponding signal conditioning cards. This would allow the system to be packaged in a container not exceeding $8 \times 9 \times 13$ inches. Weight of the system would be reduced to less than 15 lb.

Utilization of the expanded data buffer as a memory board for mass data storage offers the advantage of increasing the operating-temperature range over that imposed by the characteristics of magnetic tape. Implementation of such a board in some systems is planned to allow use of the GEOS in cold environments, such as Alaska. However, these proposed changes cannot be implemented without sacrificing beneficial attributes of the system for other applications. Utilization of the memory board reduces data capacity, data accessibility, and data transportability. Decrease in the number of channels can reduce the effective dynamic range and the usefulness of the system for studies requiring two types of three-component sensors, such as aftershock studies. Use of external batteries and external CPU for operational-parameter change eliminates the self-containment attribute of the systems and implies that full capability to reset the systems in the field would no longer involve merely selection of menu mode via the field-data-acquisition system. Nonetheless, repeated use of a large number of units for seismic-refraction experiments could justify modifying the modules to produce a subset of the GEOS for dedicated refraction use. Fortunately, the microcomputer, together with modular hardware components, provides a

general framework from which special systems with emphasis on particular attributes can be easily made.

VELOCITY AND ACCELERATION TIME HISTORIES

Time histories corresponding to the three components of ground motion detected at each location from each of the thirty shots detonated during the experiments are shown in Appendices A and B. Those time histories, termed "velocity" (Appendix A), correspond to signals detected using three-component velocity transducers (L–22; Mark Products); those termed "acceleration" (Appendix B), correspond to signals detected using three-component force-balance accelerometers (FBA–13; Kinemtrics). The analog time histories were derived using digital playback software developed by G. Maxwell and graphics software developed by E. Cranswick and C. Mueller. Conversion of data format to that used for the cassette recorder by Mooney *et al.* has been implemented by W. Kohler, for use in joint interpretation of the data sets collected on both types of recorders.

Velocity Time Histories

The velocity time histories (Appendix A) are presented in a record section format, with each section showing one of the three components of motion recorded from each shot. The record sections are arranged in groups corresponding to distinct shots. These groups are arranged in chronological order according to shot time. Each group is comprised of two sections. The figures in the first section of each group (containing usually three, occasianally six figures) show analog traces of record sections six seconds in length as recorded for each of the three components of motion. The last three figures of the group show the corresponding traces plotted for thirty seconds. For each shot the figures are labeled by a capital letter, a number, and a lower-case letter in parentheses (*e.g.*, Figure A1(a)). The first letter refers to Appendix A, the number refers to the shot number listed in the shot schedule, Table 1. The lower-case letters distinguish figures within the group corresponding to each shot.

The horizontal sensors were oriented parallel with and perpendicular, respectively to the line of deployment. Orientation of the sensors, determined using a Brunton compass,

is given in the figure captions. Actual shot-station azimuths and distances are given in Tables 3, 4 and 5. Additional instrument parameters are listed in Table 2.

In the first section of figures for a given shot, consisting of six-second records, traces are displayed with site number at the top and a range scale indicating distance from the shot point to the site at the bottom. Amplitudes are normalized to the maximum in the trace. Times are reduced using 6 km/sec. The shot time is indicated at the top of the figure in GMT. The sole exception to this format is shot number 25, a fan shot from shot point 11 into the third deployment. For this shot, the six-second recordings are presented in the same format as the 30-second recordings.

The last three figures for a given shot are the 30-second recordings. The traces in these figures are evenly spaced on the page in the same relative position as the instruments had on the deployment line. Since the stations were quite evenly spaced, the format looks similar to that for which the traces are spaced according to distance measured from the shot point. The traces are again normalized to the maximum amplitude. For all traces the zero-to-peak amplitude is indicated by the length of the arrow in the heading above the traces. The bottom of each trace is labeled with the maximum digital counts in the trace, thus allowing a comparison of relative amplitudes from site to site. A conversion factor of approximately 6×10^{-7} converts digital counts to ground motion in cm/sec for the gain setting used in all these recordings. Times start from the GMT shown in the heading. Instrument timing was determined by synchronizing internal clocks to WWVB radio signals. Spot checks were made with a master clock and it was found that the accuracy of the relative timing was better than 5 msec, except for station 300 where no time was available. The times indicated for that station are best guesses interpolated from surrounding stations.

The thirty-second record sections show several interesting features of the recorded data set that are not apparent in the more conventional and shorter record sections. They sometimes show late arrivals with amplitudes comparable to those of the first arrivals (*e.g.*, see Figures A3d and A18e) and are useful for identification of surface waves (*e.g.*, see Figure A26g).

The record sections corresponding to each of the components of horizontal motion

show that for many of the shots, energy recorded from the horizontal sensors was nearly comparable or in some cases larger than that recorded from the vertical sensors. The horizontal data is expected to assist in phase identification, especially converted phases, and to be useful for inferring shear-wave velocity structure.

Acceleration Time Histories

Near-shot accelerograms recorded on FBAs co-located with velocity sensors are presented in chronological order in Appendix B. A brief summary of the peak accelerations recorded is tabulated with shot sizes and shot-receiver distances in Table 6.

The largest acceleration recorded was in excess of one g on the vertical component at station 166 which was within 100m of a 4000lb shot. The peak accelerations were found to fall off rapidly with distance from the shot point and to scale roughly linearly with shot size as shown in Table 6.

There are five groups of accelerograms corresponding to the five shots that were near enough to the sensors to be recorded. Each figure shows the three components recorded at a particular station for a given shot. Instrument parameters are given in Table 2. As with the velocity sensors, the FBAs were placed with the horizontal components parallel with and perpendicular to the deployment line. Azimuths of the horizontal components are given in the figures next to the traces in the form 090/AZI, where AZI is the three-digit azimuth. Actual shot-station azimuths and distances are given in Tables 3, 4 and 5.

IN SITU CALIBRATION OF INSTRUMENTATION

Calibration signals for the sensors and the recording equipment were recorded for each deployment location. These signals, automatically generated by GEOS, provide a basis for accurate inference of actual ground motion as recorded at the GEOS locations. They also allow an estimate of differences in relative response for the cassette-recorder systems colocated by Fuis *et al.* (1986) and the U.C. Santa Barbara instrumentation deployed by Malin *et al.* (1986).

Fourier amplitude spectra computed from the calibration time histories recorded at each field location are shown for the velocity transducer–recording system configuration

(Appendix C), the force-balance accelerometer–recording system configuration (Appendix D) and the recording system independent of the sensors (Appendixes C and D). The calibration signals for the velocity transducers were recorded at 54 dB gain and those for the force-balance accelerometers at the gains given in Table 2.

Velocity Channels

Two signals, generated automatically by GEOS, were utilized as calibration for the data recorded on the velocity transducers. Termination of a known DC voltage applied to the main coil was used as a calibration signal for the complete sensor–recording system. An impulse voltage applied at the input of the recording system was used to provide a calibration signal for the recording system independent of the sensors. Utilization of both calibration signals allows the system response for the recording system to be estimated throughout the selected bandwidth and dynamic range of the chosen detection–recording system configuration.

The output signal recorded as a result of the termination in DC voltage to the sensor coil is rich in low-frequency content. This input signal simulates a step-function in ground acceleration applied to the mass of the seismometer. As the derivative of this input function can be approximated by a delta function, the unit impulse response of the complete sensor–recording system to ground velocity can be estimated from the Fourier transform of the recorded time history multiplied by the square of angular frequency. Examples of the Fourier amplitude spectra computed for each deployment location are shown for each of the velocity transducer channels in the left-hand column of each figure in Appendix C. These spectra emphasize that the recorded output signal is rich in low-frequency content and are most useful for estimating the unit impulse response to ground velocity for the sensor–recording system combination up to a high-frequency limit imposed by the corner of the selected anti-aliasing filter and seismic background noise levels.

The Fourier amplitude spectra computed from the output signal generated by the impulse in voltage applied at the input of the recording system is shown for each channel in the right-hand column of each figure in Appendix C. These spectra provide an estimate for the amplitude response of the recording system to ground velocity. As the input signal

and resulting output signal are especially rich in high frequencies the computed spectra are most useful for estimating the response of the recording system for frequencies greater than some low-frequency limit imposed by the relative strength of the applied impulse voltage for the selected gain setting relative to instrument noise levels.

Utilization of the information contained in each of the recorded calibration signals permits a rather detailed estimate of instrumentation response to be calculated for each deployment location. Such estimates can be used to automatically correct data recorded on GEOS for instrumentation response. Further analysis in this report shall be limited to general comments on instrumentation performance.

Inspection of the computed calibration curves for the first deployment (Figures C1 through C10) shows that the response of the recording systems (GEOS) (right-hand column of each figure) was remarkably consistent. Minor variations in the amplification level and the fall-off characteristics for the anti-aliasing filters are apparent. Knowledge of the amplitude of the applied delta function in voltage as tabulated for each GEOS system would allow correction for these variations. One channel (H = 90; Figure C7) shows an anomalous response near the corner of the anti-aliasing filter.

Comparison of the curves computed to estimate the sensor–recording system response (left-hand column; Figures C1–C10) for the first deployment shows larger variations especially for frequencies less than the natural frequency of the sensors (nominally 2 Hz). The response of the sensor used at station 162 (sensor #201, see Table 2) suggests that each component of the sensor was performing improperly. Irregularities in the response curves near the corner frequency of the anti-aliasing filters can be attributed to high seismic background noise levels at the time the calibration signals were recorded. Inspection of the calibration curves computed for the second and third deployments (Figures C11 through C19 and Figures C10 through C30, respectively) shows upon reference to Table 2 that sensor number 201 consistently showed evidence of malfunction on at least one horizontal component and GEOS recording unit number 26 consistently showed anomalous response near the anti-aliasing filter corner on channel 6. Other than these apparent partial malfunctions sensor 197 deployed at station number 214 showed a anomalous calibration for the H = 90 component, suggesting that possibly the sensor was not properly leveled at

time of deployment

Acceleration Channels

Two signals, generated by GEOS, were utilized as calibrations for the data recorded from the force-balance accelerometers (FBA). The output signal generated as the result of the termination of the application of ±12 v to the damped and undamped central lines for the FBA simulates a step function in ground acceleration applied to the FBA which can be used to estimate the response of the sensor–recorder system. An impulse in voltage, applied to the input of the GEOS, provides a calibration signal for the recording system independent of the sensor.

The effect of applying ±12 v to the damped and undamped central lines is to set a non-zero reference voltage for the servo-amplifier of the FBA, hence forcing an offset of the accelerometer mass. Resetting to zero simulates a step in acceleration. As the derivative of this input function approximates a delta function, the unit impulse response of the recording system to ground acceleration can be estimated from the Fourier transform of the recorded time history multiplied by angular frequency. Examples of the Fourier amplitude spectra computed for each deployment location for the FBAs are shown in the left-hand columns of each figure in Appendix D. These spectra show that the recorded output signal is richest in low-frequency content and consequently most useful for estimating the unit impulse response of the FBA–recording system to frequencies less than some high-frequency limit imposed by the corner of the anti-aliasing filter and noise levels. Comparison of the spectra computed for each FBA location shows that the responses are extremely similar with the exception of station 234. The apparent difference in the computed spectra is attributable to the GEOS recording configuration chosen by operator when the system was deployed. This GEOS operated at this location was set to record at 100 sps with 50 Hz anti-aliasing filters as opposed to 200 sps chosen for the other recording sites.

The Fourier amplitude spectra computed from the output signal generated by the impulse in voltage applied at the recording system is shown for each channel in the right-hand column of each figure in Appendix D. These spectra show that the computed responses are much more contaminated by noise than were those computed for the velocity

channels. This contamination is due to the low-voltage level applied at the input for the lower gain levels used for the FBA channels. *In situ* calibrations for the recording systems comparable to those shown for the velocity transducer channels could have been obtained by setting the gain levels for all channels to those used for the FBAs. This noise contamination does not indicate a system malfunction, but instead the need to improve field procedures.

ACKNOWLEDGMENTS

The data set reported for this experiment represents the combined efforts of several individuals, as indicated in part by the distributed authorship of the various sections. Compilation of this report was facilitated by efficient processing and analysis software, major portions of which were developed by G. Maxwell, E. Cranswick, and C. Mueller. The resources of the National Strong Motion Data Center, as initially implemented by L. Baker, G. Maxwell, and J. Fletcher and operated by H. Bundock permitted this large data set to be efficiently processed. W. Kohler developed software for conversion of the data set to a format compatible with data recorded on the portable cassette recorders. The talents of C. Sullivan with TEX were most helpful and are certainly appreciated.

REFERENCES CITED

Becker, F. L. and R. L. Richardson, 1969, Critical angle reflectivity, *J. Acous. Soc. Am.* **45**, 793–794.

Becker, F. L. and R. L. Richardson, 1972, Influence of material properties on Rayleigh critical-angle reflectivity, *J. Acous. Soc. Am.* **51**, 1609–1617.

Borcherdt, R. D., Glassmoyer, G., and Wennerberg, L., 1986, Influence of welded boundaries in anelastic media on energy flow and characteristics of P, S–I and S–II waves: Observational evidence for inhomogeneous body waves in low-loss solids, *submitted to J. Geophys. Res.*

Borcherdt, R. D. and L. Wennerberg, 1985, General P, type–I S, and type–II S waves in anelastic solids: Inhomogeneous wave fields in low-loss solids, *Bull. Seismol. Soc. Am.* bf 75, 1729–1763.

Borcherdt, R. D., Fletcher, J. B., Jensen, E. G., Maxwell, G. L., VanSchaack, J. R., Warrick, R. E., Cranswick, E., Johnston, M. J. S., and McClearn, R., 1985, A General Earthquake Observation System (GEOS): *Seismol. Soc. Am. Bull.* **75**, 1783–1823.

Brekhovskikh, L. M., 1960, *Waves in Layered Media*, Academic Press, New York, 34 p.

Fuis, G. S., McCarthy, J., and Howard, K. A., 1986, A seismic-refraction survey of the Whipple Mountains metamorphic core complex, southeastern California: A progress report from PACE [abs.], *Geol. Soc. America Abs. w/Prog.*, **18**, 356.

Healy, J. H., Mooney, W. D., Blank, H. R., Gettings, M. E., Kohler, W. M., Lamson, R., and Leone, L. E., 1982, Saudi Arabian seismic deep-refraction profile: Final Project Report, *U.S. Geol. Surv. Saudi Arabian Mission Open-File Report* **02–37**, 429 p.

Howard, K. A., 1986, PACE—the Pacific to Arizona crustal experiment [abs.], *Geol. Soc. America Abs. w/Prog.*, **18**, 362.

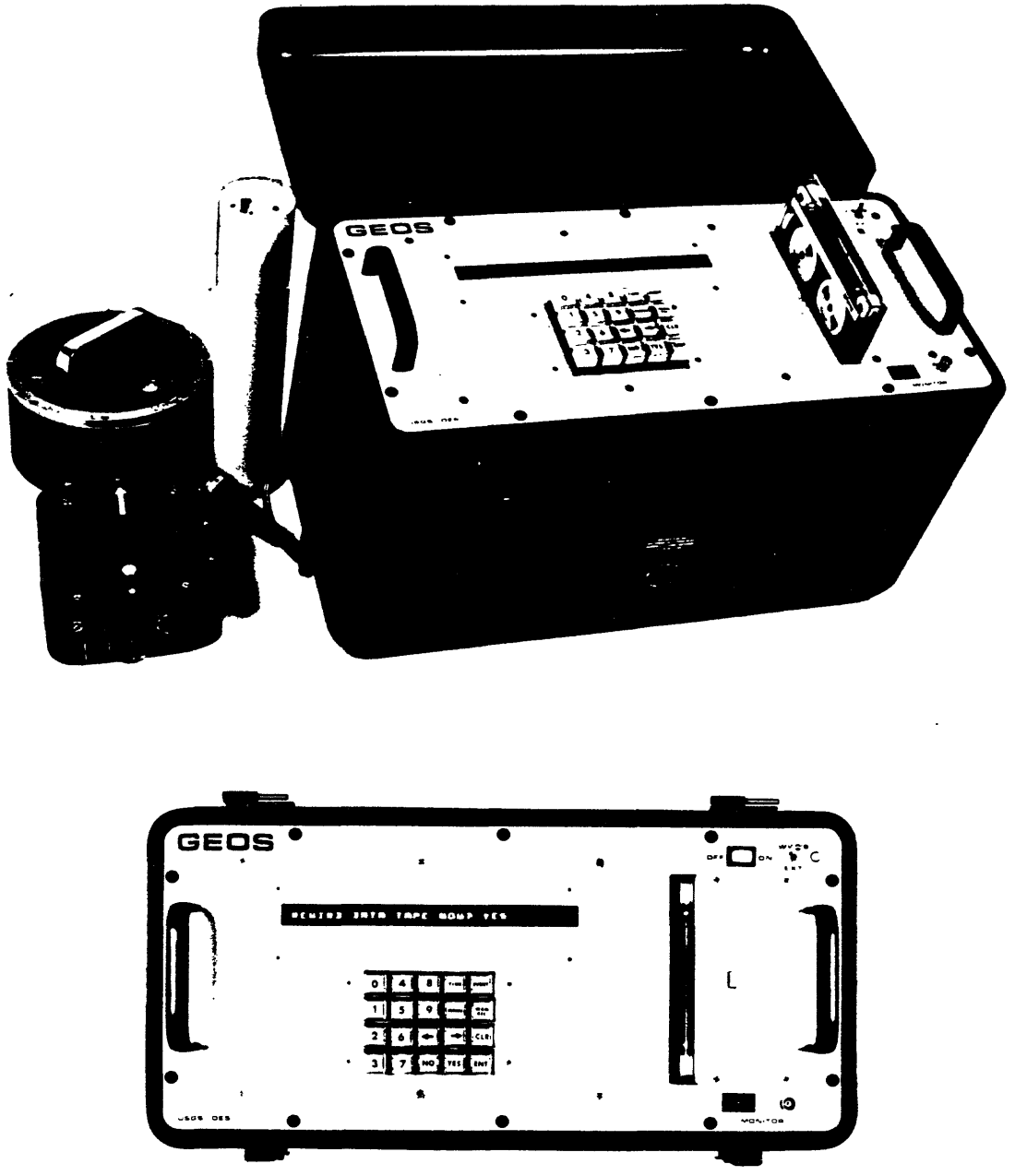

Figure 1. Side and front panel view of the General Earthquake Observation System (GEOS) together with a WWVB antenna and two sets of three-component sensors commonly used to provide more than 180 dB of linear, dynamic range. System operation for routine applications requires only initiation of power. Full capability to reconfigure system in the field is facilitated by simple operator response to english language prompts via keyboard.

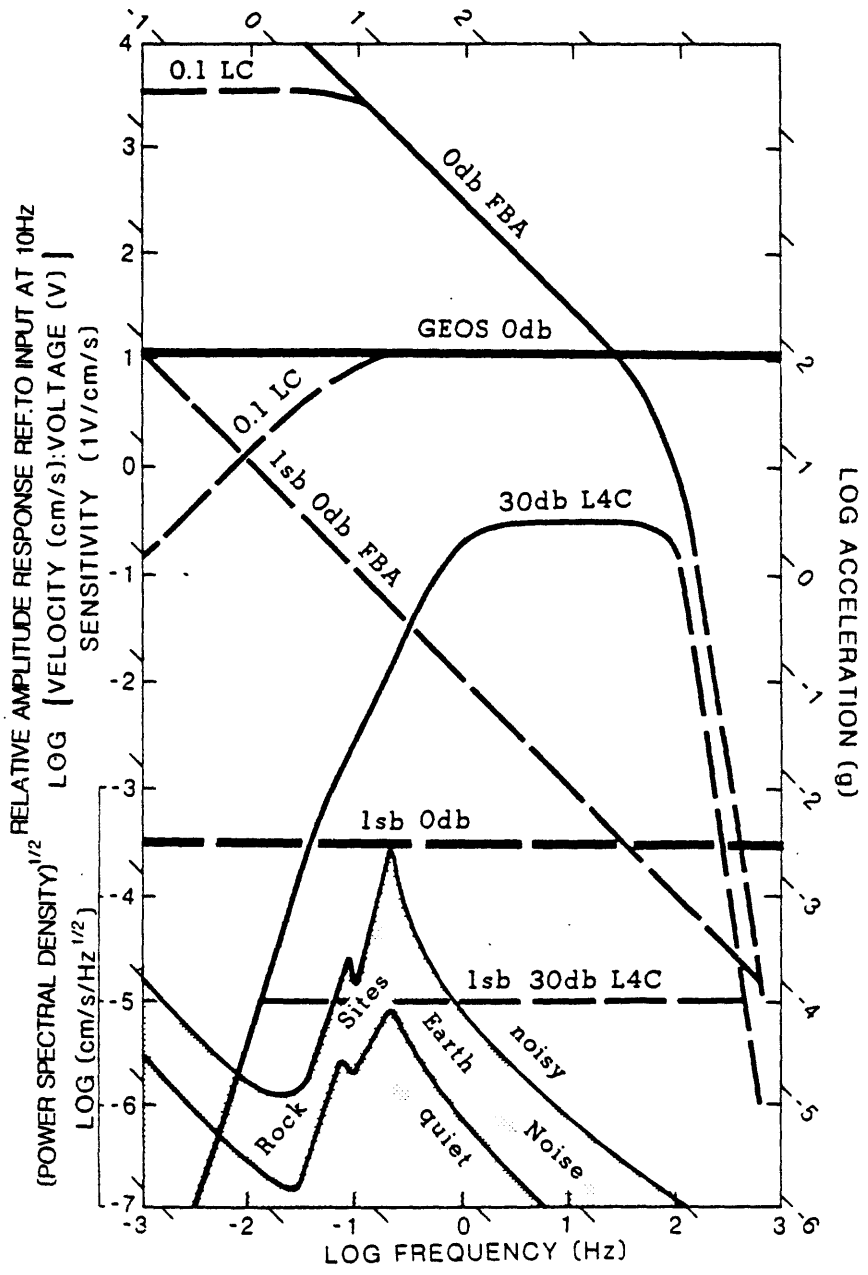

Figure 2. The unit-impulse response designed for the GEOS recorder, spectra for Earth noise (Aki and Richards, 1980), and complete system response with two types of sensors (force-balance accelerometer at 0 dB gain and L4–C velocity transducer at 30 dB gain). Two sets of sensors and linear dynamic range of 96 dB (16-bit) offers the capability to record without gain change 10 Hz signals on scale with amplitudes ranging from 20 angstroms in displacements to 2 g in acceleration.

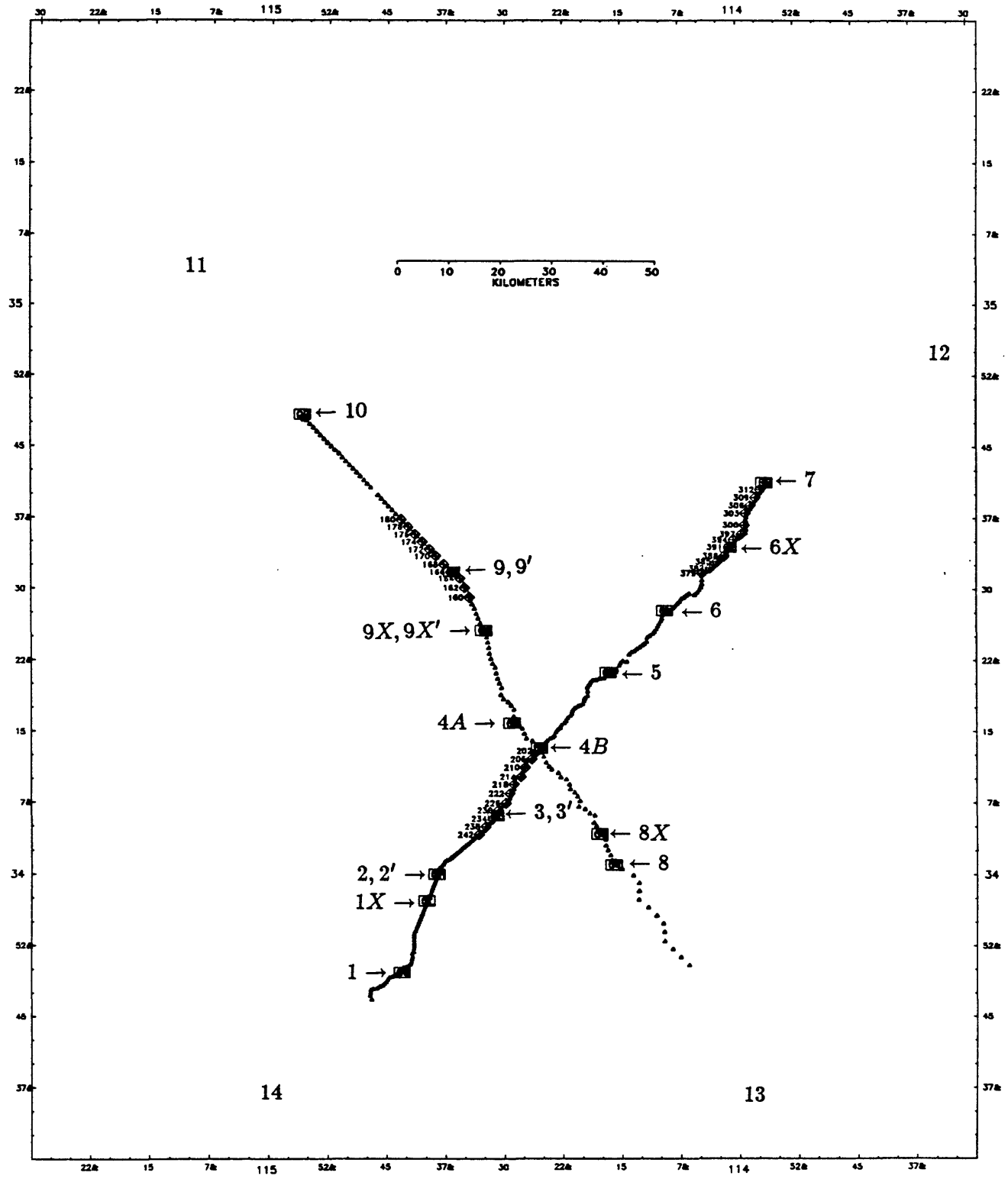

Figure 3: Map showing locations of three deployments of GEOS recorders (labeled by three digit station names) relative to cassette recorder deployments, and shots (labeled by shot point number).

Table 1:

Master Shot List

PACE - 1985

Shot Number	Shot Point	Date Shot Time	Latitude Longitude	Size (lbs)
1	8	NOV 5, 1985 309 7 0 0.011	34 1.1915 114 16.0732	3000
2	11	NOV 5, 1985 309 7 2 0.009	35 4.6421 115 9.4429	4000
3	13	NOV 5, 1985 309 7 4 0.017	33 37.5355 113 58.3179	4000
4	9	NOV 5, 1985 309 7 6 0.013	34 31.9558 114 36.7720	4000
5	9'	NOV 5, 1985 309 7 30 0.014	34 31.9558 114 36.7720	500
6	8X	NOV 5, 1985 309 9 0 0.011	34 4.4078 114 17.8740	1000
7	10	NOV 5, 1985 309 9 2 0.010	34 48.5139 114 55.9536	3000
8	4A	NOV 5, 1985 309 9 4 0.007	34 16.0713 114 29.0464	2000
9	9X	NOV 5, 1985 309 9 6 0.011	34 25.8152 114 32.6694	1000
10	9X'	NOV 5, 1985 309 9 30 0.013	34 25.8152 114 32.6694	500
11	12	NOV 7, 1985 312 6 0 0.006	34 54.5559 113 34.6748	4000
12	11	NOV 7, 1985 312 6 2 0.010	35 4.6421 115 9.4429	2000
13	14	NOV 7, 1985 312 6 4 0.008	33 37.0963 114 59.0605	2100
14	3	NOV 7, 1985 312 6 6 0.010	34 6.3268 114 31.1450	1000
15	2	NOV 7, 1985 312 6 8 0.013	34 0.1779 114 38.7549	1000
16	3'	NOV 7, 1985 312 6 30 0.011	34 6.3268 114 31.1450	500
17	2'	NOV 7, 1985 312 6 34 0.013	34 0.1779 114 38.7549	500
18	7	NOV 8, 1985 312 9 0 0.007	34 41.4065 113 56.3975	3000
19	1	NOV 8, 1985 312 9 2 0.006	33 49.8256 114 43.1675	2000

20	4B	NOV 8, 1985	34 13.4583	2000	
		312 9 4 0.010	114 25.5533		
21	1X	NOV 8, 1985	33 57.3845	500	
		312 9 6 0.013	114 40.0010		
22	12	NOV 12, 1985	34 54.5559	2400	SHOT TIME
		317 6 0 2.93	113 34.6748		NOT EXACT
23	14	NOV 12, 1985	33 37.0963	3200	
		317 6 2 0.011	114 59.0605		
24	5	NOV 12, 1985	34 21.4211	1000	(LATE)
		317 6 4 0.154	114 16.7134		
25	11	NOV 12, 1985	35 4.6421	2000	
		317 6 6 0.010	115 9.4429		
26	6X	NOV 12, 1985	34 34.5605	1000	
		317 6 8 0.010	114 1.0605		
27	7	NOV 13, 1985	34 41.4065	2000	
		317 9 0 0.008	113 56.3975		
28	1	NOV 13, 1985	33 49.8256	3000	
		317 9 2 0.011	114 43.1675		
29	4B	NOV 13, 1985	34 13.4583	2000	
		317 9 4 0.010	114 25.5533		
30	6	NOV 13, 1985	34 27.9460	720	
		317 9 8 0.010	114 9.3169		

Table 2: Station locations, instruments, and instrument recording parameters.

Station Number	Latitude	Longitude	Unit	Sample rate (ea. channel	L22 no./ gain (db)	FBA no./ gain (db)	Anti-alias filter corner freq.
160	34 29.30N	114 34.52W	18	200 sample/sec	194/60	-	50 hz.
162	34 30.31N	114 35.10W	6	200 "	201/60	-	50 hz.
164	34 31.27N	114 35.71W	32	200 "	155/60	41/18	50 hz.
166	34 31.96N	114 36.86W	30	200 "	154/60	?/6	50 hz.
168	34 32.74N	114 37.75W	23	200 "	196/60	16/18	50 hz.
170	34 33.62N	114 38.79W	4	200 "	198/60	-	50 hz.
172	34 34.32N	114 39.62W	26	200 "	186/60	-	50 hz.
174	34 35.12N	114 40.53W	3	200 "	?/60	-	50 hz.
178	34 36.72N	114 42.35W	17	200 "	145/60	-	50 hz.
180	34 37.50N	114 43.26W	7	200 "	193/60	-	50 hz.
202	34 13.15N	114 25.74W	7	200 "	185/60	42/12	50 hz.
206	34 12.29N	114 26.52W	3	200 "	186/60	-	50 hz.
210	34 11.42N	114 27.35W	18	200 "	155/60	-	50 hz.
214	34 10.43N	114 27.87W	32	200 "	197/60	-	50 hz.
218	34 09.62N	114 28.84W	6	200 "	201/60	-	50 hz.
222	34 08.65N	114 29.34W	23	200 "	154/60	-	50 hz.
226	34 07.62N	114 29.84W	30	200 "	196/60	-	50 hz.
230	34 06.88N	114 30.80W	17	200 "	194/60	12/18	50 hz.
234	34 06.00N	114 31.59W	26	100 "	193/60	28/18	50 hz.
238	34 05.19N	114 32.45W	4	200 "	162/60	-	50 hz.
242	34 04.35N	114 33.33W	22	200 "	198/60	-	50 hz.
379	34 31.85N	114 04.47W	18	400 "	201/60	-	100 hz.
382	34 32.38N	114 03.43W	3	200 "	154/60	-	50 hz.
385	34 33.06N	114 02.54W	17	200 "	196/60	-	50 hz.
388	34 33.65N	114 01.63W	4	200 "	186/60	-	50 hz.
391	34 34.58N	114 01.07W	22	200 "	185/60	42/6	50 hz.
394	34 35.37N	114 00.43W	6	200 "	194/60	-	50 hz.
397	34 35.97N	113 59.42W	12	200 "	155/60	-	50 hz.
300	34 36.95N	113 59.00W	23	200 "	200/60	-	50 hz.
303	34 38.17N	113 58.88W	26	200 "	198/60	-	50 hz.
306	34 39.00N	113 58.24W	13	200 "	188/60	-	50 hz.
309	34 39.83N	113 57.60W	30	200 "	195/60	-	50 hz.
312	34 40.66N	113 56.95W	32	200 "	159/60	-	50 hz.

Table 3: First deployment, station azimuths and distances.

Shot number 1 Shot point 8

Station	Radial azimuth	Distance (km)
160	331	59.2
162	332	61.3
164	332	63.3
166	331	65.3
168	330	67.2
170	330	69.4
172	329	71.2
174	329	73.1
176	329	75.1
178	328	77.1
180	328	79.1

Shot number 2 Shot point 11

Station	Radial azimuth	Distance (km)
160	141	84.3
162	141	82.3
164	140	80.3
166	141	78.2
168	141	76.2
170	141	74.0
172	141	72.2
174	141	70.2
176	141	68.1
178	142	66.1
180	142	64.1

Shot number 3 Shot point 13

Station	Radial azimuth	Distance (km)
160	330	110.8
162	330	112.9
164	330	114.9
166	329	116.9
168	329	118.8
170	329	121.0
172	329	122.8
174	329	124.7
176	328	126.7
178	328	128.7
180	328	130.7

Shot number 4 Shot point 9

Station	Radial azimuth	Distance (km)
160	145	6.0
162	140	4.0
164	128	2.1
166	274	0.1
168	314	2.1
170	315	4.4
172	315	6.2
174	316	8.2
176	316	10.2
178	316	12.3
180	316	14.3

Shot number 5 Shot point 9'

Station	Radial azimuth	Distance (km)
160	145	6.0
162	140	4.0
164	128	2.1
166	274	0.1
168	314	2.1
170	315	4.4
172	315	6.2
174	316	8.2
176	316	10.2
178	316	12.3
180	316	14.3

Shot number 6 Shot point 8X

Station	Radial azimuth	Distance (km)
160	331	52.7
162	331	54.7
164	331	56.7
166	330	58.7
168	330	60.6
170	329	62.9
172	329	64.6
174	329	66.6
176	328	68.6
178	328	70.6
180	328	72.5

Shot number 7 Shot point 10

Station	Radial azimuth	Distance (km)
160	138	48.3
162	137	46.3
164	136	44.4
166	137	42.3
168	137	40.3
170	137	38.0
172	137	36.2
174	137	34.2
176	137	32.1
178	137	30.1
180	137	28.1

Shot number 8 Shot point 4A

Station	Radial azimuth	Distance (km)
160	341	25.9
162	341	27.9
164	340	29.9
166	338	31.8
168	337	33.6
170	335	35.8
172	334	37.5
174	334	39.4
176	333	41.4
178	332	43.3
180	331	45.2

Shot number 9 Shot point 9X

Station	Radial azimuth	Distance (km)
160	336	7.0
162	336	9.1
164	335	11.1
166	331	13.1
168	329	15.0
170	327	17.2
172	326	19.0
174	325	21.0
176	324	23.0
178	324	25.0
180	323	27.0

Shot number 10 Shot point 9X'

Station	Radial azimuth	Distance (km)
160	336	7.0
162	336	9.1
164	335	11.1
166	331	13.1
168	329	15.0
170	327	17.2
172	326	19.0
174	325	21.0
176	324	23.0
178	324	25.0
180	323	27.0

Table 4: Second deployment, station azimuths and distances.

Shot number 11 Shot point 12

Station	Radial azimuth	Distance (km)
202	225	109.3
206	225	111.3
210	225	113.3
214	225	115.2
218	225	117.3
222	224	119.1
226	224	121.0
230	224	123.0
234	224	125.0
238	224	127.0
242	224	129.1

Shot number 12 Shot point 11

Station	Radial azimuth	Distance (km)
202	145	116.3
206	146	117.0
210	147	117.6
214	148	118.7
218	149	119.2
222	150	120.4
226	150	121.6
230	151	122.1
234	152	123.0
238	153	123.7
242	154	124.5

Shot number 13 Shot point 14

Station	Radial azimuth	Distance (km)
202	38	84.1
206	38	82.2
210	38	80.1
214	38	78.2
218	38	76.1
222	38	74.2
226	39	72.2
230	38	70.2
234	38	68.2
238	38	66.2
242	38	64.1

Shot number 14 Shot point 3

Station	Radial azimuth	Distance (km)
202	33	15.1
206	33	13.1
210	32	11.1
214	33	9.1
218	30	7.0
222	33	5.1
226	40	3.1
230	27	1.2
234	228	0.9
238	224	2.9
242	223	5.0

Shot number 15 Shot point 2

Station	Radial azimuth	Distance (km)
202	40	31.2
206	40	29.2
210	40	27.2
214	41	25.3
218	41	23.2
222	43	21.3
226	45	19.4
230	45	17.4
234	46	15.4
238	46	13.4
242	47	11.4

Shot number 16 Shot point 3'

Station	Radial azimuth	Distance (km)
202	33	15.1
206	33	13.1
210	32	11.1
214	33	9.1
218	30	7.0
222	33	5.1
226	40	3.1
230	27	1.2
234	228	0.9
238	224	2.9
242	223	5.0

Shot number 17 Shot point 2'

Station	Radial azimuth	Distance (km)
202	40	31.2
206	40	29.2
210	40	27.2
214	41	25.3
218	41	23.2
222	43	21.3
226	45	19.4
230	45	17.4
234	46	15.4
238	46	13.4
242	47	11.4

Shot number 18 Shot point 7

Station	Radial azimuth	Distance (km)
202	220	68.9
206	220	70.9
210	220	72.9
214	220	74.8
218	220	77.0
222	220	78.8
226	219	80.8
230	219	82.8
234	219	84.8
238	219	86.8
242	219	88.9

Shot number 19 Shot point 1

Station	Radial azimuth	Distance (km)
202	32	50.8
206	32	48.8
210	31	46.8
214	32	44.8
218	31	42.7
222	31	40.8
226	32	38.8
230	31	36.9
234	31	34.8
238	30	32.9
242	29	30.9

Shot number 20 Shot point 4B

Station	Radial azimuth	Distance (km)
202	207	0.6
206	214	2.6
210	216	4.7
214	212	6.6
218	215	8.7
222	213	10.6
226	211	12.7
230	213	14.6
234	214	16.6
238	215	18.6
242	215	20.6

Shot number 21 Shot point 1X

Station	Radial azimuth	Distance (km)
202	37	36.5
206	37	34.5
210	37	32.4
214	38	30.5
218	37	28.4
222	38	26.5
226	39	24.5
230	39	22.6
234	39	20.5
238	39	18.5
242	38	16.5

Table 5: Third deployment, station azimuths and distances.

Shot number 22 Shot point 12

Station	Radial azimuth	Distance (km)
379	227	61.9
382	227	60.0
385	227	58.2
388	227	56.4
391	227	54.6
394	228	52.9
397	227	51.0
300	229	49.3
303	230	47.7
306	231	46.0
309	232	44.3
312	233	42.5

Shot number 23 Shot point 14

Station	Radial azimuth	Distance (km)
379	12	103.5
382	12	104.8
385	13	106.3
388	13	107.7
391	14	109.6
394	14	111.2
397	15	112.7
300	15	114.6
303	15	116.8
306	15	118.5
309	15	120.3
312	15	122.0

Shot number 24 Shot point 5

Station	Radial azimuth	Distance (km)
379	44	26.9
382	45	28.7
385	45	30.5
388	46	32.3
391	44	34.1
394	44	35.8
397	44	37.7
300	43	39.5
303	41	41.3
306	41	43.1
309	41	44.9
312	40	46.7

Shot number 25 Shot point 11

Station	Radial azimuth	Distance (km)
379	122	116.0
382	121	116.8
385	120	117.3
388	119	118.0
391	118	117.9
394	118	118.1
397	117	118.9
300	116	118.7
303	115	117.9
306	114	118.2
309	113	118.4
312	112	118.8

Shot number 26 Shot point 6X

Station	Radial azimuth	Distance (km)
379	226	7.2
382	222	5.4
385	219	3.6
388	207	1.9
391	345	0.0
394	33	1.8
397	44	3.6
300	35	5.4
303	26	7.5
306	28	9.3
309	28	11.1
312	29	12.9

Shot number 27 Shot point 7

Station	Radial azimuth	Distance (km)
379	215	21.6
382	213	19.9
385	211	18.1
388	209	16.4
391	209	14.5
394	209	12.8
397	205	11.1
300	206	9.1
303	212	7.1
306	212	5.3
309	212	3.4
312	211	1.6

Shot number 28 Shot point 1

Station	Radial azimuth	Distance (km)
379	37	97.8
382	38	99.6
385	38	101.4
388	38	103.1
391	38	105.0
394	38	106.8
397	38	108.6
300	38	110.4
303	37	112.3
306	37	114.1
309	37	115.9
312	37	117.8

Shot number 29 Shot point 4B

Station	Radial azimuth	Distance (km)
379	44	46.9
382	44	48.7
385	44	50.5
388	44	52.3
391	44	54.1
394	44	55.9
397	44	57.7
300	43	59.5
303	42	61.3
306	42	63.1
309	41	64.9
312	41	66.7

Shot number 30 Shot point 6

Station	Radial azimuth	Distance (km)
379	46	10.3
382	48	12.2
385	48	14.0
388	48	15.8
391	46	17.6
394	45	19.3
397	45	21.2
300	43	22.9
303	40	24.7
306	40	26.5
309	39	28.4
312	39	30.2

Table 6: Maximum observed accelerations (see figures 31-35)

Distance from shot pt.	*Max acc.* (cm/sec^2)	*Shot size* (*lbs.*)	*Shot* point	*Station*
$< 50\,meters$	539	1000	6X	391
.1 km	$983 < acc. <\sim 1500^*$	4000	9	166
.1 km	322	500	9′	166
.9 km	4.1	1000	3	234
.9 km	3.5	500	3′	234
1.2 km	1.4	1000	3	230
1.2 km	1.0	500	3′	230
2.1 km	11.5	4000	9	164
2.1 km	3.8	4000	9	168
2.1 km	2.4	500	9′	164
2.1 km	1.0	500	9′	168

*Upper bound based on linear extrapolation of recorded data adjacent to clipped data point. Lower bound is maximum on scale at 6db gain. Note that the upper bound is slightly less than if ground motion at station 166 had scaled with shot size as station 164, but greater than if it had scaled as station 168.

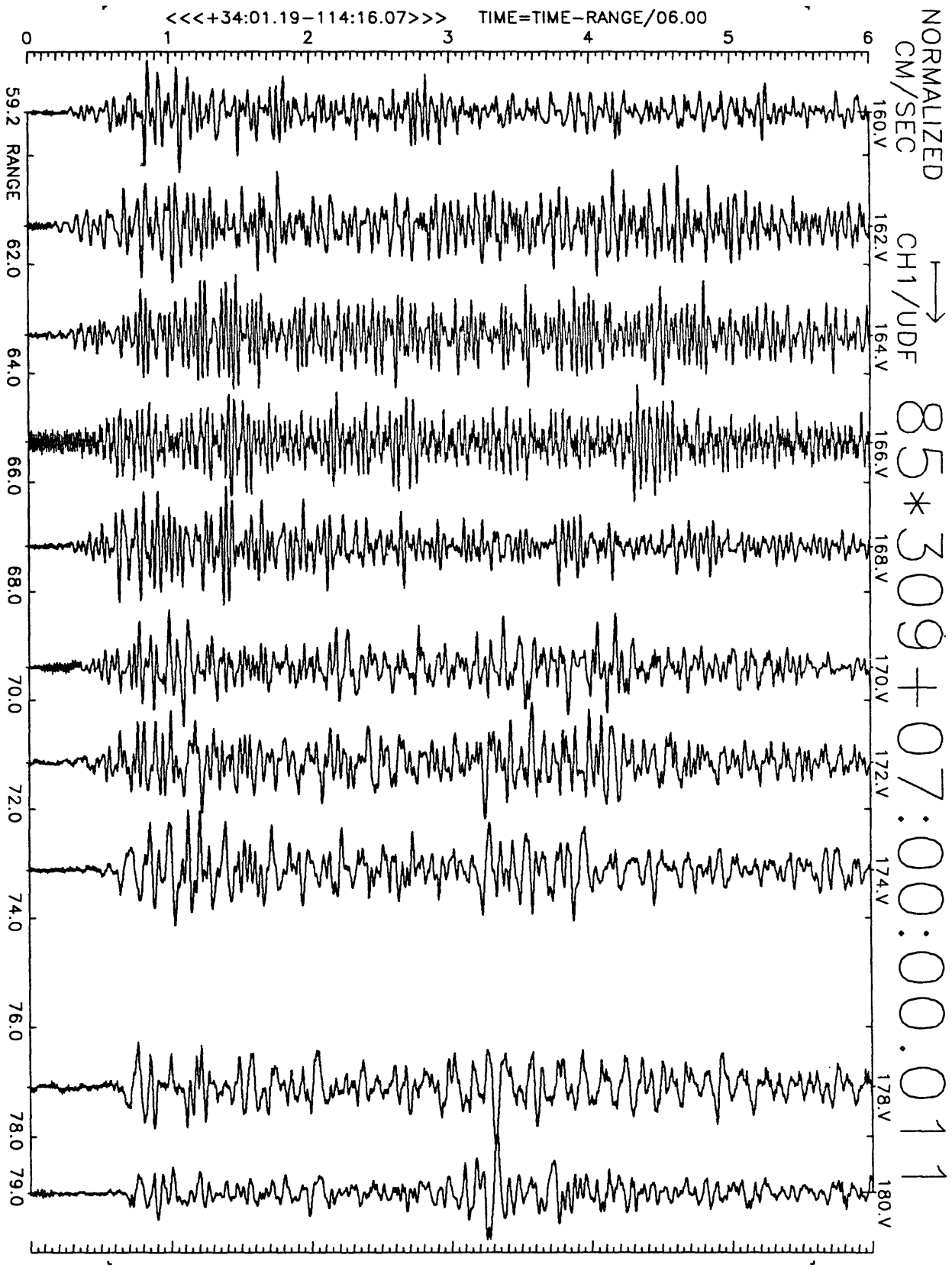

Figure A1(a), shot point 8: 6 second velocity record. Positive vertical motion is to right. Abscissa is distance to shot point. Top of trace is labeled with station number. Times are reduced by 6 km/sec. Shot time is indicated.

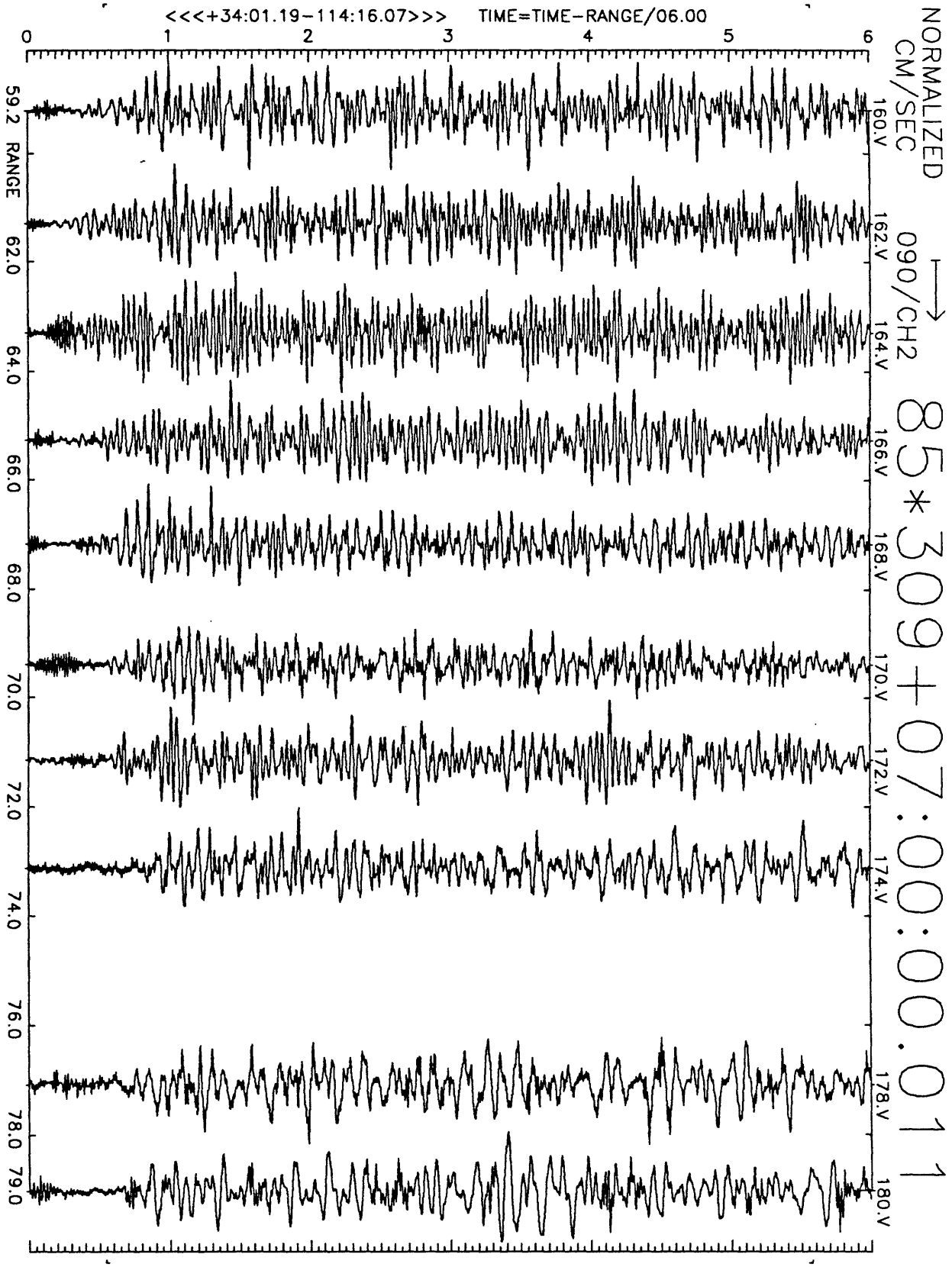

Figure A1(b), shot point 8: 6 second velocity record. Positive N33W motion is to right. Abscissa is distance to shot point. Top of trace is labeled with station number. Times are reduced by 6 km/sec. Shot time is indicated.

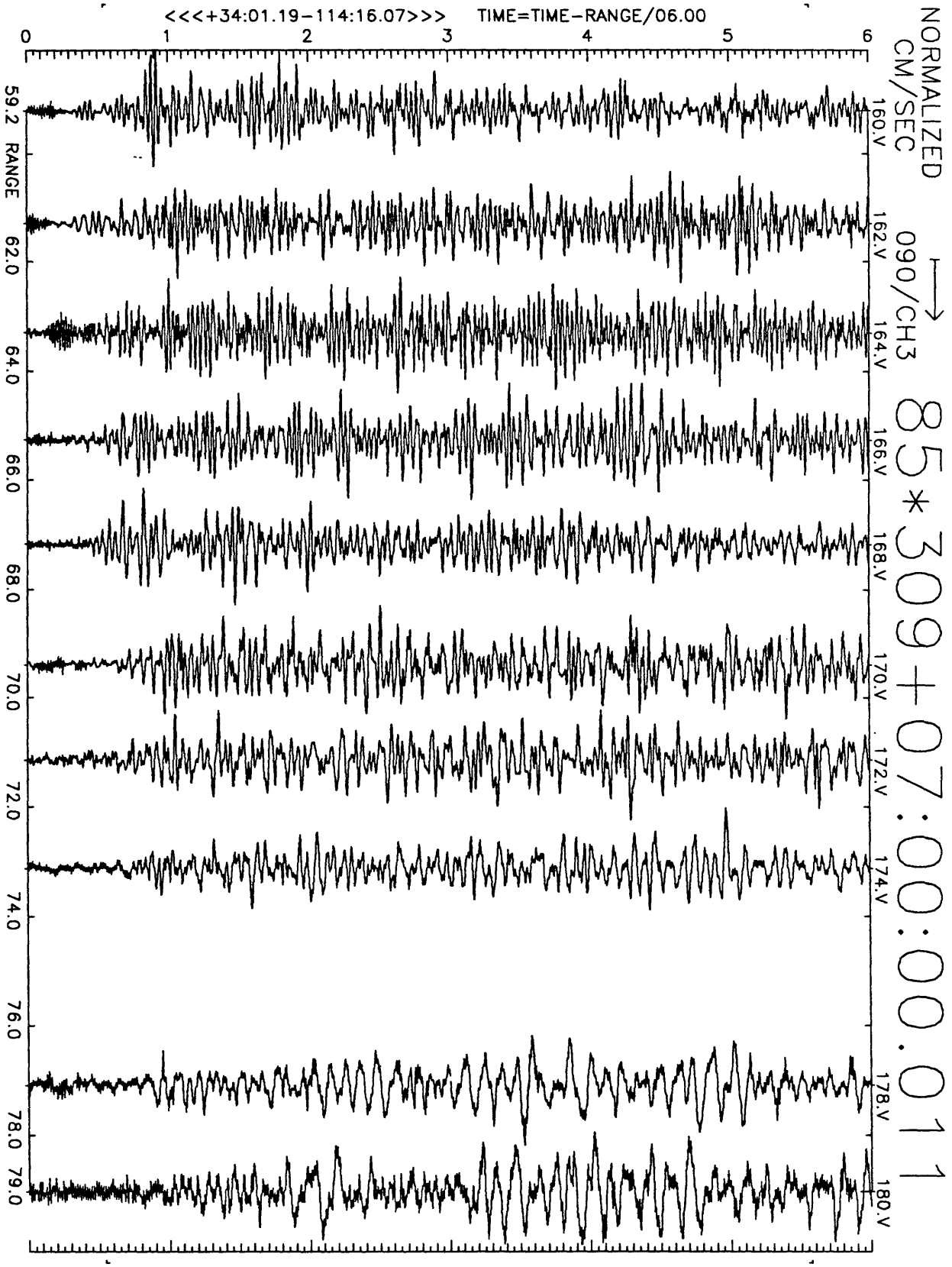

Figure A1(c), shot point 8: 6 second velocity record. Positive N57E motion is to right. Abscissa is distance to shot point. Top of trace is labeled with station number. Times are reduced by 6 km/sec. Shot time is indicated.

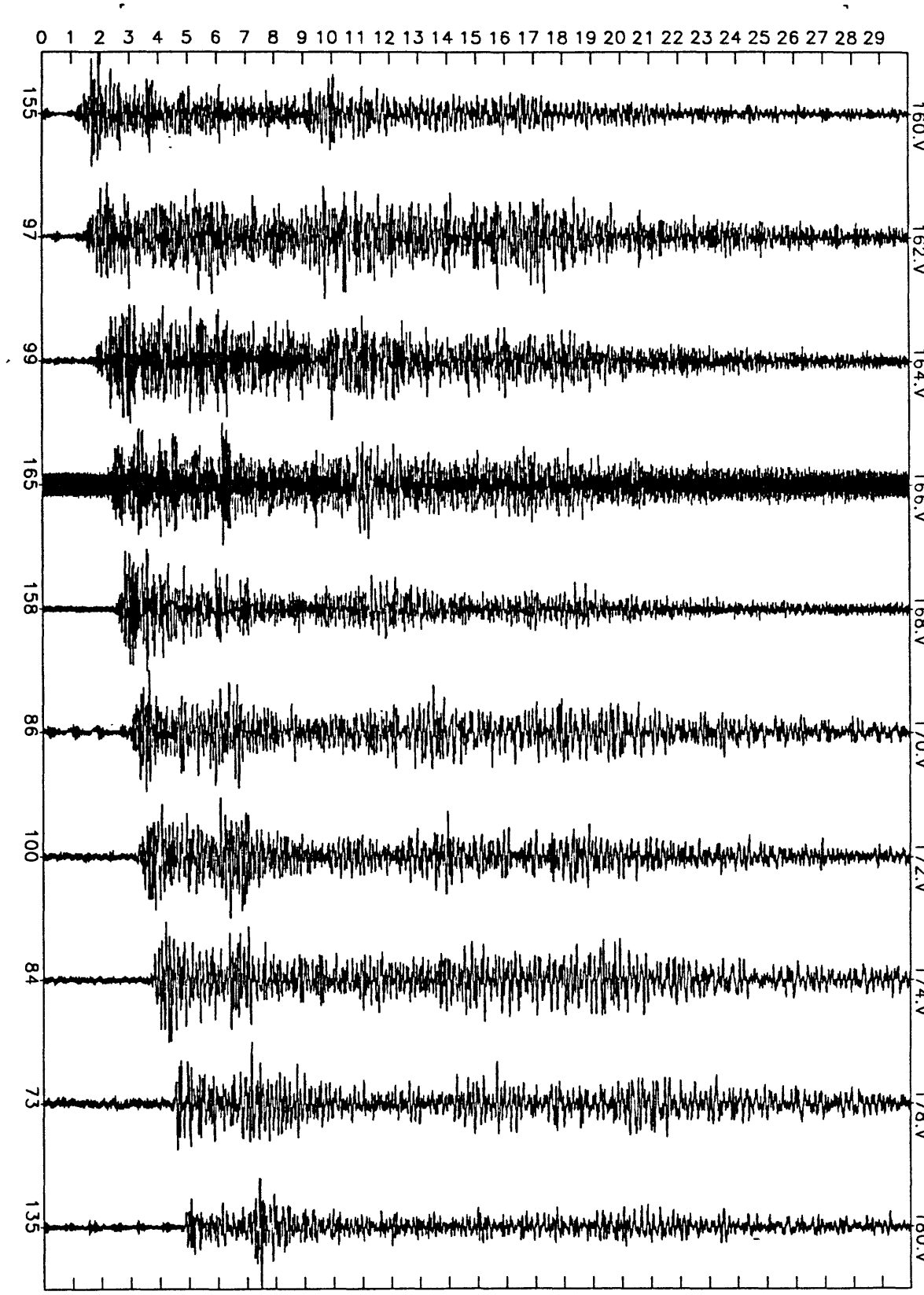

Figure A1(d), shot point 8: 30 second vertical velocity record. Abscissa is labeled with maximum counts in record (multiply by $\frac{10}{2^{24}-2^5} \approx 6 \times 10^{-7}$ to get cm/sec). Times are unreduced beginning at time indicated.

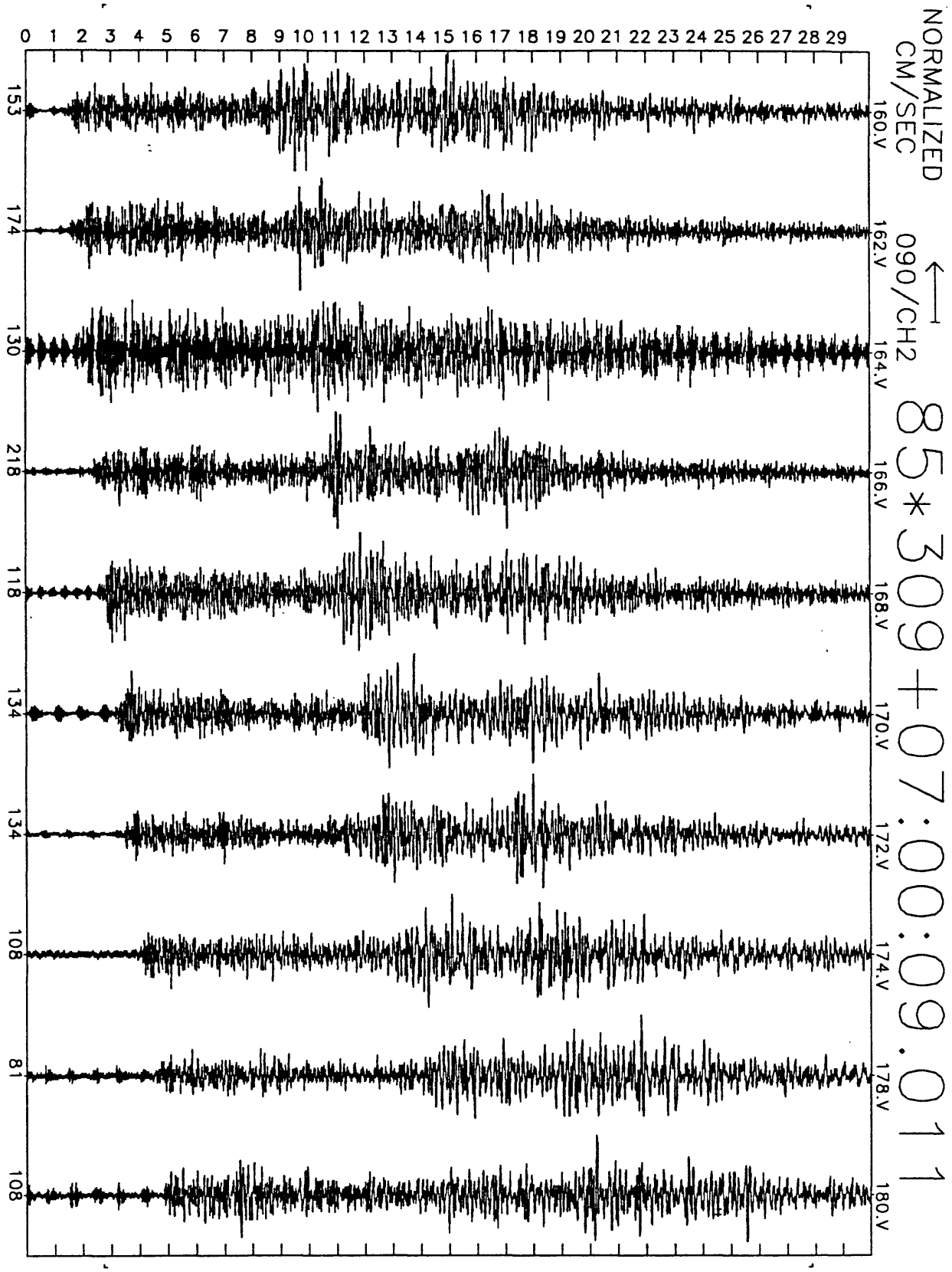

Figure A1(e), shot point 8: 30 second N33W velocity record. Abscissa is labeled with maximum counts in record (multiply by $\frac{10}{2^{24}-2^5} \approx 6 \times 10^{-7}$ to get cm/sec). Times are unreduced beginning at time indicated.

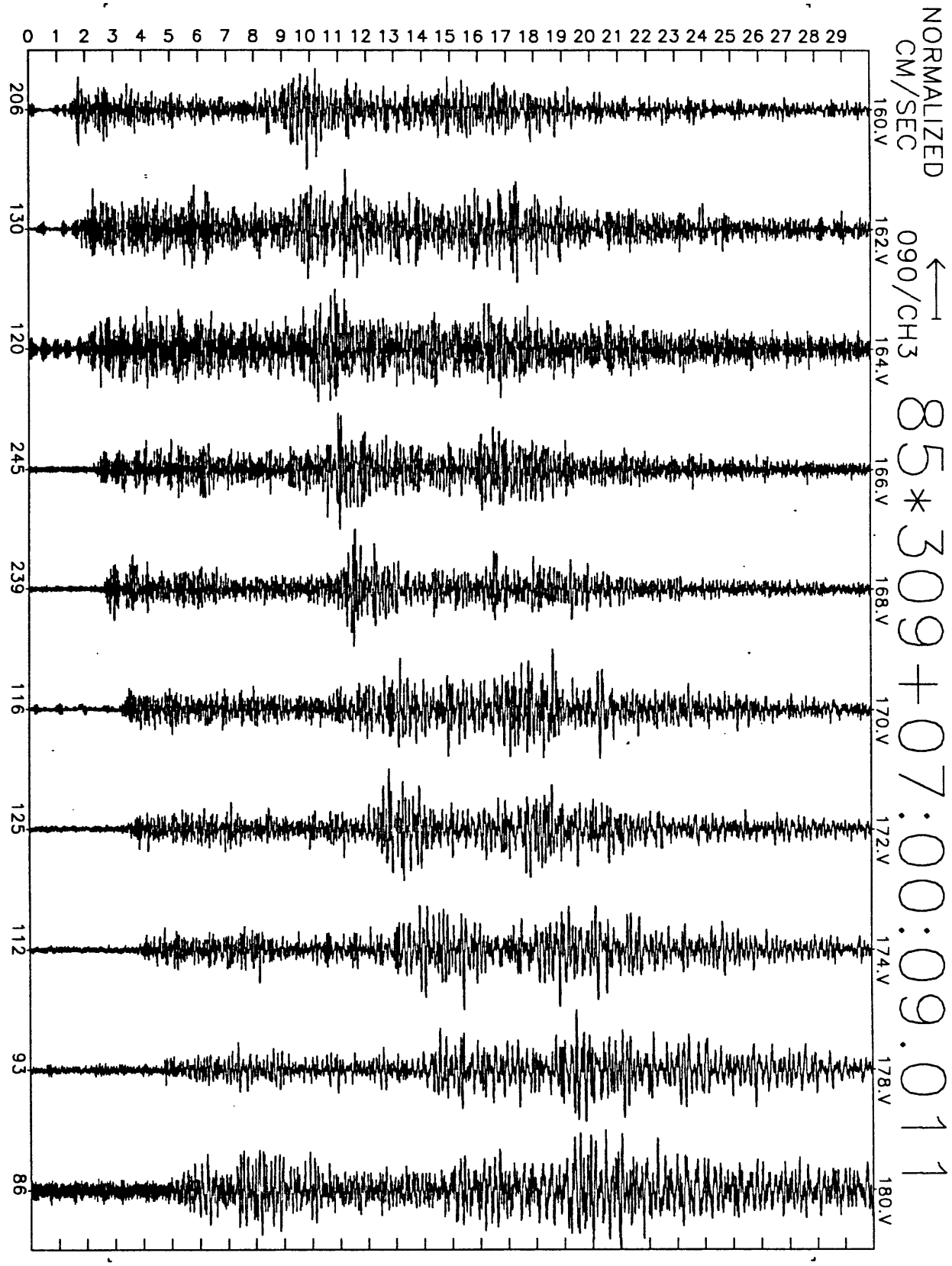

Figure A1(f), shot point 8: 30 second N57E velocity record. Abscissa is labeled with maximum counts in record (multiply by $\frac{10}{2^{24}-2^8} \approx 6 \times 10^{-7}$ to get cm/sec). Times are unreduced beginning at time indicated.

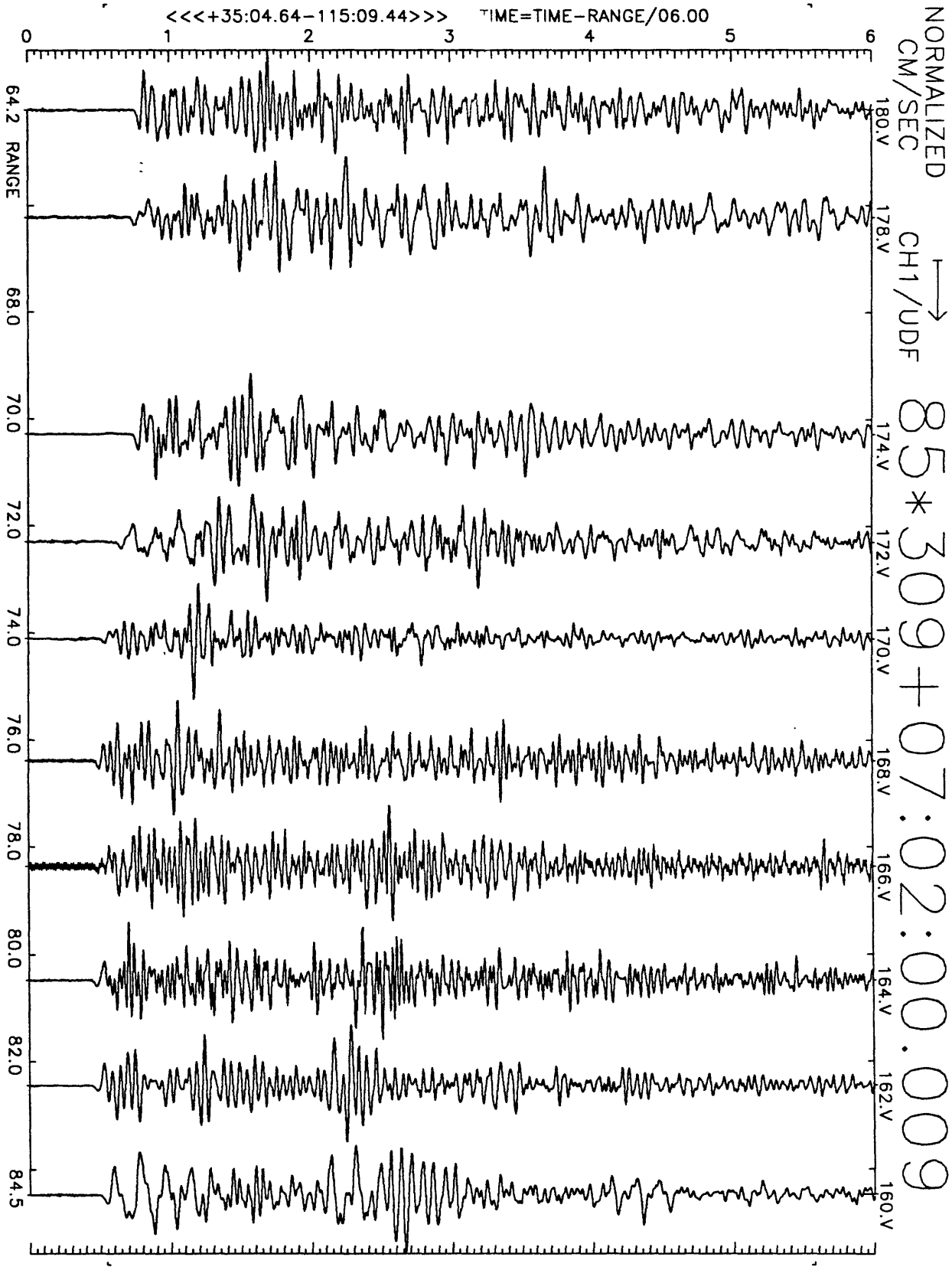

Figure A2(a), shot point 11: 6 second velocity record. Positive vertical motion is to right. Abscissa is distance to shot point. Top of trace is labeled with station number. Times are reduced by 6 km/sec. Shot time is indicated.

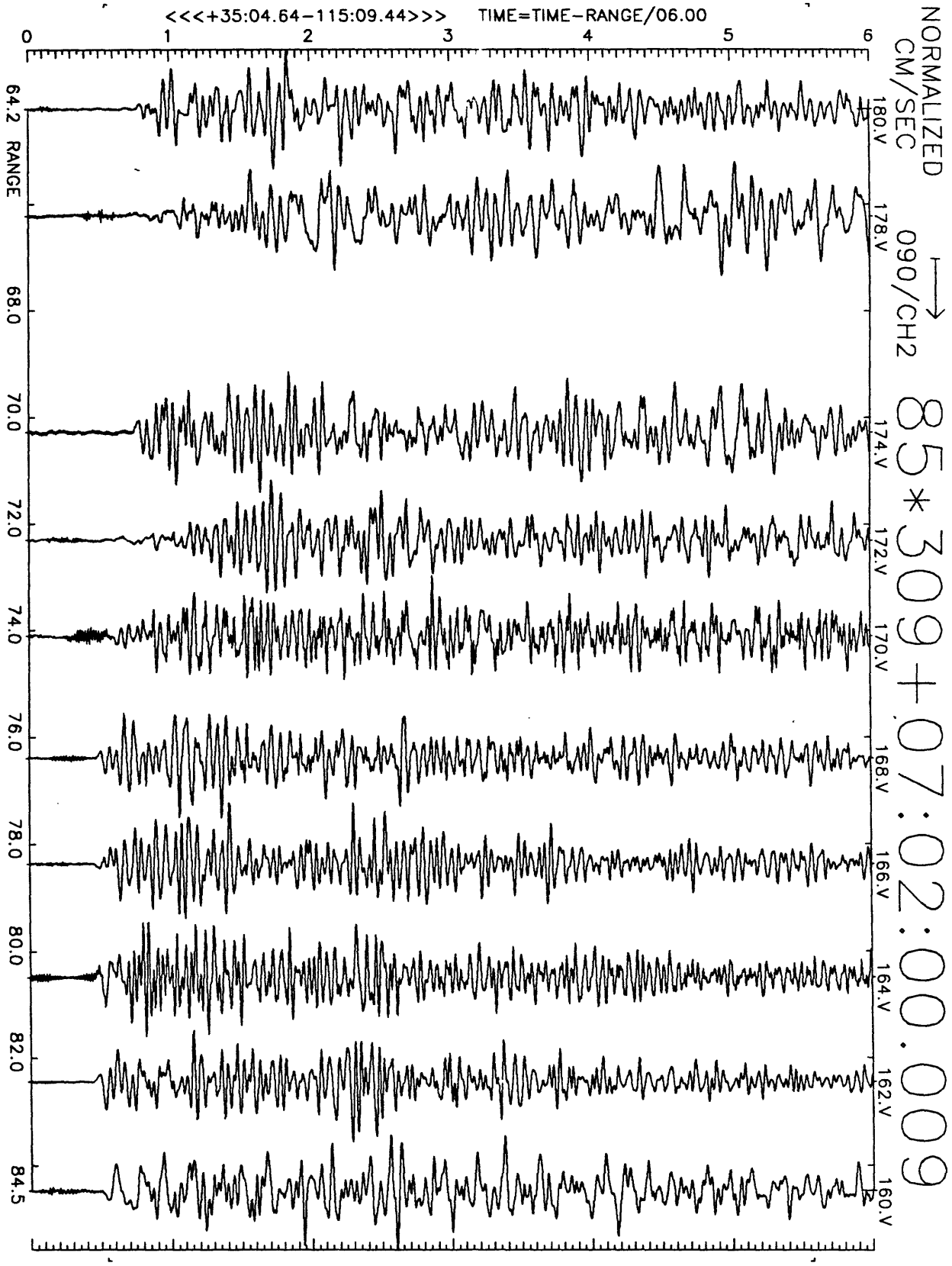

Figure A2(b), shot point 11: 6 second velocity record. Positive N33W motion is to right. Abscissa is distance to shot point. Top of trace is labeled with station number. Times are reduced by 6 km/sec. Shot time is indicated.

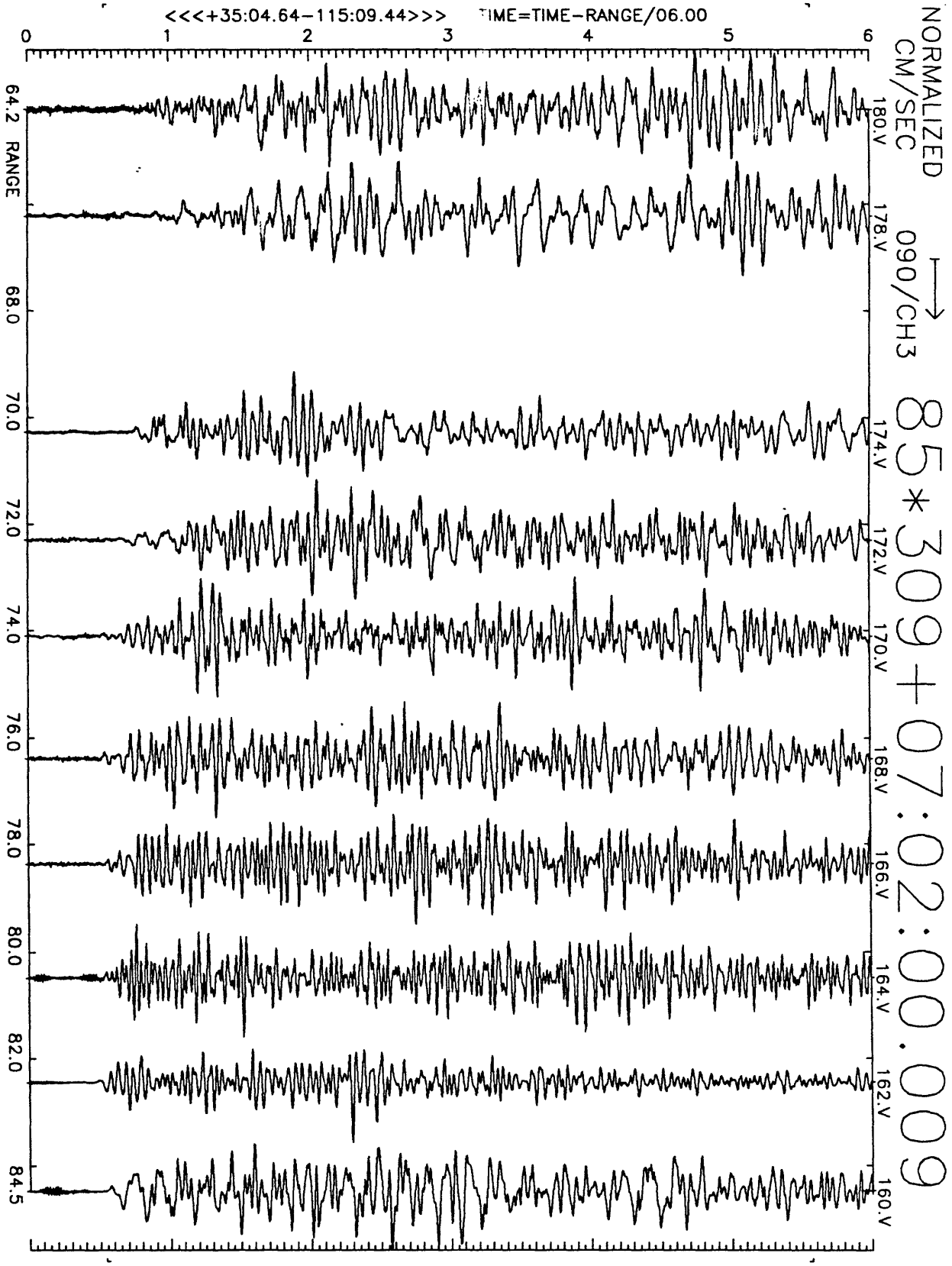

Figure A2(c), shot point 11: 6 second velocity record. Positive N57E motion is to right. Abscissa is distance to shot point. Top of trace is labeled with station number. Times are reduced by 6 km/sec. Shot time is indicated.

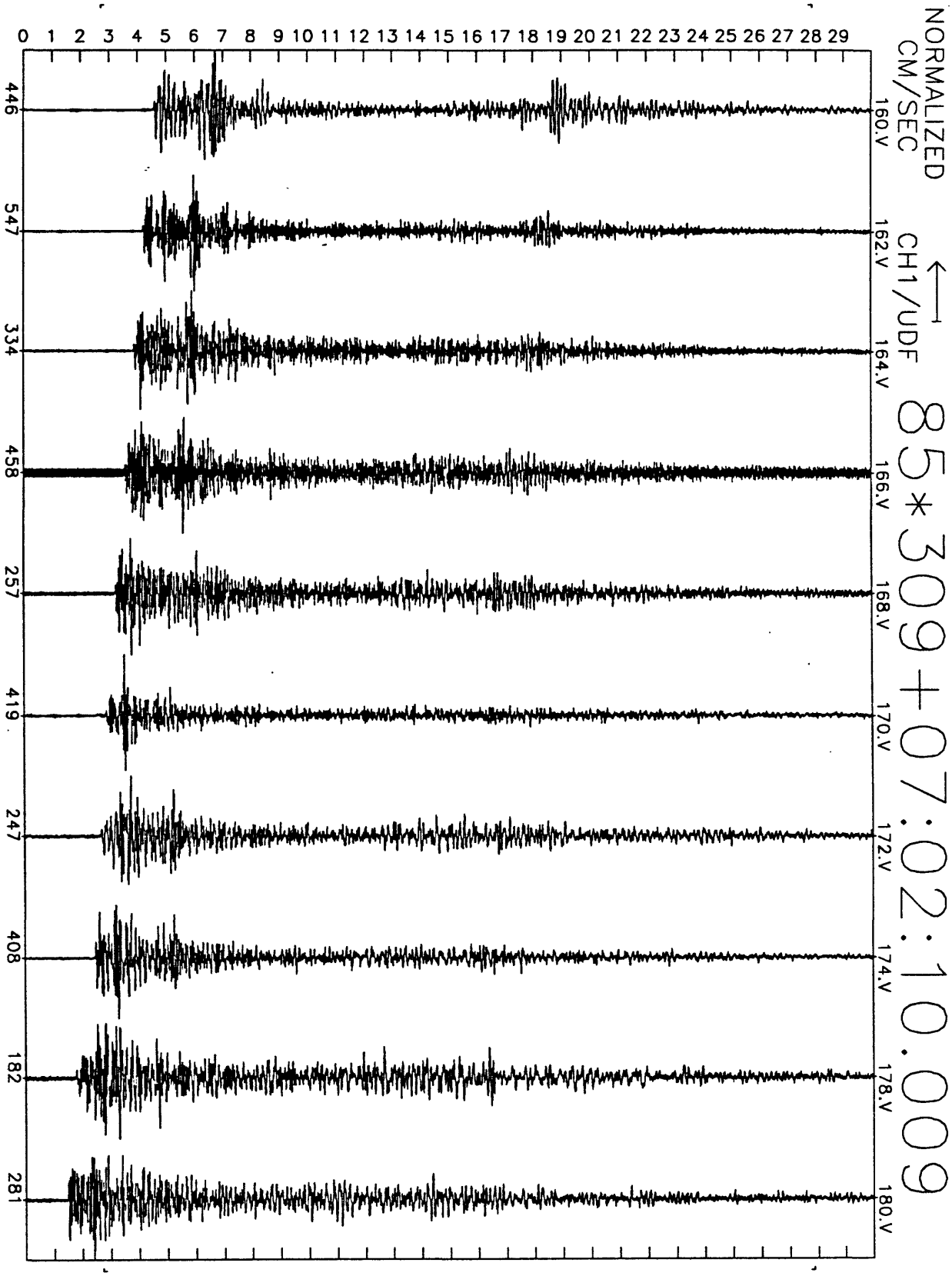

Figure A2(d), shot point 11: 30 second vertical velocity record. Abscissa is labeled with maximum counts in record (multiply by $\frac{10}{2^{24}-2^5} \approx 6 \times 10^{-7}$ to get cm/sec). Times are unreduced beginning at time indicated.

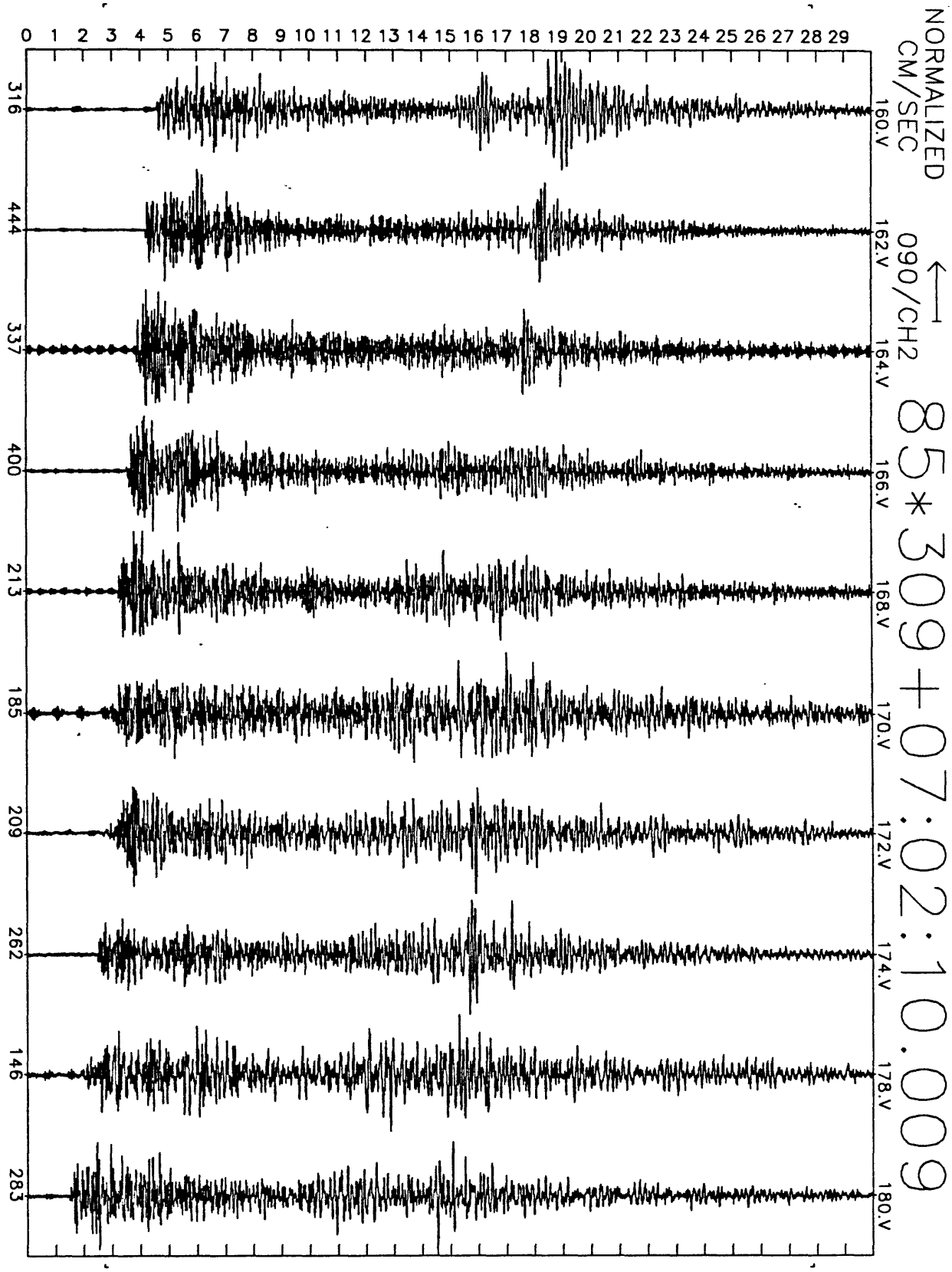

Figure A2(e), shot point 11: 30 second N33W velocity record. Abscissa is labeled with maximum counts in record (multiply by $\frac{10}{2^{24}-2^{5}} \approx 6 \times 10^{-7}$ to get cm/sec). Times are unreduced beginning at time indicated.

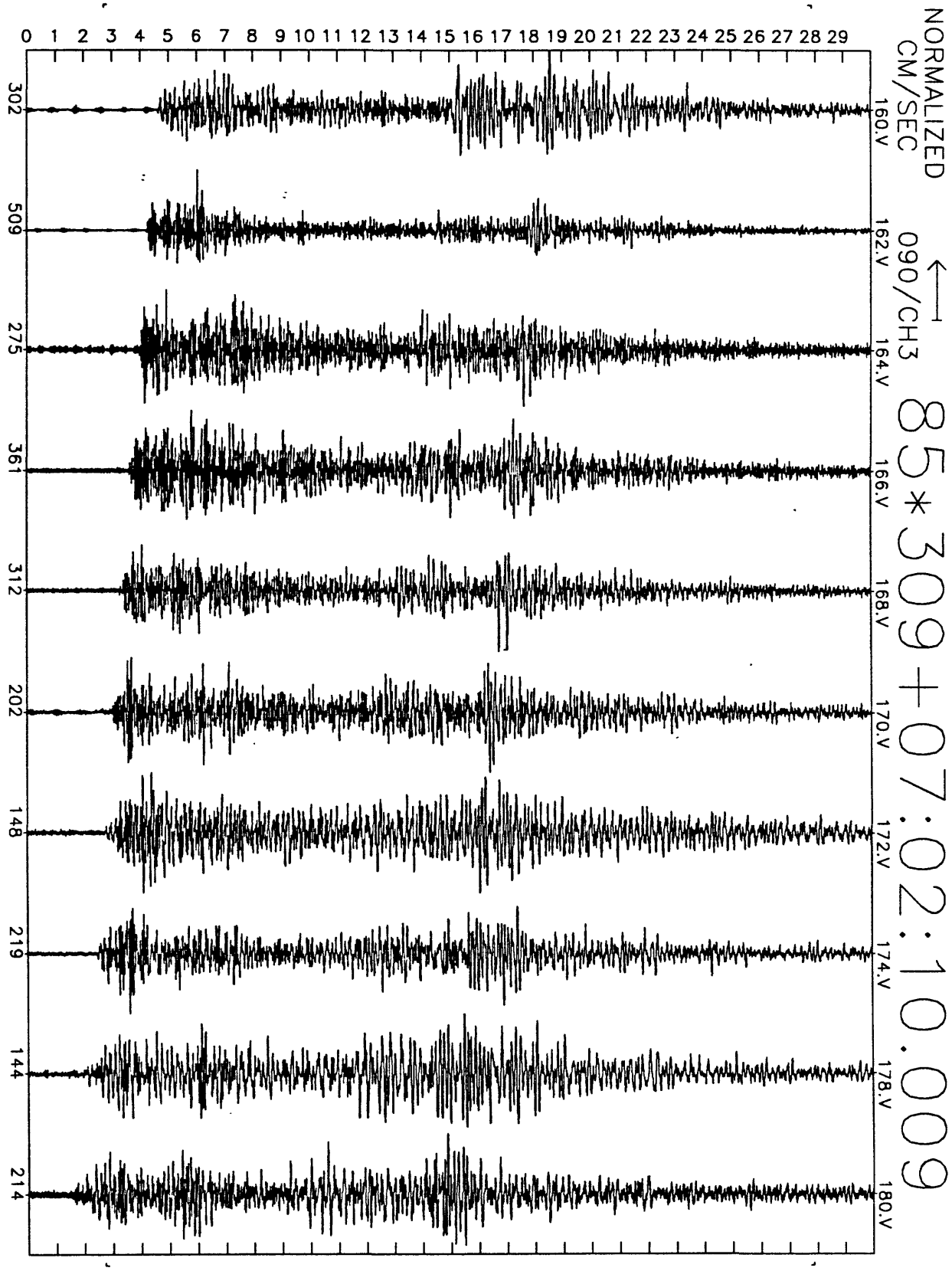

Figure A2(f), shot point 11: 30 second N57E velocity record. Abscissa is labeled with maximum counts in record (multiply by $\frac{10}{2^{24}-2^{8}} \approx 6 \times 10^{-7}$ to get cm/sec). Times are unreduced beginning at time indicated.

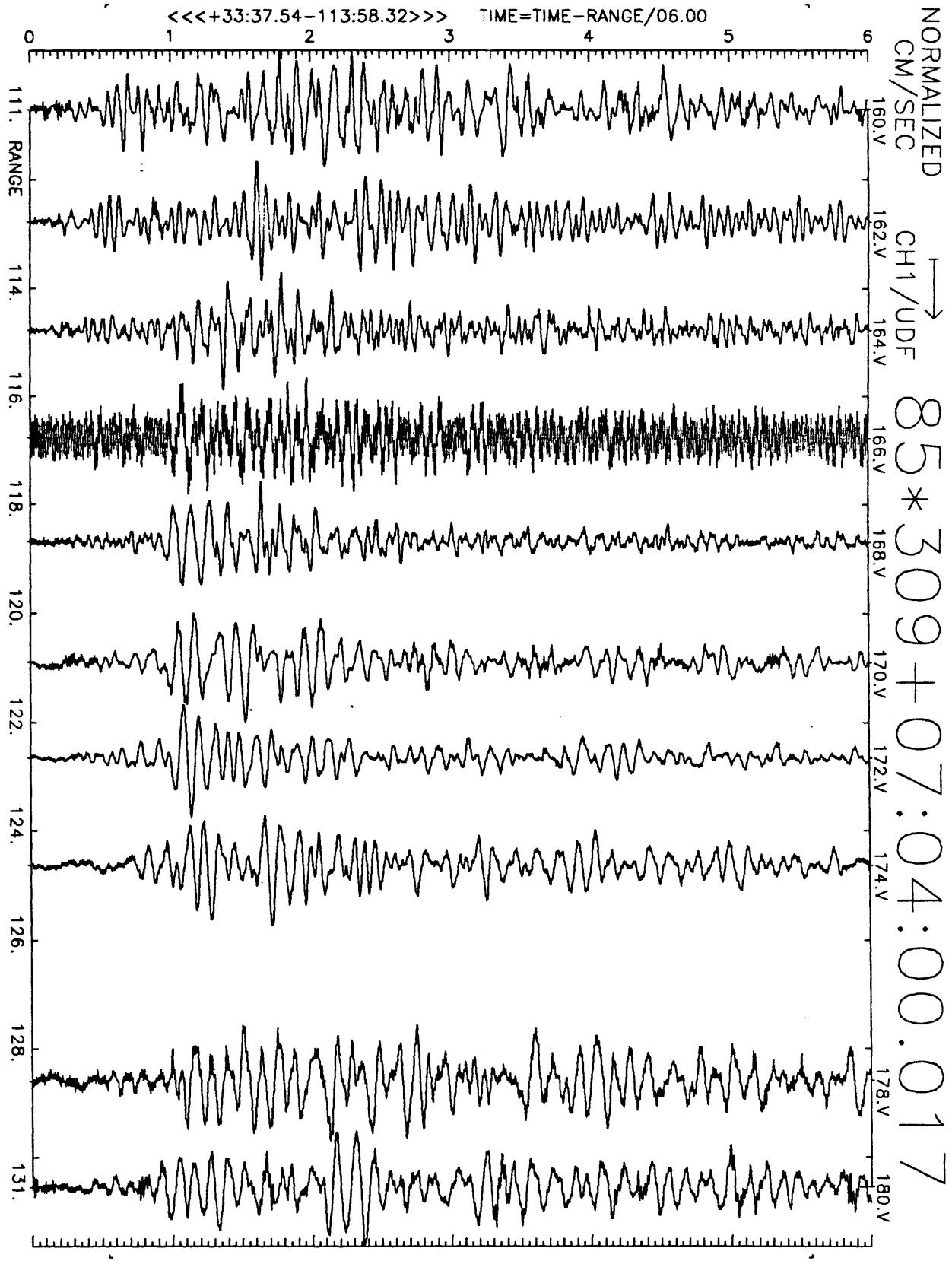

Figure A3(a), shot point 13: 6 second velocity record. Positive vertical motion is to right. Abscissa is distance to shot point. Top of trace is labeled with station number. Times are reduced by 6 km/sec. Shot time is indicated.

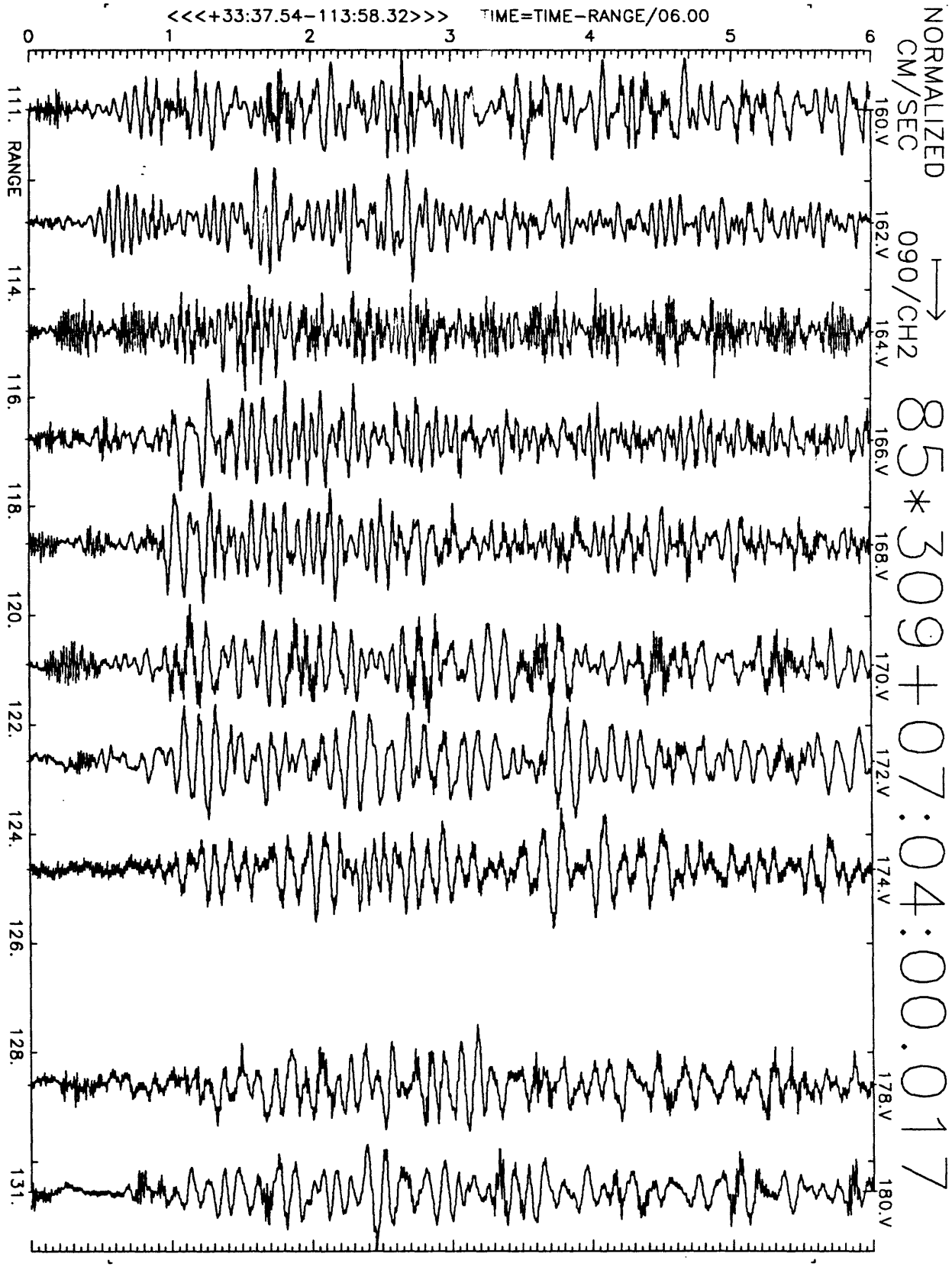

Figure A3(b), shot point 13: 6 second velocity record. Positive N33W motion is to right. Abscissa is distance to shot point. Top of trace is labeled with station number. Times are reduced by 6 km/sec. Shot time is indicated.

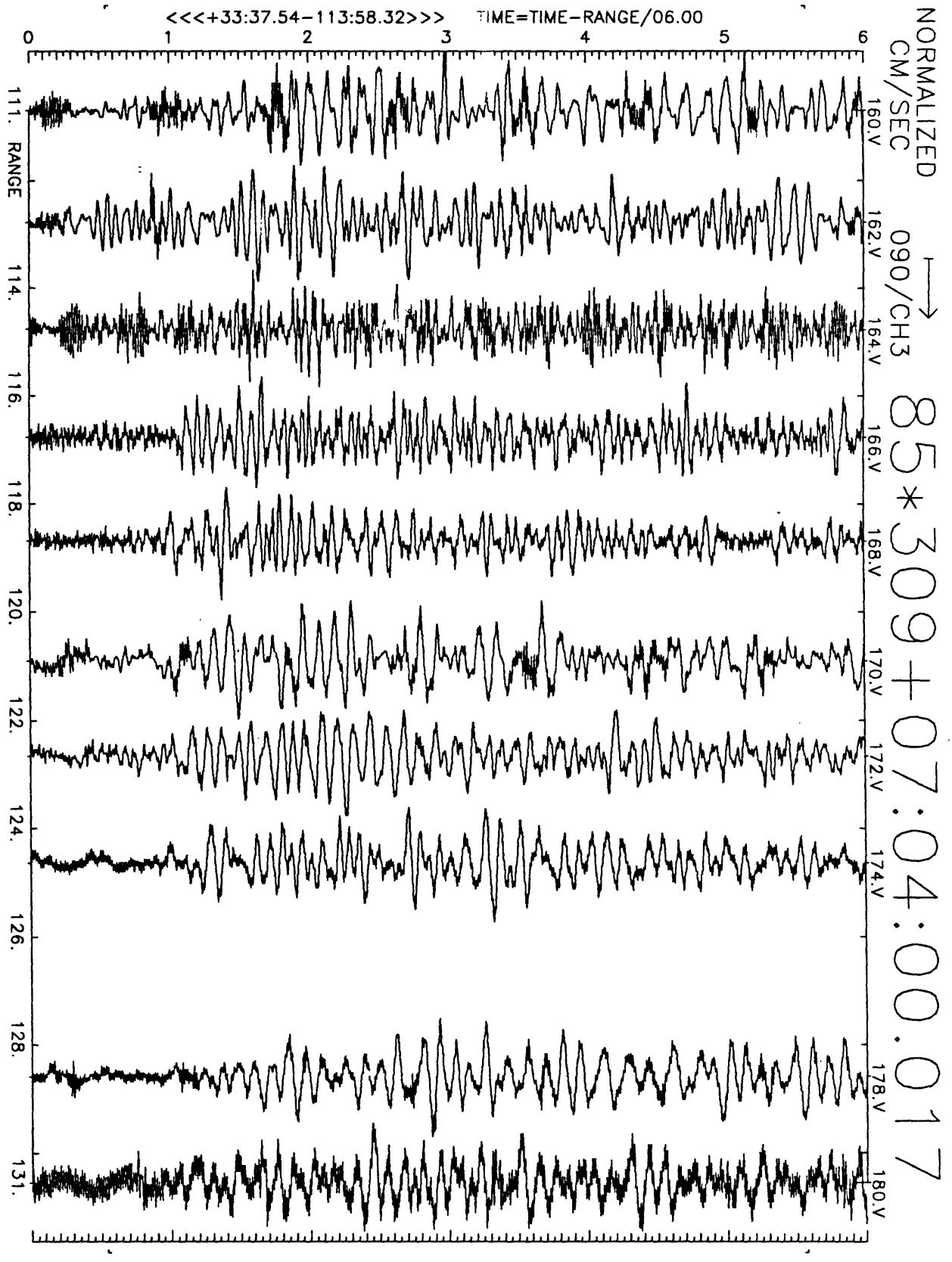

Figure A3(c), shot point 13: 6 second velocity record. Positive N57E motion is to right. Abscissa is distance to shot point. Top of trace is labeled with station number. Times are reduced by 6 km/sec. Shot time is indicated.

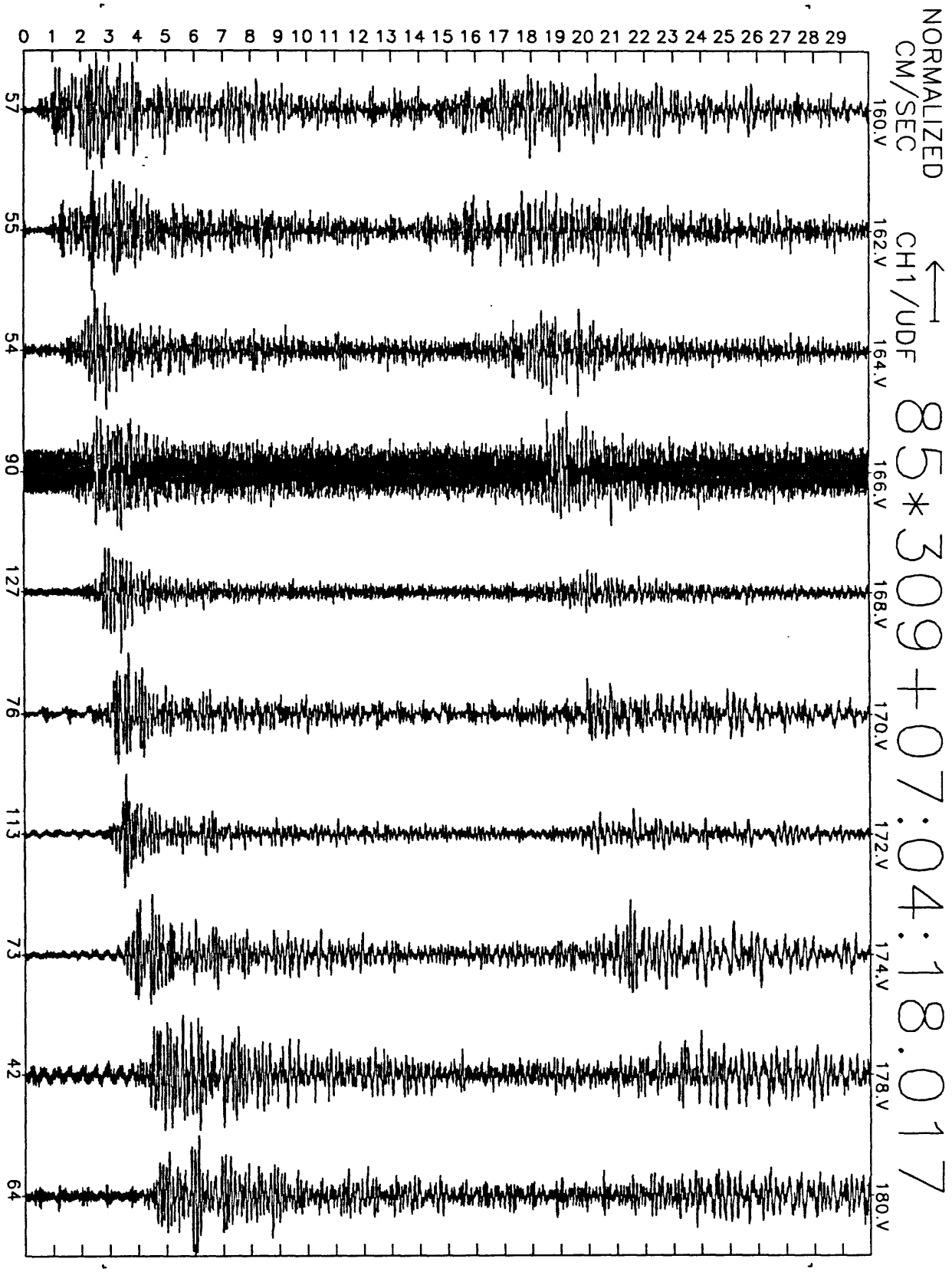

Figure A3(d), shot point 13: 30 second vertical velocity record. Abscissa is labeled with maximum counts in record (multiply by $\frac{10}{2^{24}-2^5} \approx 6 \times 10^{-7}$ to get cm/sec). Times are unreduced beginning at time indicated.

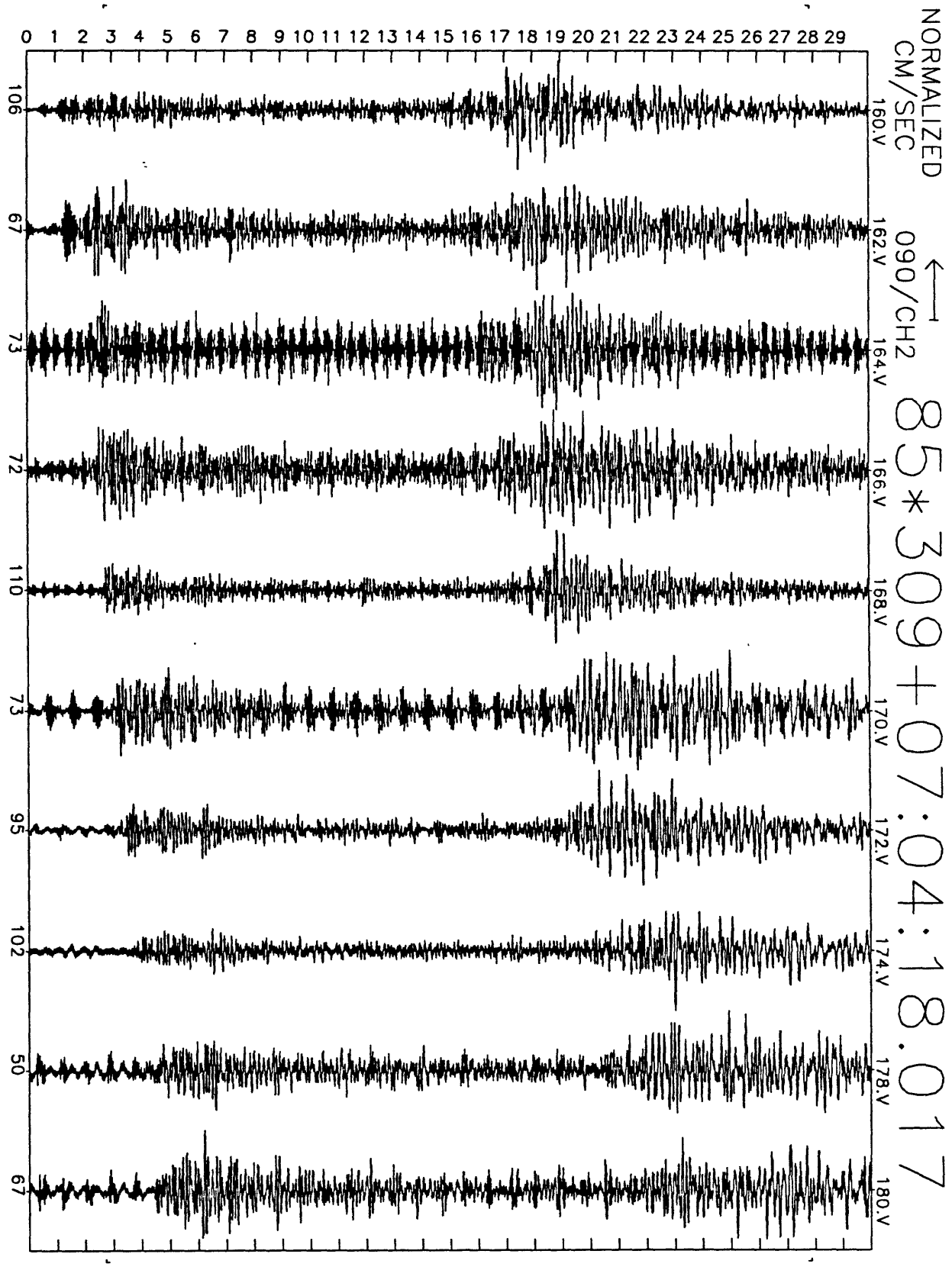

Figure A3(e), shot point 13: 30 second N33W velocity record. Abscissa is labeled with maximum counts in record (multiply by $\frac{10}{2^{24}-2^8} \approx 6 \times 10^{-7}$ to get cm/sec). Times are unreduced beginning at time indicated.

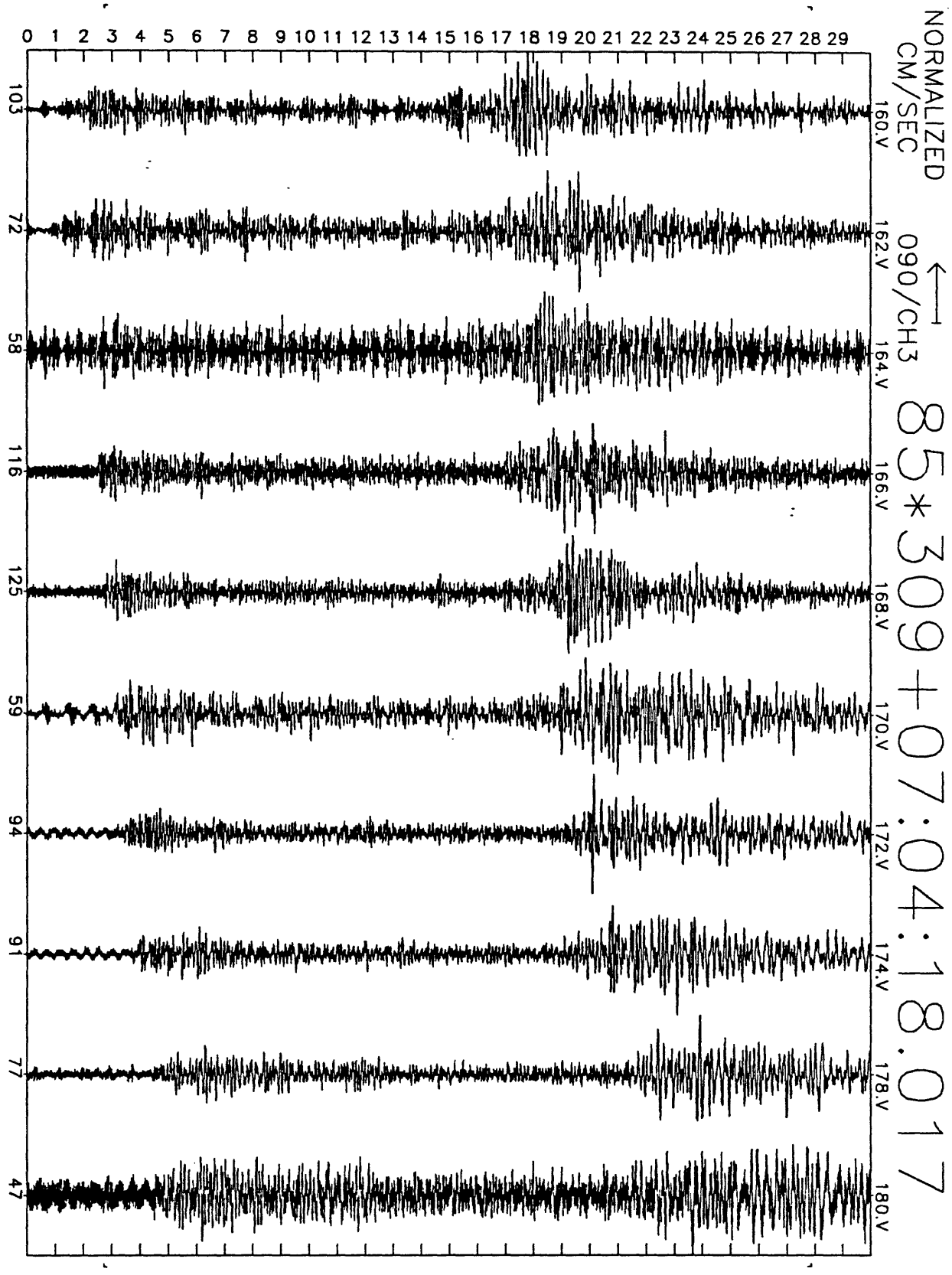

Figure A3(f), shot point 13: 30 second N57E velocity record. Abscissa is labeled with maximum counts in record (multiply by $\frac{10}{2^{24}-2^{8}} \approx 6 \times 10^{-7}$ to get cm/sec). Times are unreduced beginning at time indicated.

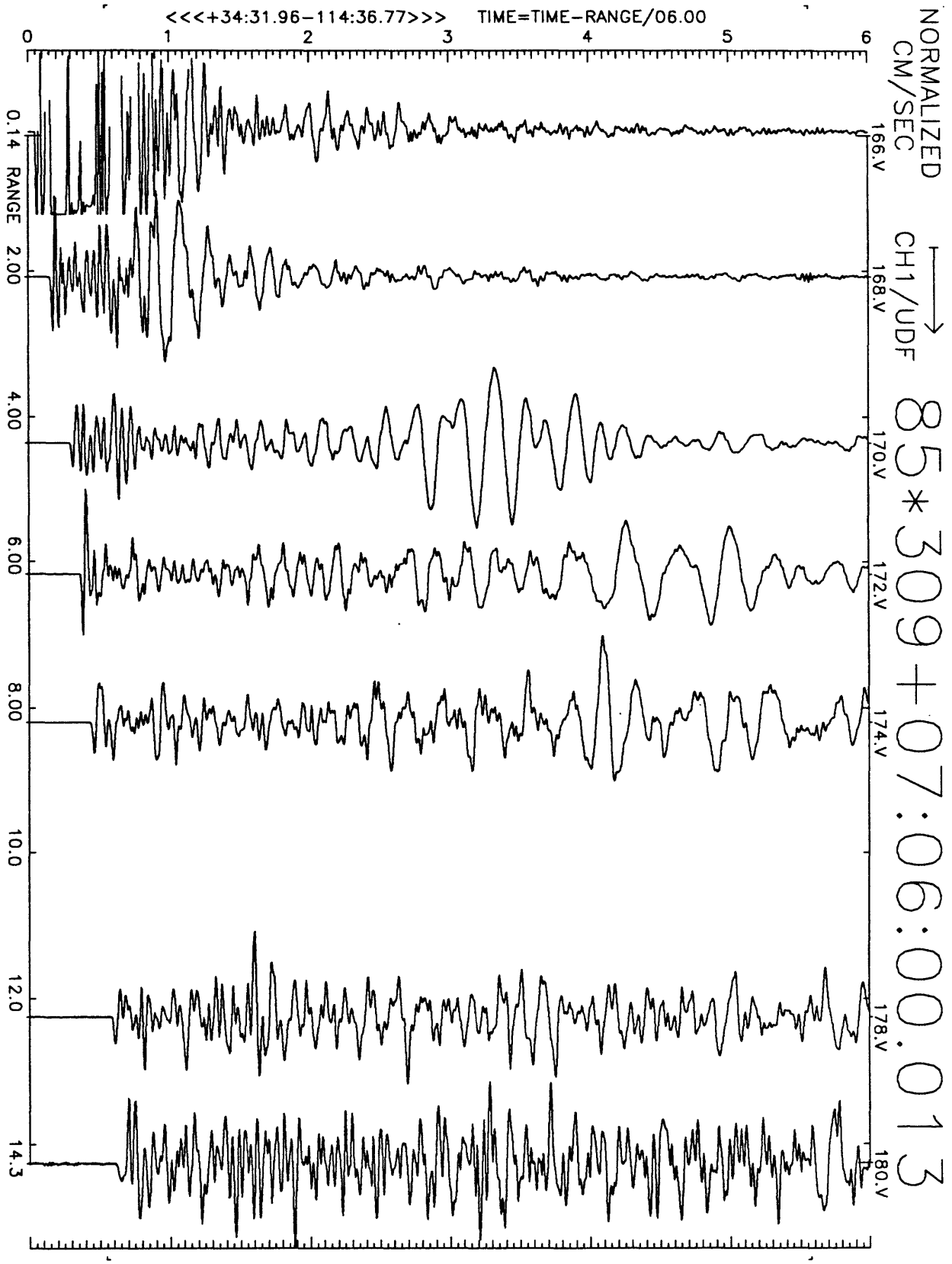

Figure A4(a), shot point 9, NW stations: 6 second velocity record. Positive vertical motion is to right. Abscissa is distance to shot point. Top of trace is labeled with station number. Times are reduced by 6 km/sec. Shot time is indicated.

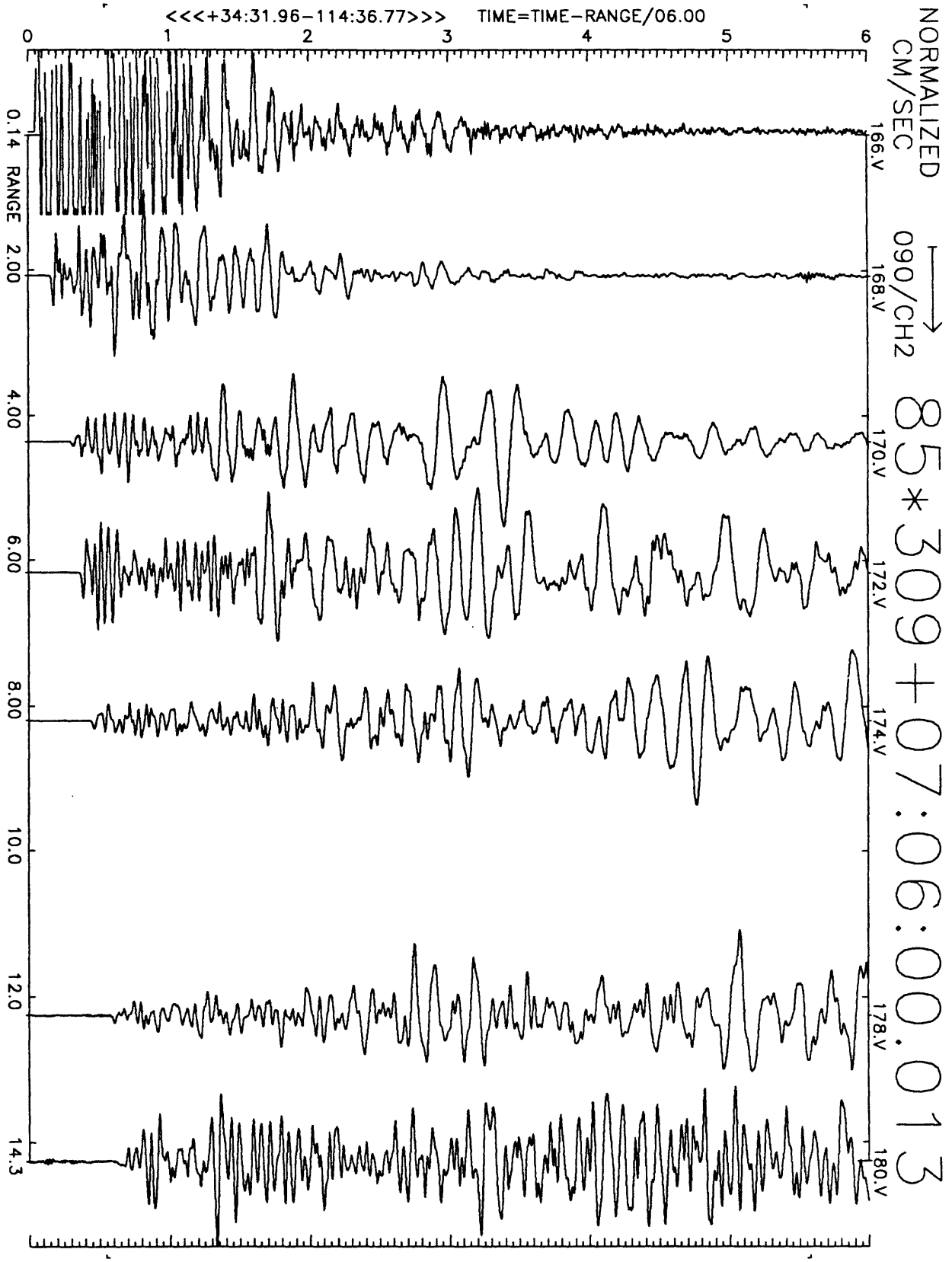

Figure A4(b), shot point 9, NW stations: 6 second velocity record. Positive N33W motion is to right. Abscissa is distance to shot point. Top of trace is labeled with station number. Times are reduced by 6 km/sec. Shot time is indicated.

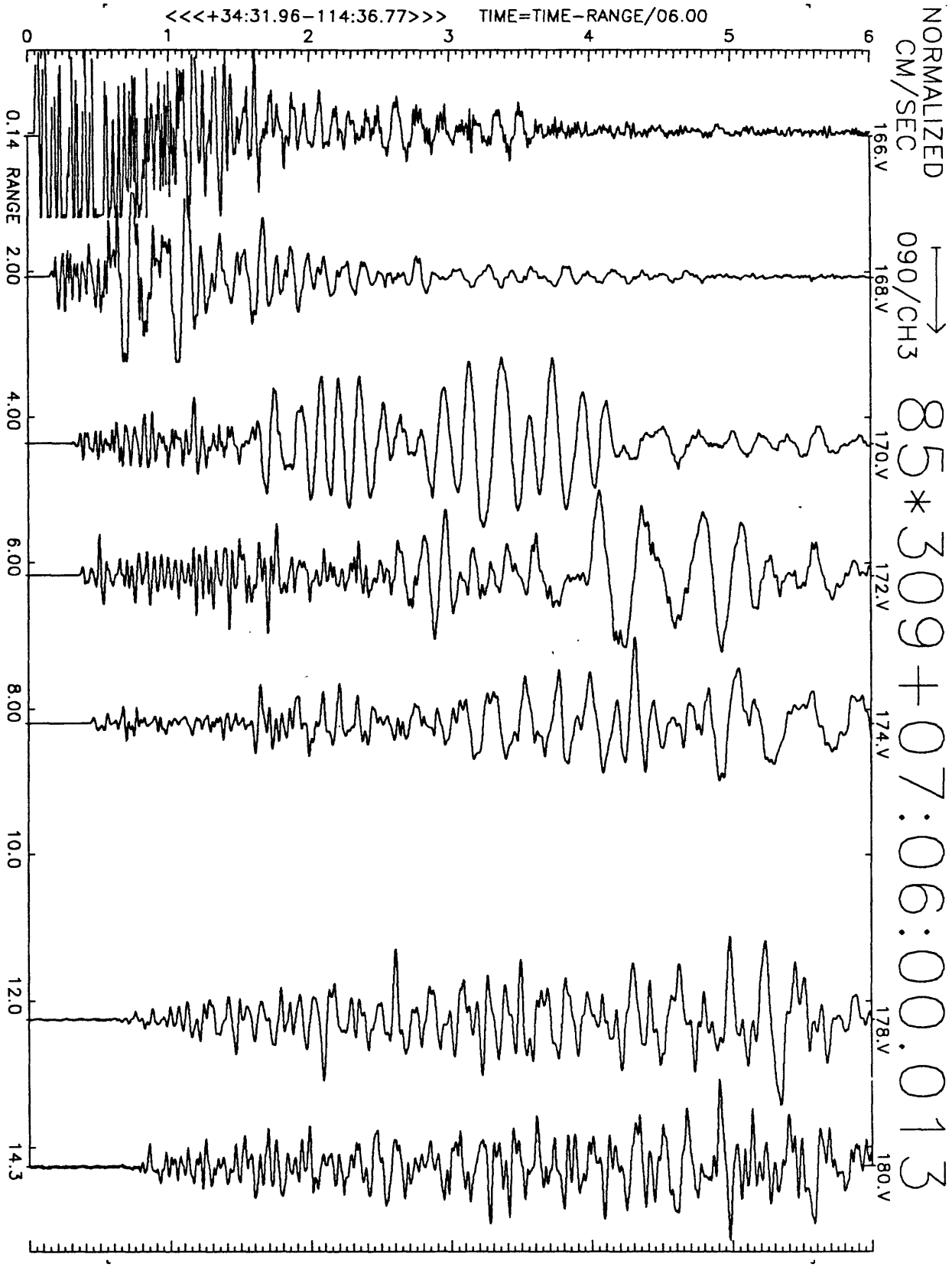

Figure A4(c), shot point 9, NW stations: 6 second velocity record. Positive N57E motion is to right. Abscissa is distance to shot point. Top of trace is labeled with station number. Times are reduced by 6 km/sec. Shot time is indicated.

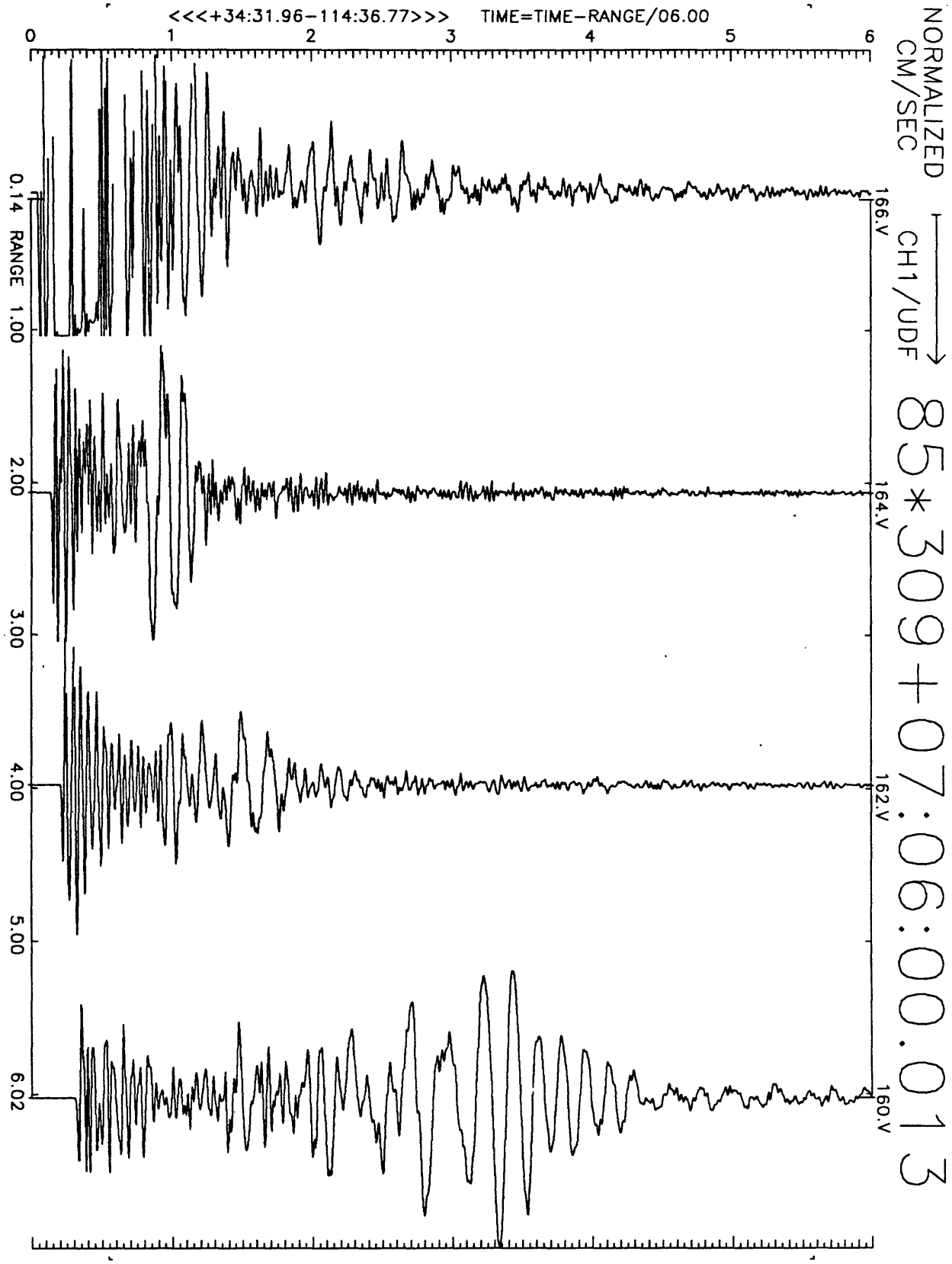

Figure A4(d), shot point 9, SE stations: 6 second velocity record. Positive vertical motion is to right. Abscissa is distance to shot point. Top of trace is labeled with station number. Times are reduced by 6 km/sec. Shot time is indicated.

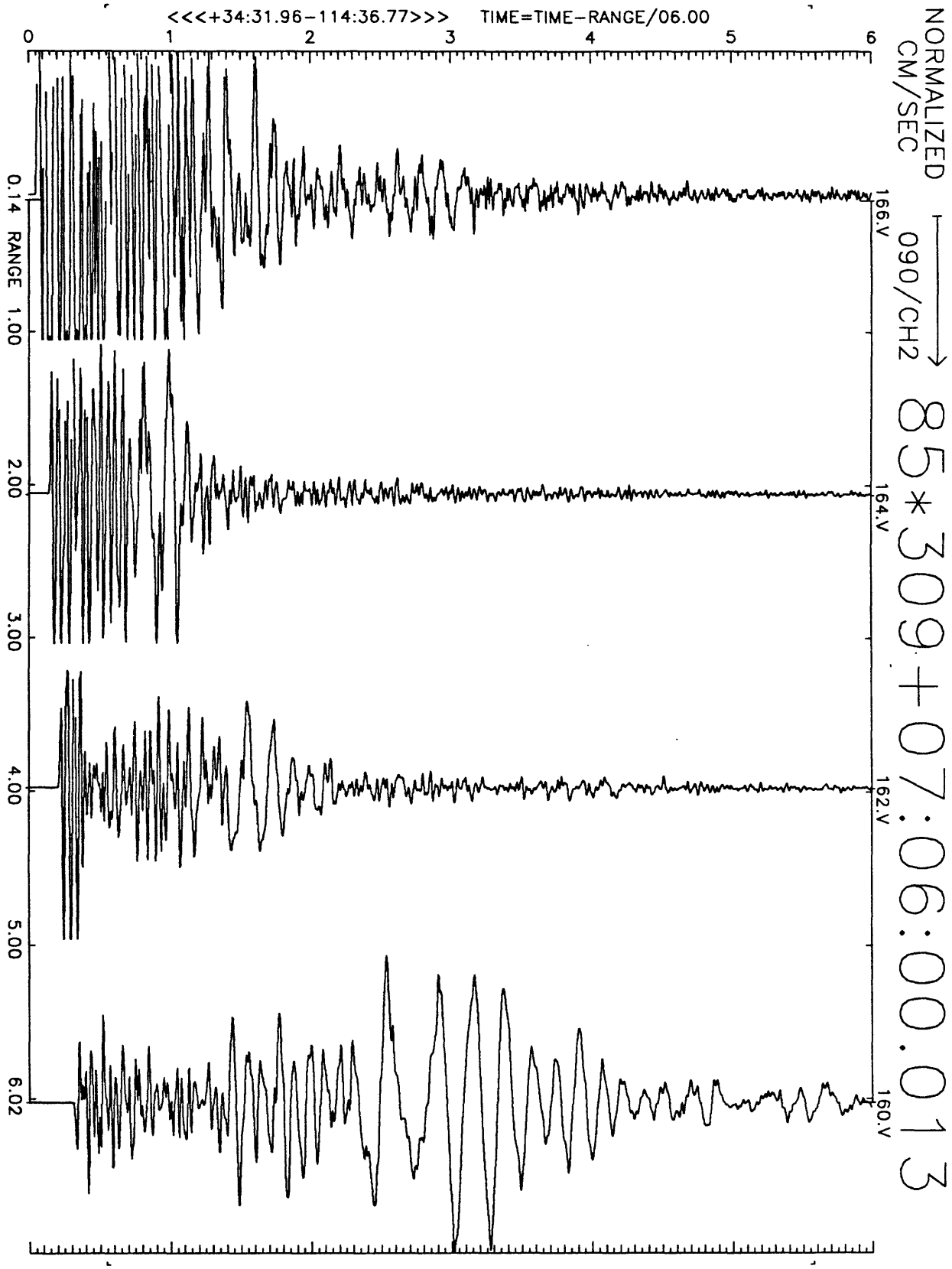

Figure A4(e), shot point 9, SE stations: 6 second velocity record. Positive N33W motion is to right. Abscissa is distance to shot point. Top of trace is labeled with station number. Times are reduced by 6 km/sec. Shot time is indicated.

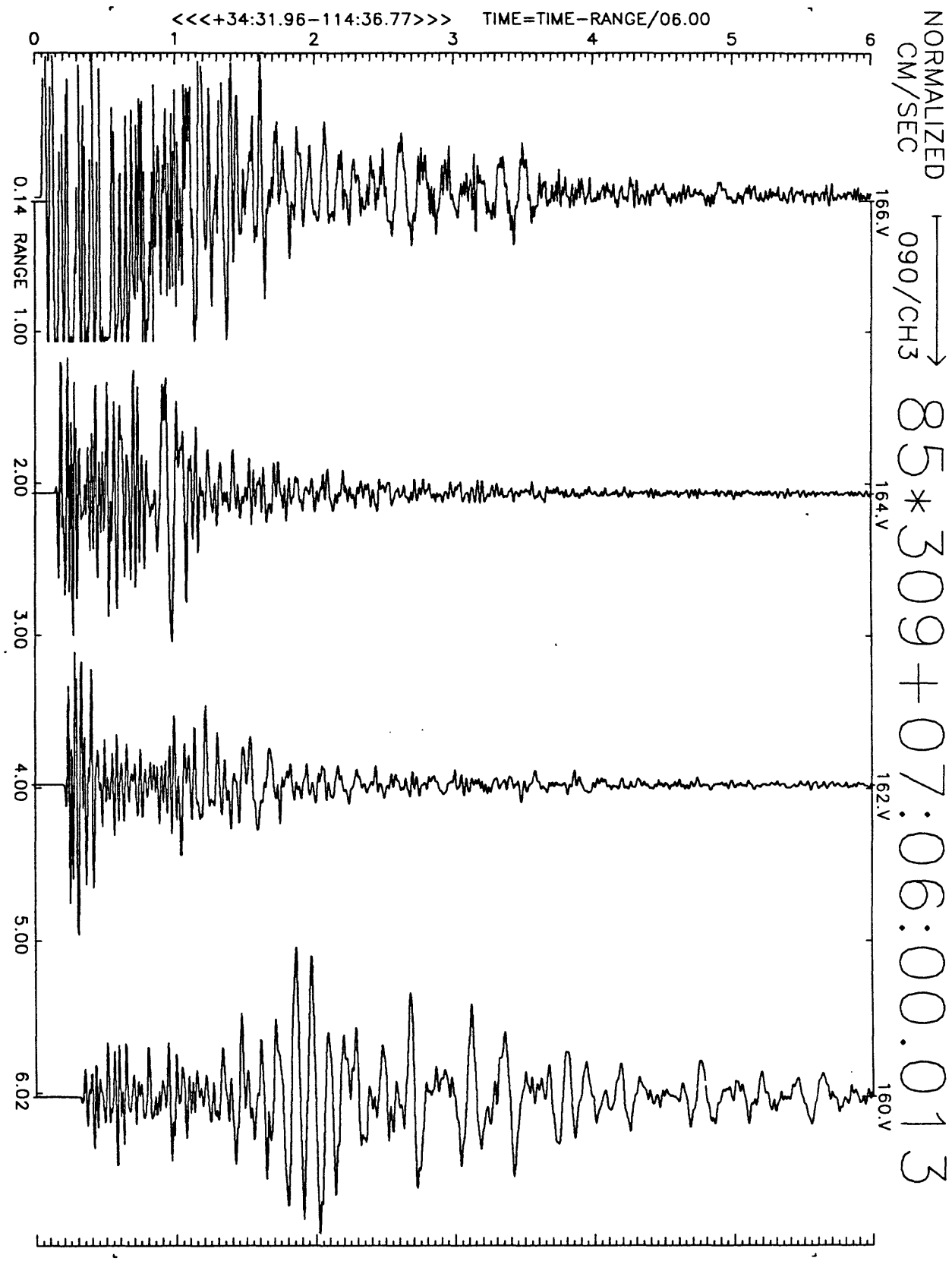

Figure A4(f), shot point 9, SE stations: 6 second velocity record. Positive N57E motion is to right. Abscissa is distance to shot point. Top of trace is labeled with station number. Times are reduced by 6 km/sec. Shot time is indicated.

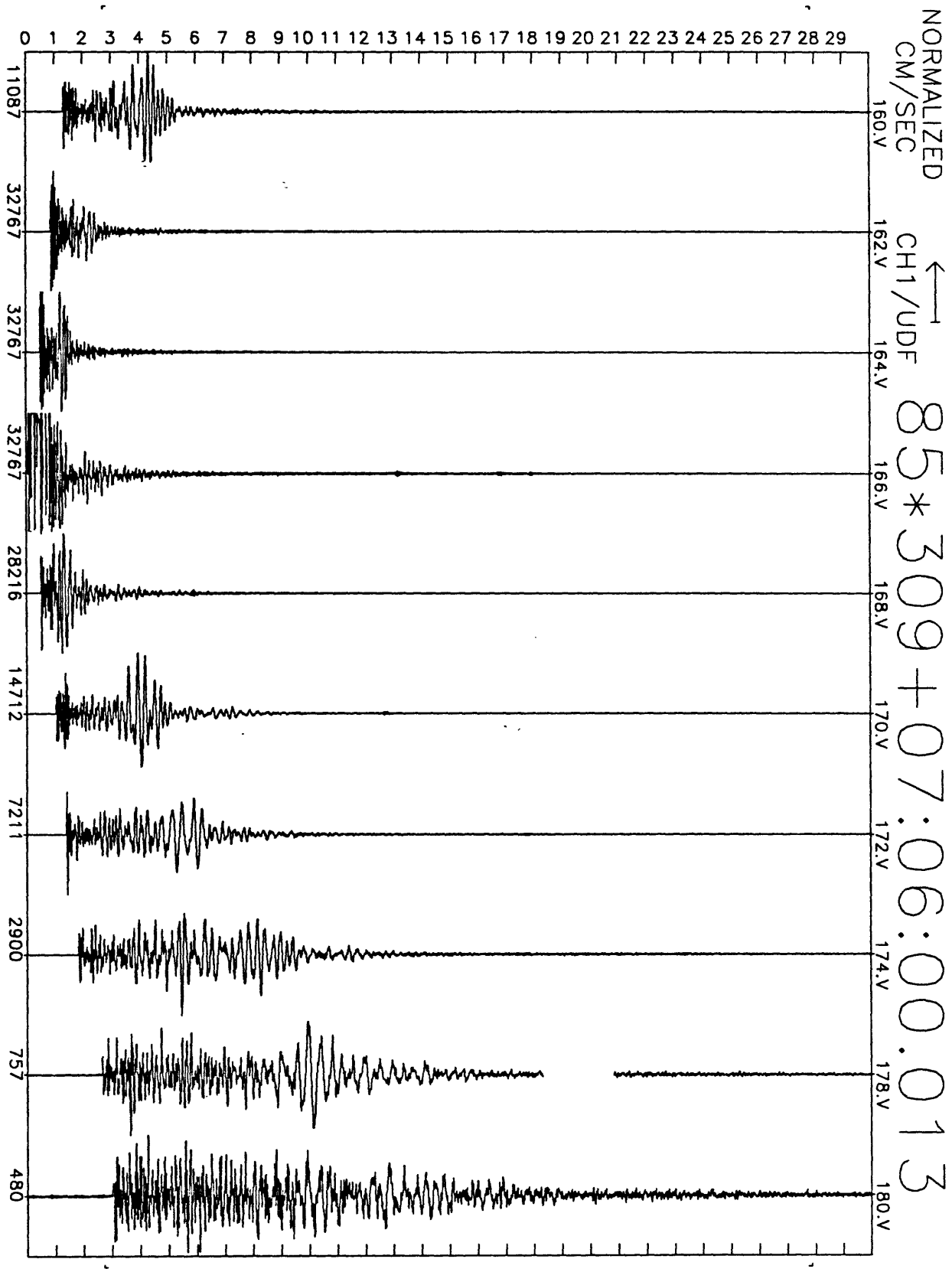

Figure A4(g), shot point 9: 30 second vertical velocity record. Abscissa is labeled with maximum counts in record (multiply by $\frac{10}{2^{24}-2^6} \approx 6 \times 10^{-7}$ to get cm/sec). Times are unreduced beginning at time indicated.

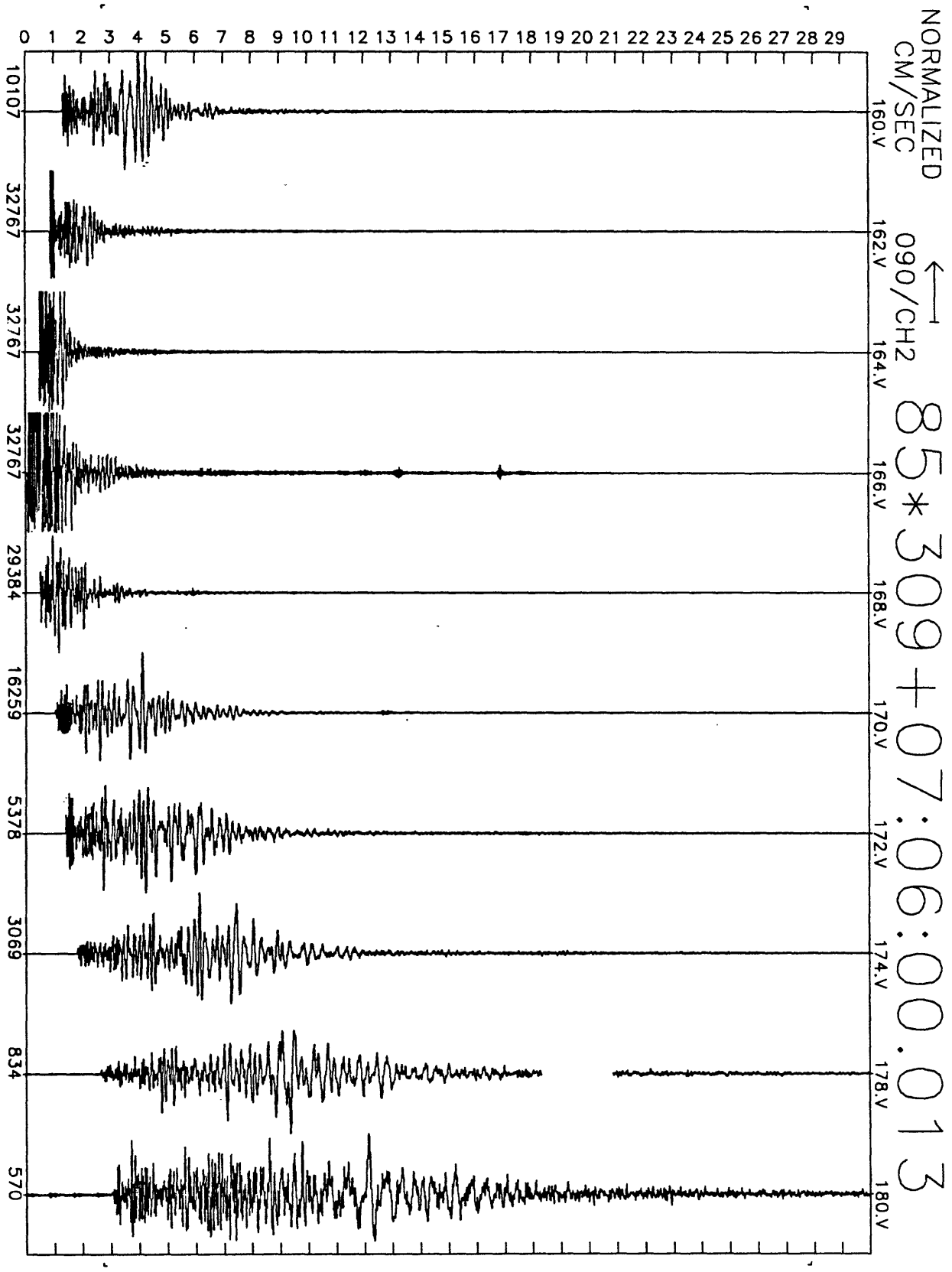

Figure A4(h), shot point 9: 30 second N33W velocity record. Abscissa is labeled with maximum counts in record (multiply by $\frac{10}{2^{24}-2^5} \approx 6 \times 10^{-7}$ to get cm/sec). Times are unreduced beginning at time indicated.

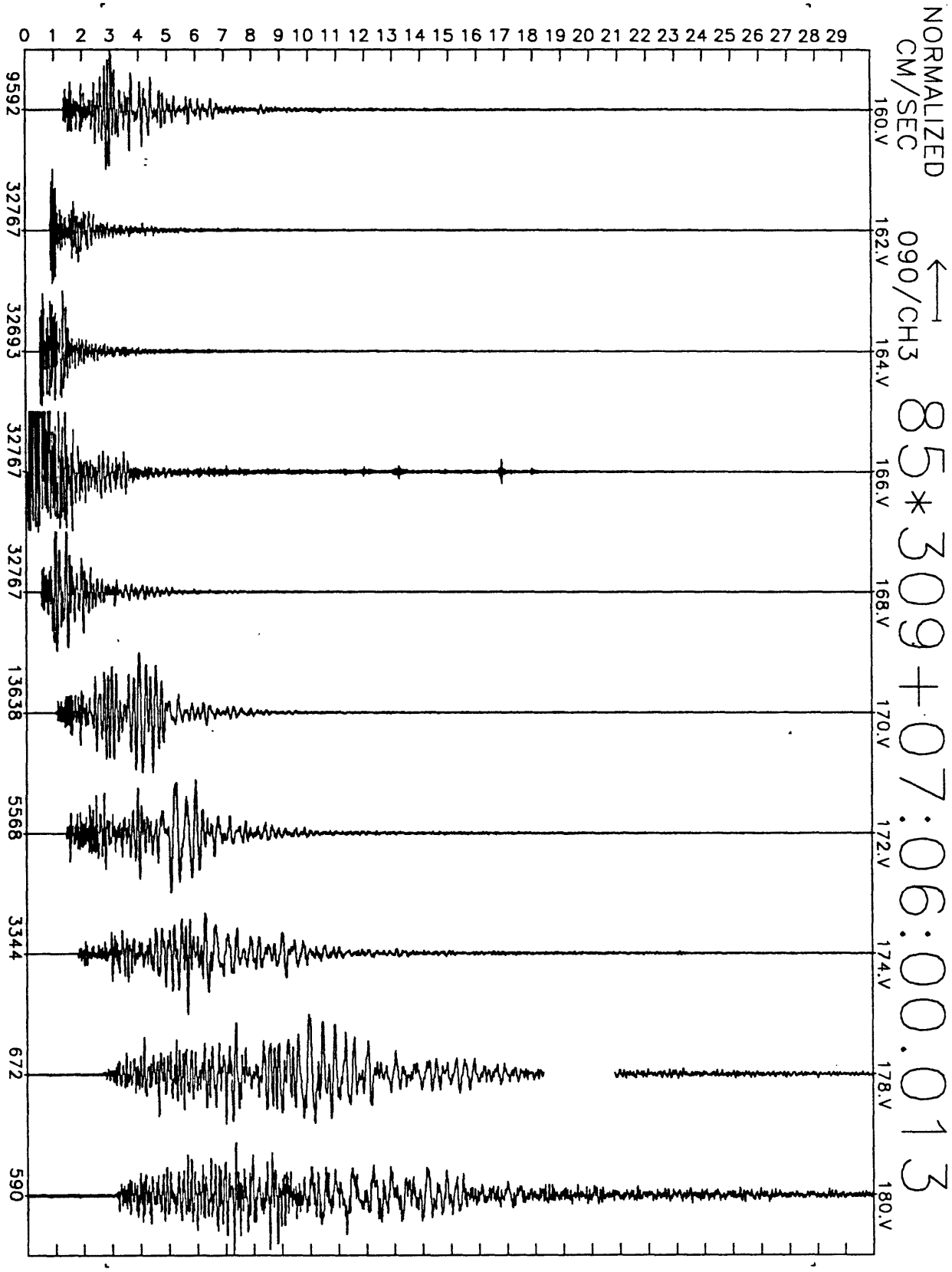

Figure A4(i), shot point 9: 30 second N57E velocity record. Abscissa is labeled with maximum counts in record (multiply by $\frac{10}{2^{24}-2^9} \approx 6 \times 10^{-7}$ to get cm/sec). Times are unreduced beginning at time indicated.

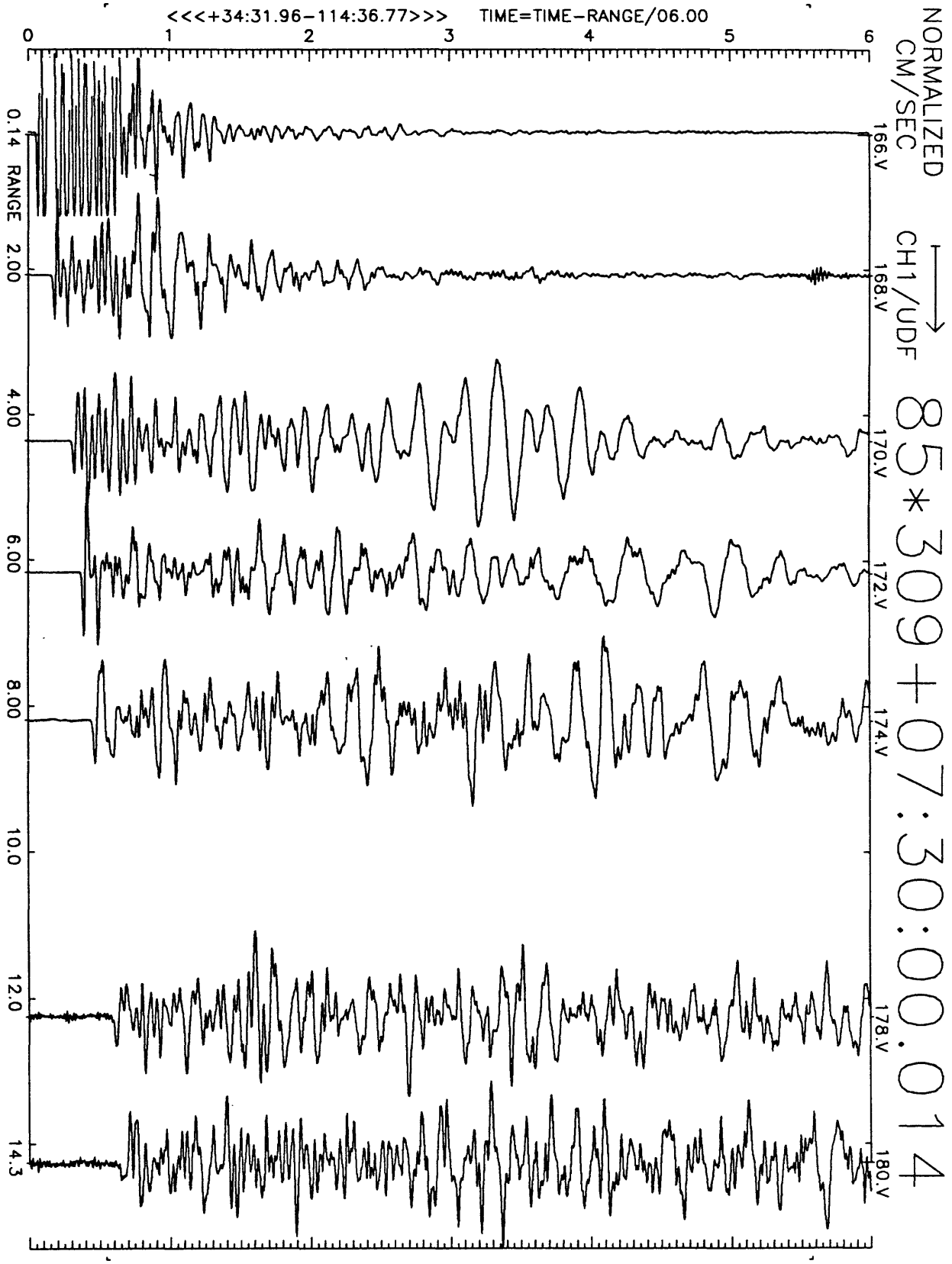

Figure A5(a), shot point 9′, NW stations: 6 second velocity record. Positive vertical motion is to right. Abscissa is distance to shot point. Top of trace is labeled with station number. Times are reduced by 6 km/sec. Shot time is indicated.

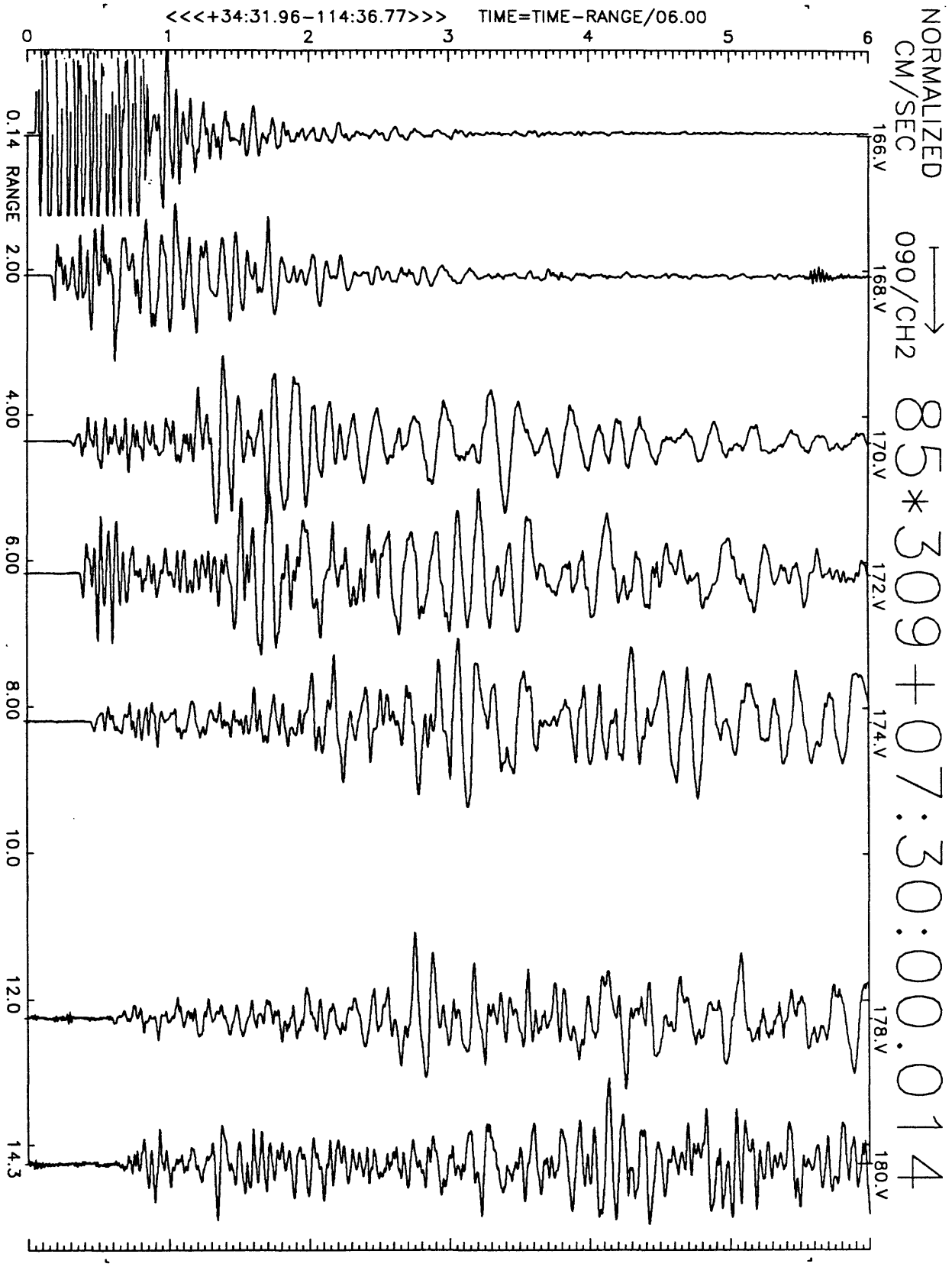

Figure A5(b), shot point 9′, NW stations: 6 second velocity record. Positive N33W motion is to right. Abscissa is distance to shot point. Top of trace is labeled with station number. Times are reduced by 6 km/sec. Shot time is indicated.

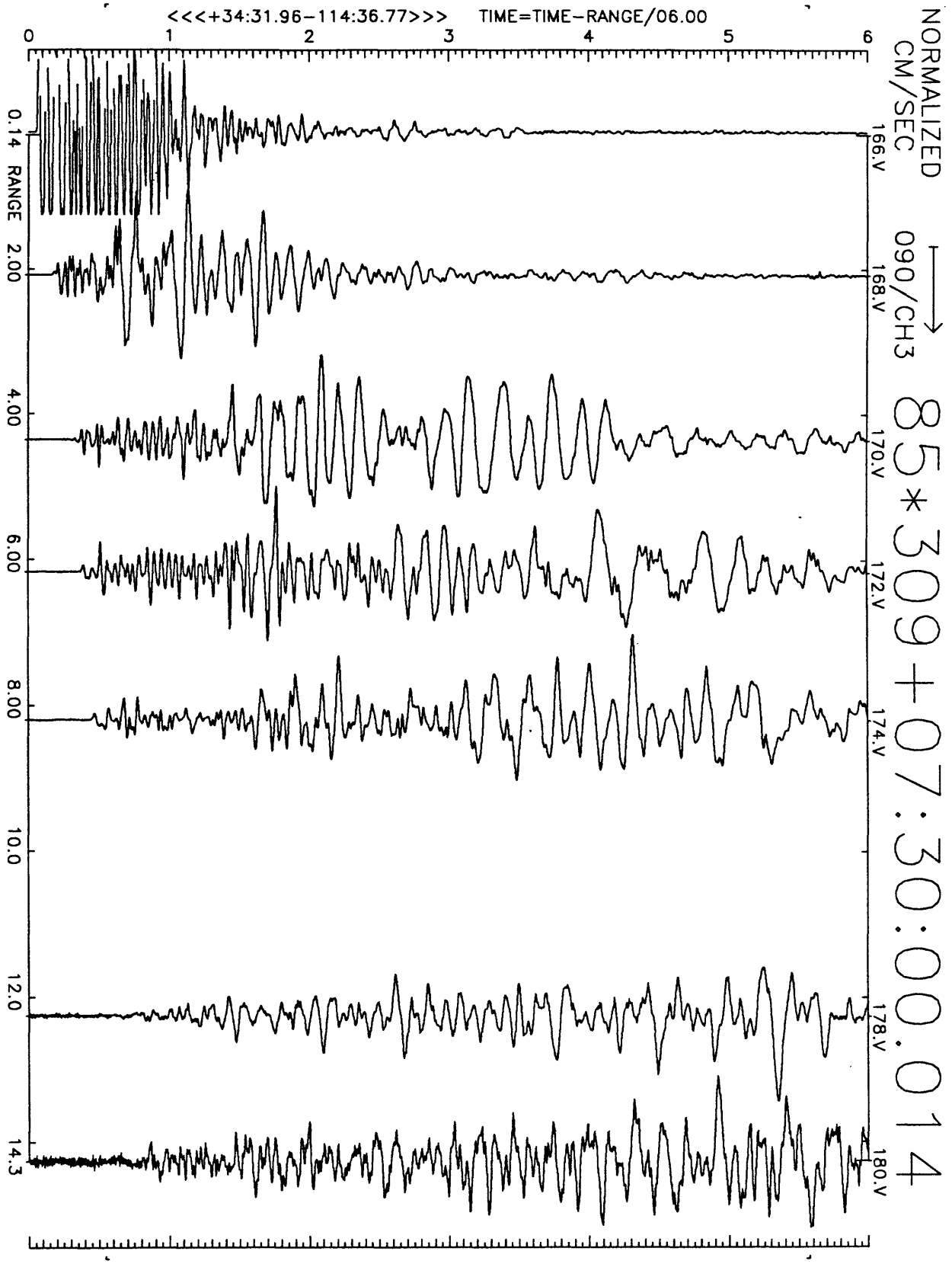

Figure A5(c), shot point 9′, NW stations: 6 second velocity record. Positive N57E motion is to right. Abscissa is distance to shot point. Top of trace is labeled with station number. Times are reduced by 6 km/sec. Shot time is indicated.

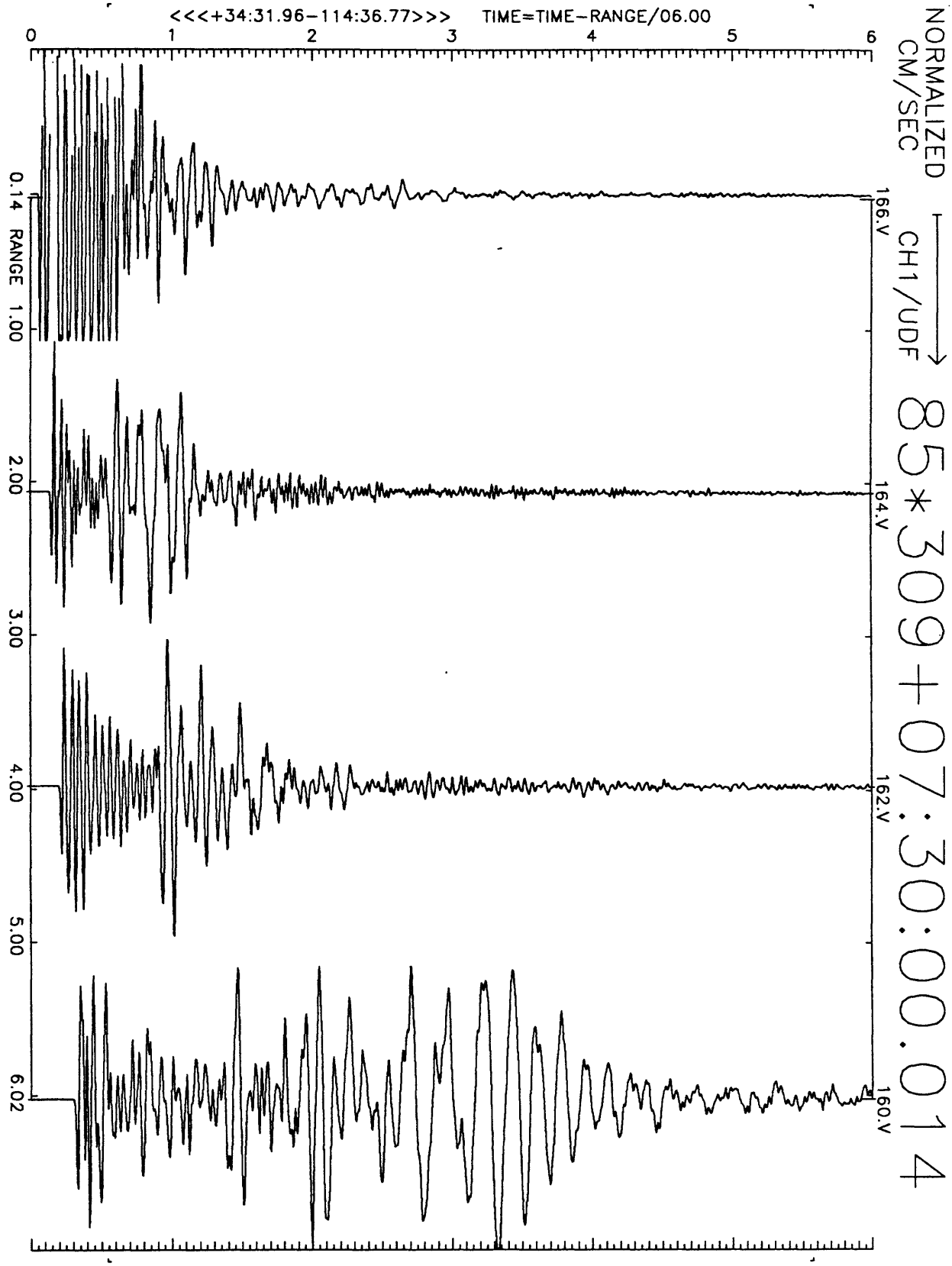

Figure A5(d), shot point 9′, SE stations: 6 second velocity record. Positive vertical motion is to right. Abscissa is distance to shot point. Top of trace is labeled with station number. Times are reduced by 6 km/sec. Shot time is indicated.

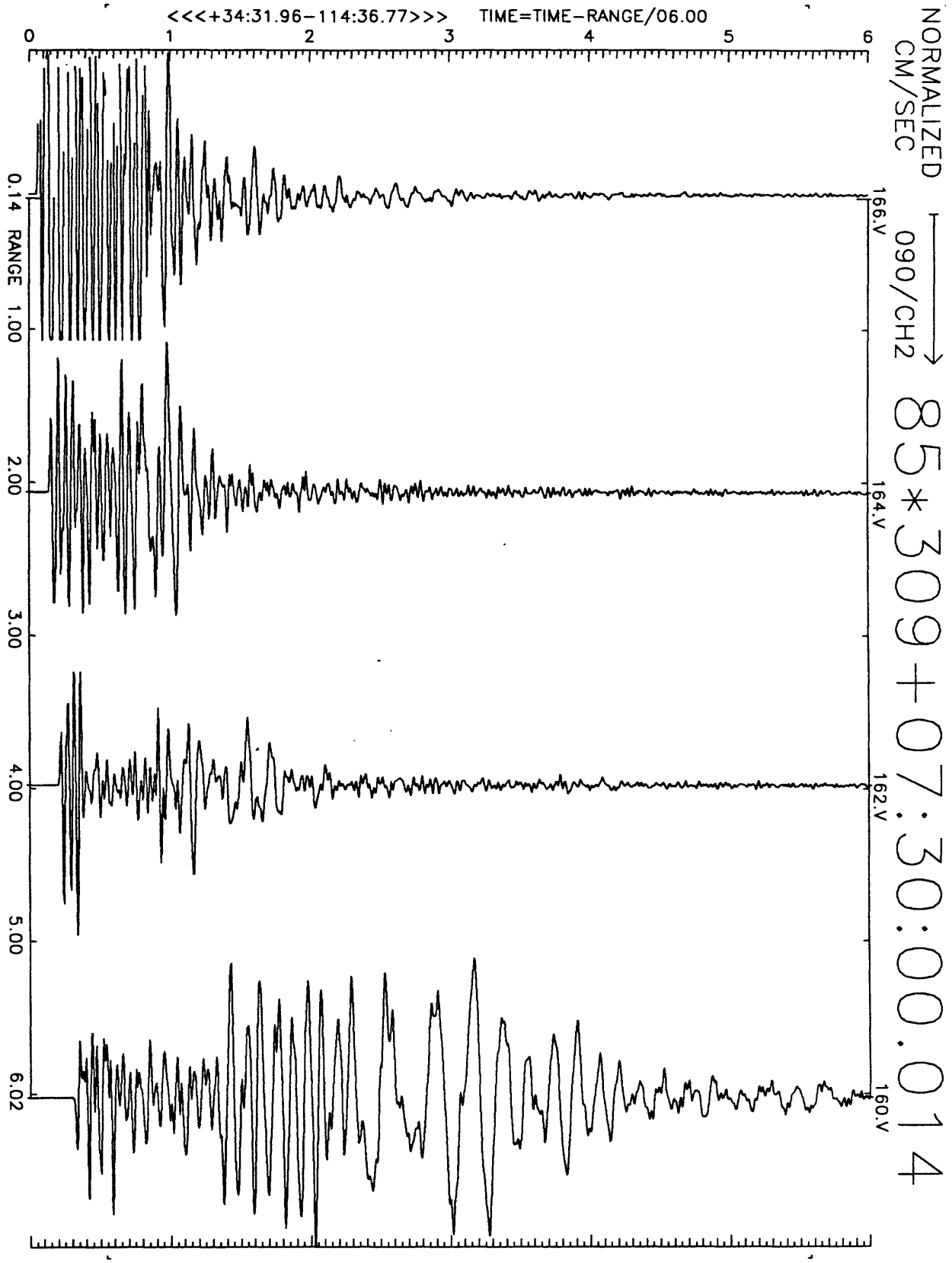

Figure A5(e), shot point 9′, SE stations: 6 second velocity record. Positive N33W motion is to right. Abscissa is distance to shot point. Top of trace is labeled with station number. Times are reduced by 6 km/sec. Shot time is indicated.

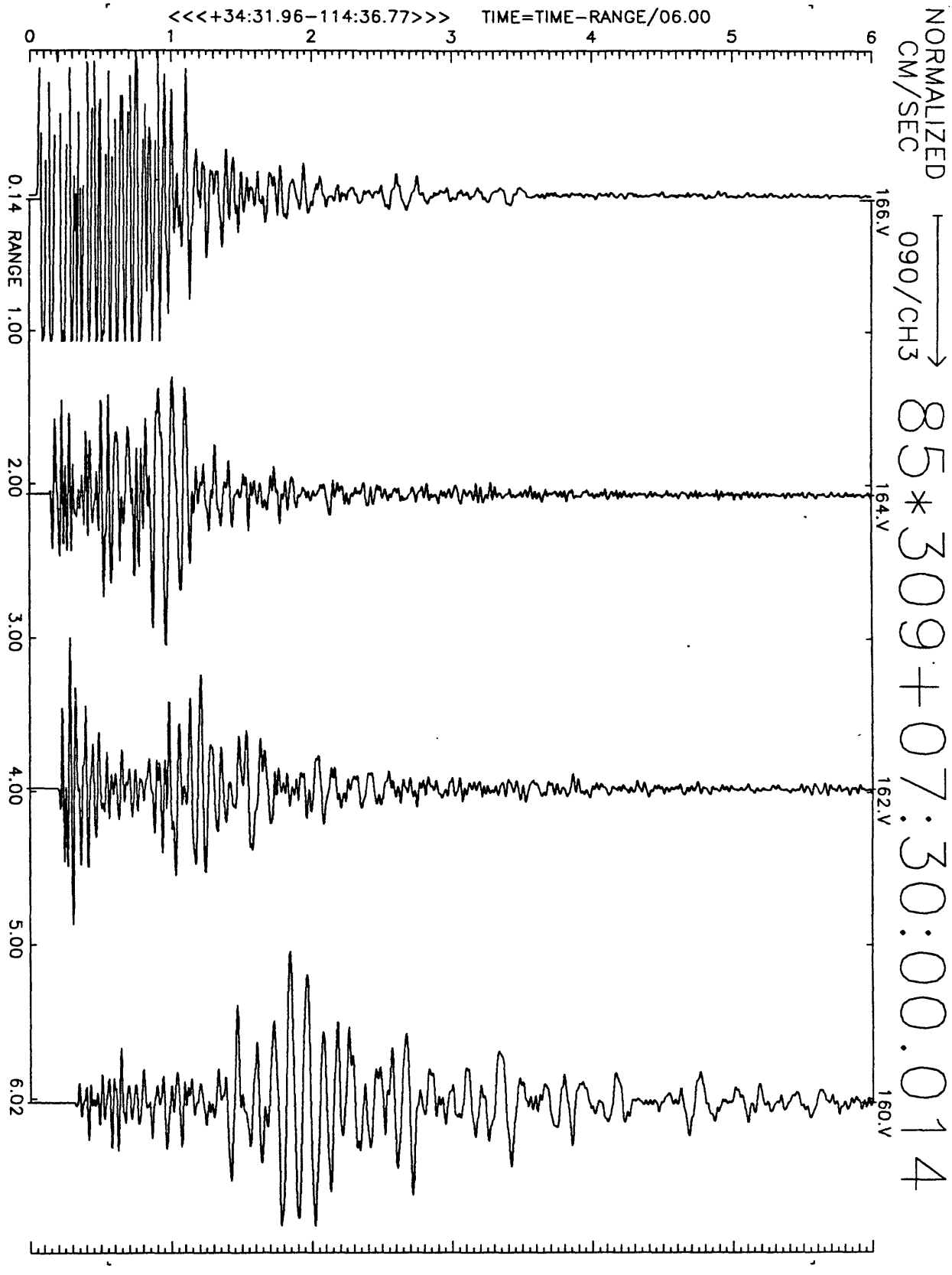

Figure A5(f), shot point 9′, SE stations: 6 second velocity record. Positive N57E motion is to right. Abscissa is distance to shot point. Top of trace is labeled with station number. Times are reduced by 6 km/sec. Shot time is indicated.

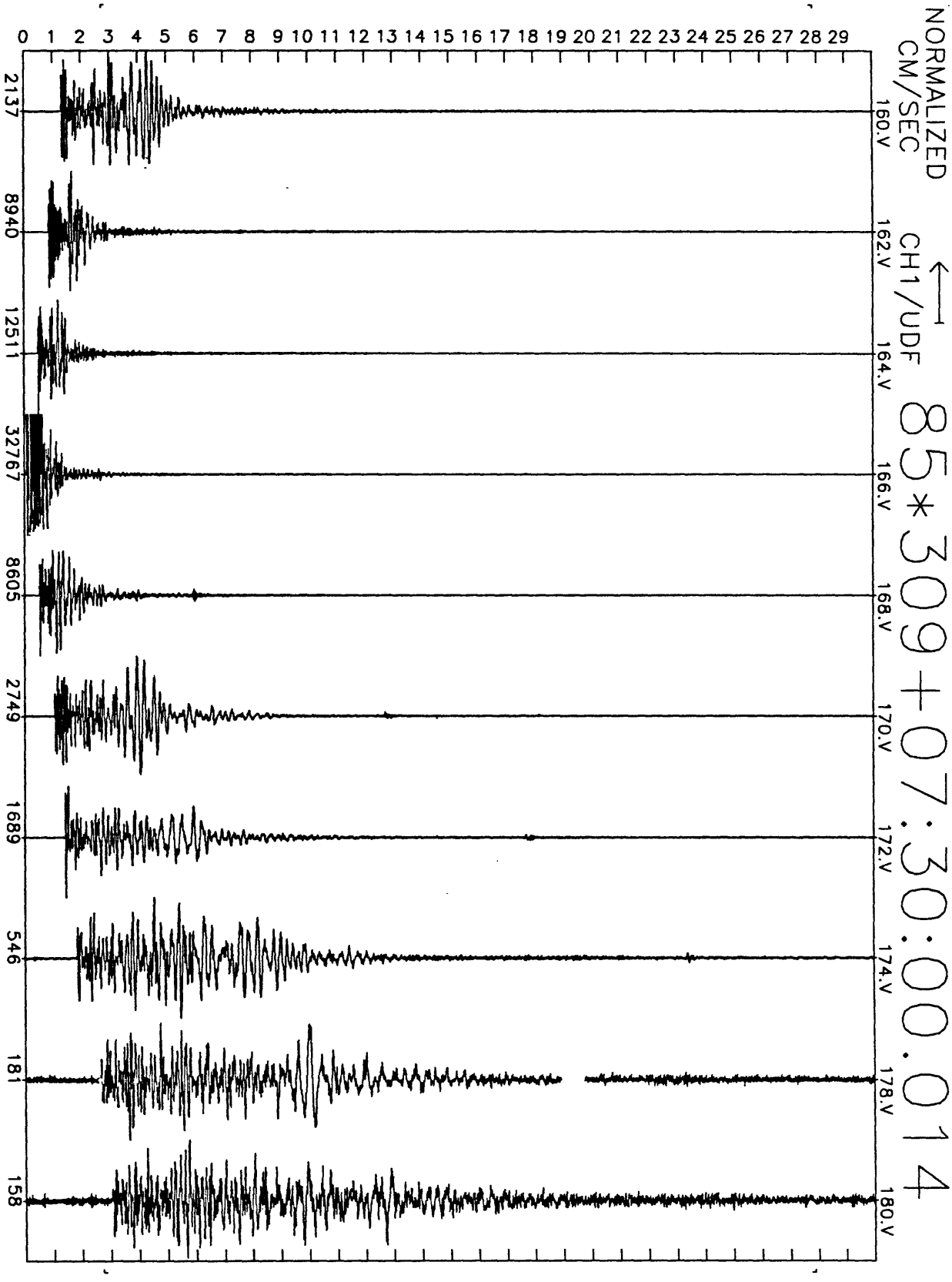

Figure A5(g), shot point 9′: 30 second vertical velocity record. Abscissa is labeled with maximum counts in record (multiply by $\frac{10}{2^{24}-2^8} \approx 6 \times 10^{-7}$ to get cm/sec). Times are unreduced beginning at time indicated.

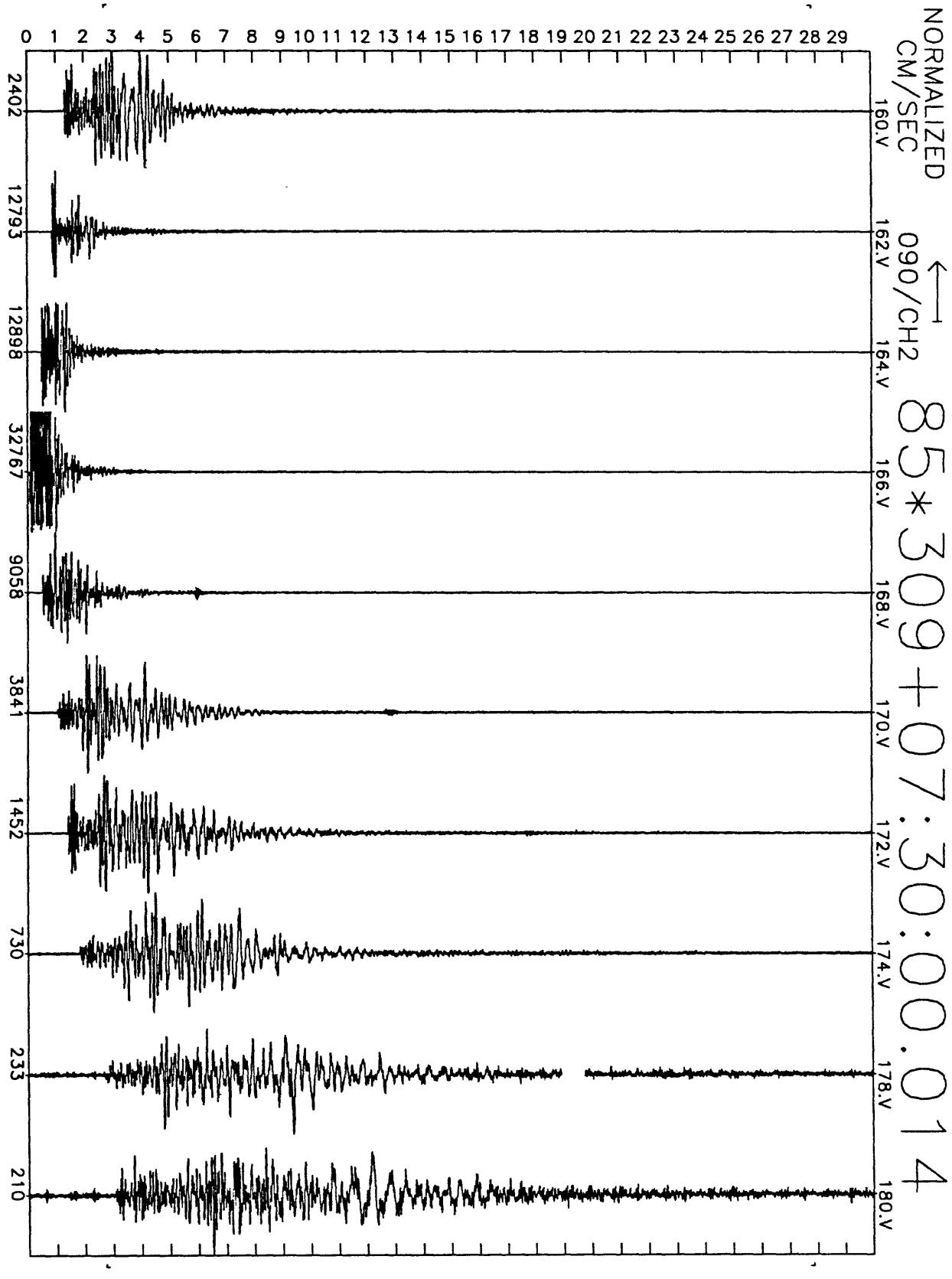

Figure A5(h), shot point 9′: 30 second N33W velocity record. Abscissa is labeled with maximum counts in record (multiply by $\frac{10}{2^{24}-2^0} \approx 6 \times 10^{-7}$ to get cm/sec). Times are unreduced beginning at time indicated.

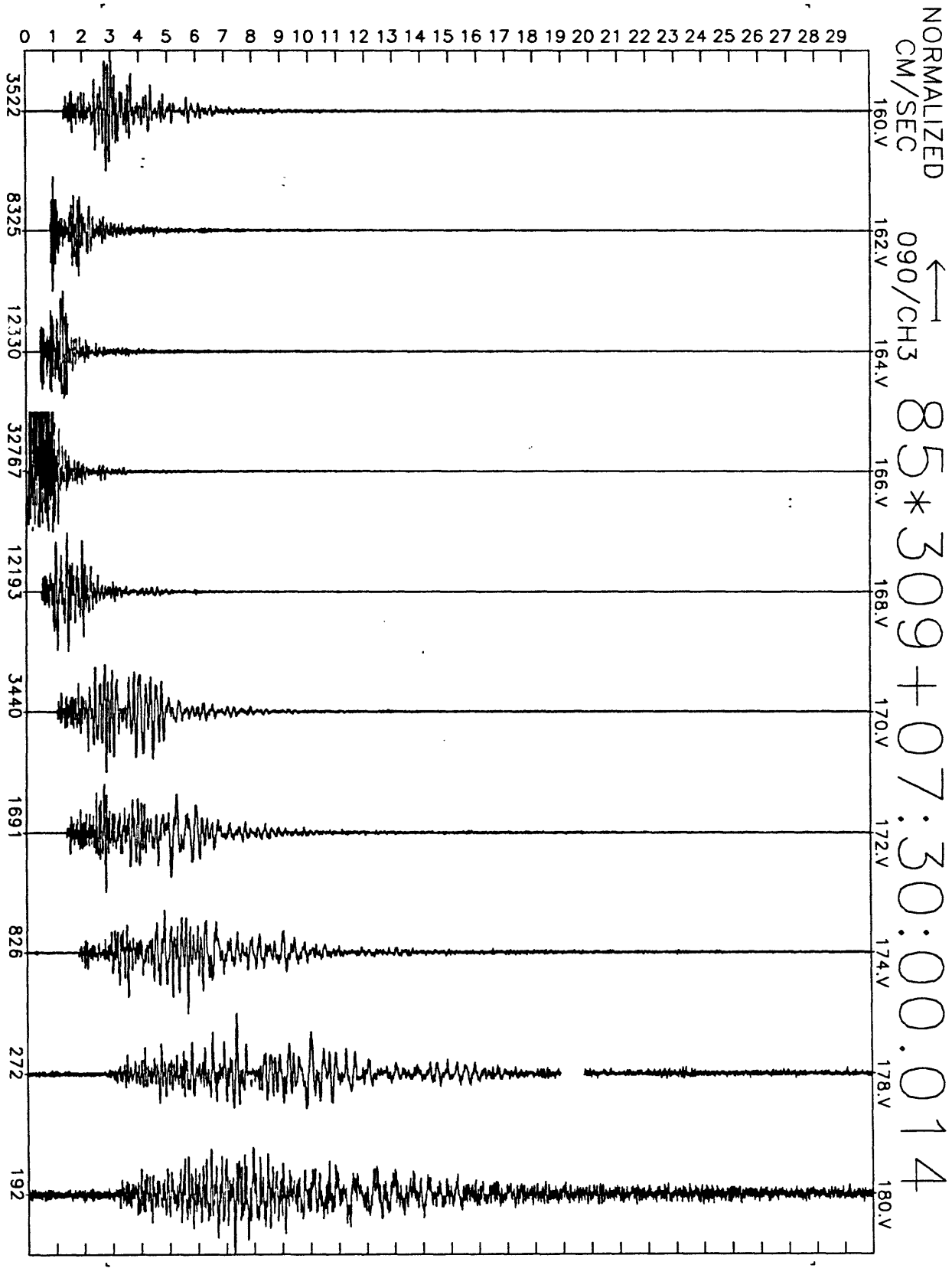

Figure A5(i), shot point 9′: 30 second N57E velocity record. Abscissa is labeled with maximum counts in record (multiply by $\frac{10}{2^{24}-2^5} \approx 6 \times 10^{-7}$ to get cm/sec). Times are unreduced beginning at time indicated.

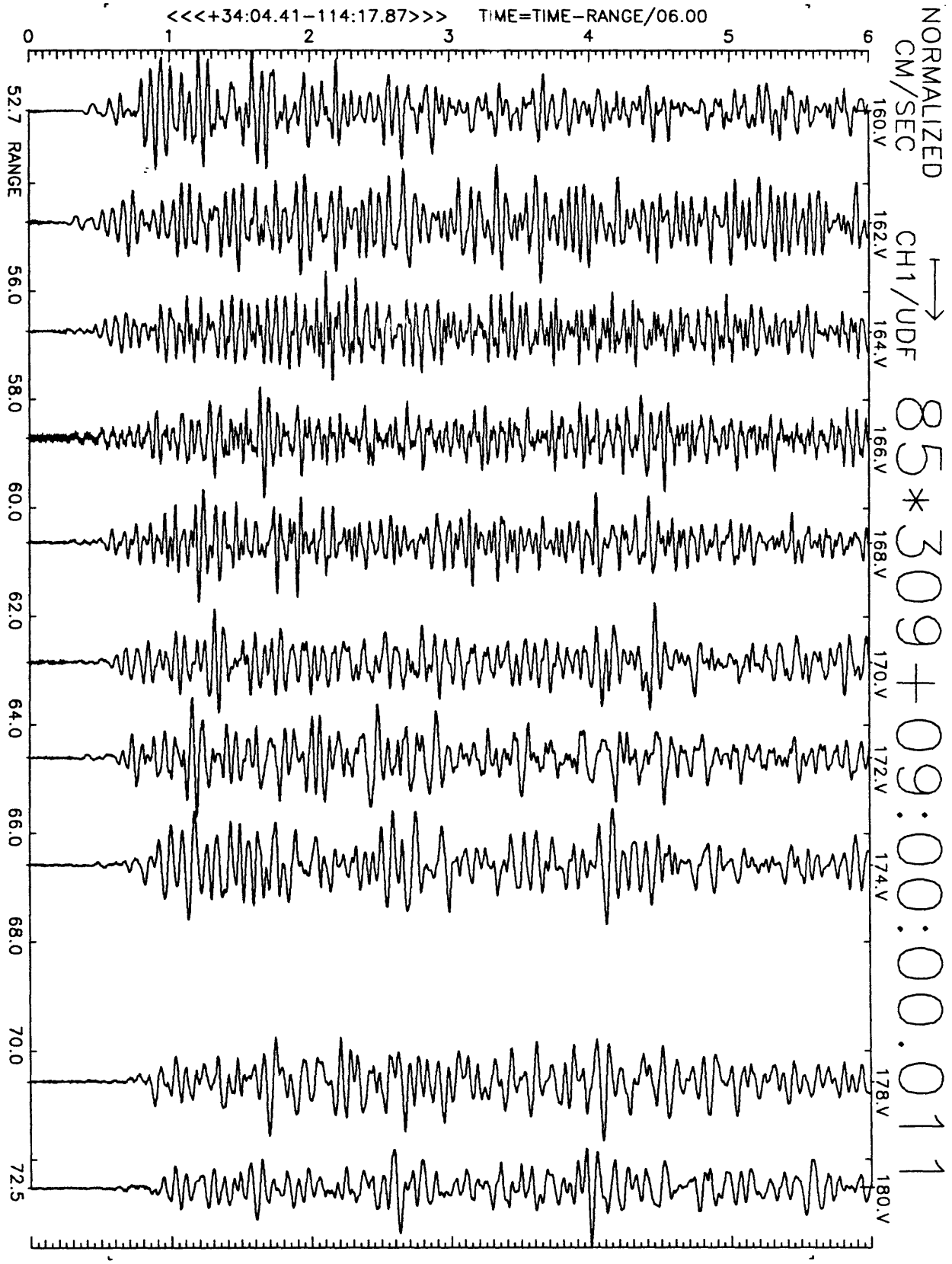

Figure A6(a), shot point 8X: 6 second velocity record. Positive vertical motion is to right. Abscissa is distance to shot point. Top of trace is labeled with station number. Times are reduced by 6 km/sec. Shot time is indicated.

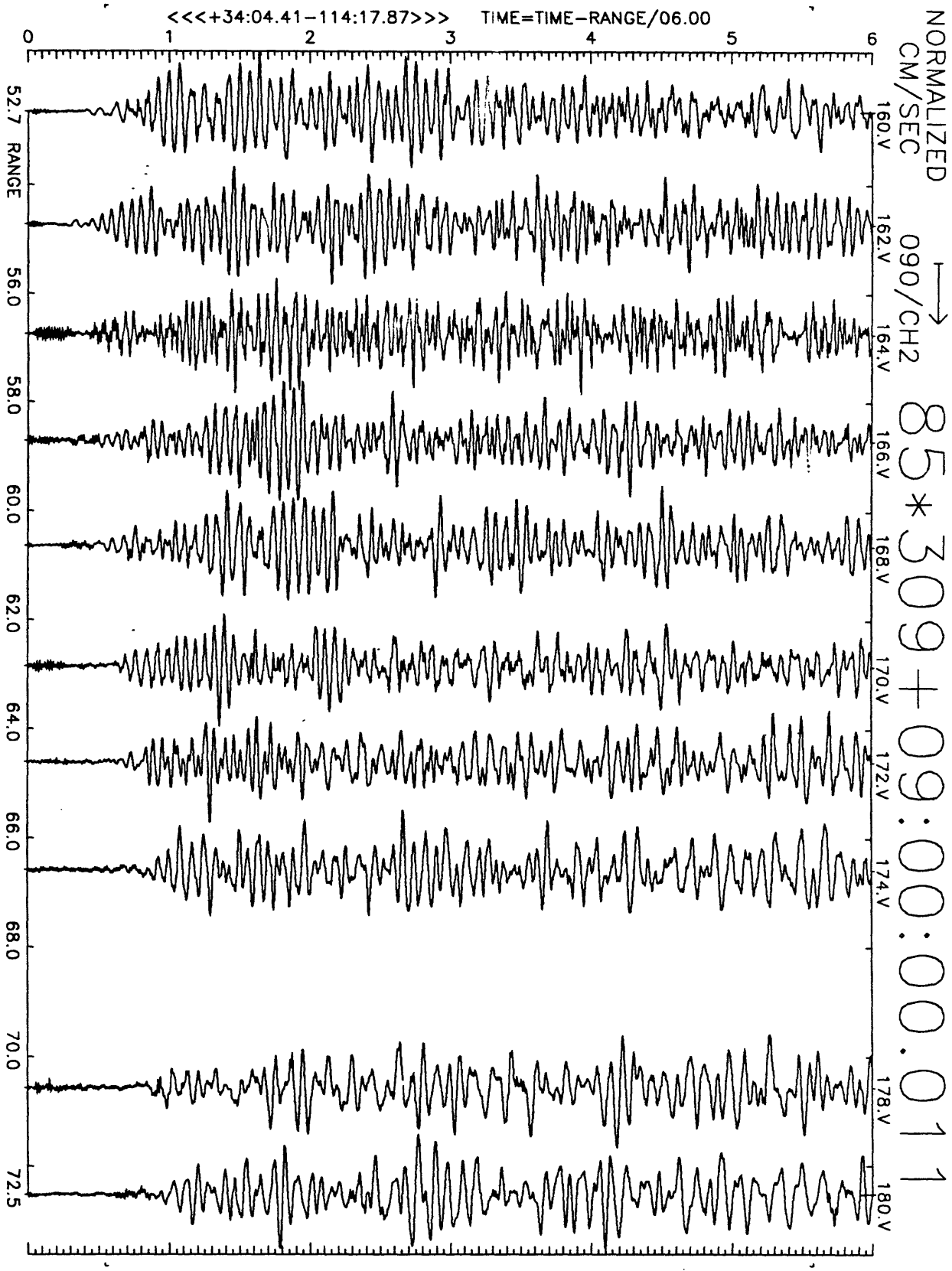

Figure A6(b), shot point 8X: 6 second velocity record. Positive N33W motion is to right. Abscissa is distance to shot point. Top of trace is labeled with station number. Times are reduced by 6 km/sec. Shot time is indicated.

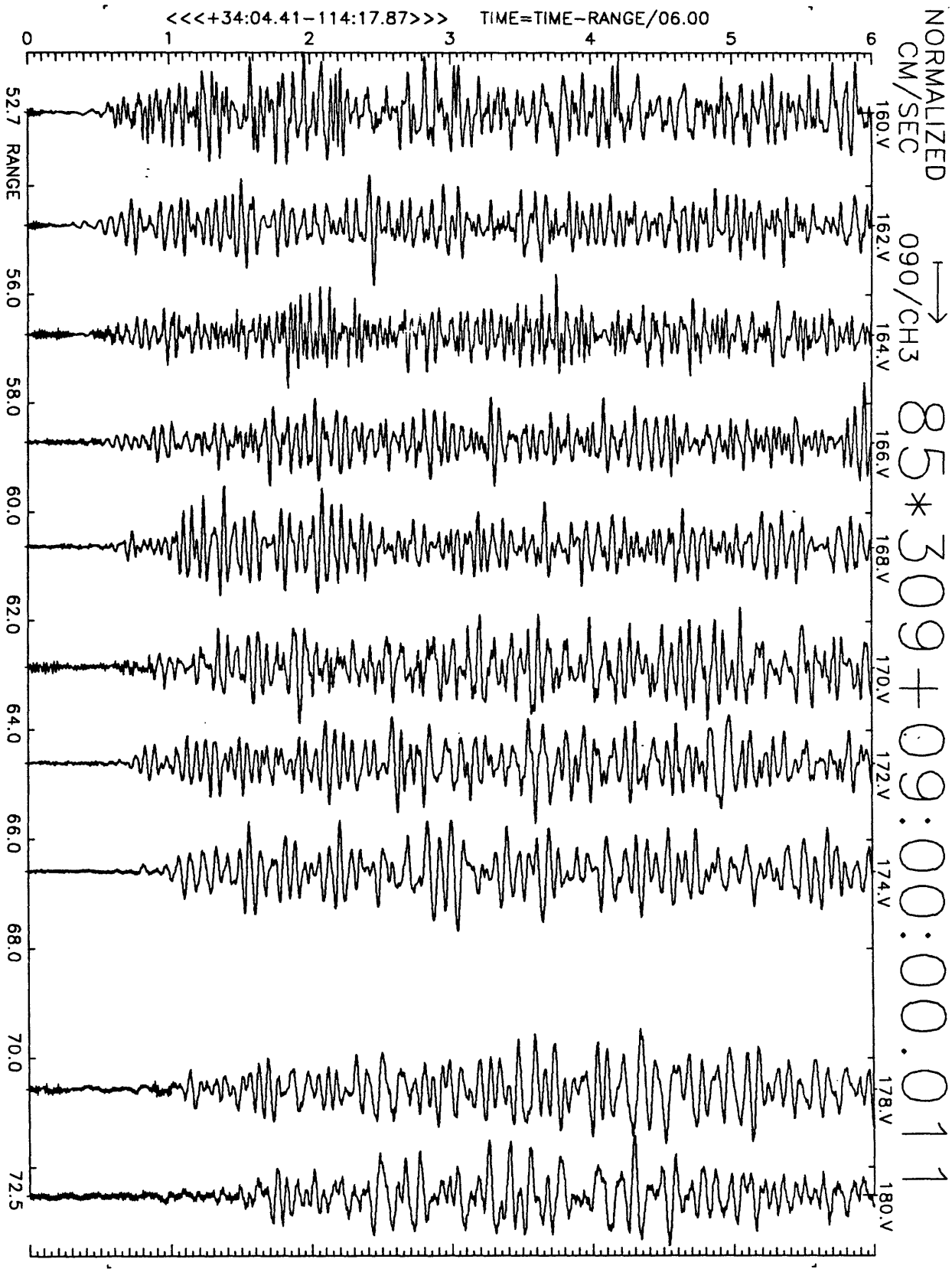

Figure A6(c), shot point 8X: 6 second velocity record. Positive N57E motion is to right. Abscissa is distance to shot point. Top of trace is labeled with station number. Times are reduced by 6 km/sec. Shot time is indicated.

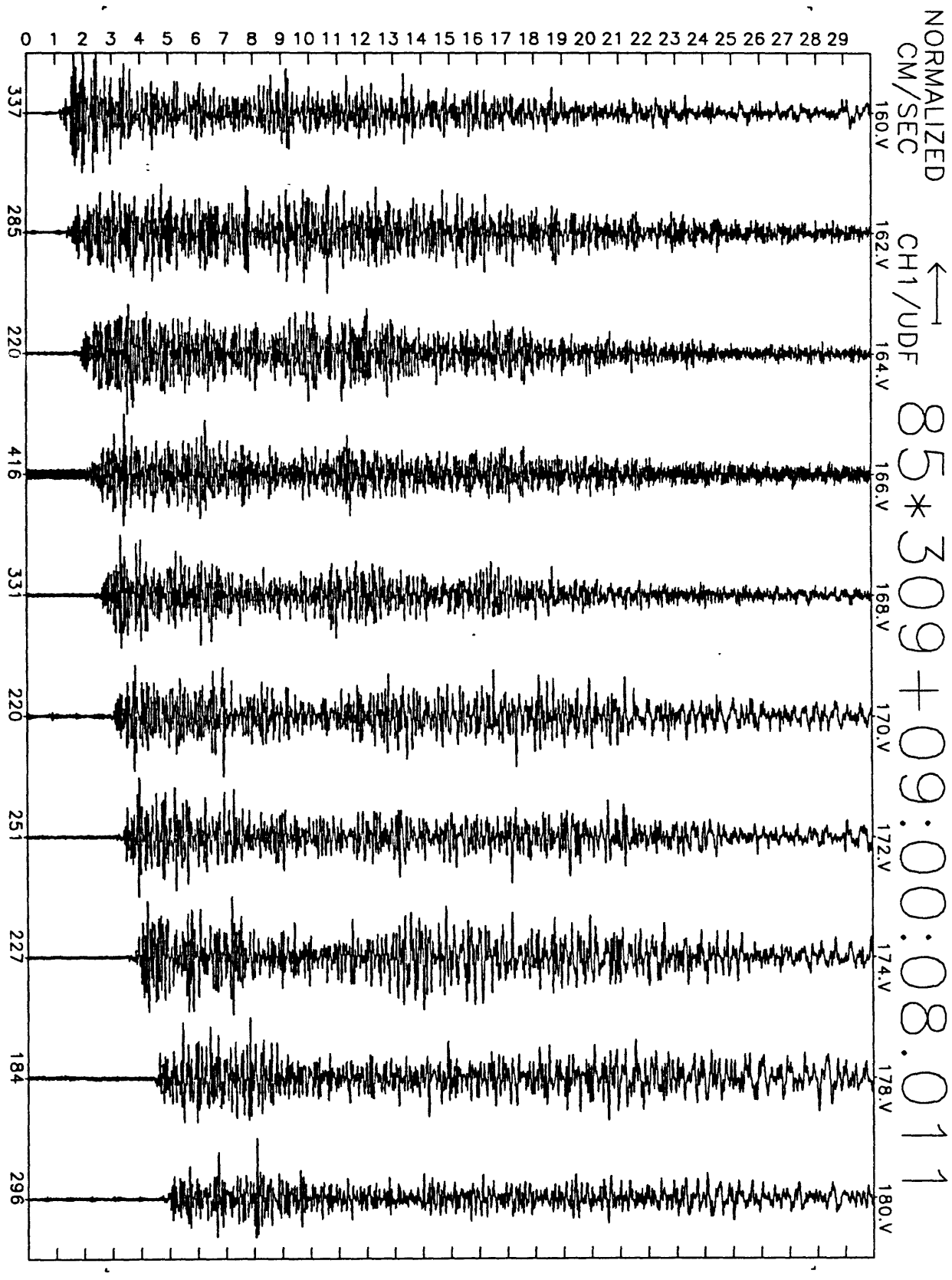

Figure A6(d), shot point 8X: 30 second vertical velocity record. Abscissa is labeled with maximum counts in record (multiply by $\frac{10}{2^{24}-2^0} \approx 6 \times 10^{-7}$ to get cm/sec). Times are unreduced beginning at time indicated.

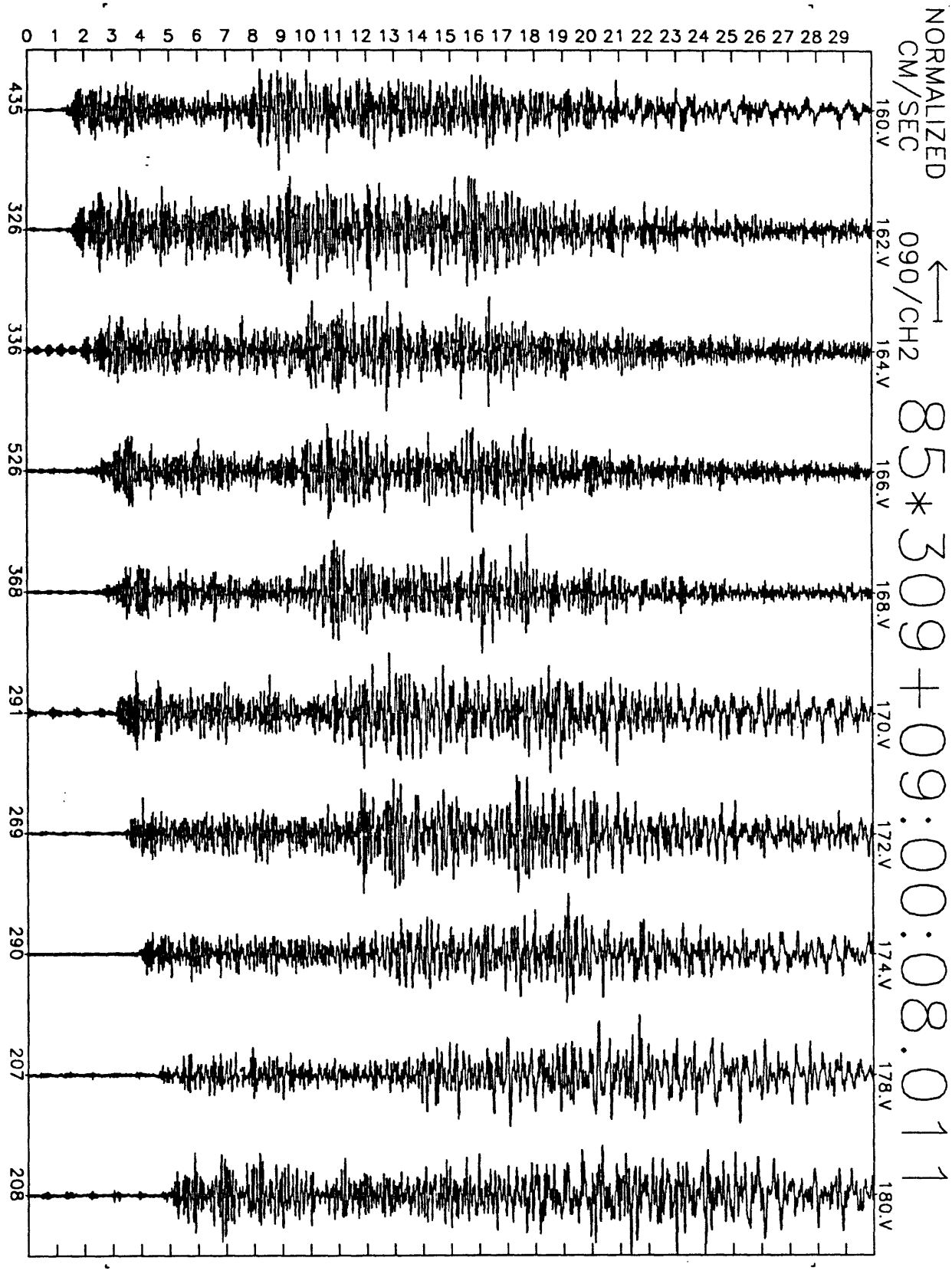

Figure A6(e), shot point 8X: 30 second N33W velocity record. Abscissa is labeled with maximum counts in record (multiply by $\frac{10}{2^{24}-2^5} \approx 6 \times 10^{-7}$ to get cm/sec). Times are unreduced beginning at time indicated.

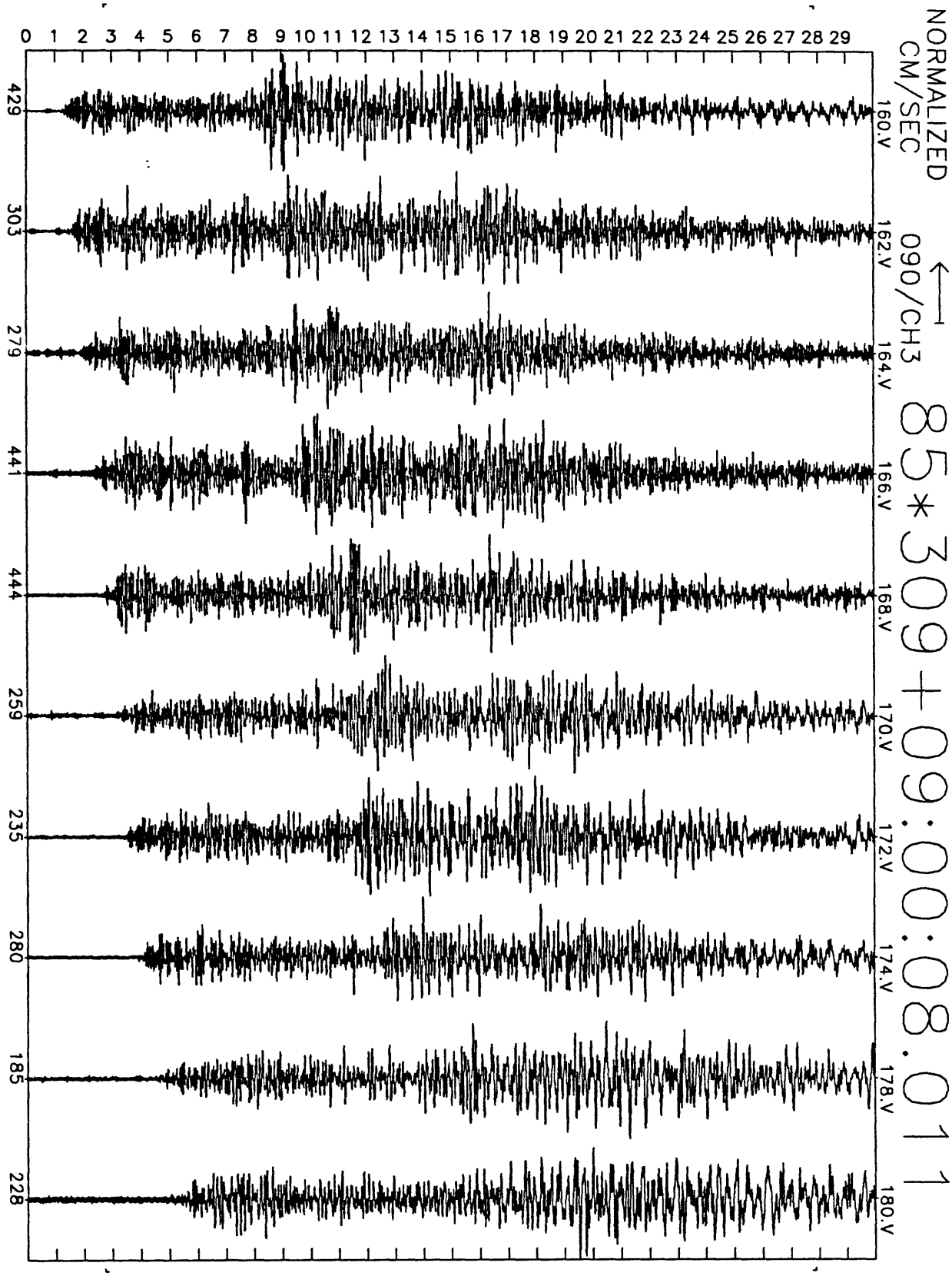

Figure A6(f), shot point 8X: 30 second N57E velocity record. Abscissa is labeled with maximum counts in record (multiply by $\frac{10}{2^{24}-2^9} \approx 6 \times 10^{-7}$ to get cm/sec). Times are unreduced beginning at time indicated.

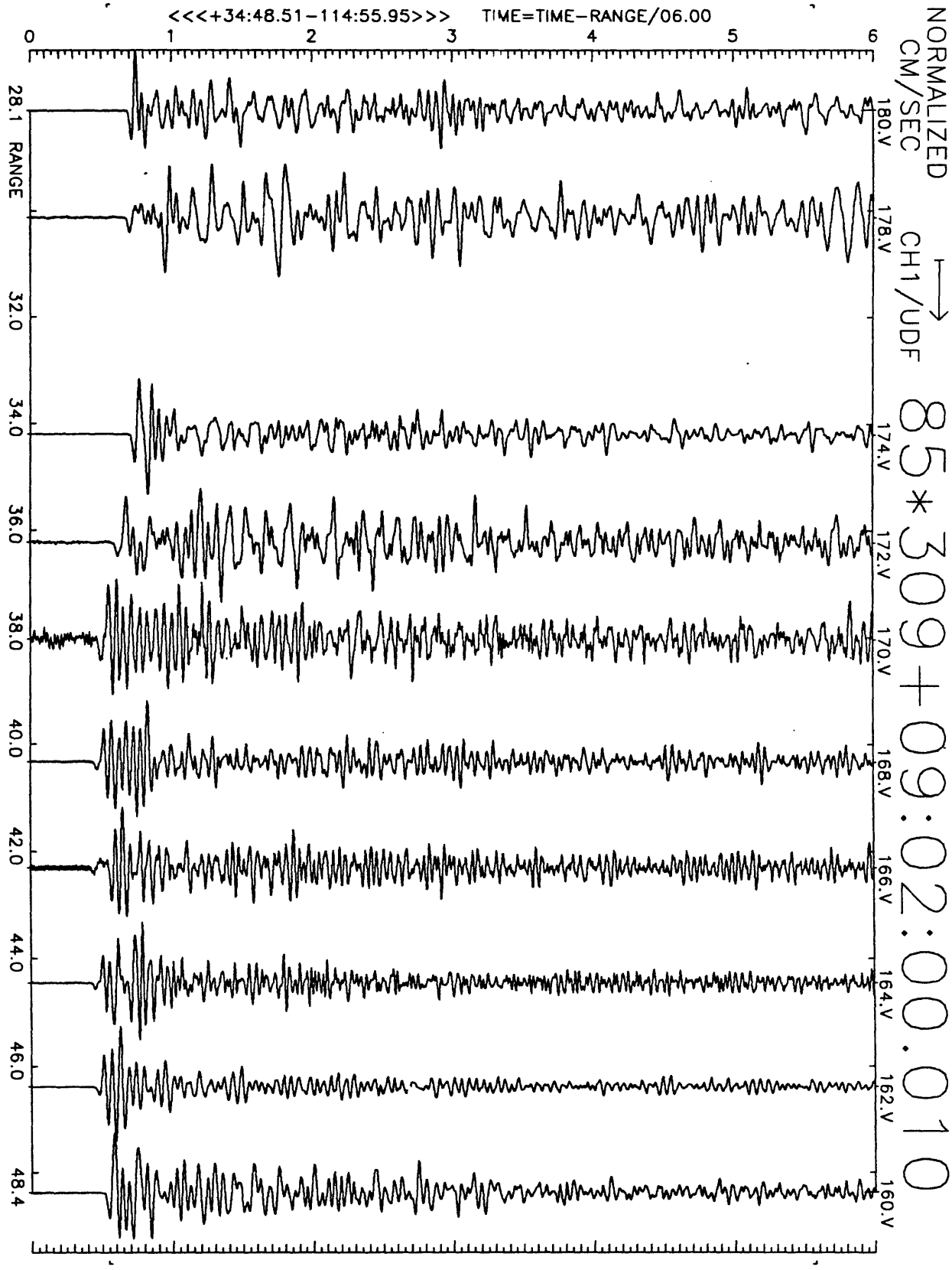

Figure A7(a), shot point 10: 6 second velocity record. Positive vertical motion is to right. Abscissa is distance to shot point. Top of trace is labeled with station number. Times are reduced by 6 km/sec. Shot time is indicated.

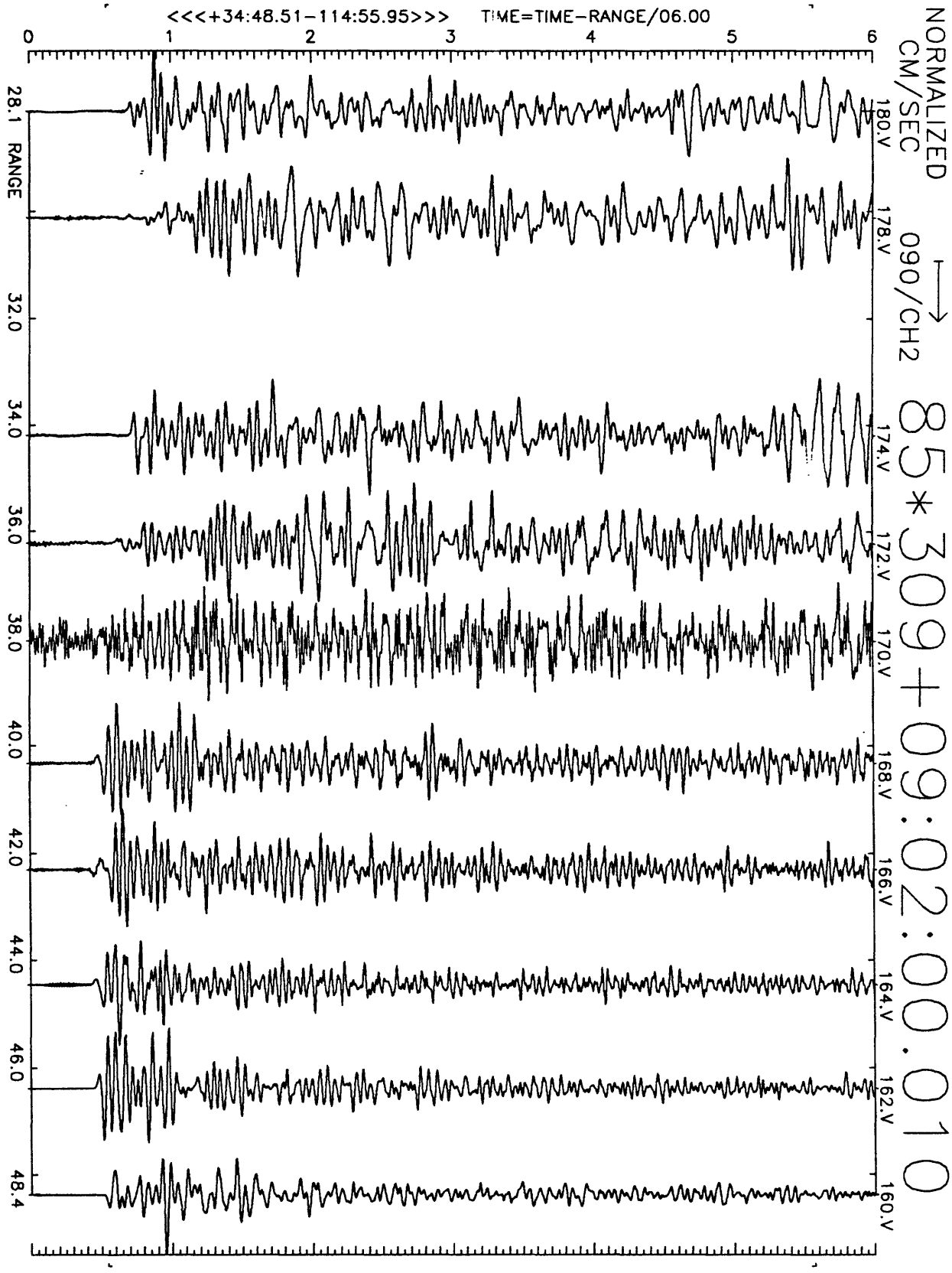

Figure A7(b), shot point 10: 6 second velocity record. Positive N33W motion is to right. Abscissa is distance to shot point. Top of trace is labeled with station number. Times are reduced by 6 km/sec. Shot time is indicated.

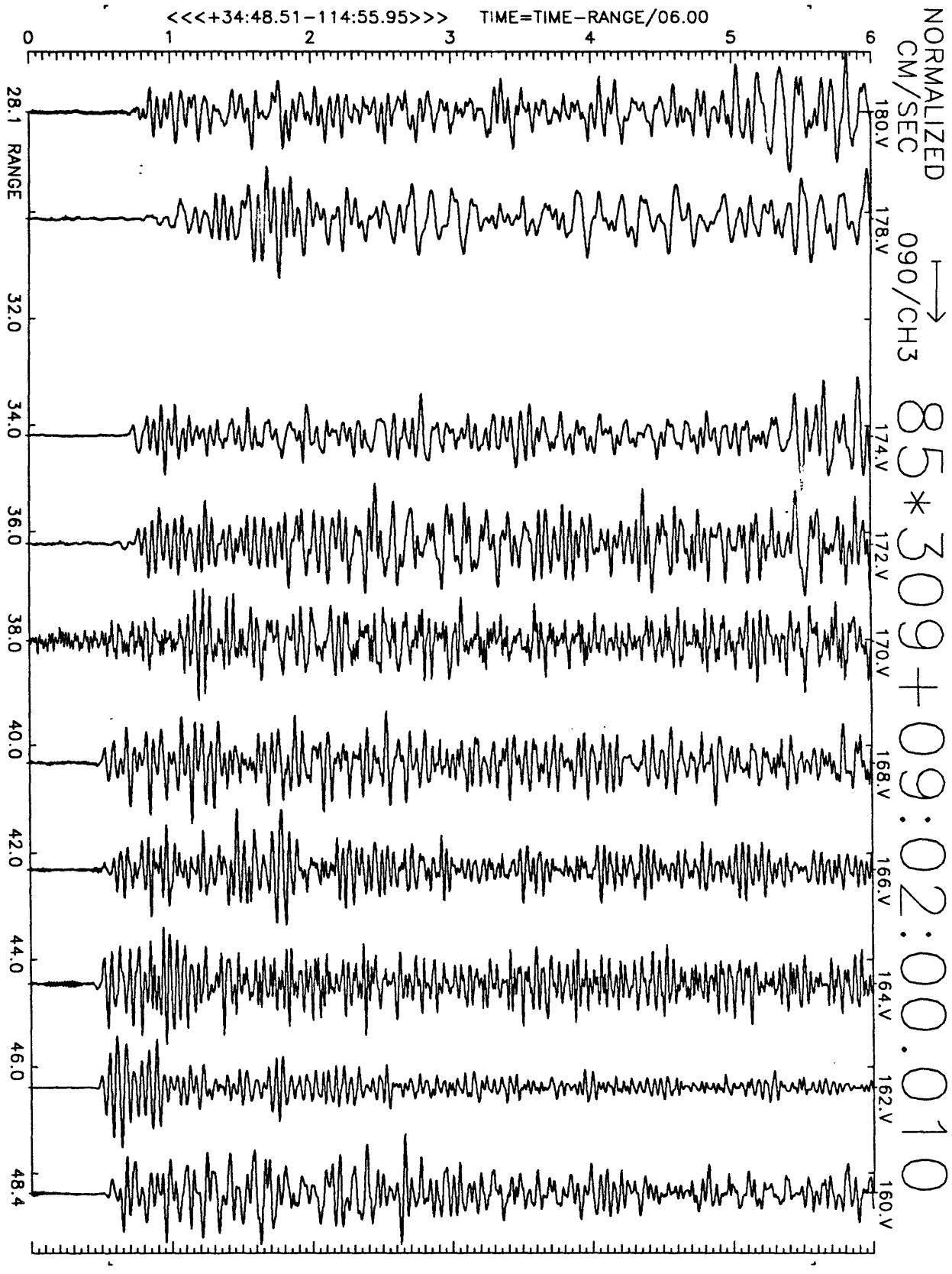

Figure A7(c), shot point 10: 6 second velocity record. Positive N57E motion is to right. Abscissa is distance to shot point. Top of trace is labeled with station number. Times are reduced by 6 km/sec. Shot time is indicated.

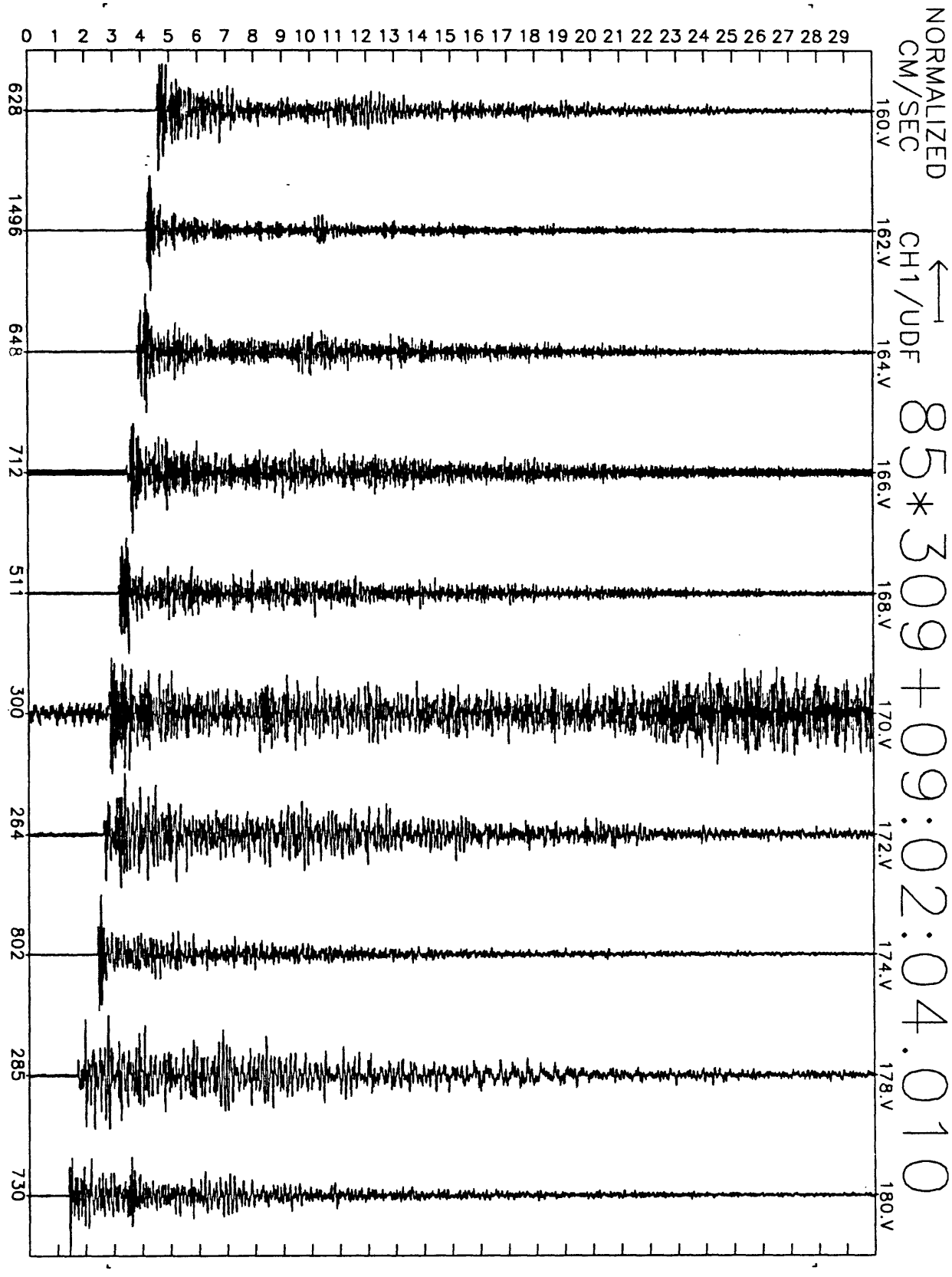

Figure A7(d), shot point 10: 30 second vertical velocity record. Abscissa is labeled with maximum counts in record (multiply by $\frac{10}{2^{24}-2^5} \approx 6 \times 10^{-7}$ to get cm/sec). Times are unreduced beginning at time indicated.

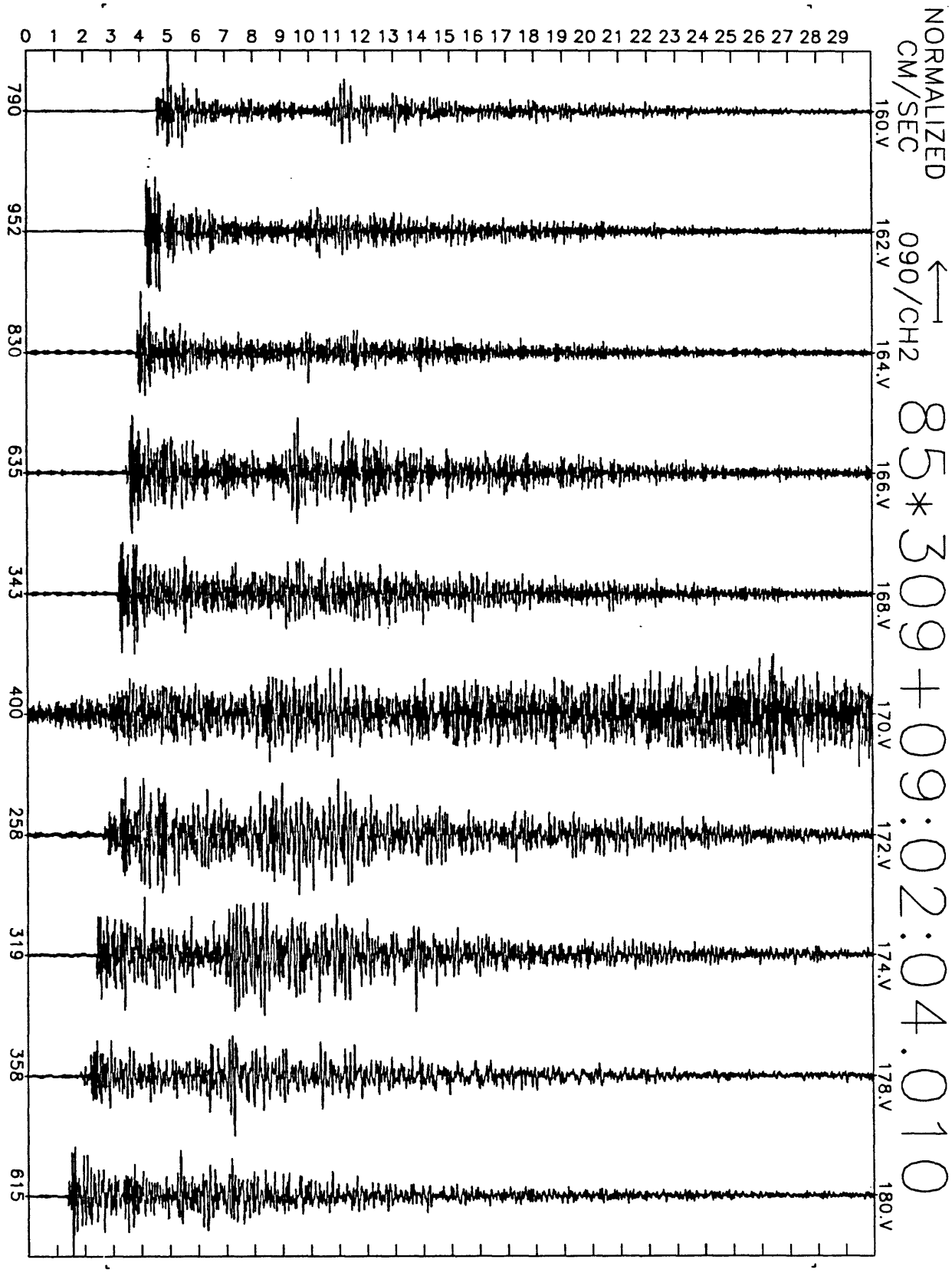

Figure A7(e), shot point 10: 30 second N33W velocity record. Abscissa is labeled with maximum counts in record (multiply by $\frac{10}{2^{24}-2^9} \approx 6 \times 10^{-7}$ to get cm/sec). Times are unreduced beginning at time indicated.

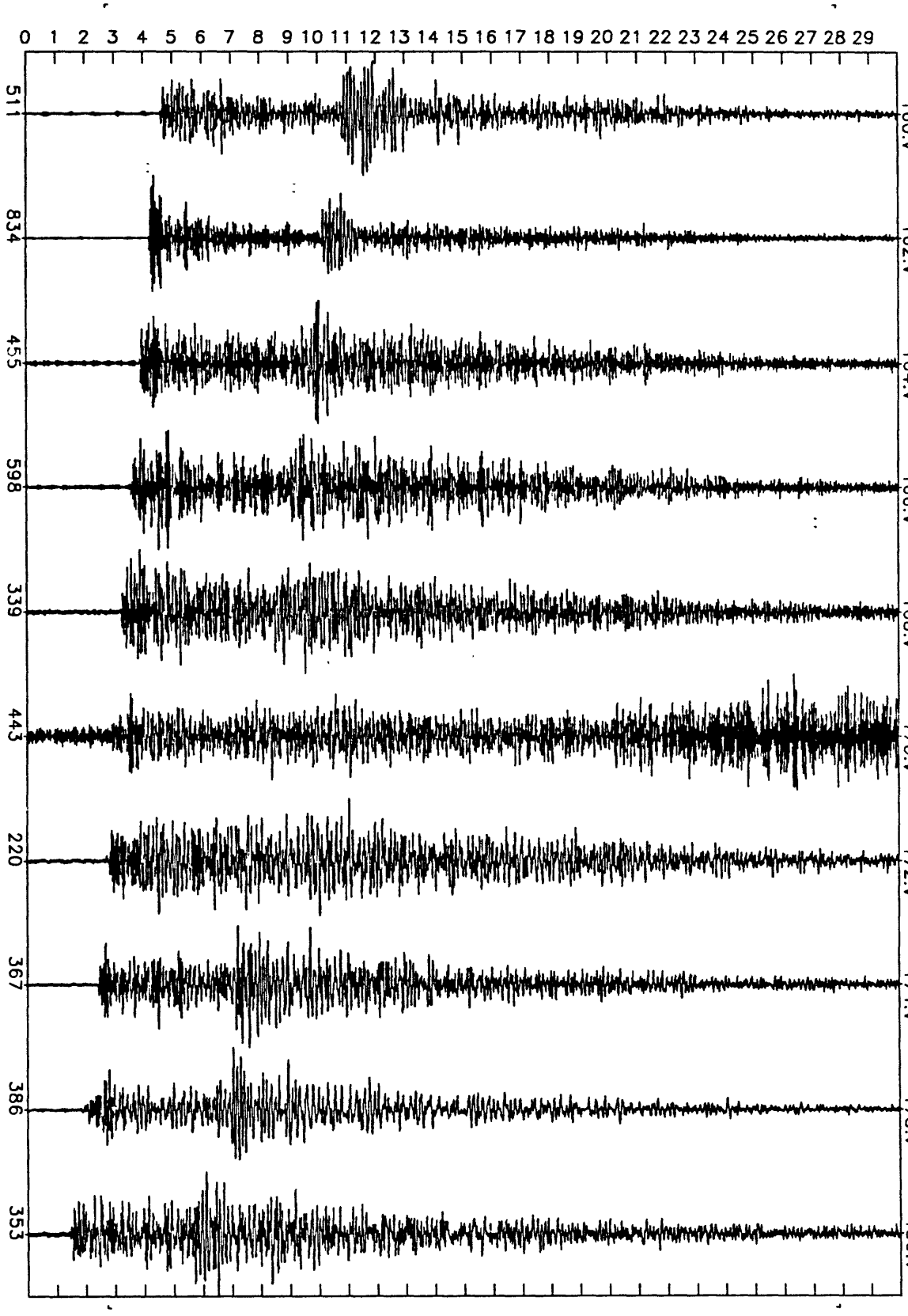

Figure A7(f), shot point 10: 30 second N57E velocity record. Abscissa is labeled with maximum counts in record (multiply by $\frac{10}{2^{24}-2^9} \approx 6 \times 10^{-7}$ to get cm/sec). Times are unreduced beginning at time indicated.

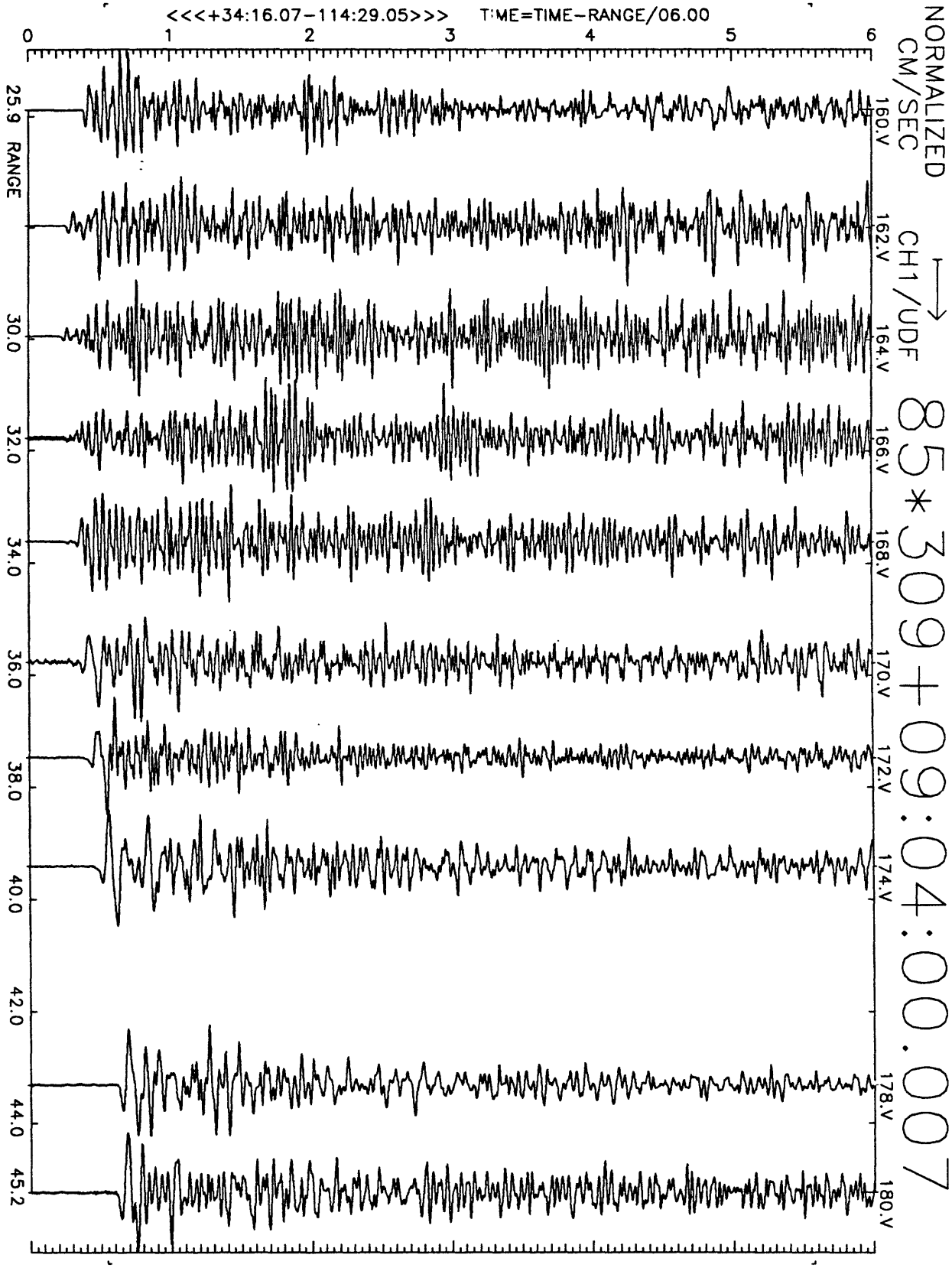

Figure A8(a), shot point 4A: 6 second velocity record. Positive vertical motion is to right. Abscissa is distance to shot point. Top of trace is labeled with station number. Times are reduced by 6 km/sec. Shot time is indicated.

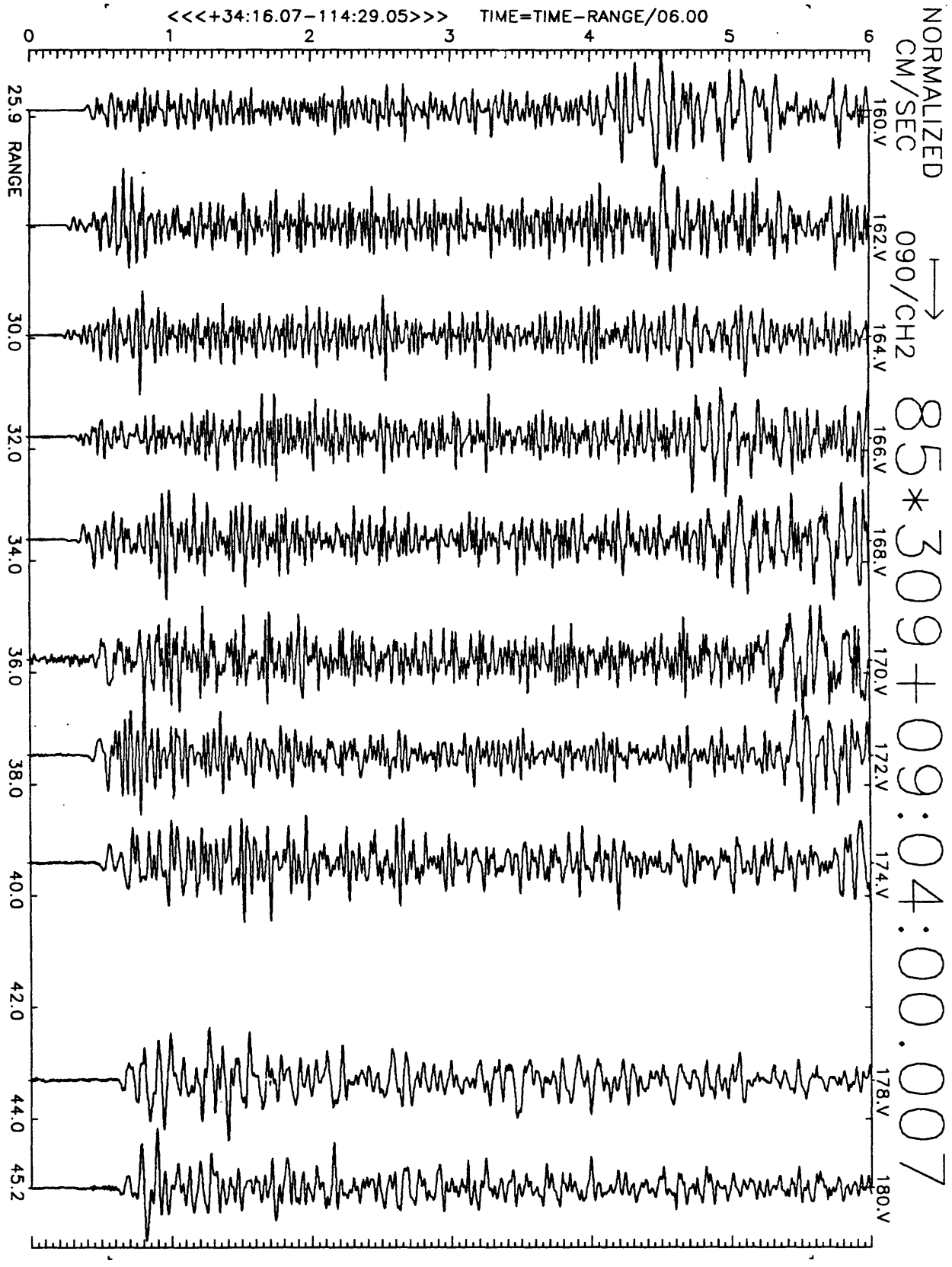

Figure A8(b), shot point 4A: 6 second velocity record. Positive N33W motion is to right. Abscissa is distance to shot point. Top of trace is labeled with station number. Times are reduced by 6 km/sec. Shot time is indicated.

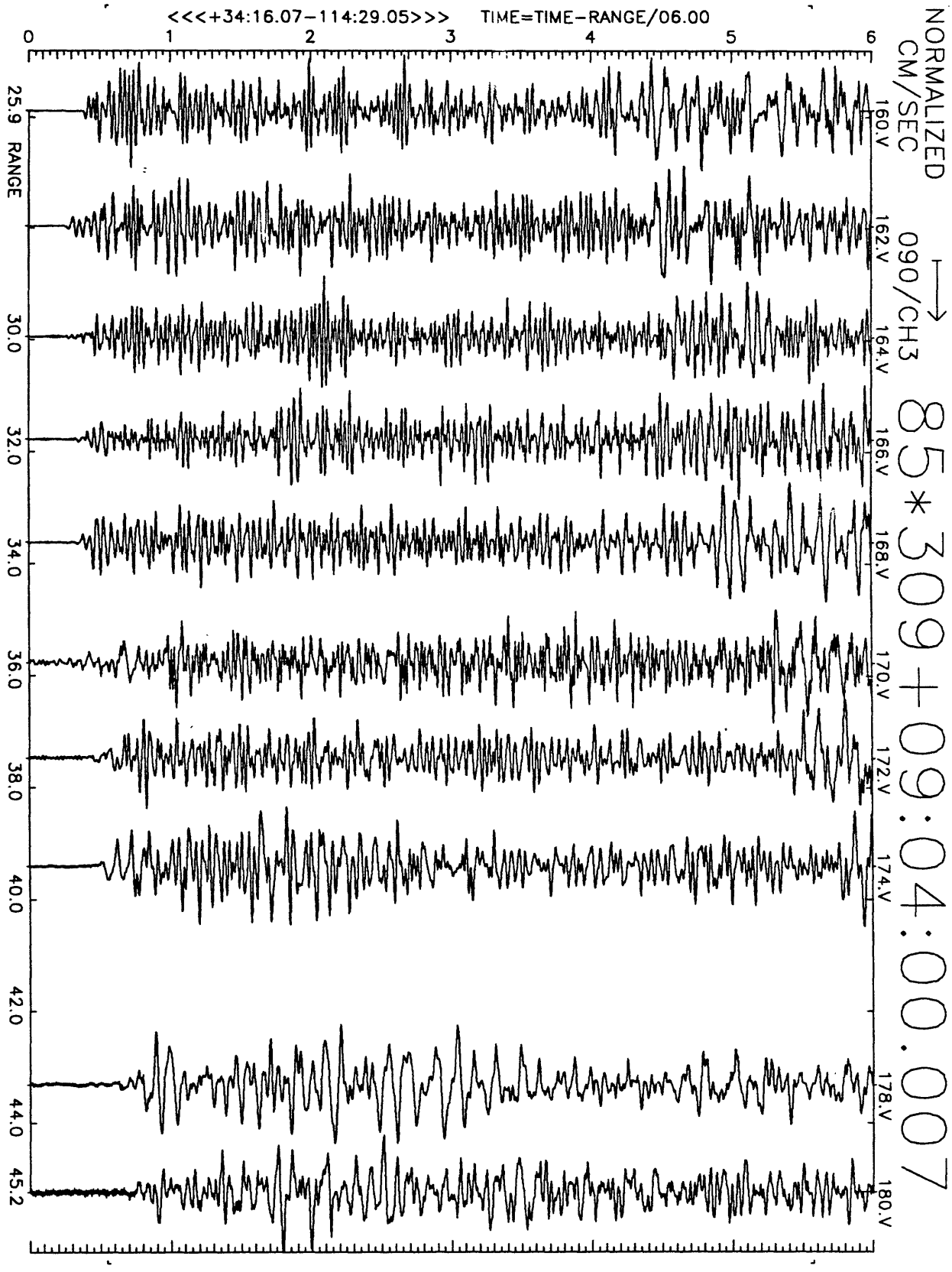

Figure A8(c), shot point 4A: 6 second velocity record. Positive N57E motion is to right. Abscissa is distance to shot point. Top of trace is labeled with station number. Times are reduced by 6 km/sec. Shot time is indicated.

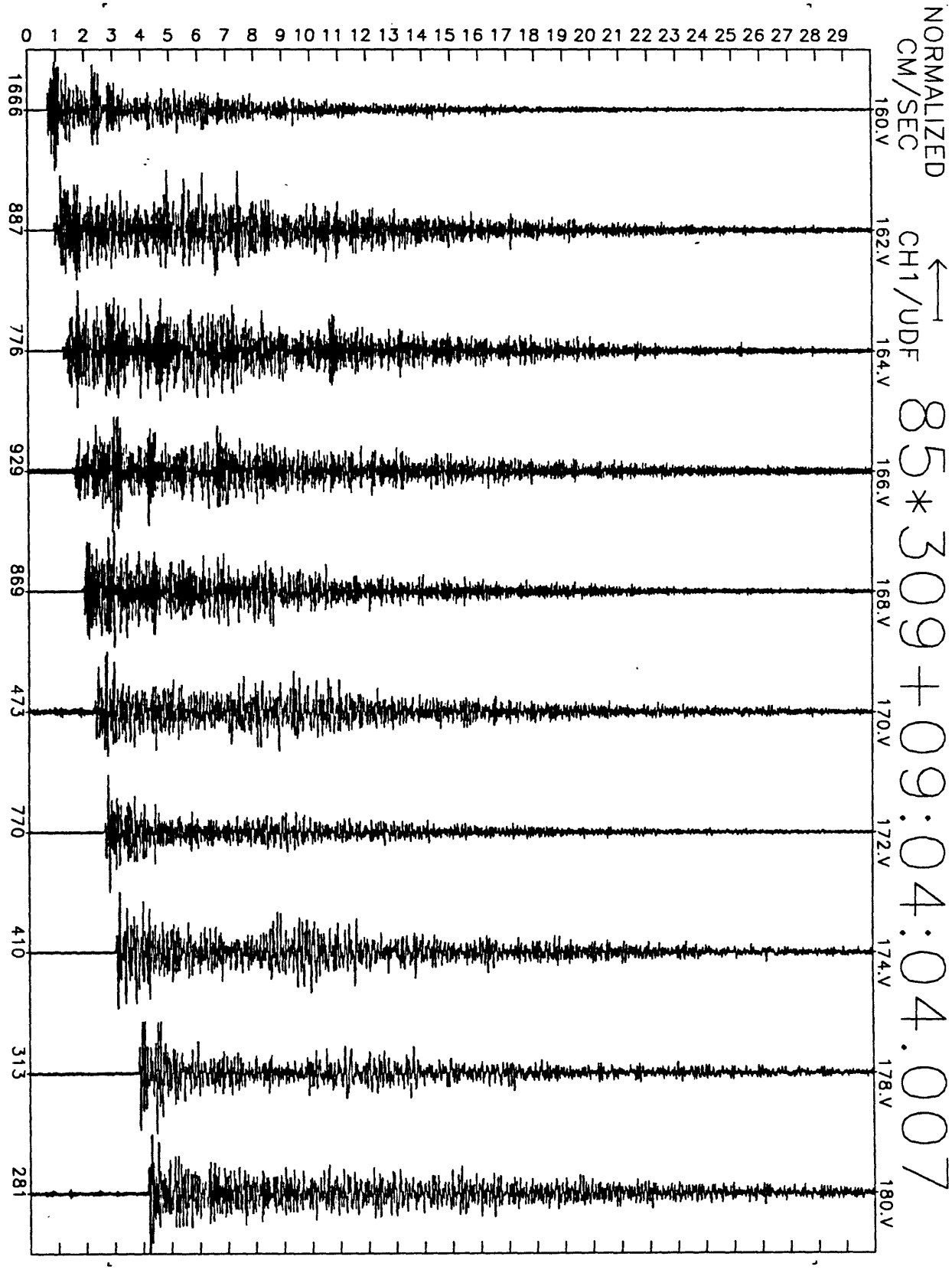

Figure A8(d), shot point 4A: 30 second vertical velocity record. Abscissa is labeled with maximum counts in record (multiply by $\frac{10}{2^{24}-2^9} \approx 6 \times 10^{-7}$ to get cm/sec). Times are unreduced beginning at time indicated.

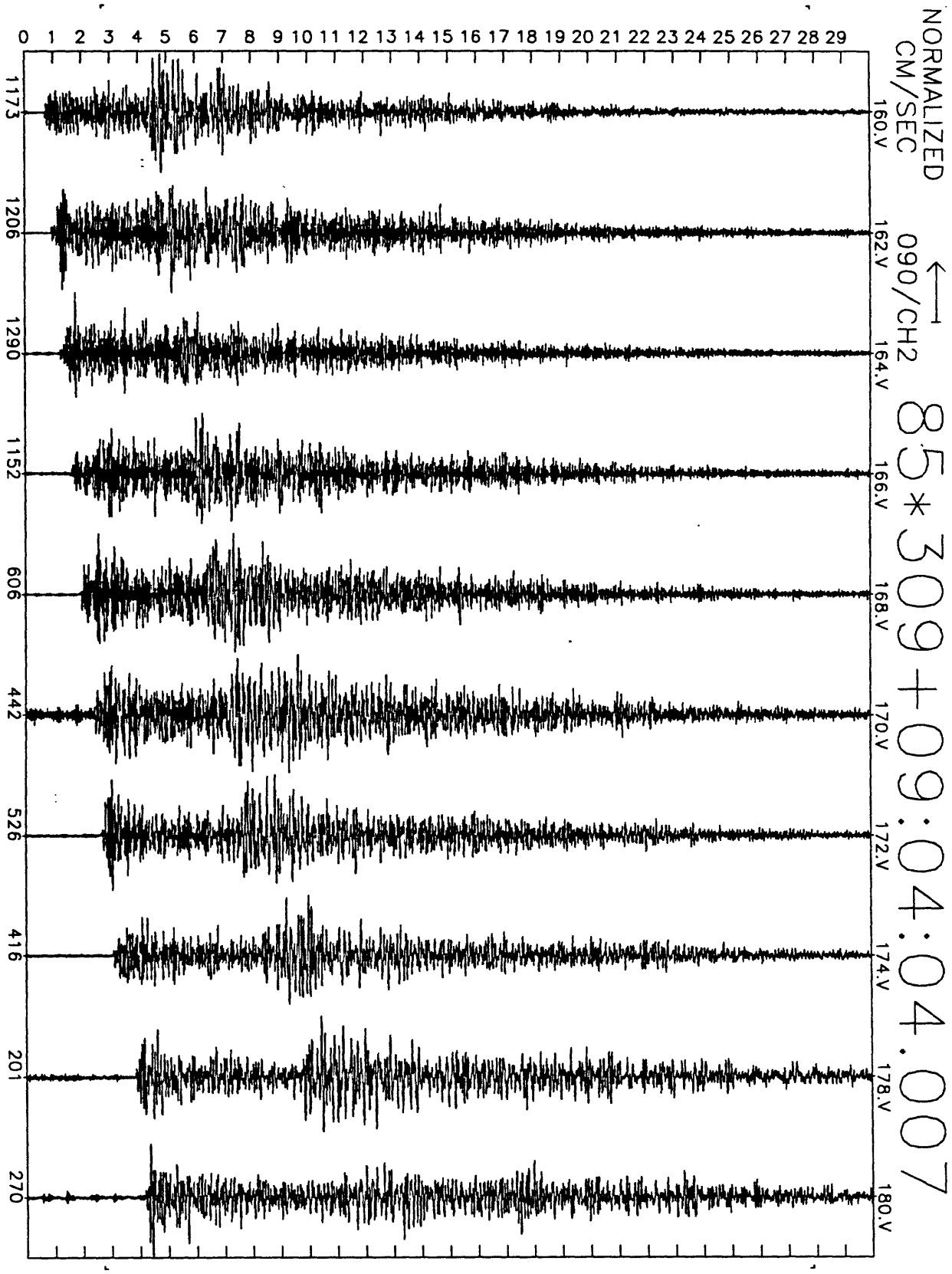

Figure A8(e), shot point 4A: 30 second N33W velocity record. Abscissa is labeled with maximum counts in record (multiply by $\frac{10}{2^{24}-2^{9}} \approx 6 \times 10^{-7}$ to get cm/sec). Times are unreduced beginning at time indicated.

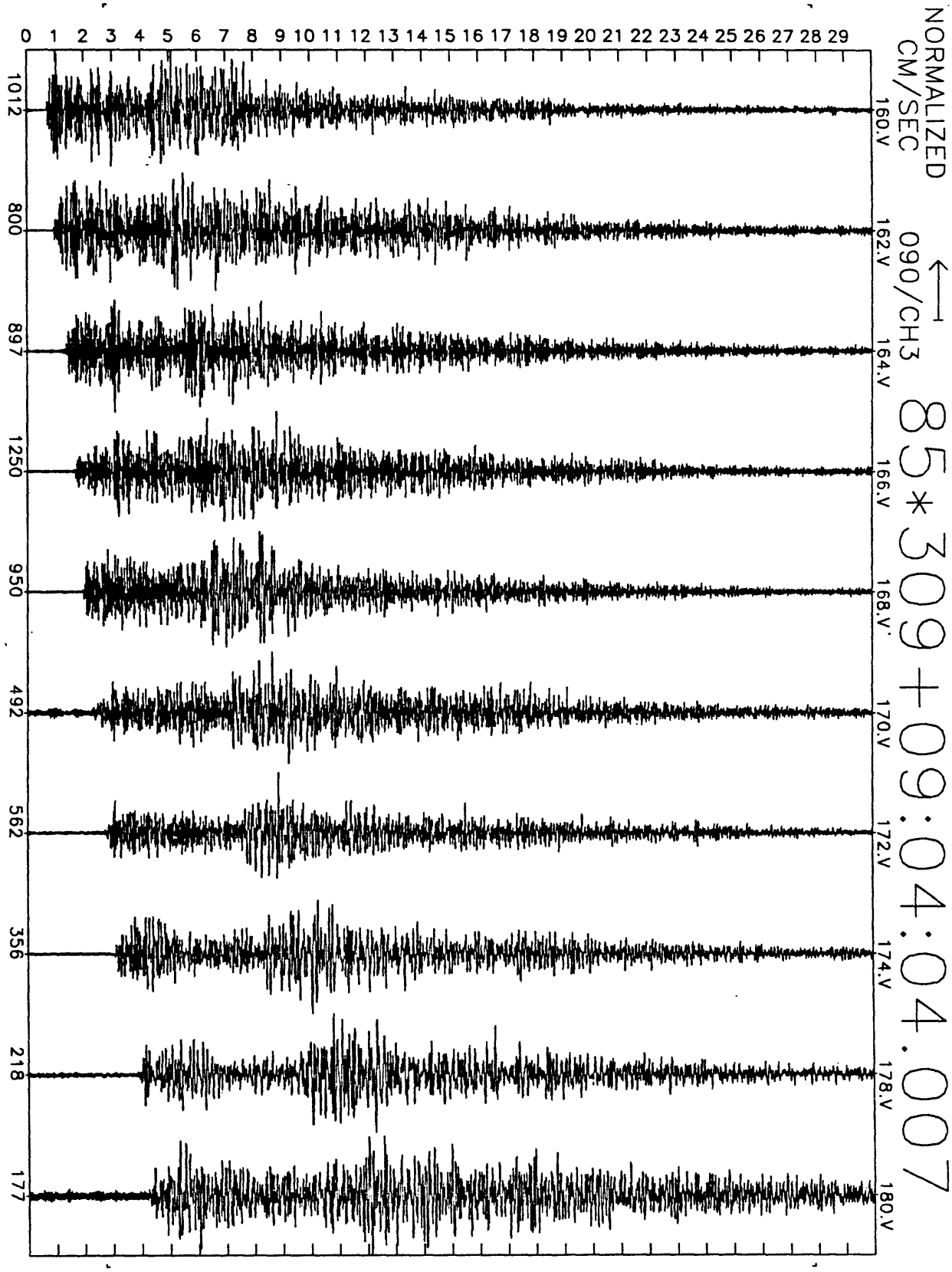

Figure A8(f), shot point 4A: 30 second N57E velocity record. Abscissa is labeled with maximum counts in record (multiply by $\frac{10}{2^{24}-2^5} \approx 6 \times 10^{-7}$ to get cm/sec). Times are unreduced beginning at time indicated.

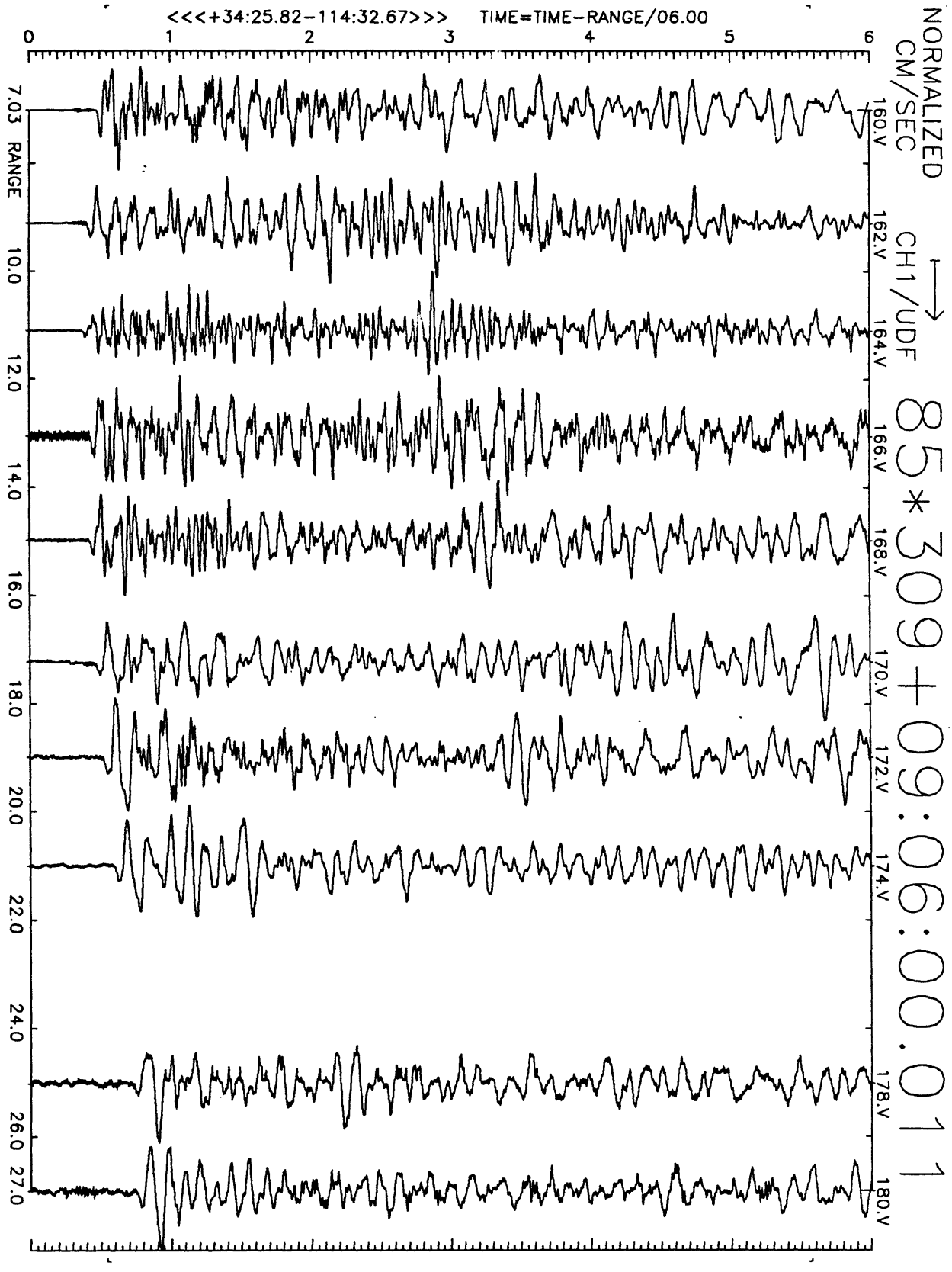

Figure A9(a), shot point 9X: 6 second velocity record. Positive vertical motion is to right. Abscissa is distance to shot point. Top of trace is labeled with station number. Times are reduced by 6 km/sec. Shot time is indicated.

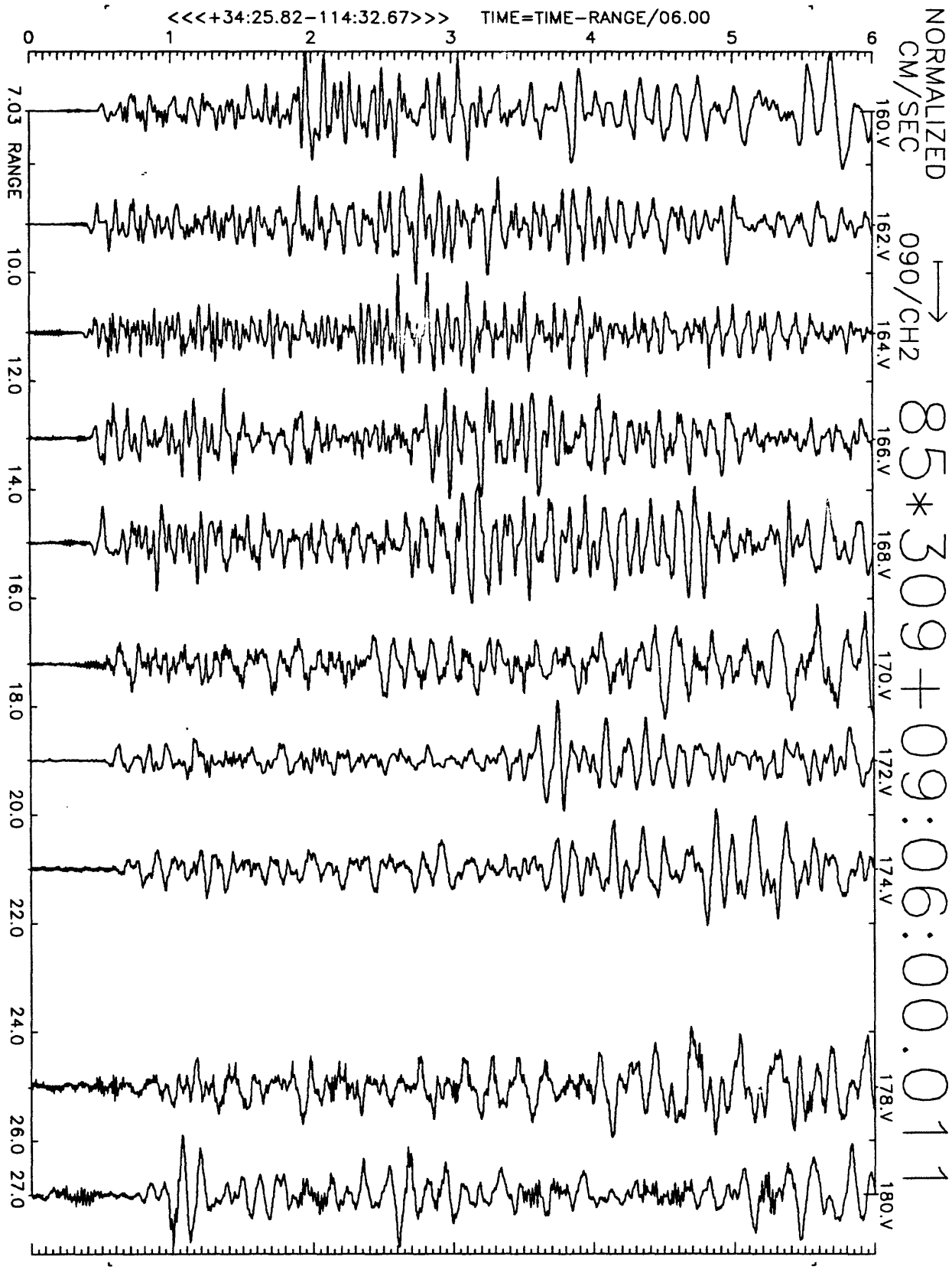

Figure A9(b), shot point 9X: 6 second velocity record. Positive N33W motion is to right. Abscissa is distance to shot point. Top of trace is labeled with station number. Times a-re reduced by 6 km/sec. Shot time is indicated.

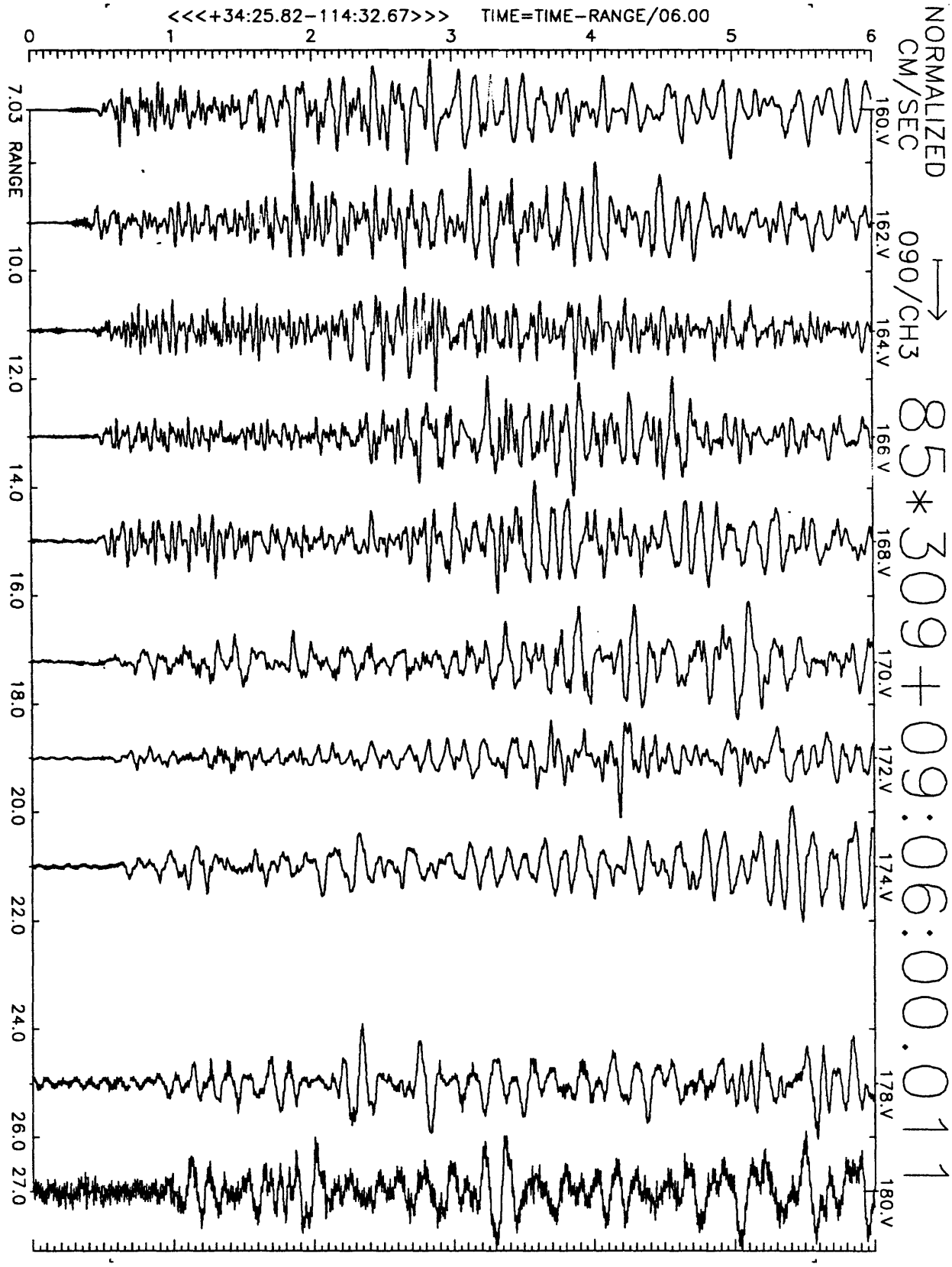

Figure A9(c), shot point 9X: 6 second velocity record. Positive N57E motion is to right. Abscissa is distance to shot point. Top of trace is labeled with station number. Times are reduced by 6 km/sec. Shot time is indicated.

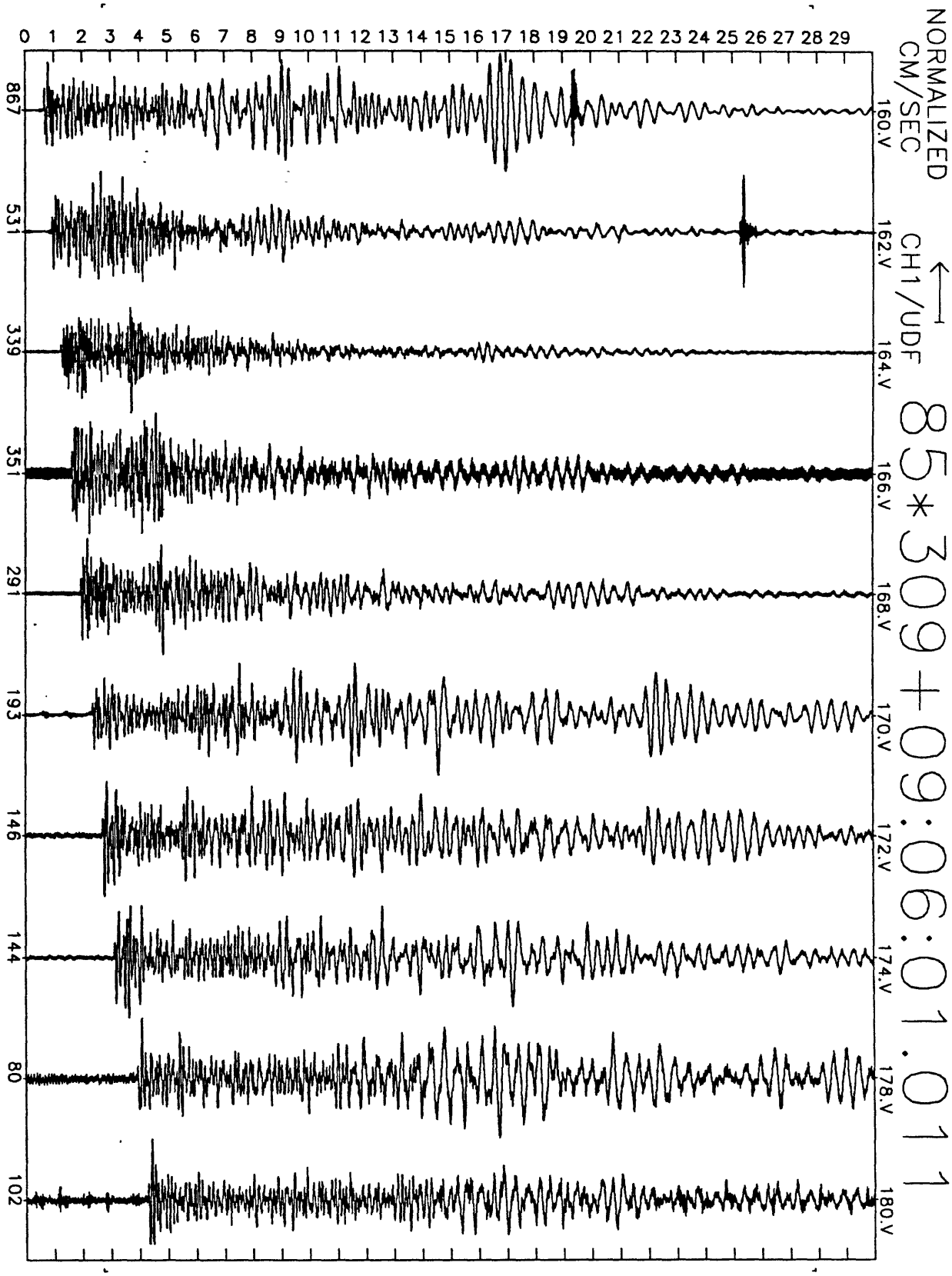

Figure A9(d), shot point 9X: 30 second vertical velocity record. Abscissa is labeled with maximum counts in record (multiply by $\frac{10}{2^{24}-2^5} \approx 6 \times 10^{-7}$ to get cm/sec). Times are unreduced beginning at time indicated.

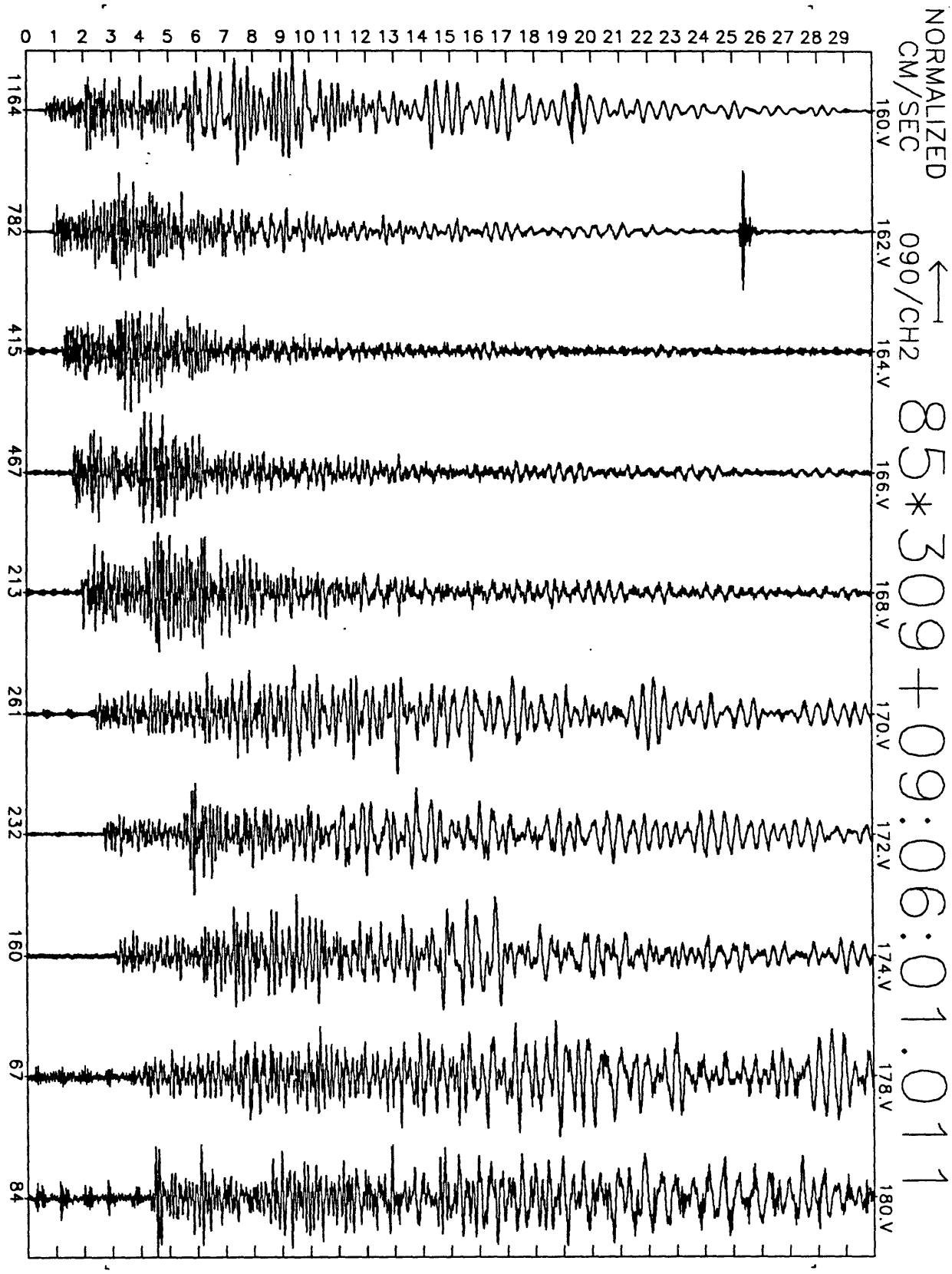

Figure A9(e), shot point 9X: 30 second N33W velocity record. Abscissa is labeled with maximum counts in record (multiply by $\frac{10}{2^{24}-2^{8}} \approx 6 \times 10^{-7}$ to get cm/sec). Times are unreduced beginning at time indicated.

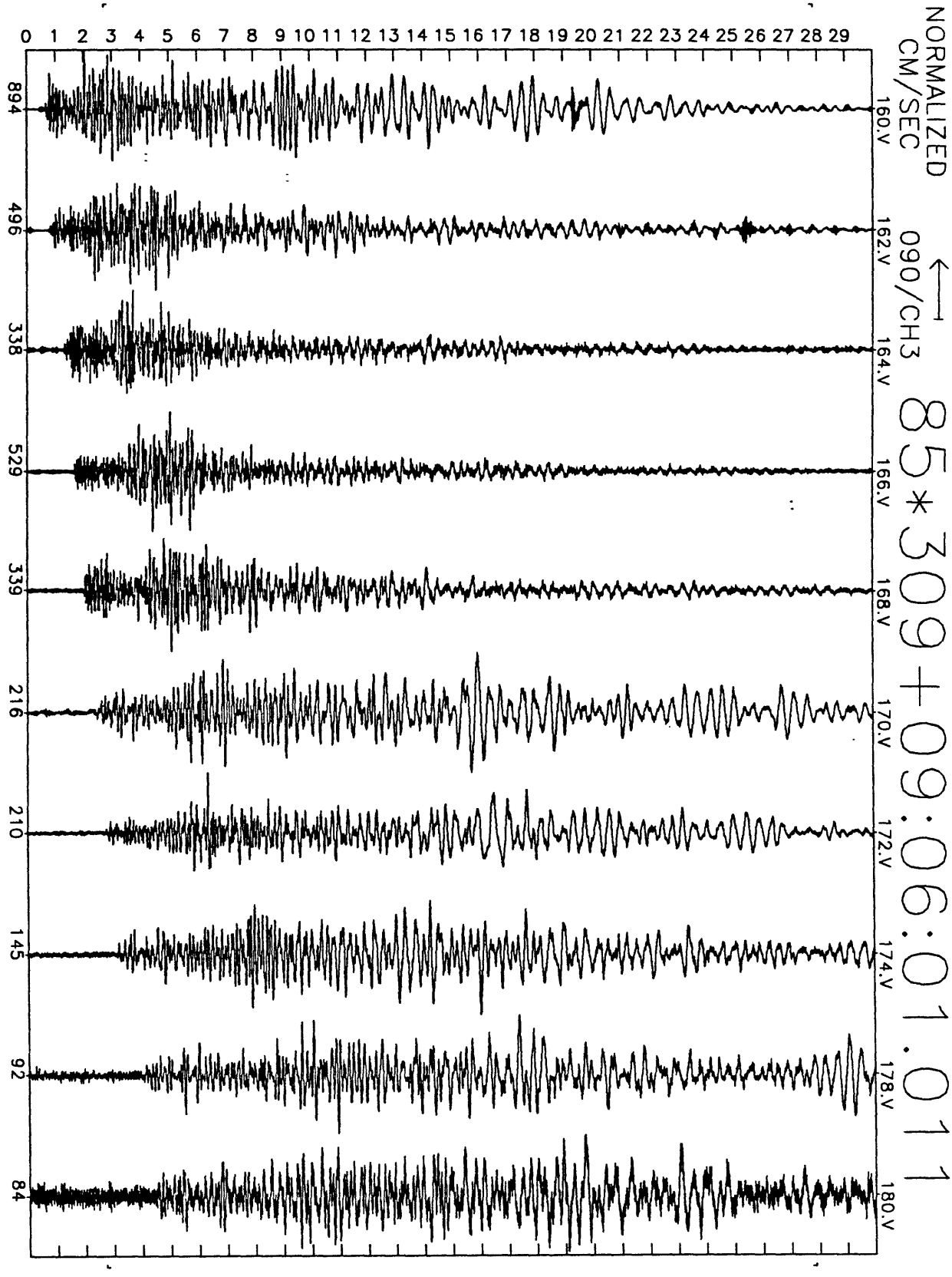

Figure A9(f), shot point 9X: 30 second N57E velocity record. Abscissa is labeled with maximum counts in record (multiply by $\frac{10}{2^{24}-2^{8}} \approx 6 \times 10^{-7}$ to get cm/sec). Times are unreduced beginning at time indicated.

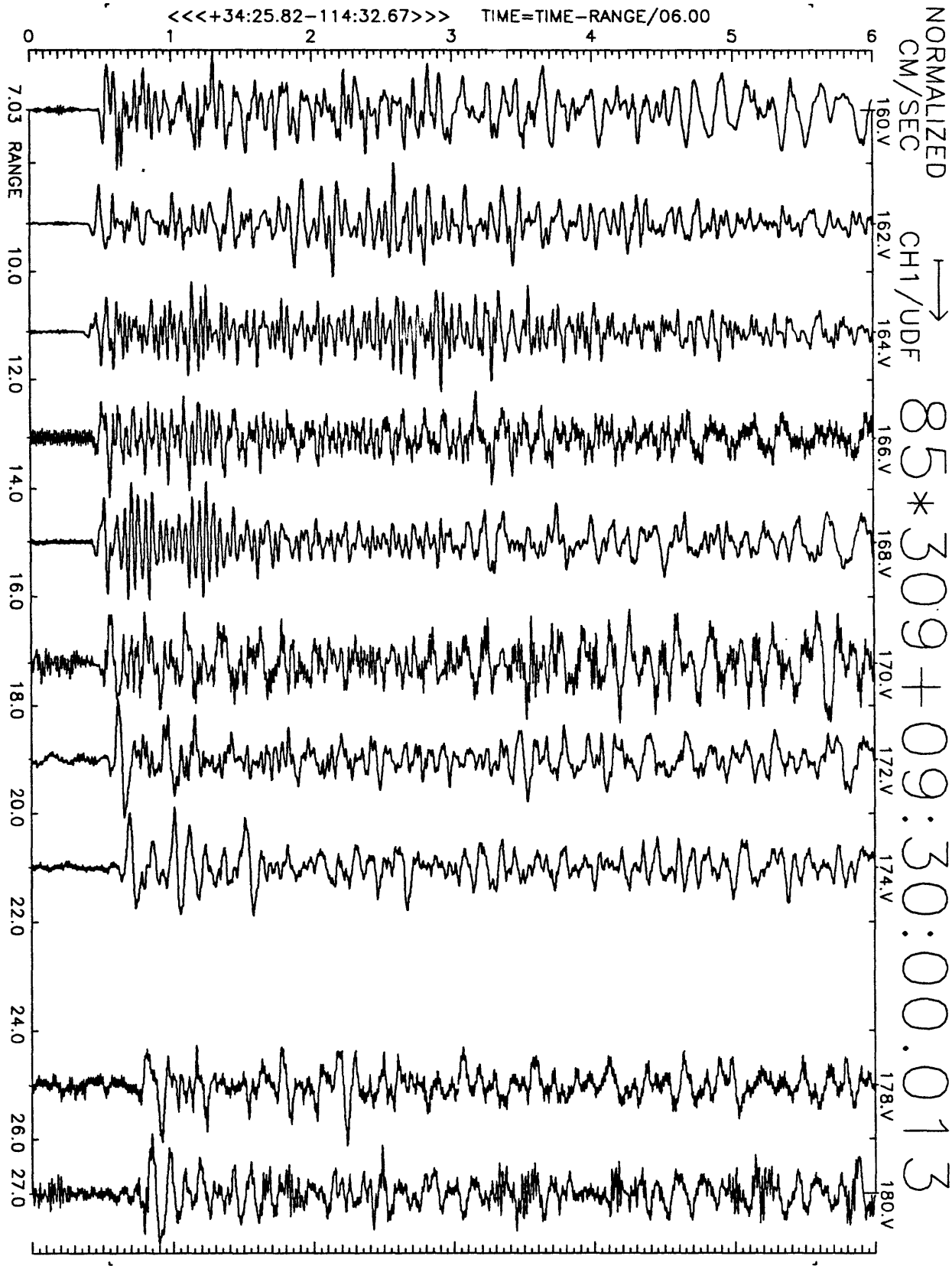

Figure A10(a), shot point $9X'$: 6 second velocity record. Positive vertical motion is to right. Abscissa is distance to shot point. Top of trace is labeled with station number. Times are reduced by 6 km/sec. Shot time is indicated.

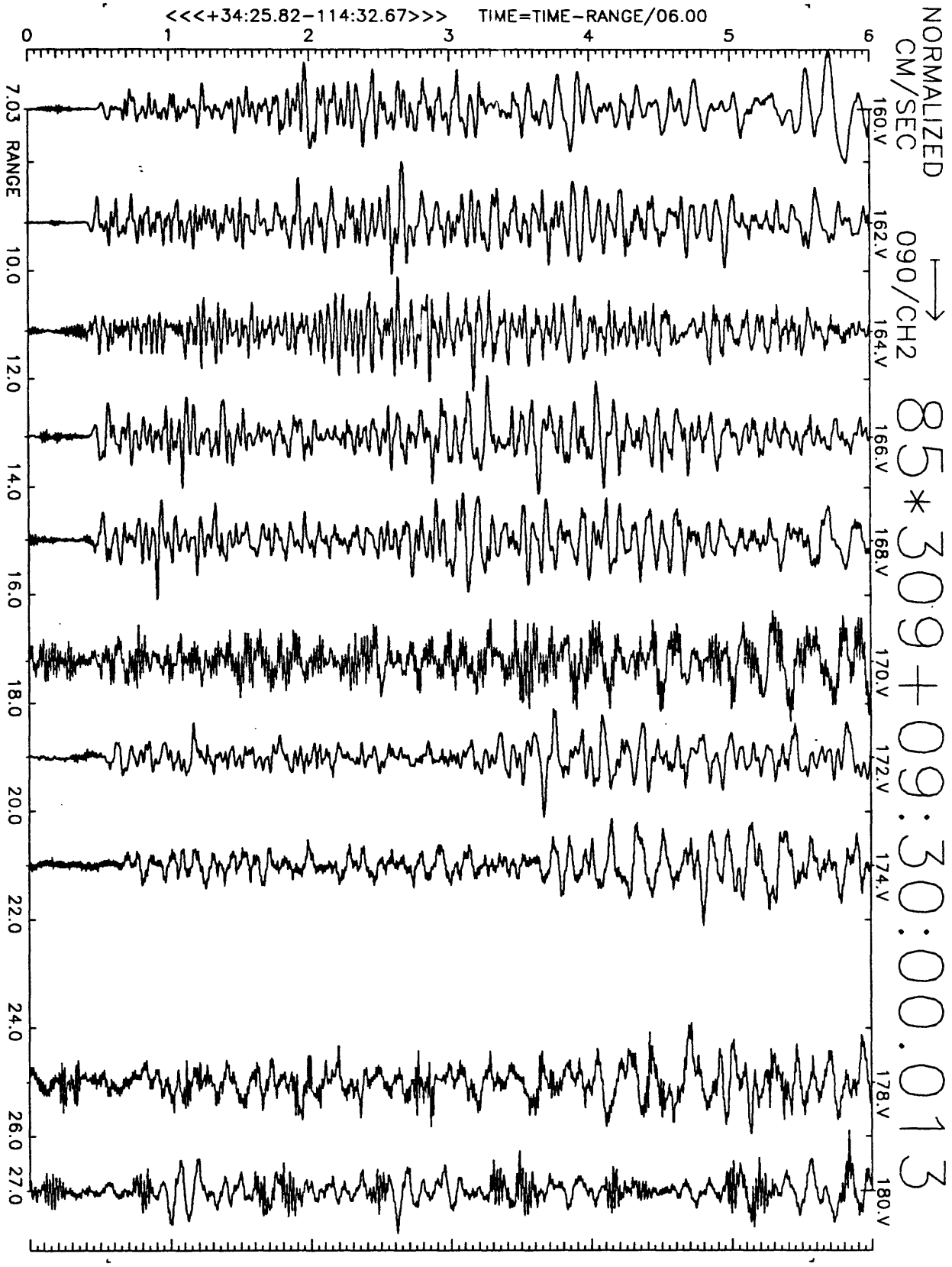

Figure A10(b), shot point $9X'$: 6 second velocity record. Positive N33W motion is to right. Abscissa is distance to shot point. Top of trace is labeled with station number. Times are reduced by 6 km/sec. Shot time is indicated.

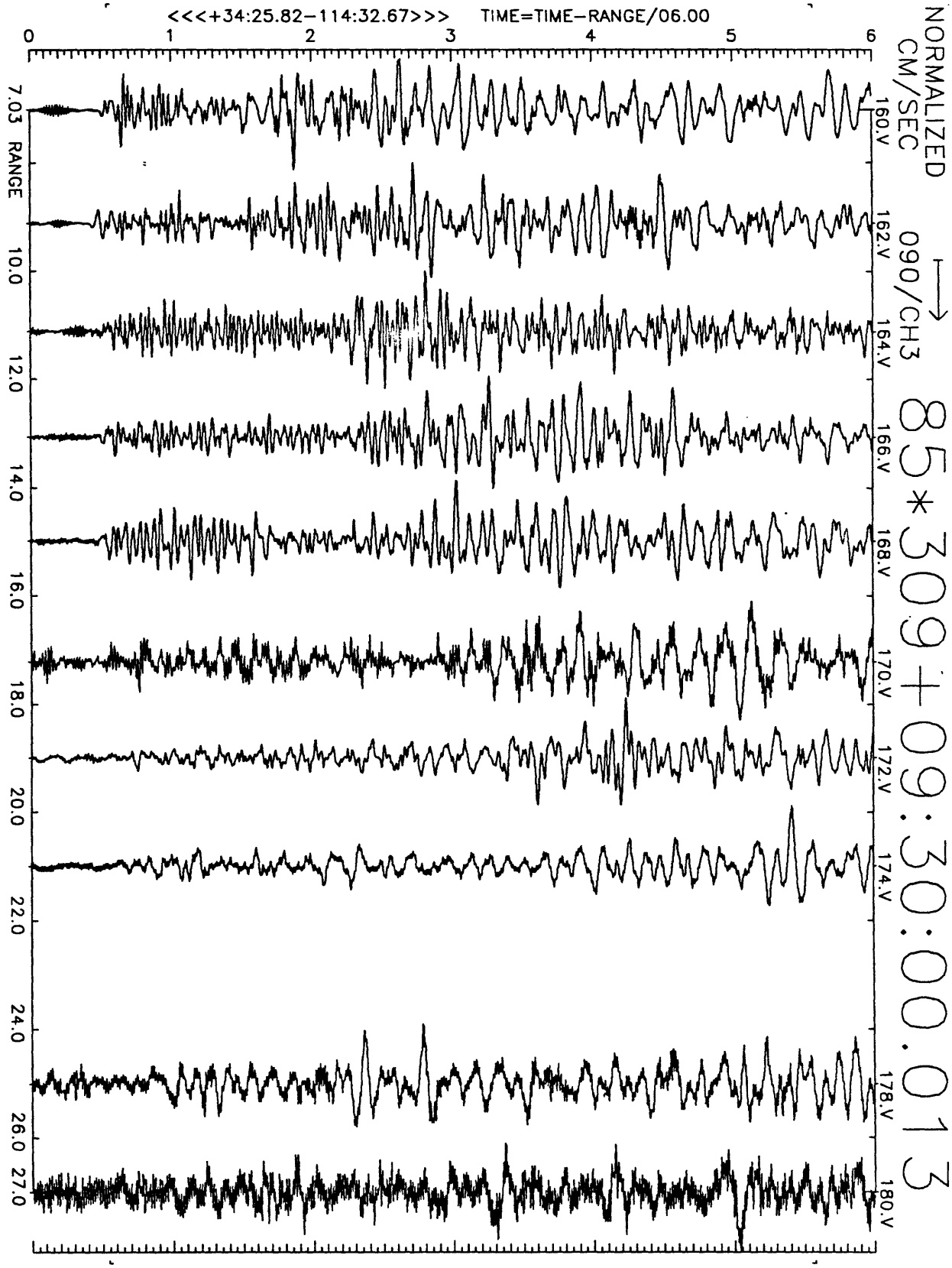

Figure A10(c), shot point $9X'$: 6 second velocity record. Positive N57E motion is to right. Abscissa is distance to shot point. Top of trace is labeled with station number. Times are reduced by 6 km/sec. Shot time is indicated.

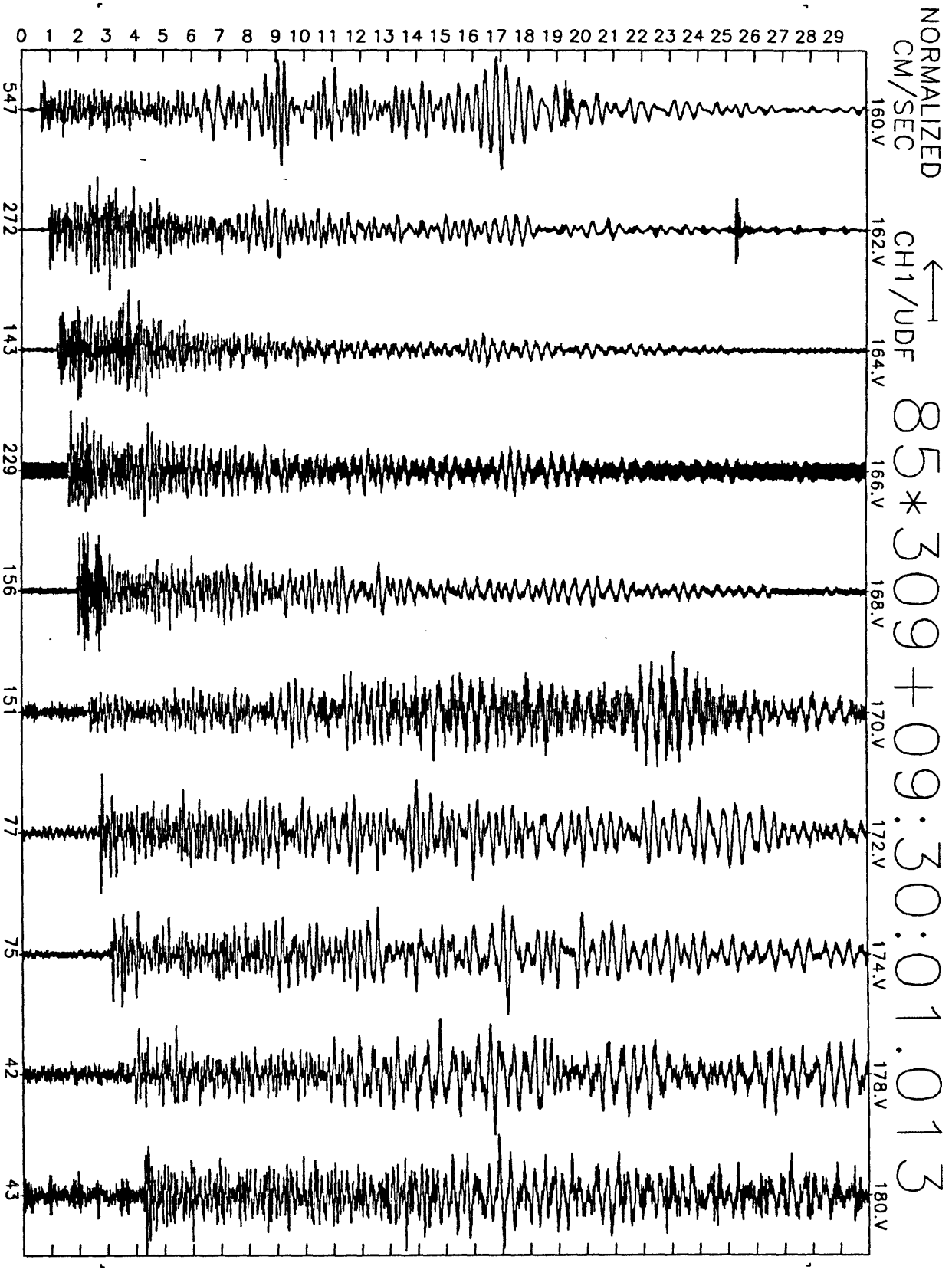

Figure A10(d), shot point $9X'$: 30 second vertical velocity record. Abscissa is labeled with maximum counts in record (multiply by $\frac{10}{2^{24}-2^5} \approx 6 \times 10^{-7}$ to get cm/sec). Times are unreduced beginning at time indicated.

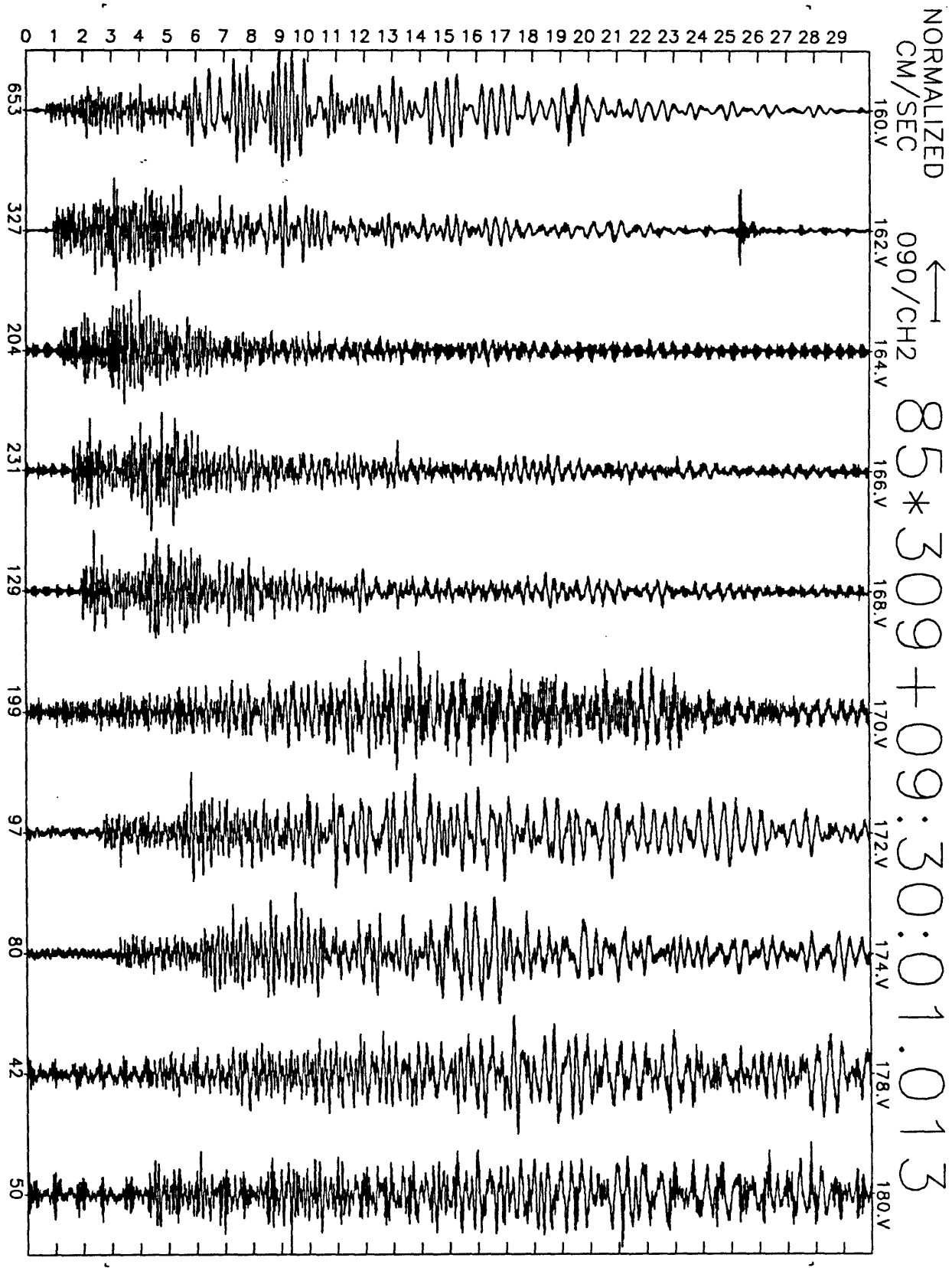

Figure A10(e), shot point $9X'$: 30 second N33W velocity record. Abscissa is labeled with maximum counts in record (multiply by $\frac{10}{2^{24}-2^5} \approx 6 \times 10^{-7}$ to get cm/sec). Times are unreduced beginning at time indicated.

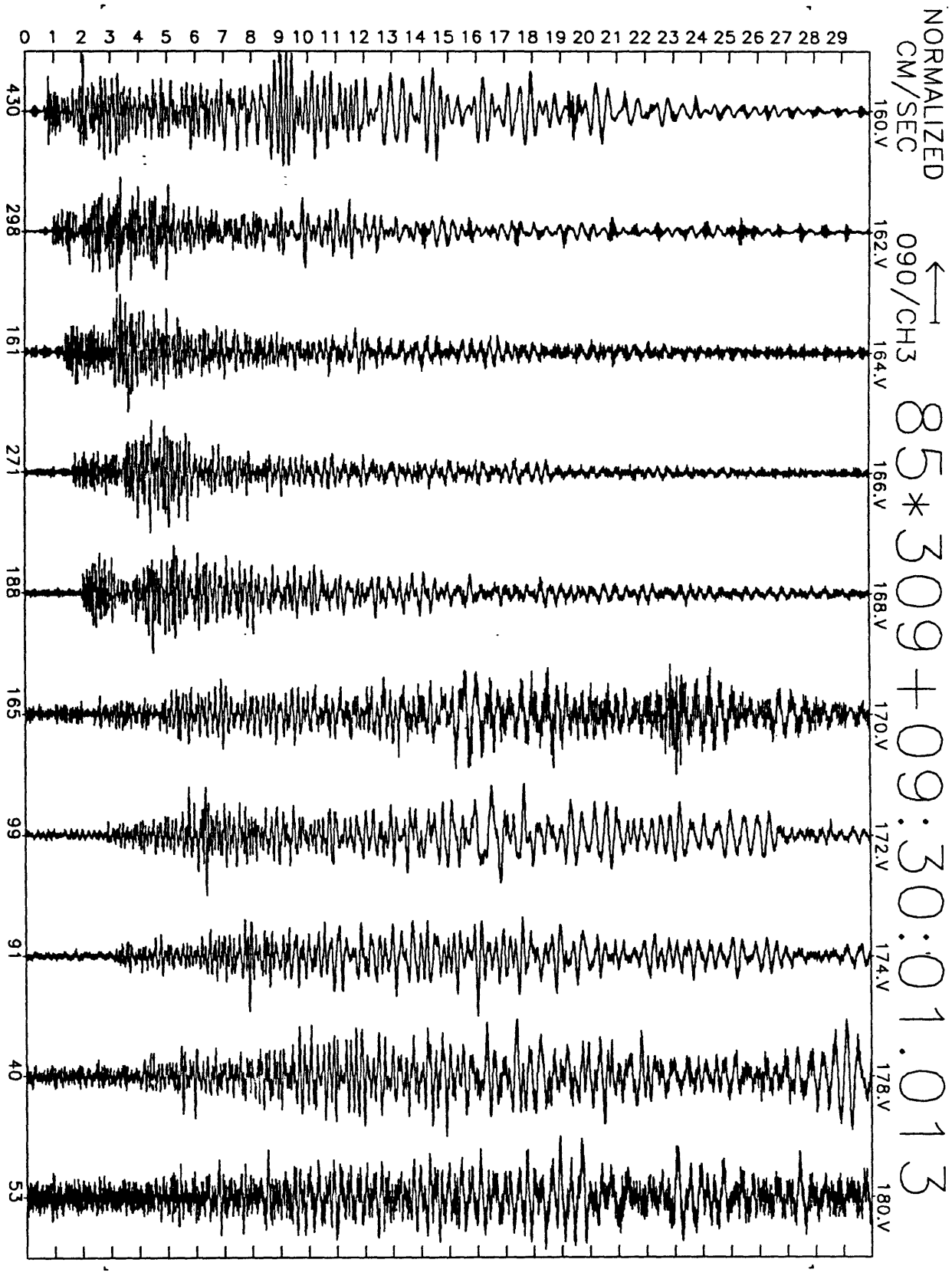

Figure A10(f), shot point $9X'$: 30 second N57E velocity record. Abscissa is labeled with maximum counts in record (multiply by $\frac{10}{2^{24}-2^{9}} \approx 6 \times 10^{-7}$ to get cm/sec). Times are unreduced beginning at time indicated.

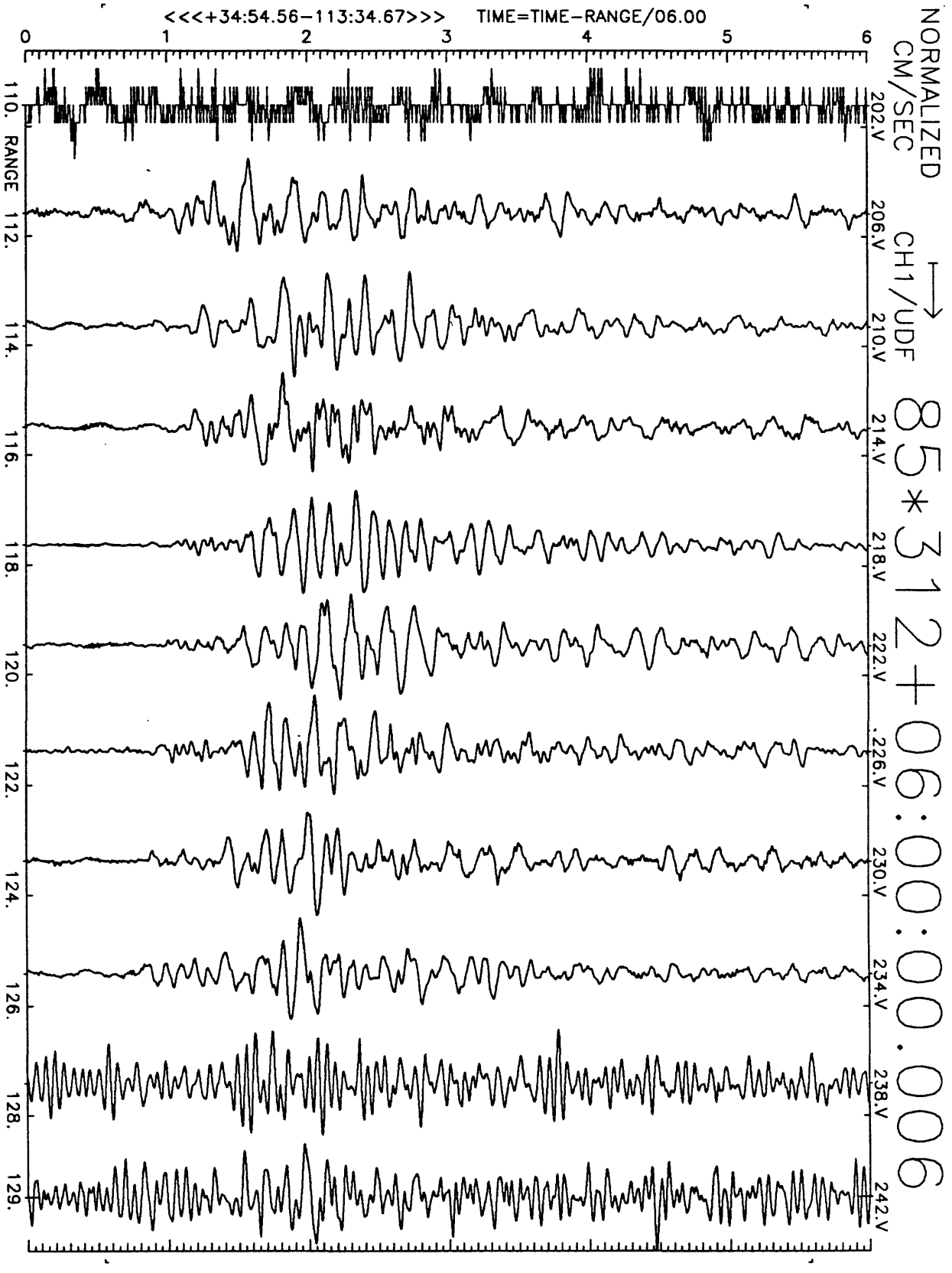

Figure A11(a), shot point 12: 6 second velocity record. Positive vertical motion is to right. Abscissa is distance to shot point. Top of trace is labeled with station number. Times are reduced by 6 km/sec. Shot time is indicated.

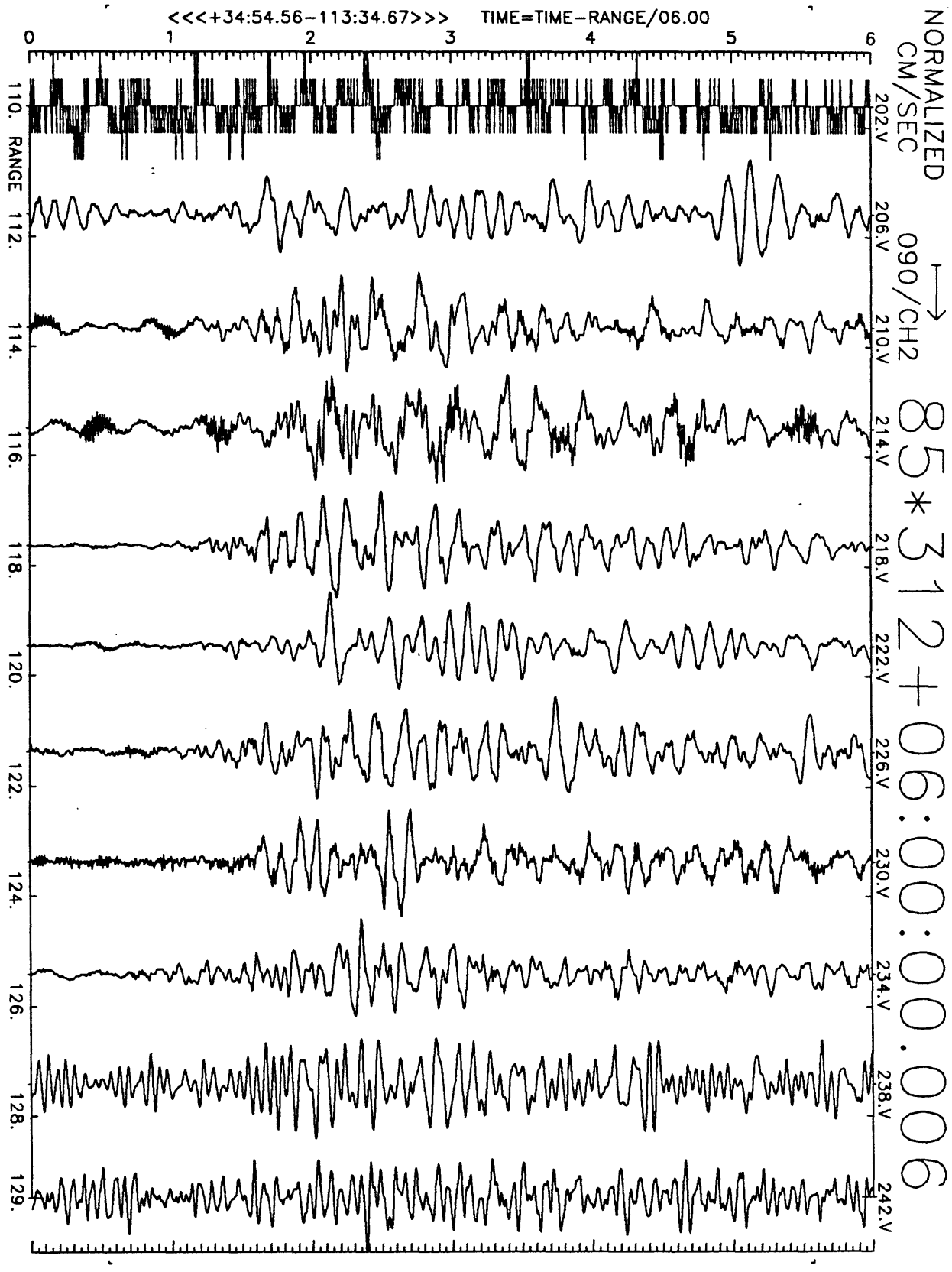

Figure A11(b), shot point 12: 6 second velocity record. Positive N20E motion is to right. Abscissa is distance to shot point. Top of trace is labeled with station number. Times are reduced by 6 km/sec. Shot time is indicated.

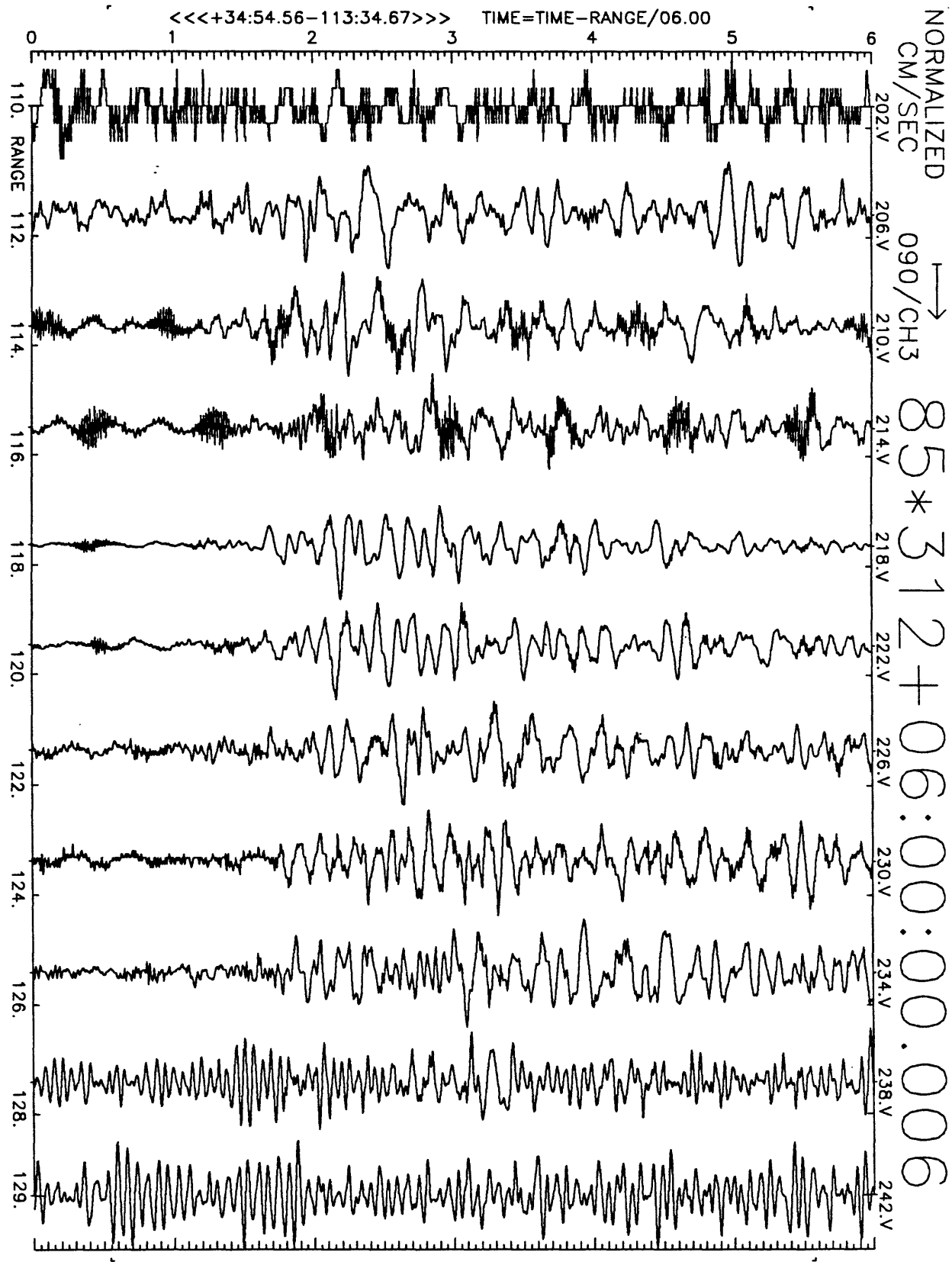

Figure A11(c), shot point 12: 6 second velocity record. Positive N110E motion is to right. Abscissa is distance to shot point. Top of trace is labeled with station number. Times are reduced by 6 km/sec. Shot time is indicated.

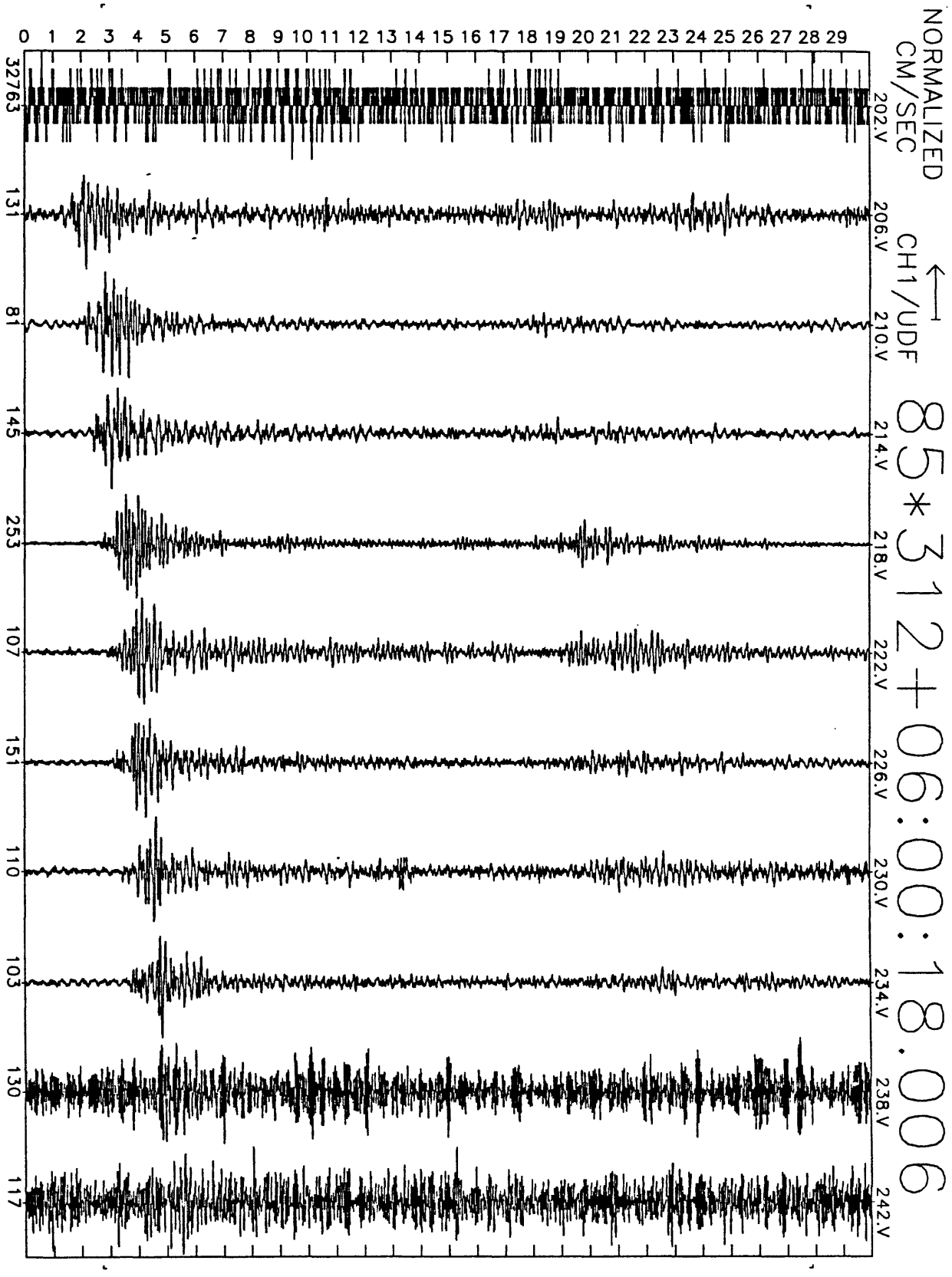

Figure A11(d), shot point 12: 30 second vertical velocity record. Abscissa is labeled with maximum counts in record (multiply by $\frac{10}{2^{24}-2^5} \approx 6 \times 10^{-7}$ to get cm/sec). Times are unreduced beginning at time indicated.

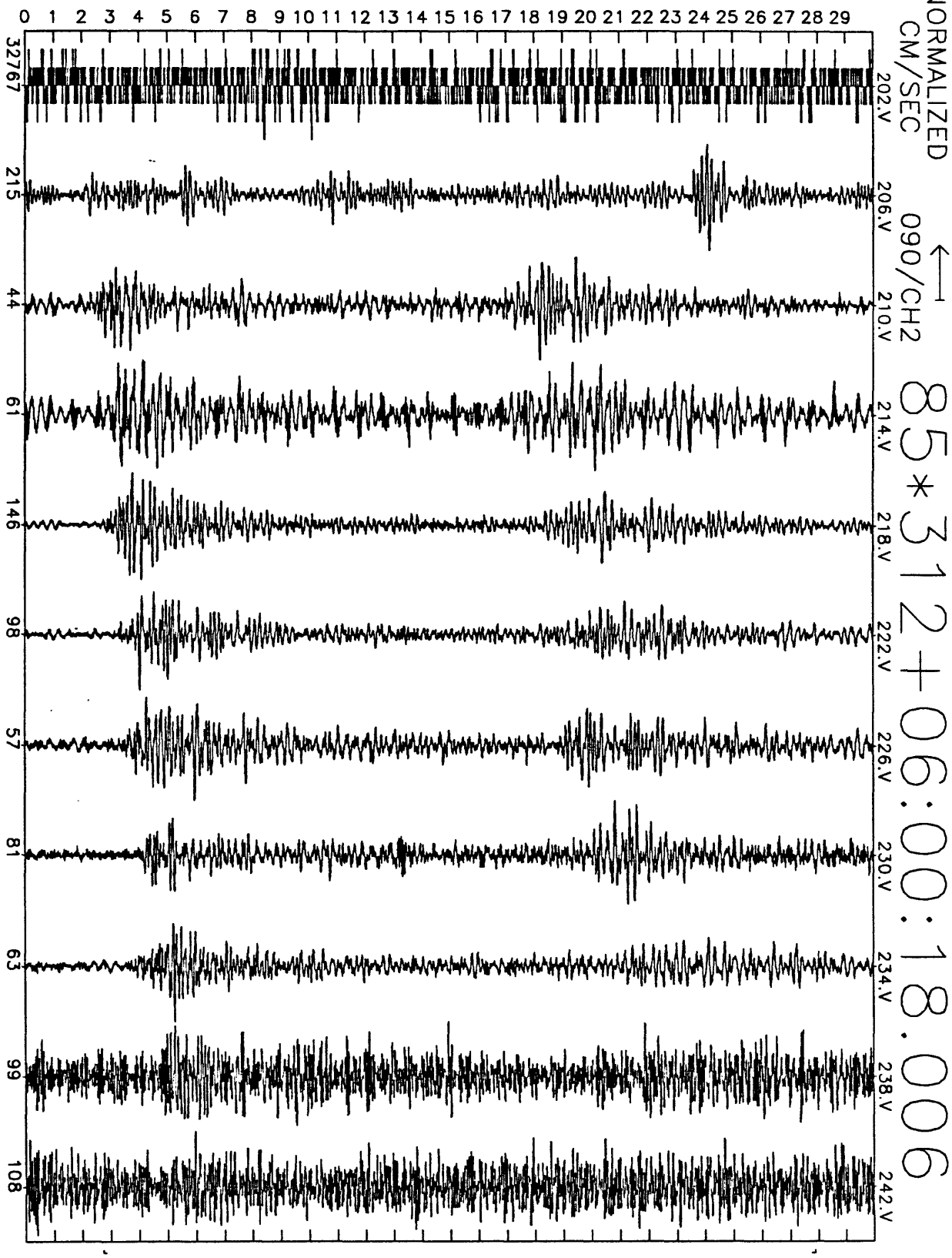

Figure A11(e), shot point 12: 30 second N20E velocity record. Abscissa is labeled with maximum counts in record (multiply by $\frac{10}{2^{24}-2^5} \approx 6 \times 10^{-7}$ to get cm/sec). Times are unreduced beginning at time indicated.

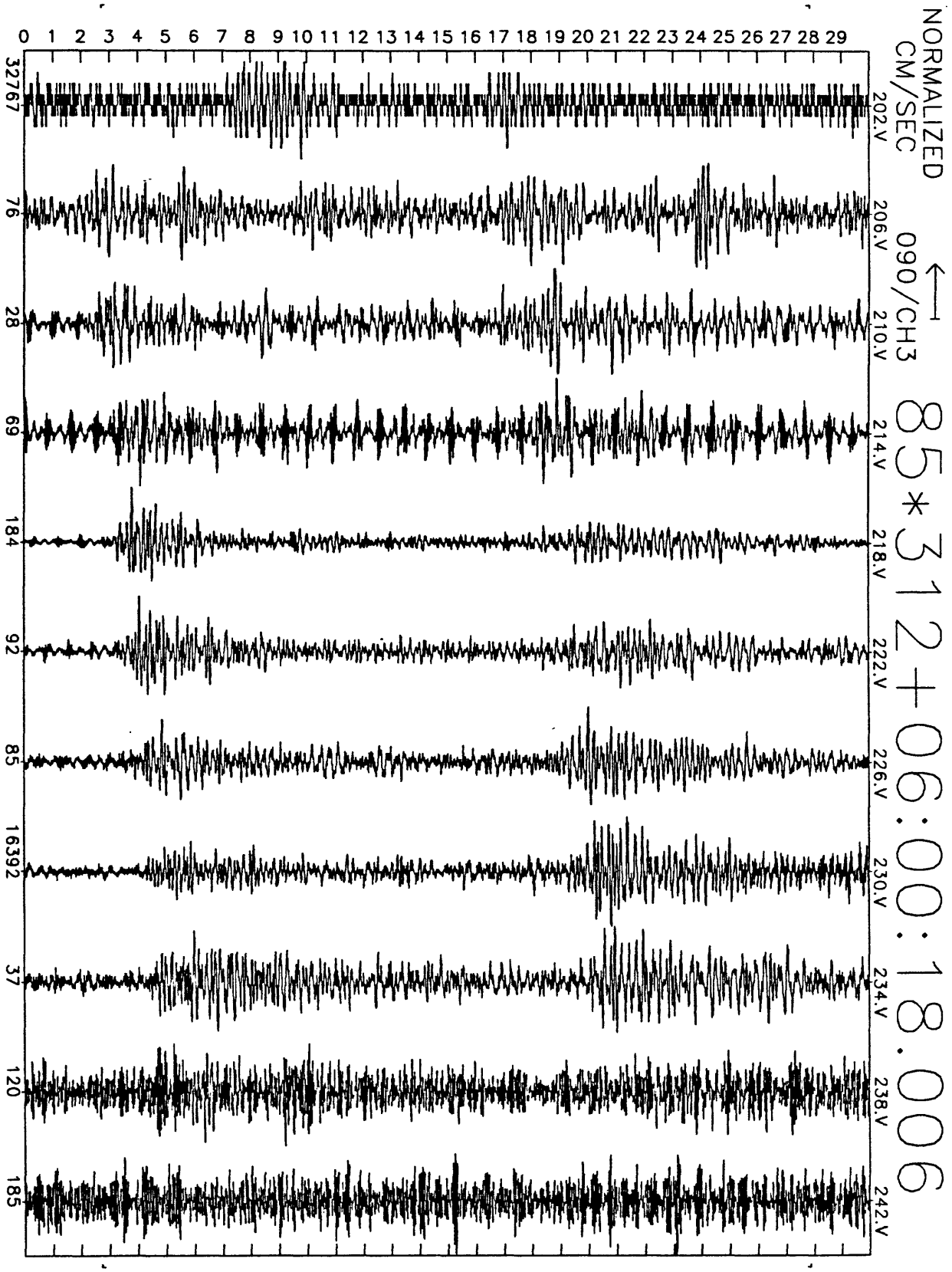

Figure A11(f), shot point 12: 30 second N110E velocity record. Abscissa is labeled with maximum counts in record (multiply by $\frac{10}{2^{24}-2^5} \approx 6 \times 10^{-7}$ to get cm/sec). Times are unreduced beginning at time indicated.

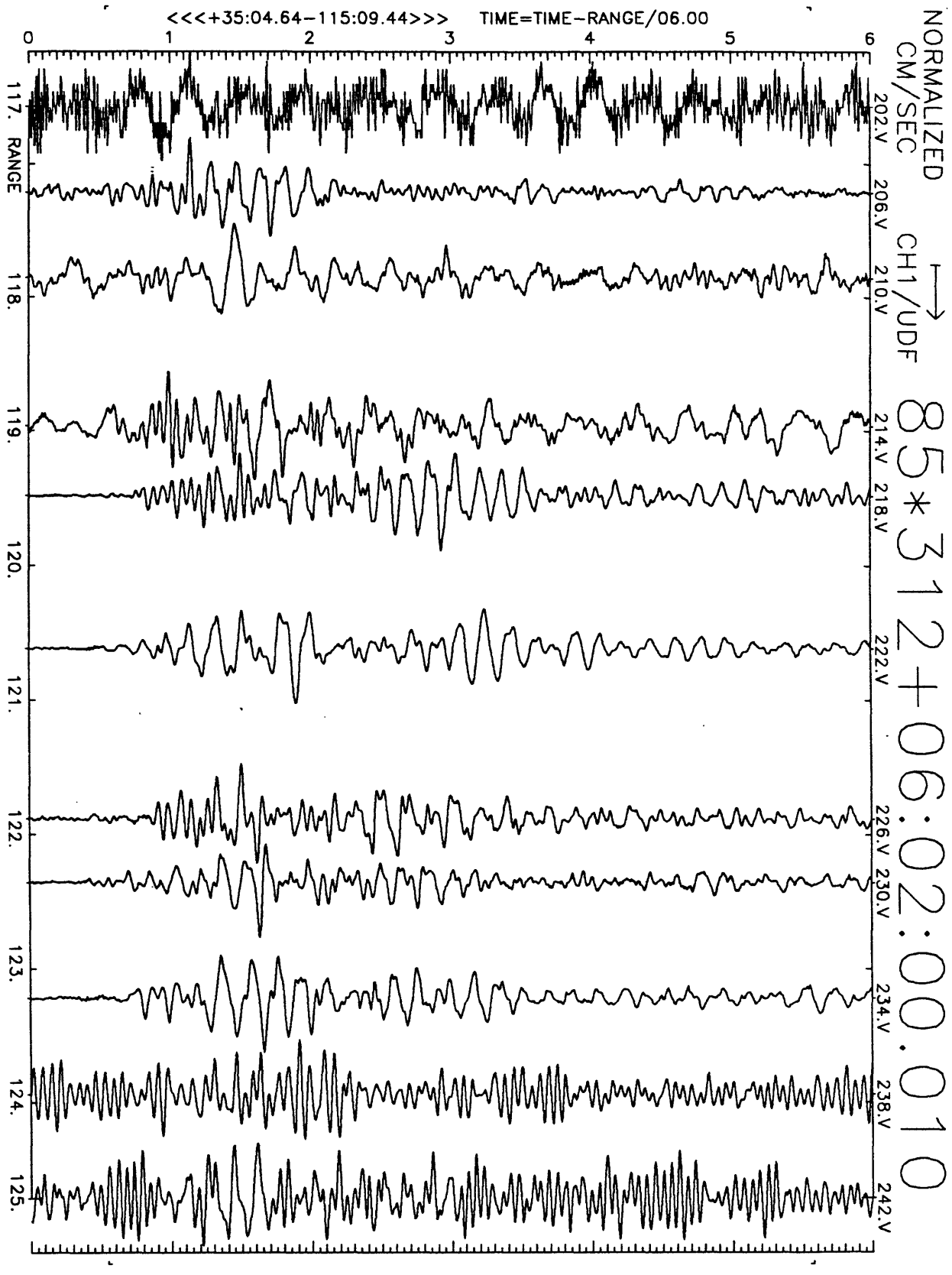

Figure A12(a), shot point 11: 6 second velocity record. Positive vertical motion is to right. Abscissa is distance to shot point. Top of trace is labeled with station number. Times are reduced by 6 km/sec. Shot time is indicated.

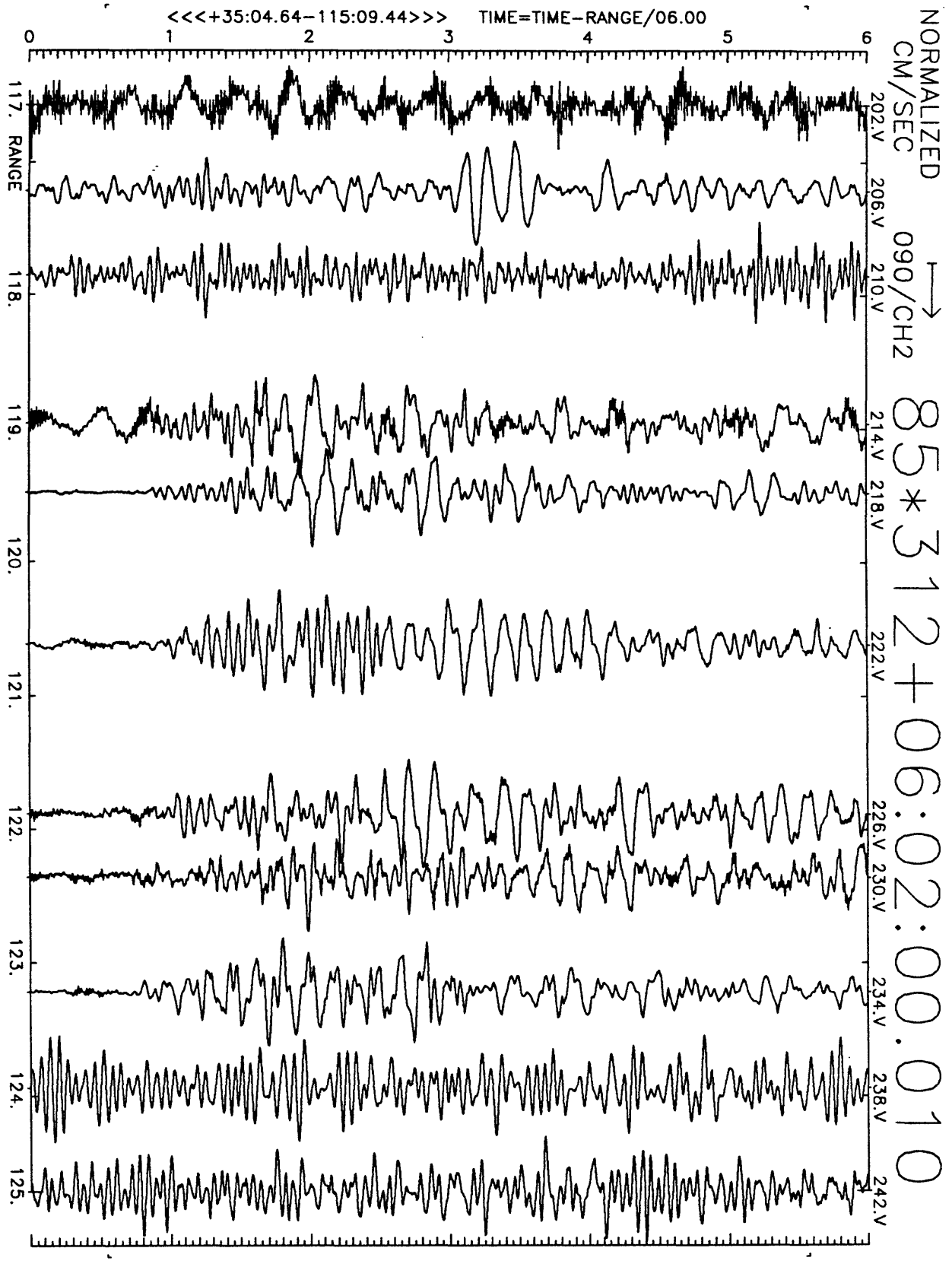

Figure A12(b), shot point 11: 6 second velocity record. Positive N20E motion is to right. Abscissa is distance to shot point. Top of trace is labeled with station number. Times are reduced by 6 km/sec. Shot time is indicated.

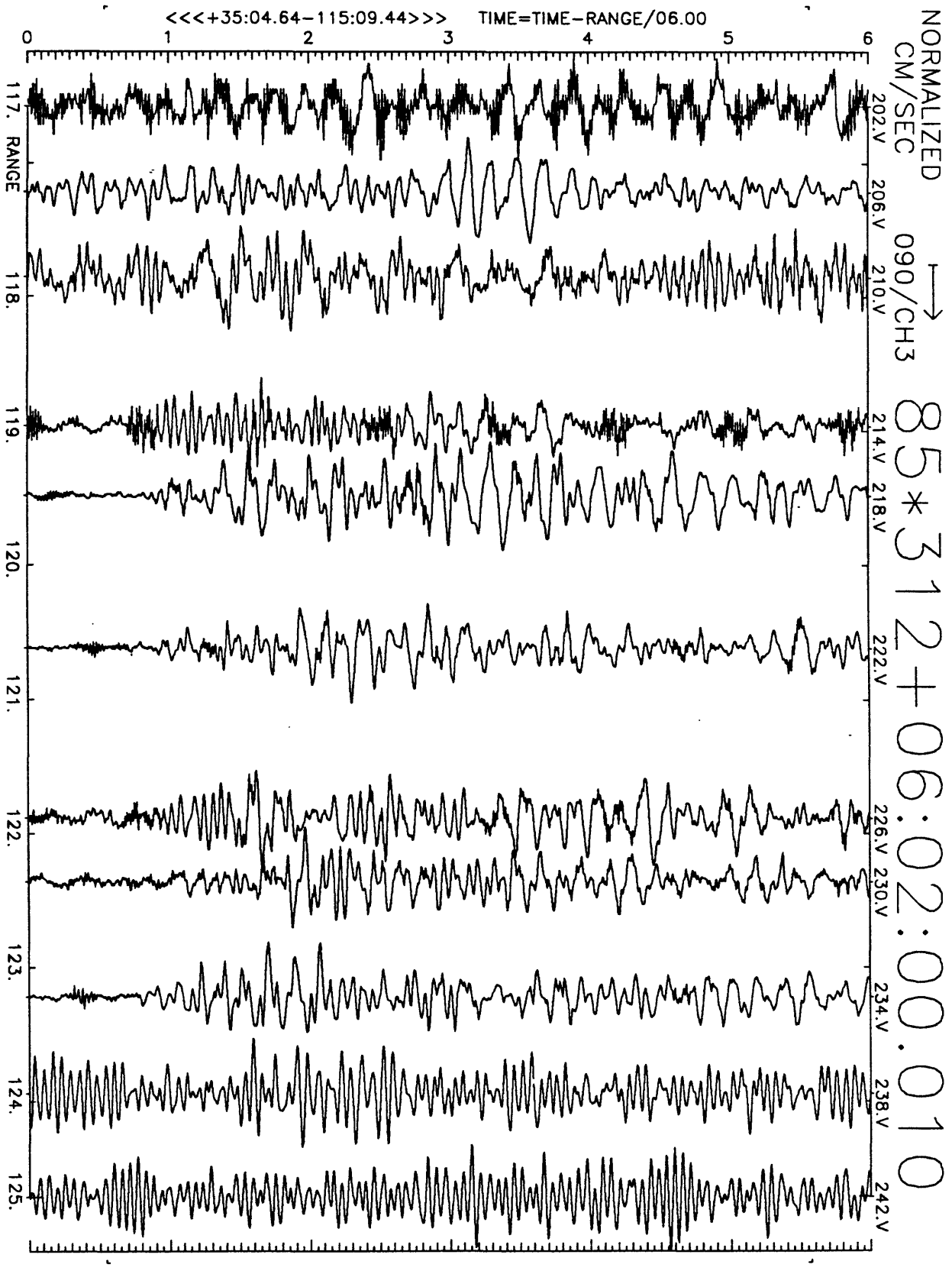

Figure A12(c), shot point 11: 6 second velocity record. Positive N110E motion is to right. Abscissa is distance to shot point. Top of trace is labeled with station number. Times are reduced by 6 km/sec. Shot time is indicated.

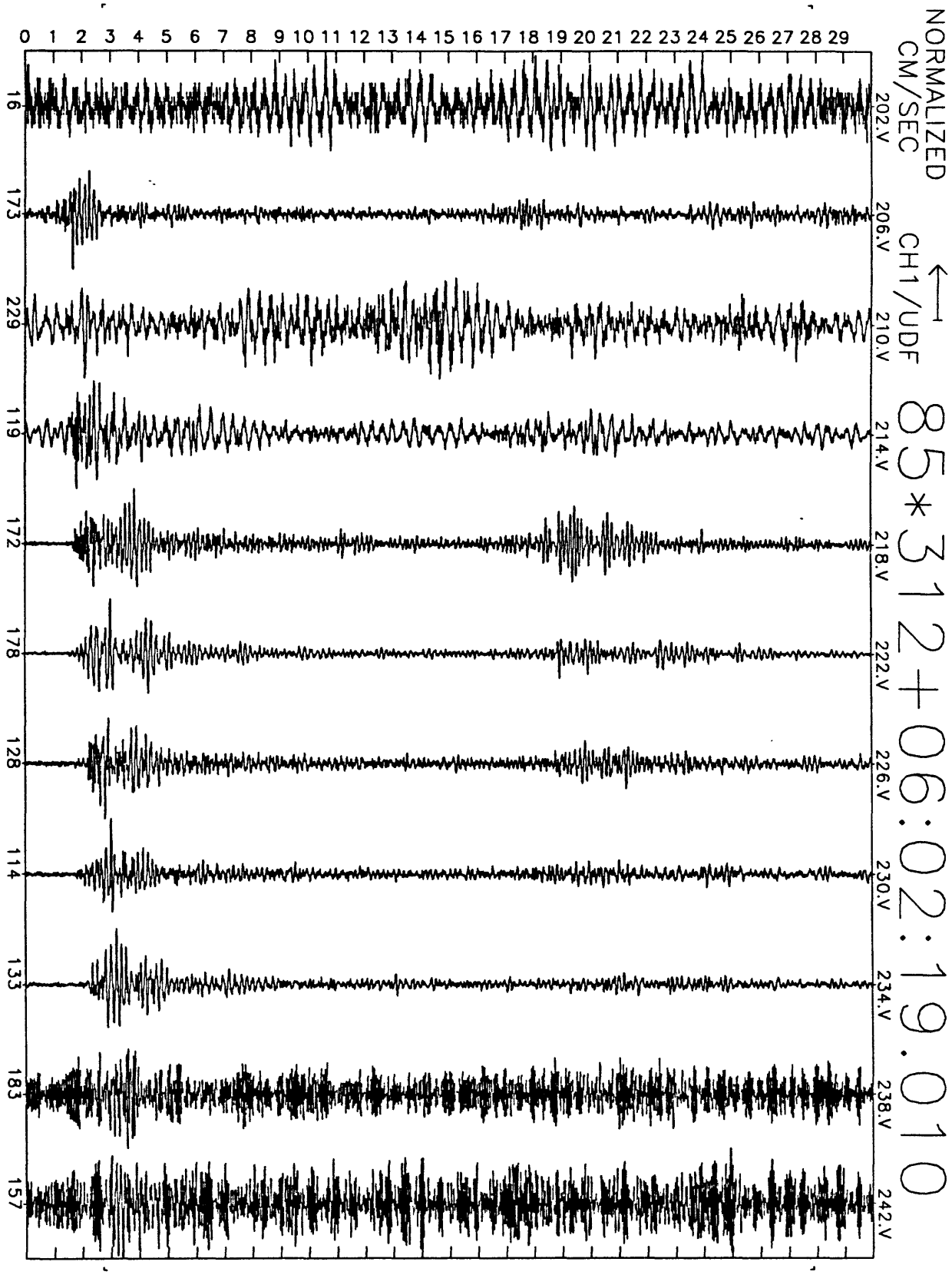

Figure A12(d), shot point 11: 30 second vertical velocity record. Abscissa is labeled with maximum counts in record (multiply by $\frac{10}{2^{24}-2^5} \approx 6 \times 10^{-7}$ to get cm/sec). Times are unreduced beginning at time indicated.

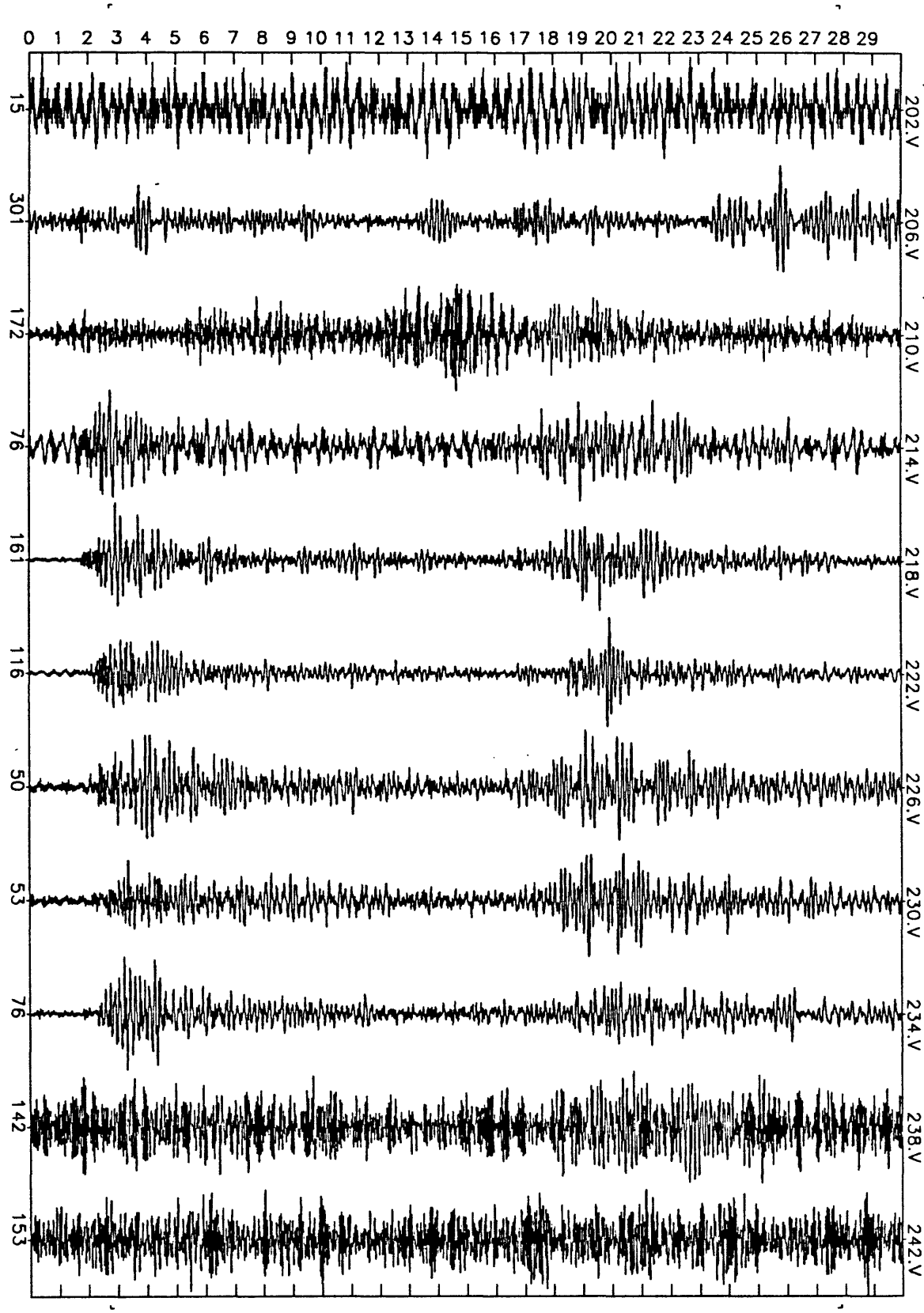

Figure A12(e), shot point 11: 30 second N20E velocity record. Abscissa is labeled with maximum counts in record (multiply by $\frac{10}{2^{24}-2^{9}} \approx 6 \times 10^{-7}$ to get cm/sec). Times are unreduced beginning at time indicated.

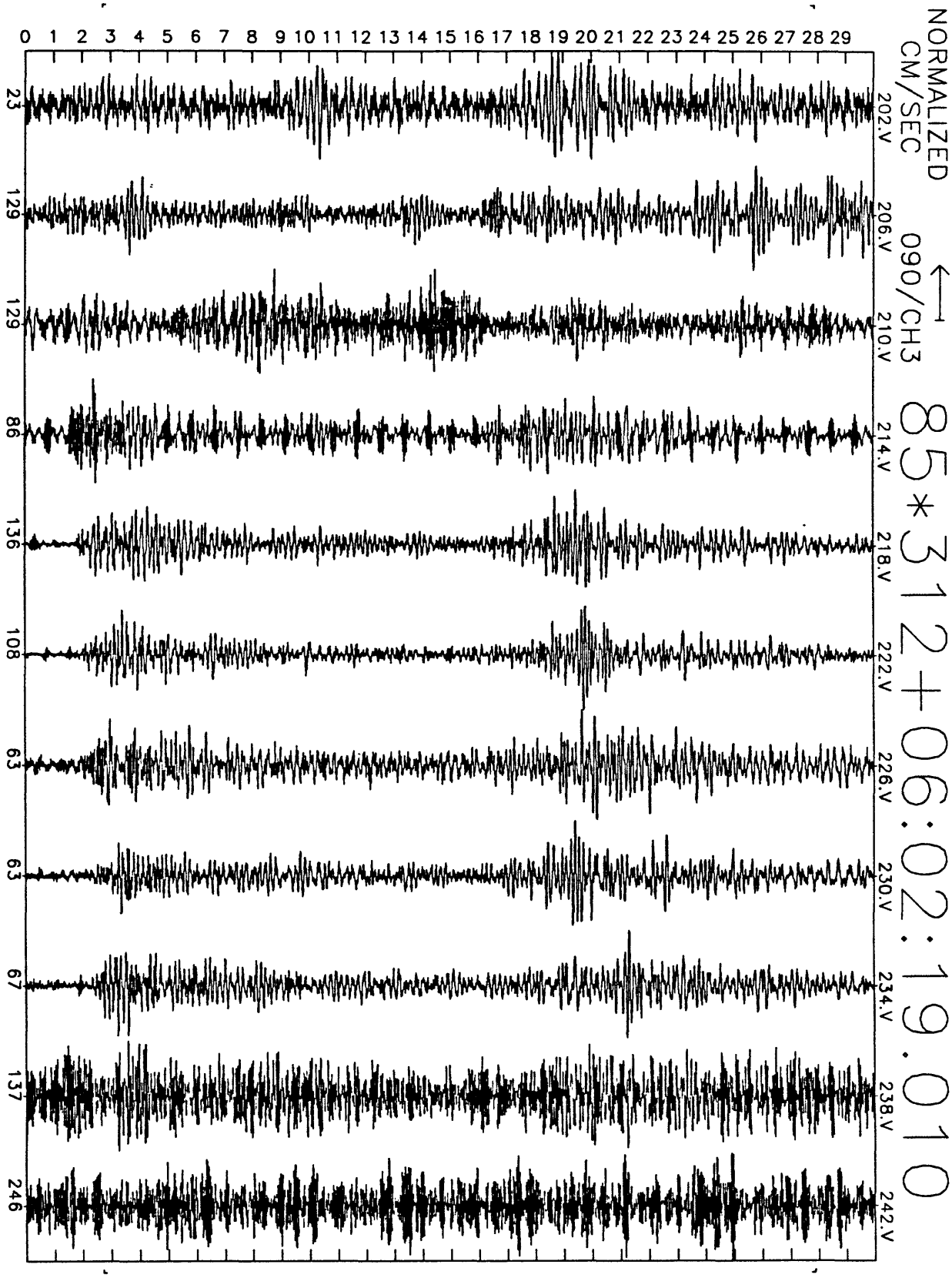

Figure A12(f), shot point 11: 30 second N110E velocity record. Abscissa is labeled with maximum counts in record (multiply by $\frac{10}{2^{24}-2^5} \approx 6 \times 10^{-7}$ to get cm/sec). Times are unreduced beginning at time indicated.

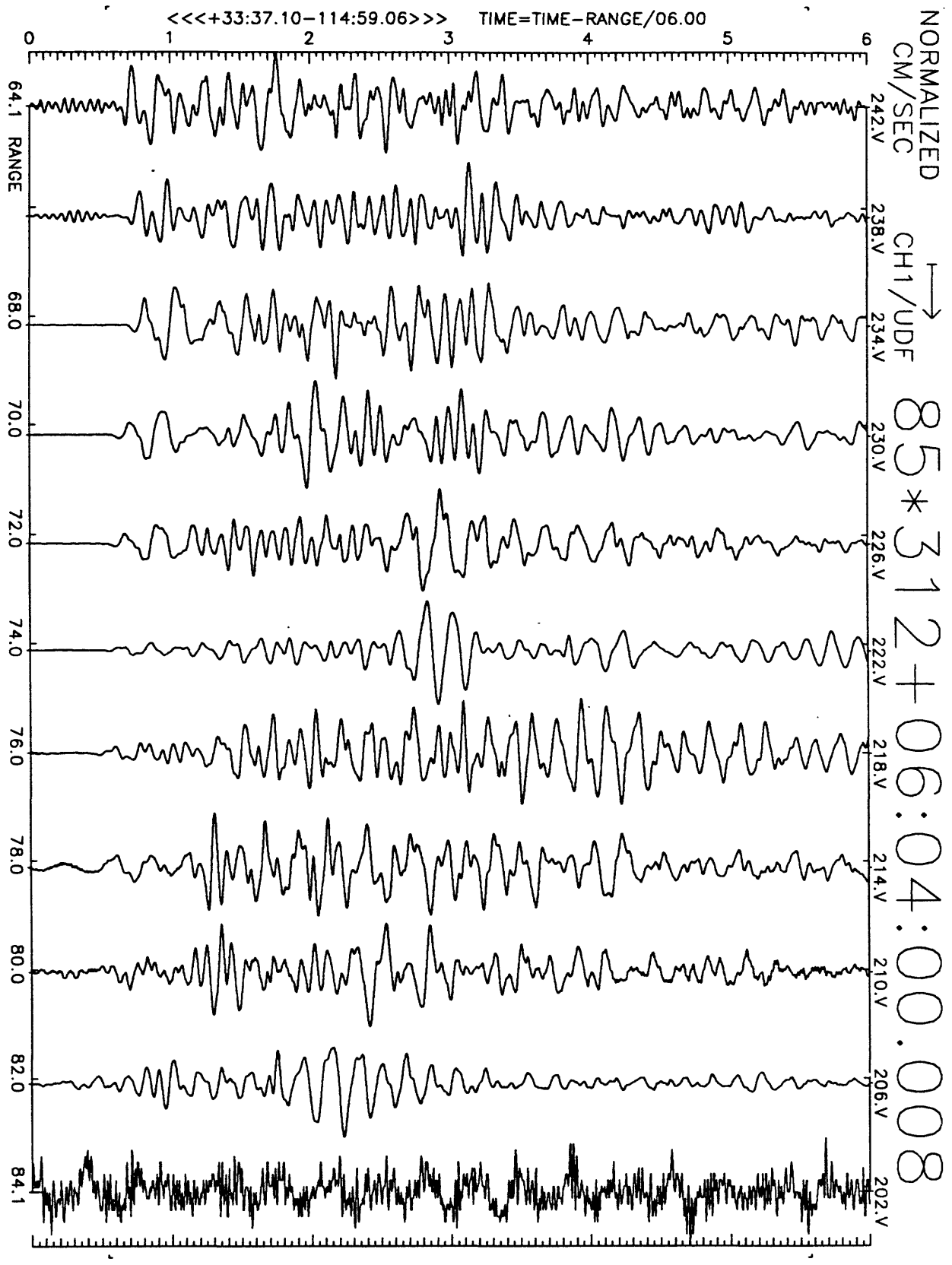

Figure A13(a), shot point 14: 6 second velocity record. Positive vertical motion is to right. Abscissa is distance to shot point. Top of trace is labeled with station number. Times are reduced by 6 km/sec. Shot time is indicated.

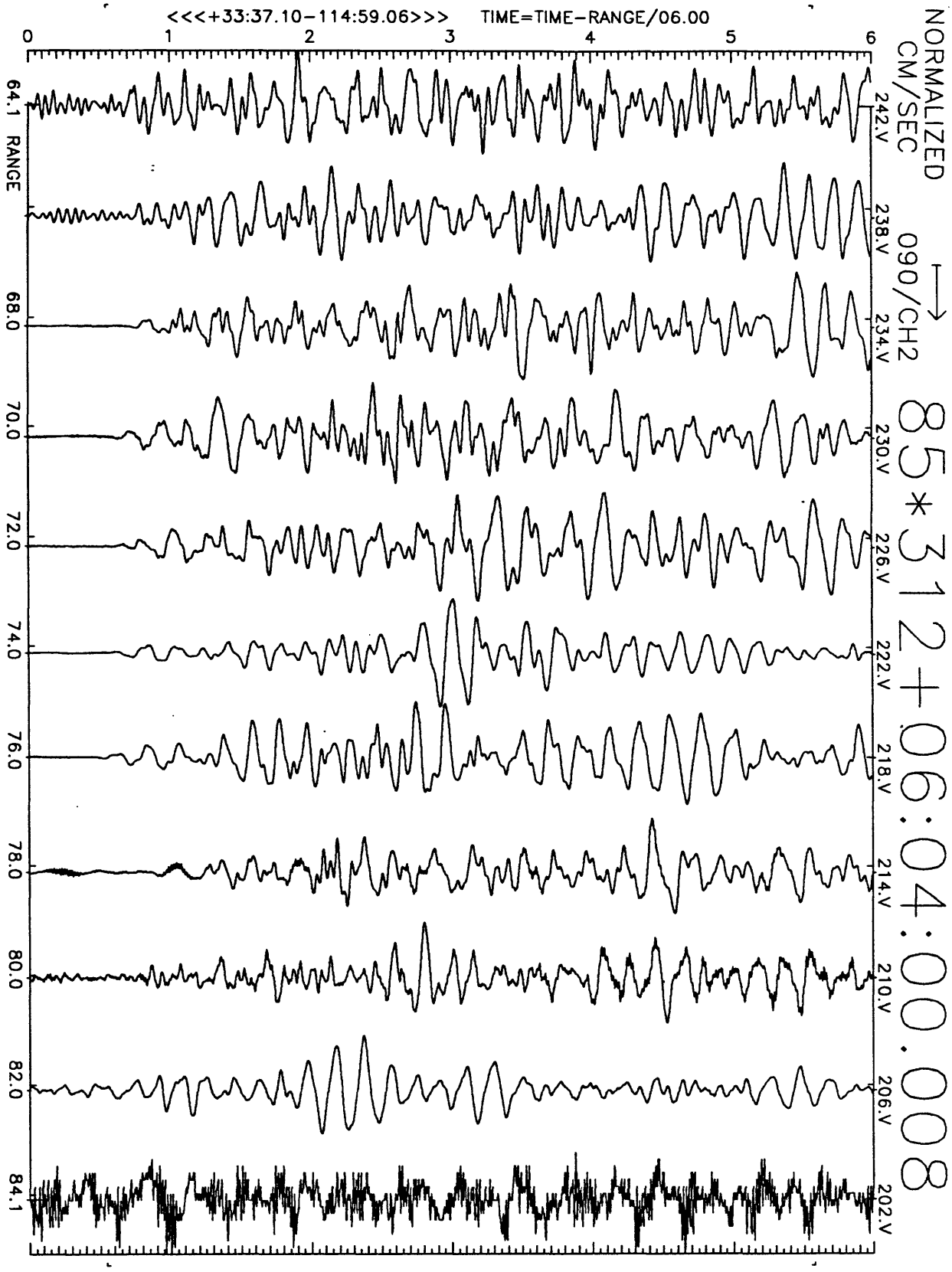

Figure A13(b), shot point 14: 6 second velocity record. Positive N20E motion is to right. Abscissa is distance to shot point. Top of trace is labeled with station number. Times are reduced by 6 km/sec. Shot time is indicated.

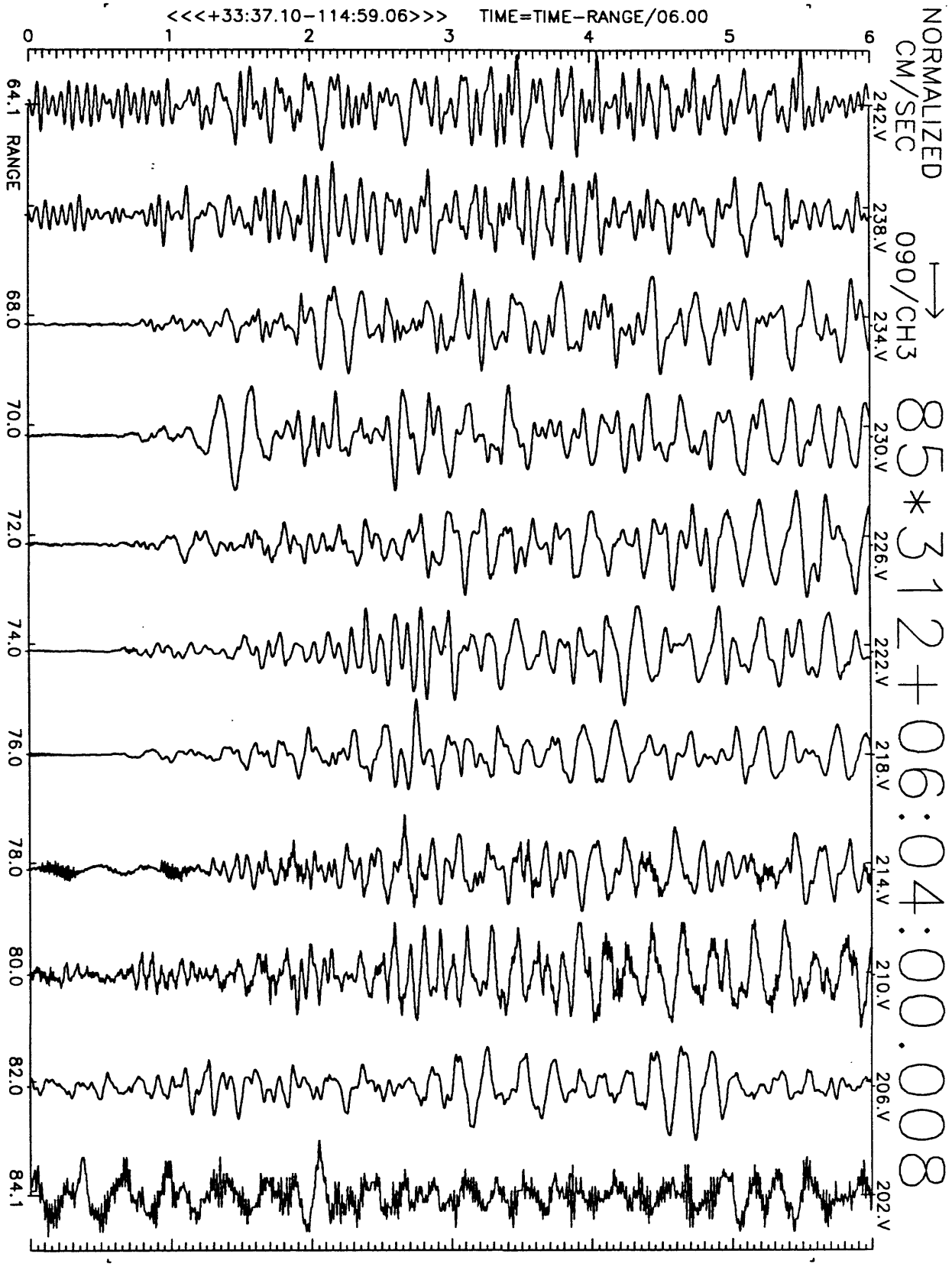

Figure A13(c), shot point 14: 6 second velocity record. Positive N110E motion is to right. Abscissa is distance to shot point. Top of trace is labeled with station number. Times are reduced by 6 km/sec. Shot time is indicated.

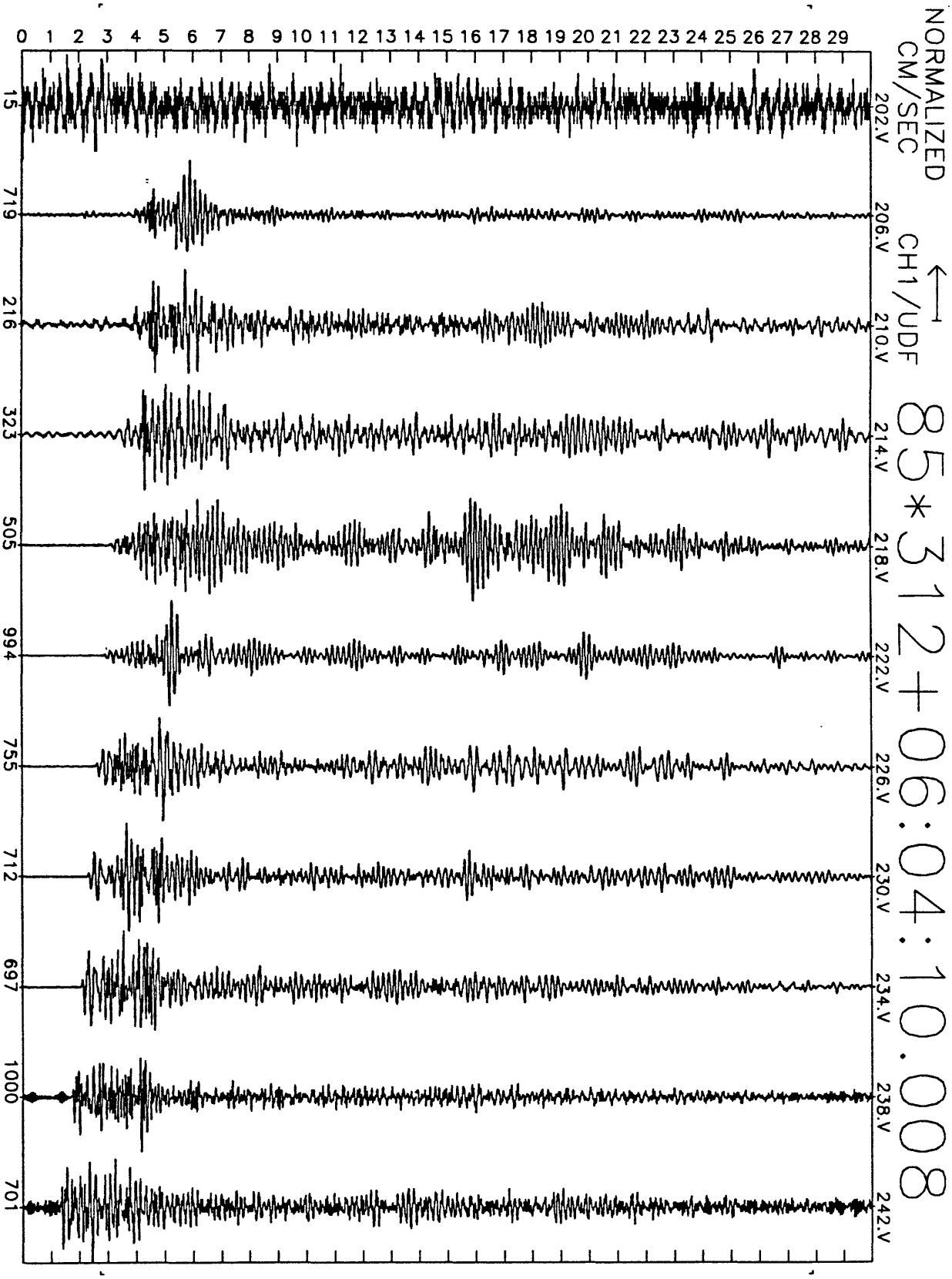

Figure A13(d), shot point 14: 30 second vertical velocity record. Abscissa is labeled with maximum counts in record (multiply by $\frac{10}{2^{24}-2^5} \approx 6 \times 10^{-7}$ to get cm/sec). Times are unreduced beginning at time indicated.

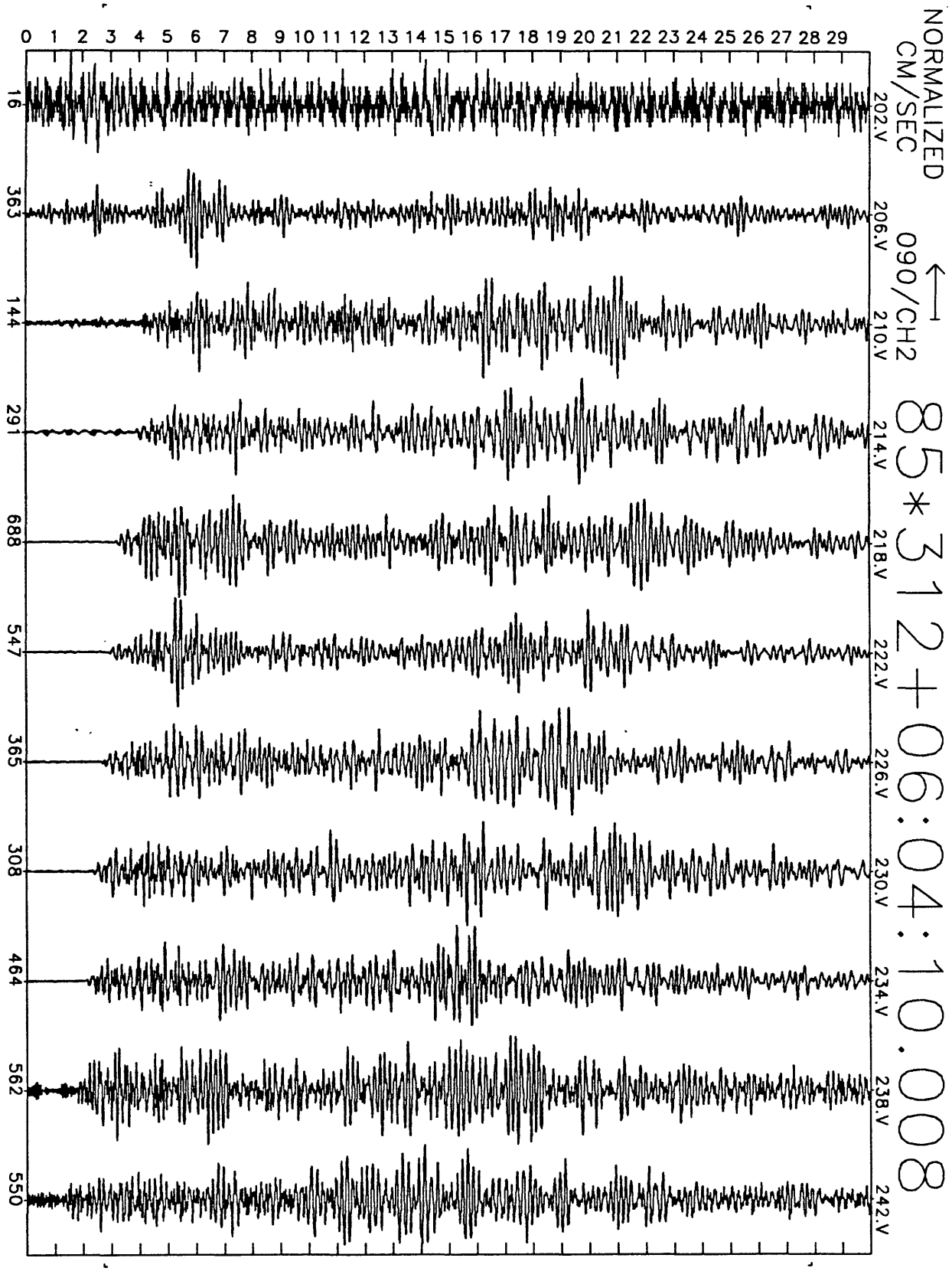

Figure A13(e), shot point 14: 30 second N20E velocity record. Abscissa is labeled with maximum counts in record (multiply by $\frac{10}{2^{24}-2^{5}} \approx 6 \times 10^{-7}$ to get cm/sec). Times are unreduced beginning at time indicated.

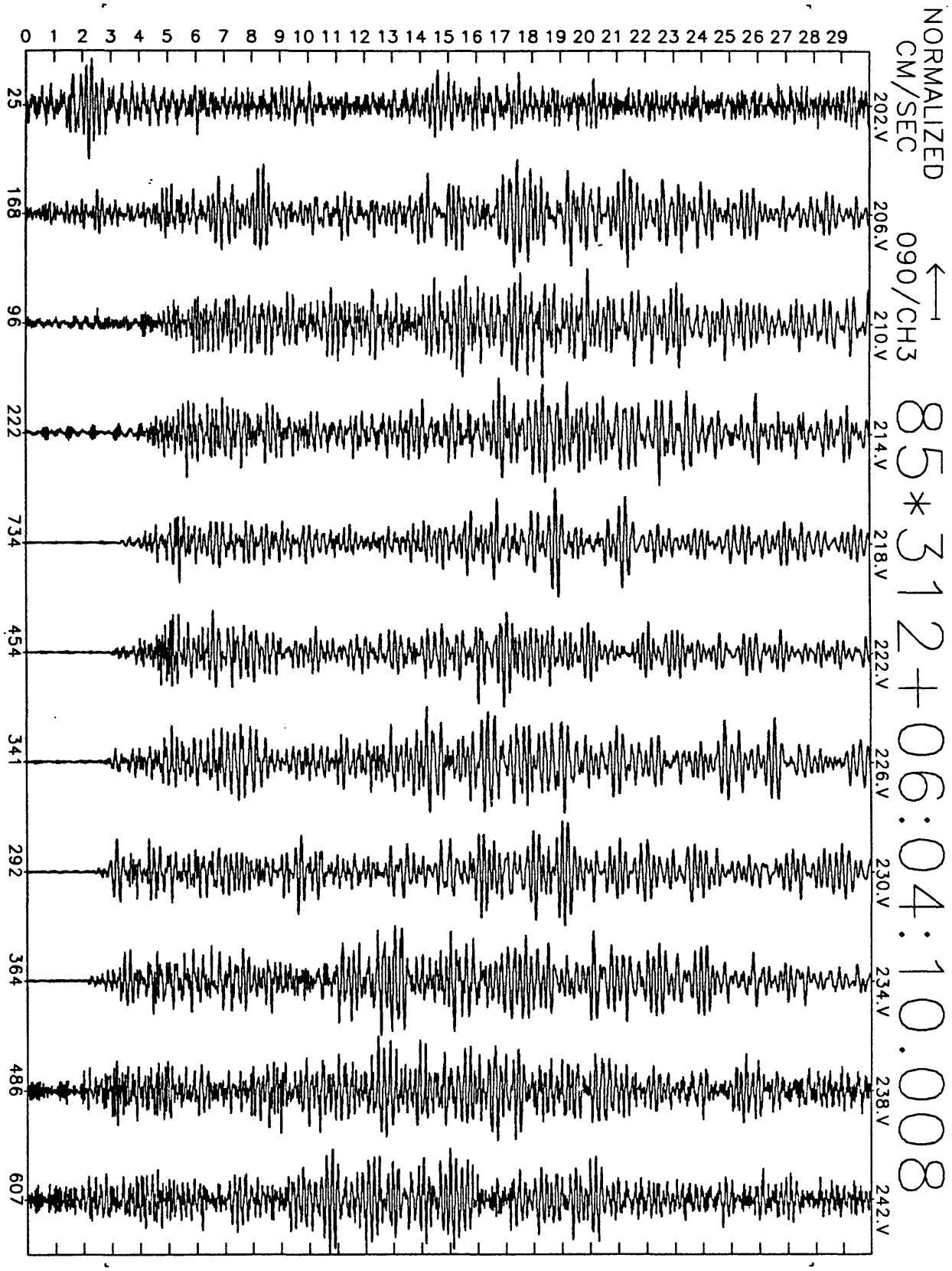

Figure A13(f), shot point 14: 30 second N110E velocity record. Abscissa is labeled with maximum counts in record (multiply by $\frac{10}{2^{24}-2^5} \approx 6 \times 10^{-7}$ to get cm/sec). Times are unreduced beginning at time indicated.

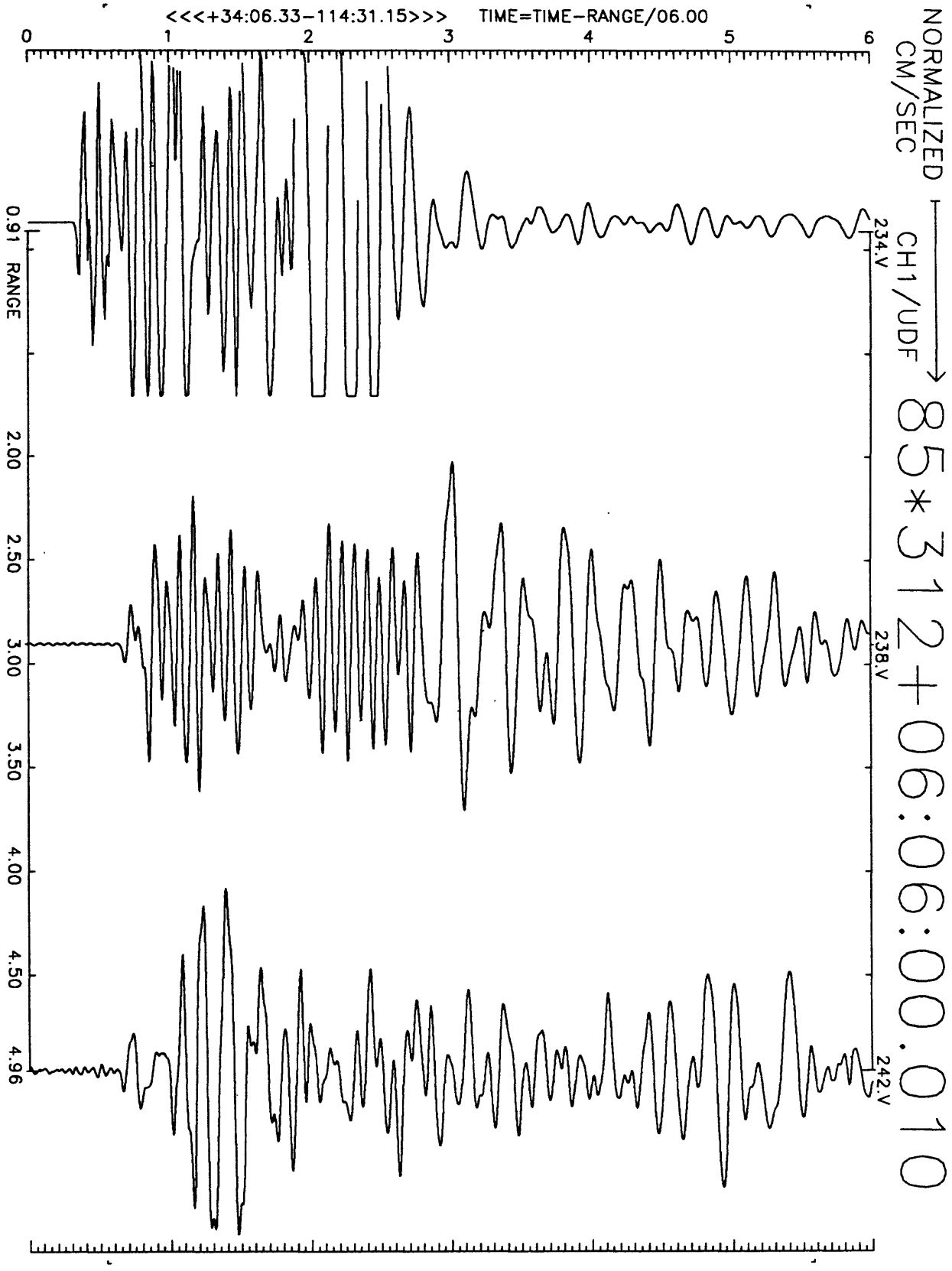

Figure A14(a), shot point 3, SW stations: 6 second velocity record. Positive vertical motion is to right. Abscissa is distance to shot point. Top of trace is labeled with station number. Times are reduced by 6 km/sec. Shot time is indicated.

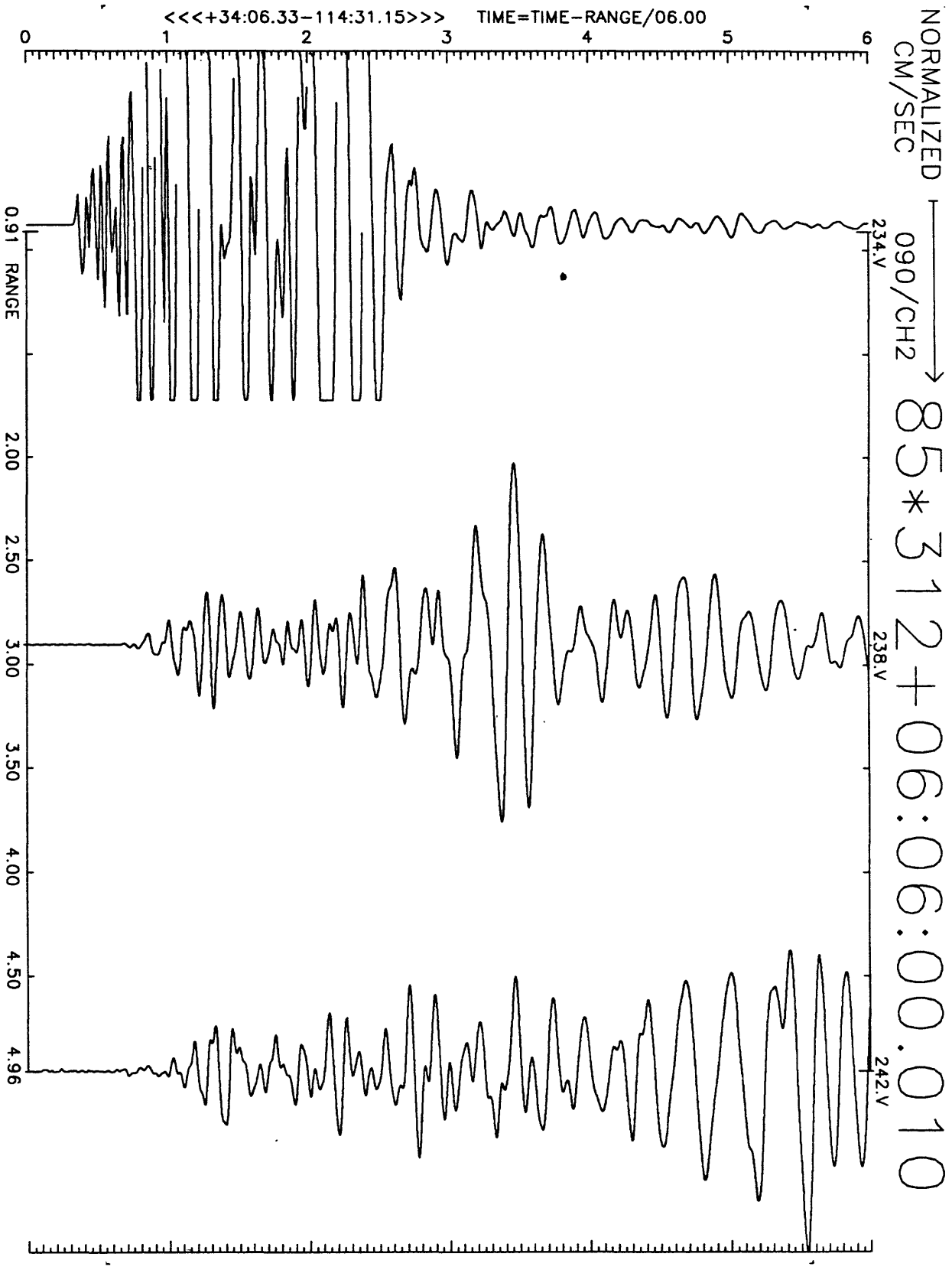

Figure A14(b), shot point 3, SW stations: 6 second velocity record. Positive N20E motion is to right. Abscissa is distance to shot point. Top of trace is labeled with station number. Times are reduced by 6 km/sec. Shot time is indicated.

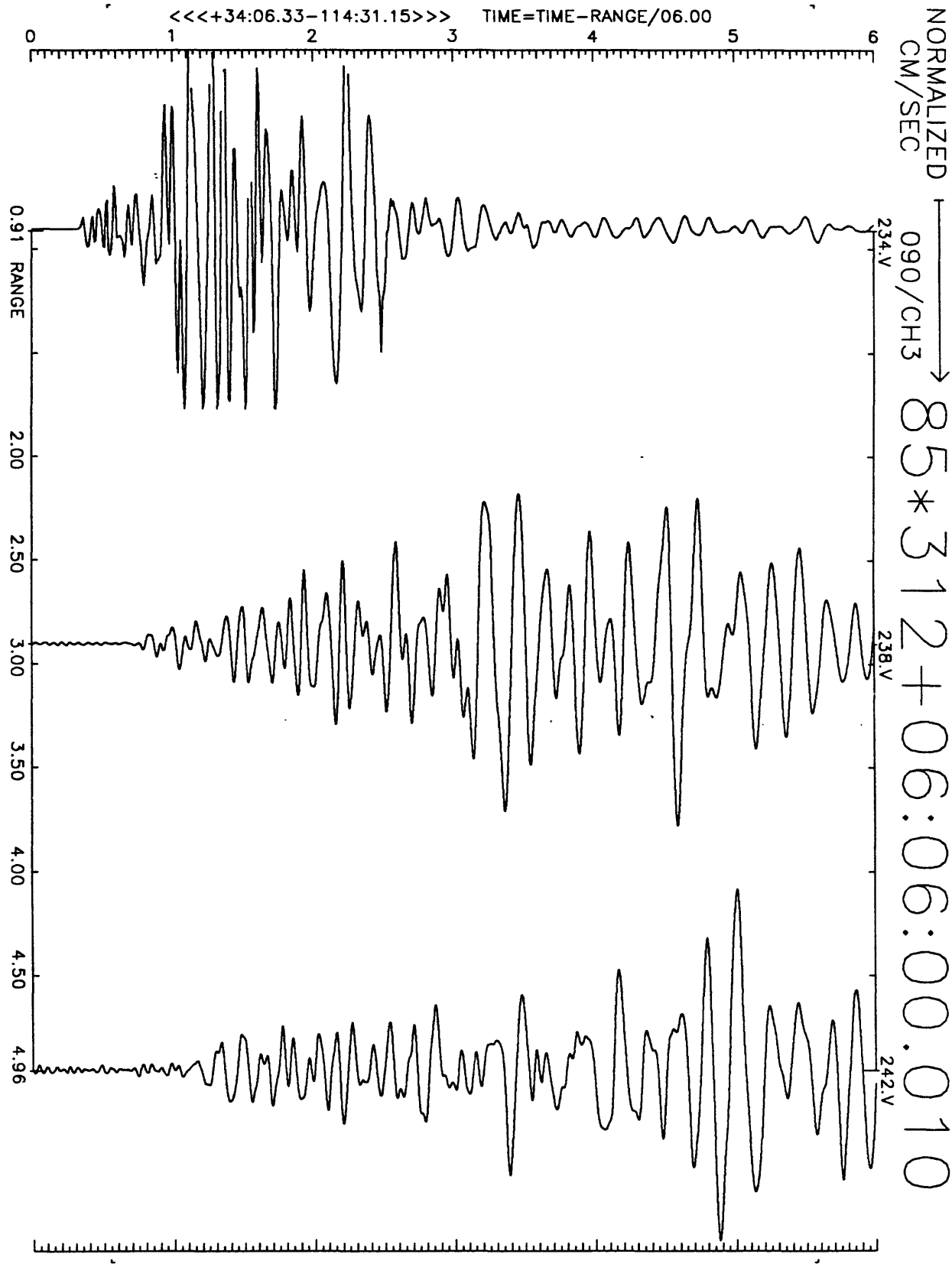

Figure A14(c), shot point 3, SW stations: 6 second velocity record. Positive N110E motion is to right. Abscissa is distance to shot point. Top of trace is labeled with station number. Times are reduced by 6 km/sec. Shot time is indicated.

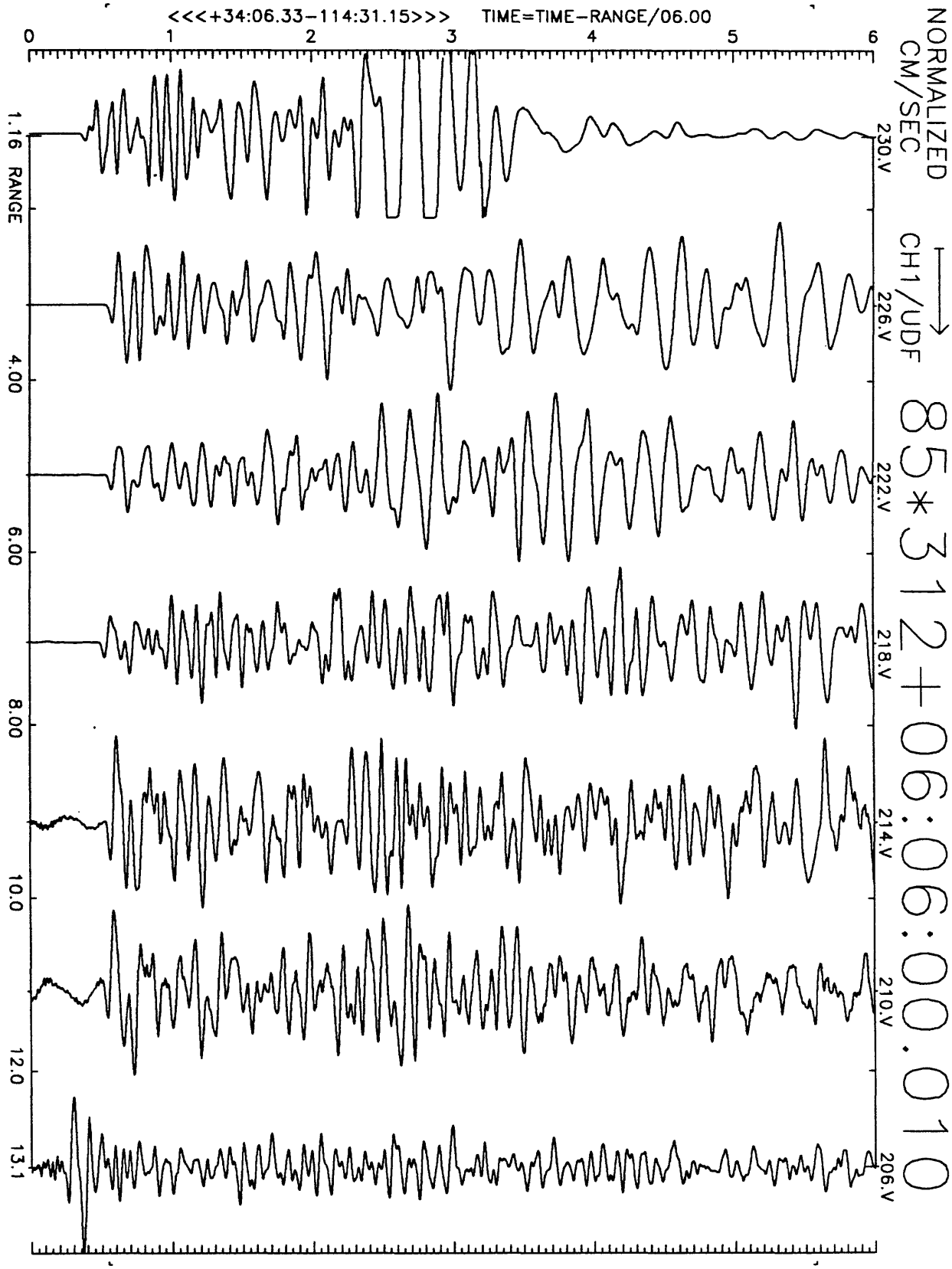

Figure A14(d), shot point 3, NE stations: 6 second velocity record. Positive vertical motion is to right. Abscissa is distance to shot point. Top of trace is labeled with station number. Times are reduced by 6 km/sec. Shot time is indicated.

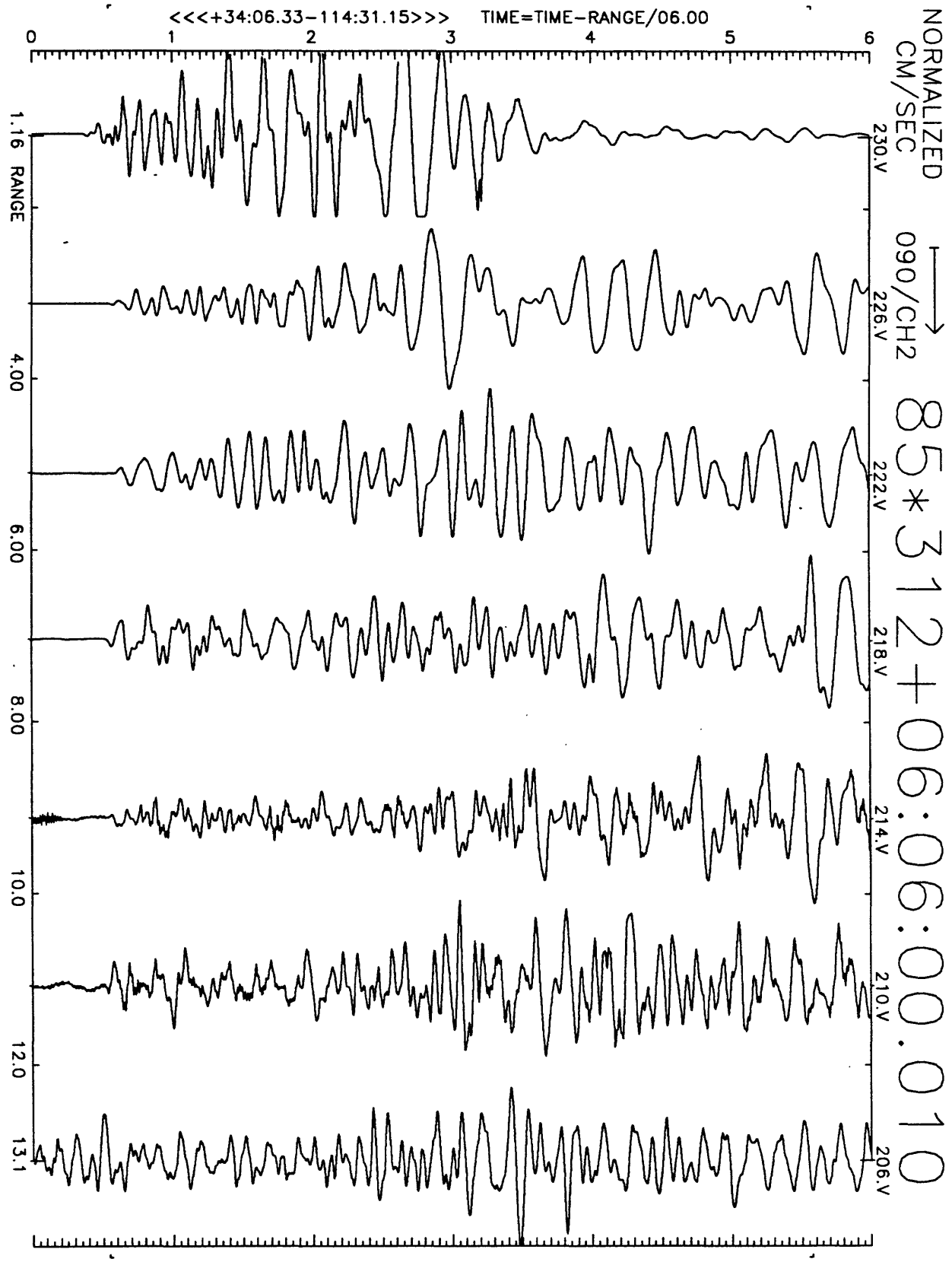

Figure A14(e), shot point 3, NE stations: 6 second velocity record. Positive N20E motion is to right. Abscissa is distance to shot point. Top of trace is labeled with station number. Times are reduced by 6 km/sec. Shot time is indicated.

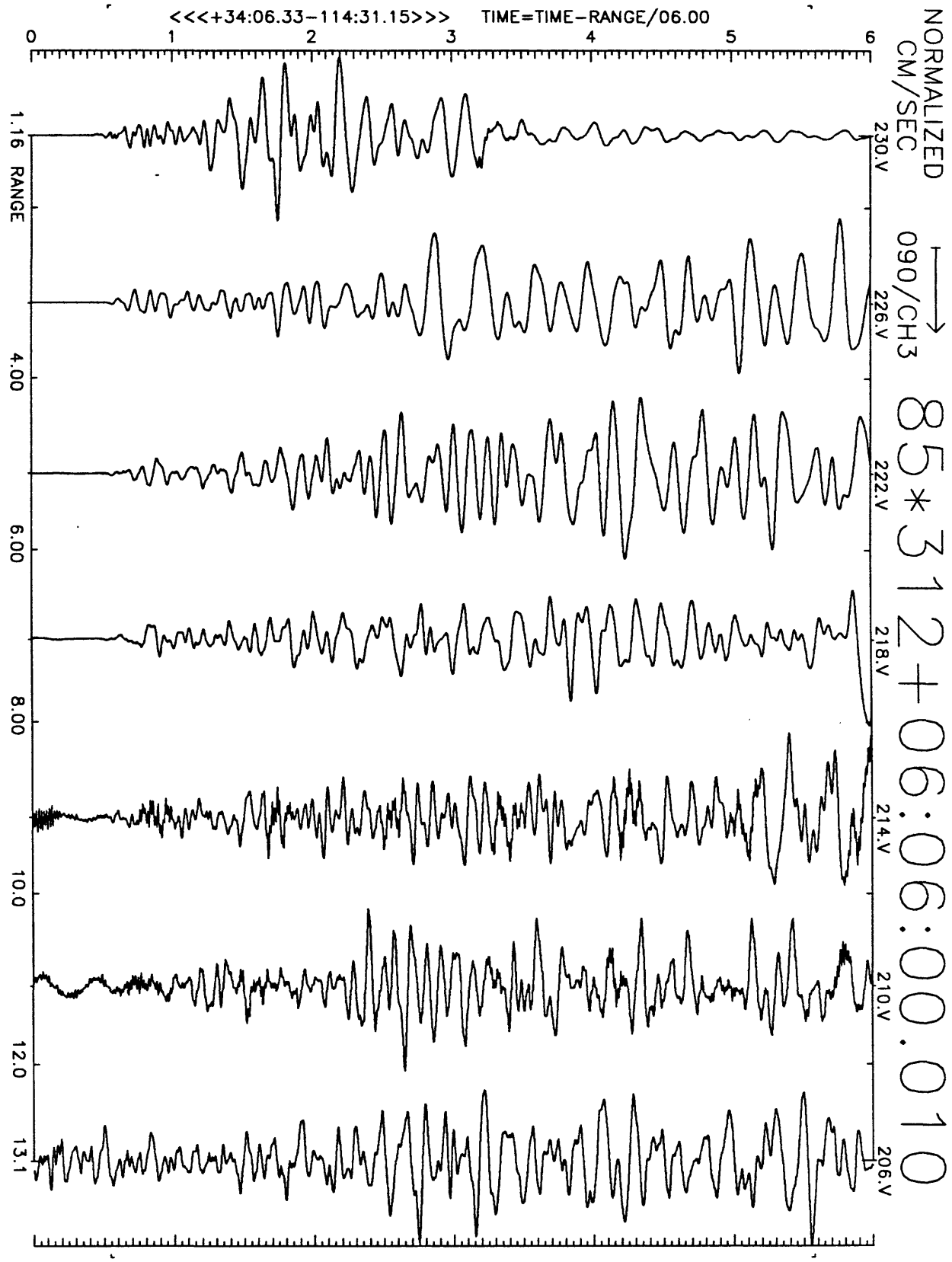

Figure A14(f), shot point 3, NE stations: 6 second velocity record. Positive N110E motion is to right. Abscissa is distance to shot point. Top of trace is labeled with station number. Times are reduced by 6 km/sec. Shot time is indicated.

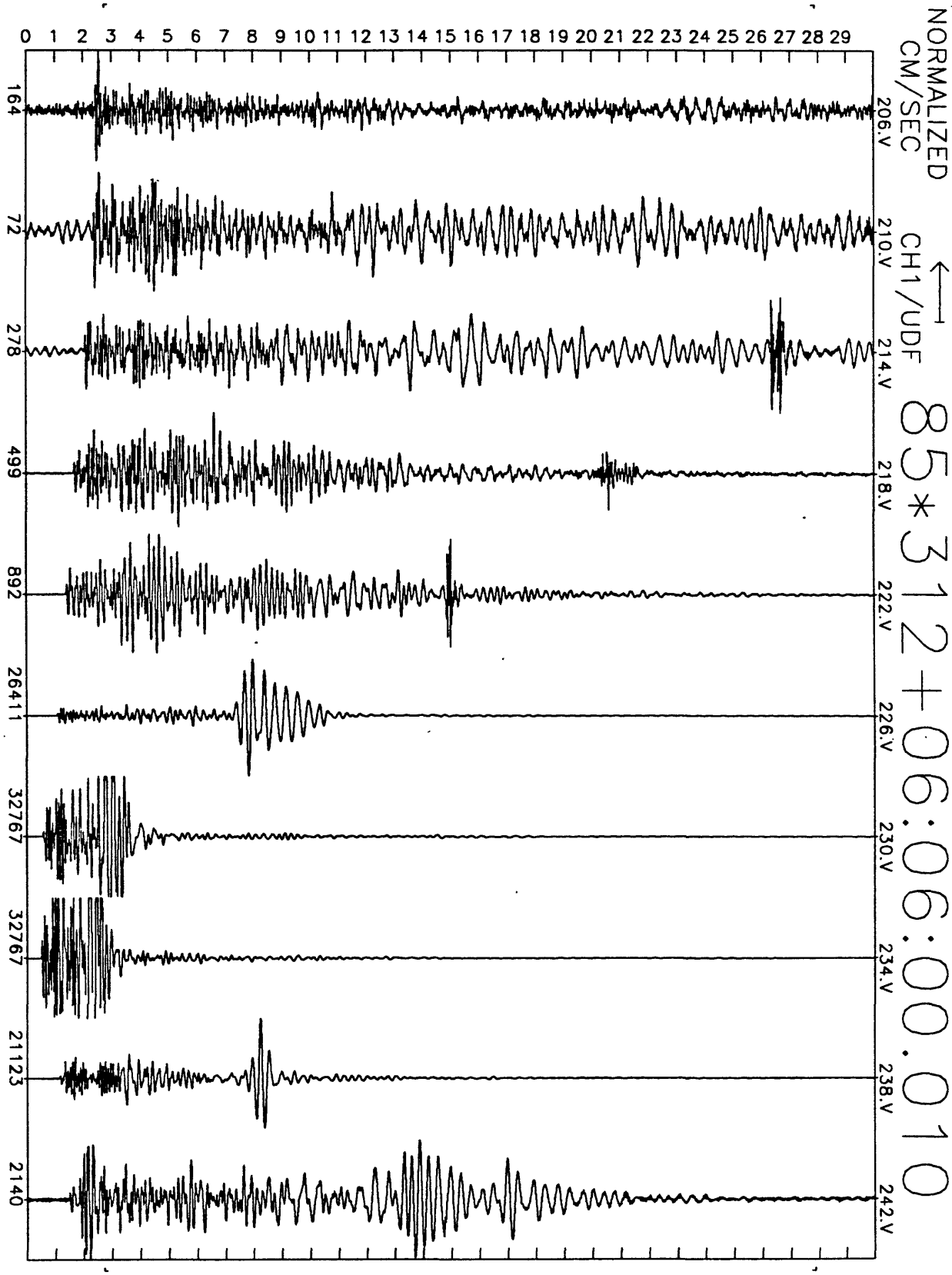

Figure A14(g), shot point 3: 30 second vertical velocity record. Abscissa is labeled with maximum counts in record (multiply by $\frac{10}{2^{24}-2^5} \approx 6 \times 10^{-7}$ to get cm/sec). Times are unreduced beginning at time indicated.

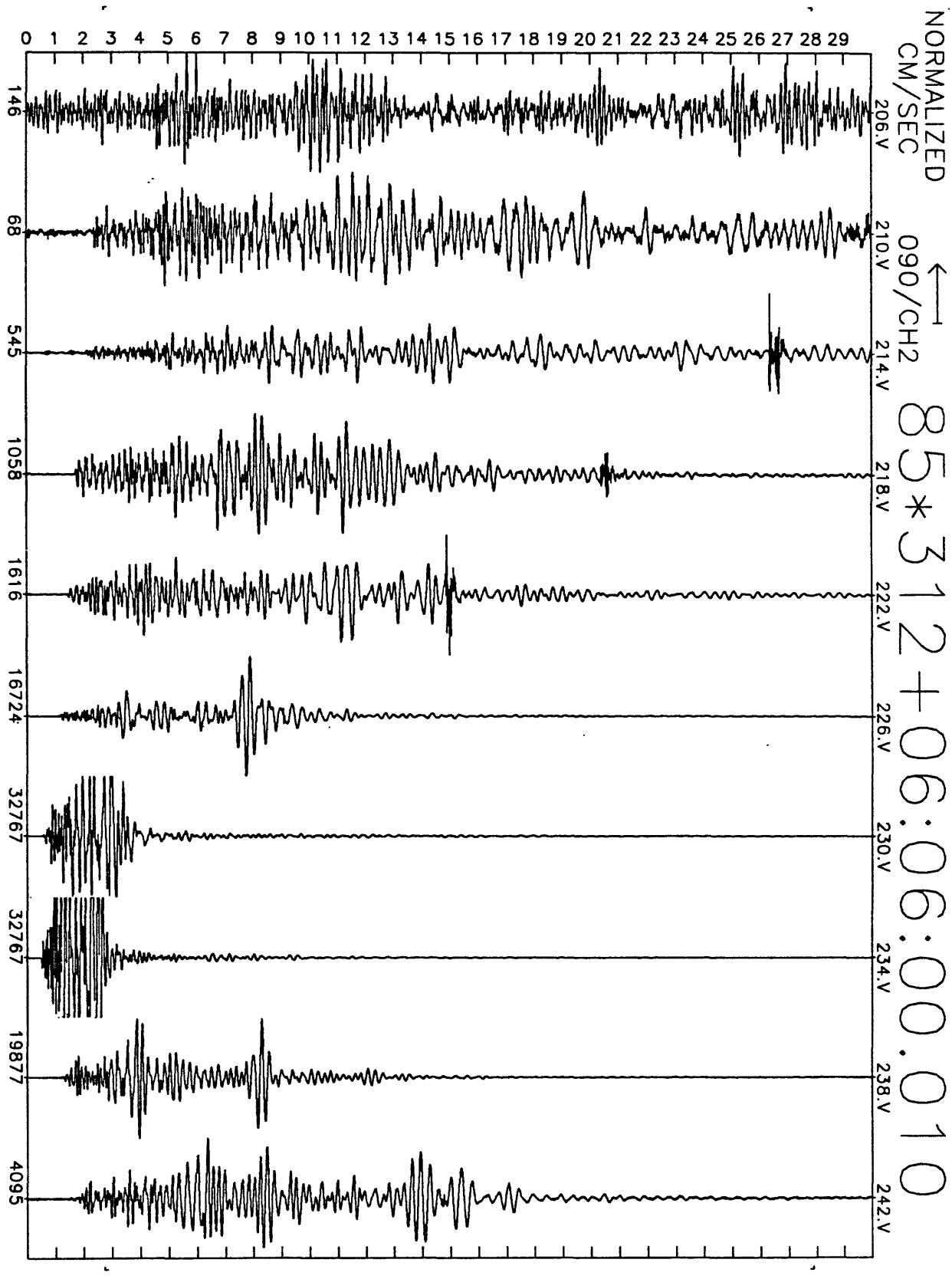

Figure A14(h), shot point 3: 30 second N20E velocity record. Abscissa is labeled with maximum counts in record (multiply by $\frac{10}{2^{24}-2^5} \approx 6 \times 10^{-7}$ to get cm/sec). Times are unreduced beginning at time indicated.

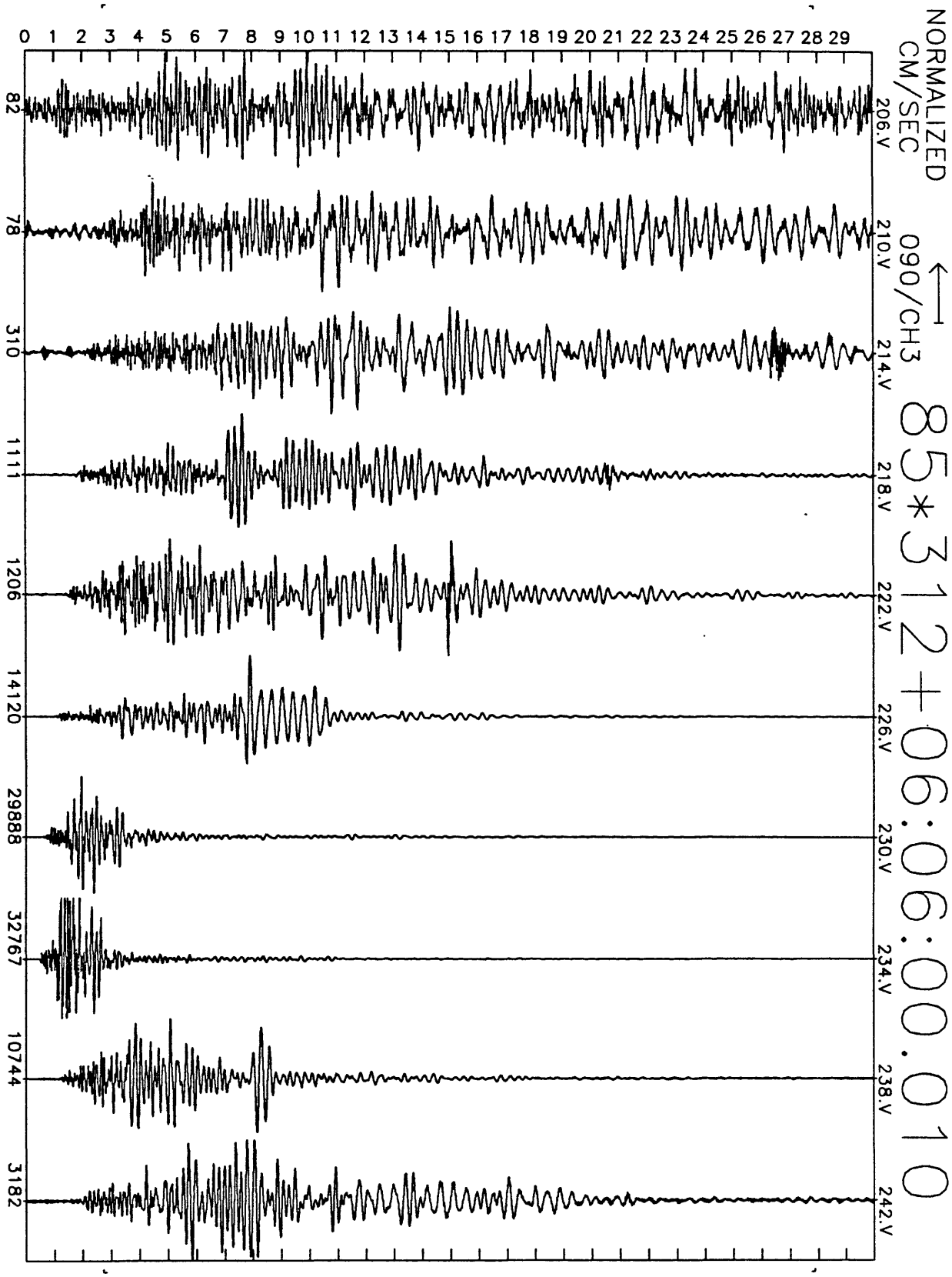

Figure A14(i), shot point 3: 30 second N110E velocity record. Abscissa is labeled with maximum counts in record (multiply by $\frac{10}{2^{24}-2^5} \approx 6 \times 10^{-7}$ to get cm/sec). Times are unreduced beginning at time indicated.

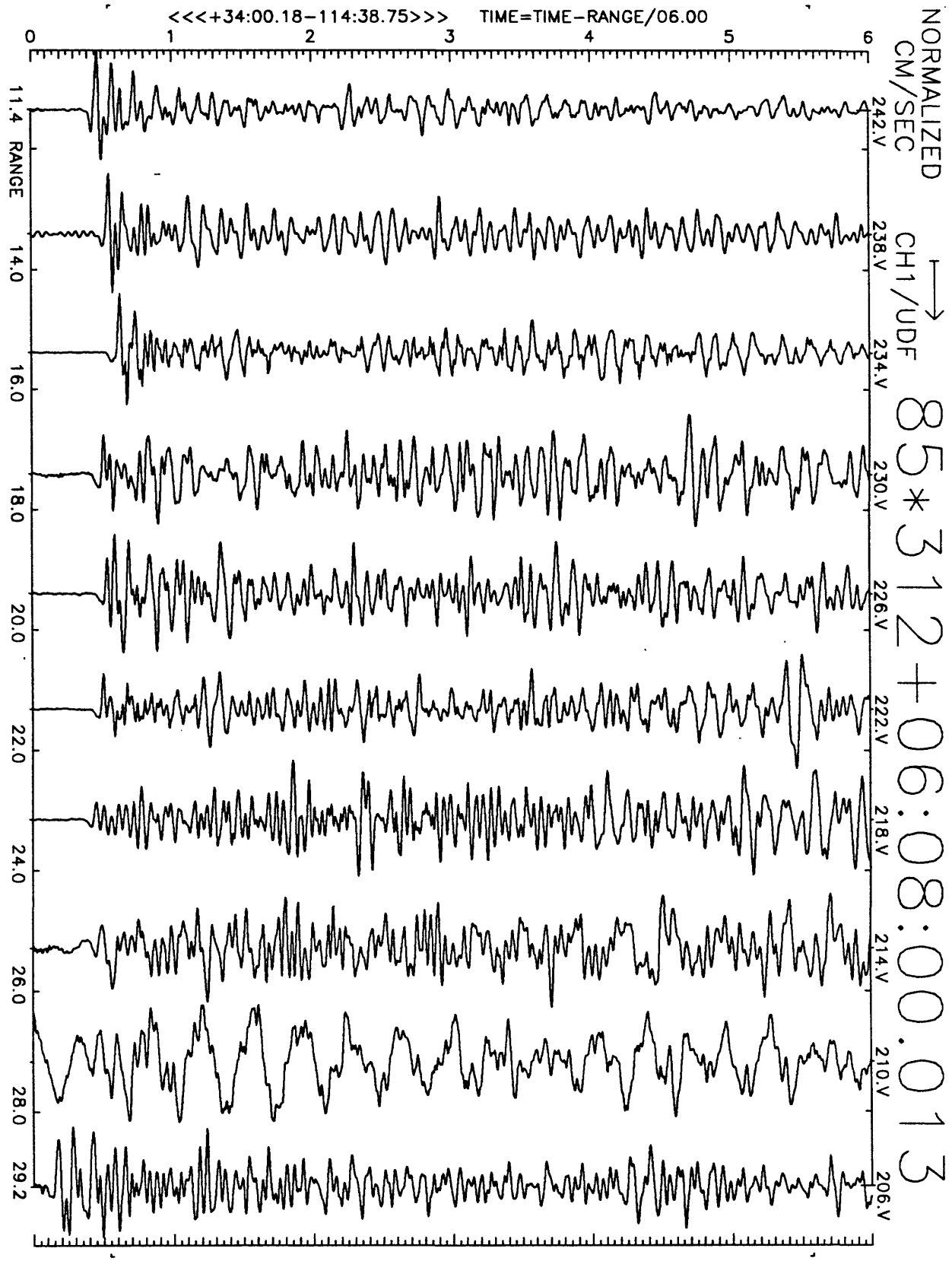

Figure A15(a), shot point 2: 6 second velocity record. Positive vertical motion is to right. Abscissa is distance to shot point. Top of trace is labeled with station number. Times are reduced by 6 km/sec. Shot time is indicated.

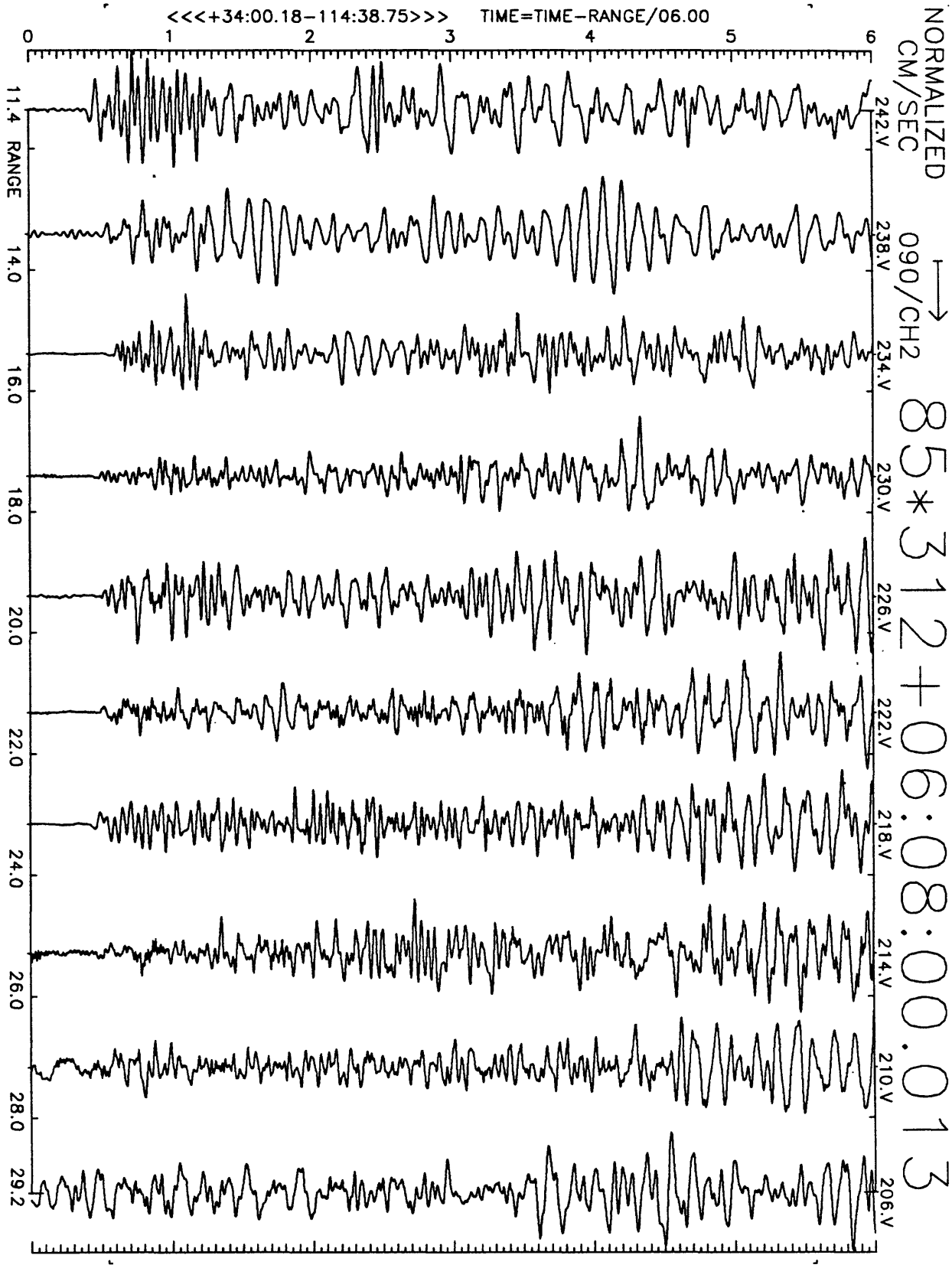

Figure A15(b), shot point 2: 6 second velocity record. Positive N20E motion is to right. Abscissa is distance to shot point. Top of trace is labeled with station number. Times are reduced by 6 km/sec. Shot time is indicated.

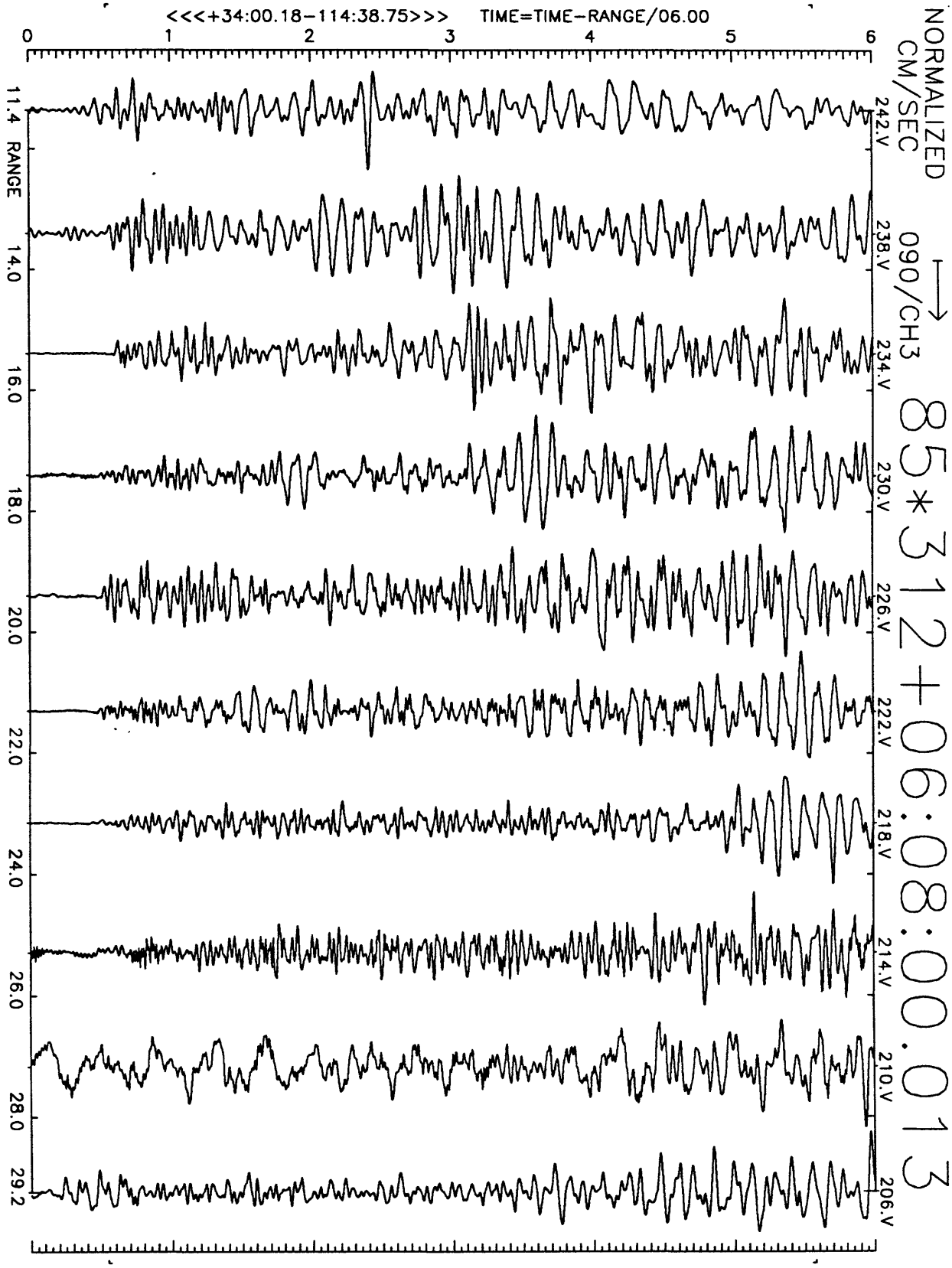

Figure A15(c), shot point 2: 6 second velocity record. Positive N110E motion is to right. Abscissa is distance to shot point. Top of trace is labeled with station number. Times are reduced by 6 km/sec. Shot time is indicated.

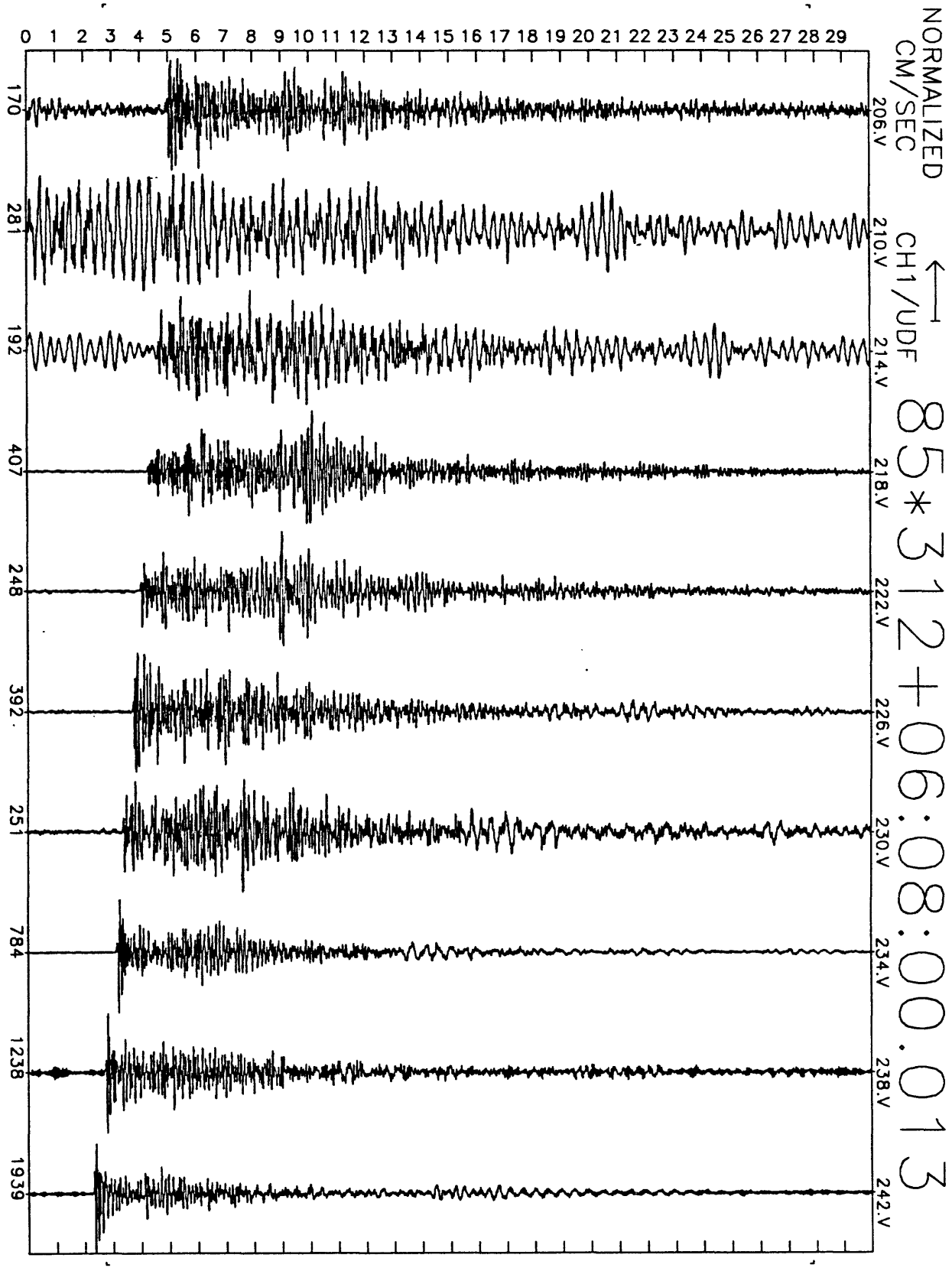

Figure A15(d), shot point 2: 30 second vertical velocity record. Abscissa is labeled with maximum counts in record (multiply by $\frac{10}{2^{24}-2^5} \approx 6 \times 10^{-7}$ to get cm/sec). Times are unreduced beginning at time indicated.

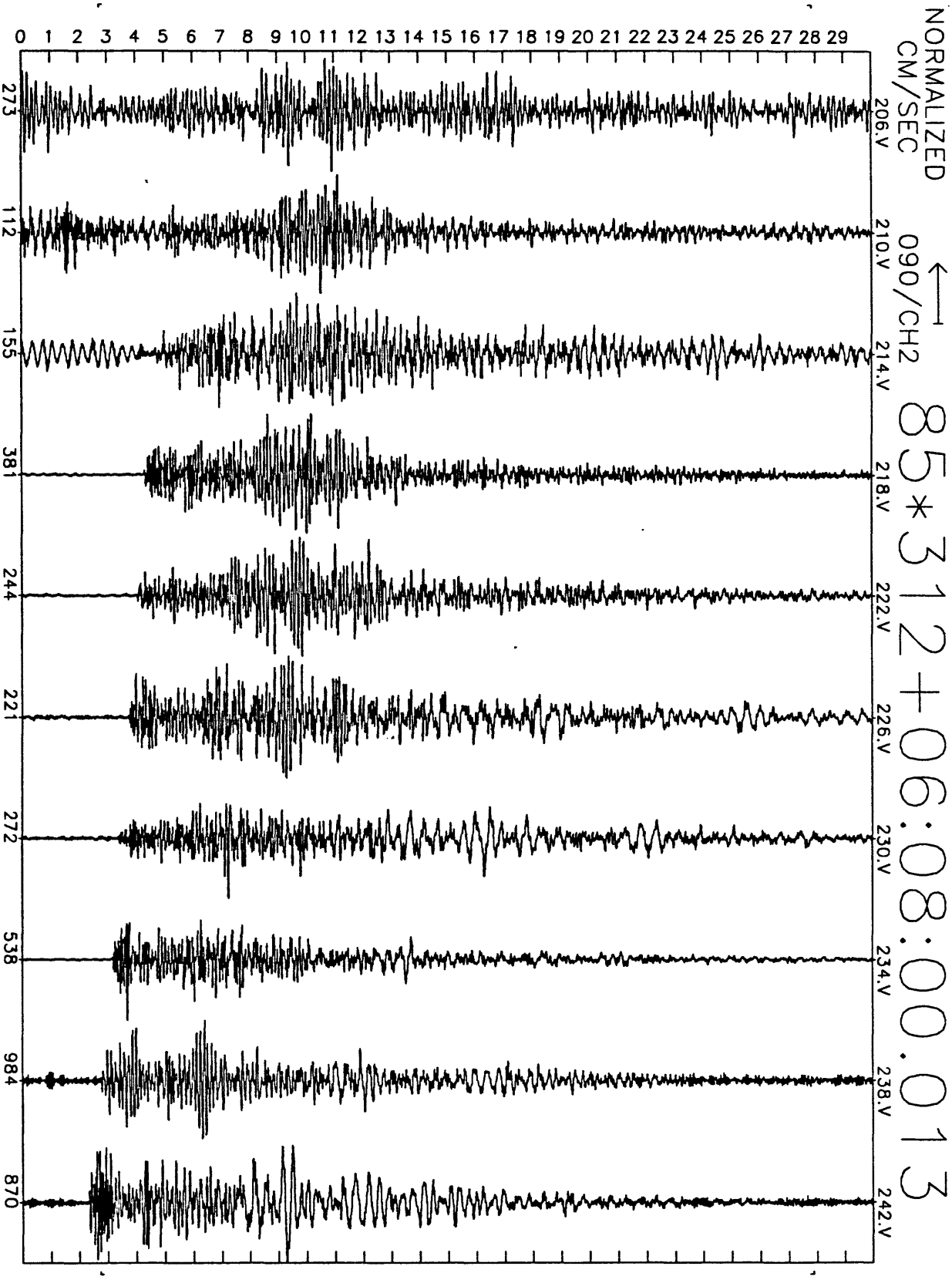

Figure A15(e), shot point 2: 30 second N20E velocity record. Abscissa is labeled with maximum counts in record (multiply by $\frac{10}{2^{24}-2^{9}} \approx 6 \times 10^{-7}$ to get cm/sec). Times are unreduced beginning at time indicated.

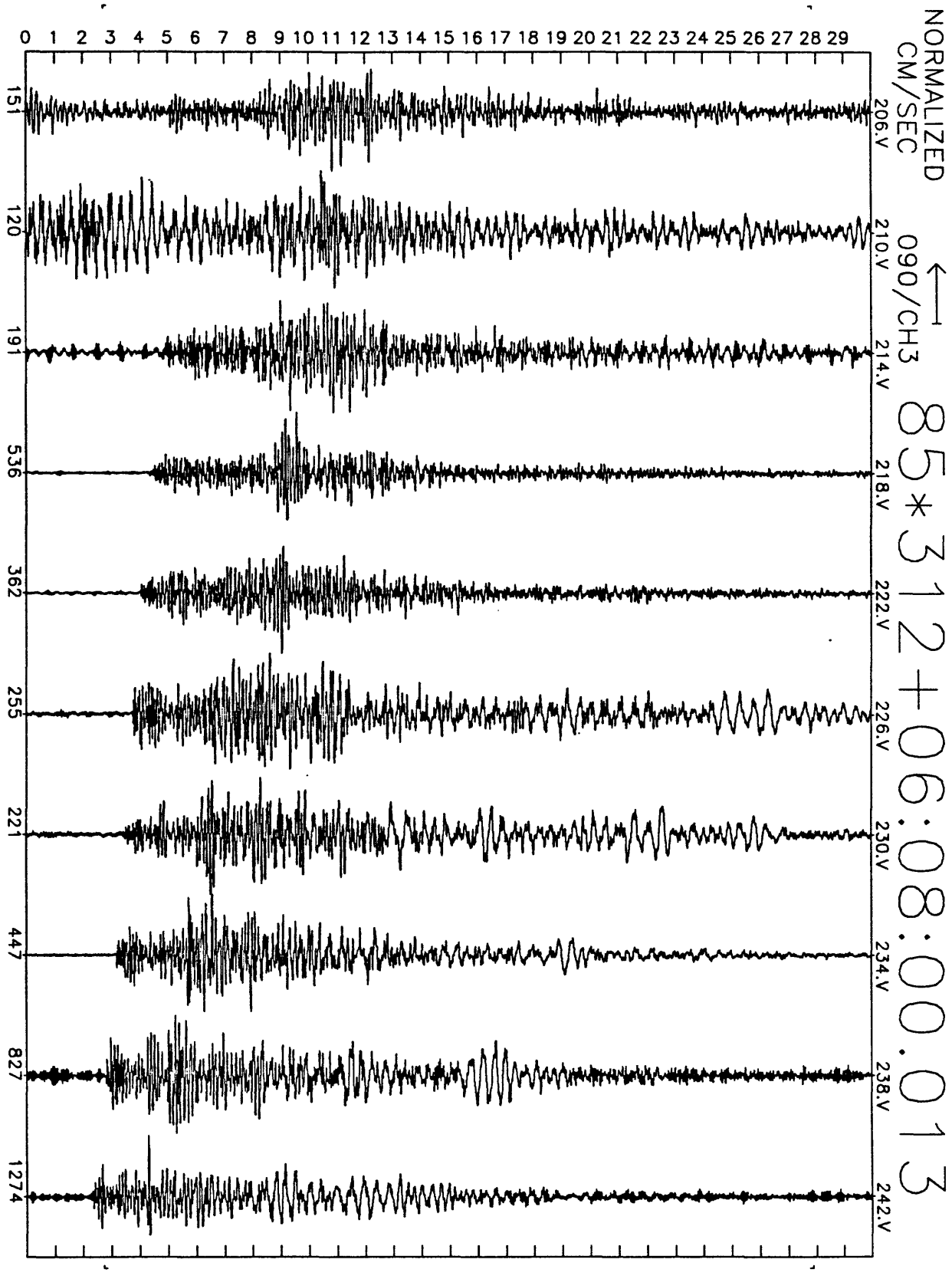

Figure A15(f), shot point 2: 30 second N110E velocity record. Abscissa is labeled with maximum counts in record (multiply by $\frac{10}{2^{24}-2^5} \approx 6 \times 10^{-7}$ to get cm/sec). Times are unreduced beginning at time indicated.

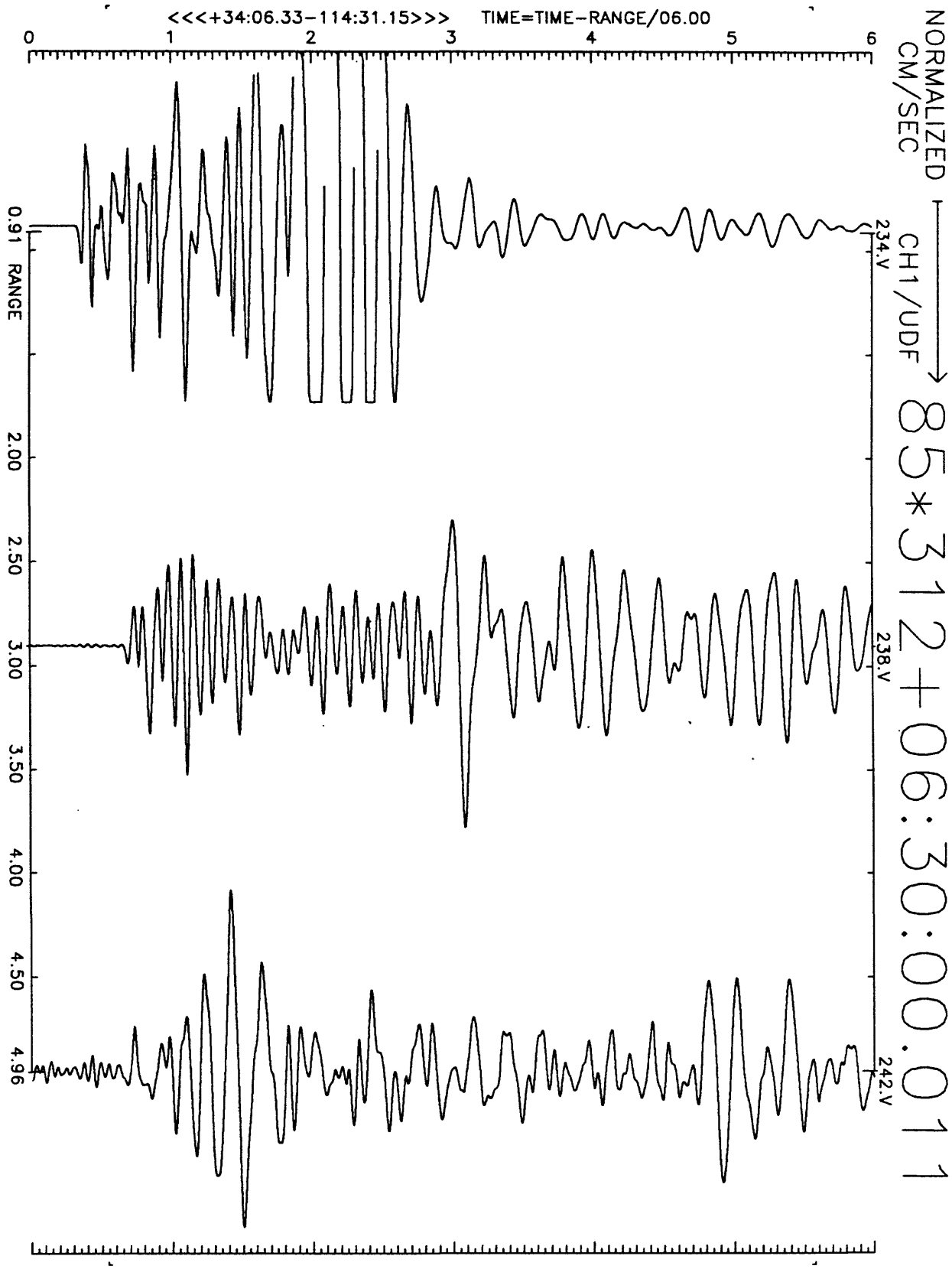

Figure A16(a), shot point 3′, SW stations: 6 second velocity record. Positive vertical motion is to right. Abscissa is distance to shot point. Top of trace is labeled with station number. Times are reduced by 6 km/sec. Shot time is indicated.

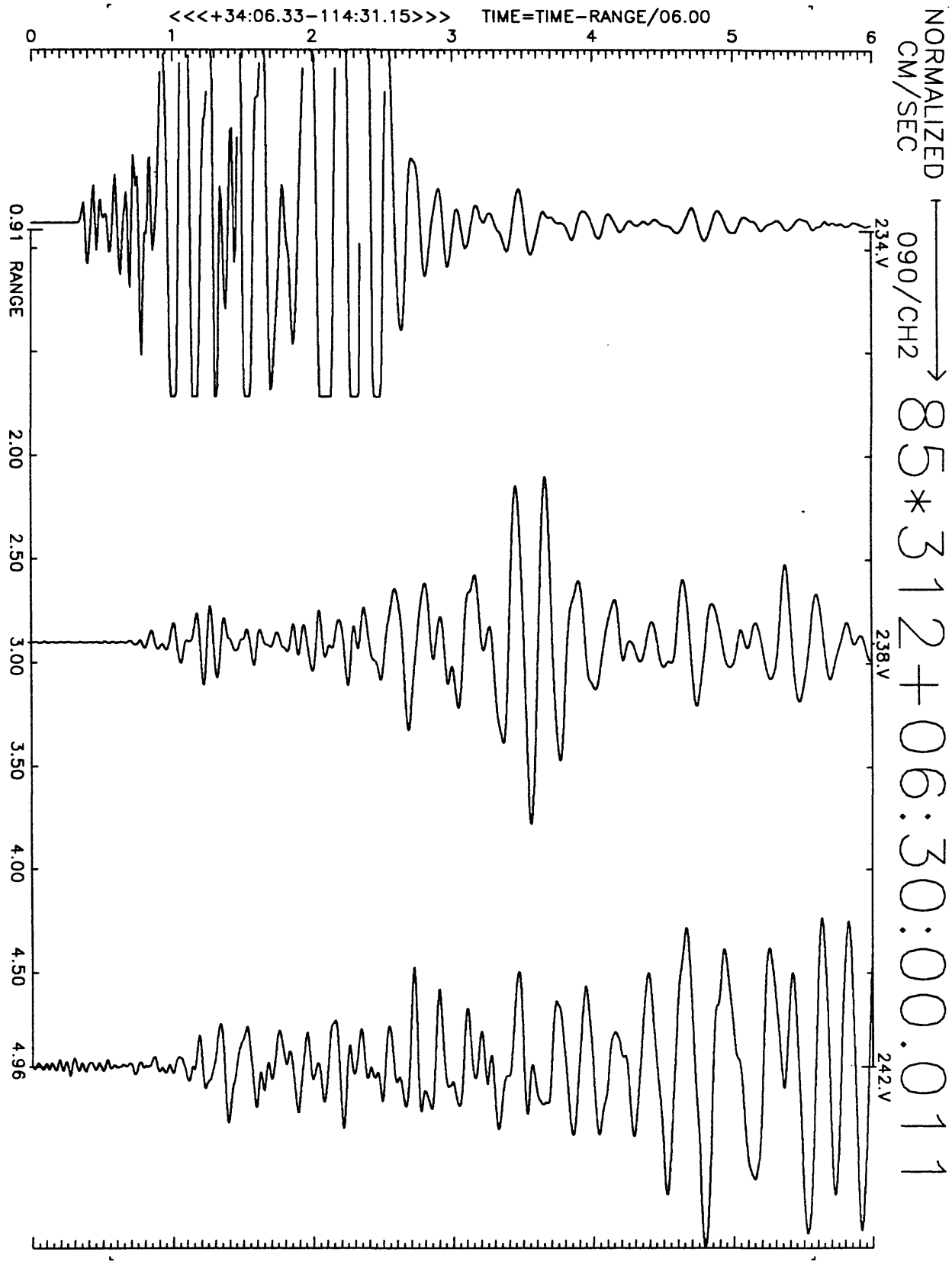

Figure A16(b), shot point 3′, SW stations: 6 second velocity record. Positive N20E motion is to right. Abscissa is distance to shot point. Top of trace is labeled with station number. Times are reduced by 6 km/sec. Shot time is indicated.

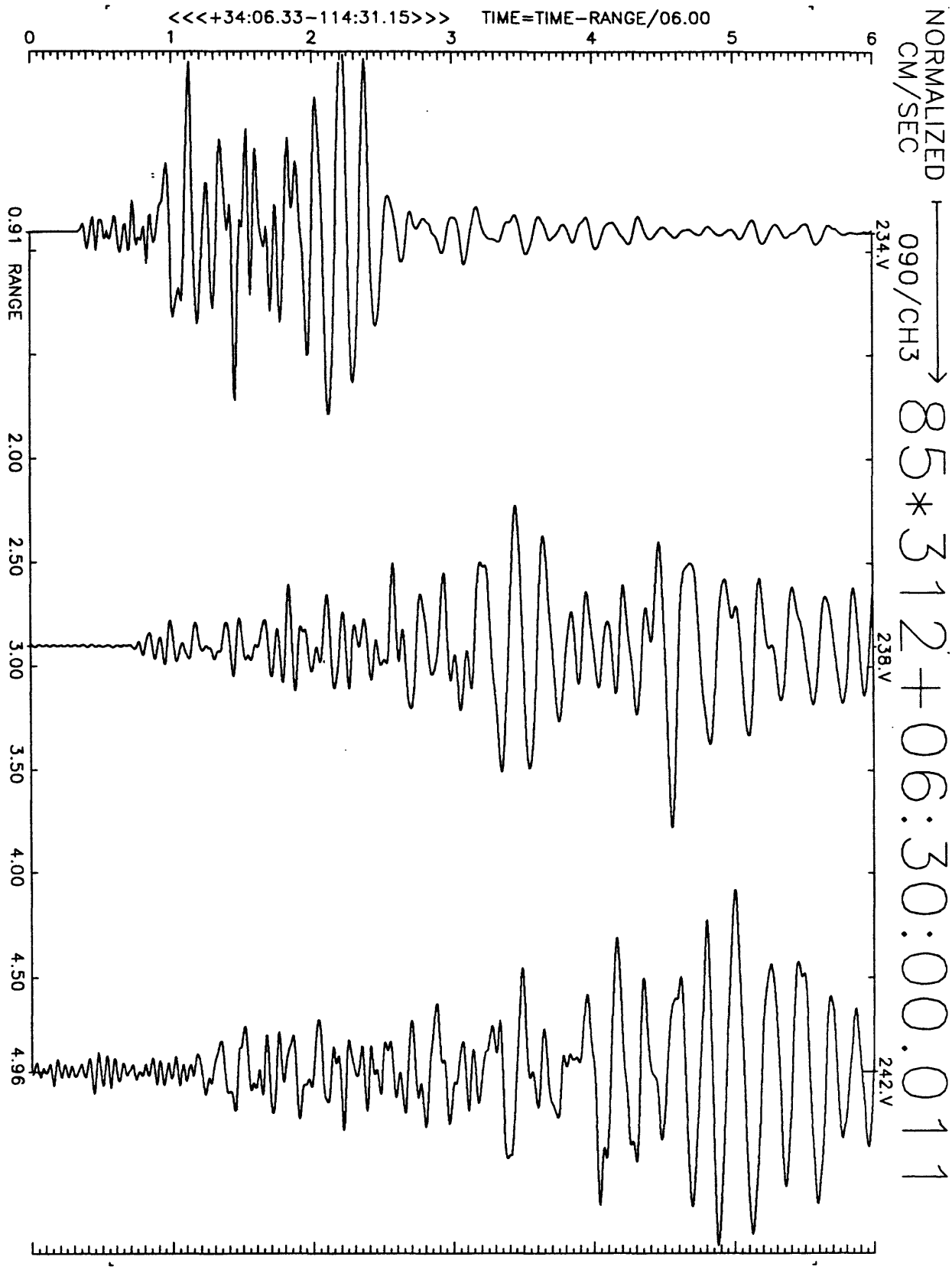

Figure A16(c), shot point 3′, SW stations: 6 second velocity record. Positive N110E motion is to right. Abscissa is distance to shot point. Top of trace is labeled with station number. Times are reduced by 6 km/sec. Shot time is indicated.

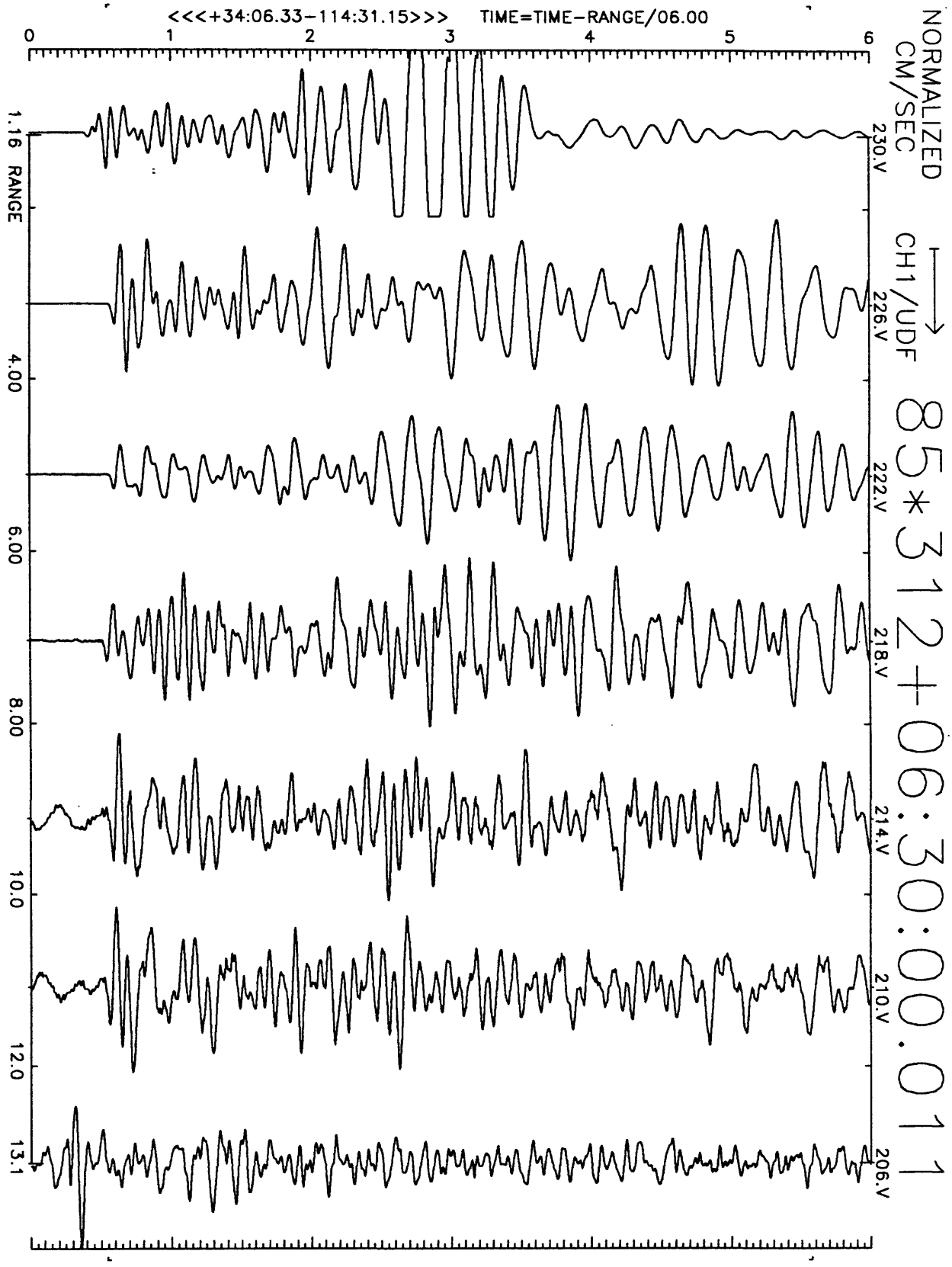

Figure A16(d), shot point 3′, NE stations: 6 second velocity record. Positive vertical motion is to right. Abscissa is distance to shot point. Top of trace is labeled with station number. Times are reduced by 6 km/sec. Shot time is indicated.

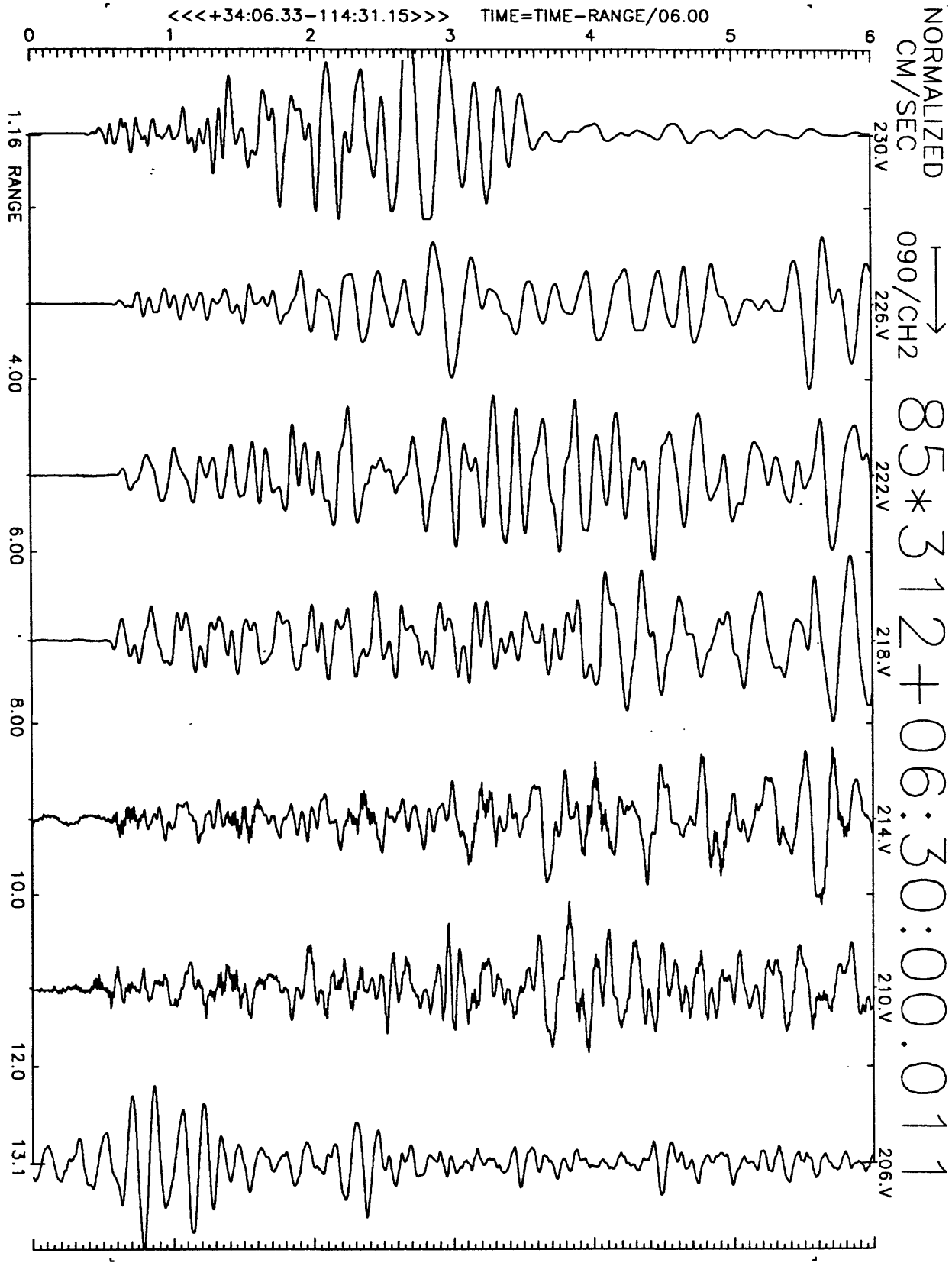

Figure A16(e), shot point 3′, NE stations: 6 second velocity record. Positive N20E motion is to right. Abscissa is distance to shot point. Top of trace is labeled with station number. Times are reduced by 6 km/sec. Shot time is indicated.

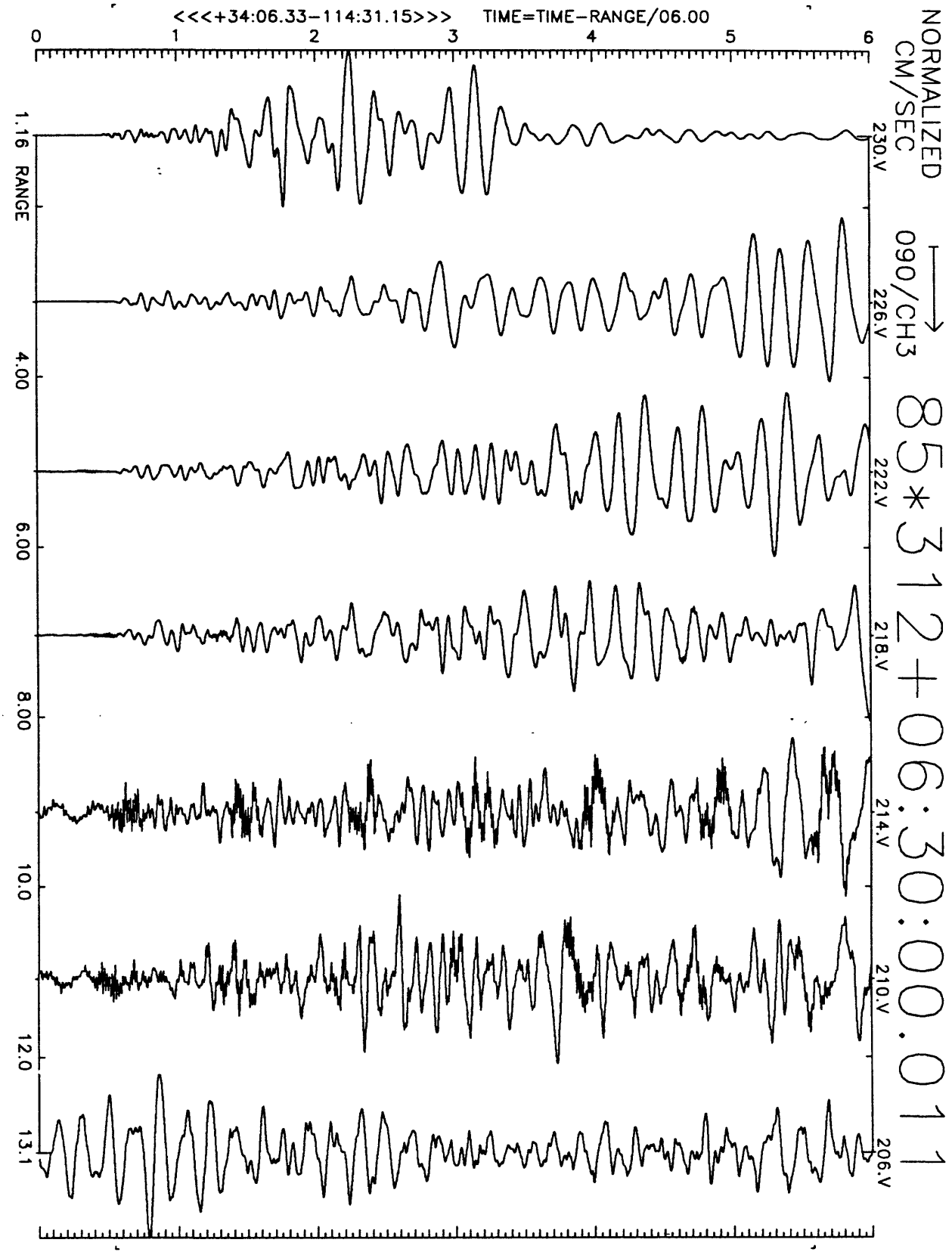

Figure A16(f), shot point 3′, NE stations: 6 second velocity record. Positive N110E motion is to right. Abscissa is distance to shot point. Top of trace is labeled with station number. Times are reduced by 6 km/sec. Shot time is indicated.

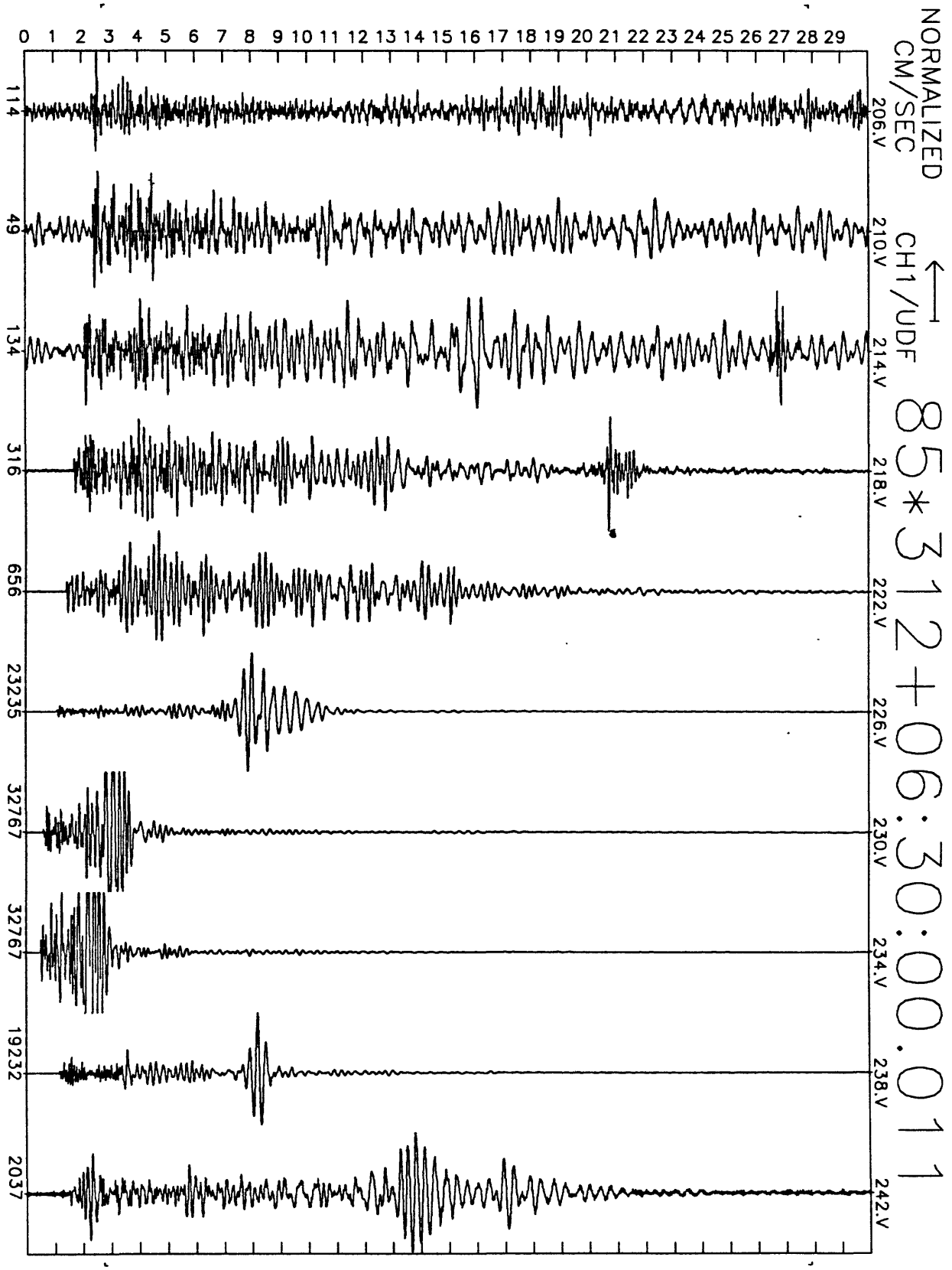

Figure A16(g), shot point 3′: 30 second vertical velocity record. Abscissa is labeled with maximum counts in record (multiply by $\frac{10}{2^{24}-2^5} \approx 6 \times 10^{-7}$ to get cm/sec). Times are unreduced beginning at time indicated.

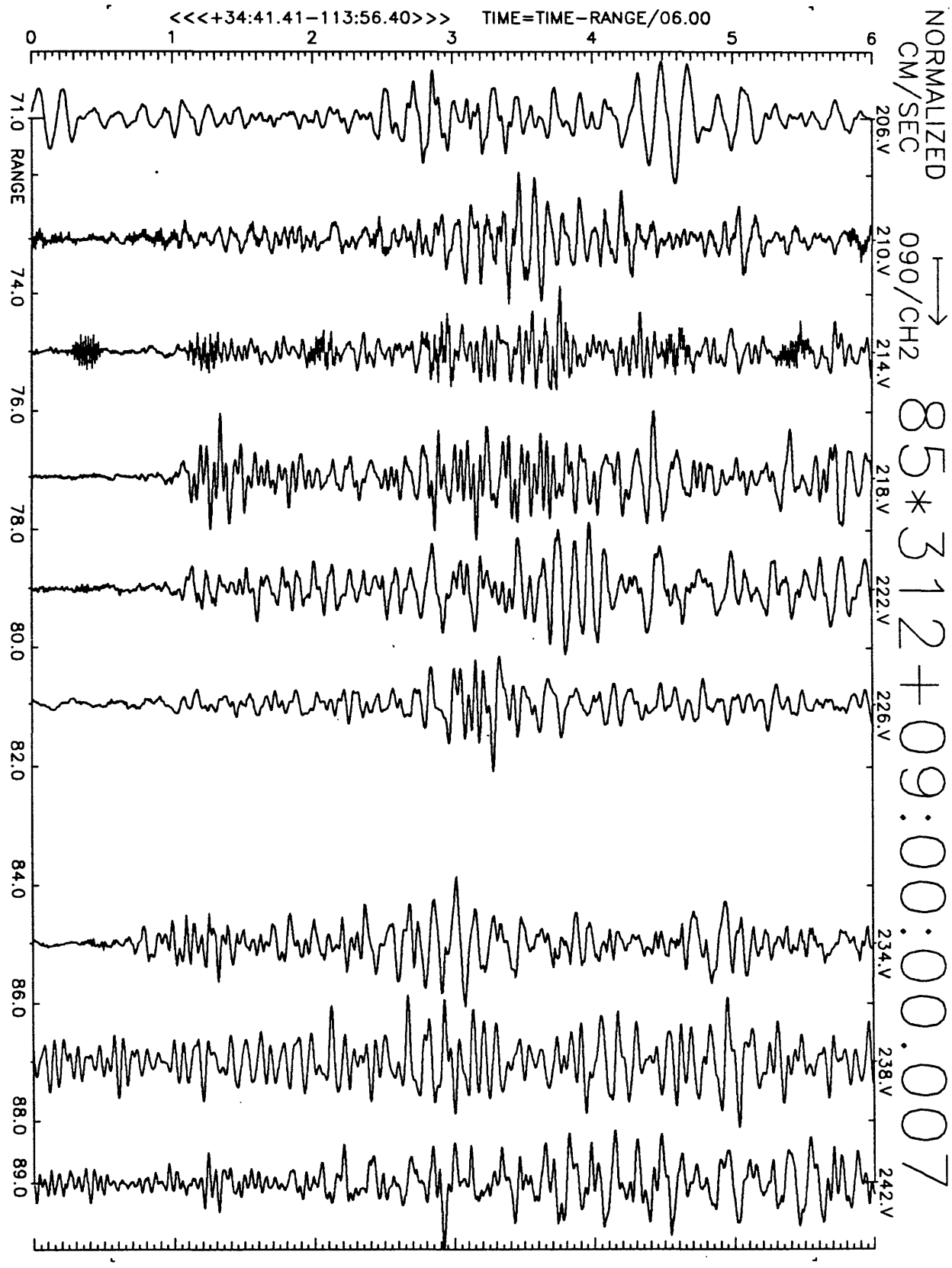

Figure A18(b), shot point 7: 6 second velocity record. Positive N20E motion is to right. Abscissa is distance to shot point. Top of trace is labeled with station number. Times are reduced by 6 km/sec. Shot time is indicated.

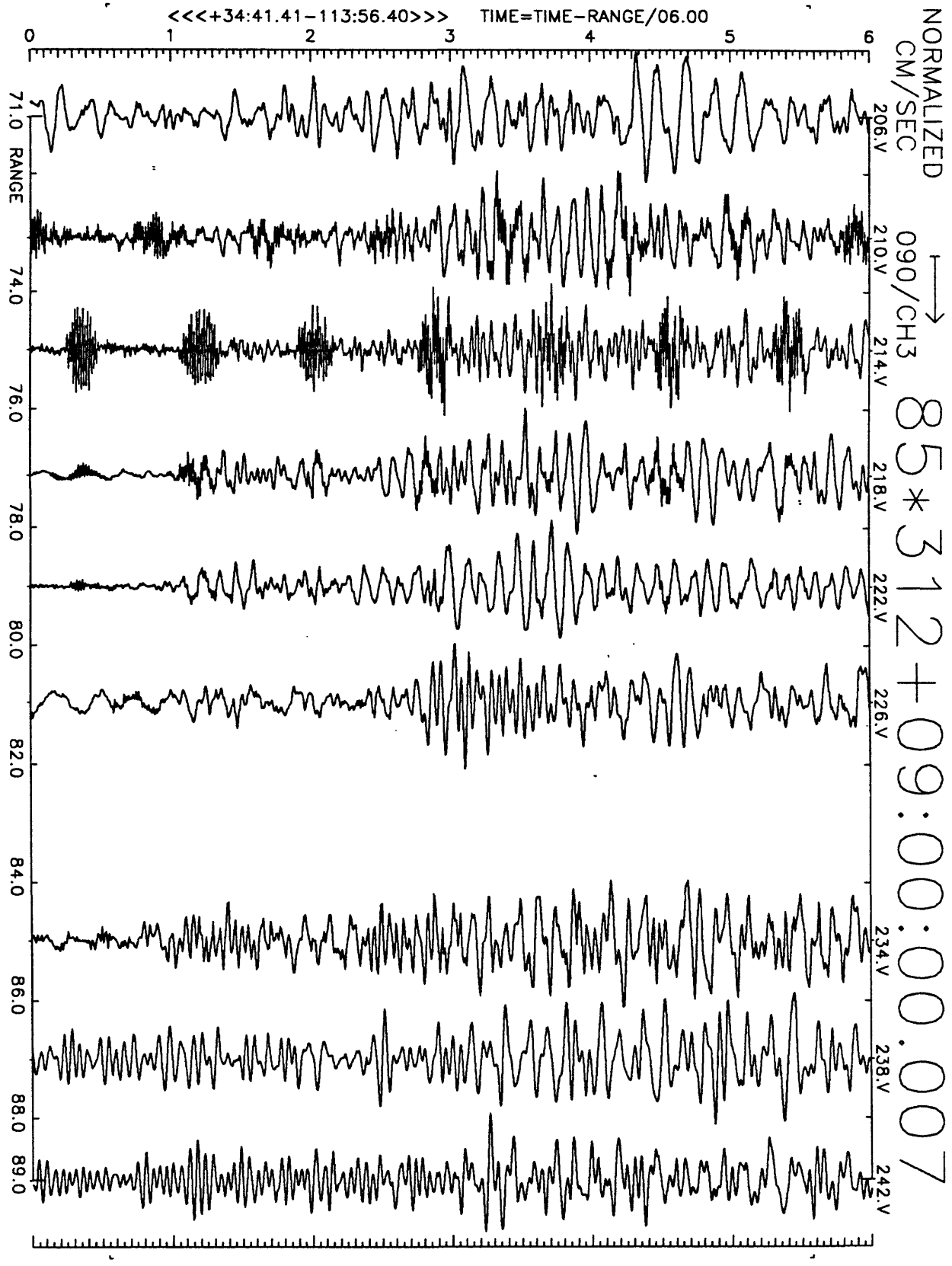

Figure A18(c), shot point 7: 6 second velocity record. Positive N110E motion is to right. Abscissa is distance to shot point. Top of trace is labeled with station number. Times are reduced by 6 km/sec. Shot time is indicated.

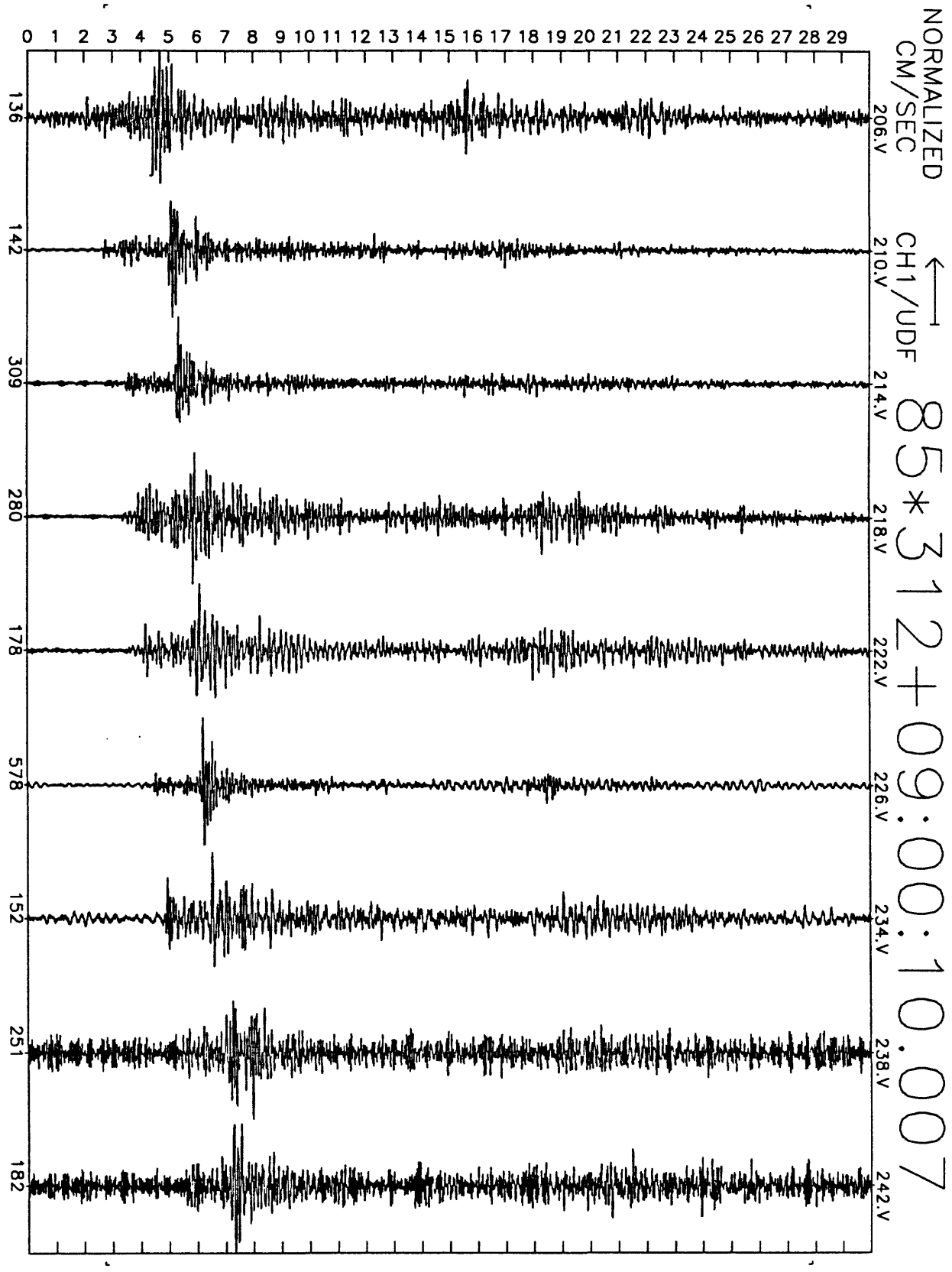

Figure A18(d), shot point 7: 30 second vertical velocity record. Abscissa is labeled with maximum counts in record (multiply by $\frac{10}{2^{24}-2^{9}} \approx 6 \times 10^{-7}$ to get cm/sec). Times are unreduced beginning at time indicated.

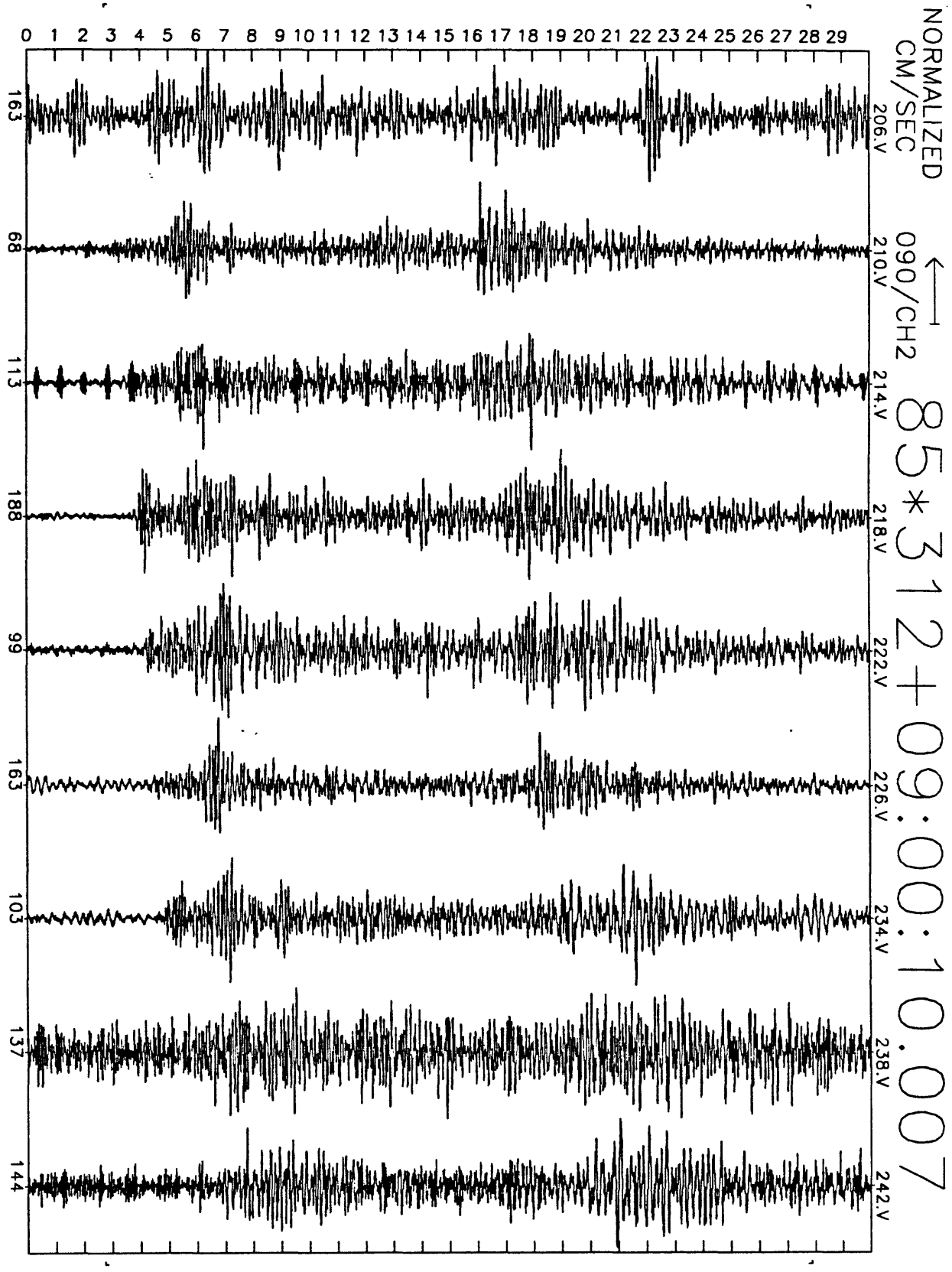

Figure A18(e), shot point 7: 30 second N20E velocity record. Abscissa is labeled with maximum counts in record (multiply by $\frac{10}{2^{24}-2^5} \approx 6 \times 10^{-7}$ to get cm/sec). Times are unreduced beginning at time indicated.

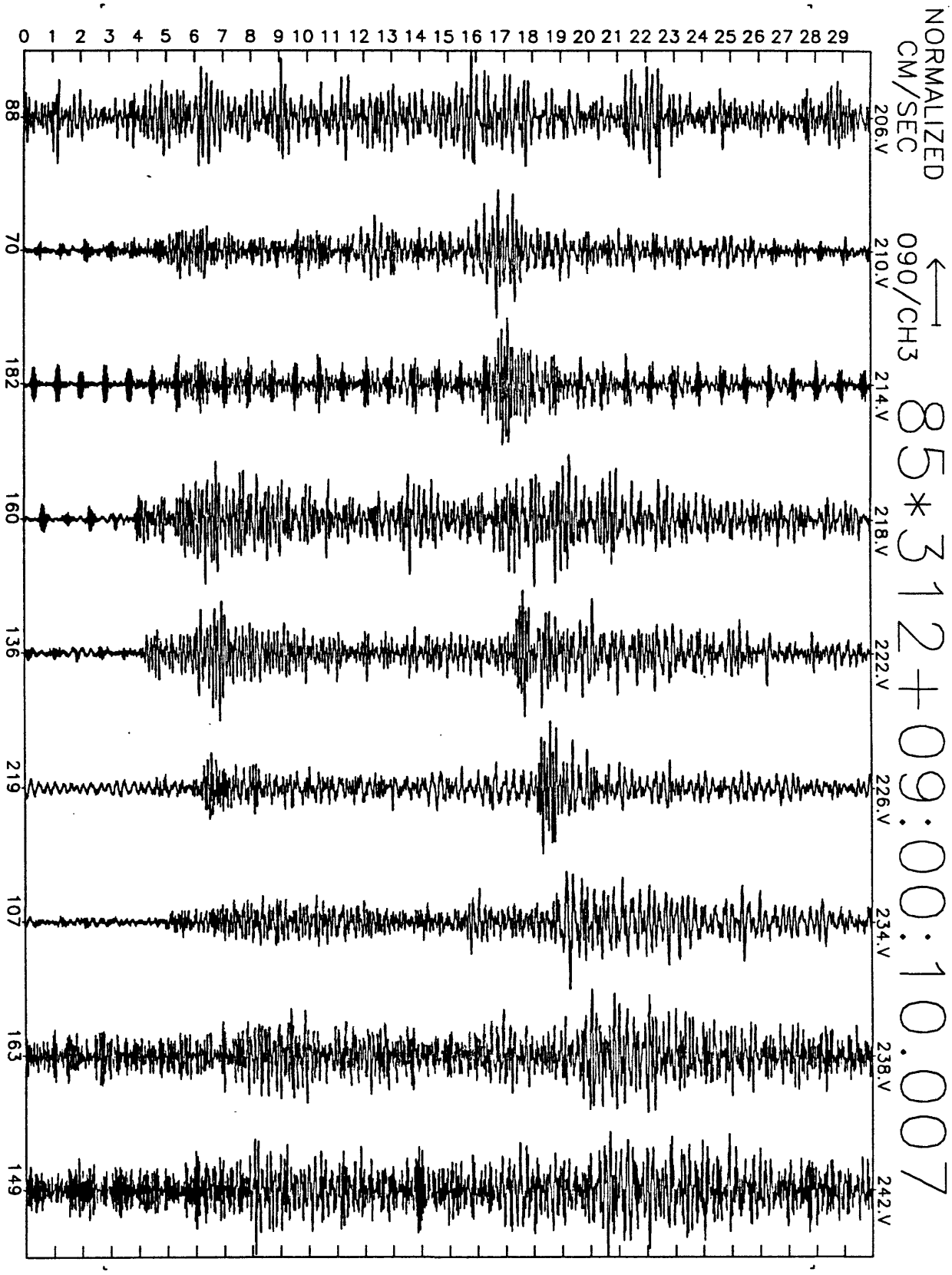

Figure A18(f), shot point 7: 30 second N110E velocity record. Abscissa is labeled with maximum counts in record (multiply by $\frac{10}{2^{24}-2^{9}} \approx 6 \times 10^{-7}$ to get cm/sec). Times are unreduced beginning at time indicated.

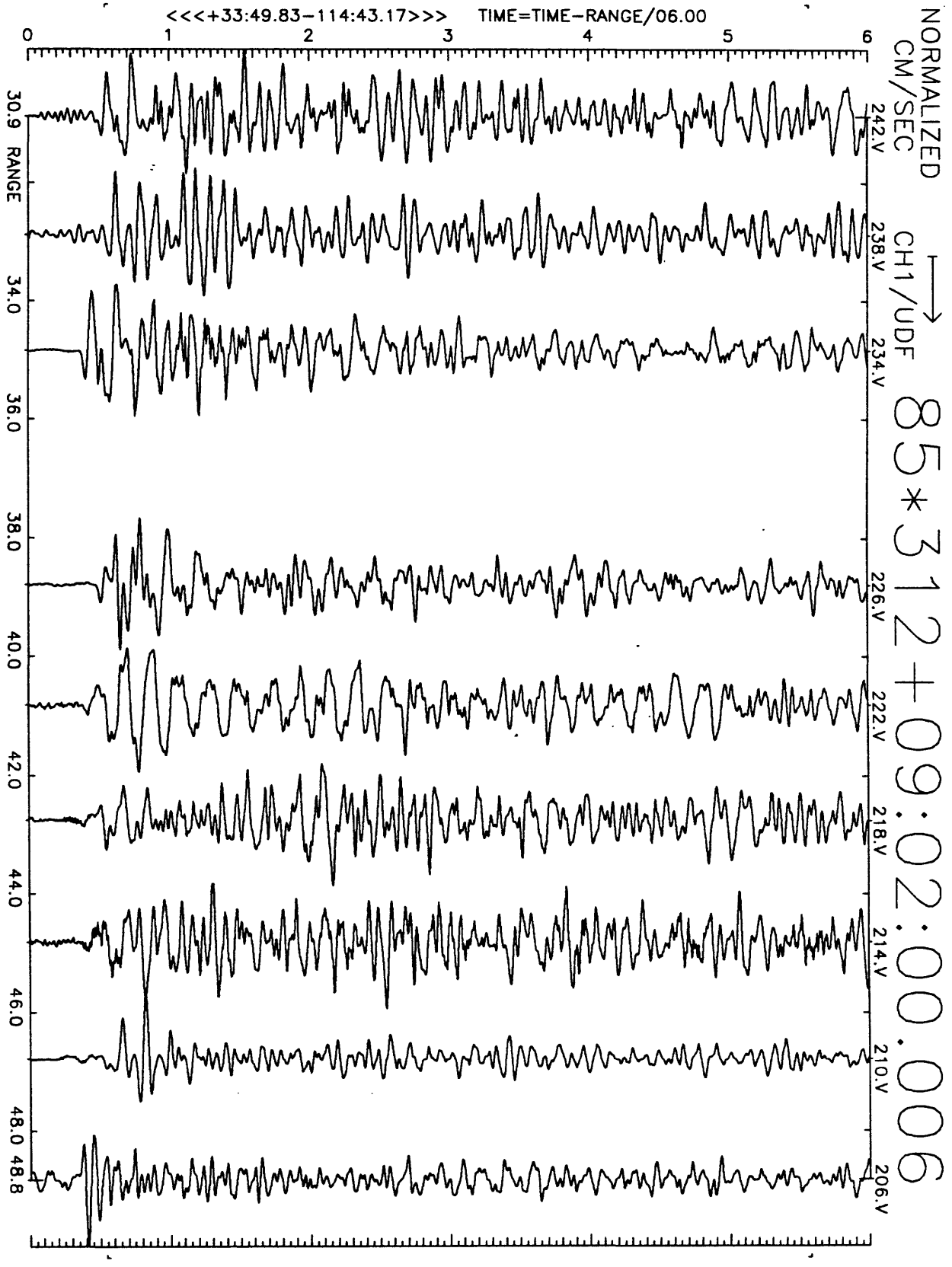

Figure A19(a), shot point 1: 6 second velocity record. Positive vertical motion is to right. Abscissa is distance to shot point. Top of trace is labeled with station number. Times are reduced by 6 km/sec. Shot time is indicated.

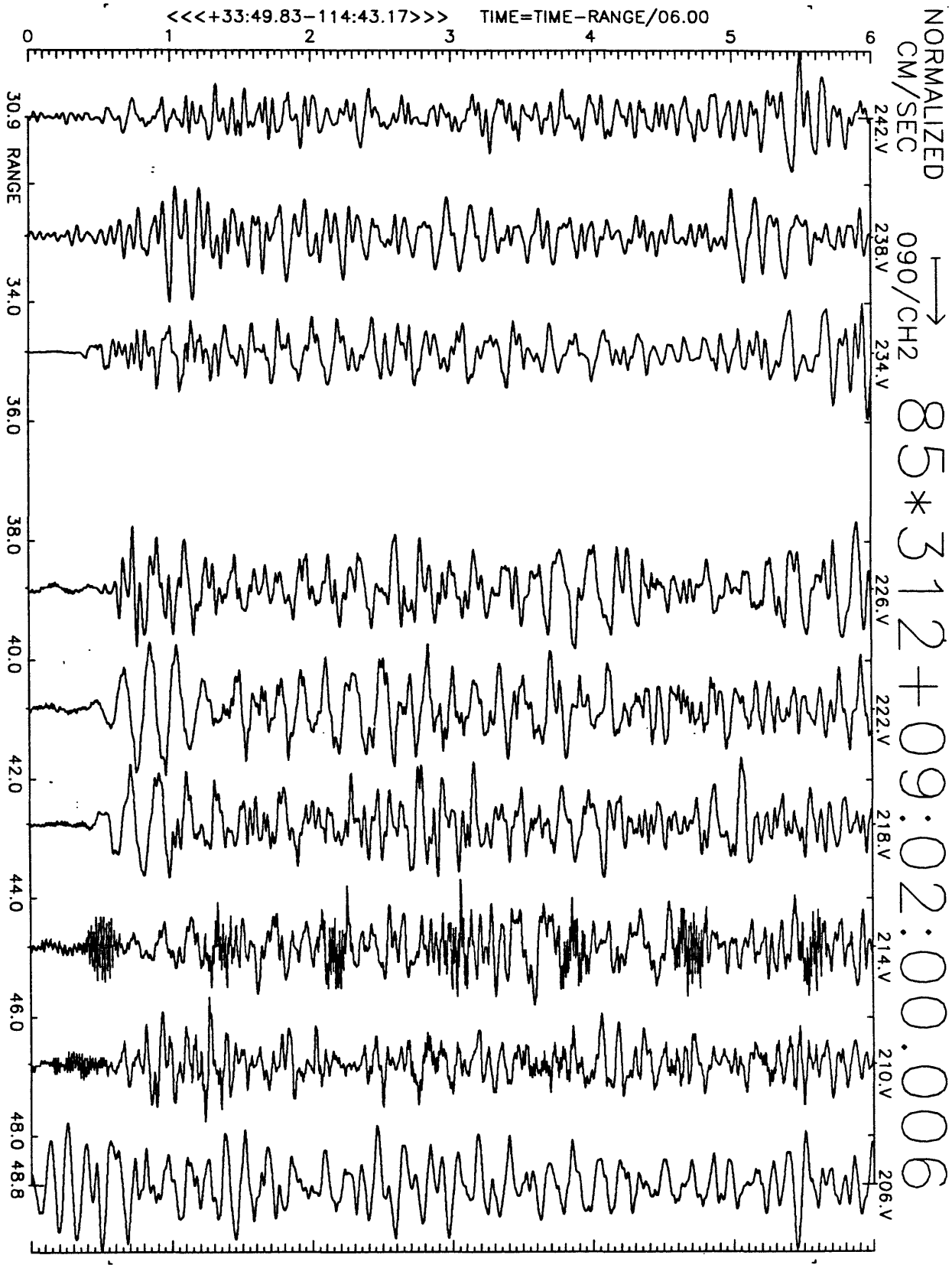

Figure A19(b), shot point 1: 6 second velocity record. Positive N20E motion is to right. Abscissa is distance to shot point. Top of trace is labeled with station number. Times are reduced by 6 km/sec. Shot time is indicated.

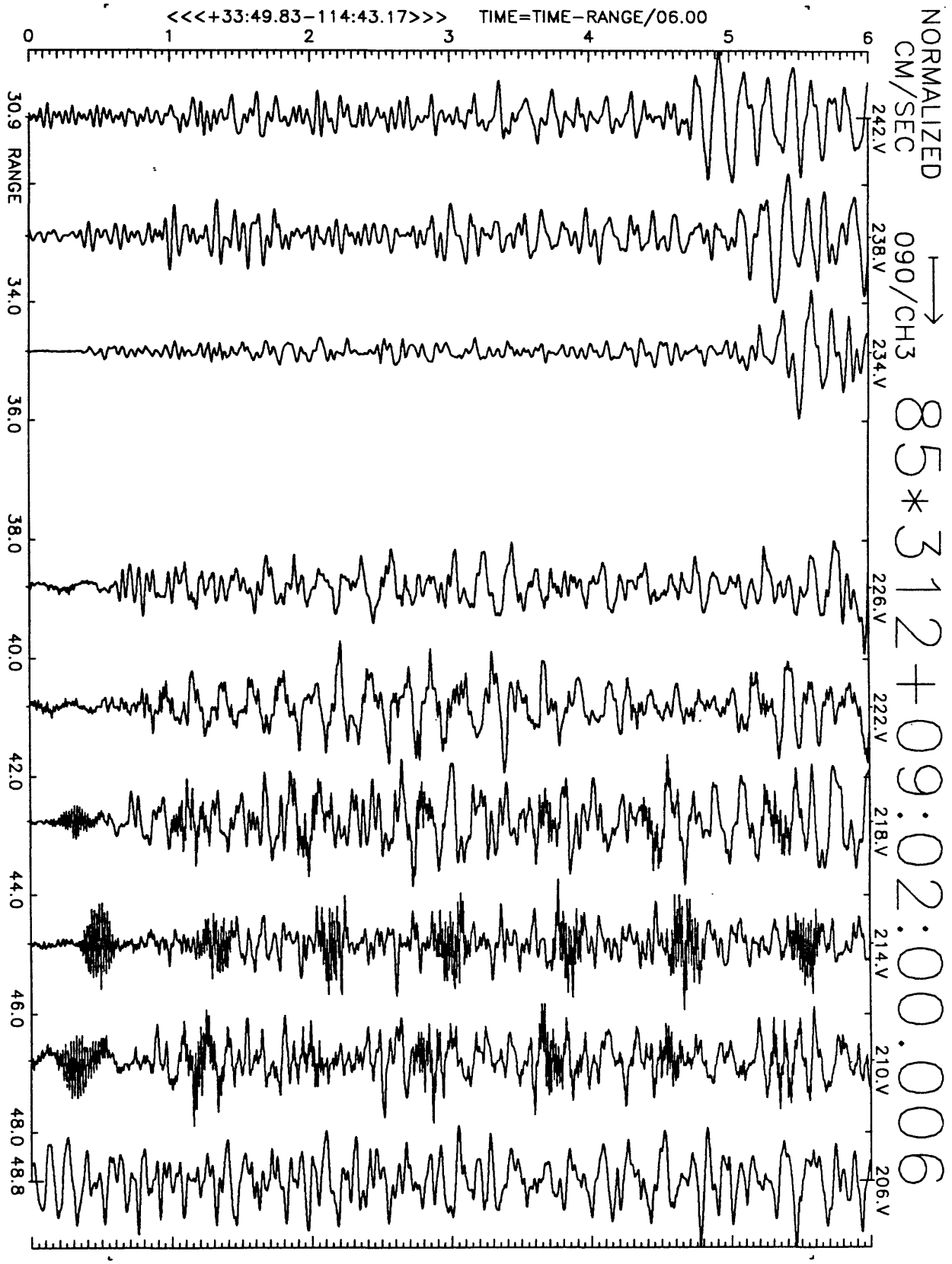

Figure A19(c), shot point 1: 6 second velocity record. Positive N110E motion is to right. Abscissa is distance to shot point. Top of trace is labeled with station number. Times are reduced by 6 km/sec. Shot time is indicated.

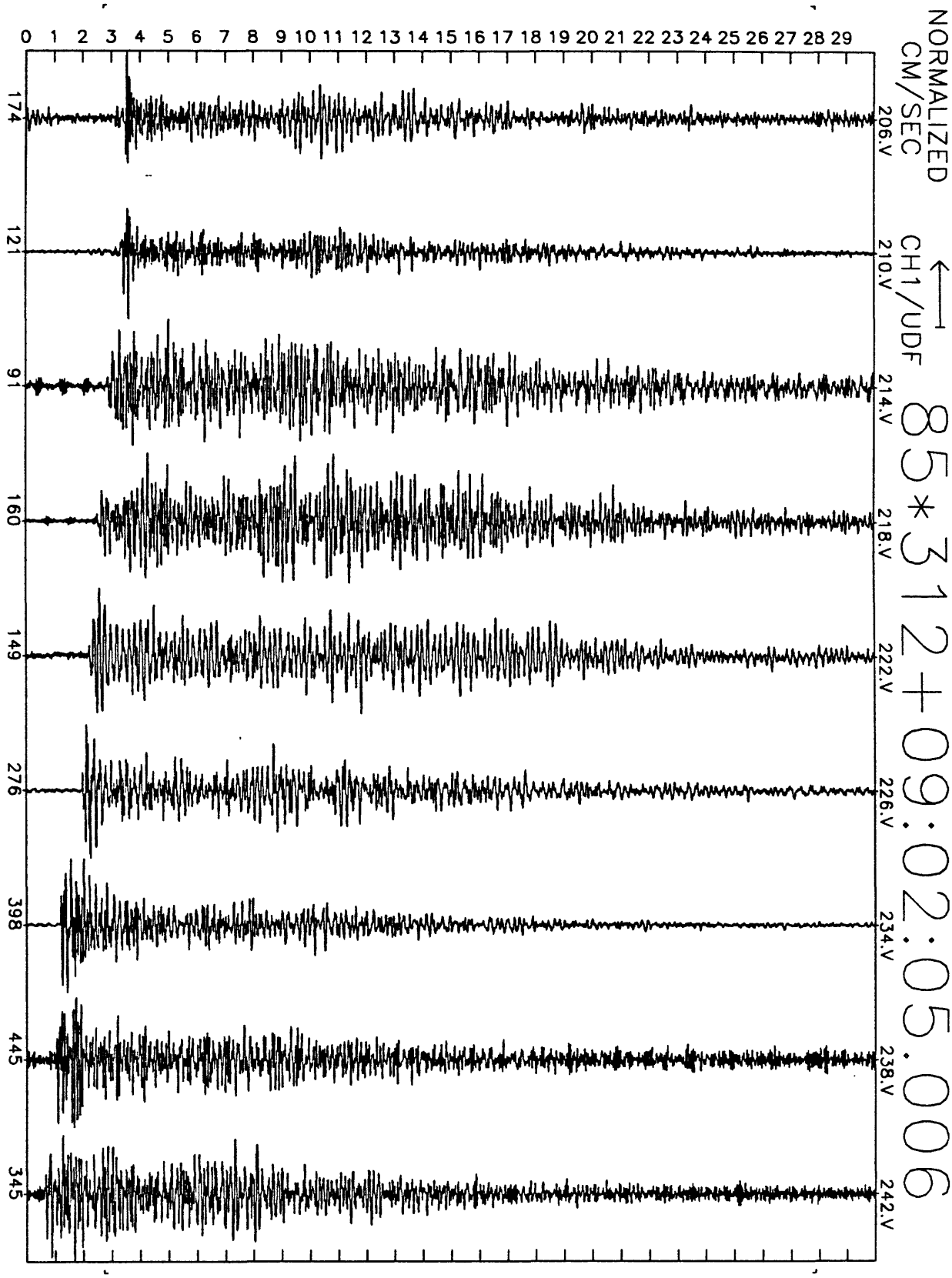

Figure A19(d), shot point 1: 30 second vertical velocity record. Abscissa is labeled with maximum counts in record (multiply by $\frac{10}{2^{24}-2^5} \approx 6 \times 10^{-7}$ to get cm/sec). Times are unreduced beginning at time indicated.

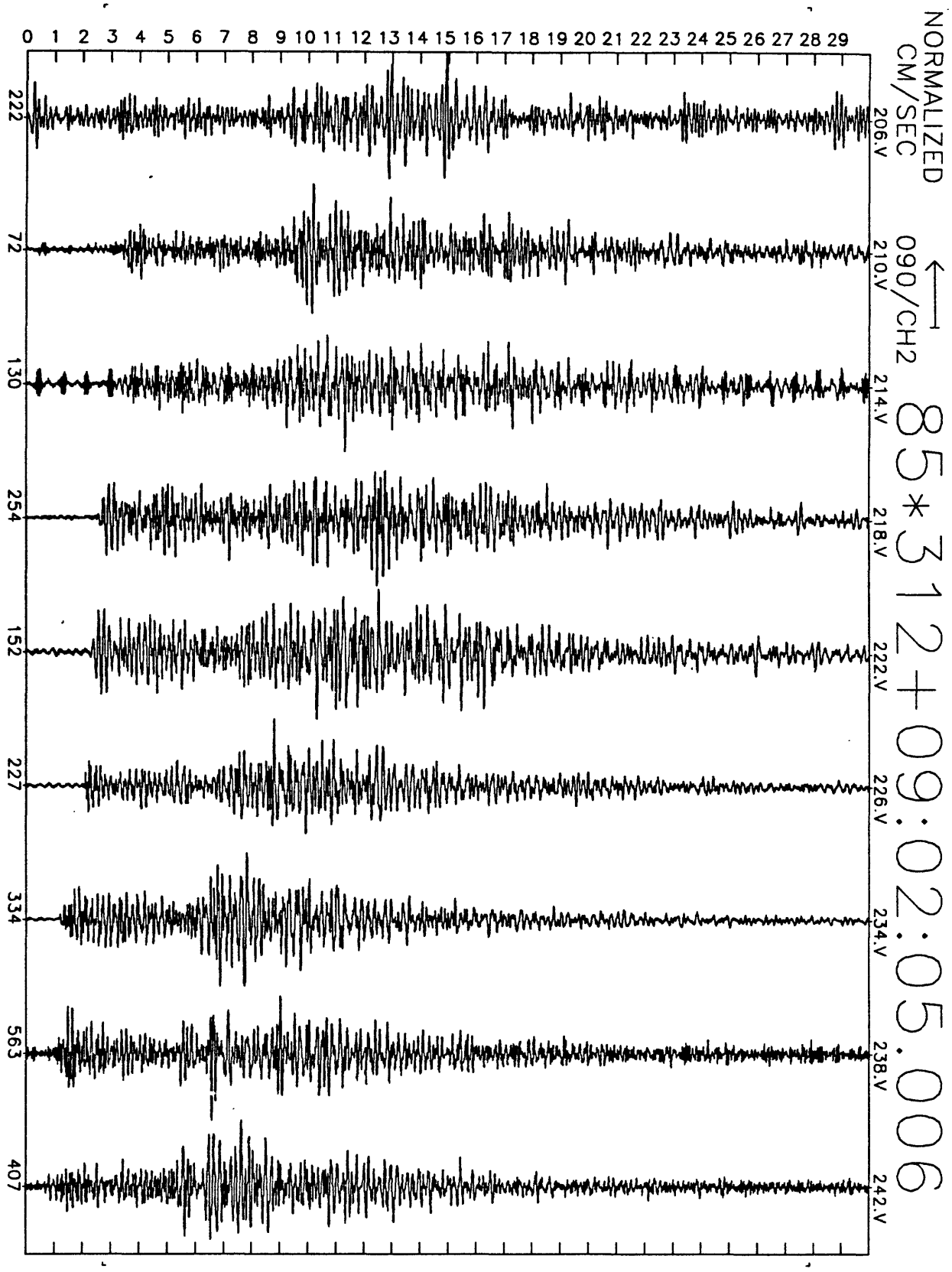

Figure A19(e), shot point 1: 30 second N20E velocity record. Abscissa is labeled with maximum counts in record (multiply by $\frac{10}{2^{24}-2^{9}} \approx 6 \times 10^{-7}$ to get cm/sec). Times are unreduced beginning at time indicated.

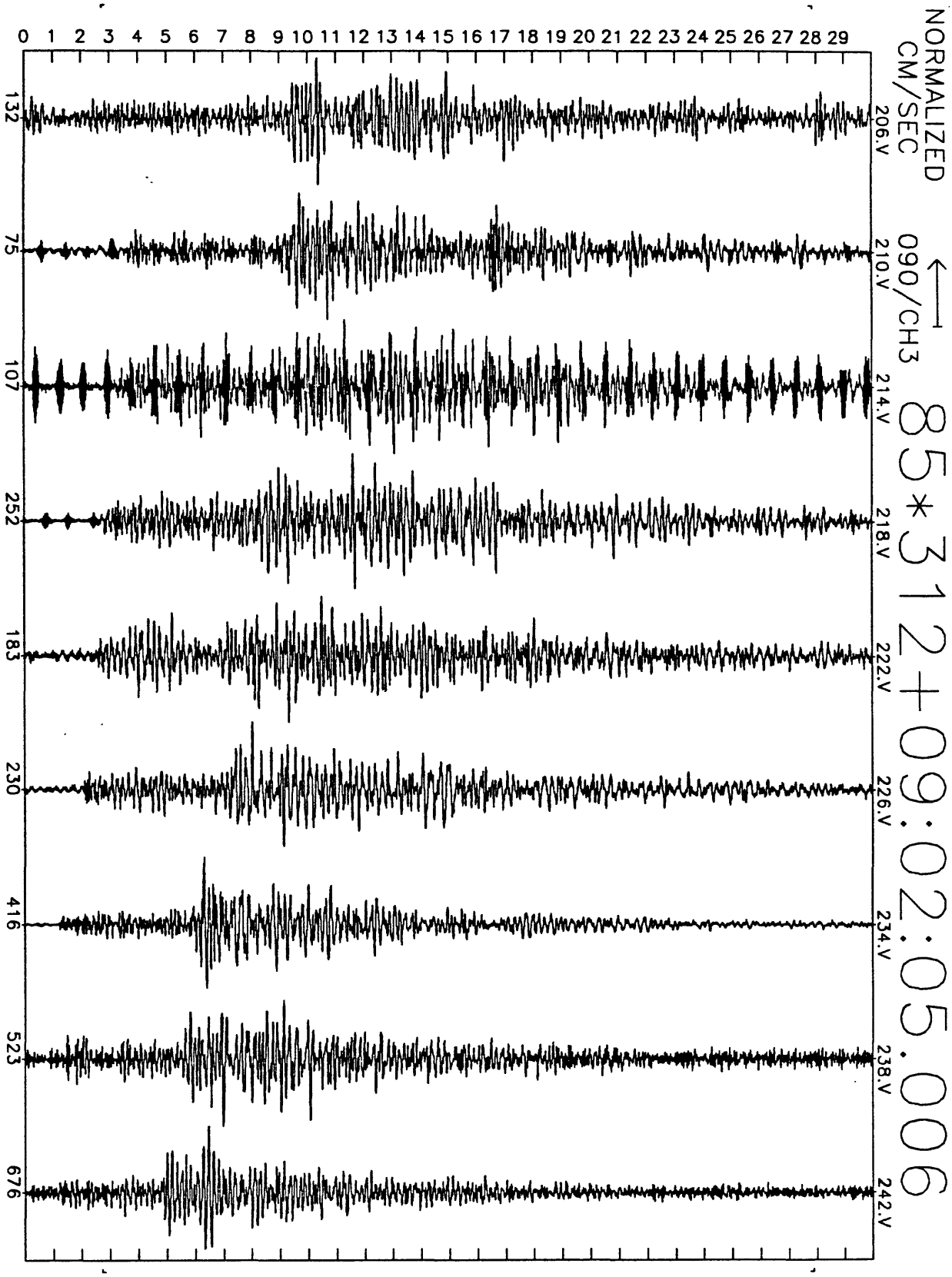

Figure A19(f), shot point 1: 30 second N110E velocity record. Abscissa is labeled with maximum counts in record (multiply by $\frac{10}{2^{24}-2^8} \approx 6 \times 10^{-7}$ to get cm/sec). Times are unreduced beginning at time indicated.

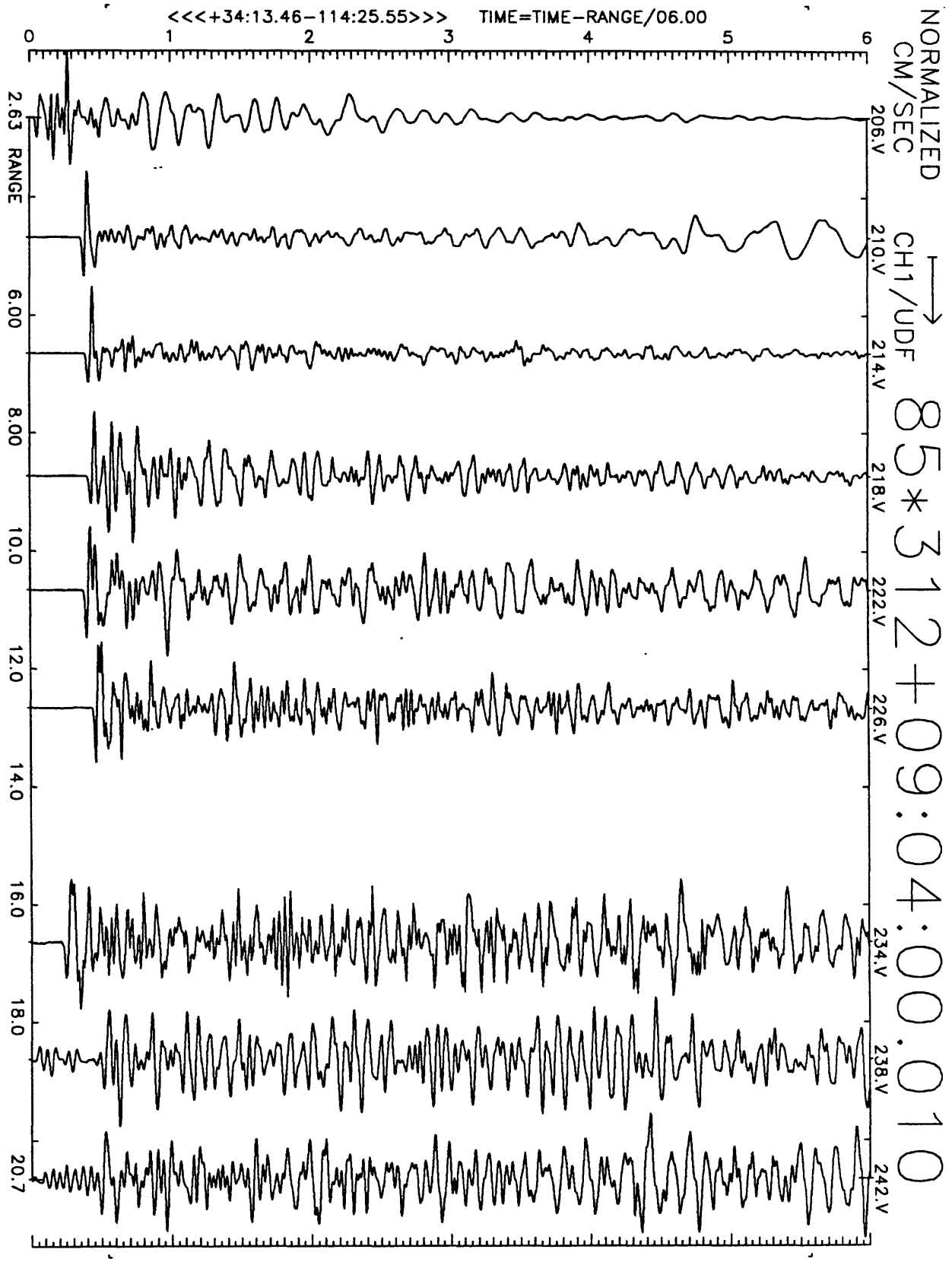

Figure A20(a), shot point 4B: 6 second velocity record. Positive vertical motion is to right. Abscissa is distance to shot point. Top of trace is labeled with station number. Times are reduced by 6 km/sec. Shot time is indicated.

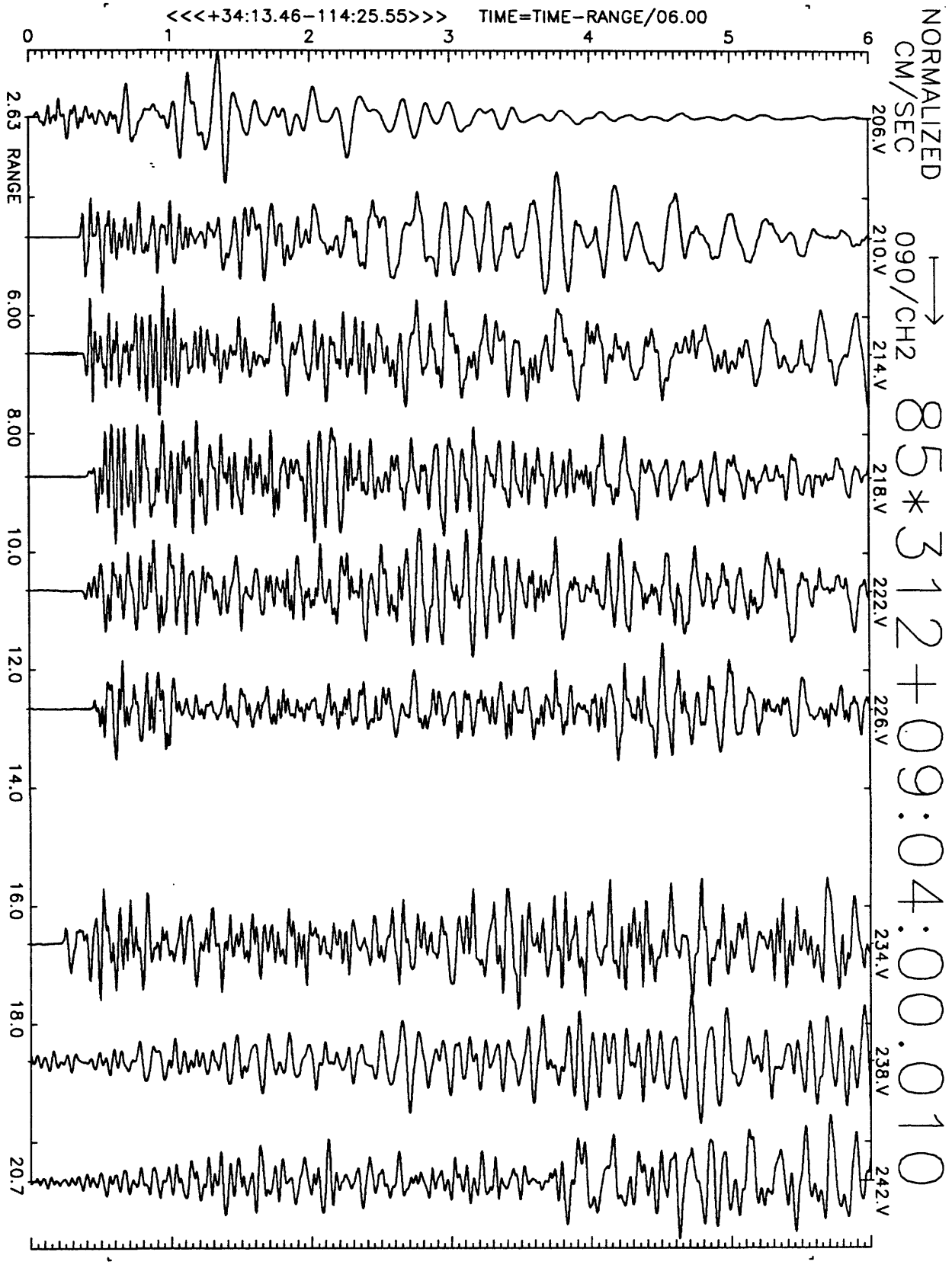

Figure A20(b), shot point 4B: 6 second velocity record. Positive N20E motion is to right. Abscissa is distance to shot point. Top of trace is labeled with station number. Times are reduced by 6 km/sec. Shot time is indicated.

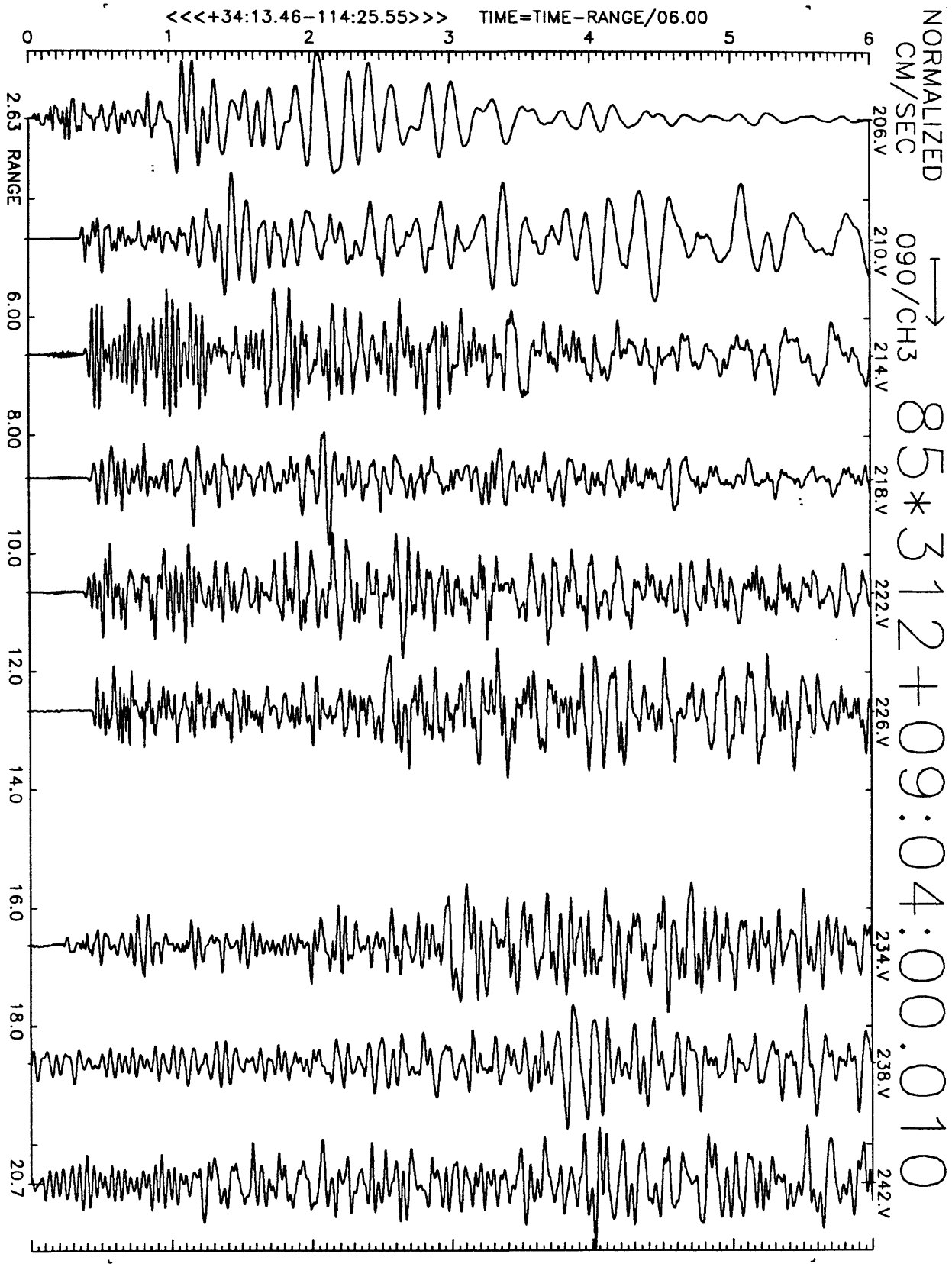

Figure A20(c), shot point 4B: 6 second velocity record. Positive N110E motion is to right. Abscissa is distance to shot point. Top of trace is labeled with station number. Times are reduced by 6 km/sec. Shot time is indicated.

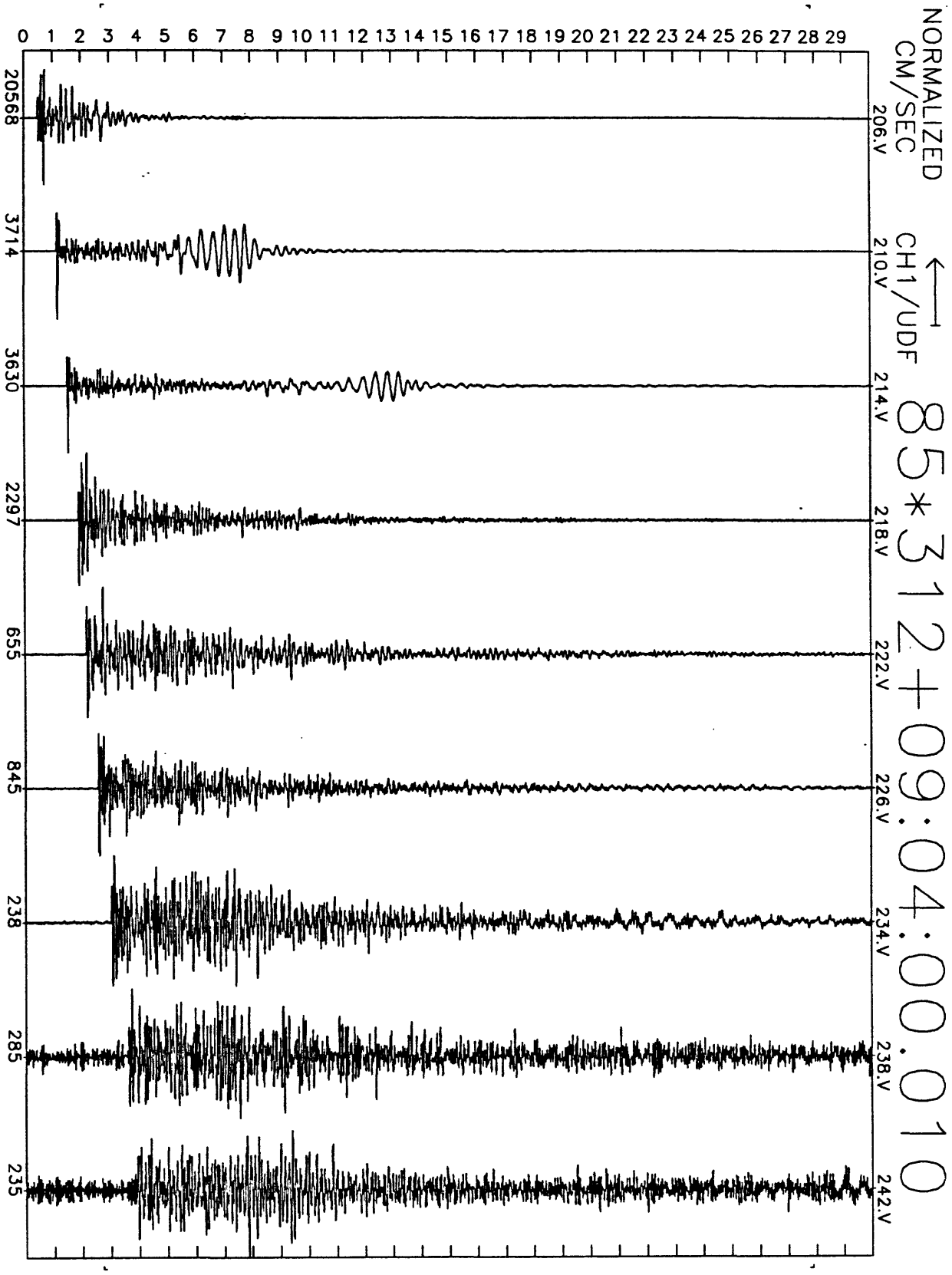

Figure A20(d), shot point 4B: 30 second vertical velocity record. Abscissa is labeled with maximum counts in record (multiply by $\frac{10}{2^{24}-2^9} \approx 6 \times 10^{-7}$ to get cm/sec). Times are unreduced beginning at time indicated.

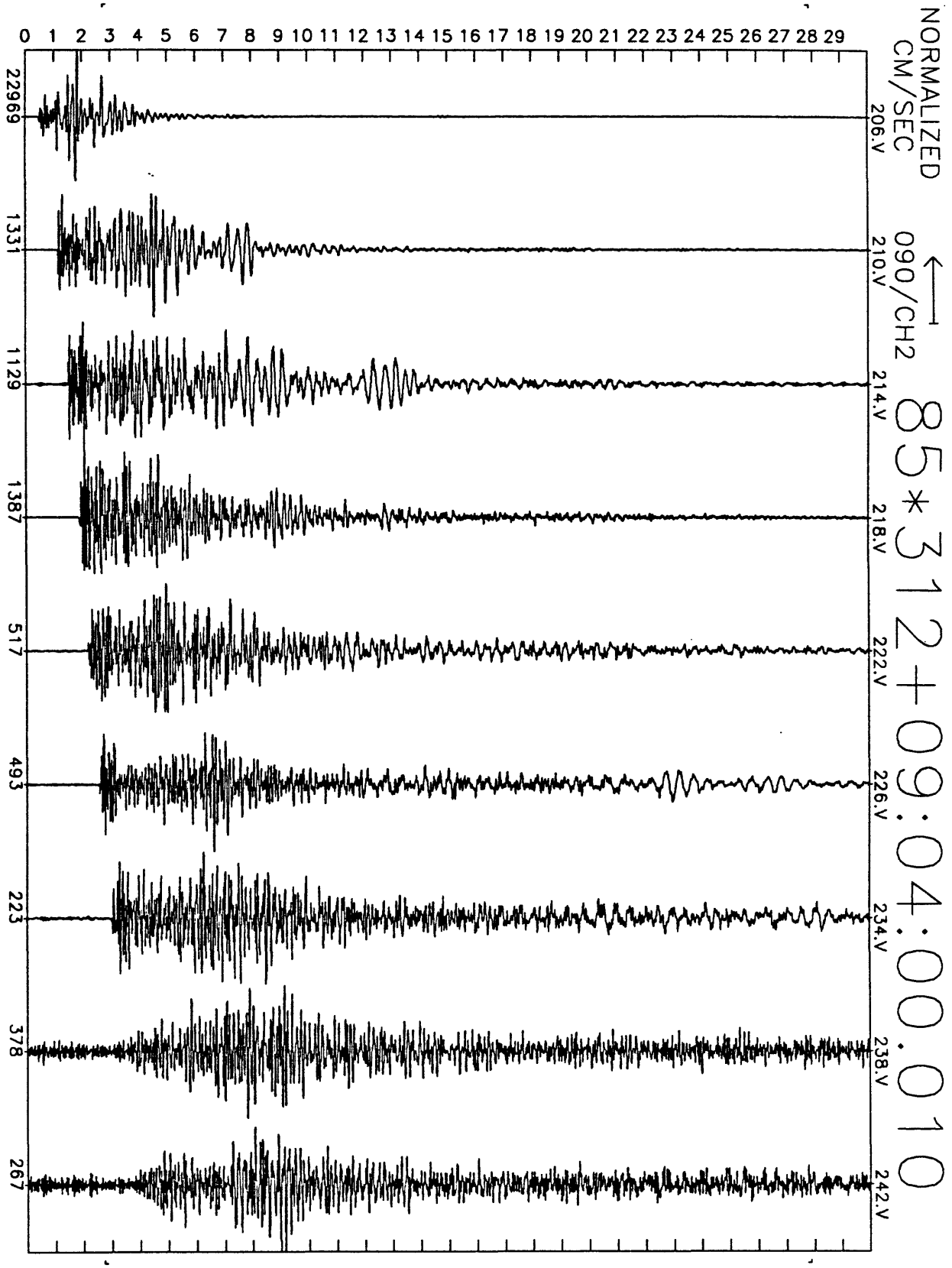

Figure A20(e), shot point 4B: 30 second N20E velocity record. Abscissa is labeled with maximum counts in record (multiply by $\frac{10}{2^{24}-2^5} \approx 6 \times 10^{-7}$ to get cm/sec). Times are unreduced beginning at time indicated.

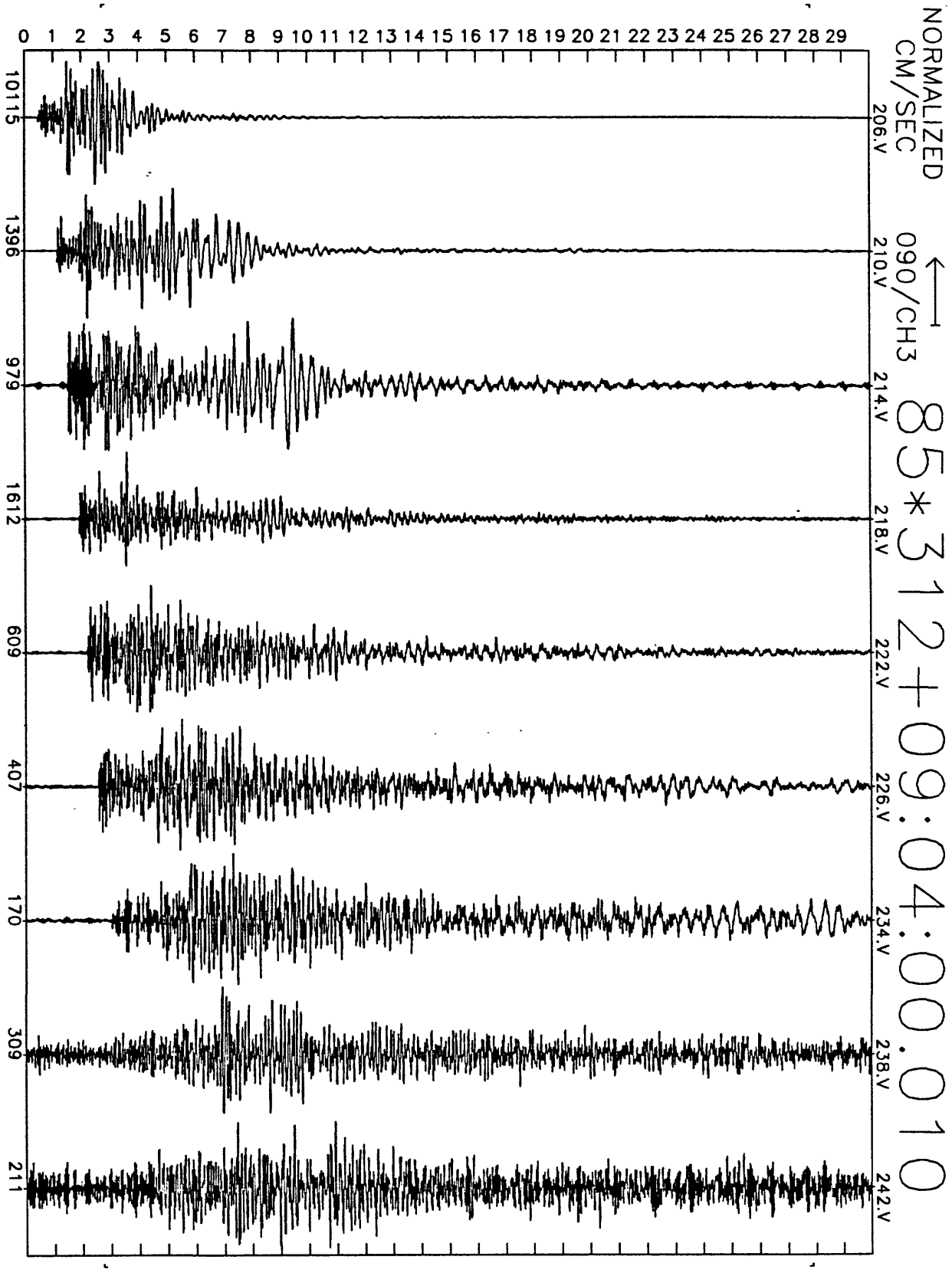

Figure A20(f), shot point 4B: 30 second N110E velocity record. Abscissa is labeled with maximum counts in record (multiply by $\frac{10}{2^{24}-2^{9}} \approx 6 \times 10^{-7}$ to get cm/sec). Times are unreduced beginning at time indicated.

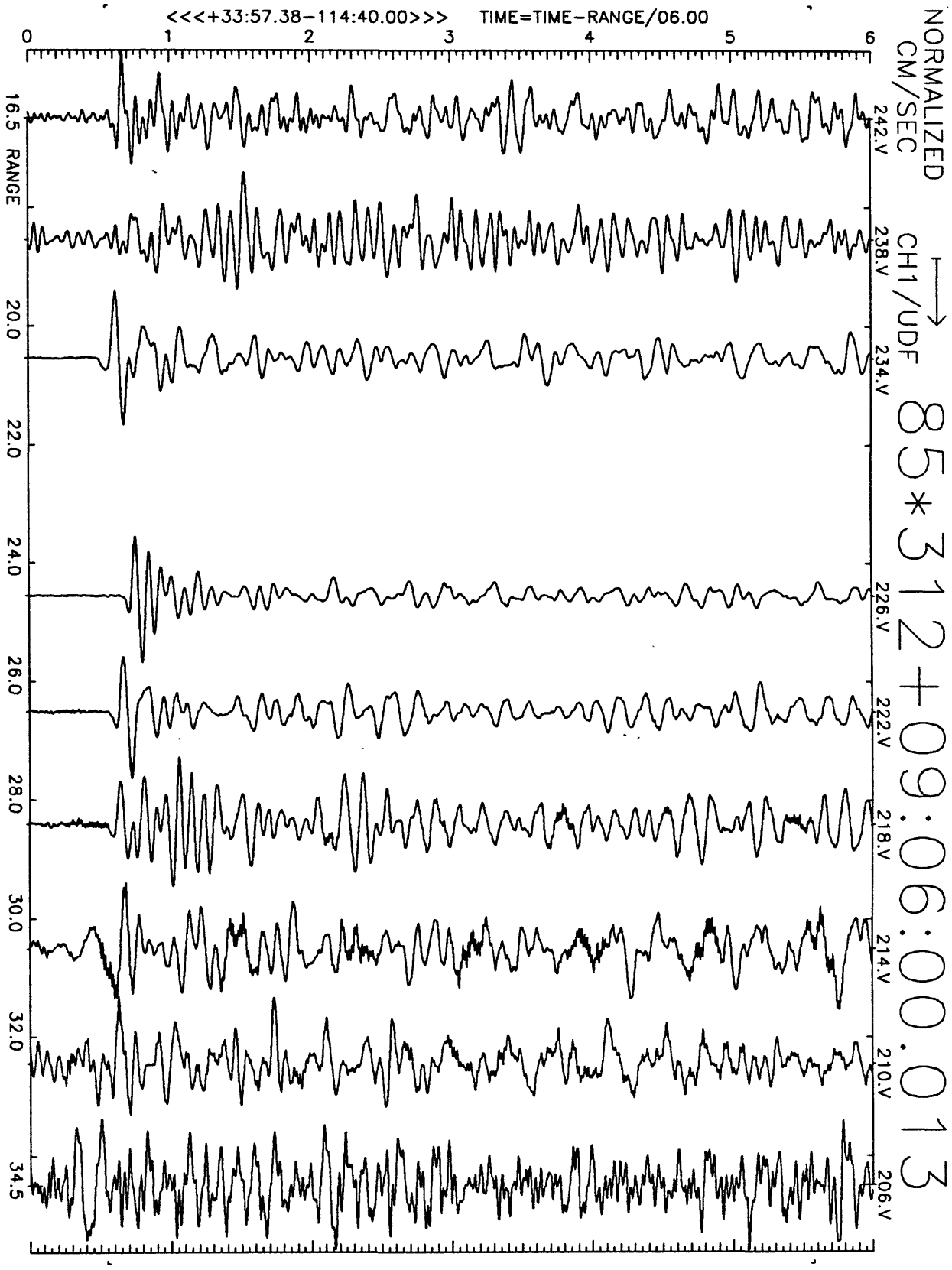

Figure A21(a), shot point 1X: 6 second velocity record. Positive vertical motion is to right. Abscissa is distance to shot point. Top of trace is labeled with station number. Times are reduced by 6 km/sec. Shot time is indicated.

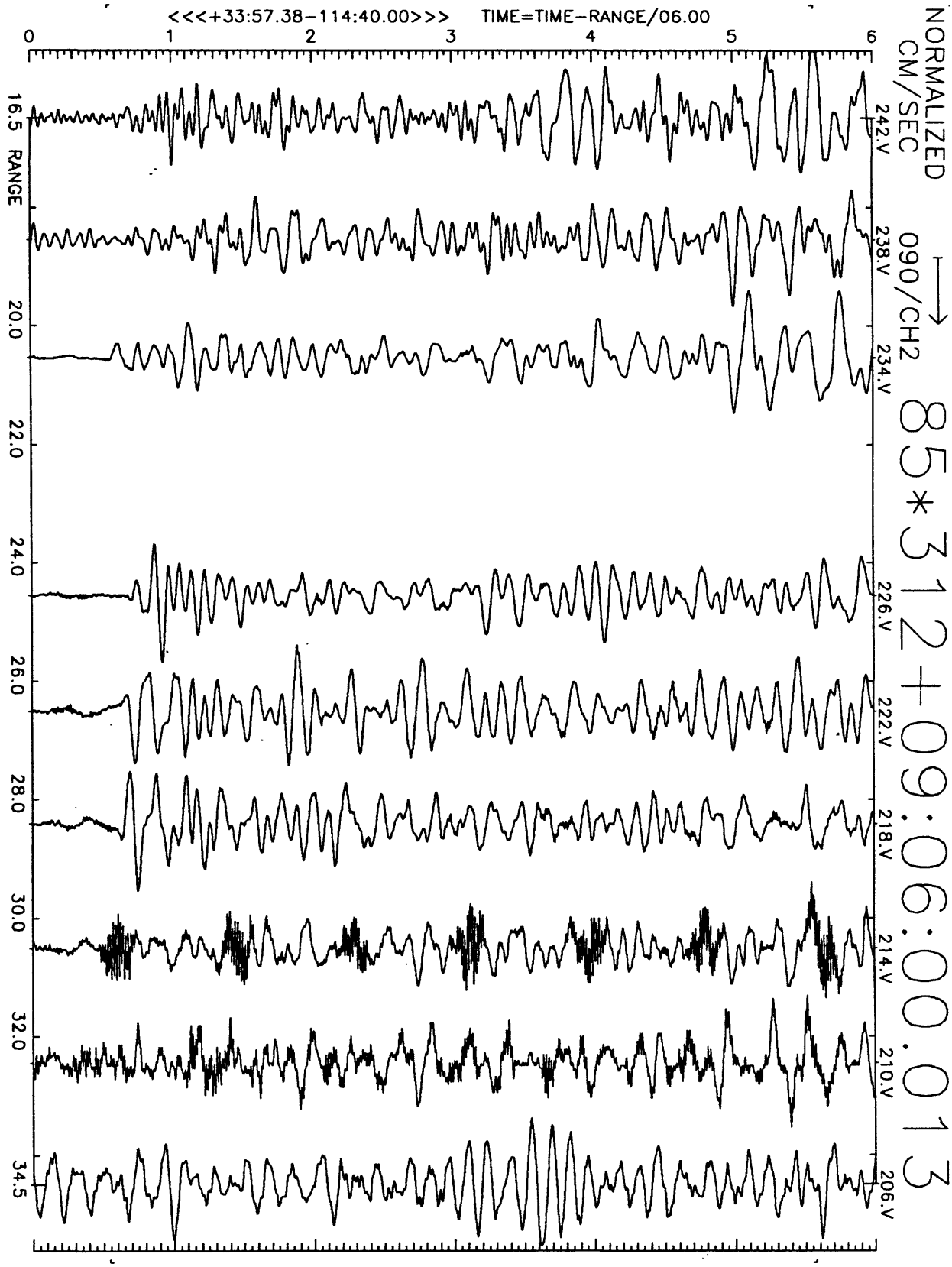

Figure A21(b), shot point 1X: 6 second velocity record. Positive N20E motion is to right. Abscissa is distance to shot point. Top of trace is labeled with station number. Times are reduced by 6 km/sec. Shot time is indicated.

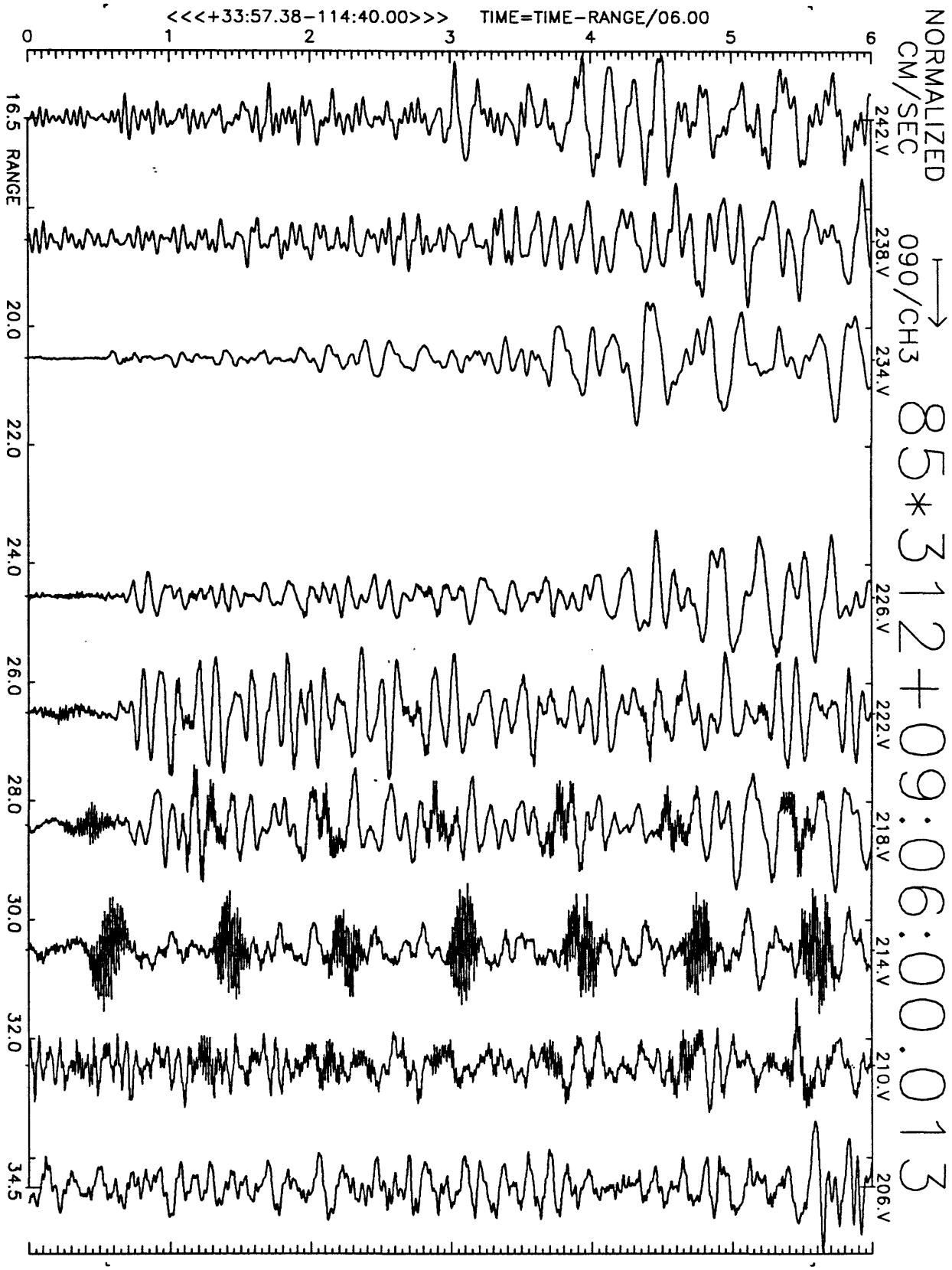

Figure A21(c), shot point 1X: 6 second velocity record. Positive N110E motion is to right. Abscissa is distance to shot point. Top of trace is labeled with station number. Times are reduced by 6 km/sec. Shot time is indicated.

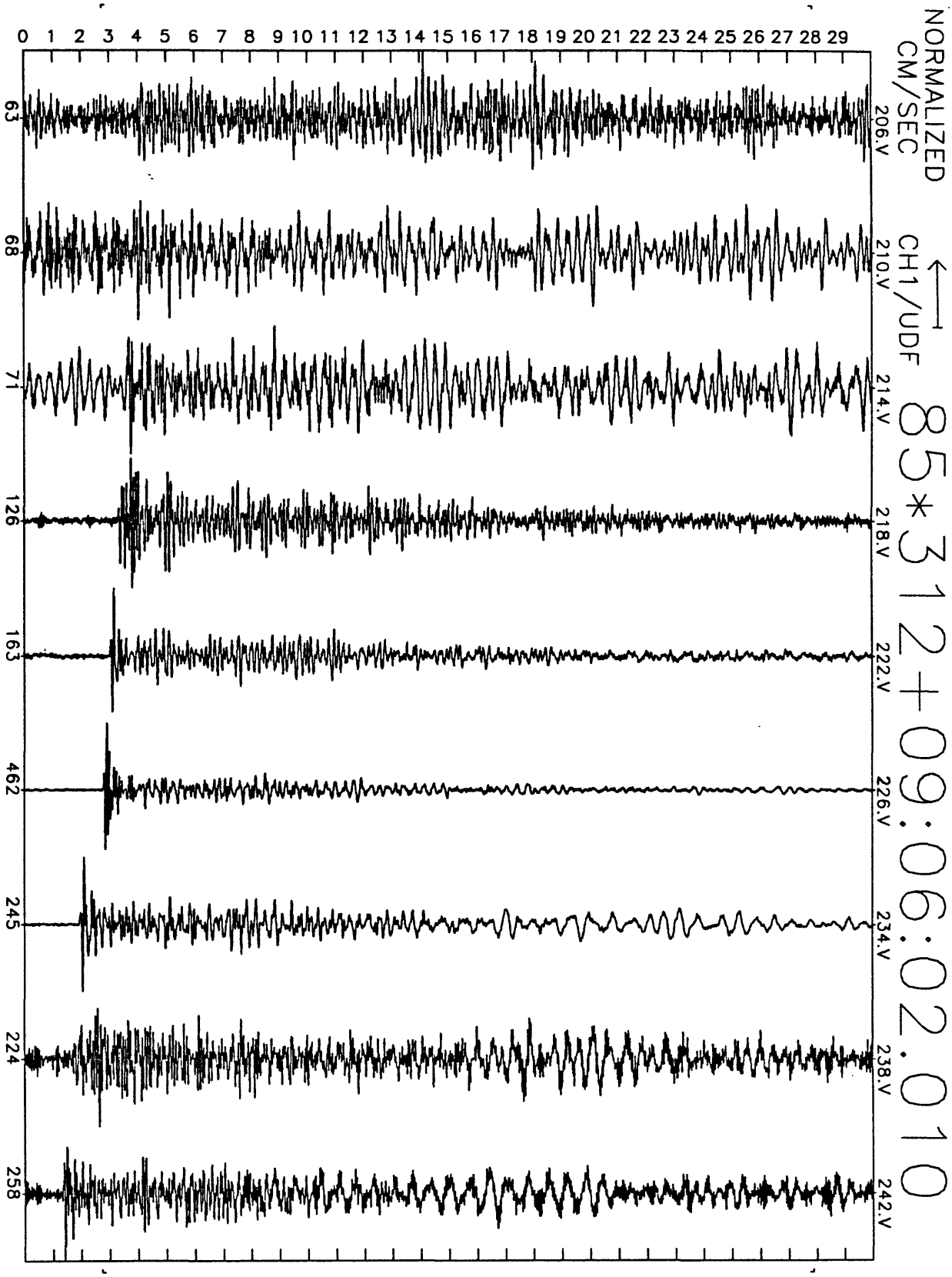

Figure A21(d), shot point 1X: 30 second vertical velocity record. Abscissa is labeled with maximum counts in record (multiply by $\frac{10}{2^{24}-2^9} \approx 6 \times 10^{-7}$ to get cm/sec). Times are unreduced beginning at time indicated.

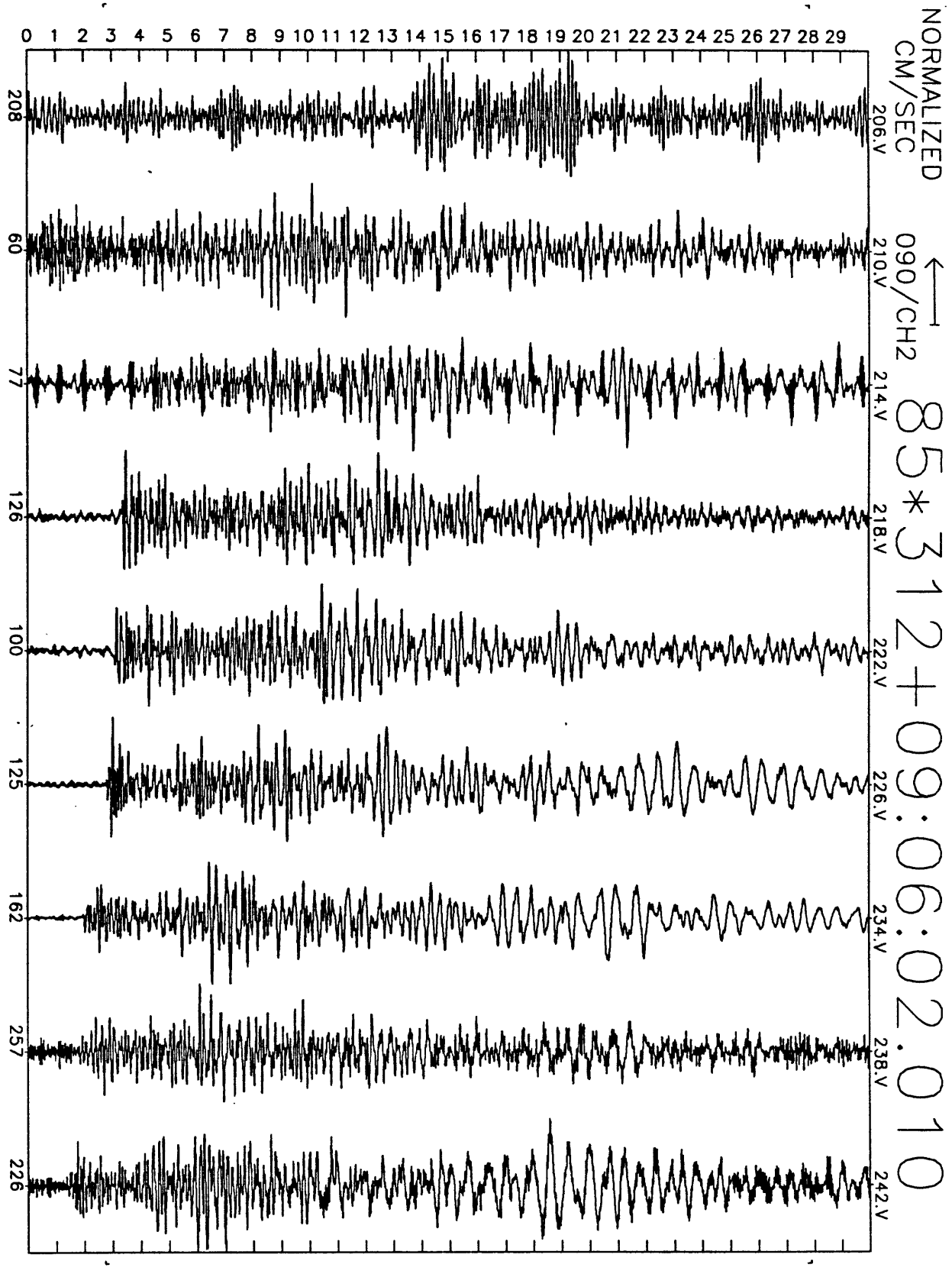

Figure A21(e), shot point 1X: 30 second N20E velocity record. Abscissa is labeled with maximum counts in record (multiply by $\frac{10}{2^{24}-2^0} \approx 6 \times 10^{-7}$ to get cm/sec). Times are unreduced beginning at time indicated.

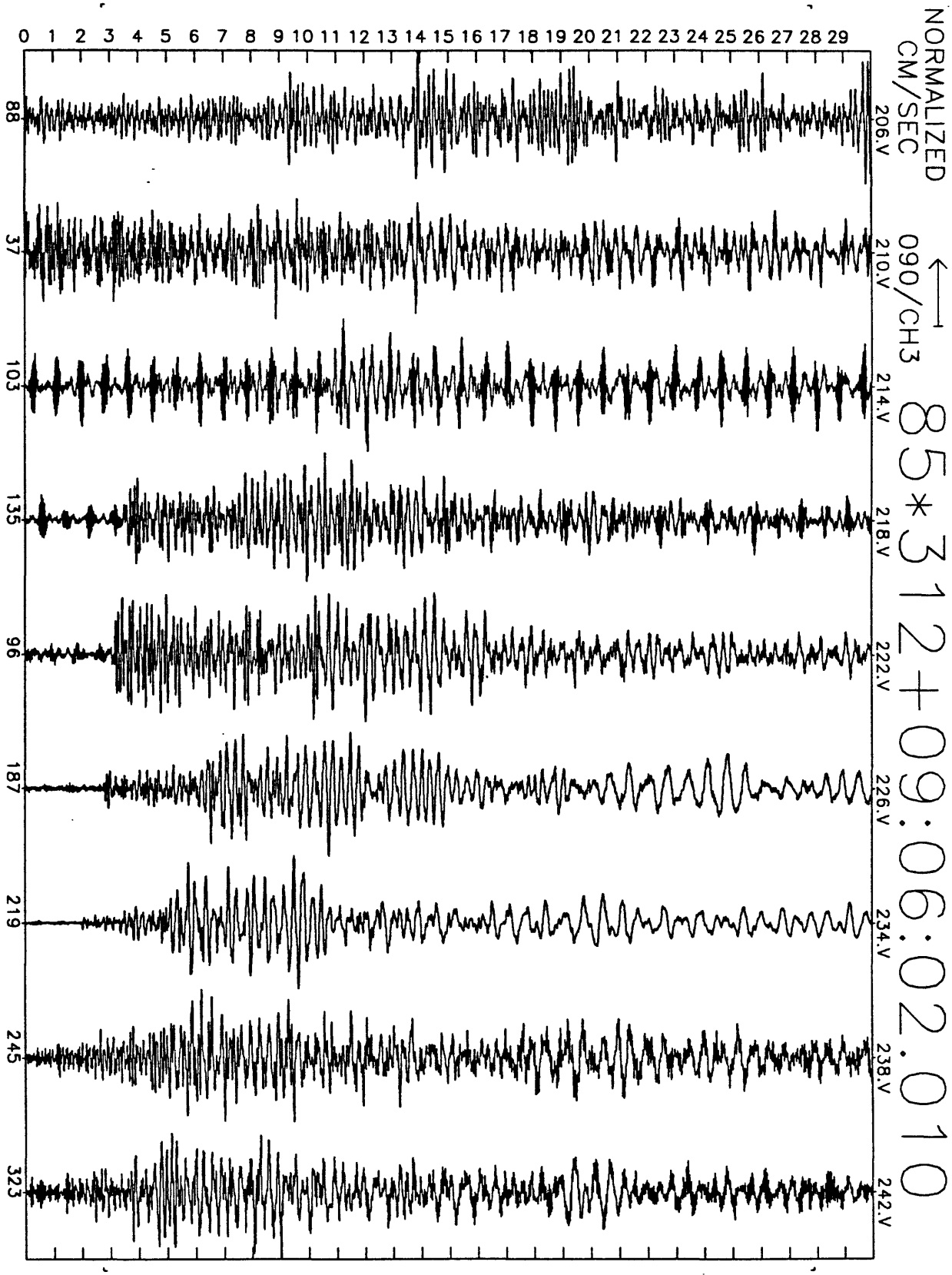

Figure A21(f), shot point 1X: 30 second N110E velocity record. Abscissa is labeled with maximum counts in record (multiply by $\frac{10}{2^{24}-2^{9}} \approx 6 \times 10^{-7}$ to get cm/sec). Times are unreduced beginning at time indicated.

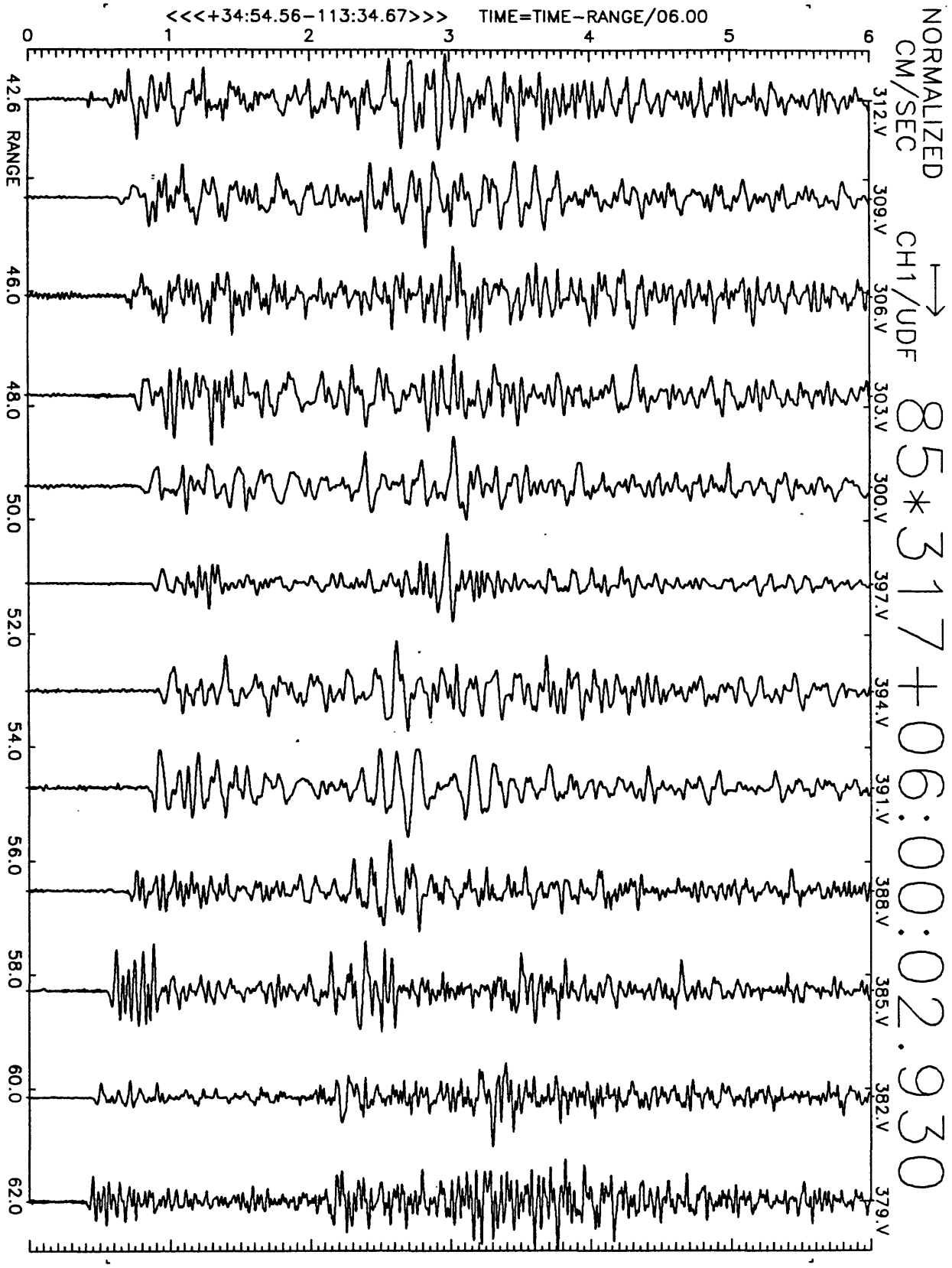

Figure A22(a), shot point 12: 6 second velocity record. Positive vertical motion is to right. Abscissa is distance to shot point. Top of trace is labeled with station number. Times are reduced by 6 km/sec. Shot time is indicated.

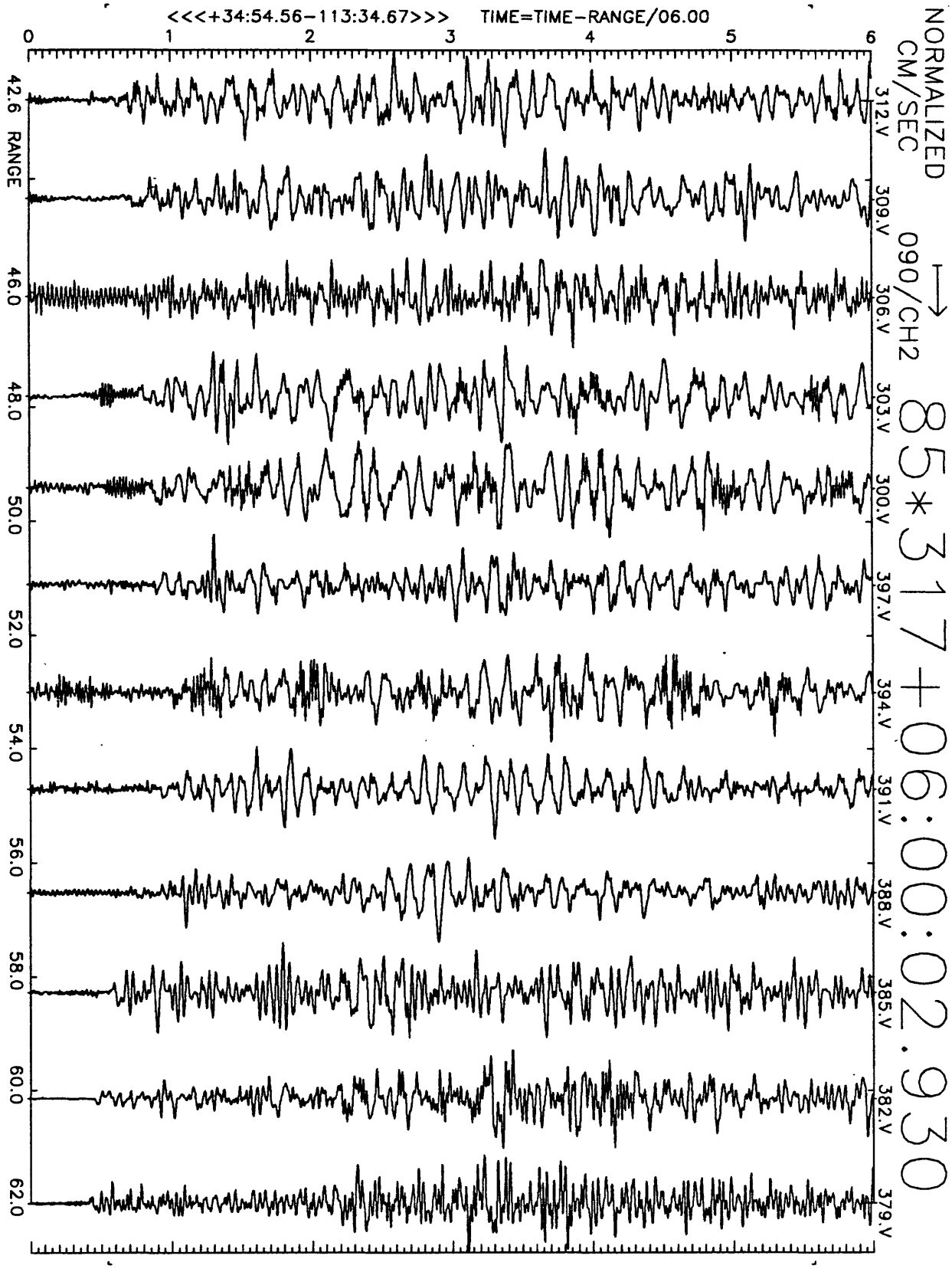

Figure A22(b), shot point 12: 6 second velocity record. Positive N25E motion is to right. Abscissa is distance to shot point. Top of trace is labeled with station number. Times are reduced by 6 km/sec. Shot time is indicated.

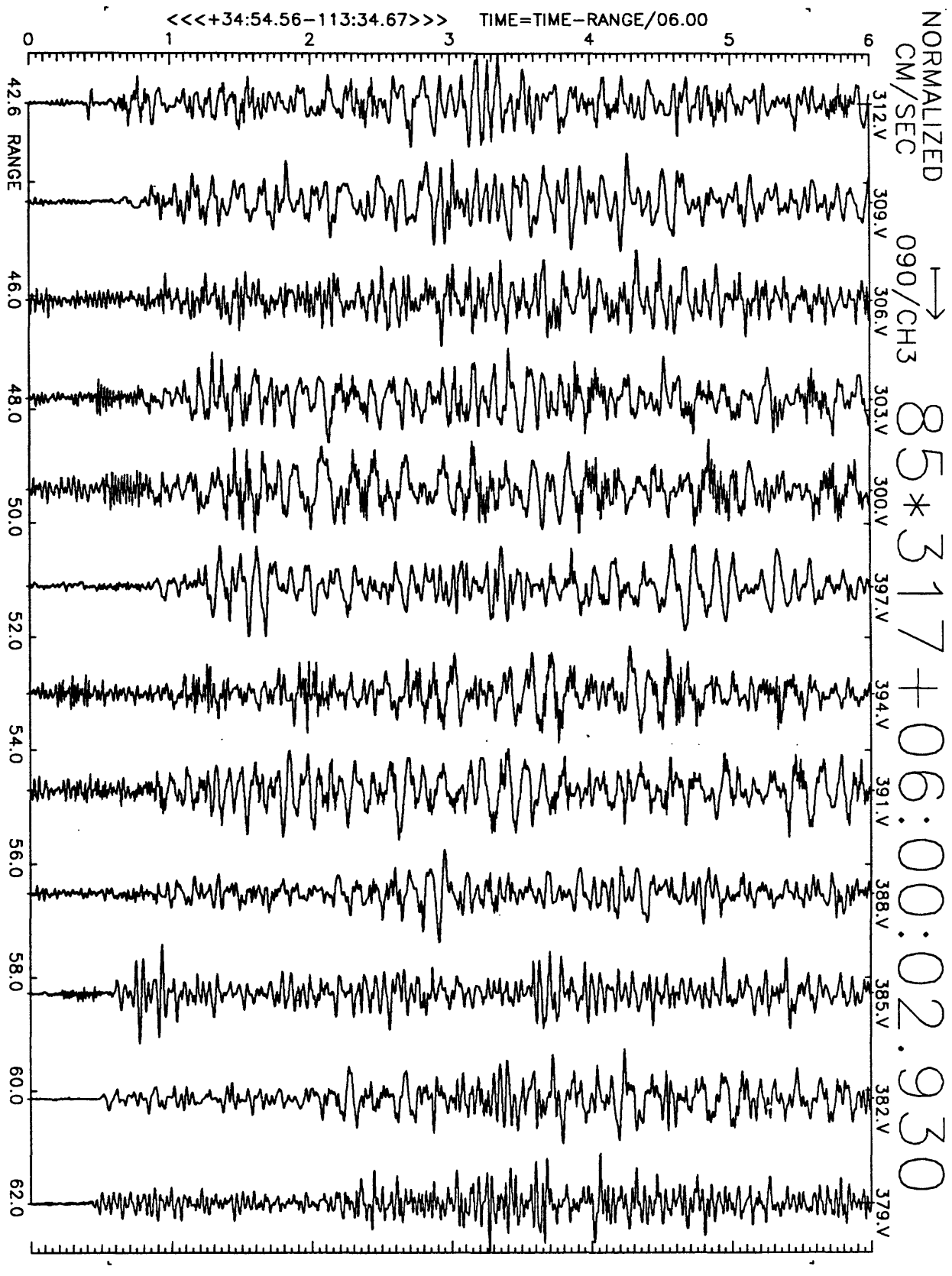

Figure A22(c), shot point 12: 6 second velocity record. Positive N115E motion is to right. Abscissa is distance to shot point. Top of trace is labeled with station number. Times are reduced by 6 km/sec. Shot time is indicated.

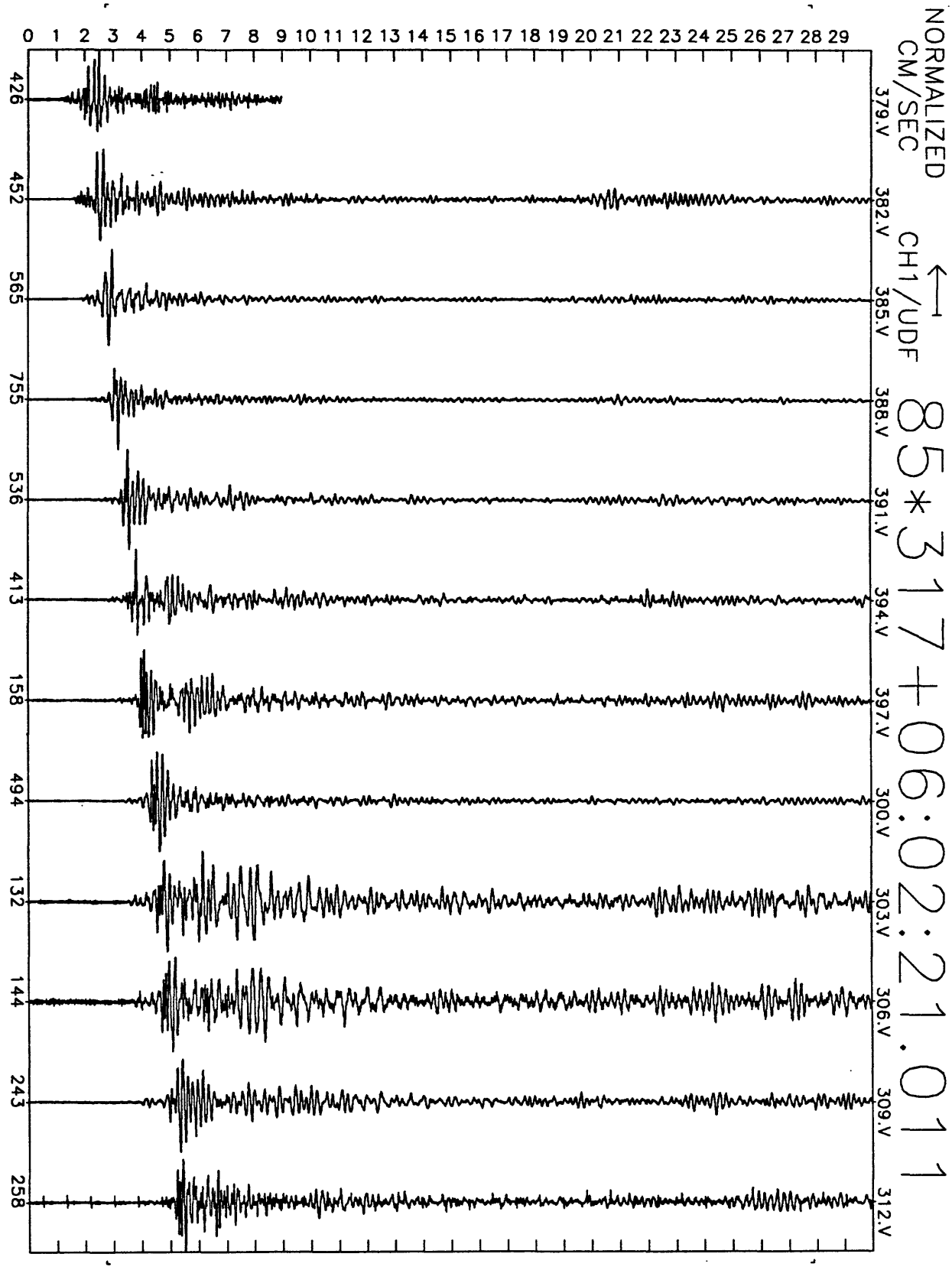

Figure A22(d), shot point 12: 30 second vertical velocity record. Abscissa is labeled with maximum counts in record (multiply by $\frac{10}{2^{24}-2^5} \approx 6 \times 10^{-7}$ to get cm/sec). Times are unreduced beginning at time indicated.

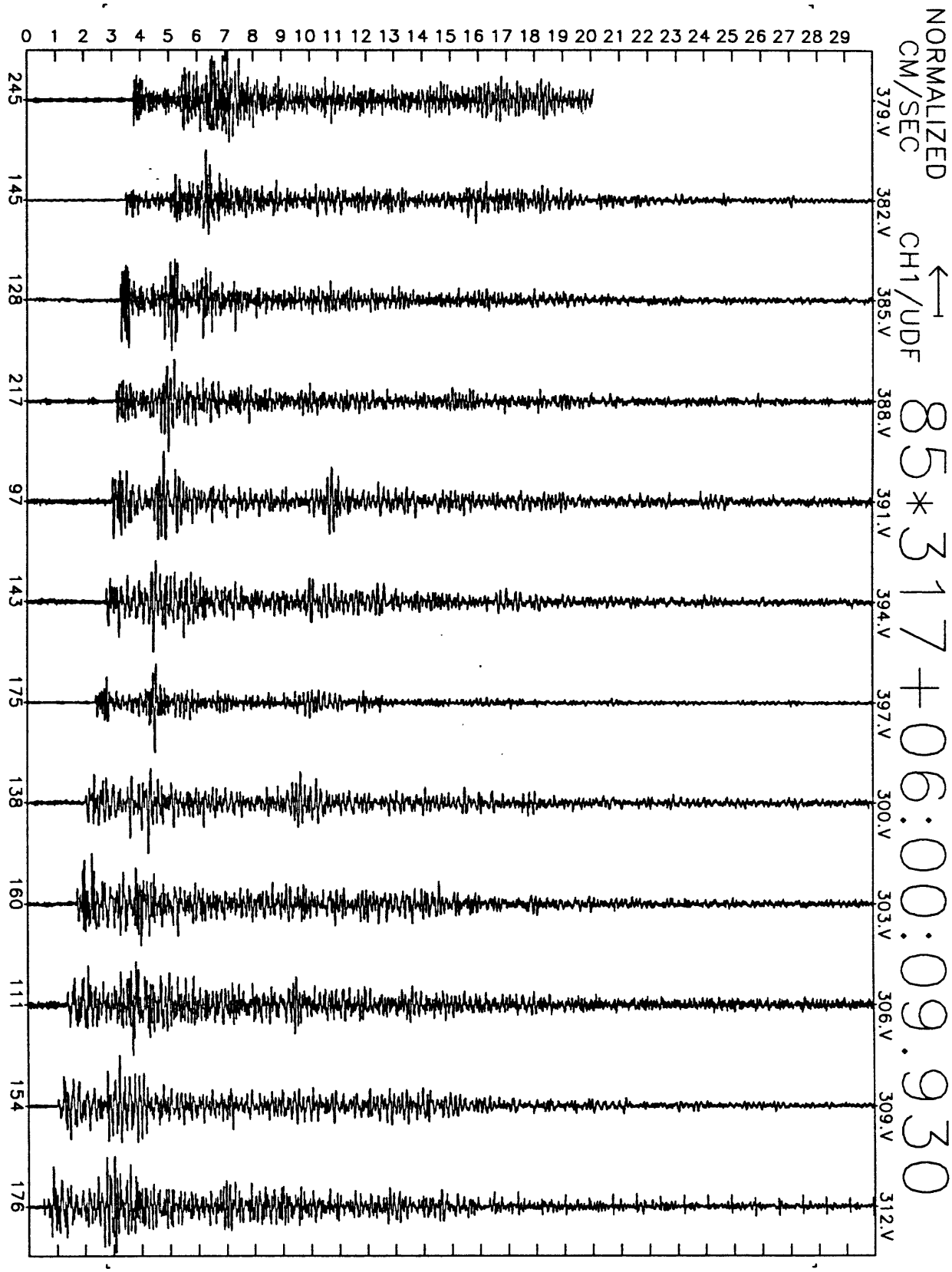

Figure A22(e), shot point 12: 30 second N25E velocity record. Abscissa is labeled with maximum counts in record (multiply by $\frac{10}{2^{24}-2^5} \approx 6 \times 10^{-7}$ to get cm/sec). Times are unreduced beginning at time indicated.

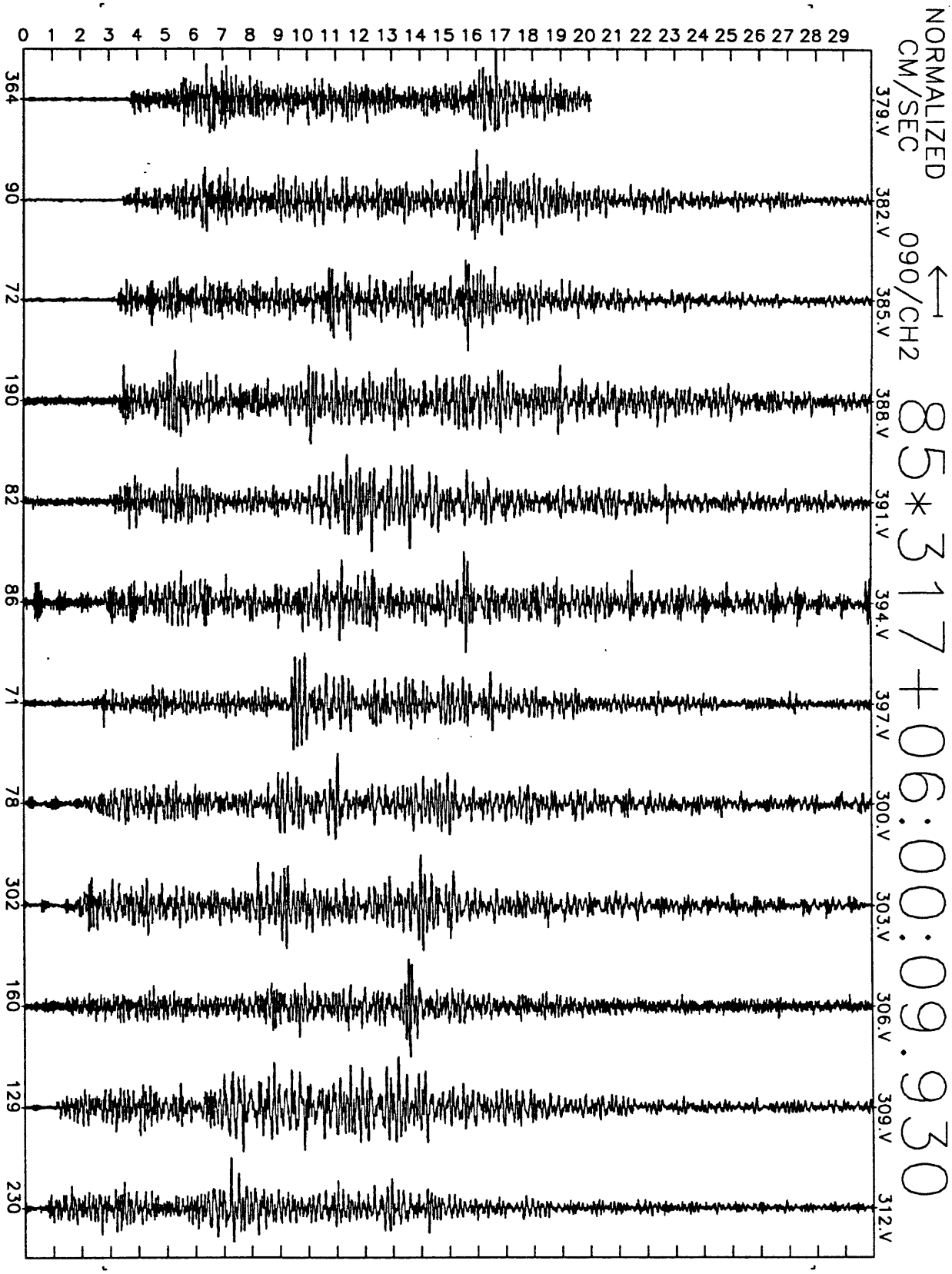

Figure A22(f), shot point 12: 30 second N115E velocity record. Abscissa is labeled with maximum counts in record (multiply by $\frac{10}{2^{24}-2^0} \approx 6 \times 10^{-7}$ to get cm/sec). Times are unreduced beginning at time indicated.

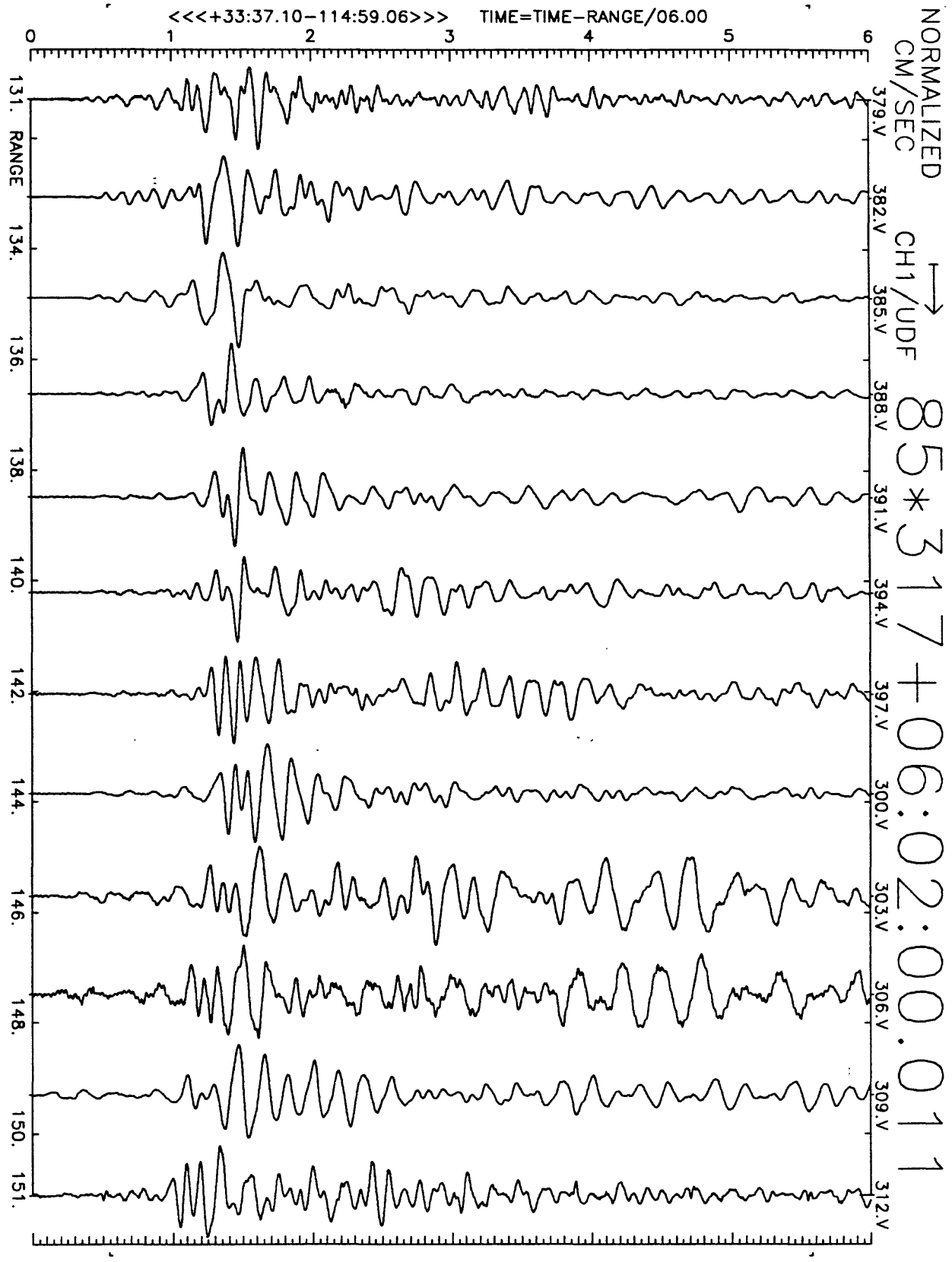

Figure A23(a), shot point 14: 6 second velocity record. Positive vertical motion is to right. Abscissa is distance to shot point. Top of trace is labeled with station number. Times are reduced by 6 km/sec. Shot time is indicated.

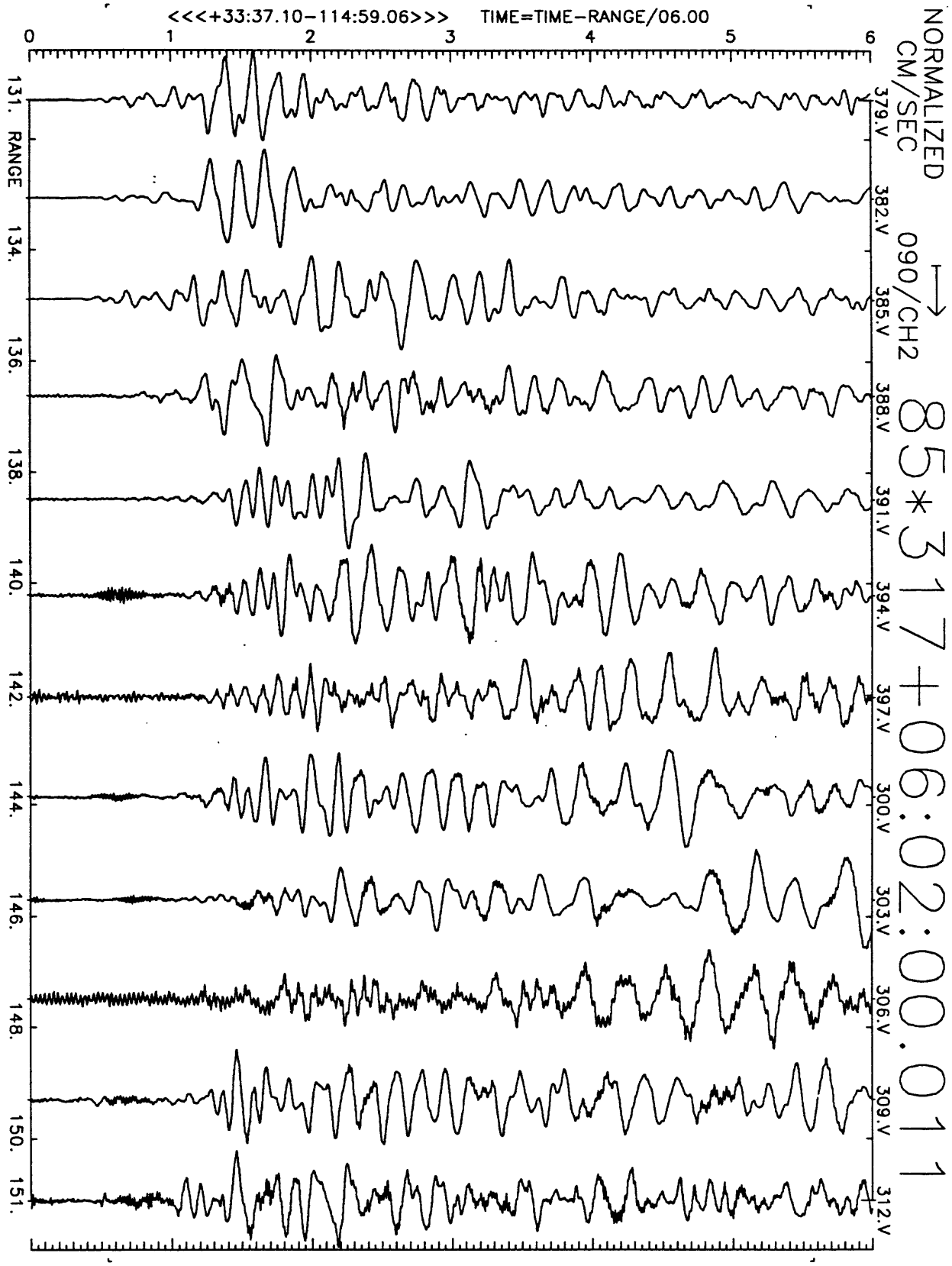

Figure A23(b), shot point 14: 6 second velocity record. Positive N25E motion is to right. Abscissa is distance to shot point. Top of trace is labeled with station number. Times are reduced by 6 km/sec. Shot time is indicated.

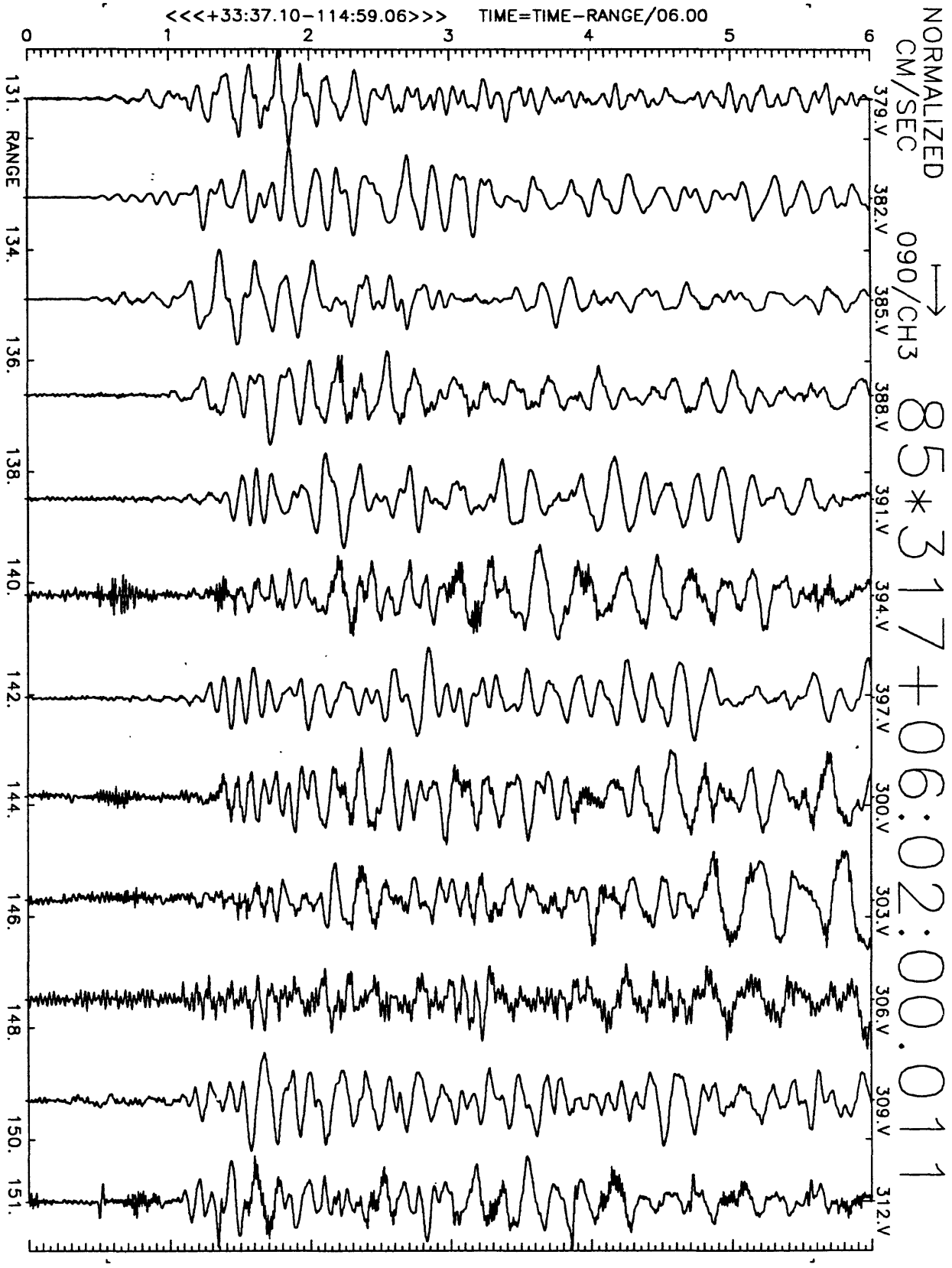

Figure A23(c), shot point 14: 6 second velocity record. Positive N115E motion is to right. Abscissa is distance to shot point. Top of trace is labeled with station number. Times are reduced by 6 km/sec. Shot time is indicated.

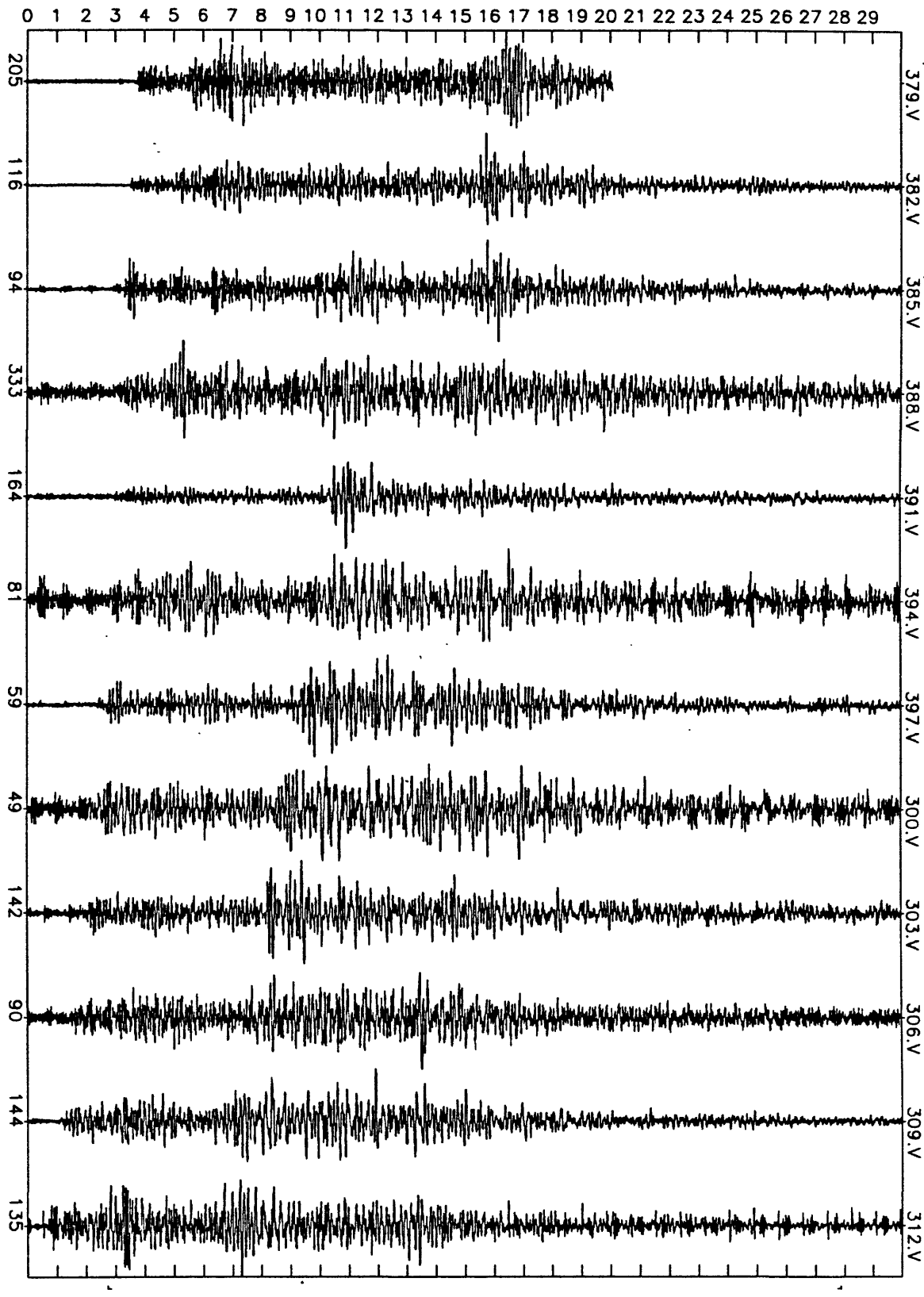

Figure A23(d), shot point 14: 30 second vertical velocity record. Abscissa is labeled with maximum counts in record (multiply by $\frac{10}{2^{24}-2^9} \approx 6 \times 10^{-7}$ to get cm/sec). Times are unreduced beginning at time indicated.

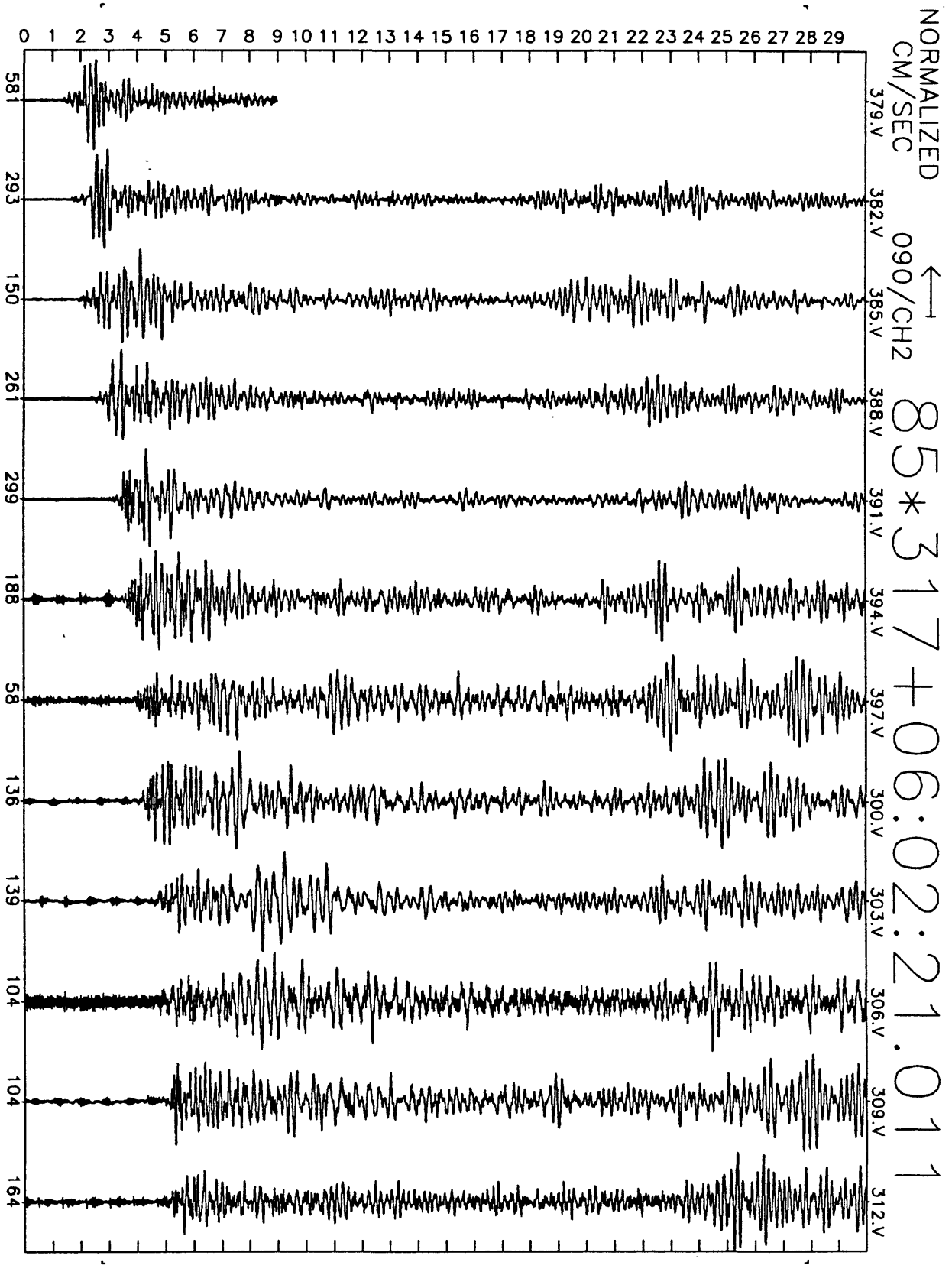

Figure A23(e), shot point 14: 30 second N25E velocity record. Abscissa is labeled with maximum counts in record (multiply by $\frac{10}{2^{24}-2^{5}} \approx 6 \times 10^{-7}$ to get cm/sec). Times are unreduced beginning at time indicated.

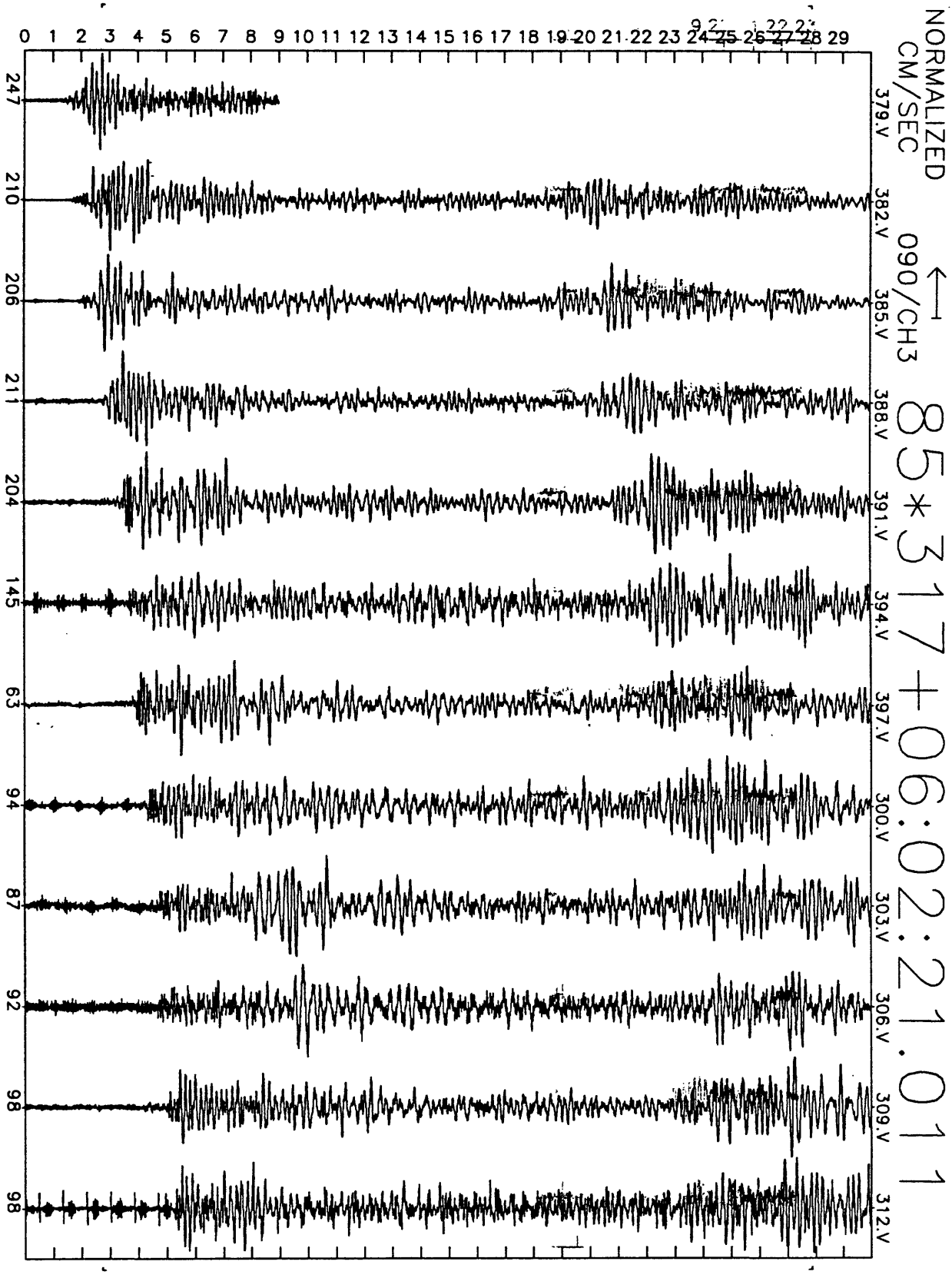

Figure A23(f), shot point 14: 30 second N115E velocity record. Abscissa is labeled with maximum counts in record (multiply by $\frac{10}{2^{24}-2^5} \approx 6 \times 10^{-7}$ to get cm/sec). Times are unreduced beginning at time indicated.

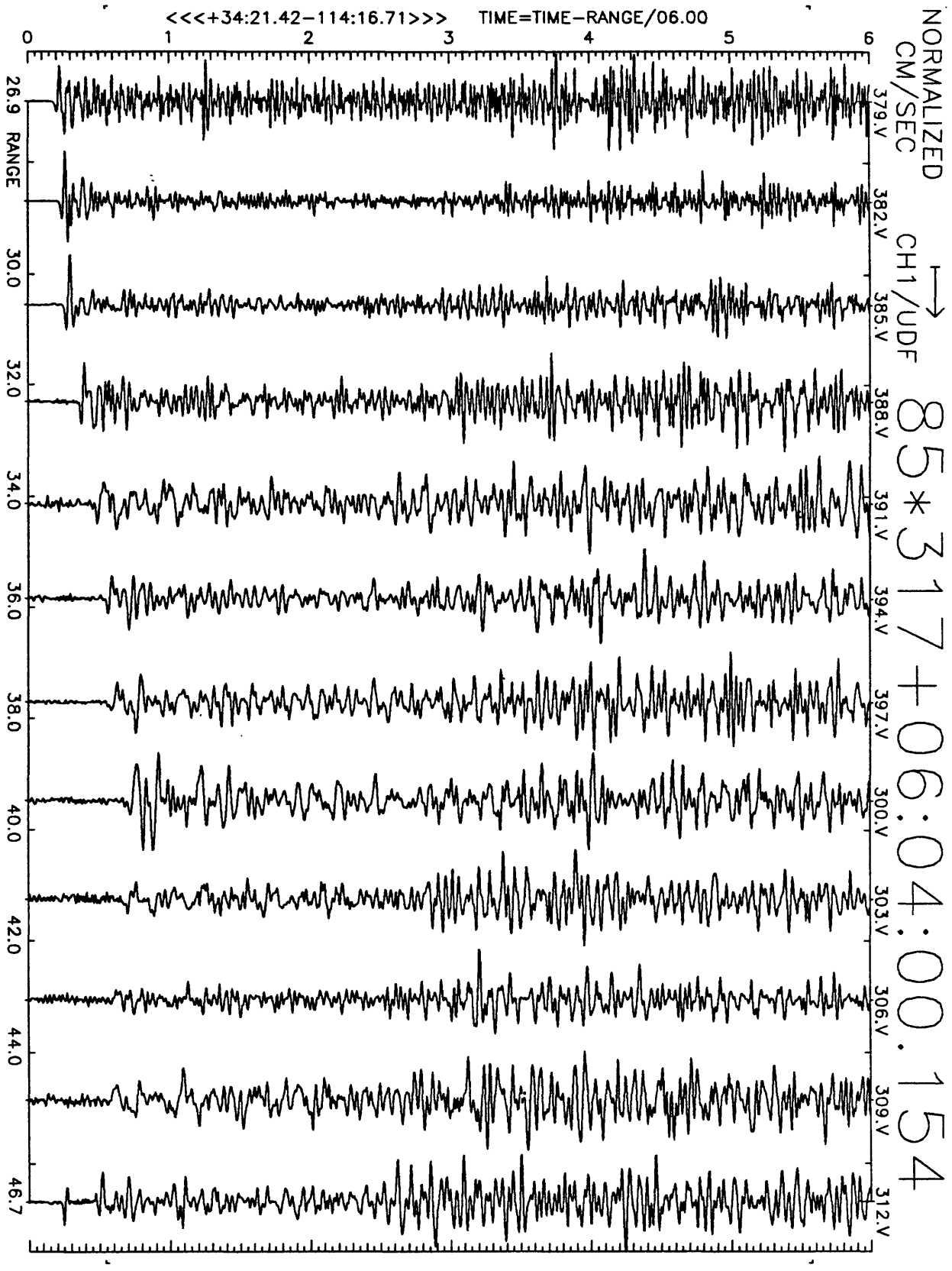

Figure A24(a), shot point 5: 6 second velocity record. Positive vertical motion is to right. Abscissa is distance to shot point. Top of trace is labeled with station number. Times are reduced by 6 km/sec. Shot time is indicated.

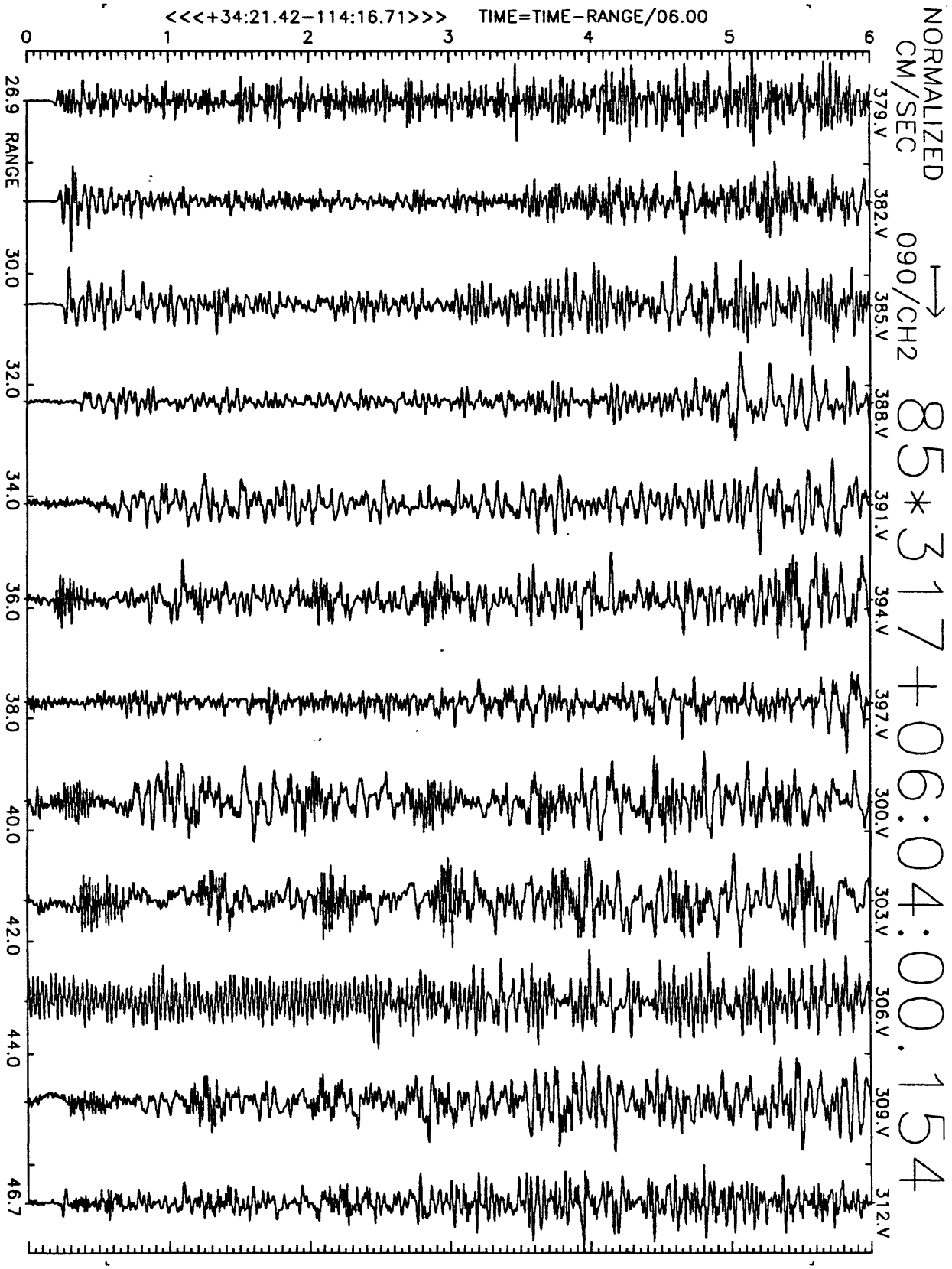

Figure A24(b), shot point 5: 6 second velocity record. Positive N25E motion is to right. Abscissa is distance to shot point. Top of trace is labeled with station number. Times are reduced by 6 km/sec. Shot time is indicated.

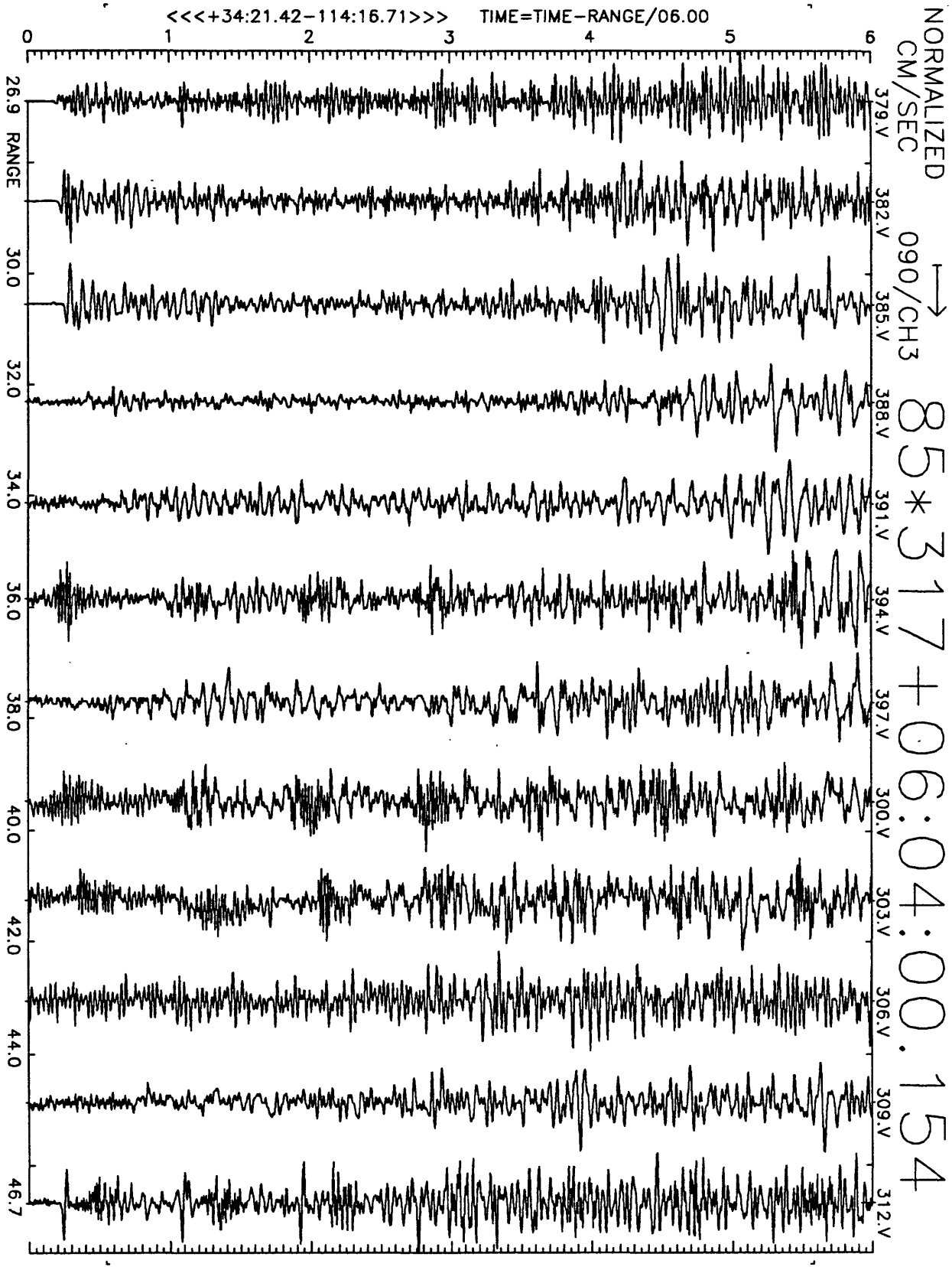

Figure A24(c), shot point 5: 6 second velocity record. Positive N115E motion is to right. Abscissa is distance to shot point. Top of trace is labeled with station number. Times are reduced by 6 km/sec. Shot time is indicated.

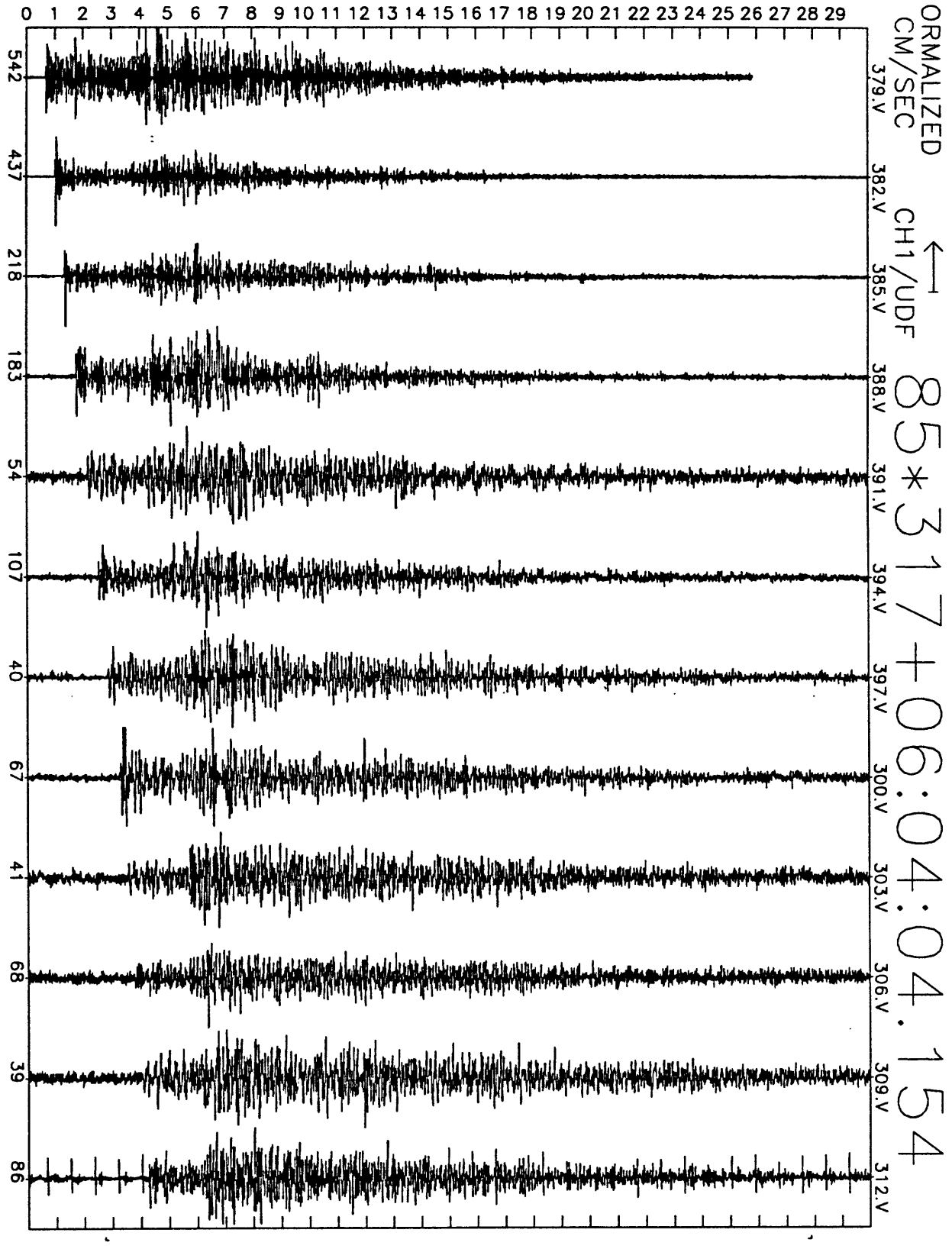

Figure A24(d), shot point 5: 30 second vertical velocity record. Abscissa is labeled with maximum counts in record (multiply by $\frac{10}{2^{24}-2^5} \approx 6 \times 10^{-7}$ to get cm/sec). Times are unreduced beginning at time indicated.

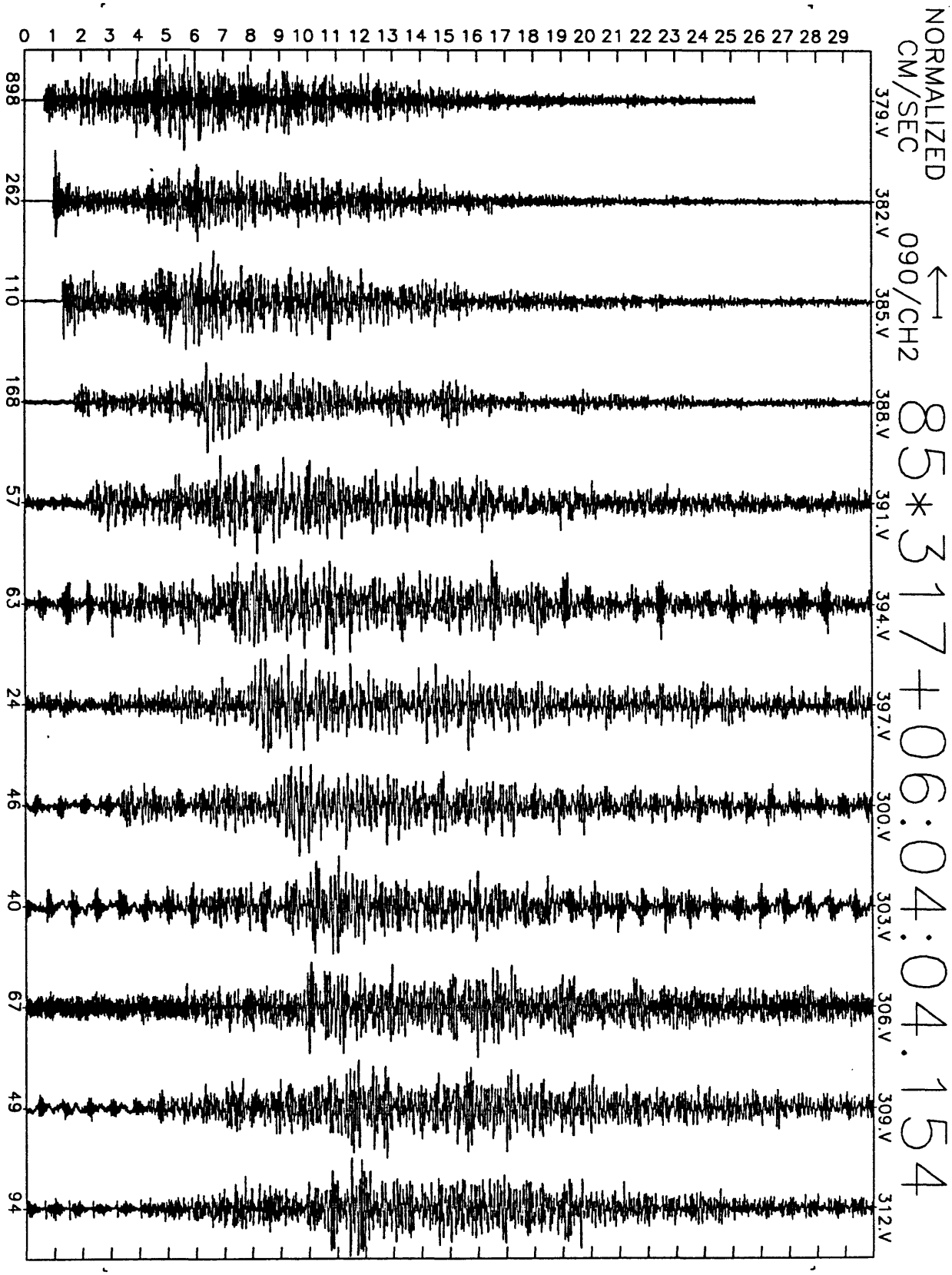

Figure A24(e), shot point 5: 30 second N25E velocity record. Abscissa is labeled with maximum counts in record (multiply by $\frac{10}{2^{24}-2^5} \approx 6 \times 10^{-7}$ to get cm/sec). Times are unreduced beginning at time indicated.

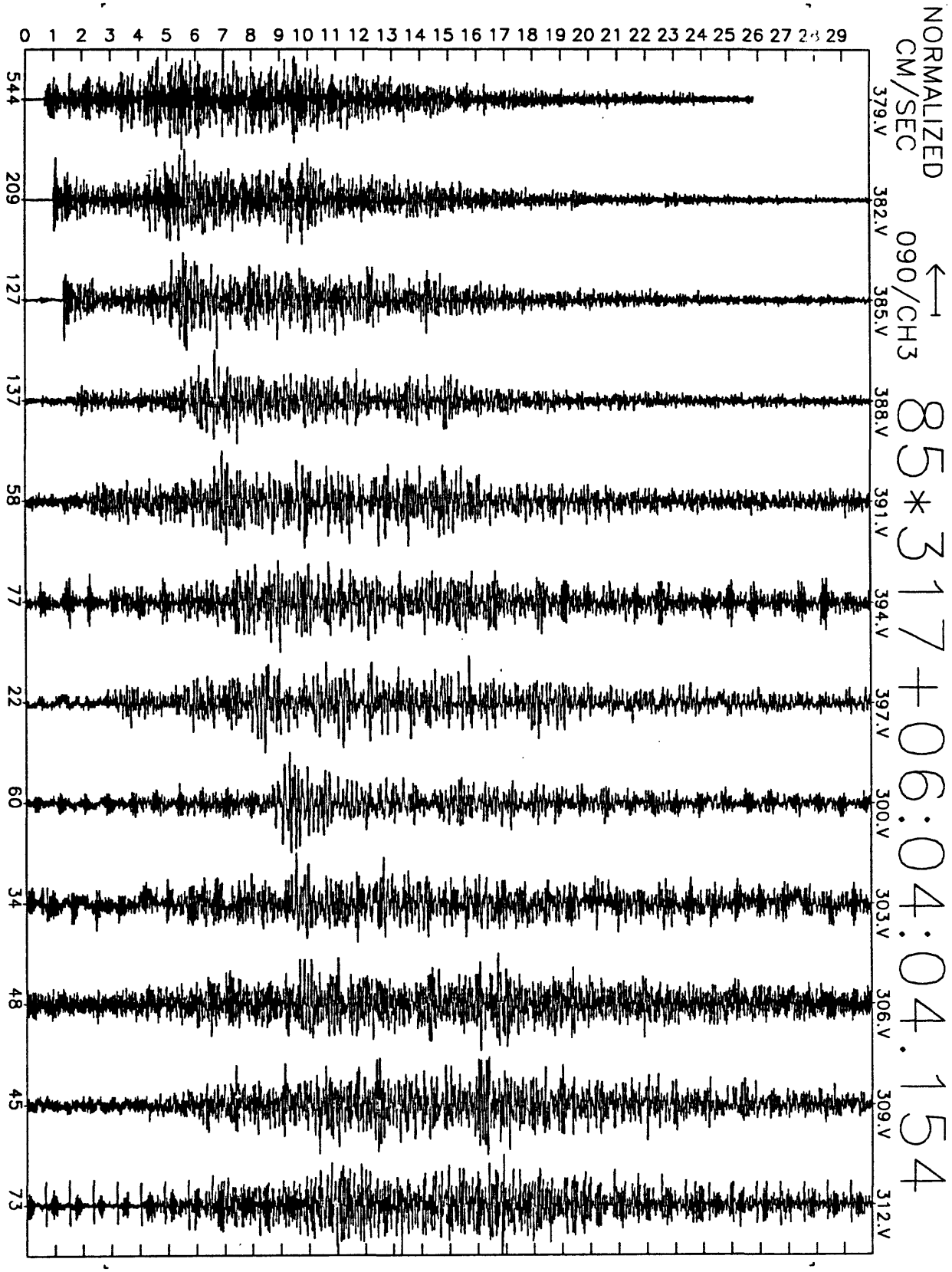

Figure A24(f), shot point 5: 30 second N115E velocity record. Abscissa is labeled with maximum counts in record (multiply by $\frac{10}{2^{24}-2^5} \approx 6 \times 10^{-7}$ to get cm/sec). Times are unreduced beginning at time indicated.

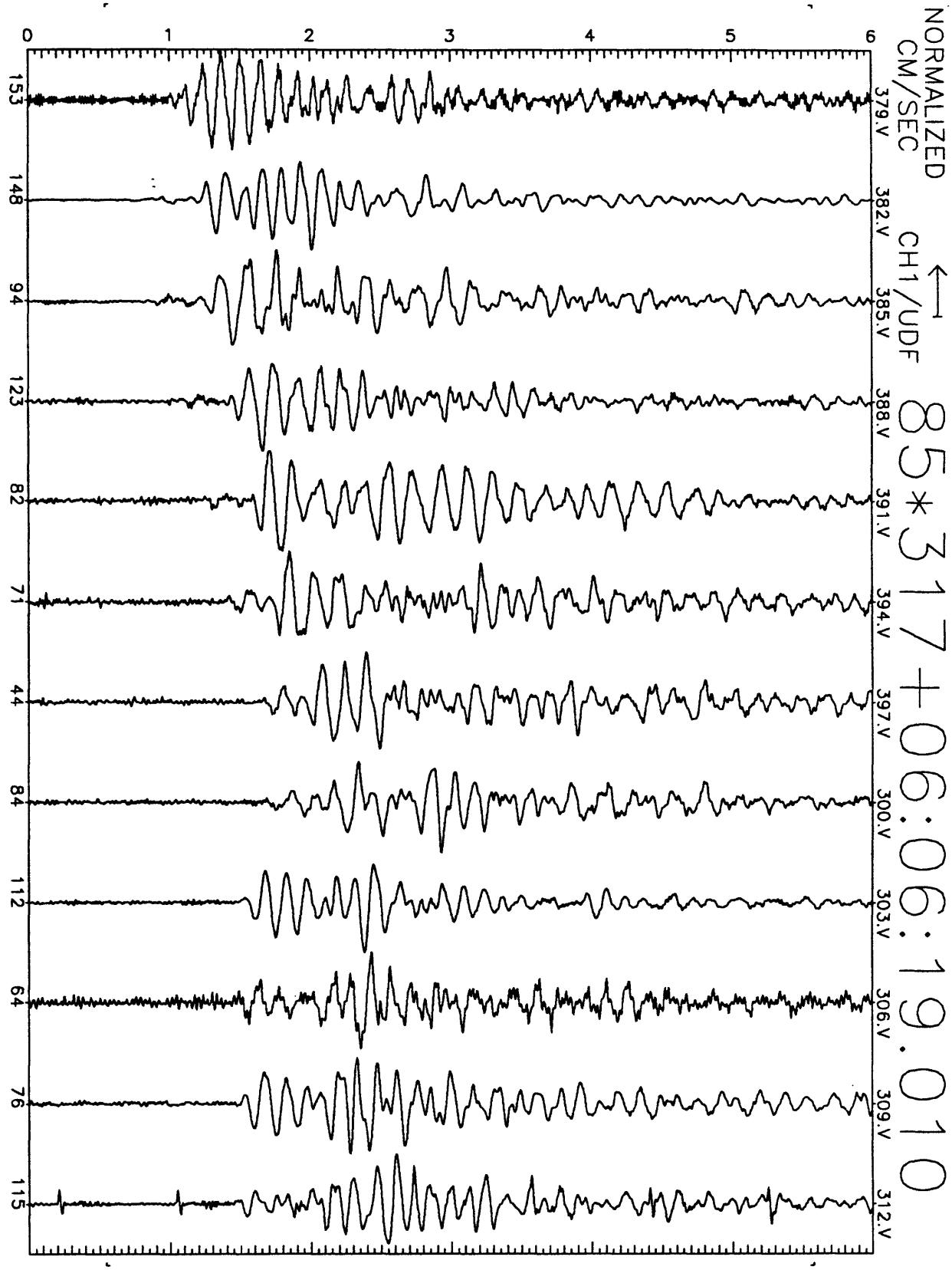

Figure A25(a), shot point 11 (fan shot): 6 second velocity record. Positive vertical motion is to left. Abscissa is labeled with maximum counts in record. Distances are $\sim 117.5 \pm 1.5 km$. Times are unreduced beginning at shot time + 19 seconds.

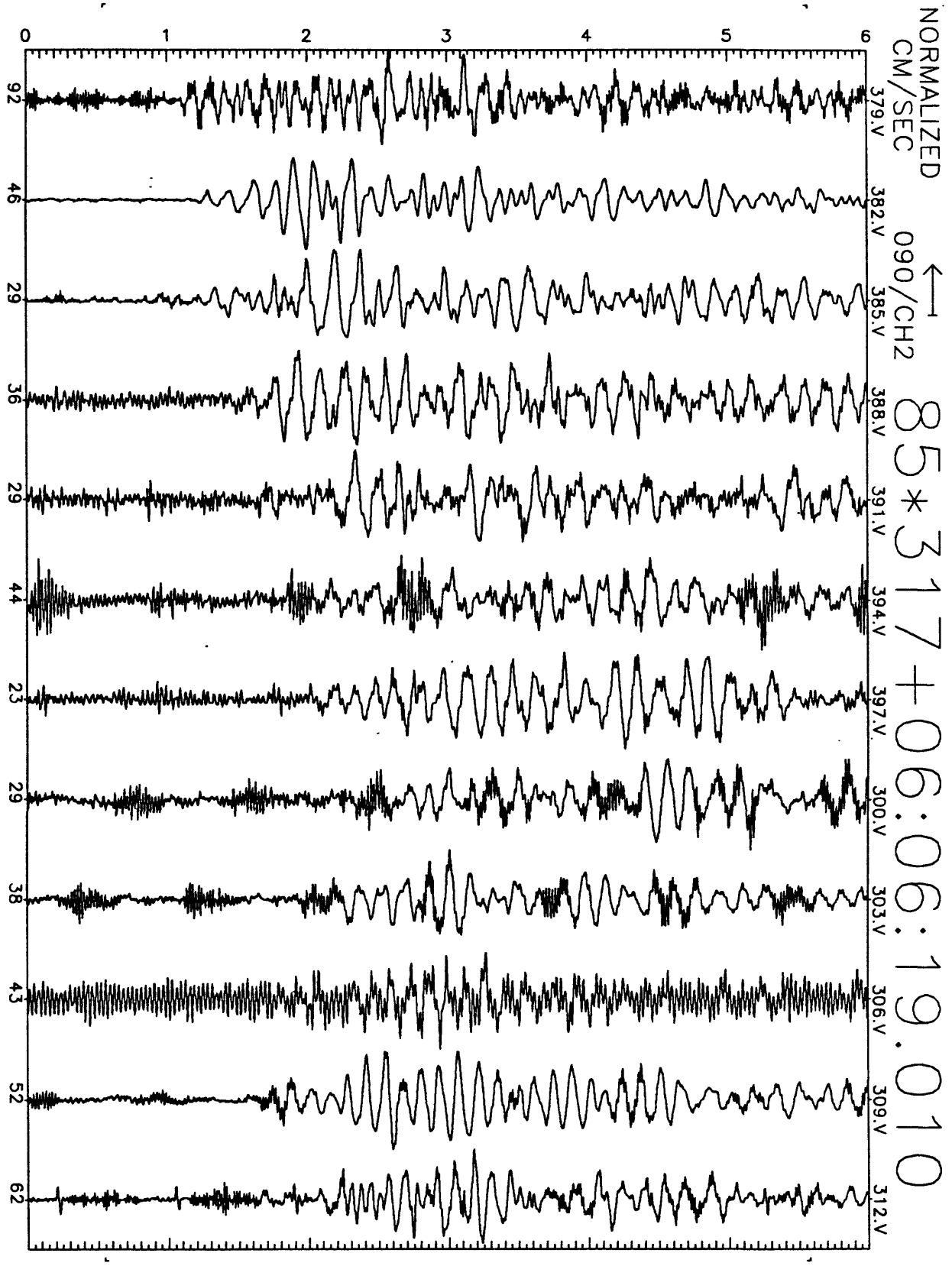

Figure A25(b), shot point 11 (fan shot): 6 second velocity record. Positive N25E motion is to left. Abscissa is labeled with maximum counts in record. Distances are $\sim 117.5 \pm 1.5 km$. Times are unreduced beginning at shot time + 19 seconds.

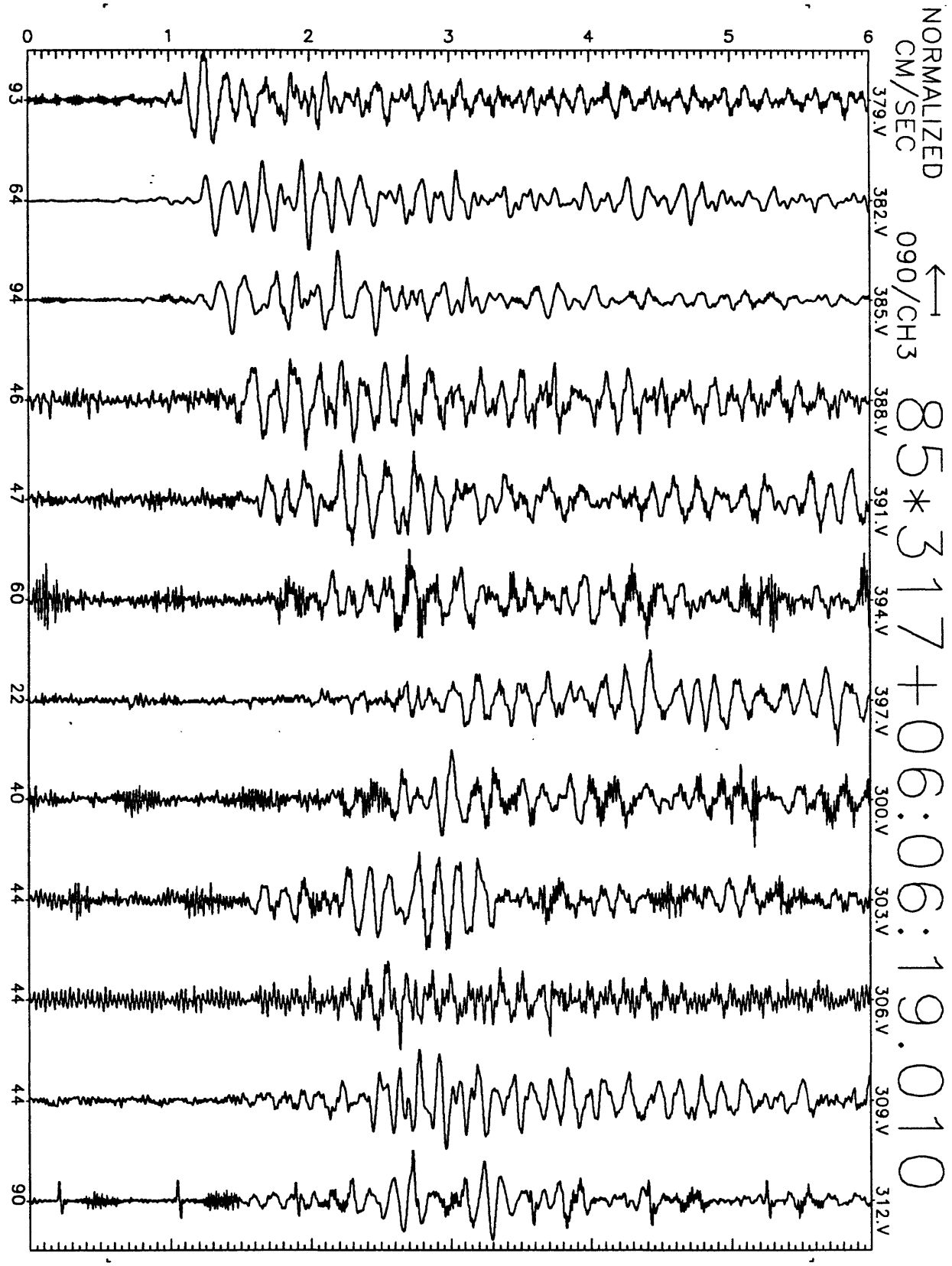

Figure A25(c), shot point 11 (fan shot): 6 second velocity record. Positive N115E motion is to left. Abscissa is labeled with maximum counts in record. Distances are $\sim 117.5 \pm 1.5 km$. Times are unreduced beginning at shot time + 19 seconds.

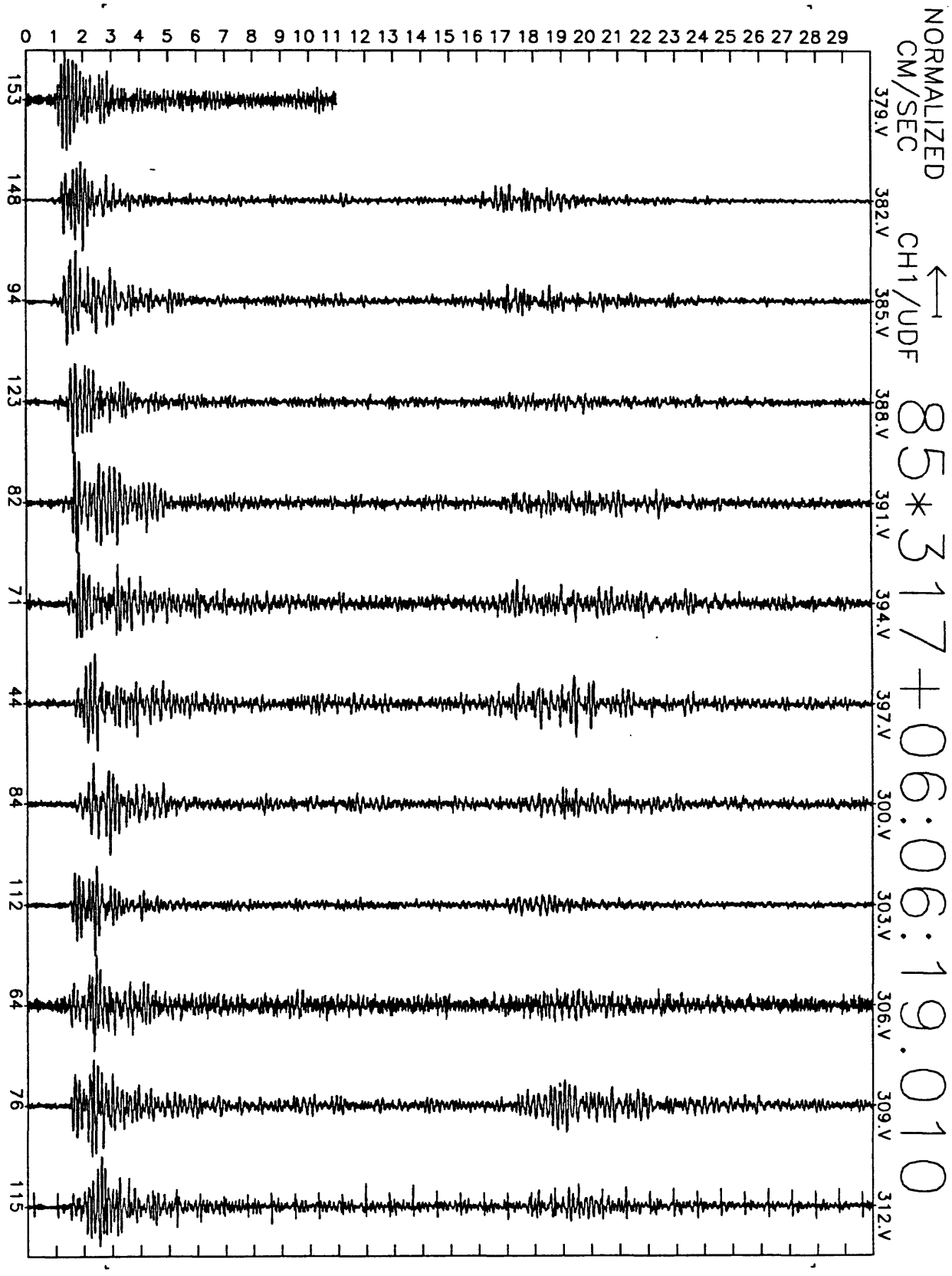

Figure A25(d), shot point 11: 30 second vertical velocity record. Abscissa is labeled with maximum counts in record (multiply by $\frac{10}{2^{24}-2^5} \approx 6 \times 10^{-7}$ to get cm/sec). Times are unreduced beginning at time indicated.

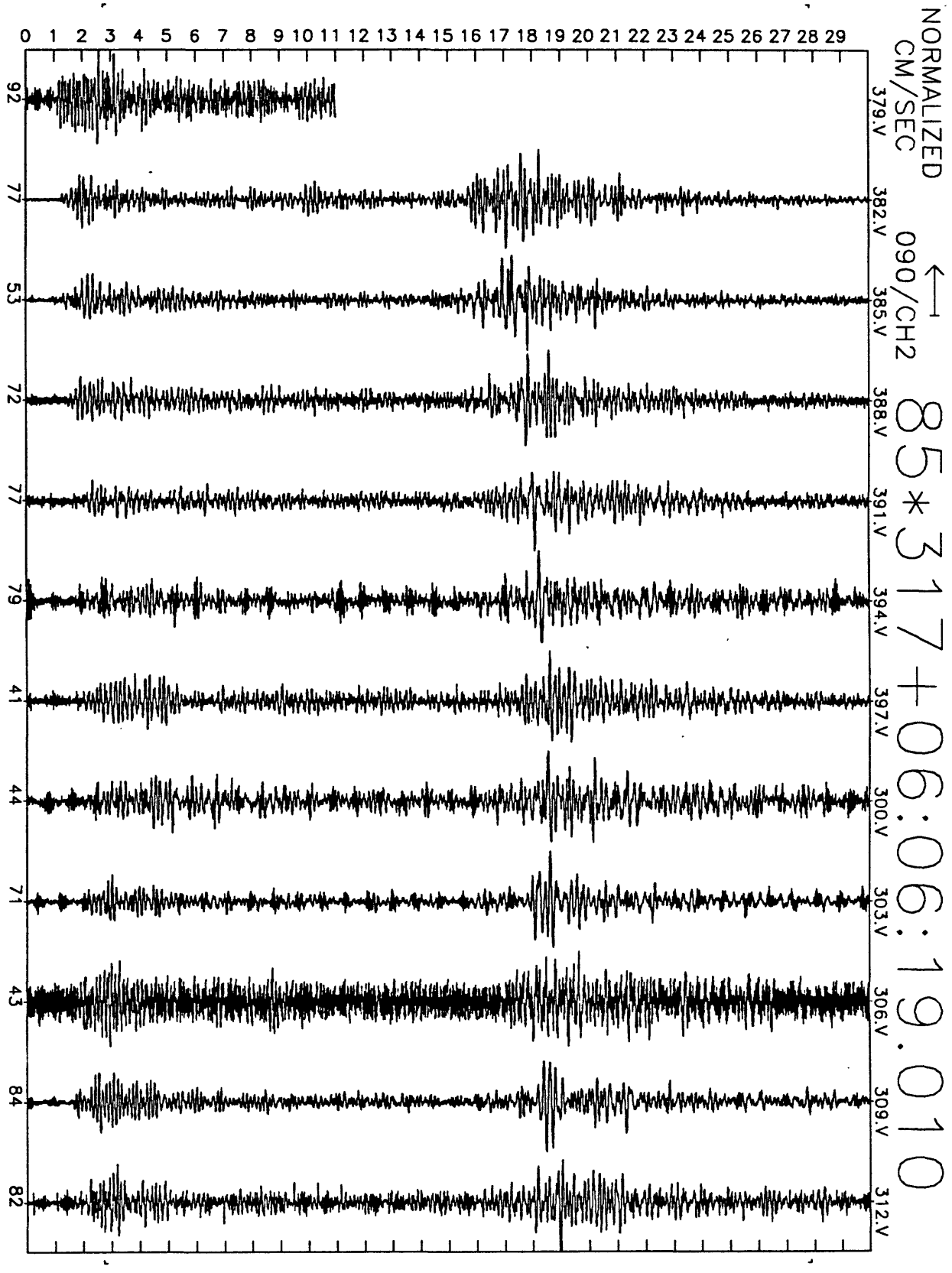

Figure A25(e), shot point 11: 30 second N25E velocity record. Abscissa is labeled with maximum counts in record (multiply by $\frac{10}{2^{24}-2^5} \approx 6 \times 10^{-7}$ to get cm/sec). Times are unreduced beginning at time indicated.

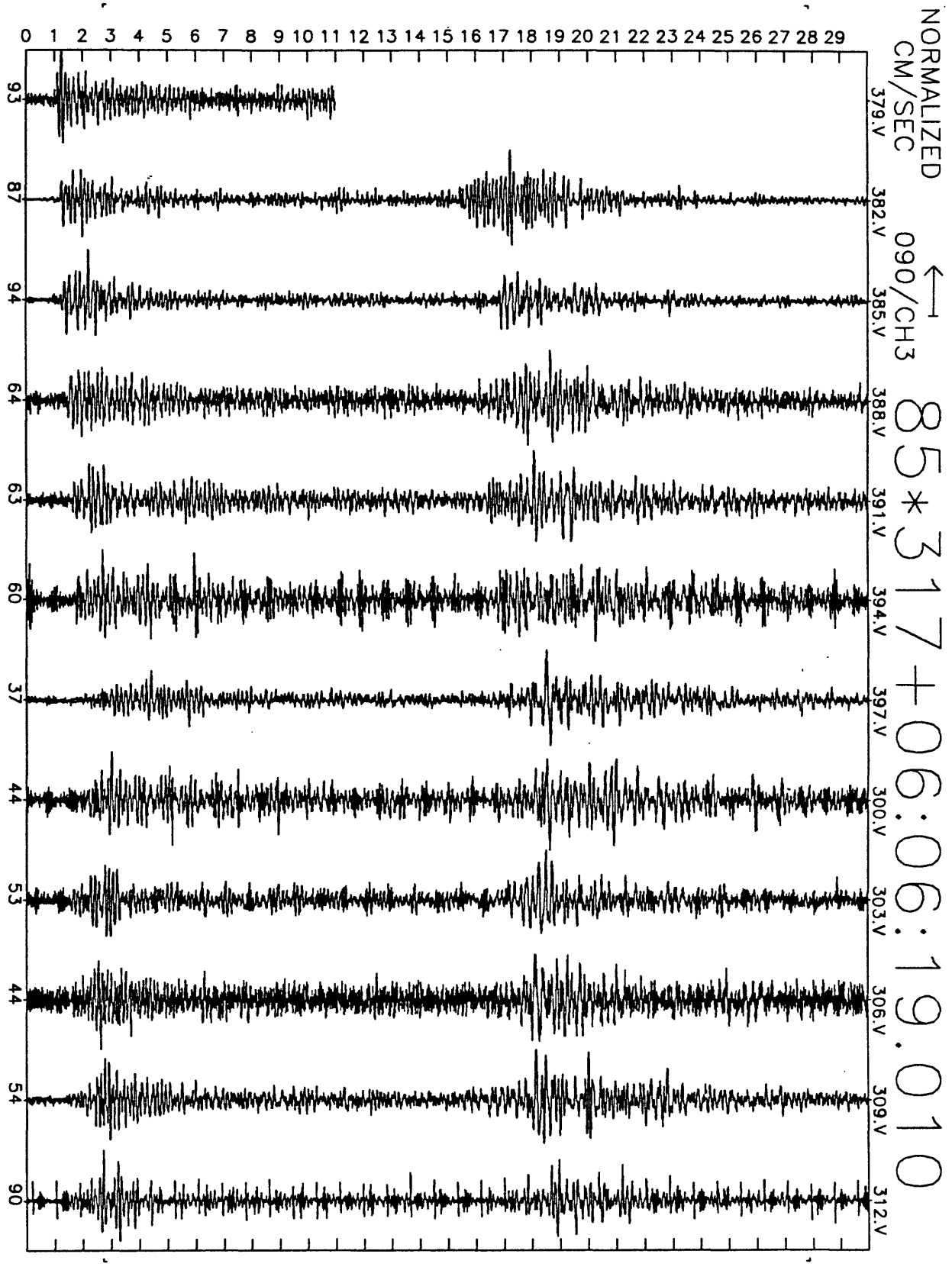

Figure A25(f), shot point 11: 30 second N115E velocity record. Abscissa is labeled with maximum counts in record (multiply by $\frac{10}{2^{24}-2^5} \approx 6 \times 10^{-7}$ to get cm/sec). Times are unreduced beginning at time indicated.

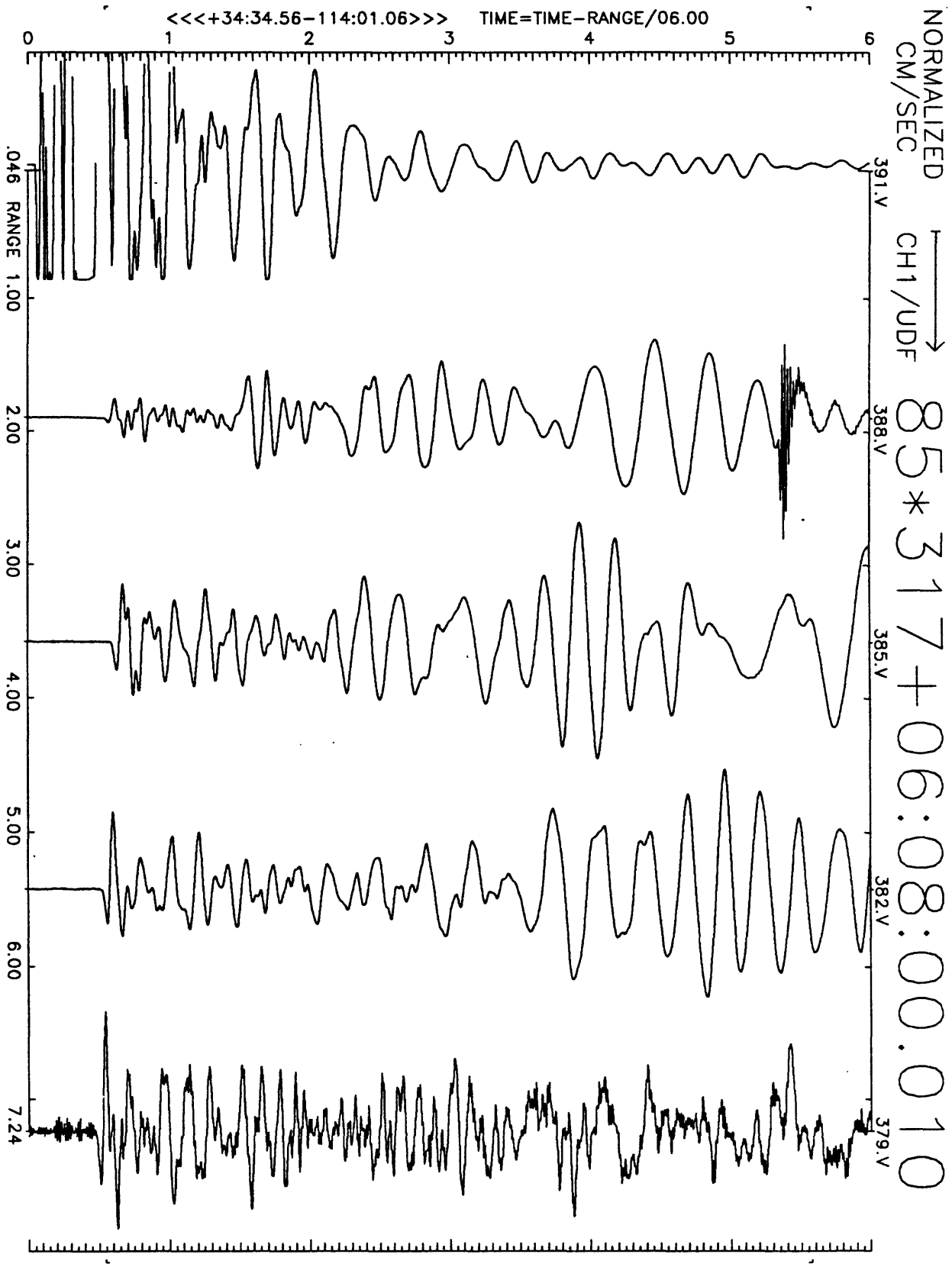

Figure A26(a), shot point 6X, SW stations: 6 second velocity record. Positive vertical motion is to right. Abscissa is distance to shot point. Top of trace is labeled with station number. Times are reduced by 6 km/sec. Shot time is indicated.

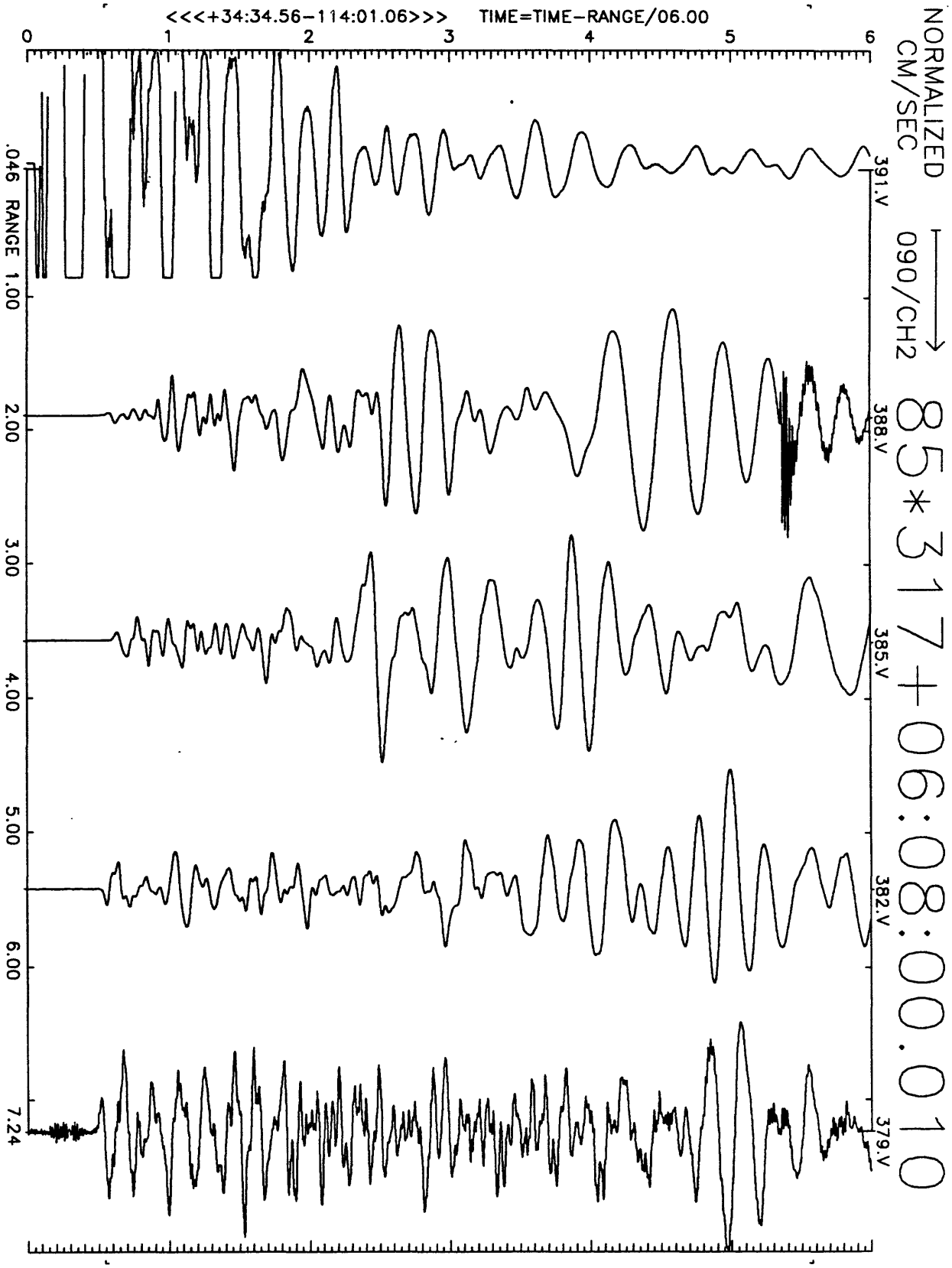

Figure A26(b), shot point 6X, SW stations: 6 second velocity record. Positive N25E motion is to right. Abscissa is distance to shot point. Top of trace is labeled with station number. Times are reduced by 6 km/sec. Shot time is indicated.

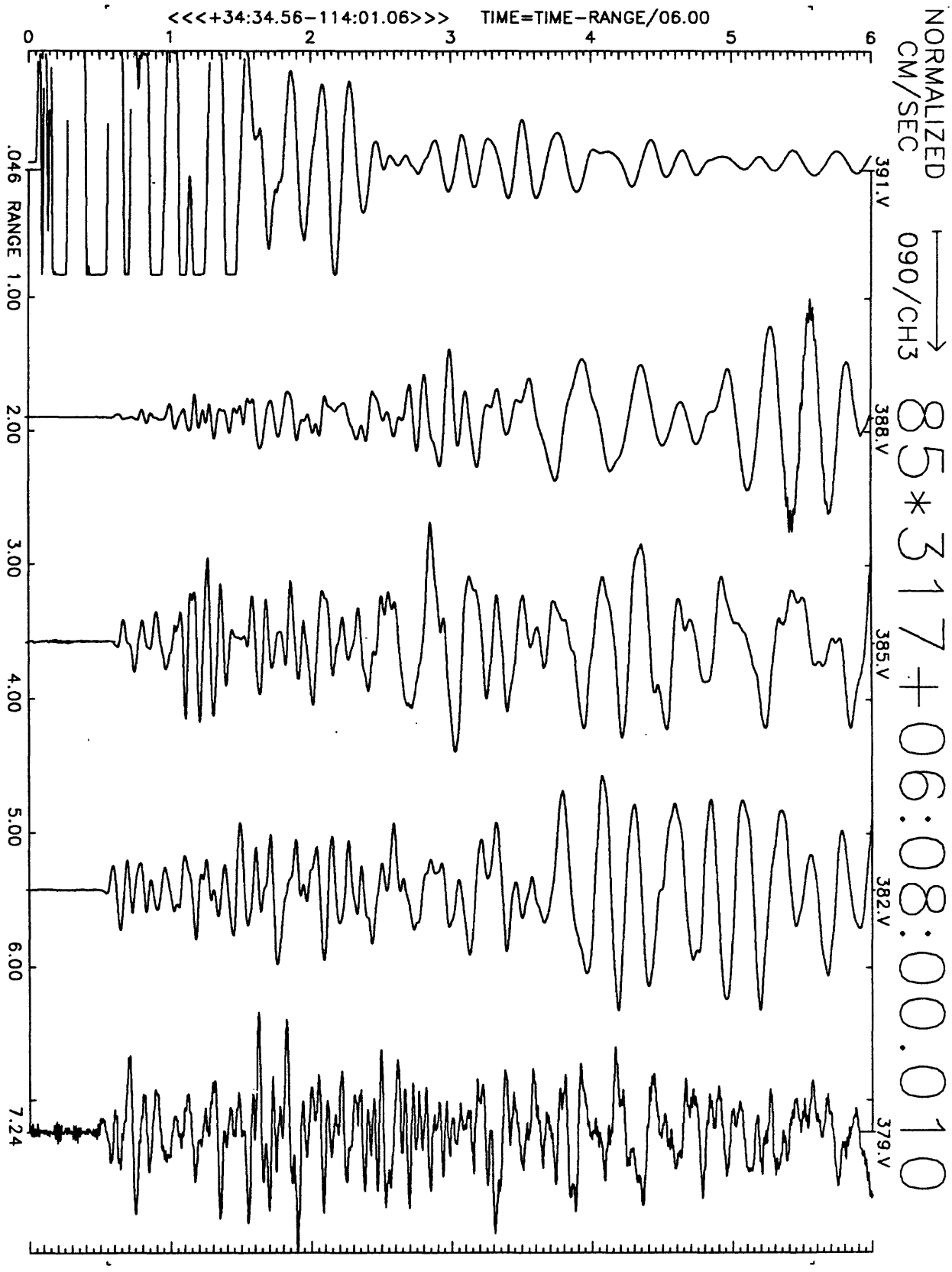

Figure A26(c), shot point 6X, SW stations: 6 second velocity record. Positive N115E motion is to right. Abscissa is distance to shot point. Top of trace is labeled with station number. Times are reduced by 6 km/sec. Shot time is indicated.

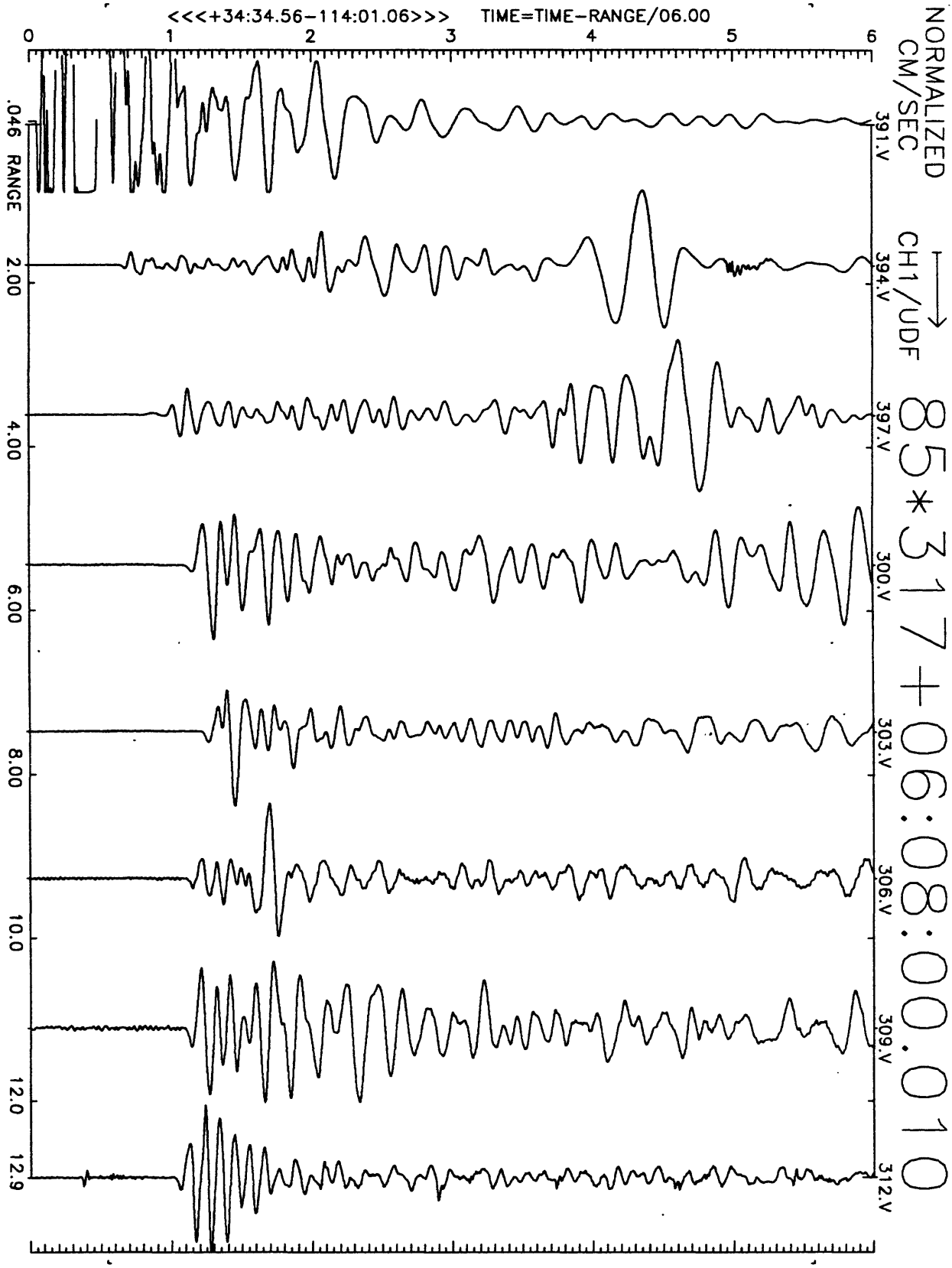

Figure A26(d), shot point 6X, NE stations: 6 second velocity record. Positive vertical motion is to right. Abscissa is distance to shot point. Top of trace is labeled with station number. Times are reduced by 6 km/sec. Shot time is indicated.

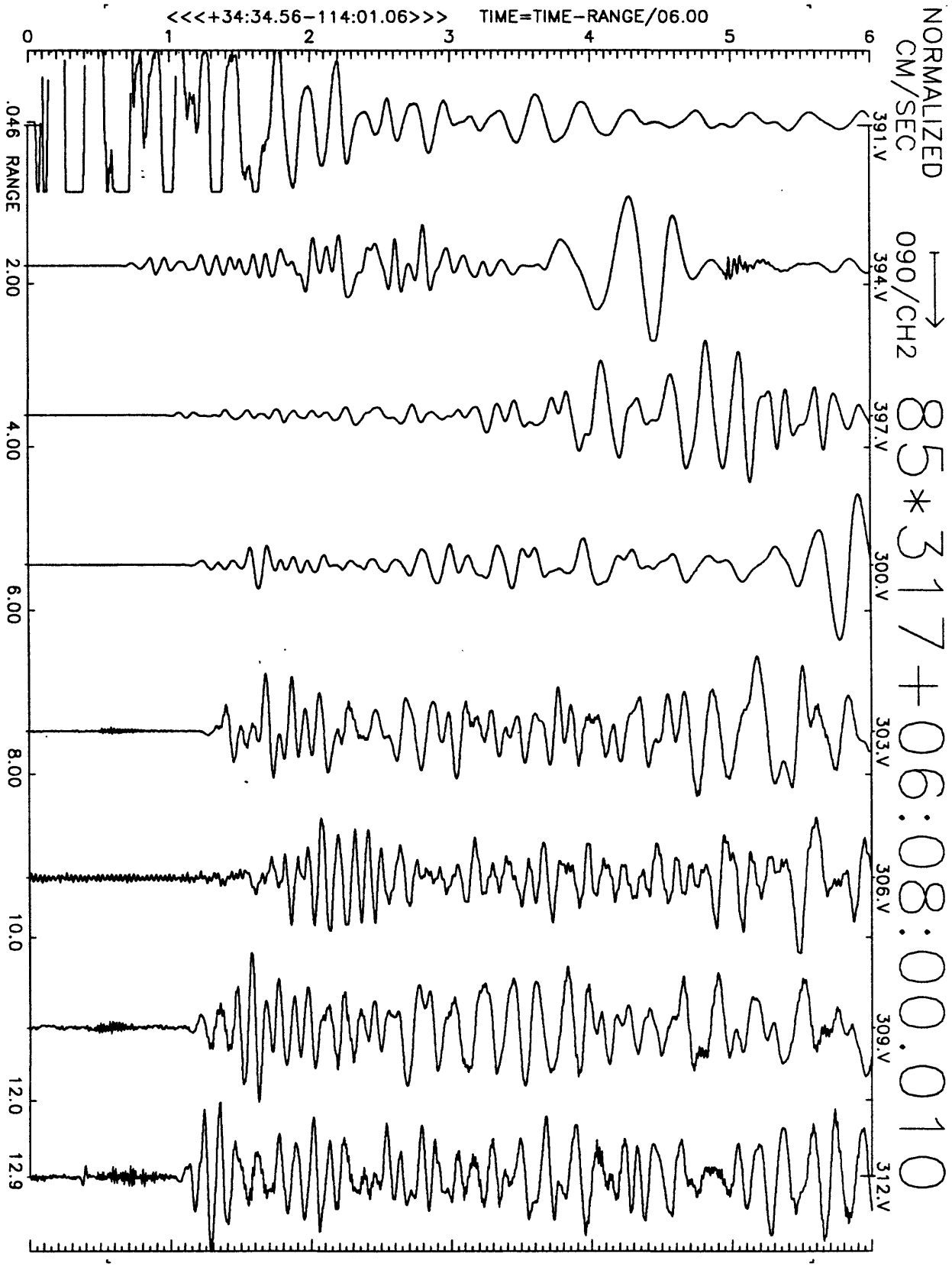

Figure A26(e), shot point 6X, NE stations: 6 second velocity record. Positive N25E motion is to right. Abscissa is distance to shot point. Top of trace is labeled with station number. Times are reduced by 6 km/sec. Shot time is indicated.

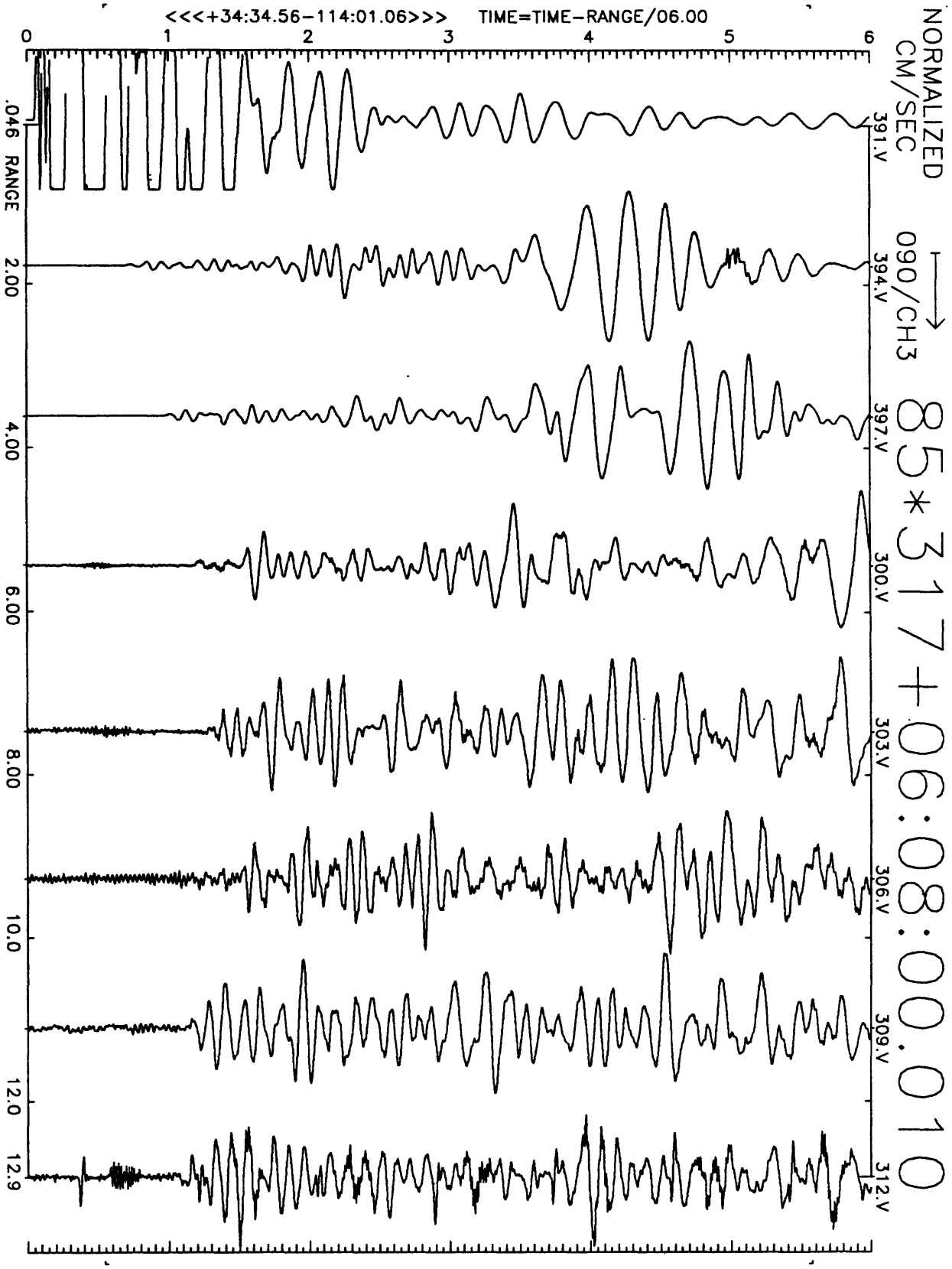

Figure A26(f), shot point 6X, NE stations: 6 second velocity record. Positive N115E motion is to right. Abscissa is distance to shot point. Top of trace is labeled with station number. Times are reduced by 6 km/sec. Shot time is indicated.

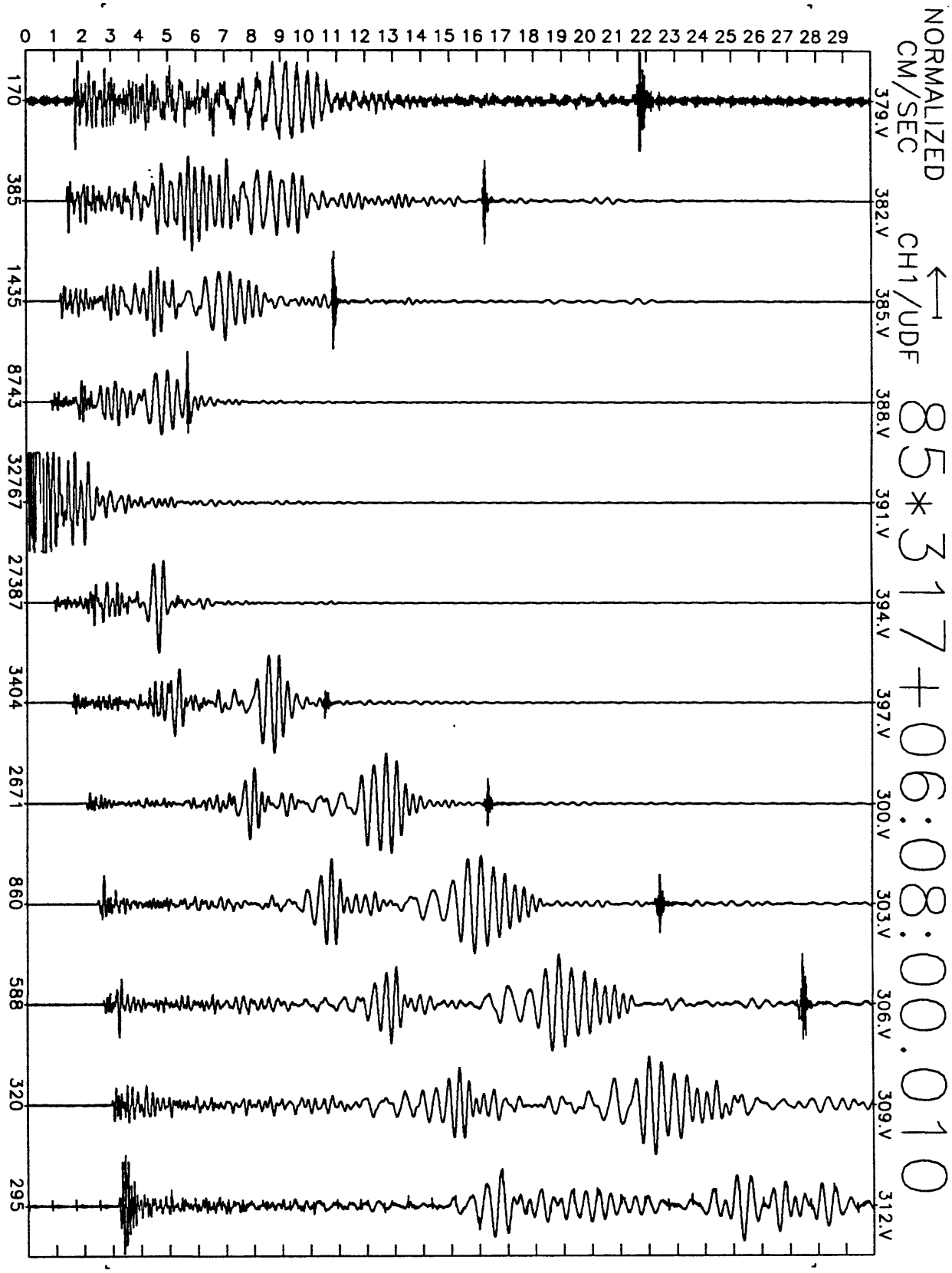

Figure A26(g), shot point 6X: 30 second vertical velocity record. Abscissa is labeled with maximum counts in record (multiply by $\frac{10}{2^{24}-2^5} \approx 6 \times 10^{-7}$ to get cm/sec). Times are unreduced beginning at time indicated.

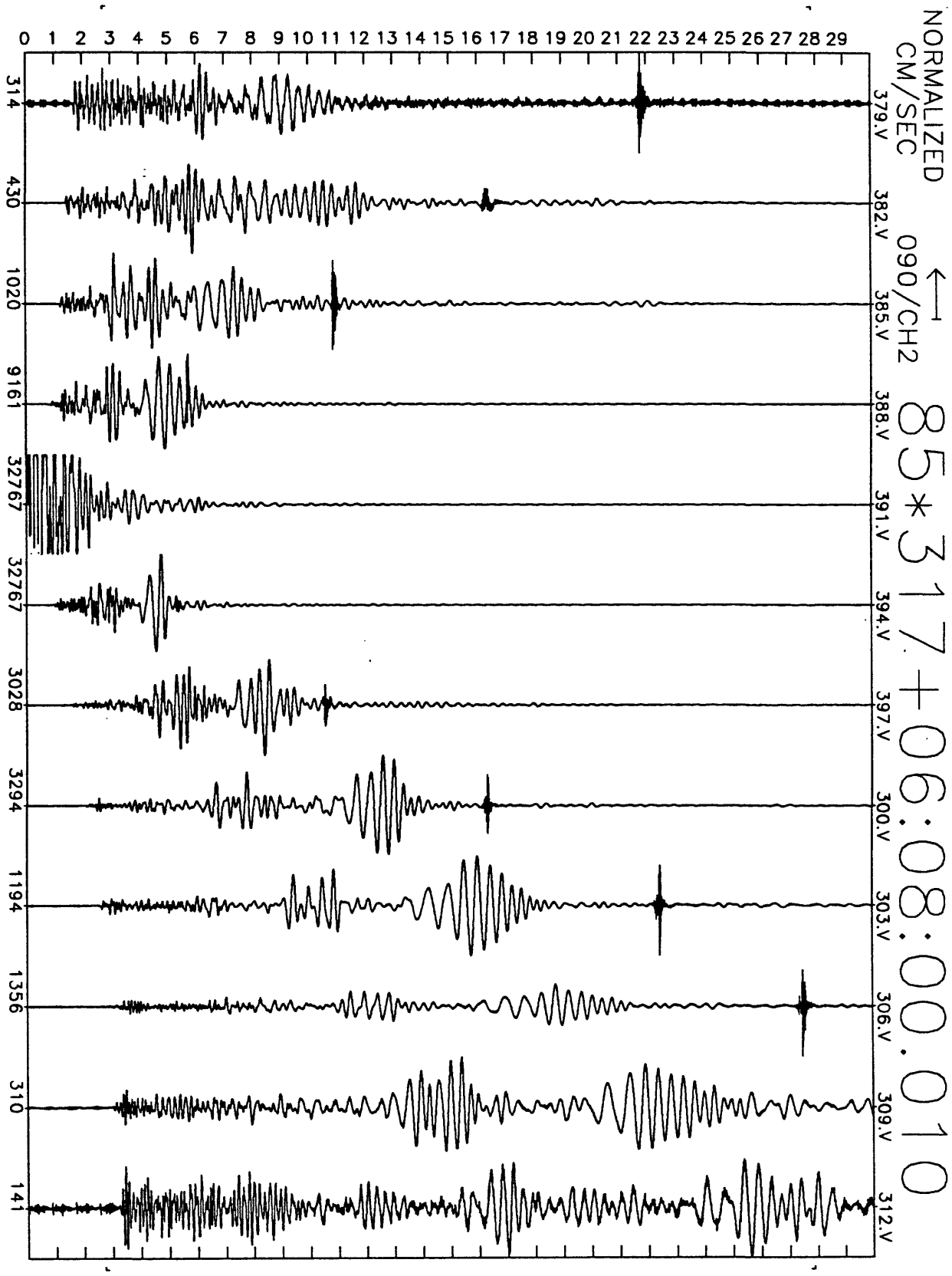

Figure A26(h), shot point 6X: 30 second N25E velocity record. Abscissa is labeled with maximum counts in record (multiply by $\frac{10}{2^{24}-2^5} \approx 6 \times 10^{-7}$ to get cm/sec). Times are unreduced beginning at time indicated.

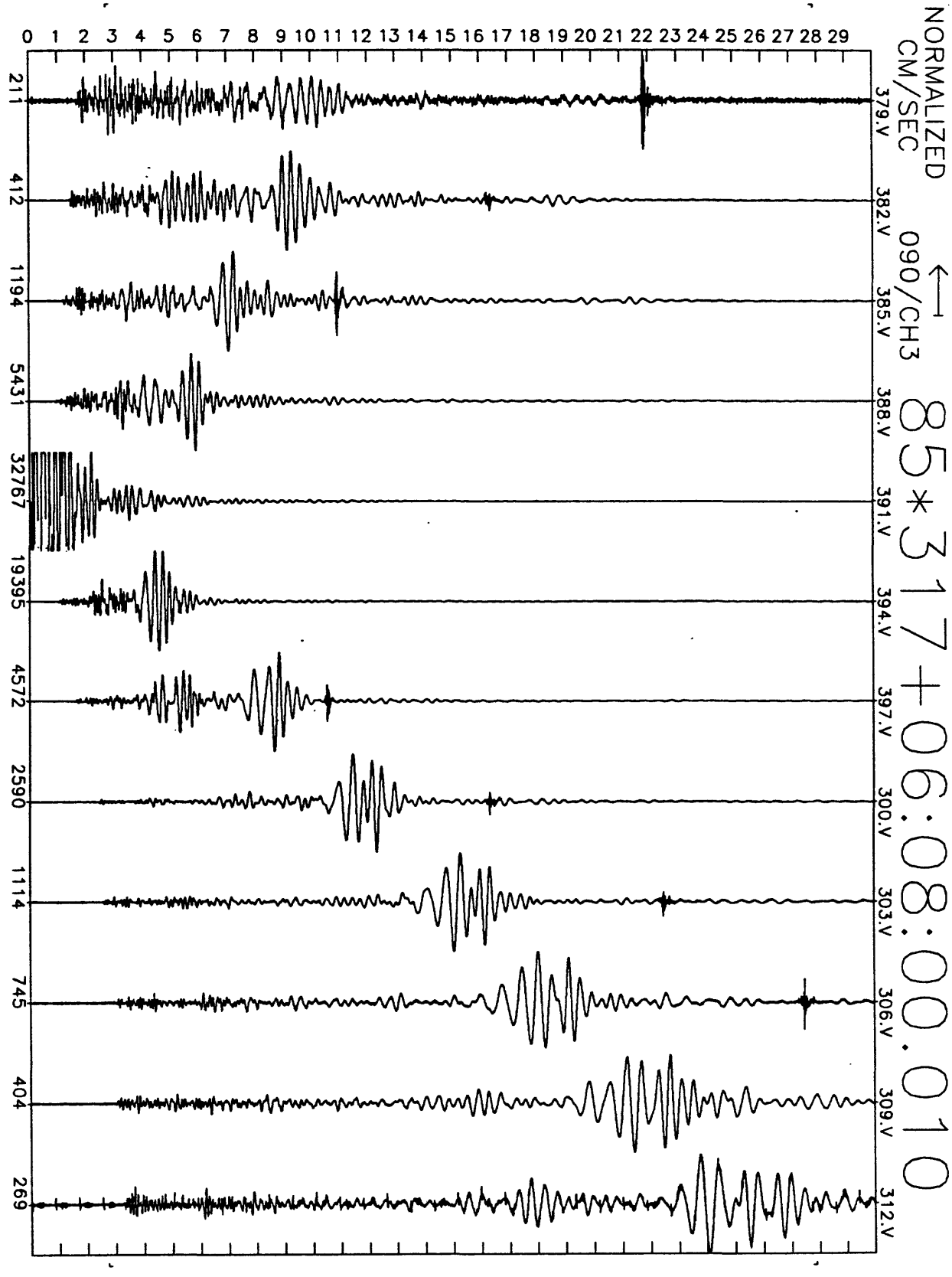

Figure A26(i), shot point 6X: 30 second N115E velocity record. Abscissa is labeled with maximum counts in record (multiply by $\frac{10}{2^{24}-2^9} \approx 6 \times 10^{-7}$ to get cm/sec). Times are unreduced beginning at time indicated.

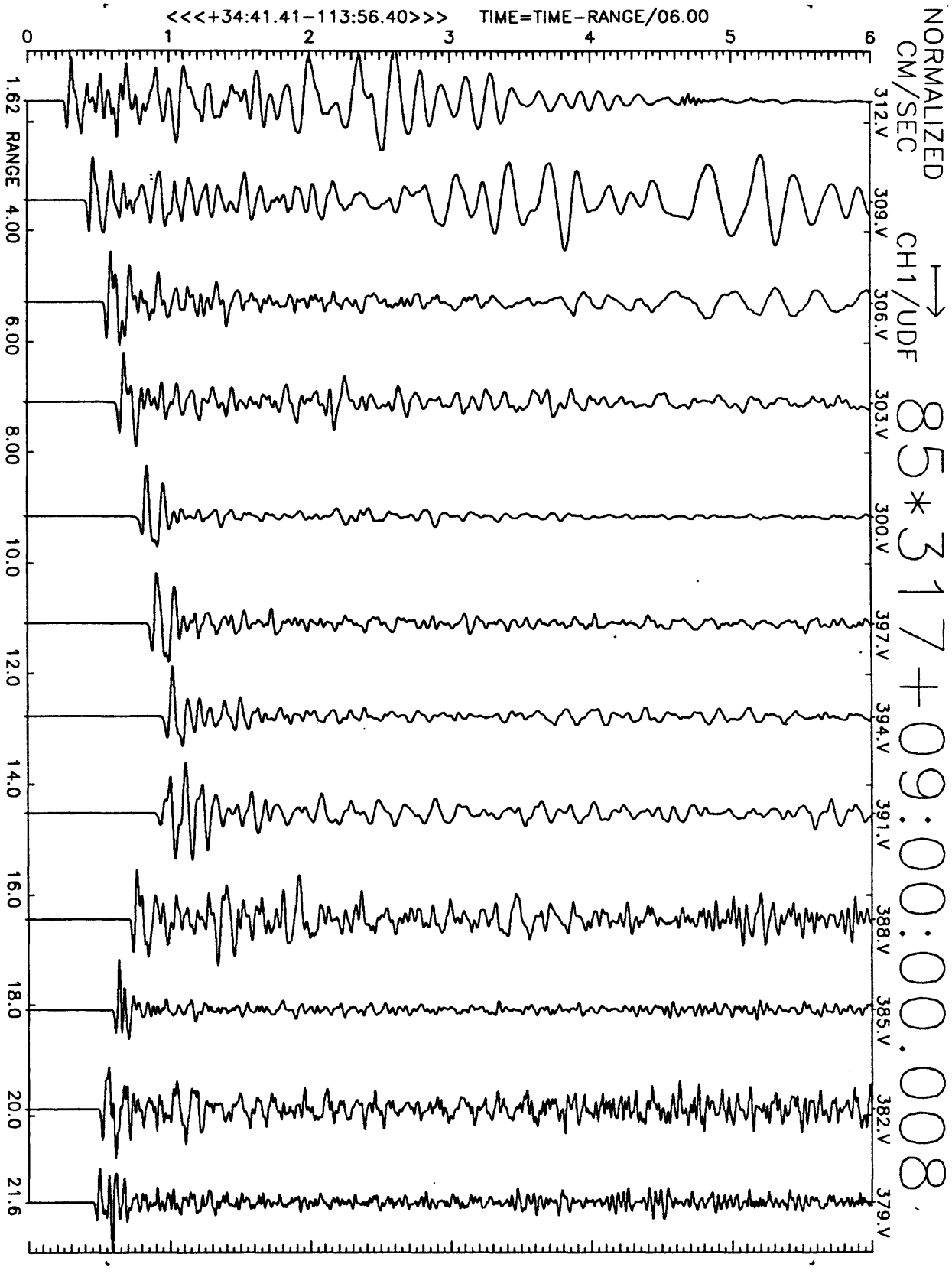

Figure A27(a), shot point 7: 6 second velocity record. Positive vertical motion is to right. Abscissa is distance to shot point. Top of trace is labeled with station number. Times are reduced by 6 km/sec. Shot time is indicated.

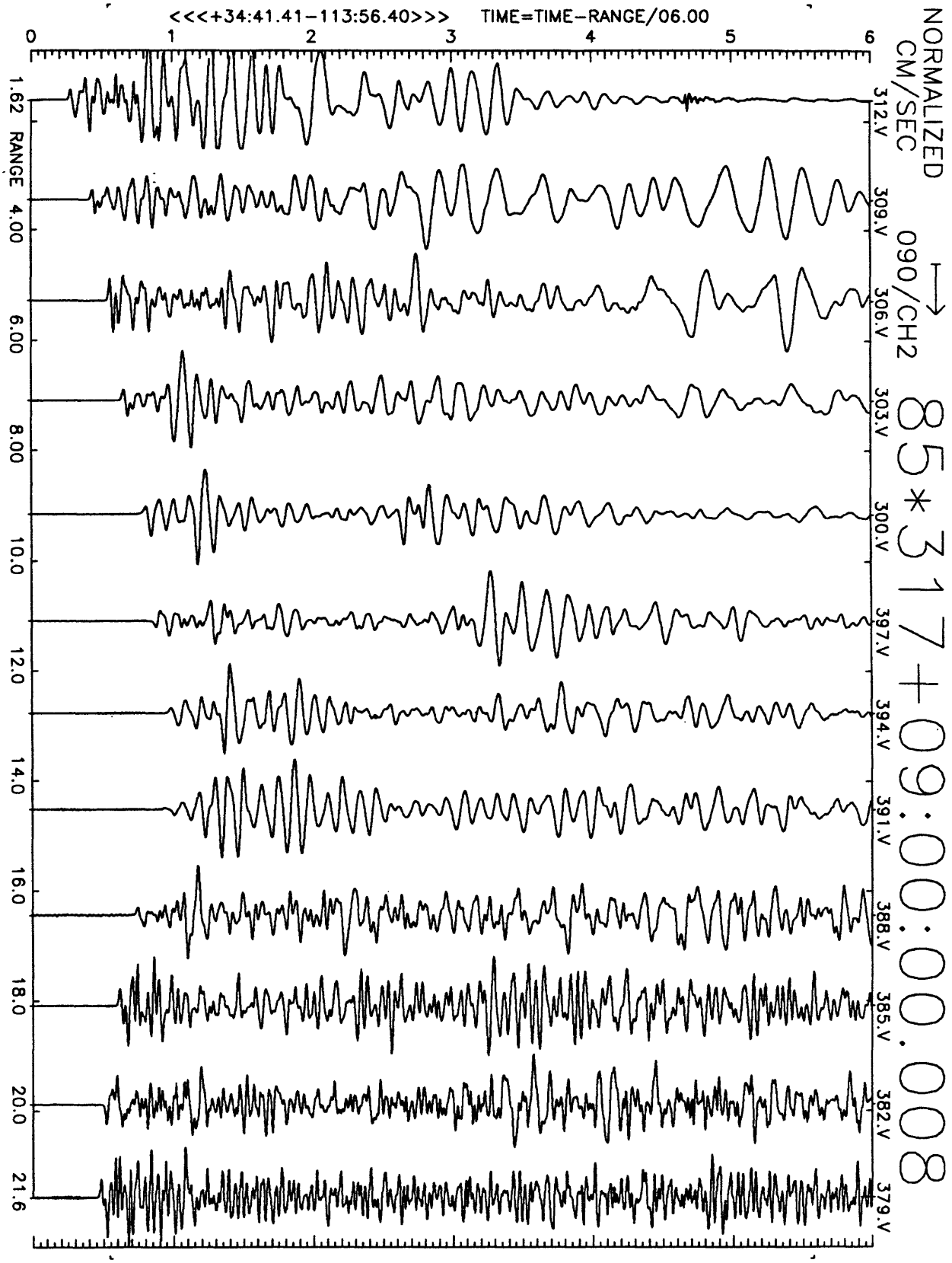

Figure A27(b), shot point 7: 6 second velocity record. Positive N25E motion is to right. Abscissa is distance to shot point. Top of trace is labeled with station number. Times are reduced by 6 km/sec. Shot time is indicated.

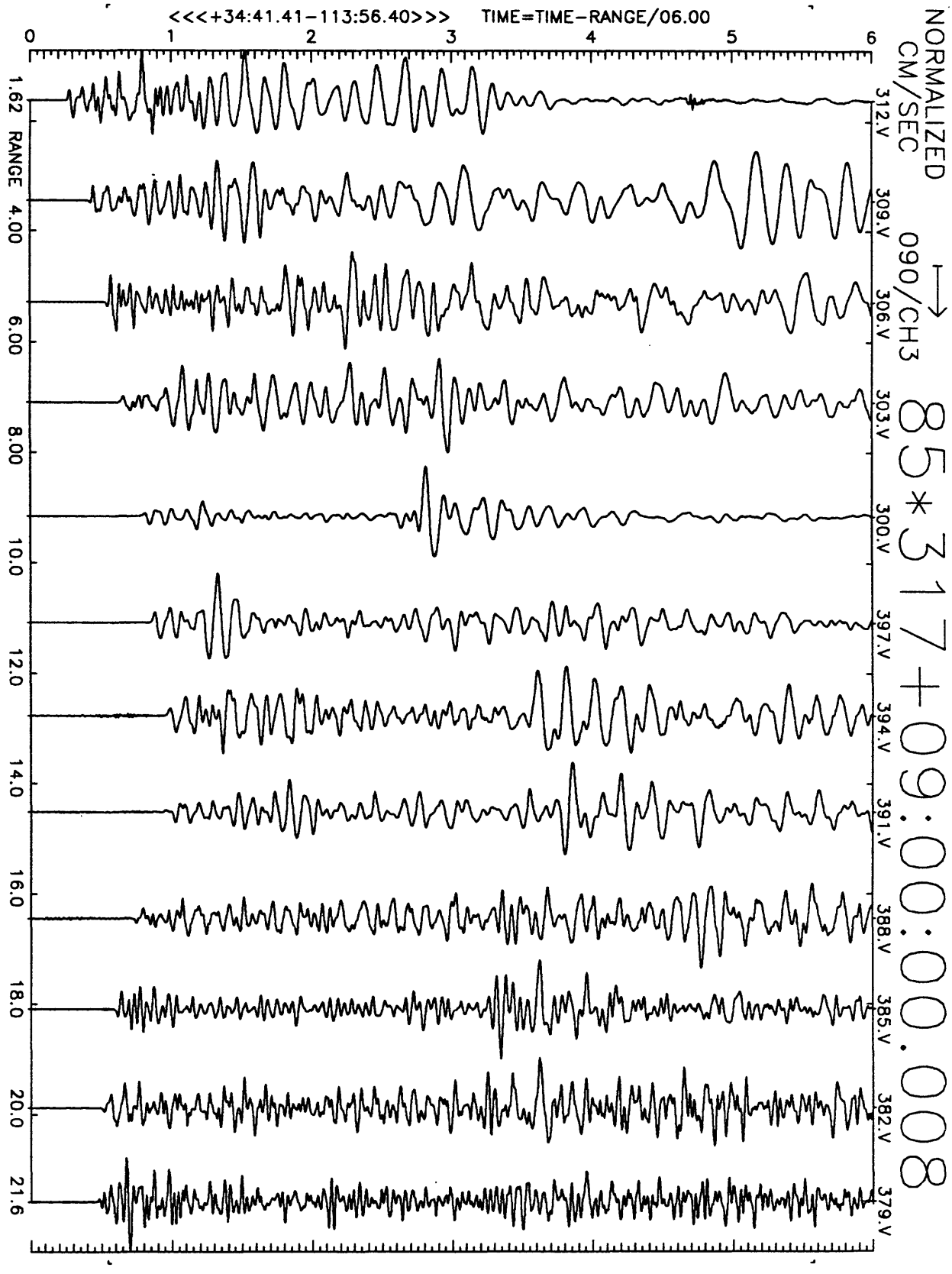

Figure A27(c), shot point 7: 6 second velocity record. Positive N115E motion is to right. Abscissa is distance to shot point. Top of trace is labeled with station number. Times are reduced by 6 km/sec. Shot time is indicated.

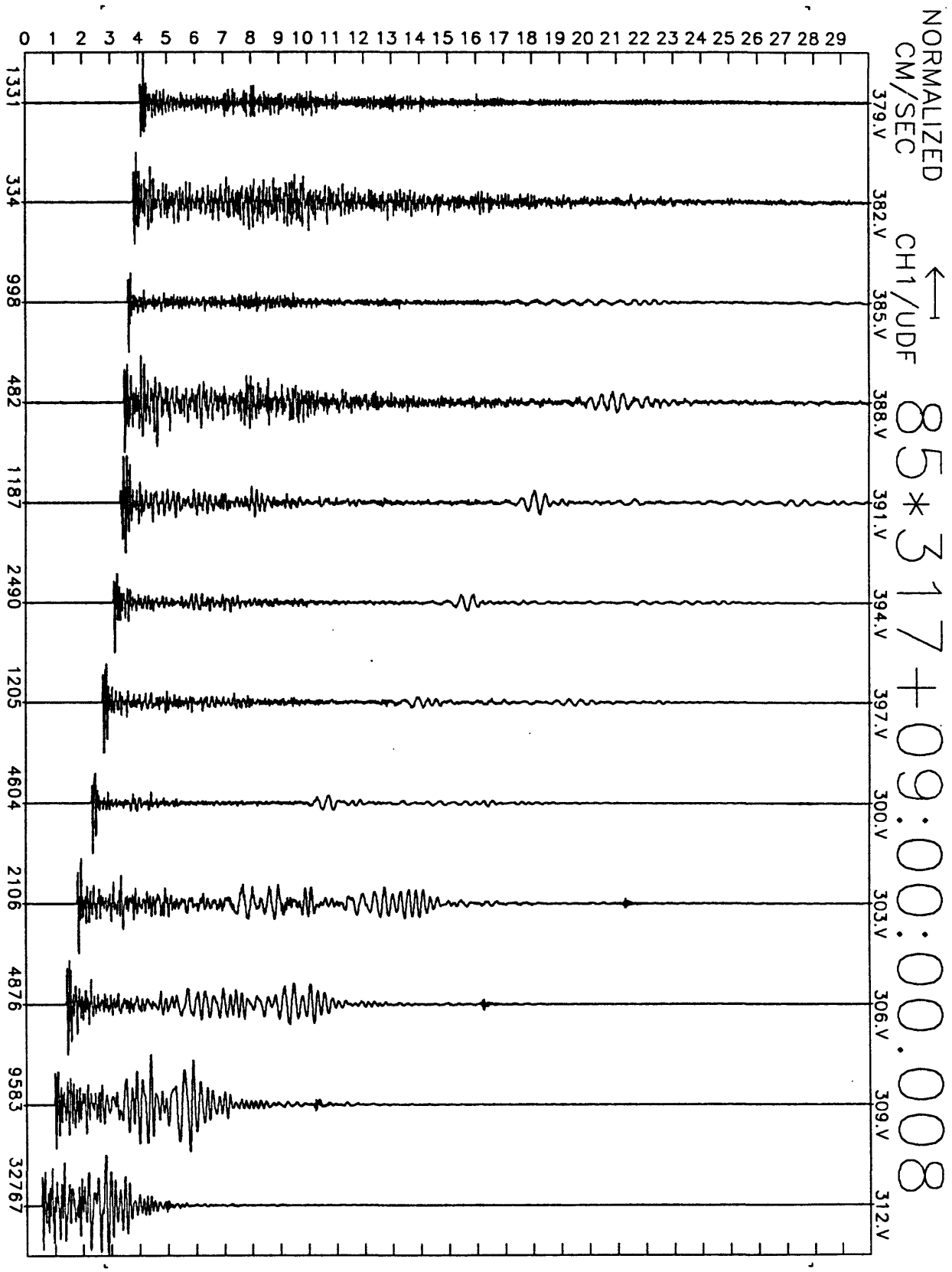

Figure A27(d), shot point 7: 30 second vertical velocity record. Abscissa is labeled with maximum counts in record (multiply by $\frac{10}{2^{24}-2^5} \approx 6 \times 10^{-7}$ to get cm/sec). Times are unreduced beginning at time indicated.

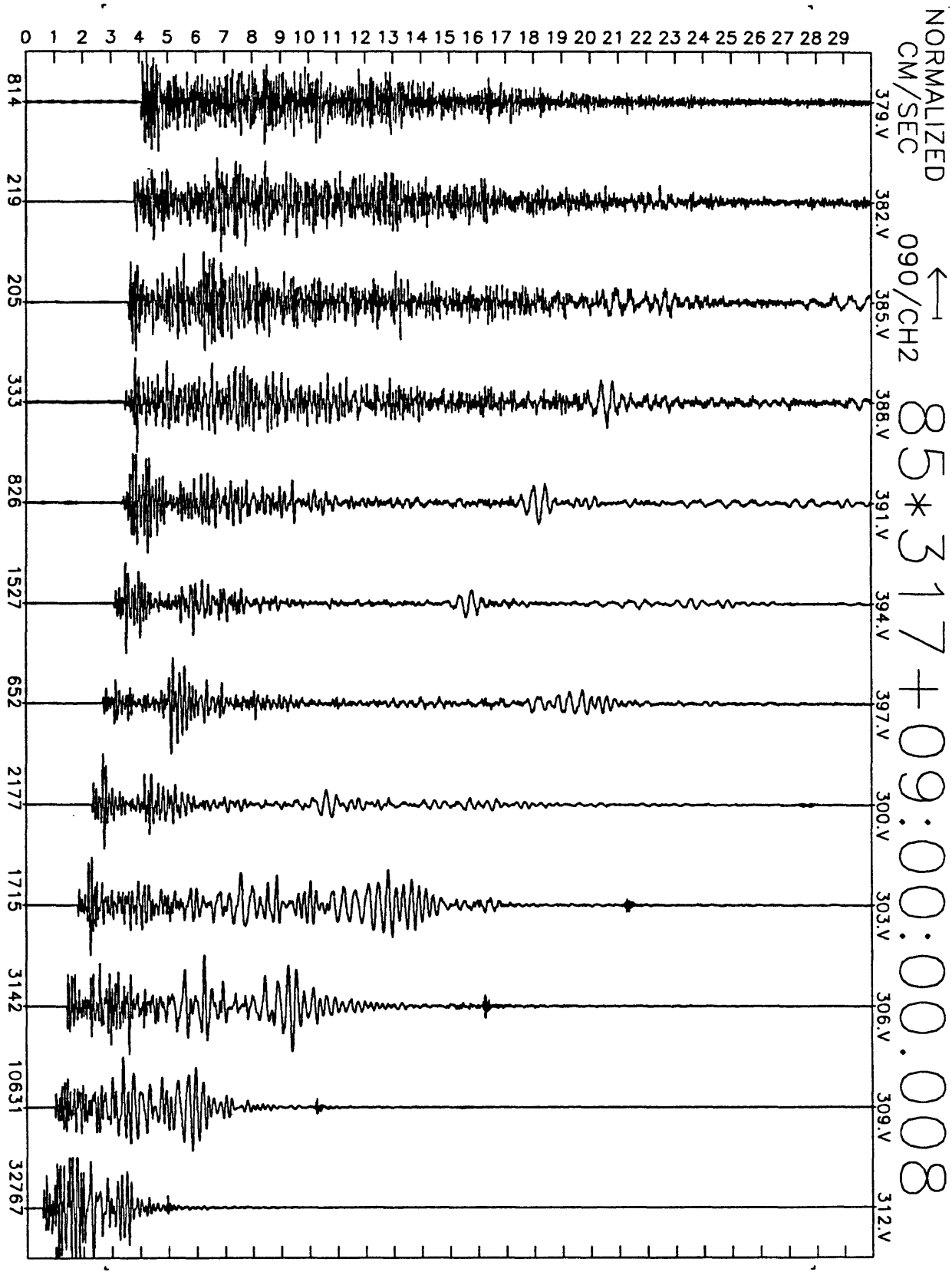

Figure A27(e), shot point 7: 30 second N25E velocity record. Abscissa is labeled with maximum counts in record (multiply by $\frac{10}{2^{24}-2^8} \approx 6 \times 10^{-7}$ to get cm/sec). Times are unreduced beginning at time indicated.

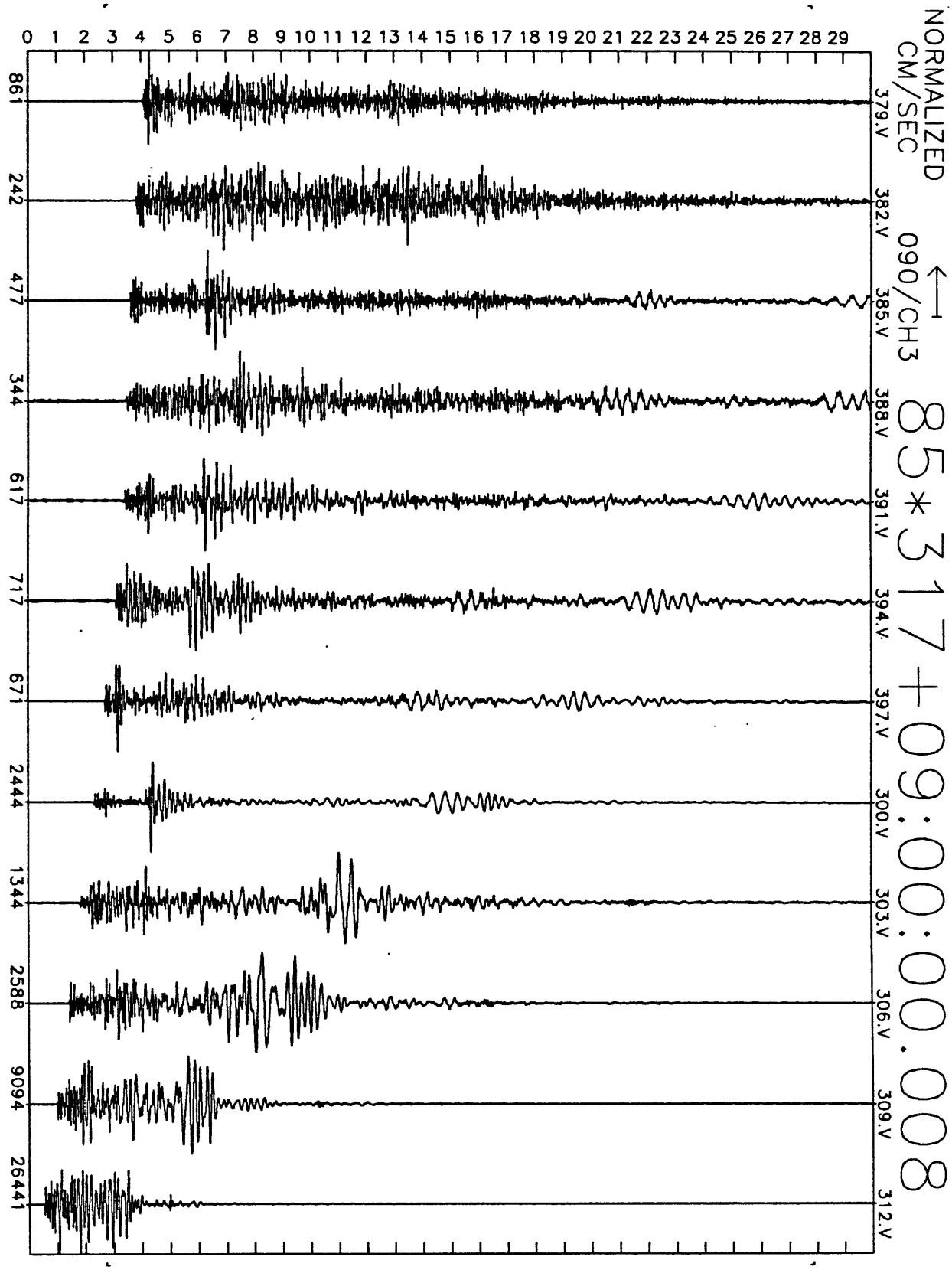

Figure A27(f), shot point 7: 30 second N115E velocity record. Abscissa is labeled with maximum counts in record (multiply by $\frac{10}{2^{24}-2^{9}} \approx 6 \times 10^{-7}$ to get cm/sec). Times are unreduced beginning at time indicated.

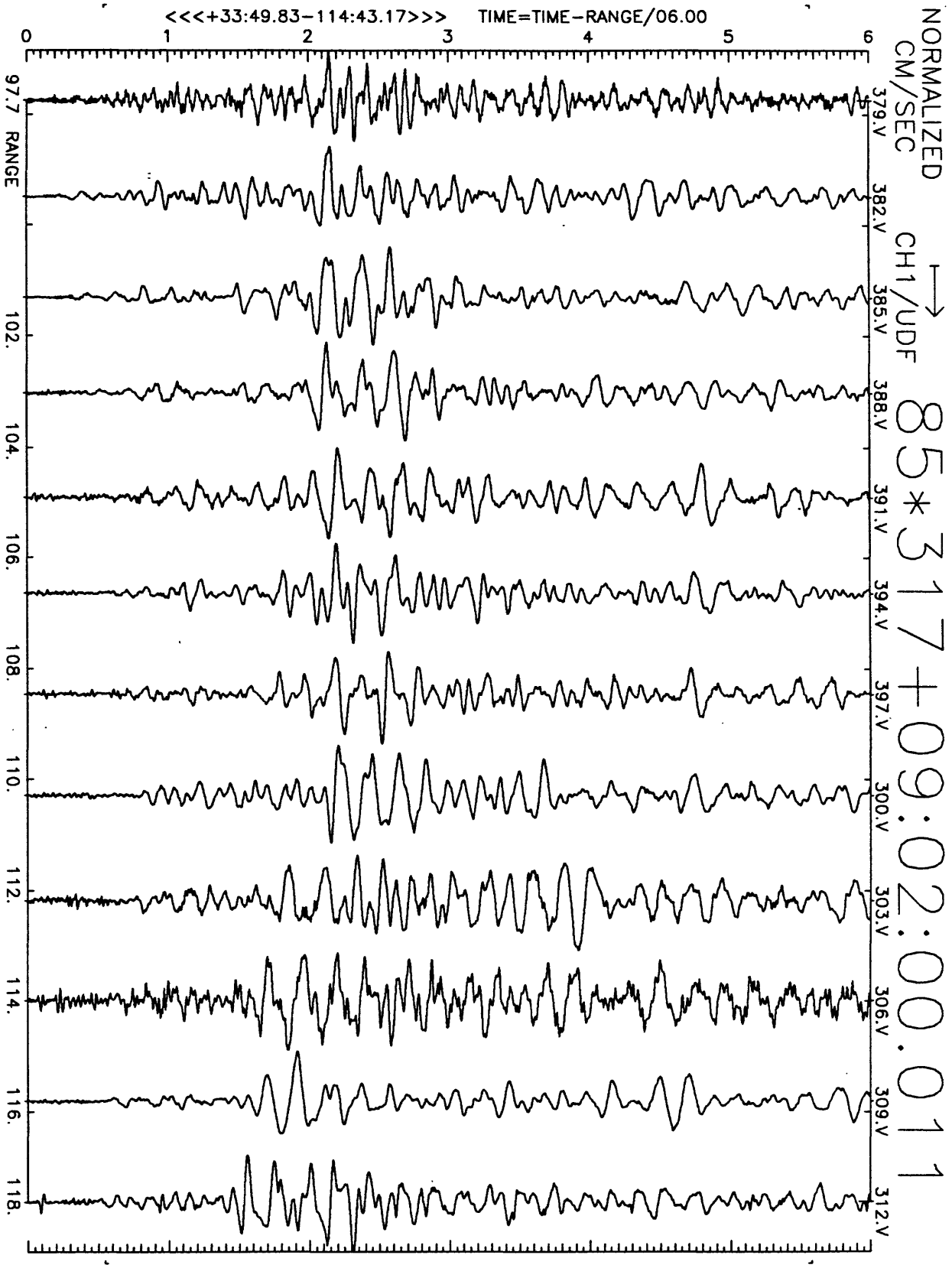

Figure A28(a), shot point 1: 6 second velocity record. Positive vertical motion is to right. Abscissa is distance to shot point. Top of trace is labeled with station number. Times are reduced by 6 km/sec. Shot time is indicated.

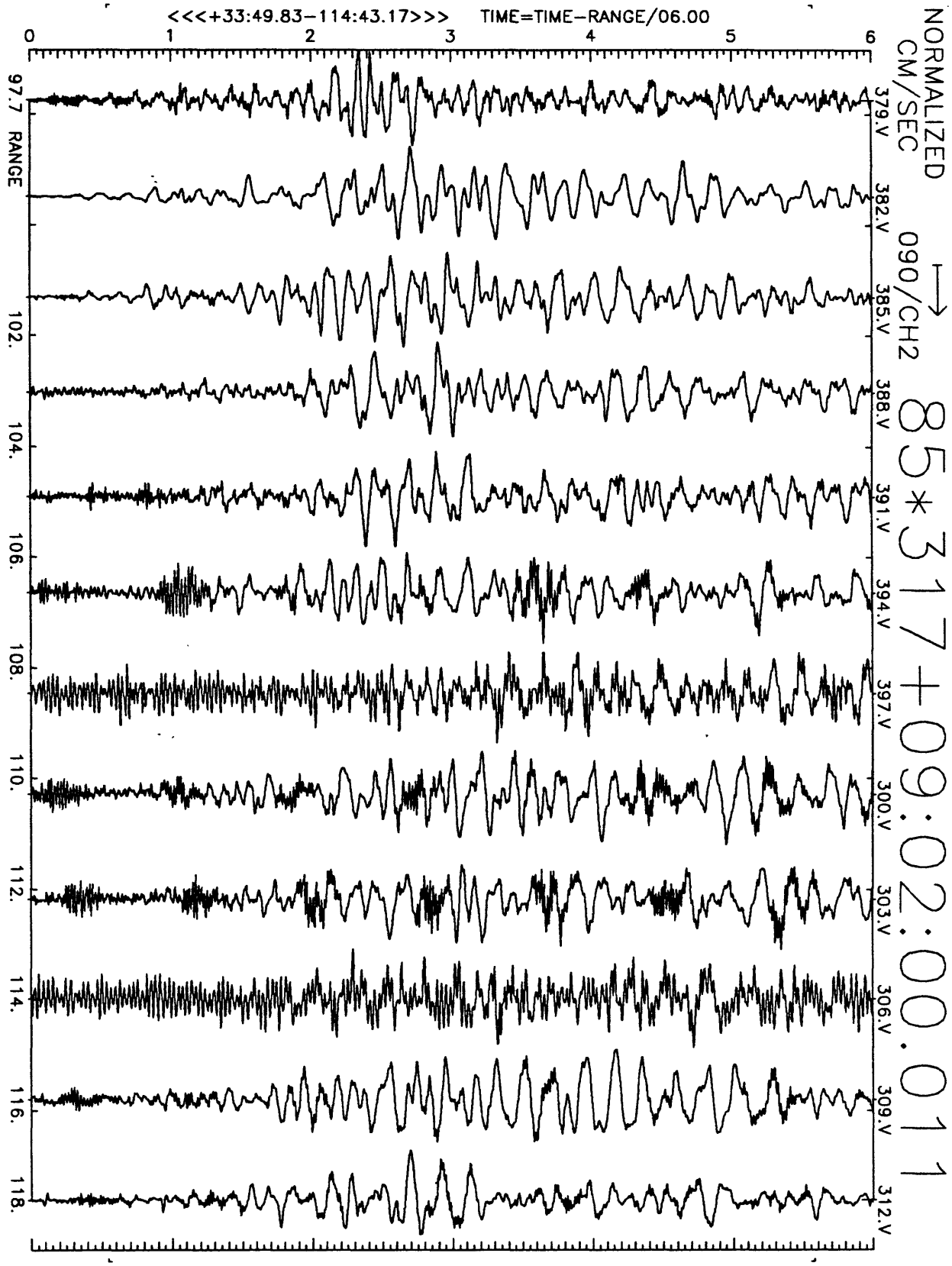

Figure A28(b), shot point 1: 6 second velocity record. Positive N25E motion is to right. Abscissa is distance to shot point. Top of trace is labeled with station number. Times are reduced by 6 km/sec. Shot time is indicated.

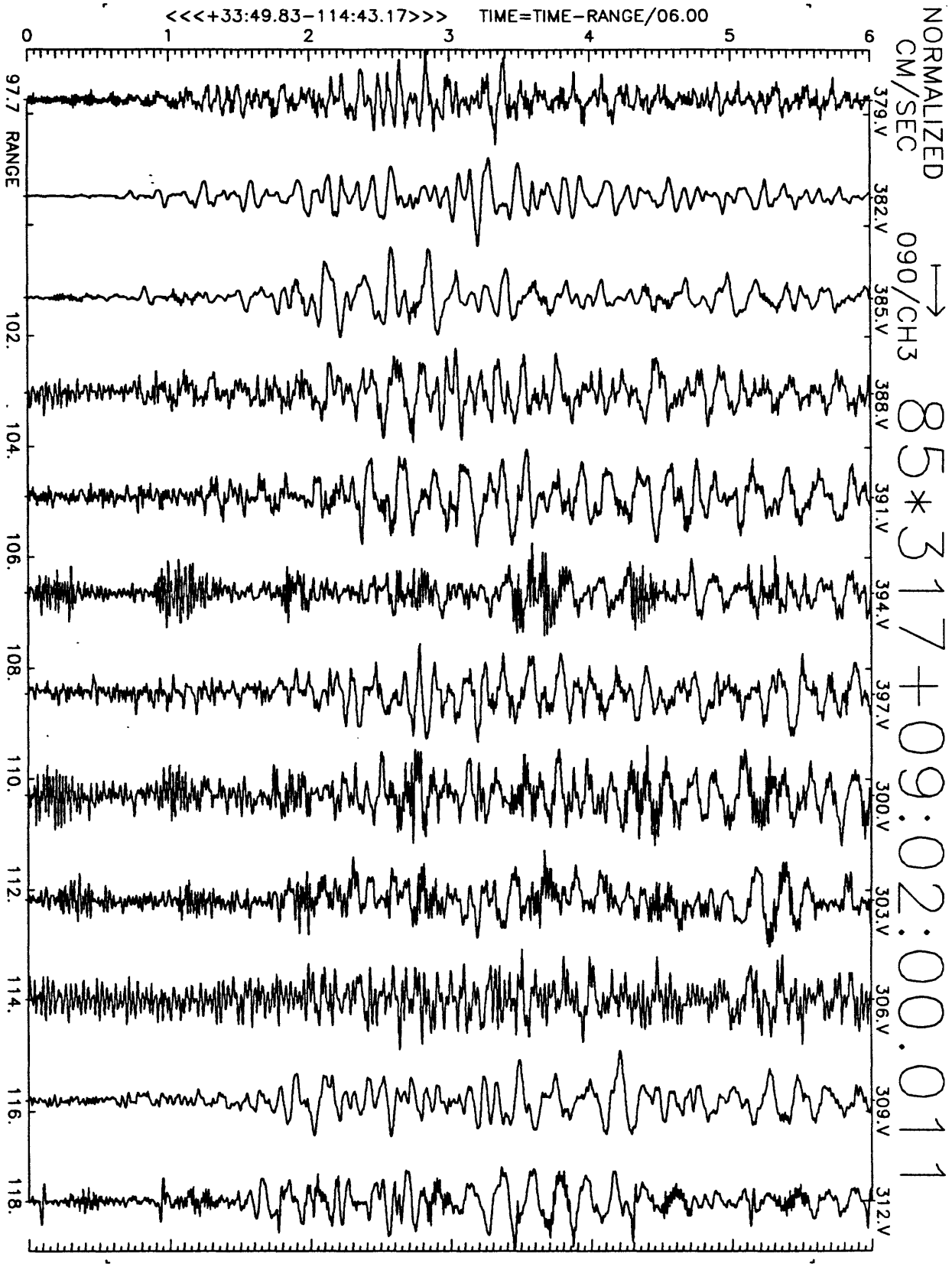

Figure A28(c), shot point 1: 6 second velocity record. Positive N115E motion is to right. Abscissa is distance to shot point. Top of trace is labeled with station number. Times are reduced by 6 km/sec. Shot time is indicated.

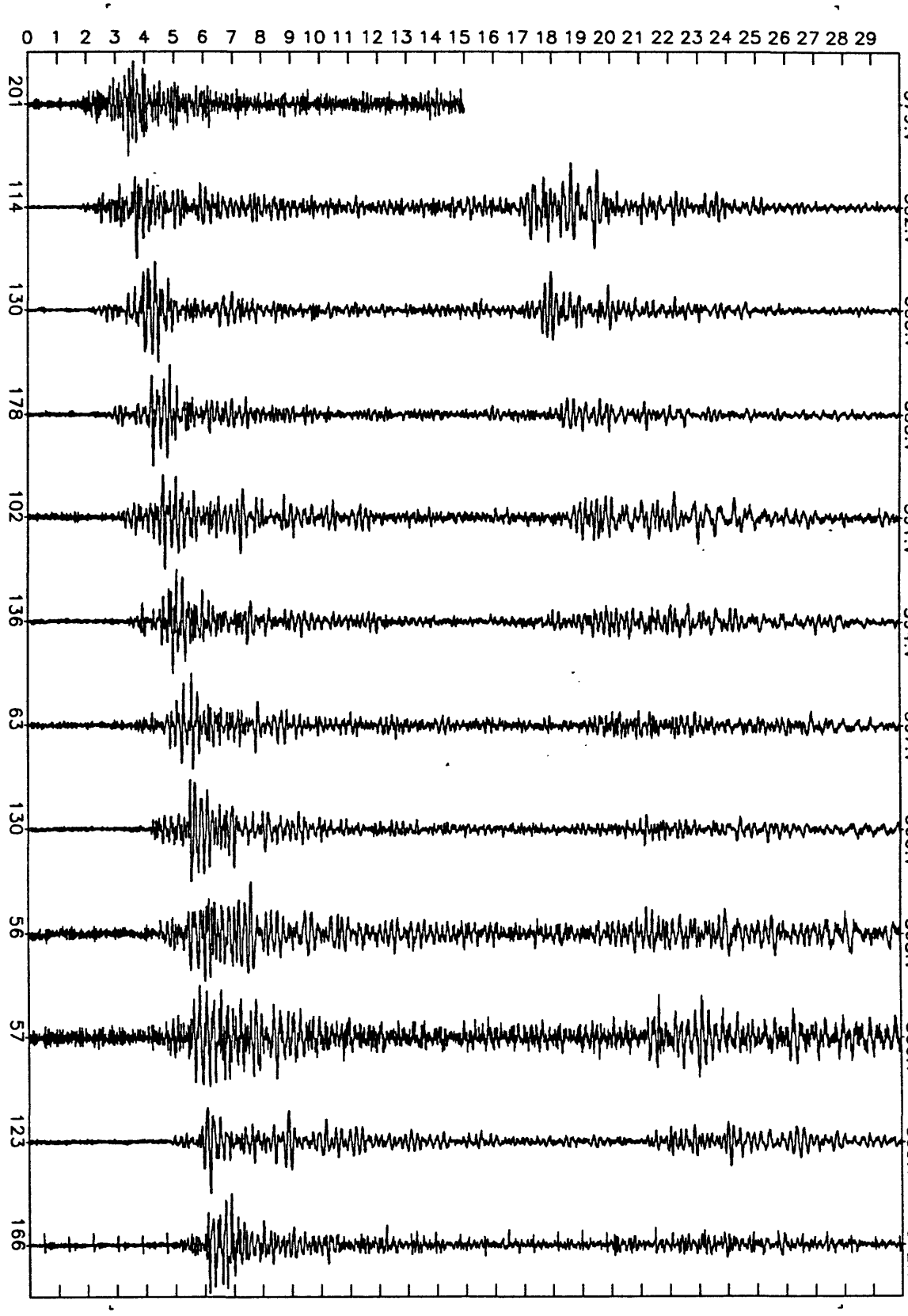

Figure A28(d), shot point 1: 30 second vertical velocity record. Abscissa is labeled with maximum counts in record (multiply by $\frac{10}{2^{24}-2^0} \approx 6 \times 10^{-7}$ to get cm/sec). Times are unreduced beginning at time indicated.

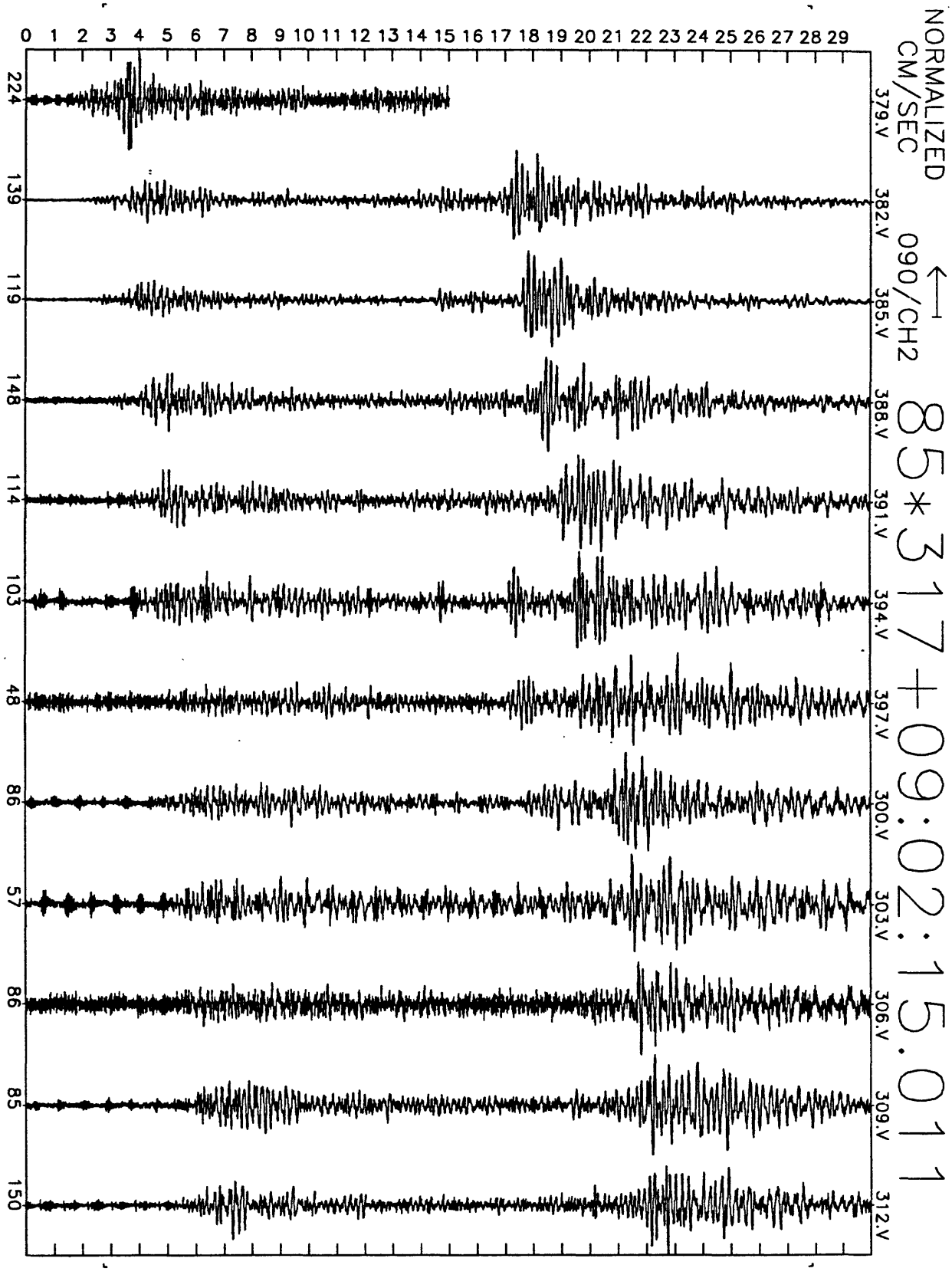

Figure A28(e), shot point 1: 30 second N25E velocity record. Abscissa is labeled with maximum counts in record (multiply by $\frac{10}{2^{24}-2^5} \approx 6 \times 10^{-7}$ to get cm/sec). Times are unreduced beginning at time indicated.

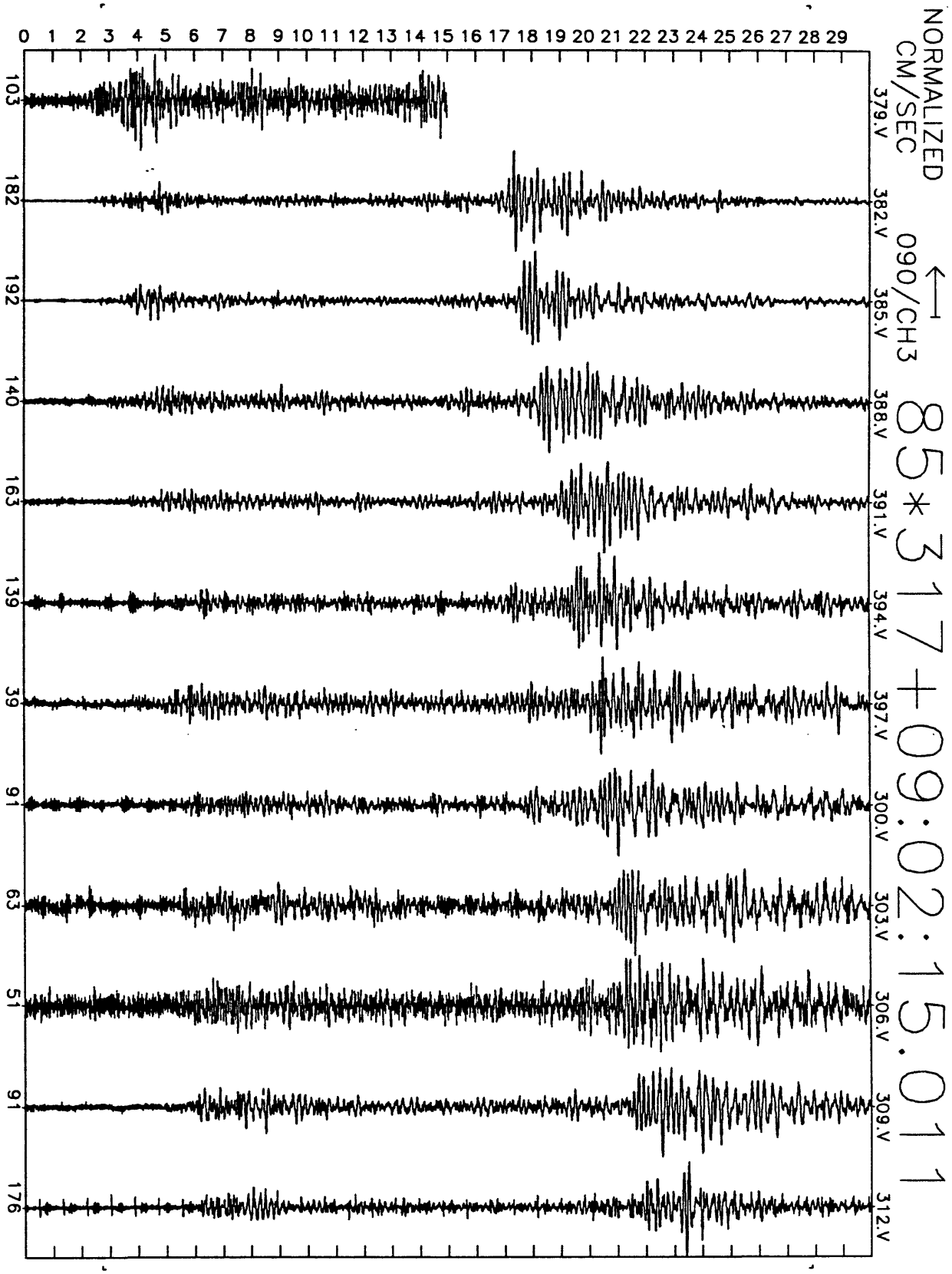

Figure A28(f), shot point 1: 30 second N115E velocity record. Abscissa is labeled with maximum counts in record (multiply by $\frac{10}{2^{24}-2^5} \approx 6 \times 10^{-7}$ to get cm/sec). Times are unreduced beginning at time indicated.

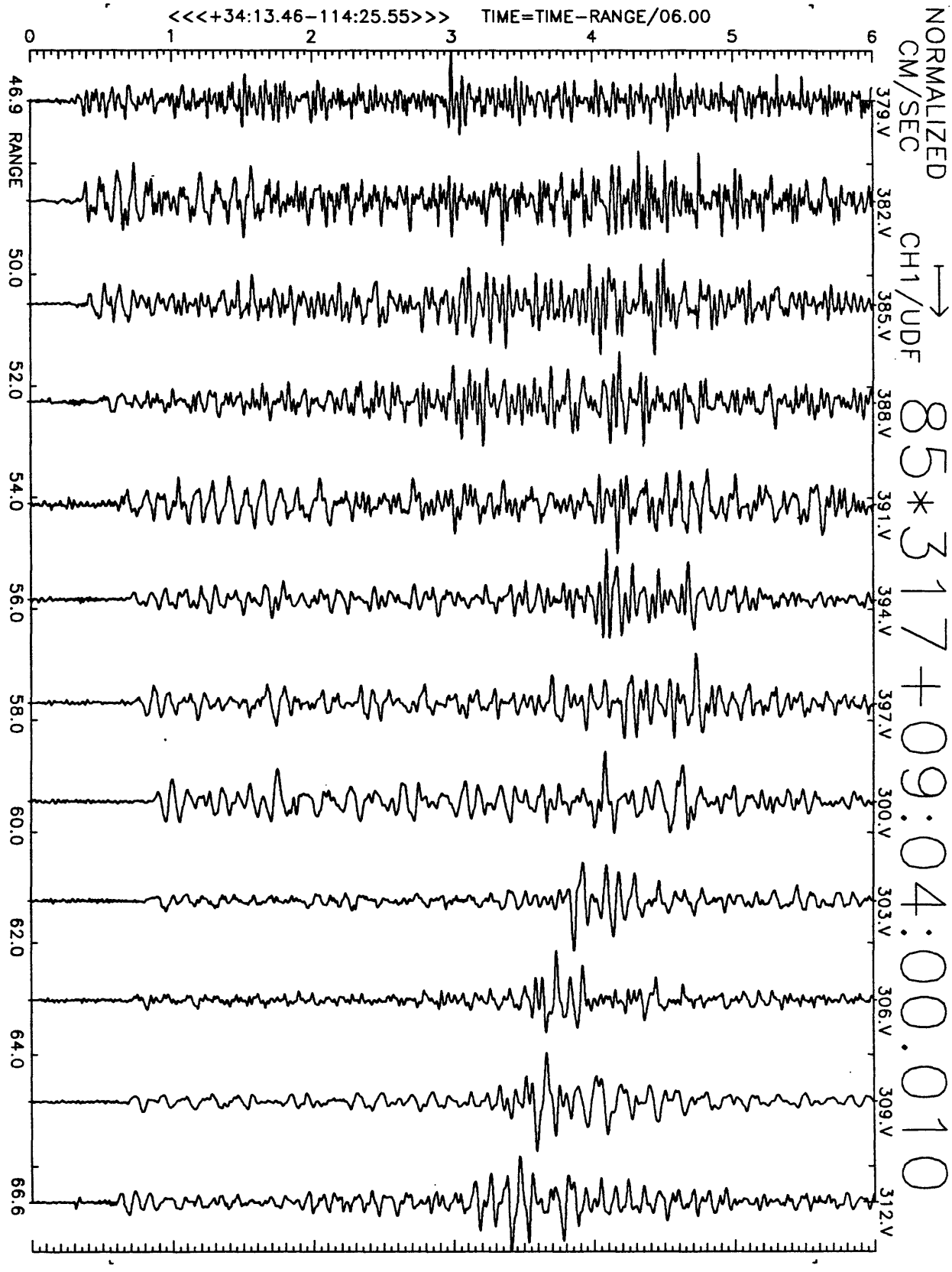

Figure A29(a), shot point 4B: 6 second velocity record. Positive vertical motion is to right. Abscissa is distance to shot point. Top of trace is labeled with station number. Times are reduced by 6 km/sec. Shot time is indicated.

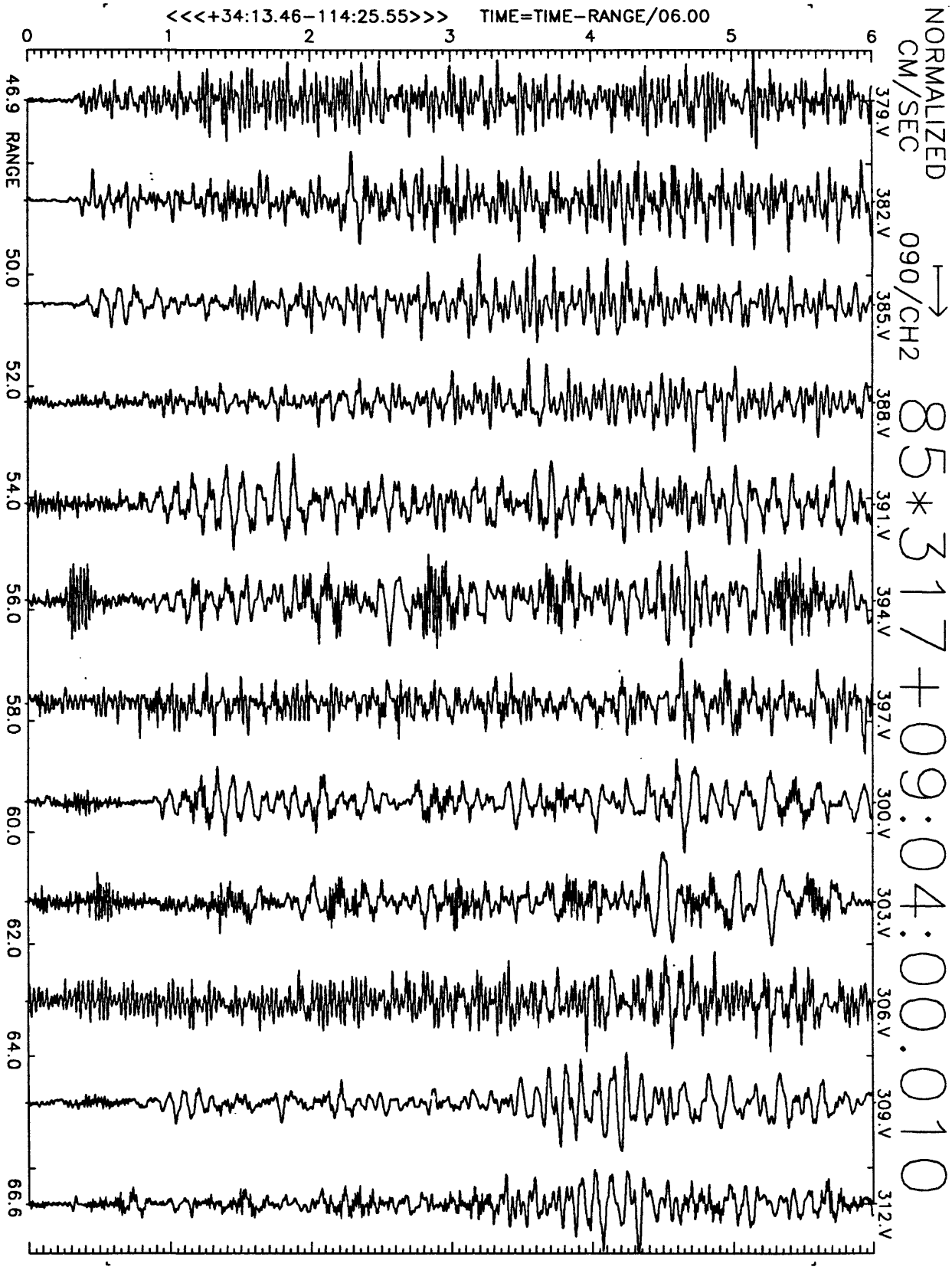

Figure A29(b), shot point 4B: 6 second velocity record. Positive N25E motion is to right. Abscissa is distance to shot point. Top of trace is labeled with station number. Times are reduced by 6 km/sec. Shot time is indicated.

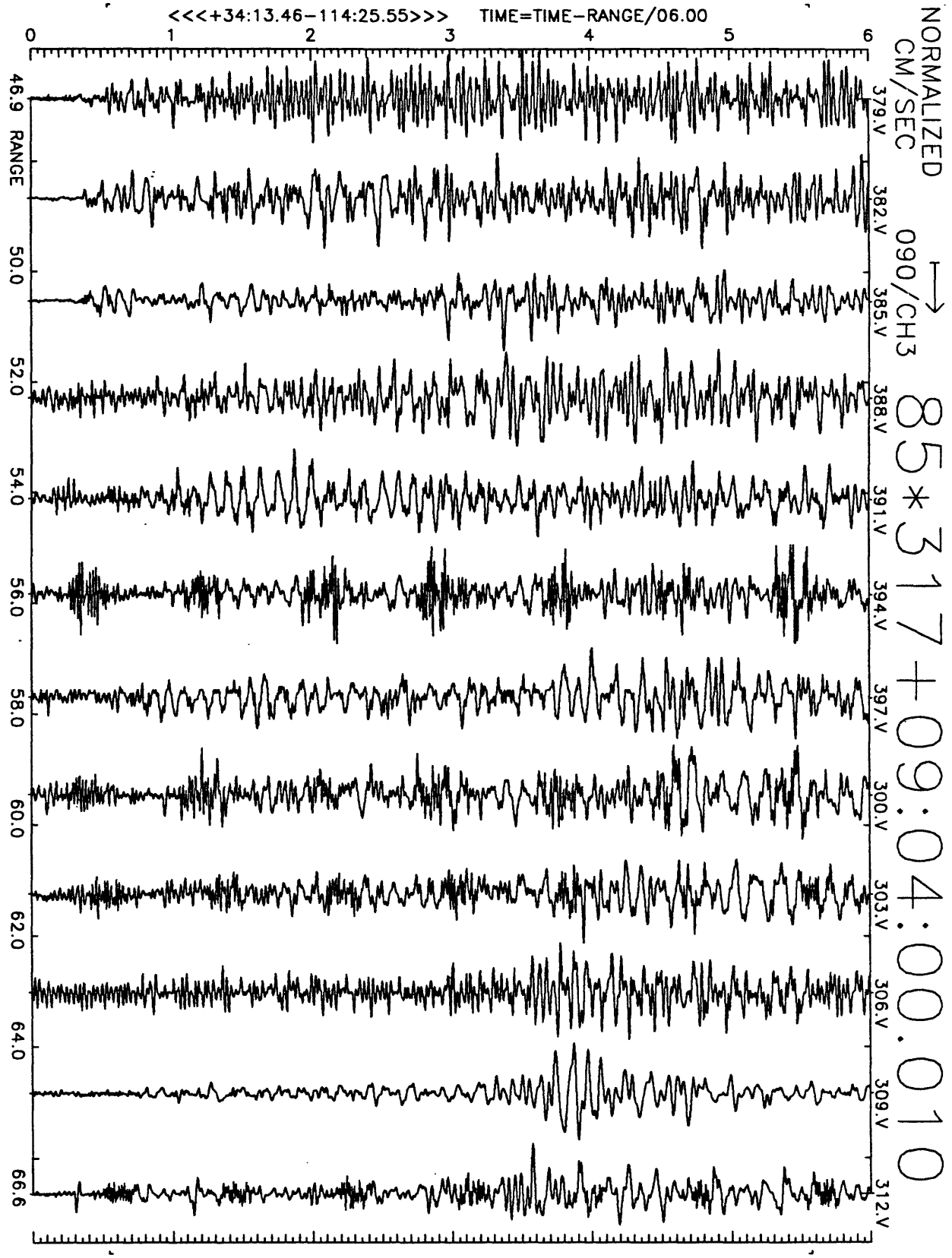

Figure A29(c), shot point 4B: 6 second velocity record. Positive N115E motion is to right. Abscissa is distance to shot point. Top of trace is labeled with station number. Times are reduced by 6 km/sec. Shot time is indicated.

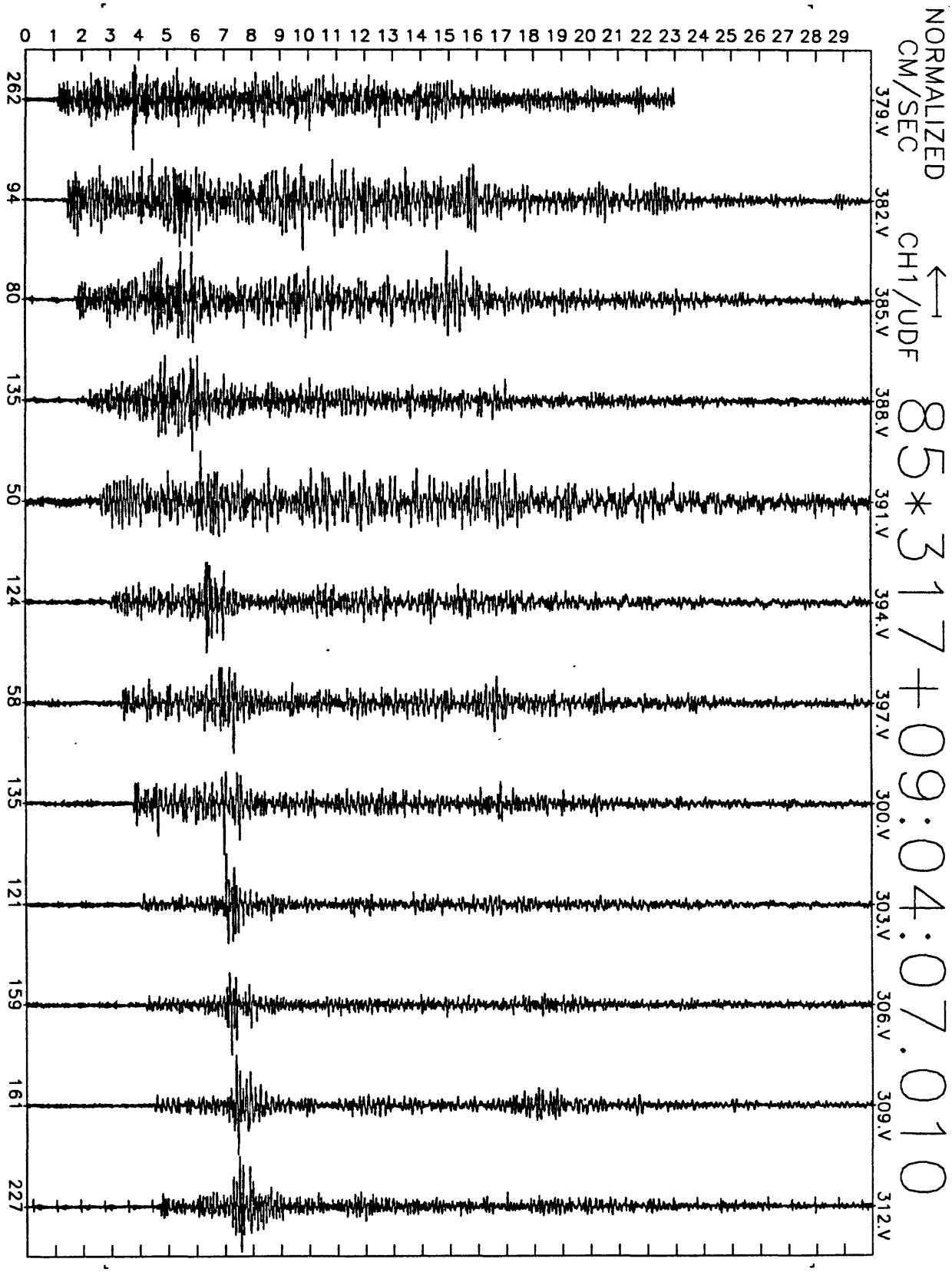

Figure A29(d), shot point 4B: 30 second vertical velocity record. Abscissa is labeled with maximum counts in record (multiply by $\frac{10}{2^{24}-2^{5}} \approx 6 \times 10^{-7}$ to get cm/sec). Times are unreduced beginning at time indicated.

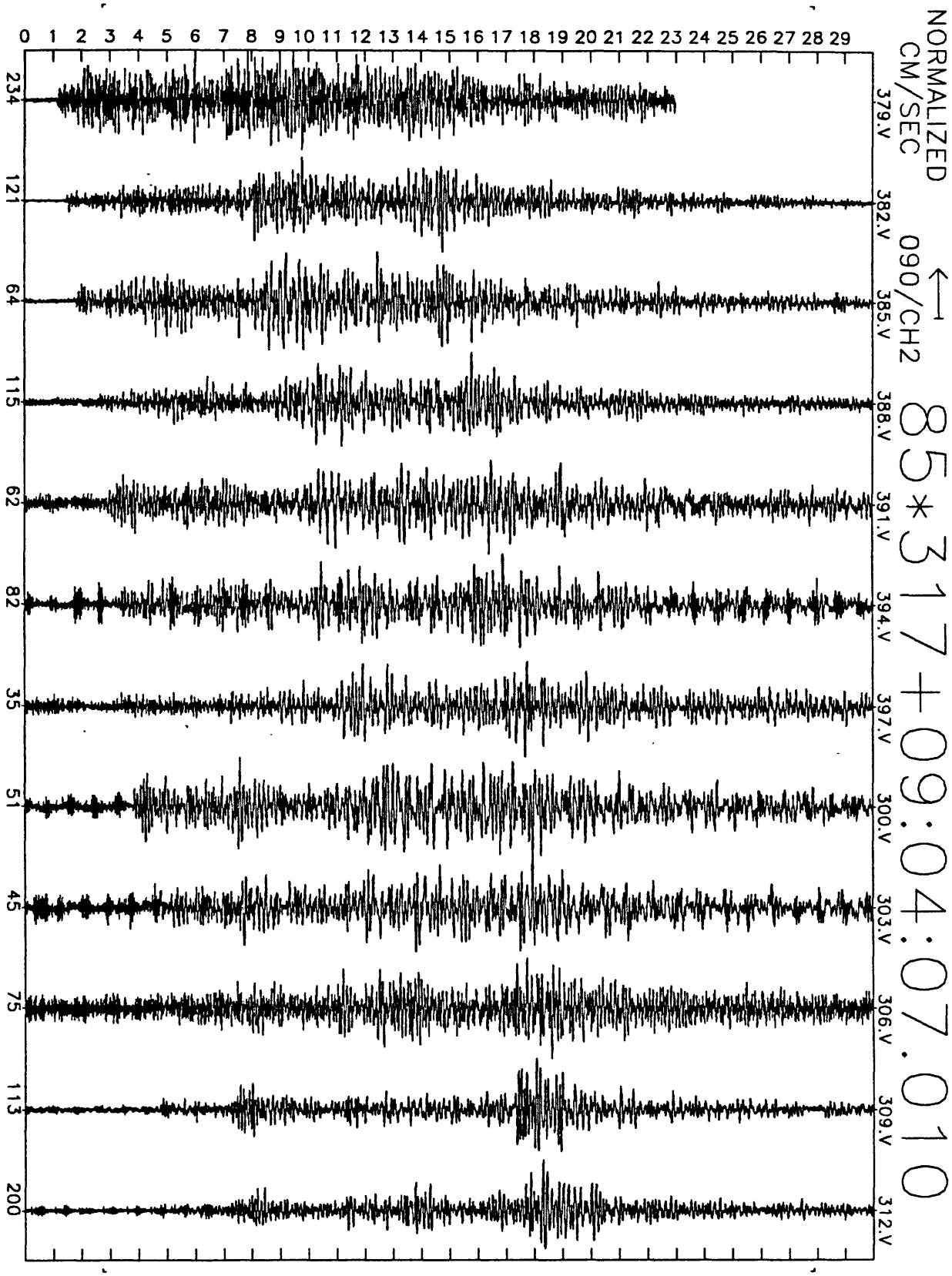

Figure A29(e), shot point 4B: 30 second N25E velocity record. Abscissa is labeled with maximum counts in record (multiply by $\frac{10}{2^{24}-2^9} \approx 6 \times 10^{-7}$ to get cm/sec). Times are unreduced beginning at time indicated.

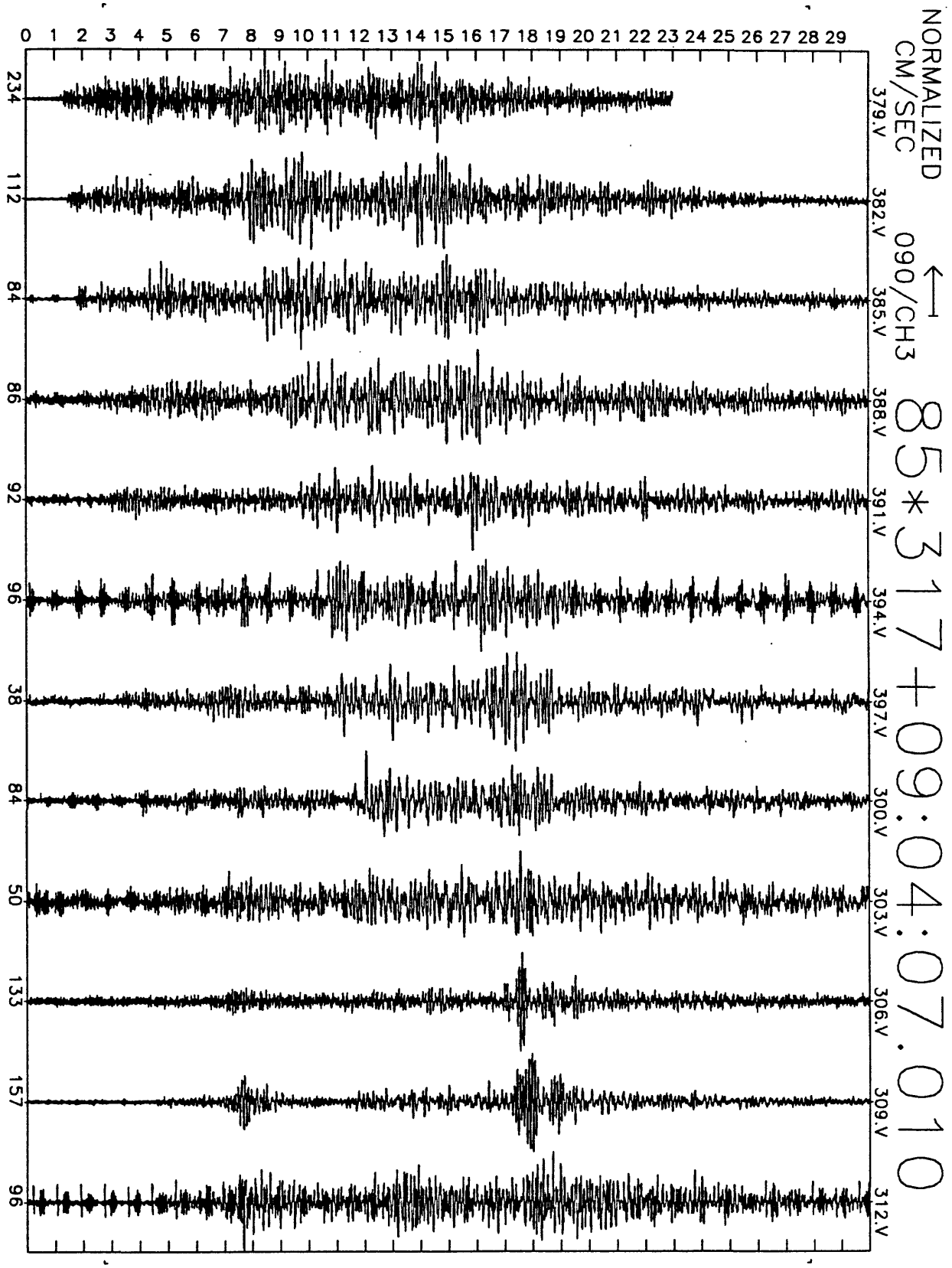

Figure A29(f), shot point 4B: 30 second N115E velocity record. Abscissa is labeled with maximum counts in record (multiply by $\frac{10}{2^{24}-2^8} \approx 6 \times 10^{-7}$ to get cm/sec). Times are unreduced beginning at time indicated.

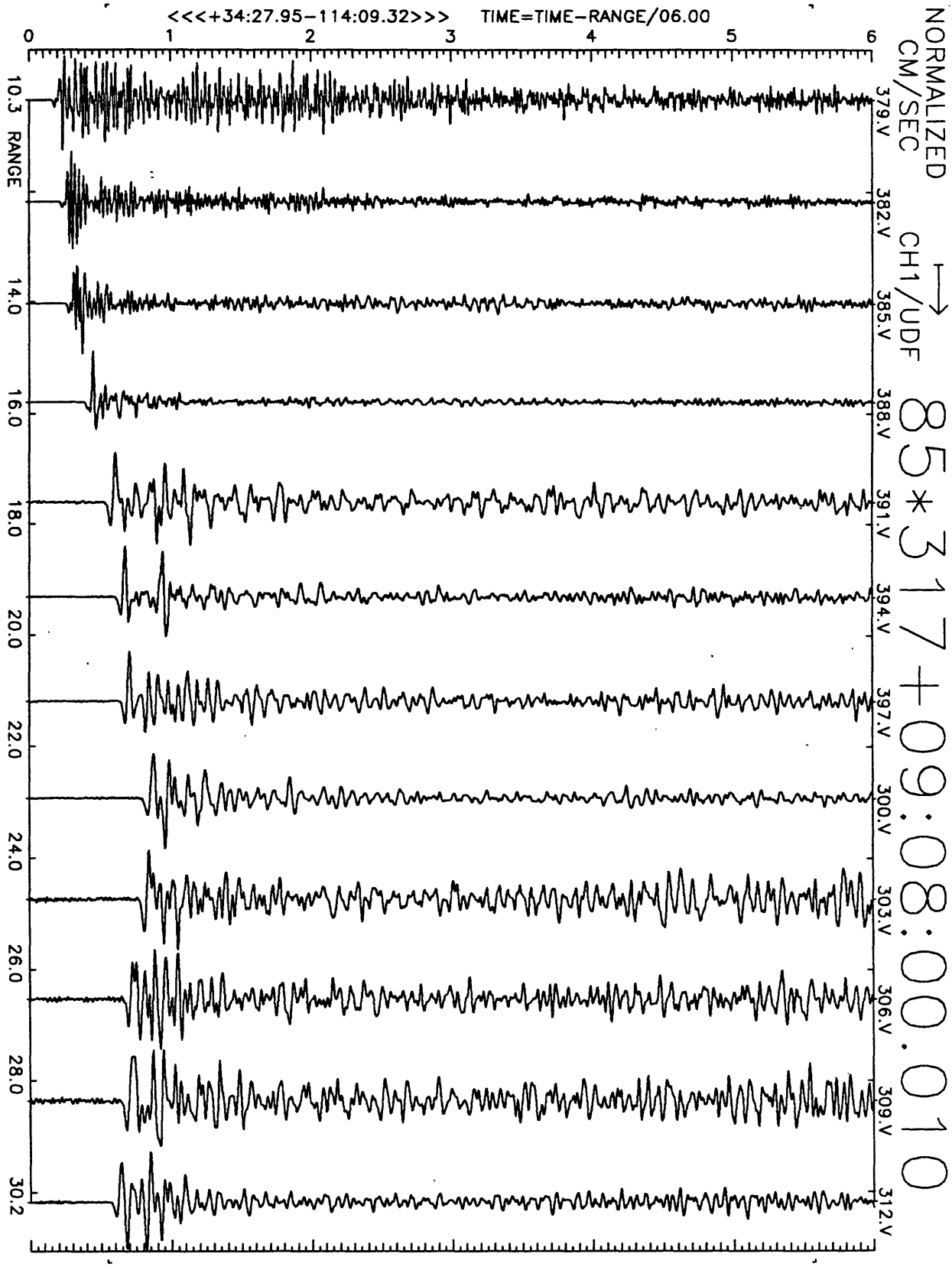

Figure A30(a), shot point 6: 6 second velocity record. Positive vertical motion is to right. Abscissa is distance to shot point. Top of trace is labeled with station number. Times are reduced by 6 km/sec. Shot time is indicated.

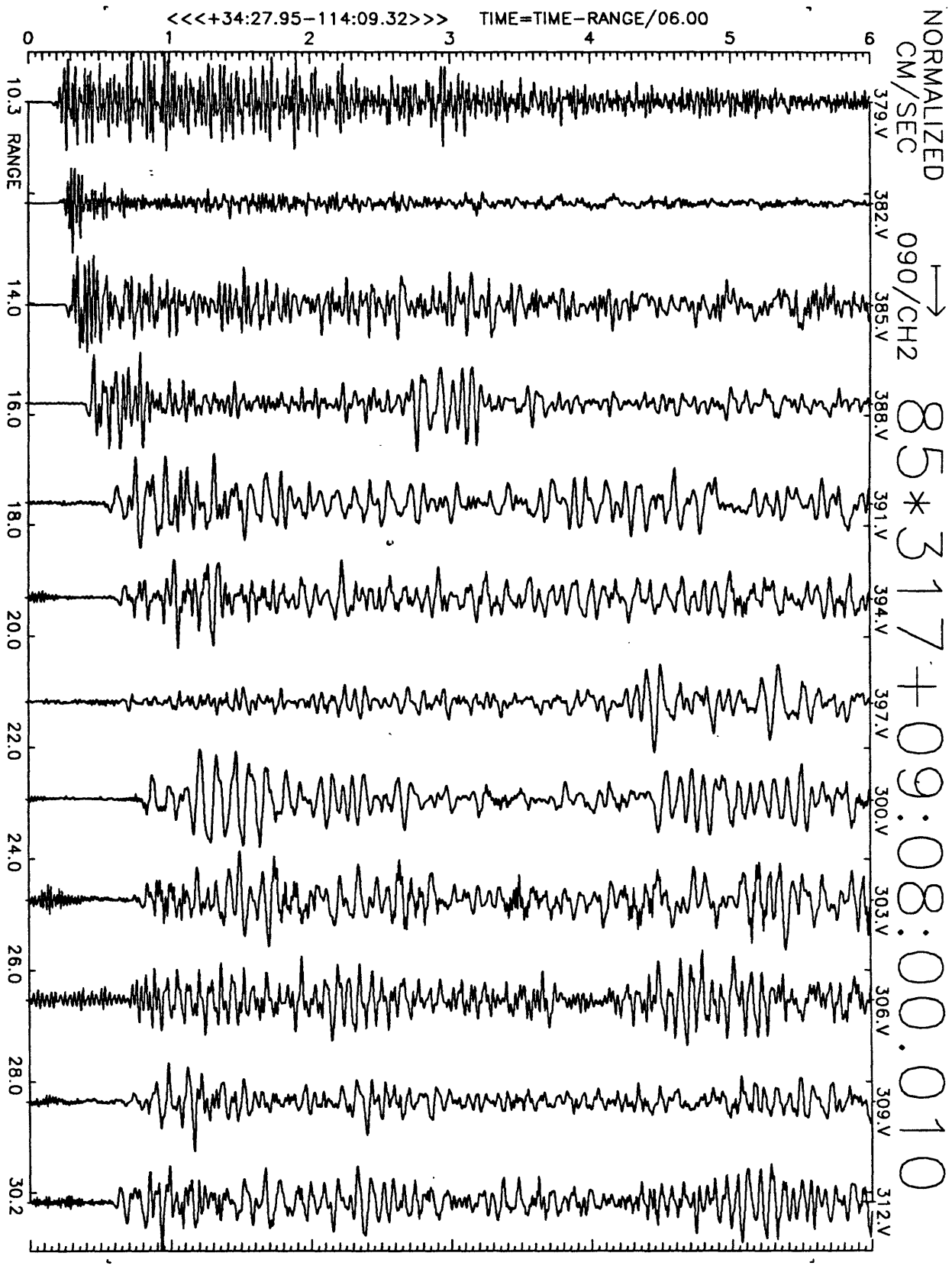

Figure A30(b), shot point 6: 6 second velocity record. Positive N25E motion is to right. Abscissa is distance to shot point. Top of trace is labeled with station number. Times are reduced by 6 km/sec. Shot time is indicated.

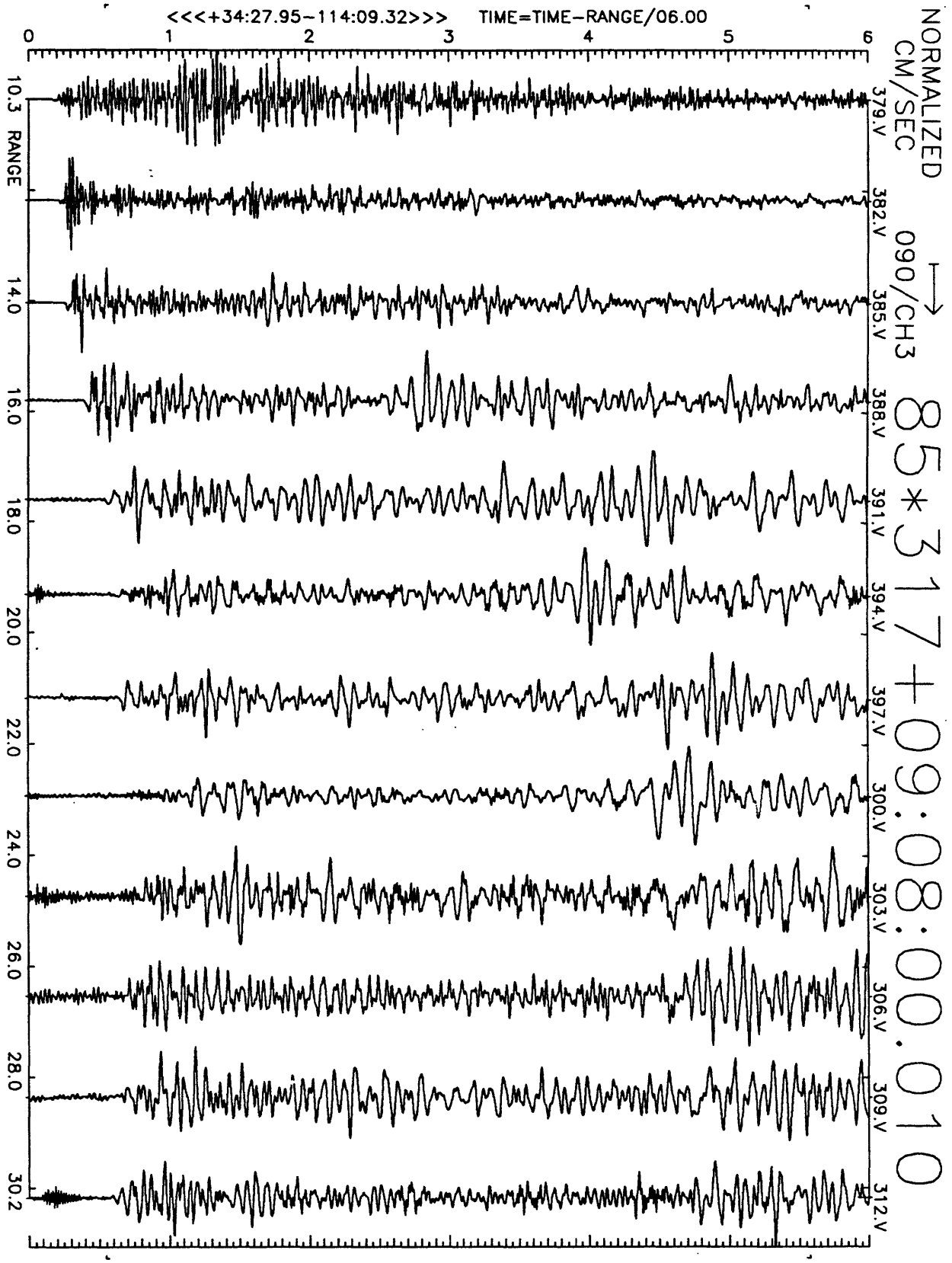

Figure A30(c), shot point 6: 6 second velocity record. Positive N115E motion is to right. Abscissa is distance to shot point. Top of trace is labeled with station number. Times are reduced by 6 km/sec. Shot time is indicated.

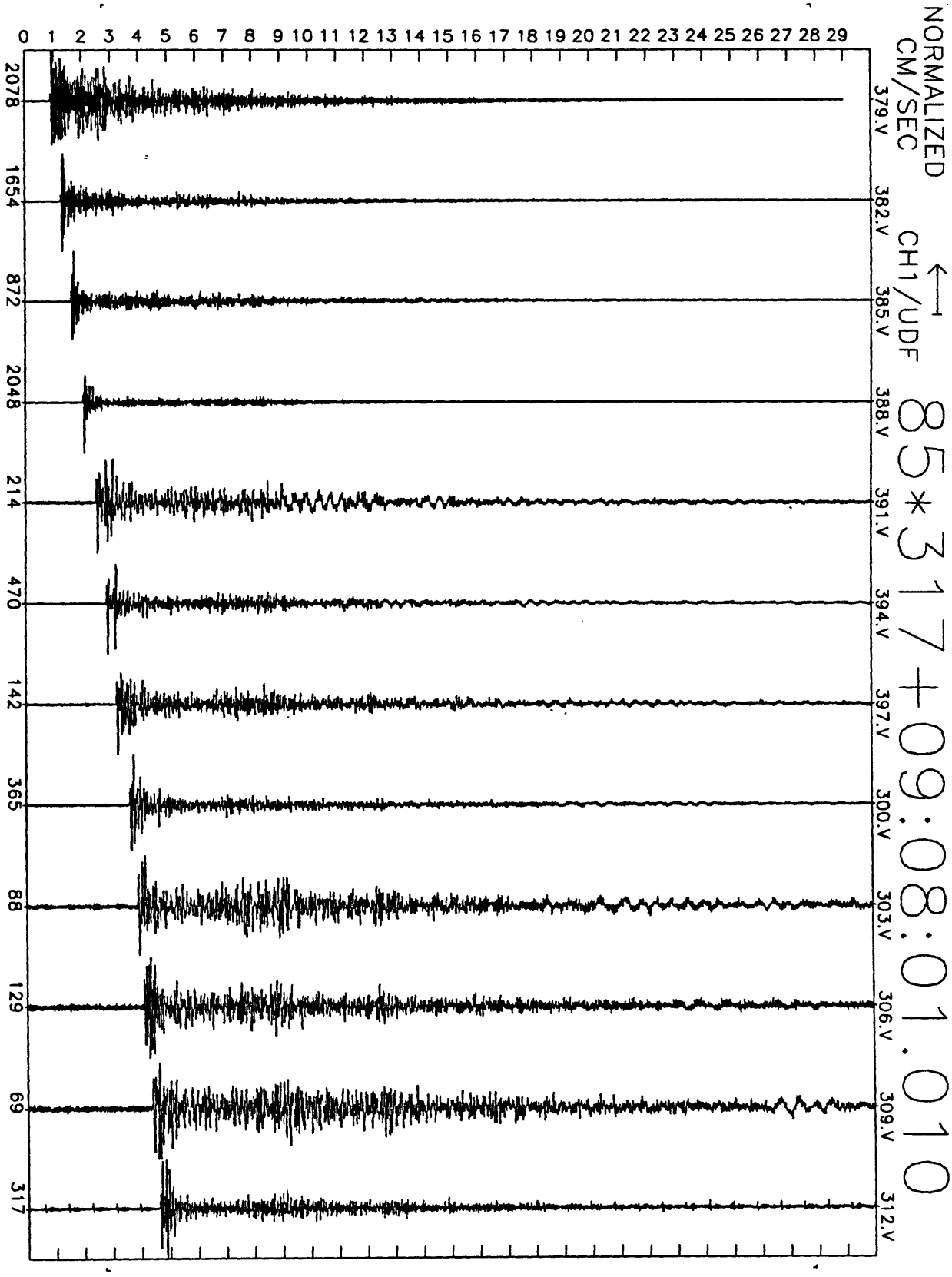

Figure A30(d), shot point 6: 30 second vertical velocity record. Abscissa is labeled with maximum counts in record (multiply by $\frac{10}{2^{24}-2^5} \approx 6 \times 10^{-7}$ to get cm/sec). Times are unreduced beginning at time indicated.

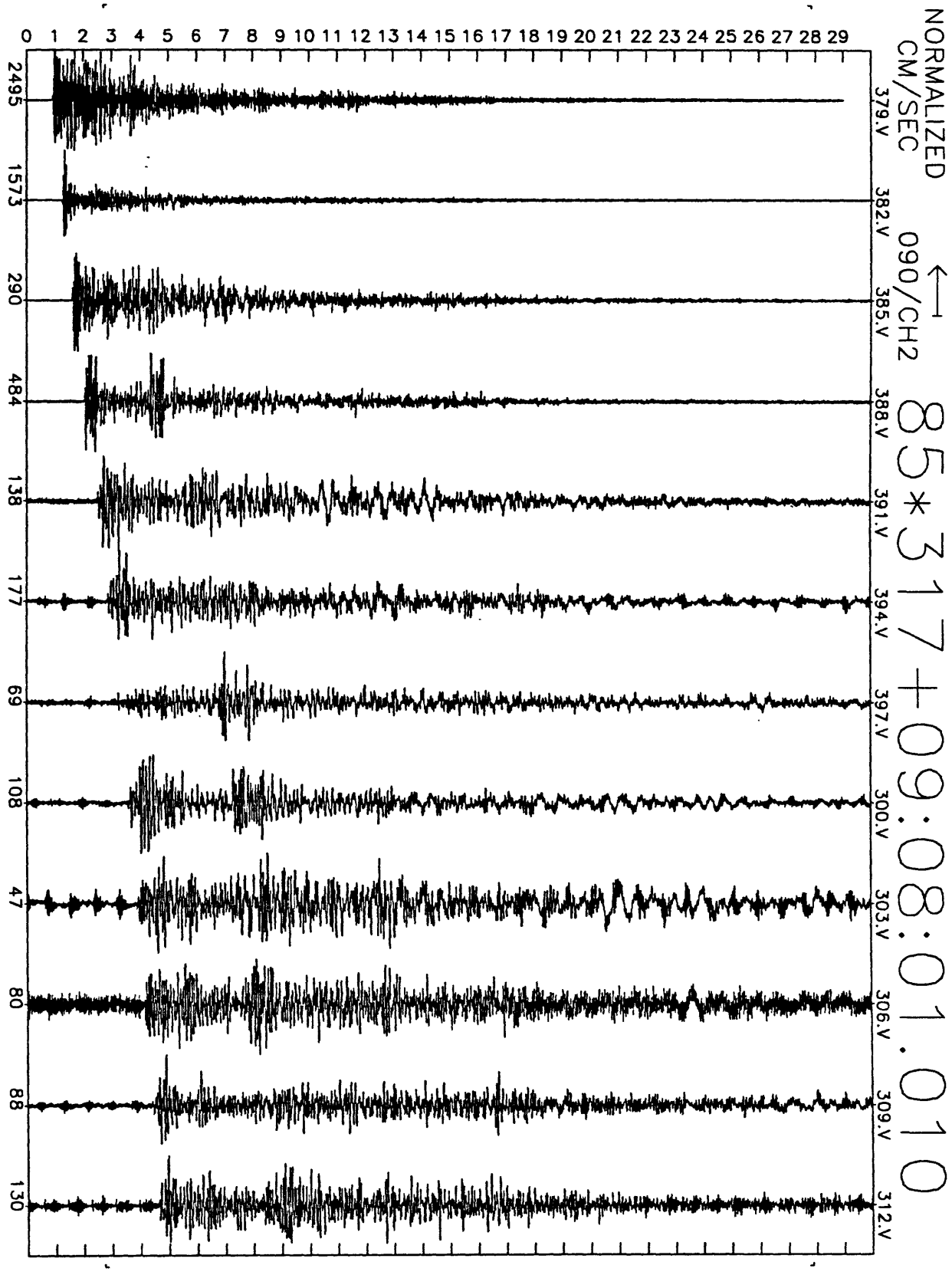

Figure A30(e), shot point 6: 30 second N25E velocity record. Abscissa is labeled with maximum counts in record (multiply by $\frac{10}{2^{24}-2^{9}} \approx 6 \times 10^{-7}$ to get cm/sec). Times are unreduced beginning at time indicated.

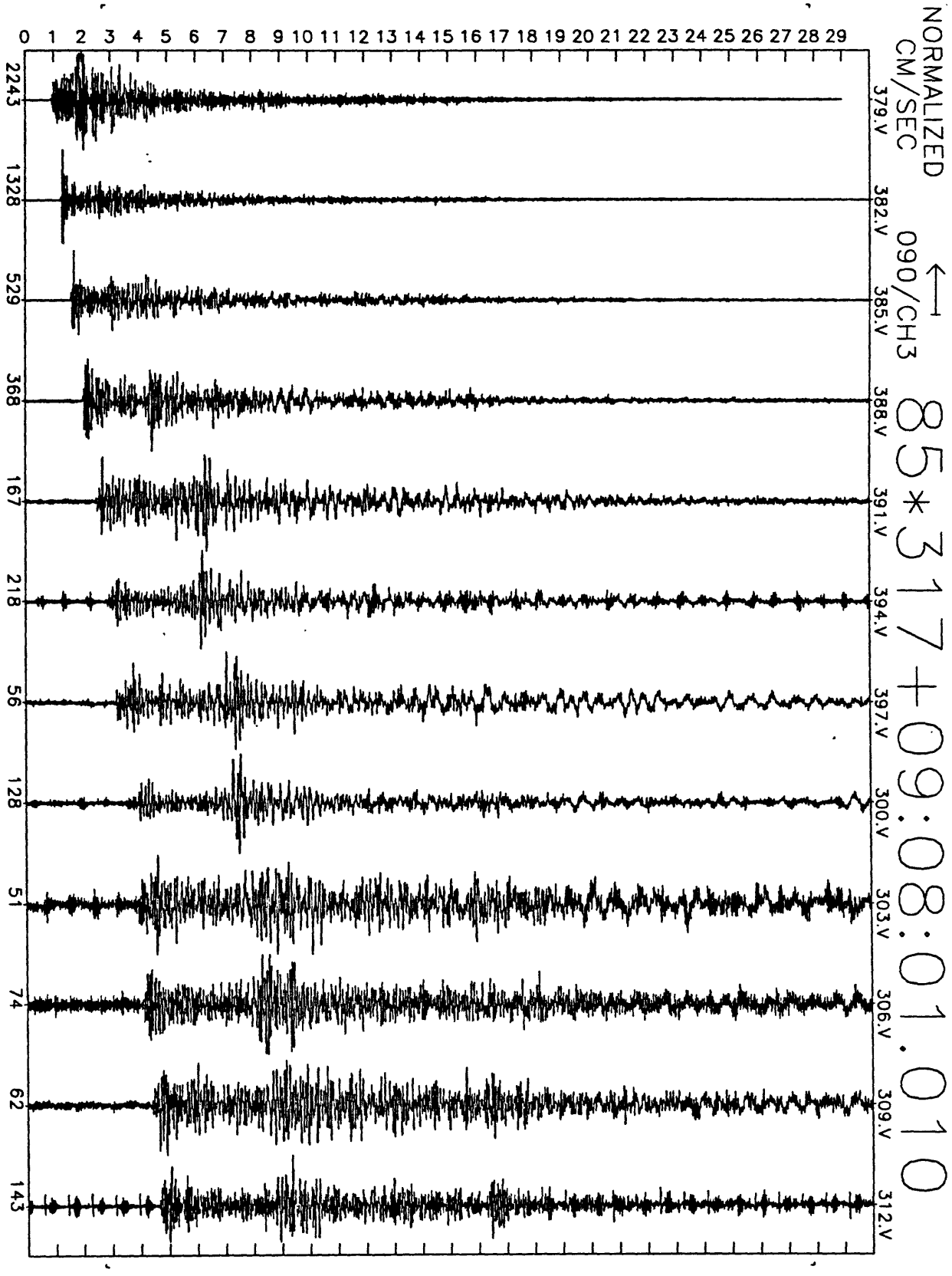

Figure A30(f), shot point 6: 30 second N115E velocity record. Abscissa is labeled with maximum counts in record (multiply by $\frac{10}{2^{24}-2^{0}} \approx 6 \times 10^{-7}$ to get cm/sec). Times are unreduced beginning at time indicated.

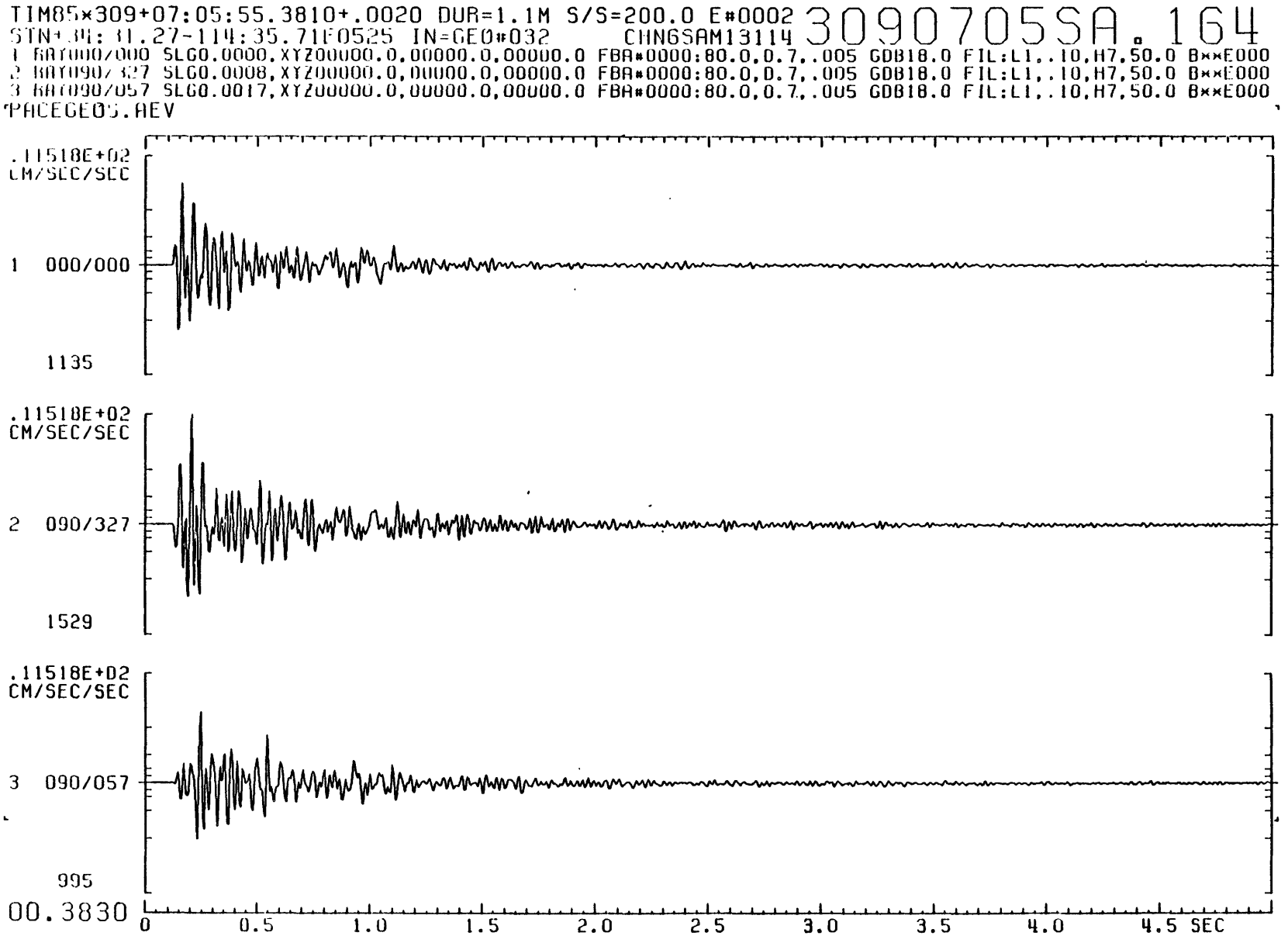

Figure B1(a), shot point 9: Three component accelerogram for station 164. Lower traces show horizontal motion. Azimuths are indicated imediately to the left of the traces. Start time is arbitrary.

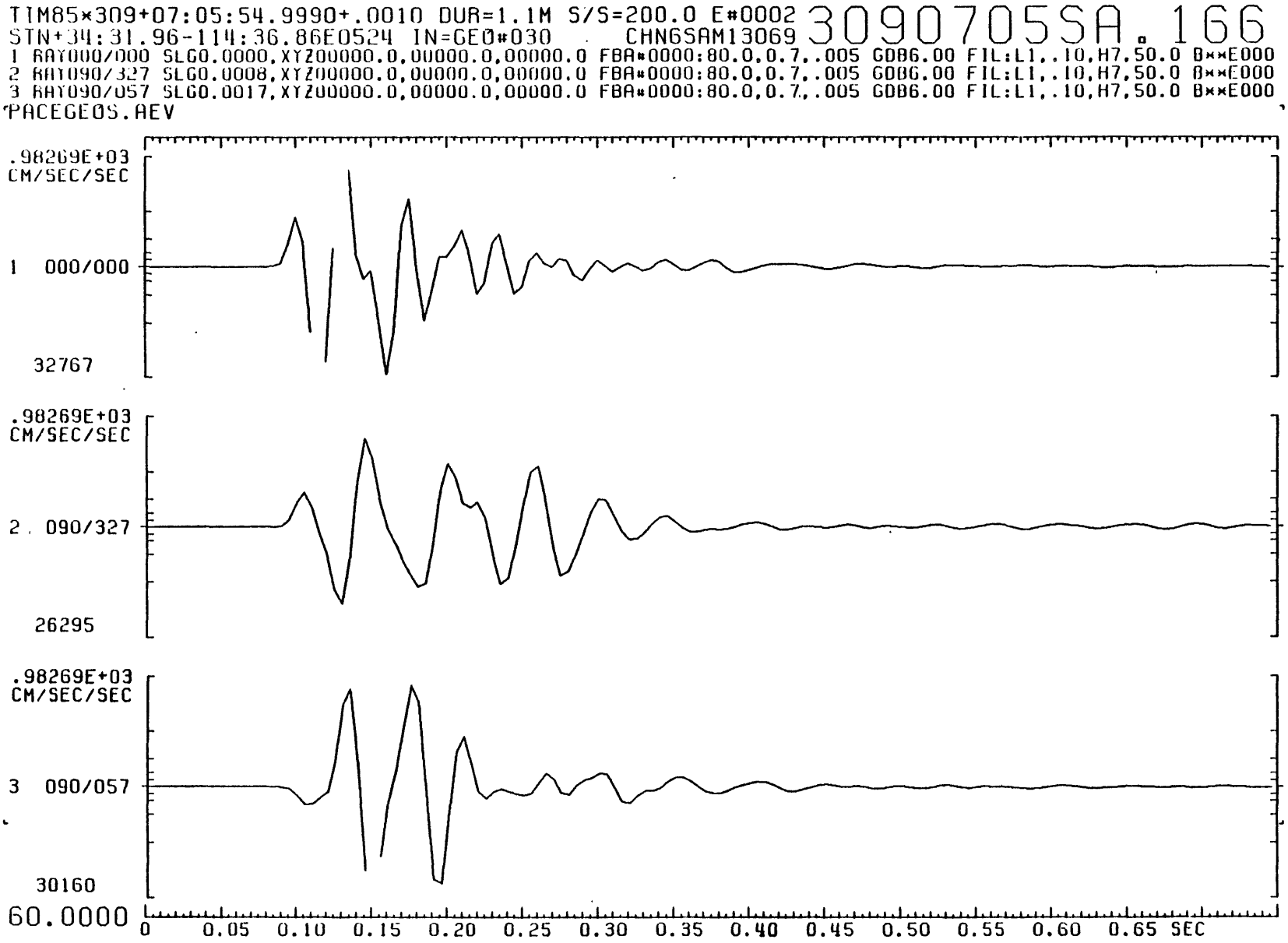

Figure B1(b), shot point 9: Three component accelerogram for station 166. Lower traces show horizontal motion. Azimuths are indicated imediately to the left of the traces. Start time is arbitrary. Only on scale data points are plotted.

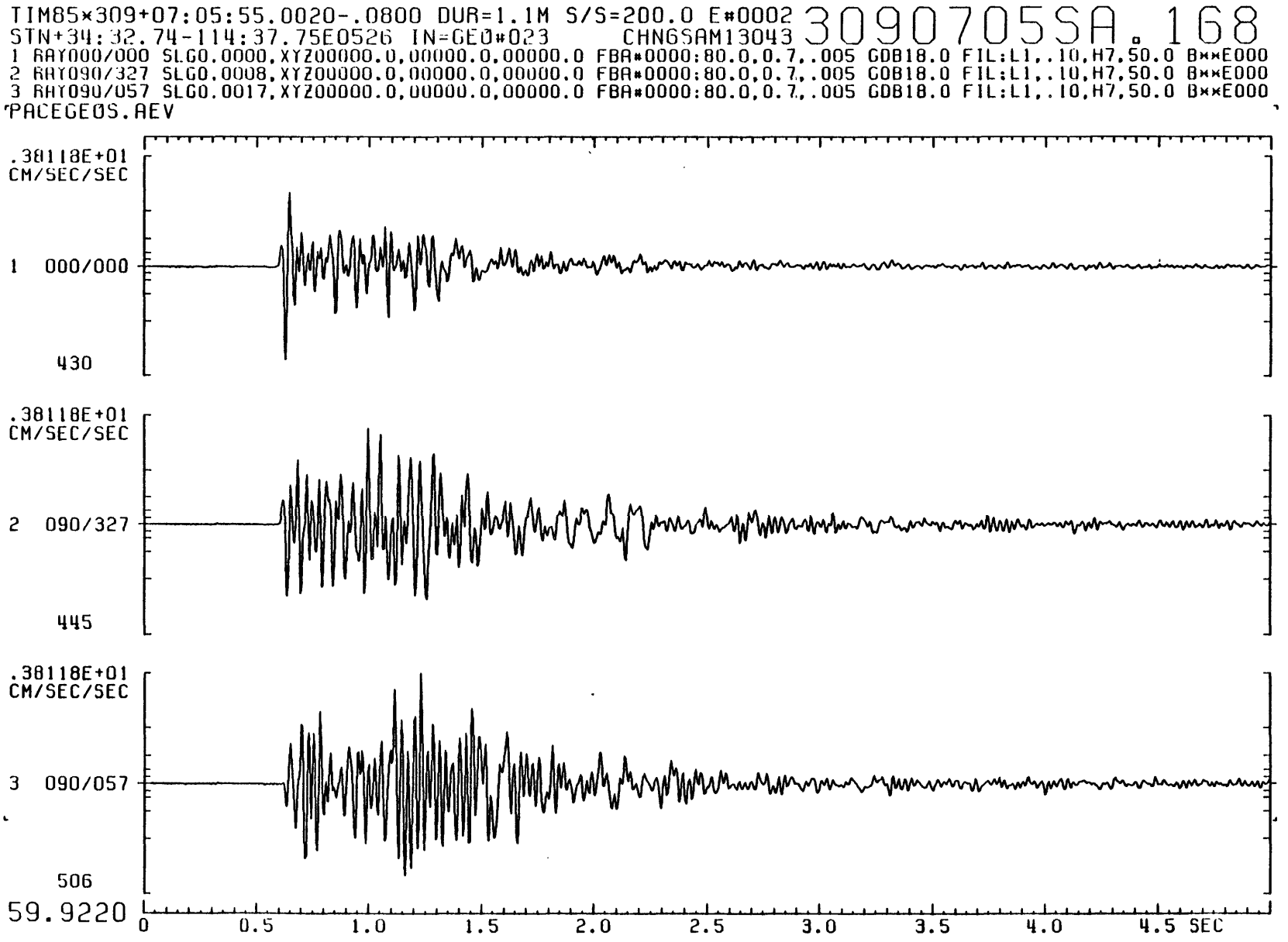

Figure B1(c), shot point 9: Three component accelerogram for station 168. Lower traces show horizontal motion. Azimuths are indicated imediately to the left of the traces. Start time is arbitrary.

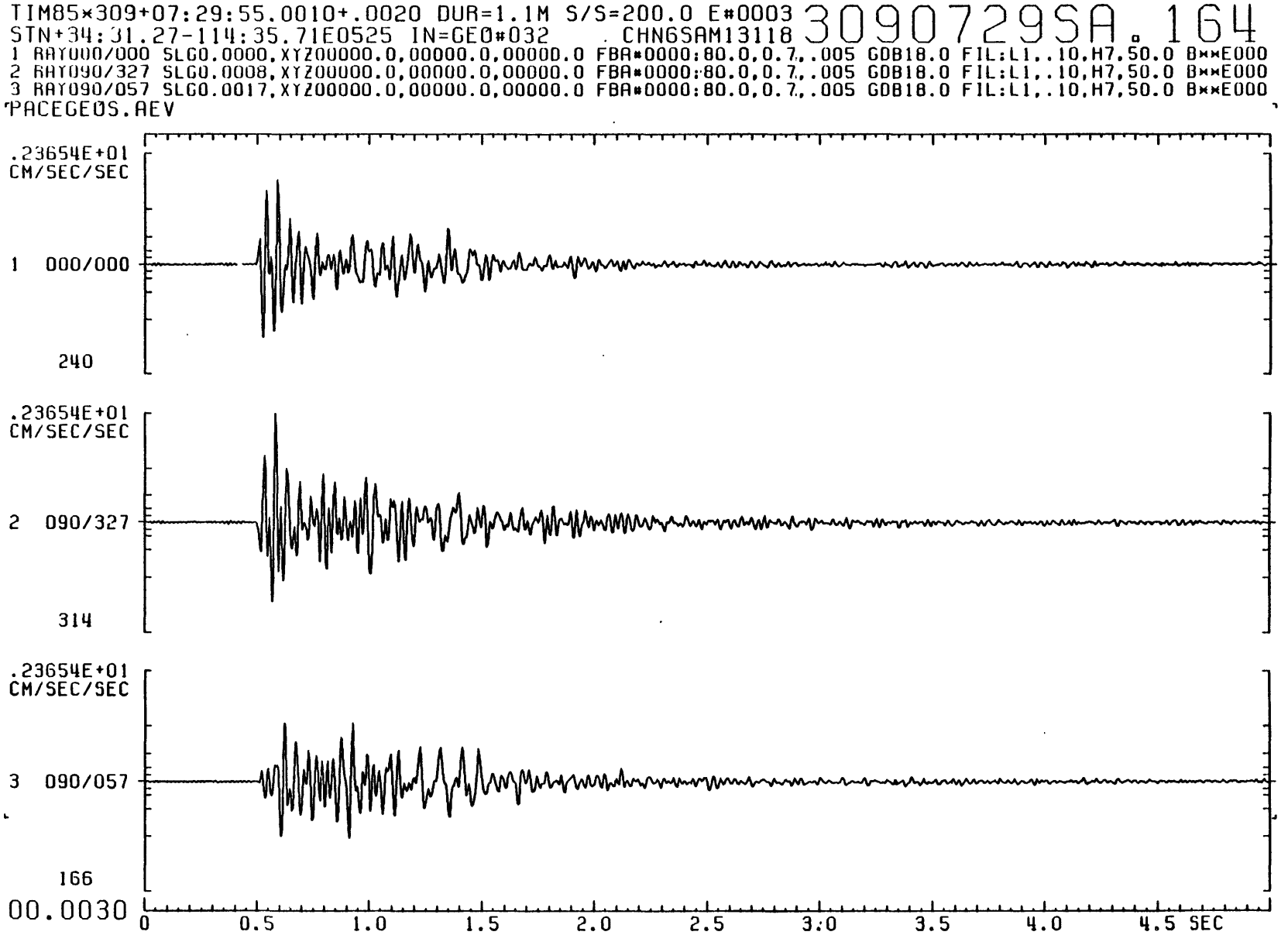

Figure B2(a), shot point 9′: Three component accelerogram for station 164. Lower traces show horizontal motion. Azimuths are indicated imediately to the left of the traces. Start time is arbitrary.

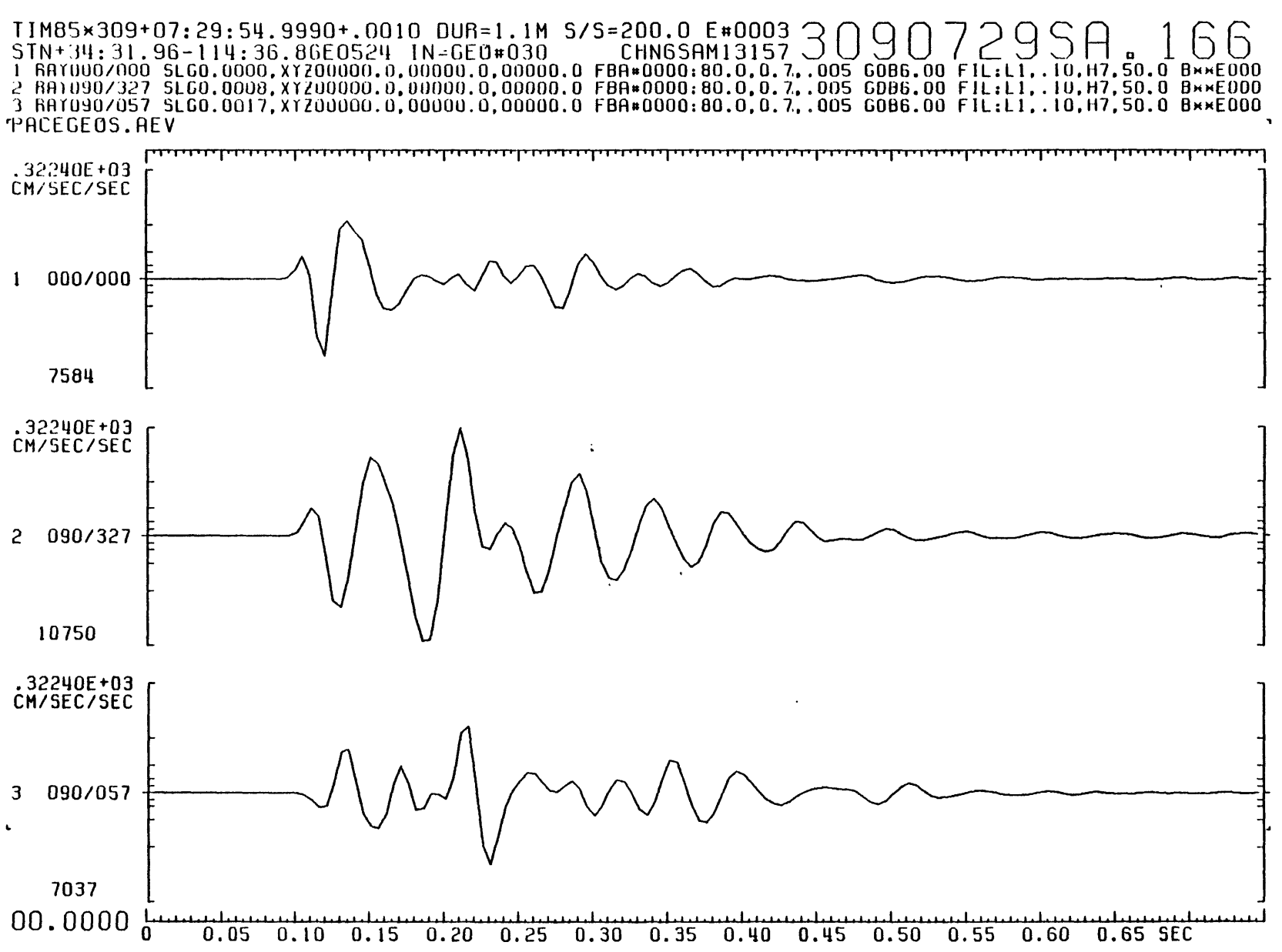

Figure B2(b), shot point 9′: Three component accelerogram for station 166. Lower traces show horizontal motion. Azimuths are indicated imediately to the left of the traces. Start time is arbitrary.

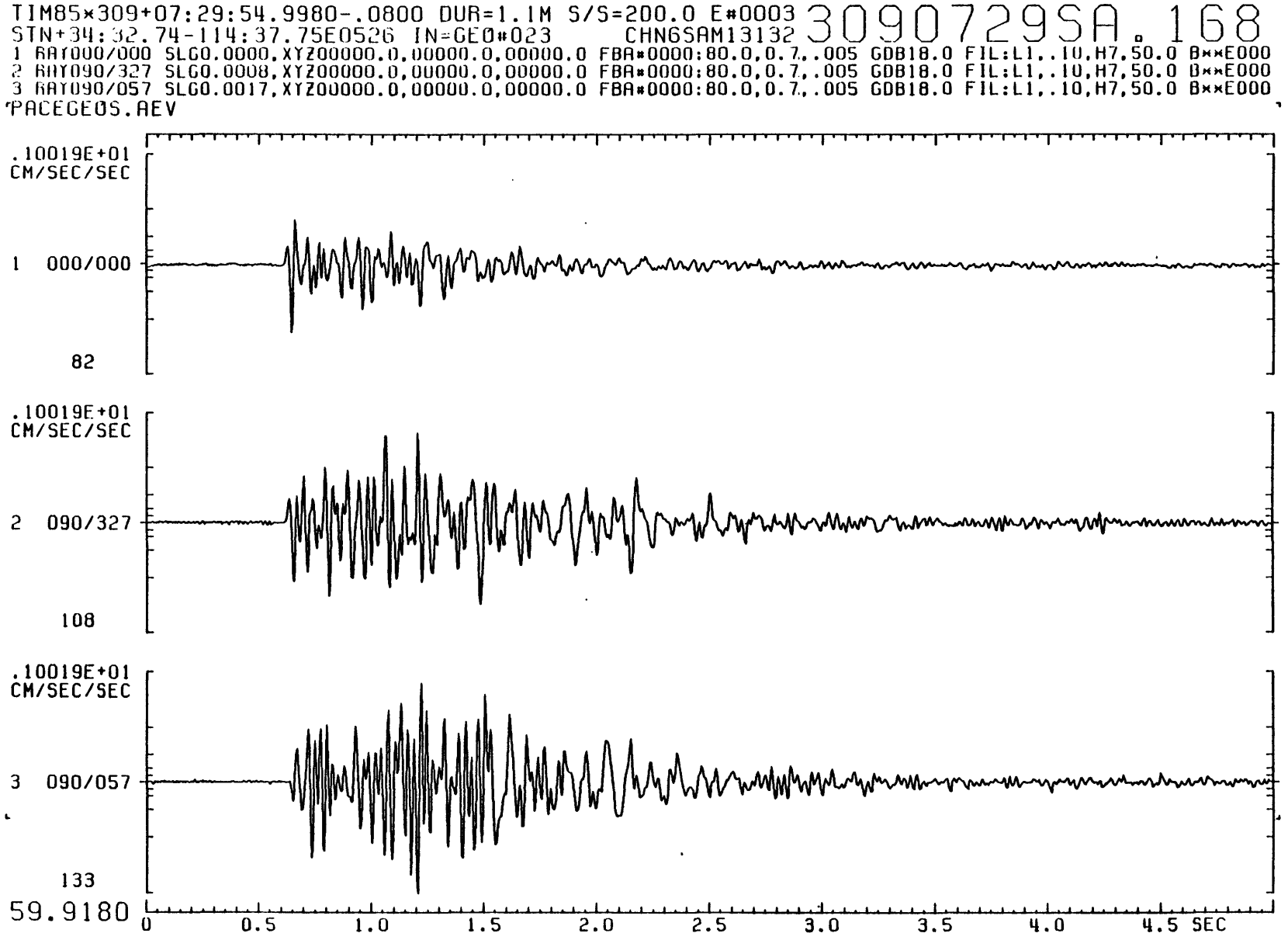

Figure B2(c), shot point 9′: Three component accelerogram for station 168. Lower traces show horizontal motion. Azimuths are indicated imediately to the left of the traces. Start time is arbitrary.

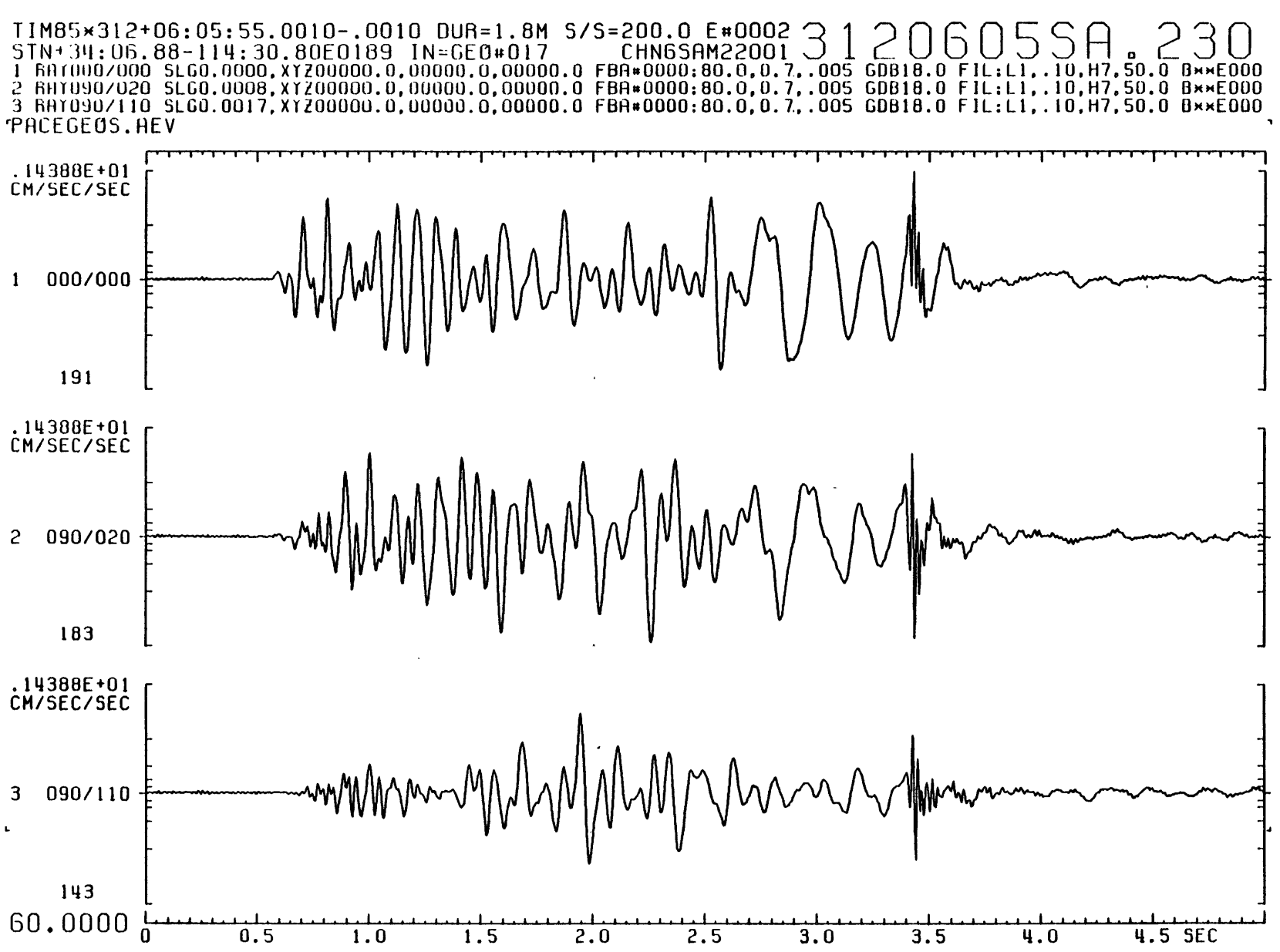

Figure B3(a), shot point 3: Three component accelerogram for station 230. Lower traces show horizontal motion. Azimuths are indicated imediately to the left of the traces. Start time is arbitrary.

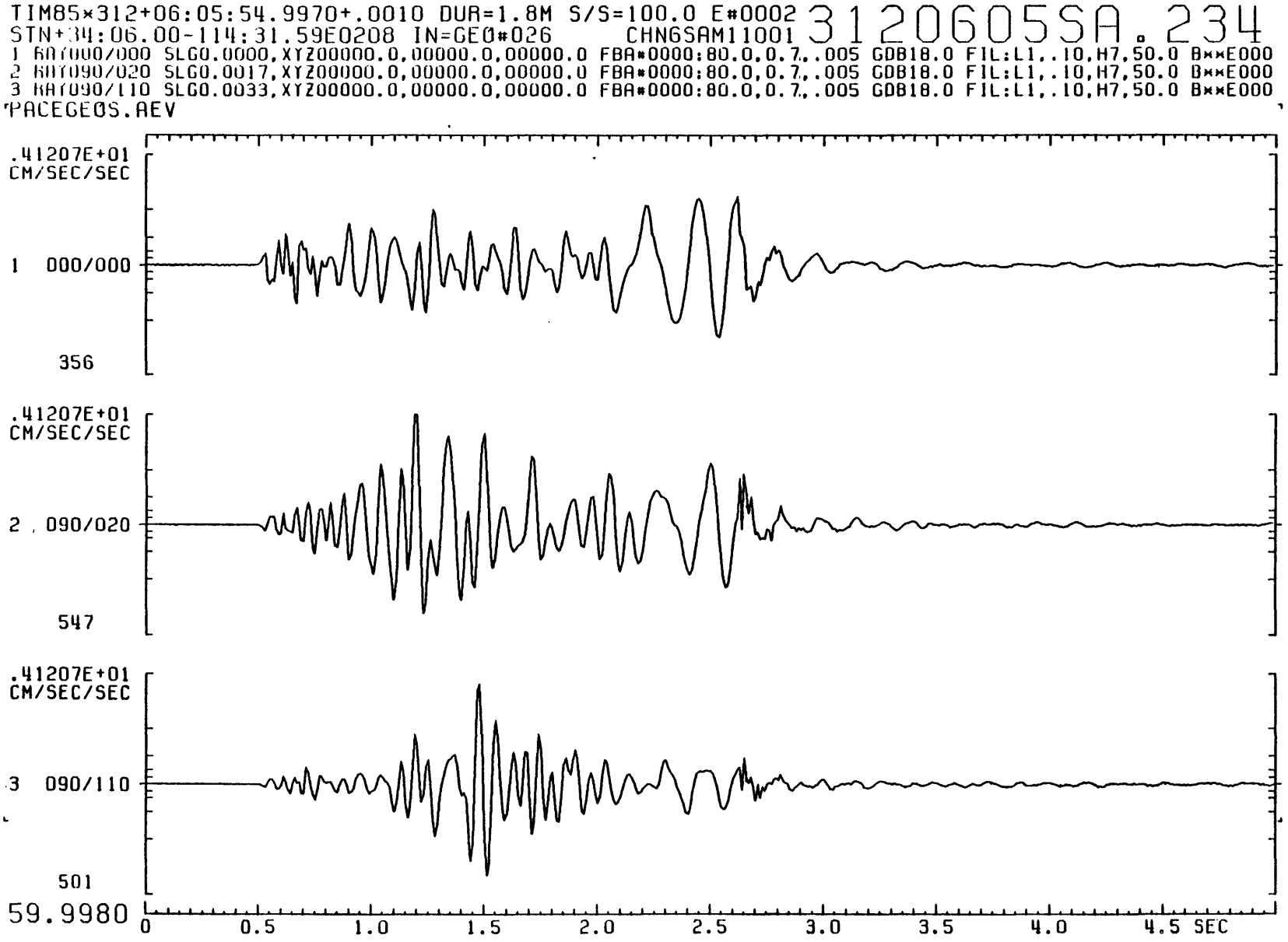

Figure B3(b), shot point 3: Three component accelerogram for station 234. Lower traces show horizontal motion. Azimuths are indicated imediately to the left of the traces. Start time is arbitrary.

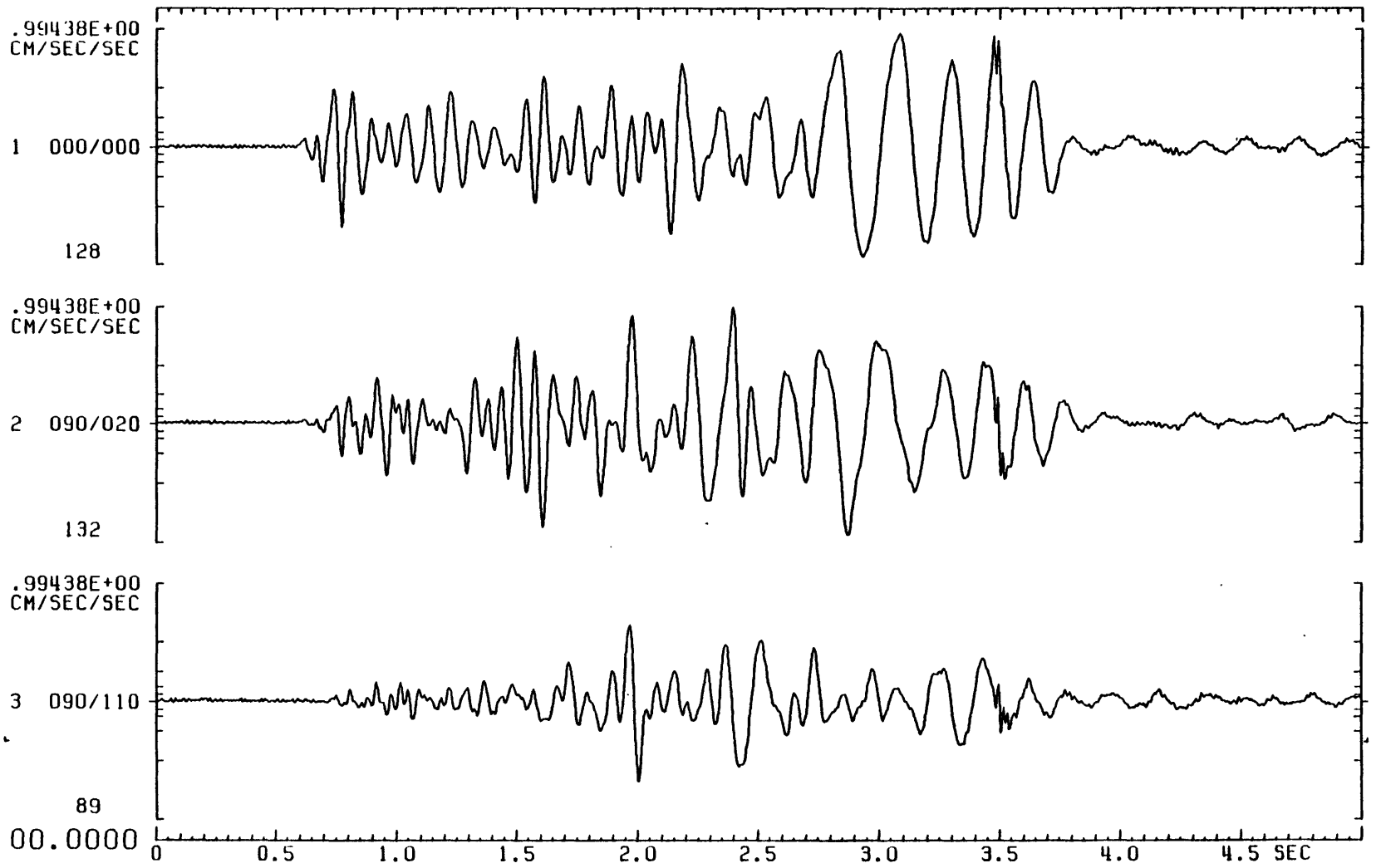

Figure B4(a), shot point 3′: Three component accelerogram for station 230. Lower traces show horizontal motion. Azimuths are indicated imediately to the left of the traces. Start time is arbitrary.

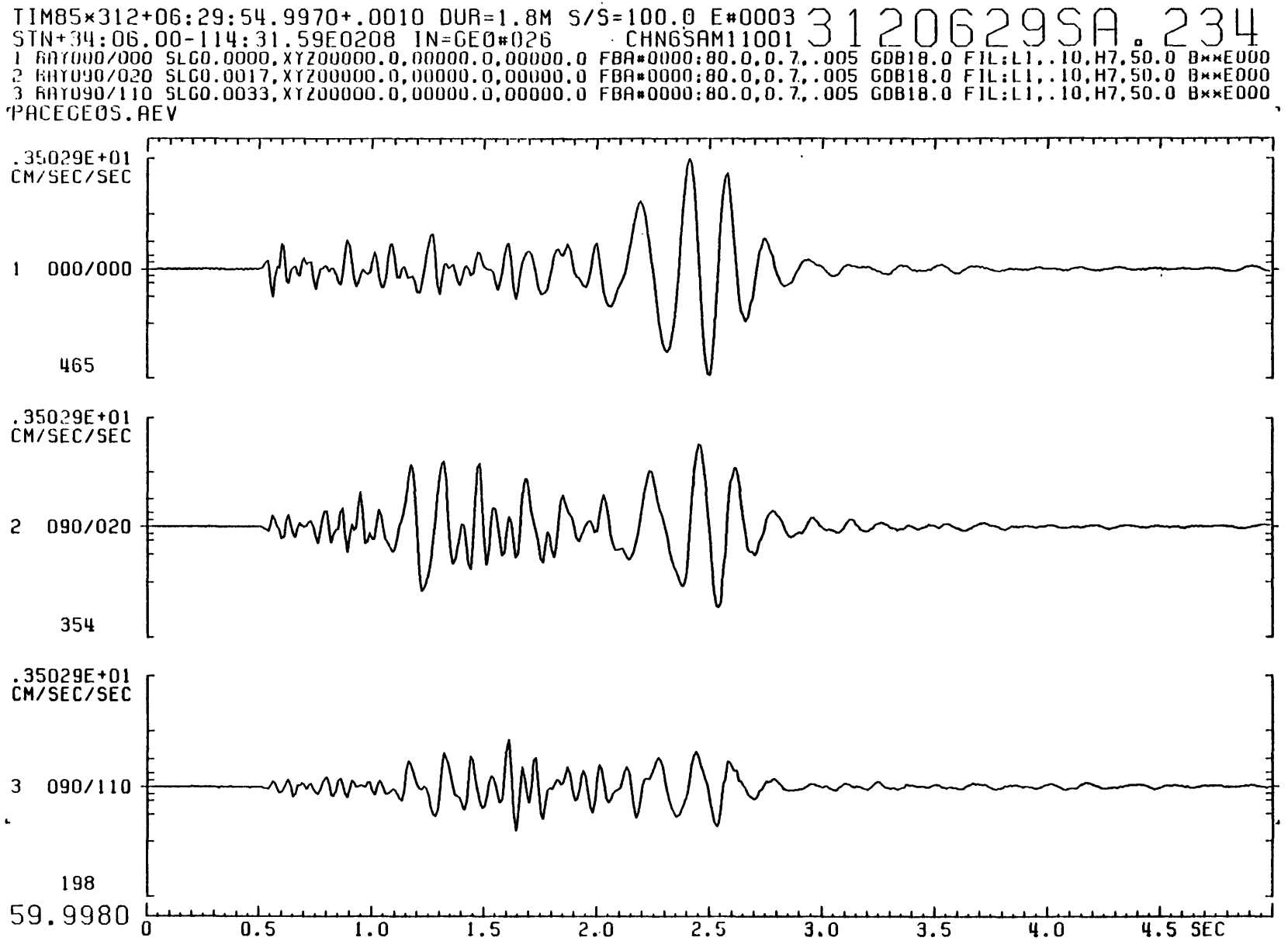

Figure B4(b), shot point 3′: Three component accelerogram for station 234. Lower traces show horizontal motion. Azimuths are indicated imediately to the left of the traces. Start time is arbitrary.

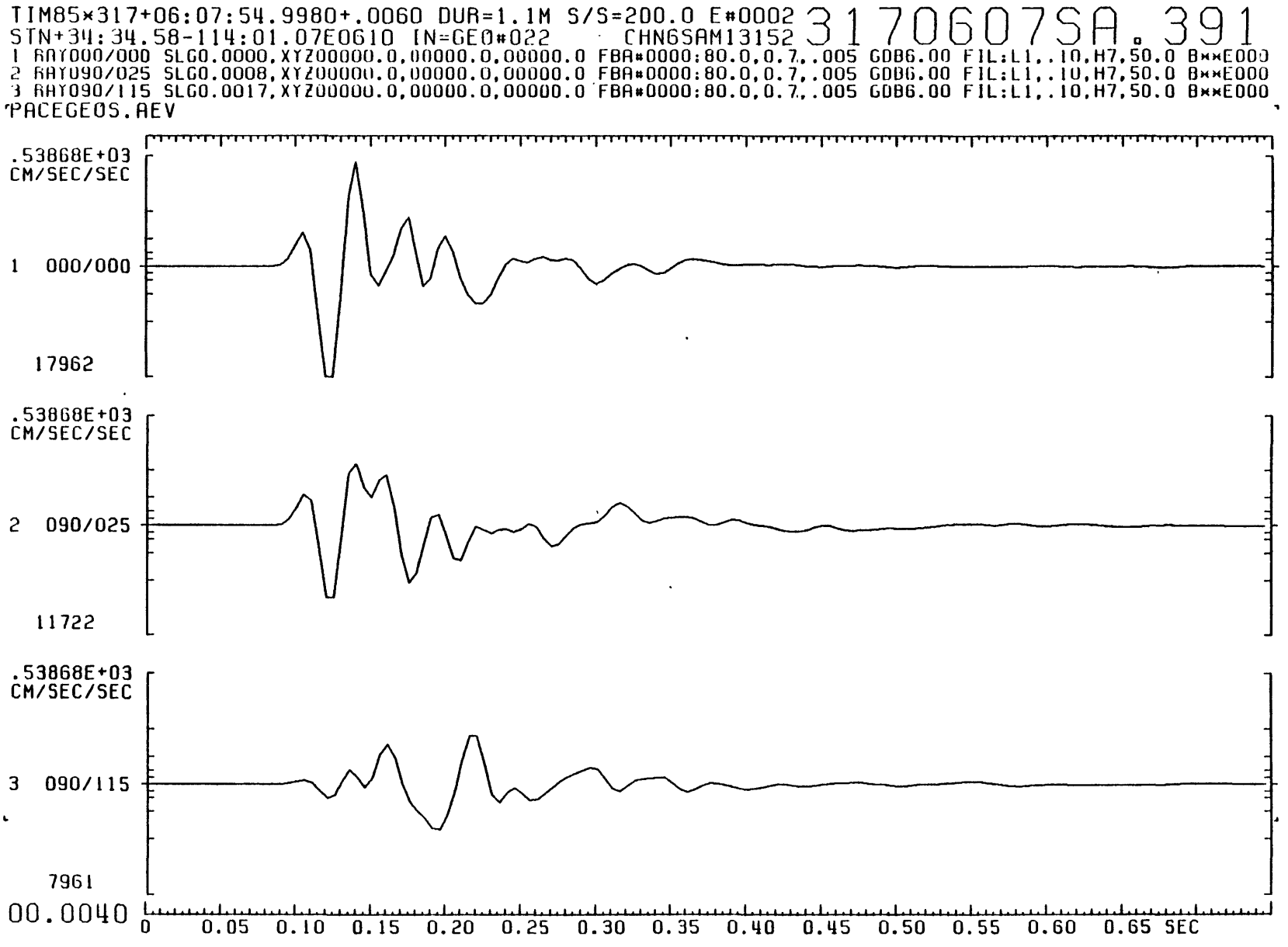

Figure B5, shot point 6X: Three component accelerogram for station 391. Lower traces show horizontal motion. Azimuths are indicated imediately to the left of the traces. Start time is arbitrary.

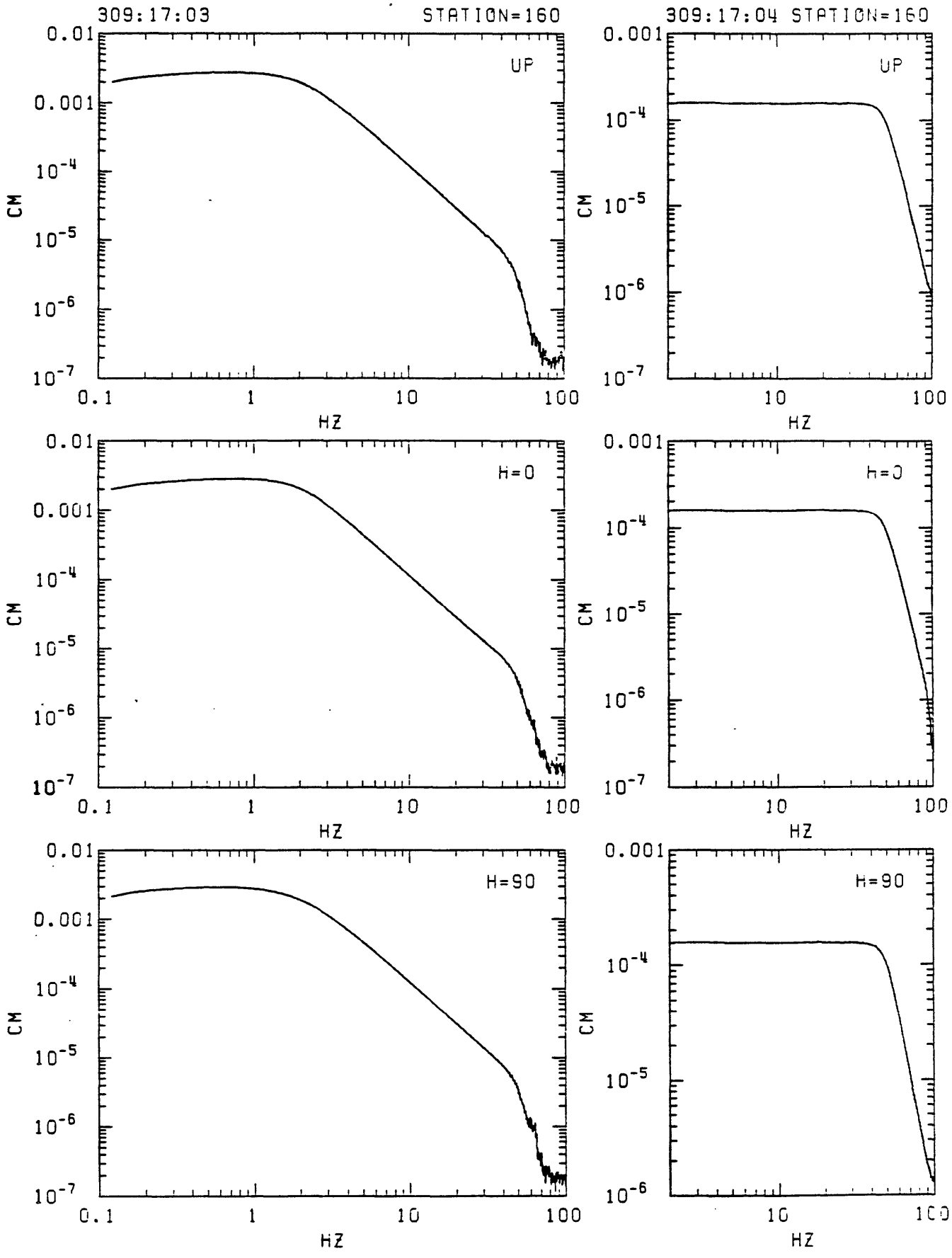

Figure C1. Station 160 in-situ velocity calibration spectra. Left: response to step in acceleration (seismometer mass released from rest at offset position). Right: response to delta function in velocity (voltage impulse applied to recorder input). From top: vertical, N33W and N57E.

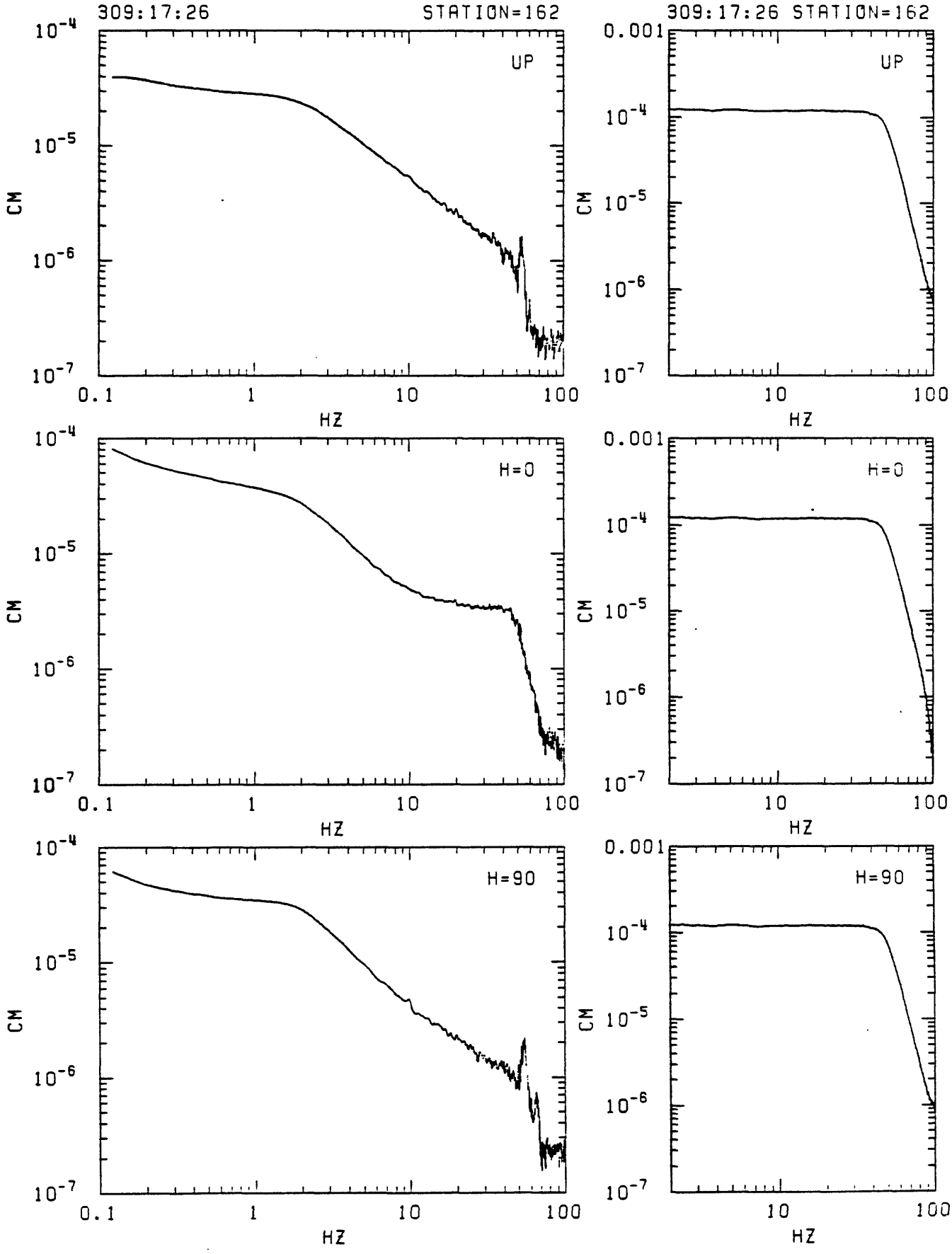

Figure C2. Station 162 in-situ velocity calibration spectra. Left: response to step in acceleration (seismometer mass released from rest at offset position). Right: response to delta function in velocity (voltage impulse applied to recorder input). From top: vertical, N33W and N57E.

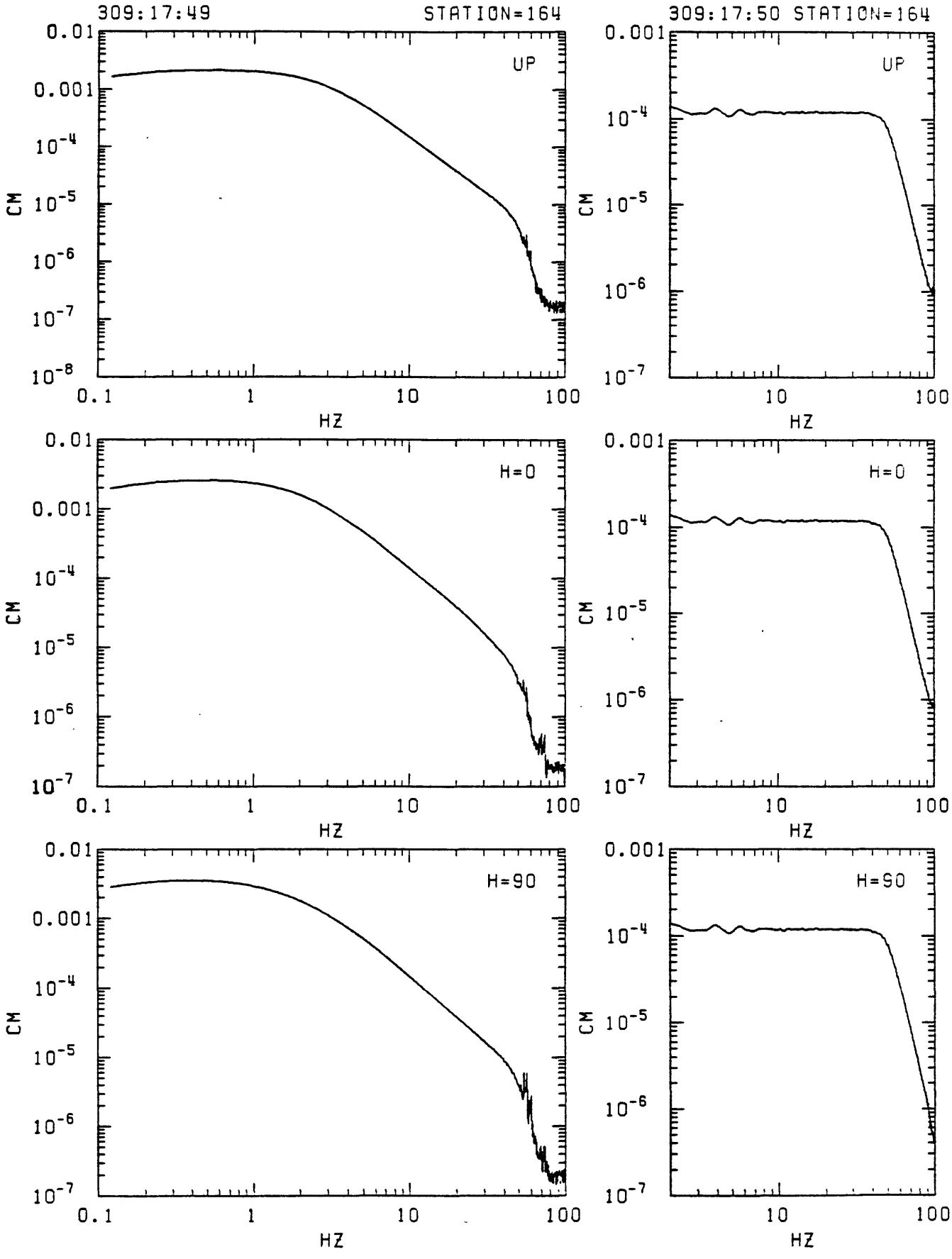

Figure C3. Station 164 in-situ velocity calibration spectra. Left: response to step in acceleration (seismometer mass released from rest at offset position). Right: response to delta function in velocity (voltage impulse applied to recorder input). From top: vertical, N33W and N57E.

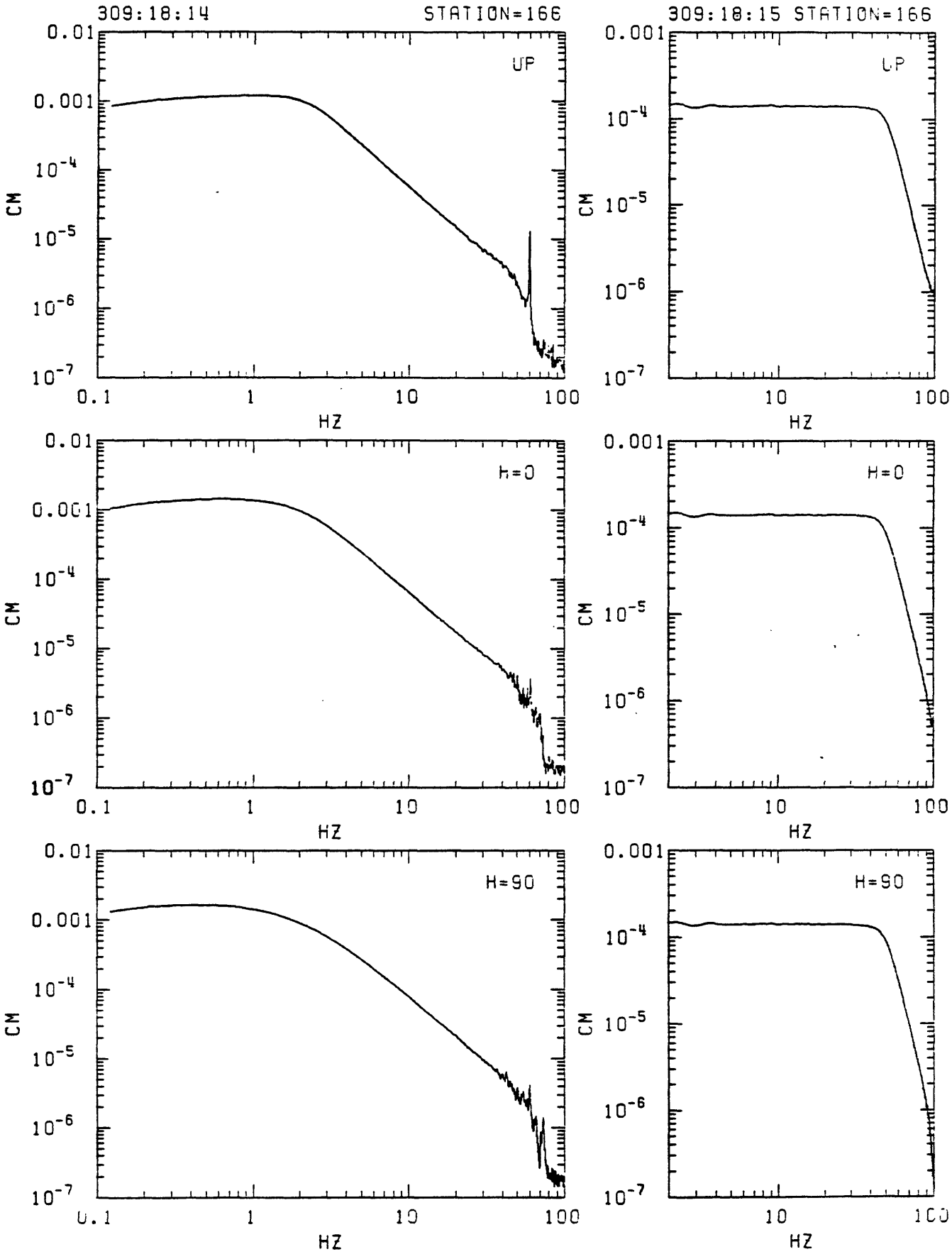

Figure C4. Station 166 in-situ velocity calibration spectra. Left: response to step in acceleration (seismometer mass released from rest at offset position). Right: response to delta function in velocity (voltage impulse applied to recorder input). From top: vertical, N33W and N57E.

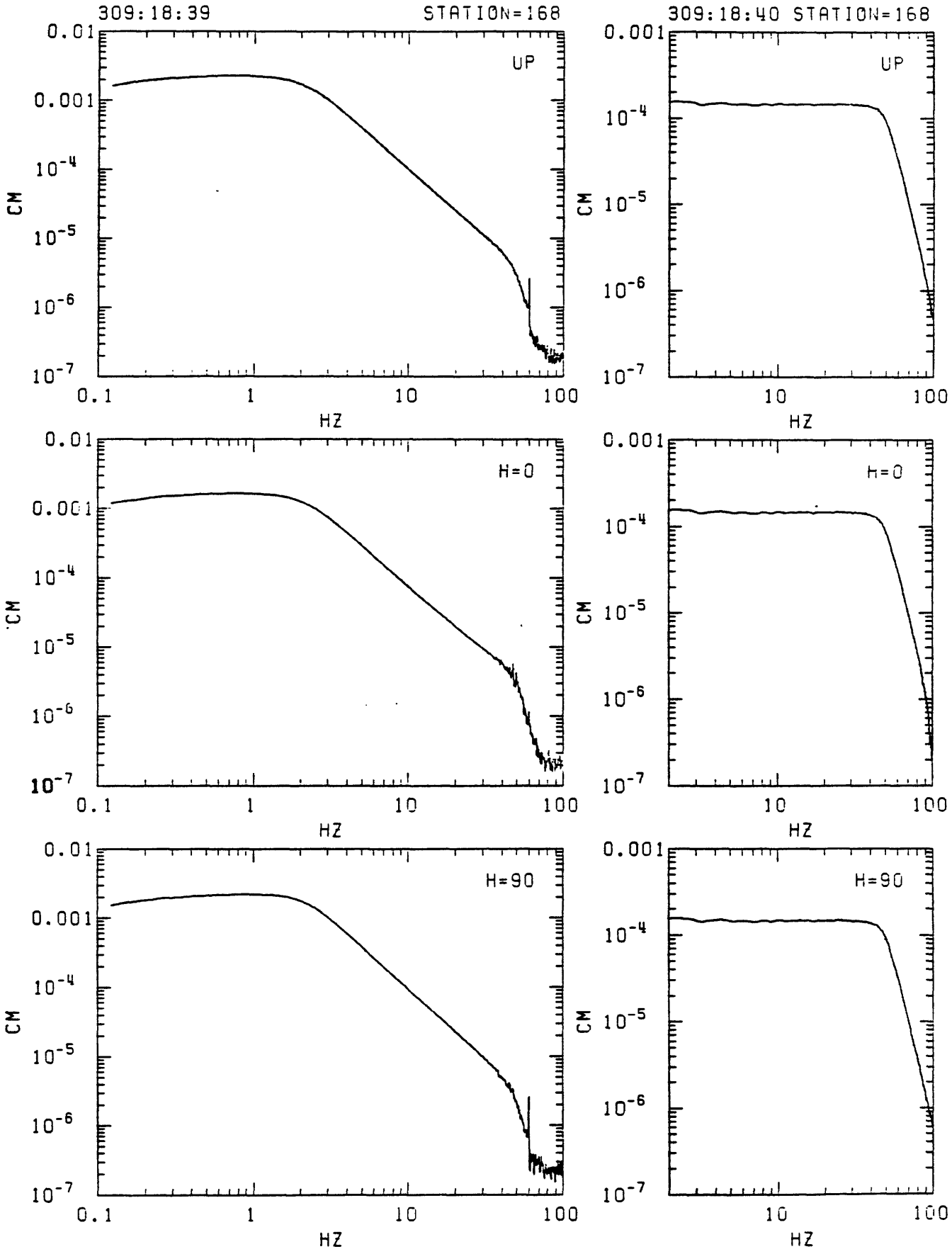

Figure C5. Station 168 in-situ velocity calibration spectra. Left: response to step in acceleration (seismometer mass released from rest at offset position). Right: response to delta function in velocity (voltage impulse applied to recorder input). From top: vertical, N33W and N57E.

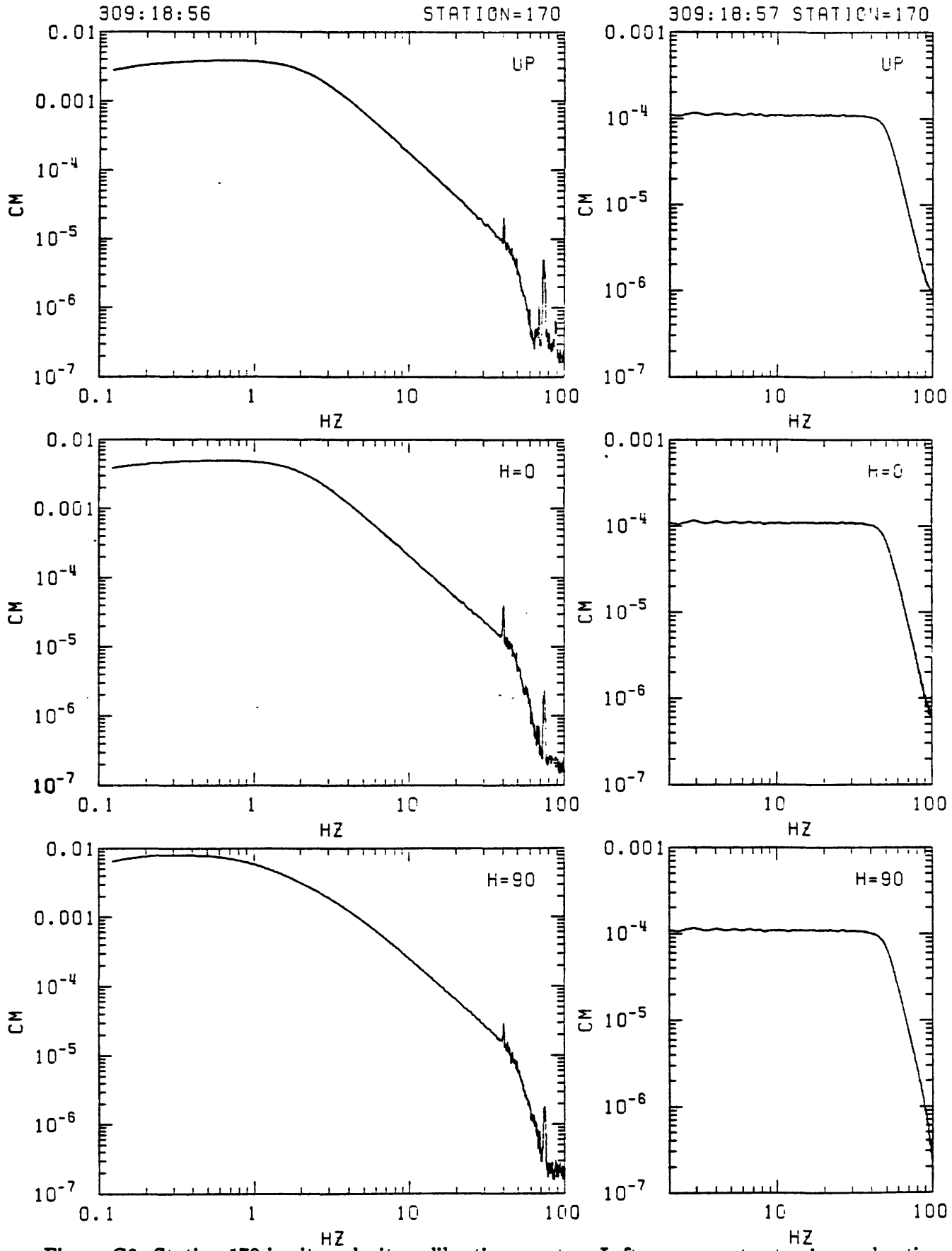

Figure C6. Station 170 in-situ velocity calibration spectra. Left: response to step in acceleration (seismometer mass released from rest at offset position). Right: response to delta function in velocity (voltage impulse applied to recorder input). From top: vertical, N33W and N57E.

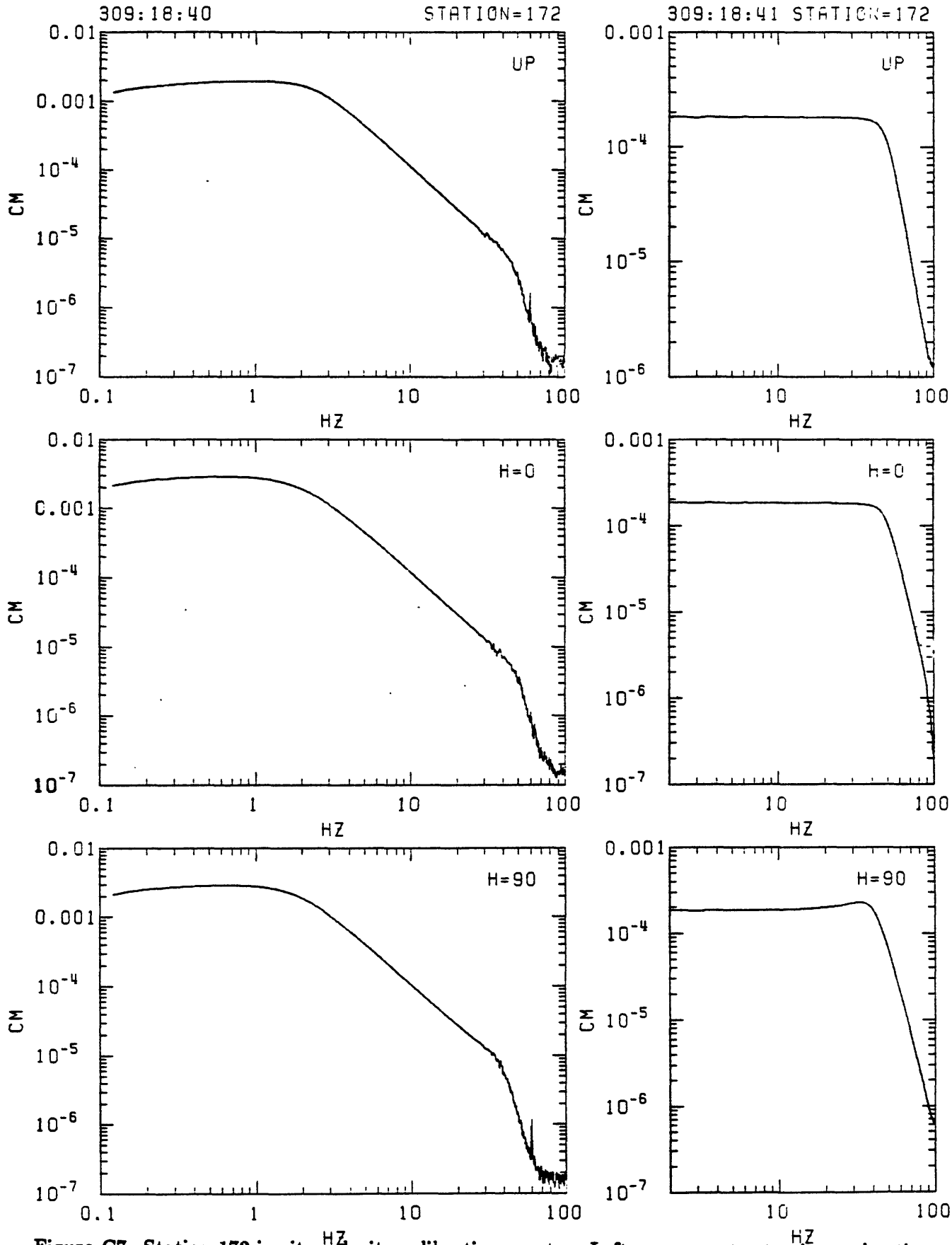

Figure C7. Station 172 in-situ velocity calibration spectra. Left: response to step in acceleration (seismometer mass released from rest at offset position). Right: response to delta function in velocity (voltage impulse applied to recorder input). From top: vertical, N33W and N57E.

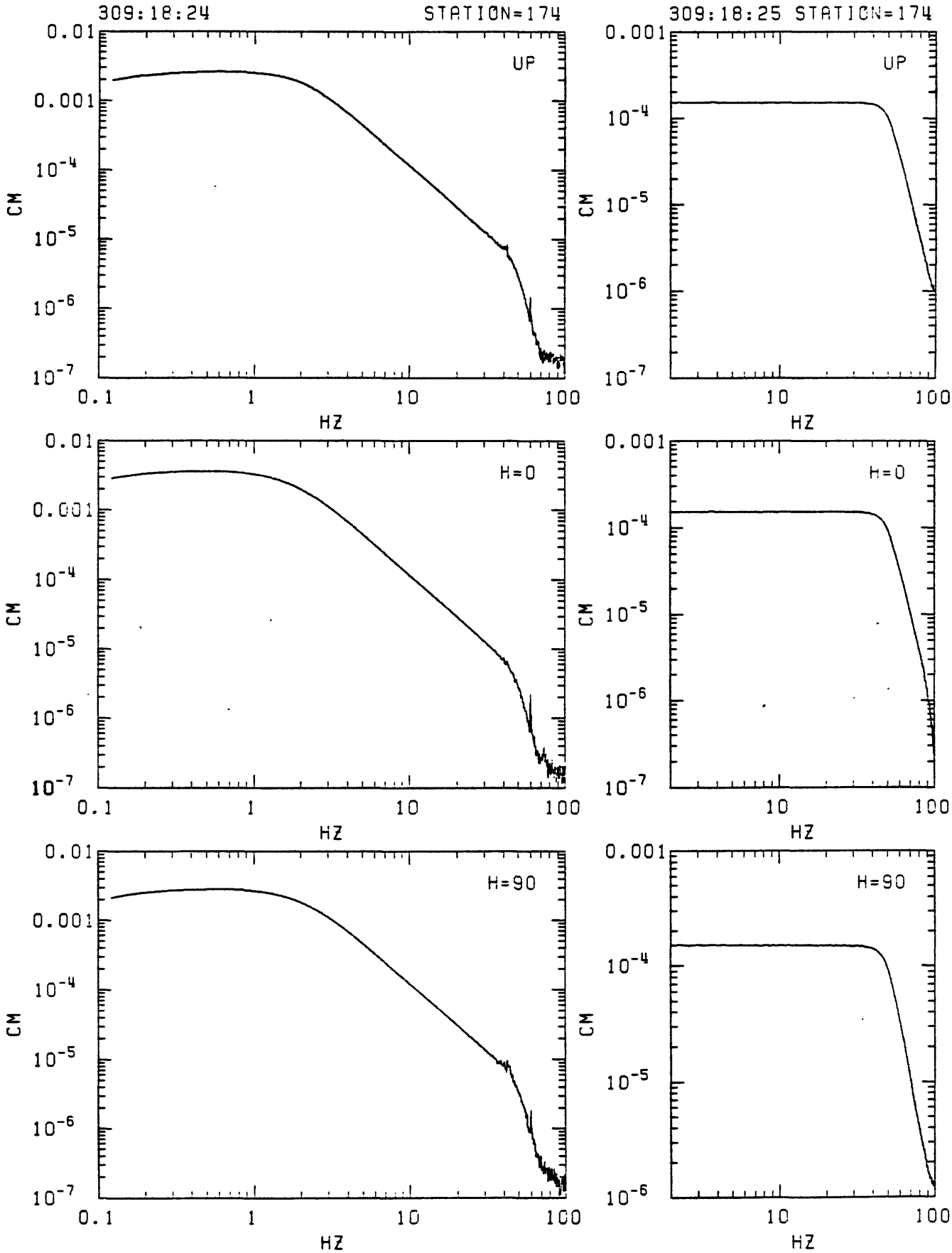

Figure C8. Station 174 in-situ velocity calibration spectra. Left: response to step in acceleration (seismometer mass released from rest at offset position). Right: response to delta function in velocity (voltage impulse applied to recorder input). From top: vertical, N33W and N57E.

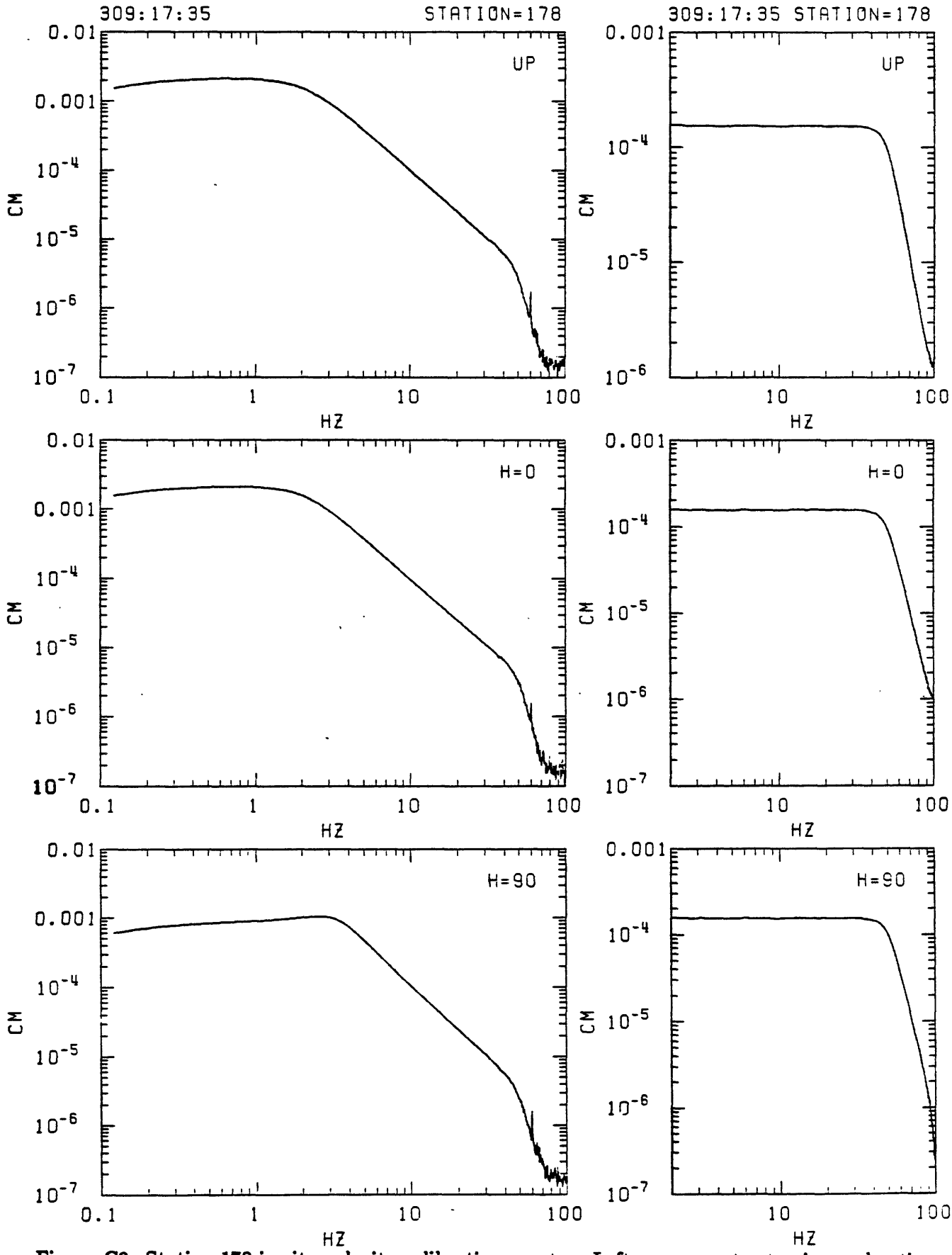

Figure C9. Station 178 in-situ velocity calibration spectra. Left: response to step in acceleration (seismometer mass released from rest at offset position). Right: response to delta function in velocity (voltage impulse applied to recorder input). From top: vertical, N33W and N57E.

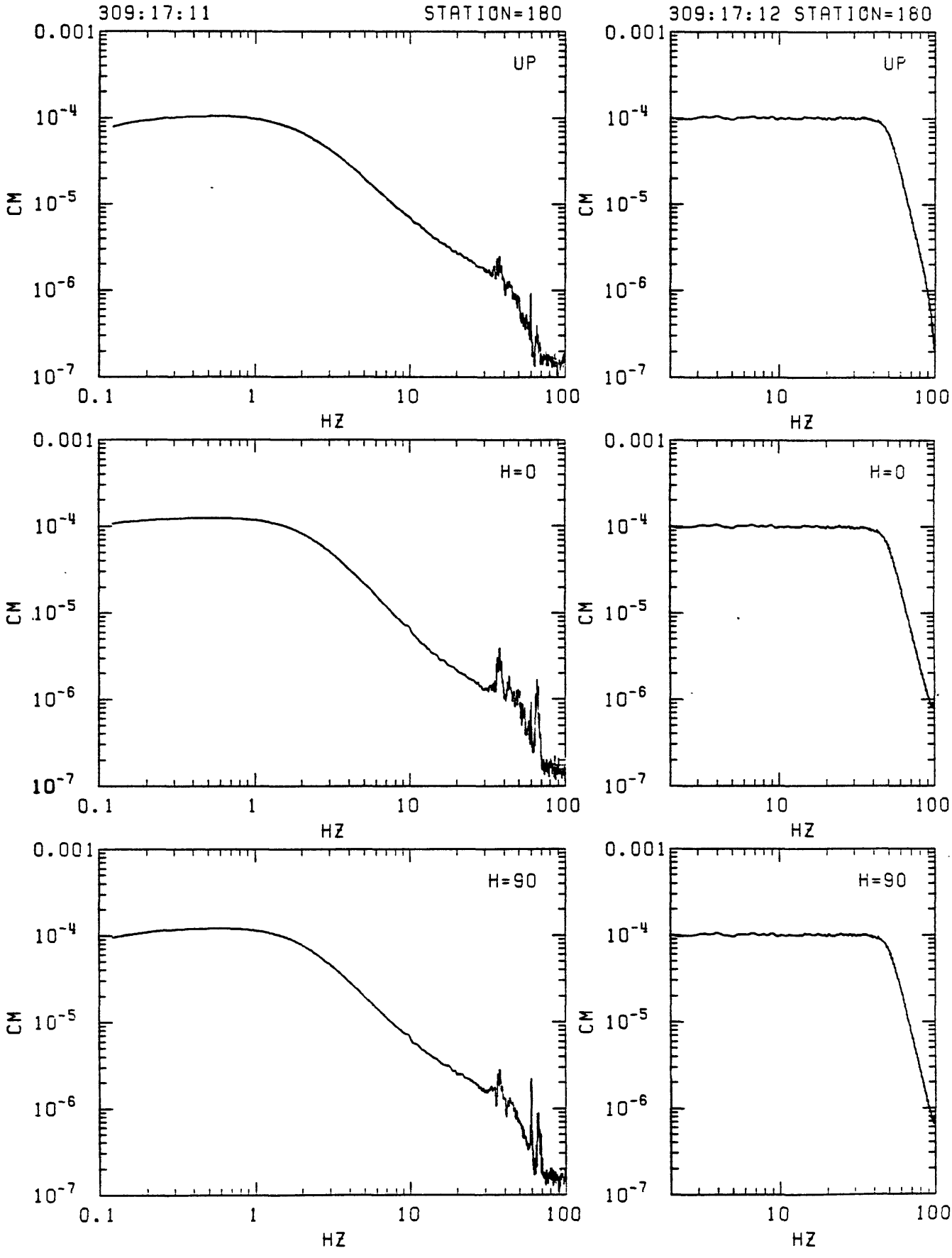

Figure C10. Station 180 in-situ velocity calibration spectra. Left: response to step in acceleration (seismometer mass released from rest at offset position). Right: response to delta function in velocity (voltage impulse applied to recorder input). From top: vertical, N33W and N57E.

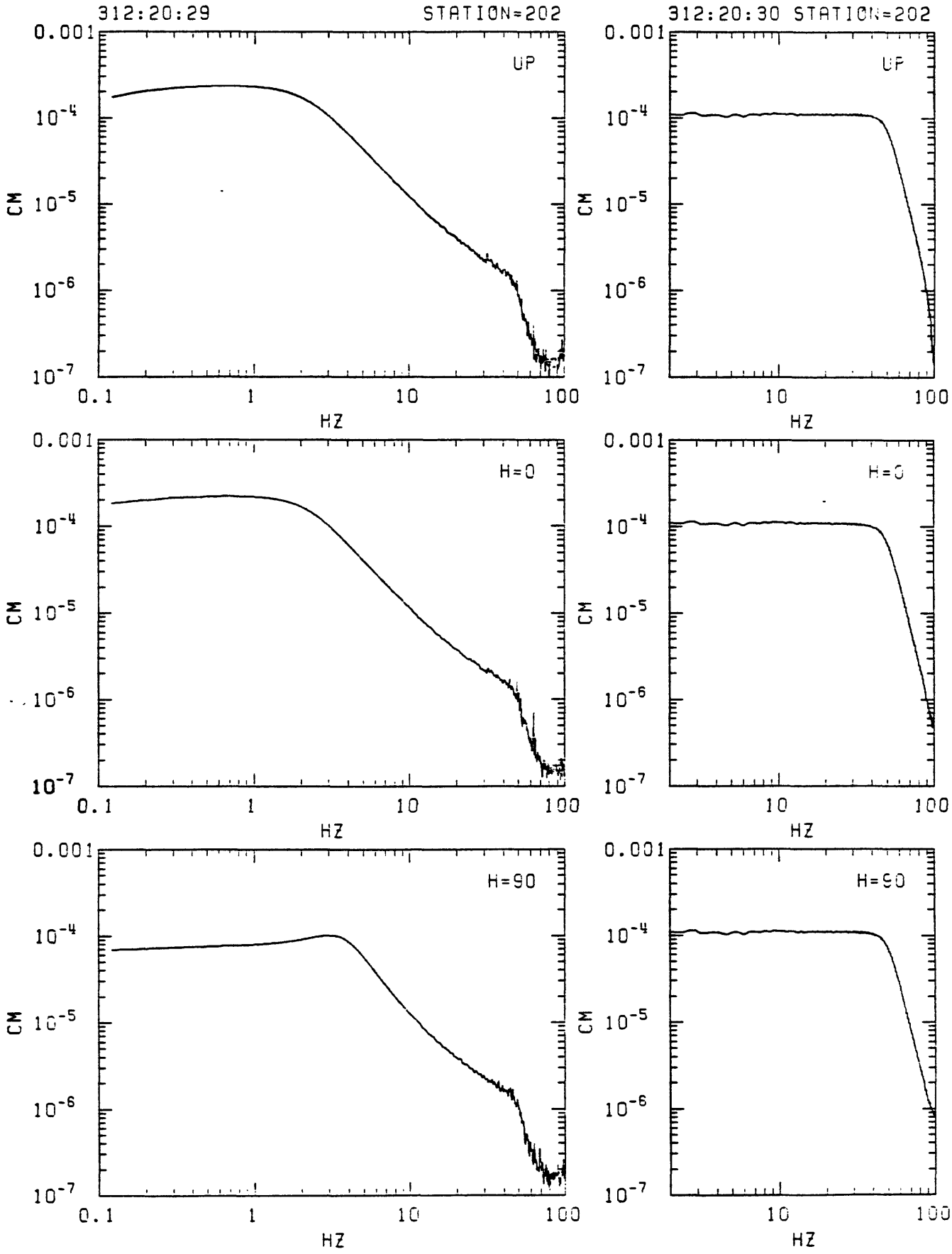

Figure C11. Station 202 in-situ velocity calibration spectra. Left: response to step in acceleration (seismometer mass released from rest at offset position). Right: response to delta function in velocity (voltage impulse applied to recorder input). From top: vertical, N20E and N110E.

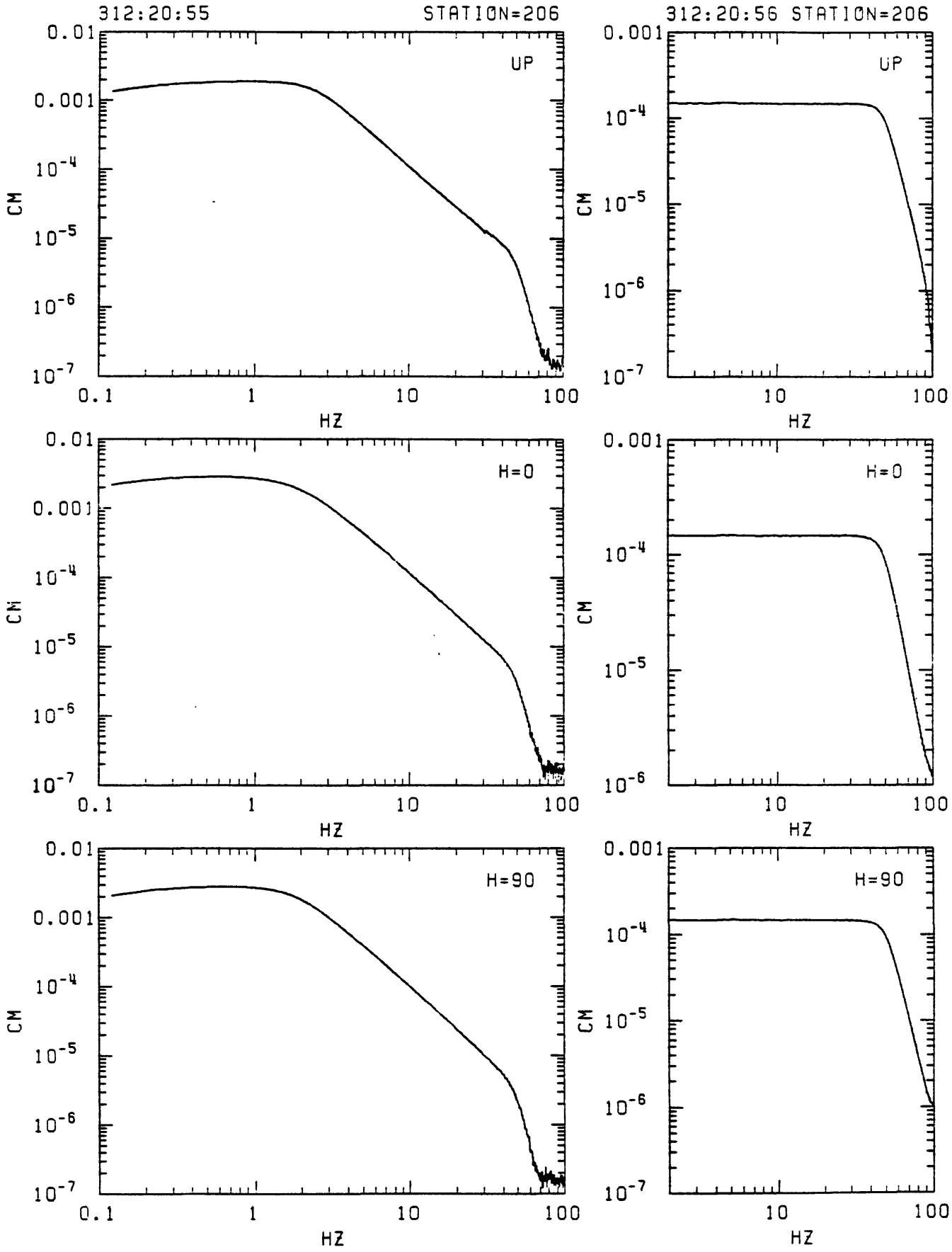

Figure C12. Station 206 in-situ velocity calibration spectra. Left: response to step in acceleration (seismometer mass released from rest at offset position). Right: response to delta function in velocity (voltage impulse applied to recorder input). From top: vertical, N20E and N110E.

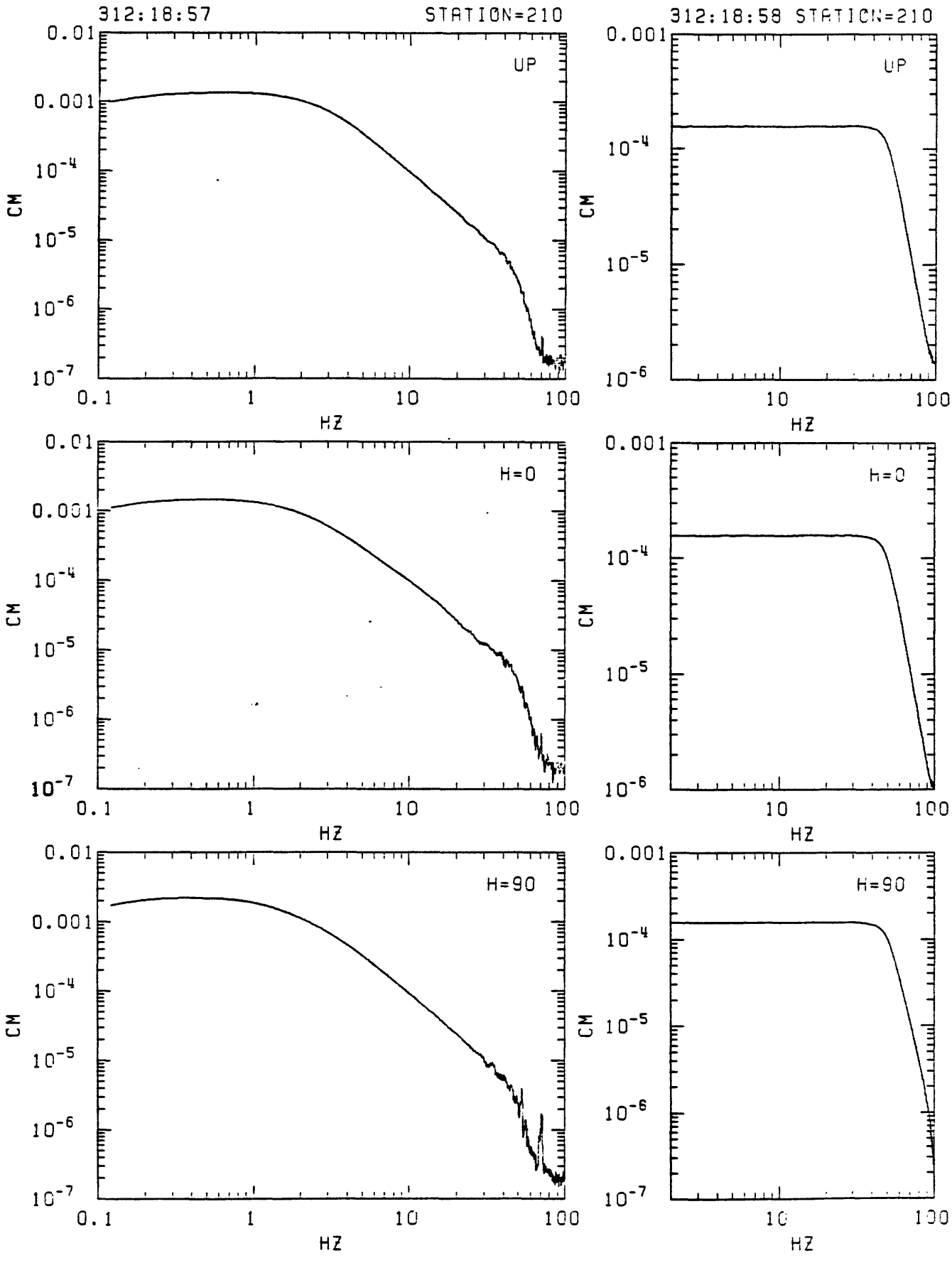

Figure C13. Station 210 in-situ velocity calibration spectra. Left: response to step in acceleration (seismometer mass released from rest at offset position). Right: response to delta function in velocity (voltage impulse applied to recorder input). From top: vertical, N20E and N110E.

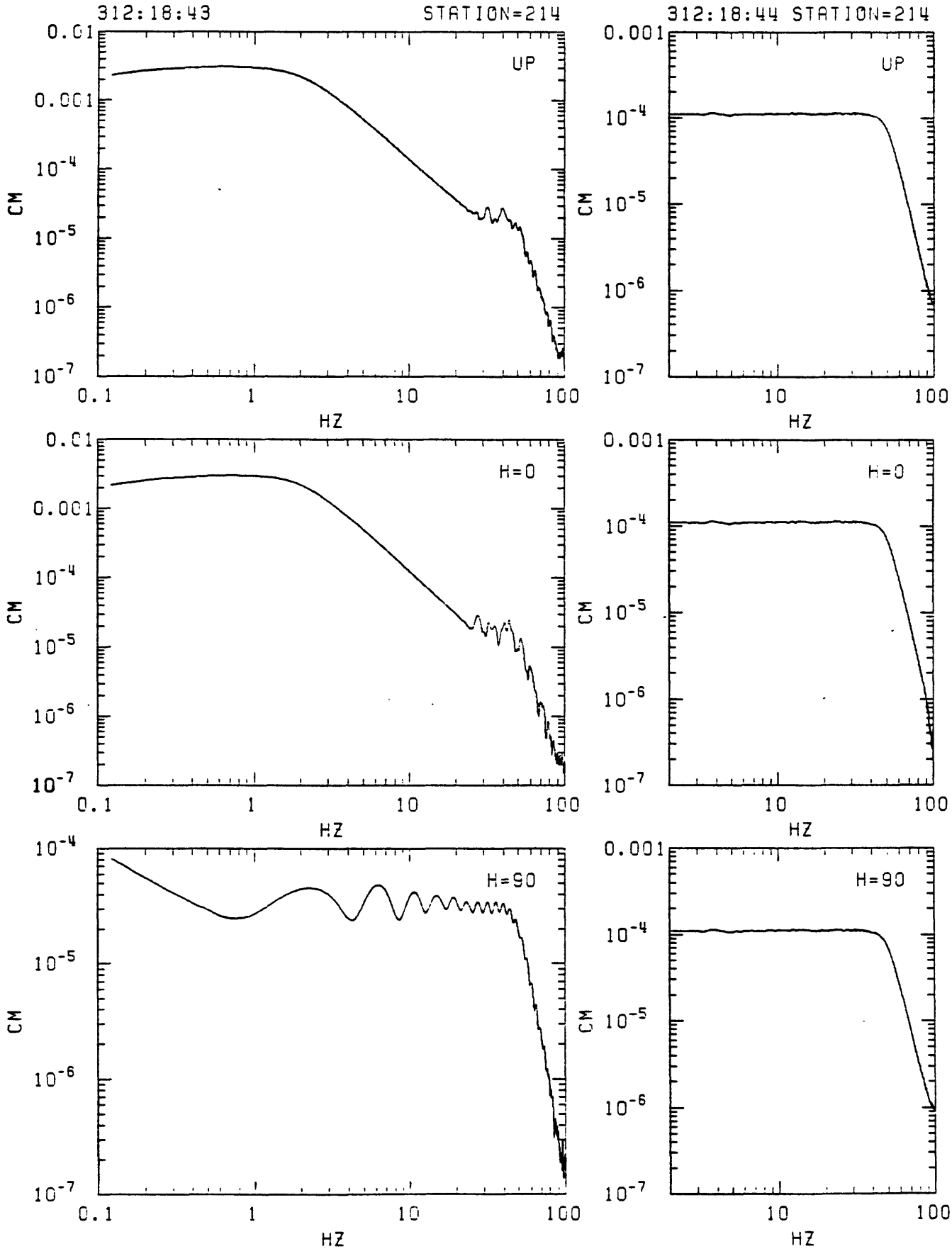

Figure C14. Station 214 in-situ velocity calibration spectra. Left: response to step in acceleration (seismometer mass released from rest at offset position). Right: response to delta function in velocity (voltage impulse applied to recorder input). From top: vertical, N20E and N110E.

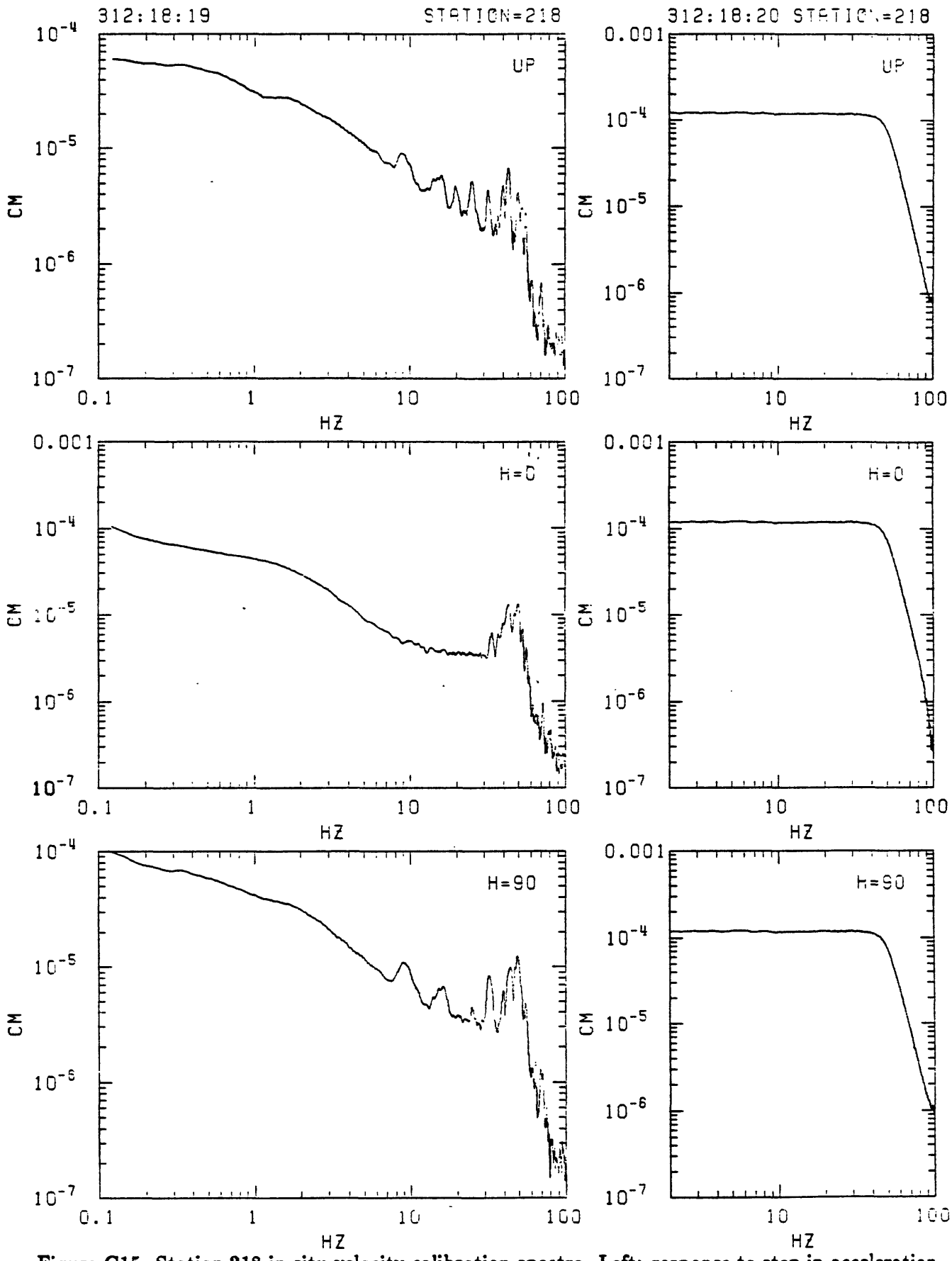

Figure C15. Station 218 in-situ velocity calibration spectra. Left: response to step in acceleration (seismometer mass released from rest at offset position). Right: response to delta function in velocity (voltage impulse applied to recorder input). From top: vertical, N20E and N110E.

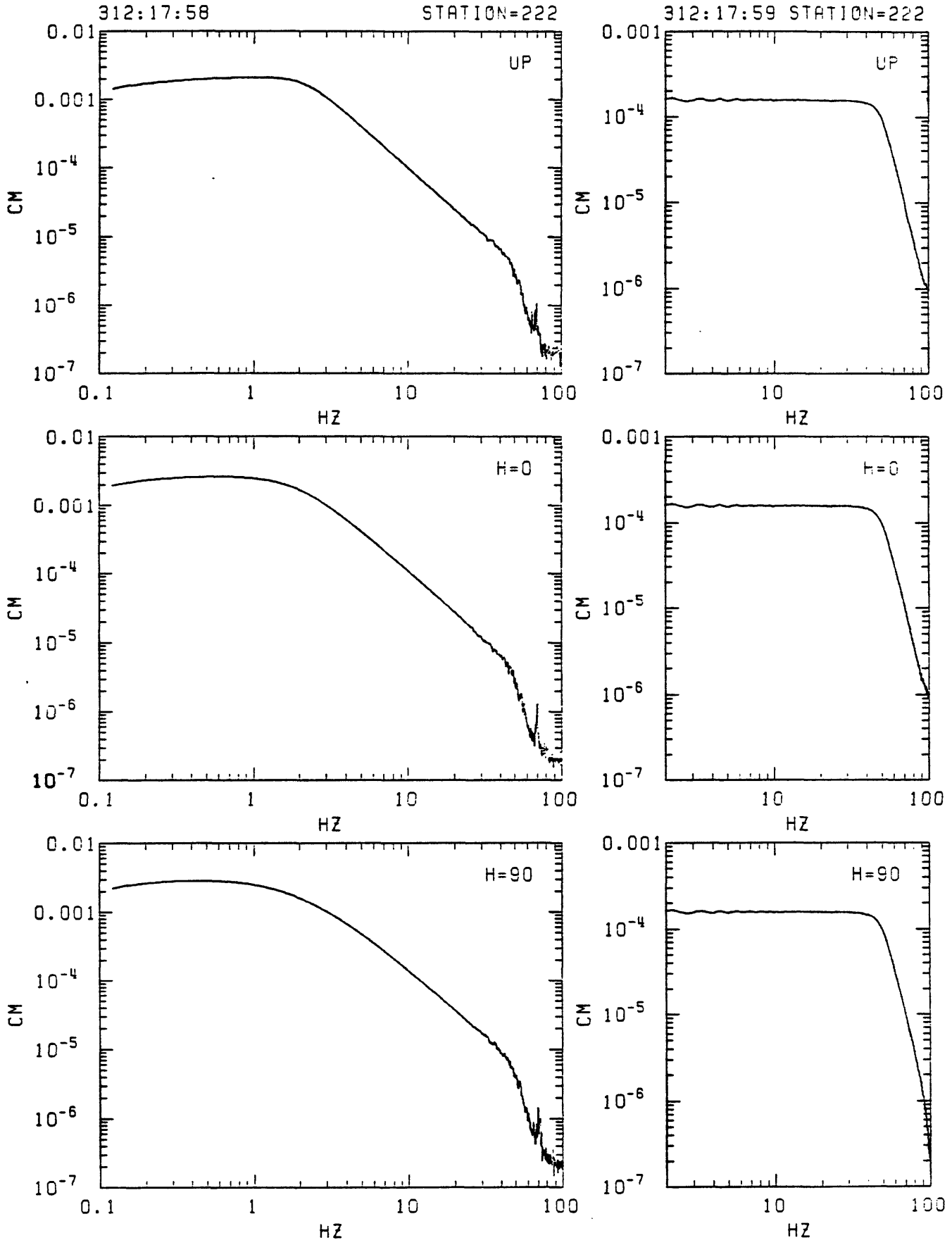

Figure C16. Station 222 in-situ velocity calibration spectra. Left: response to step in acceleration (seismometer mass released from rest at offset position). Right: response to delta function in velocity (voltage impulse applied to recorder input). From top: vertical, N20E and N110E.

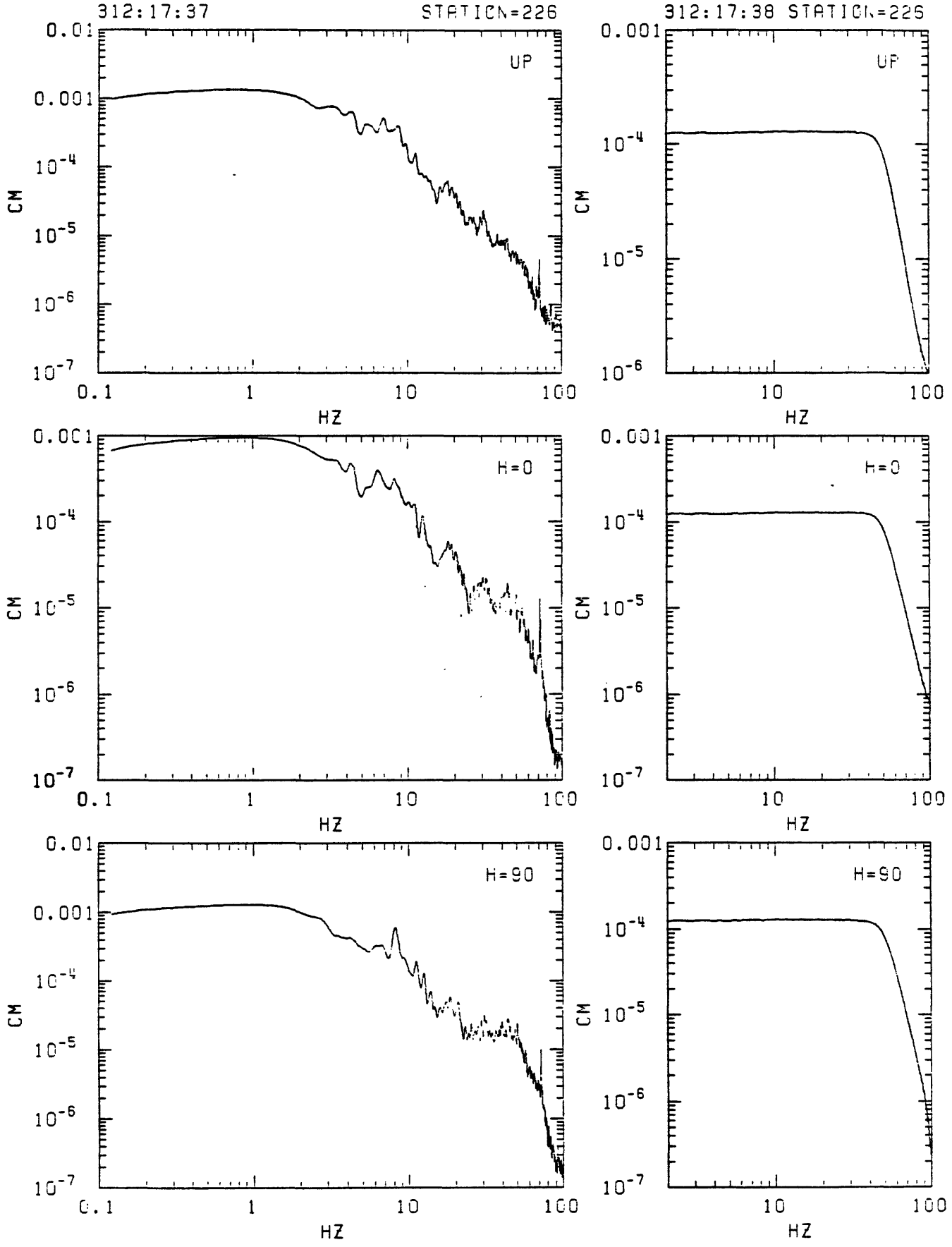

Figure C17. Station 226 in-situ velocity calibration spectra. Left: response to step in acceleration (seismometer mass released from rest at offset position). Right: response to delta function in velocity (voltage impulse applied to recorder input). From top: vertical, N20E and N110E.

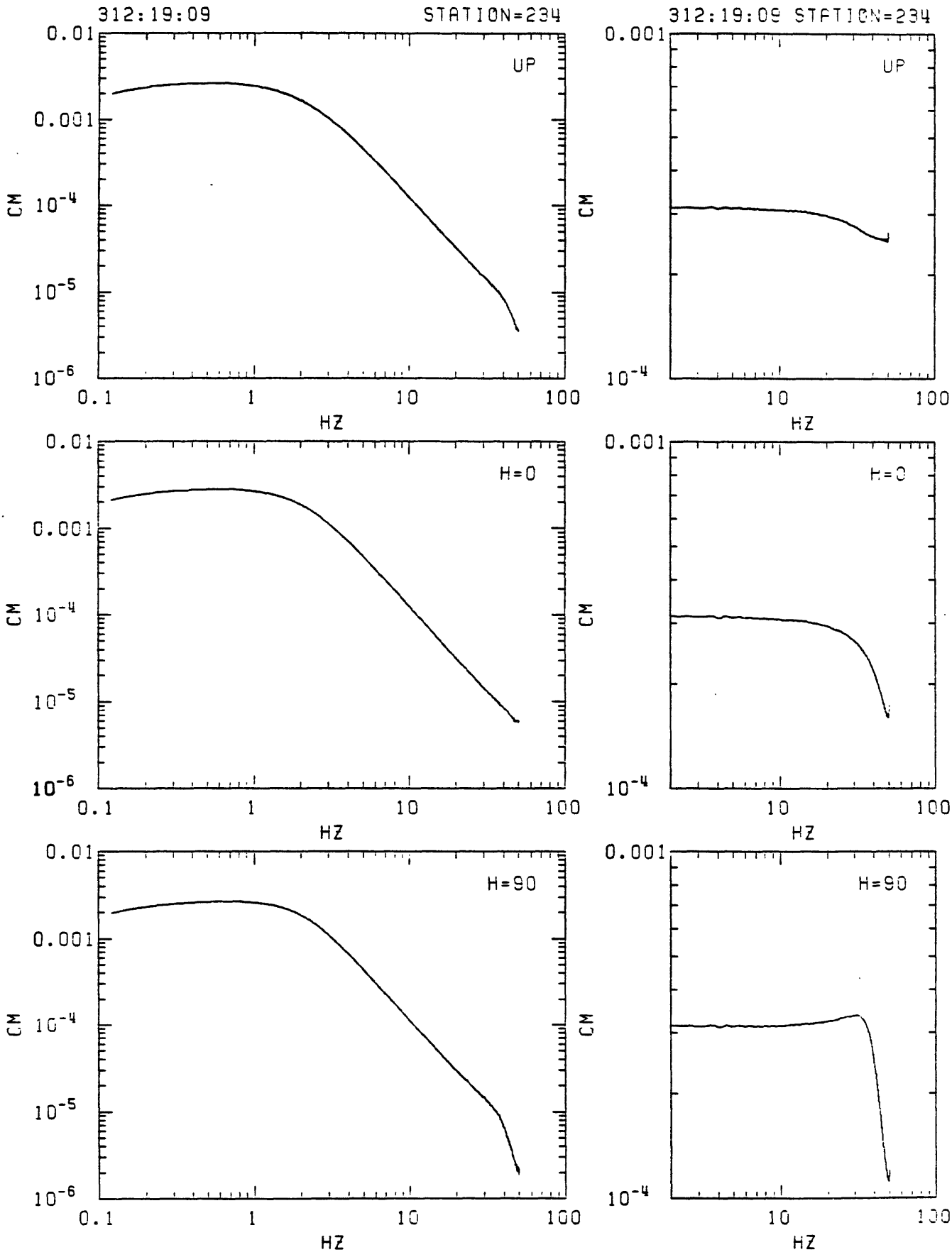

Figure C18. Station 234 in-situ velocity calibration spectra. Left: response to step in acceleration (seismometer mass released from rest at offset position). Right: response to delta function in velocity (voltage impulse applied to recorder input). From top: vertical, N20E and N110E.

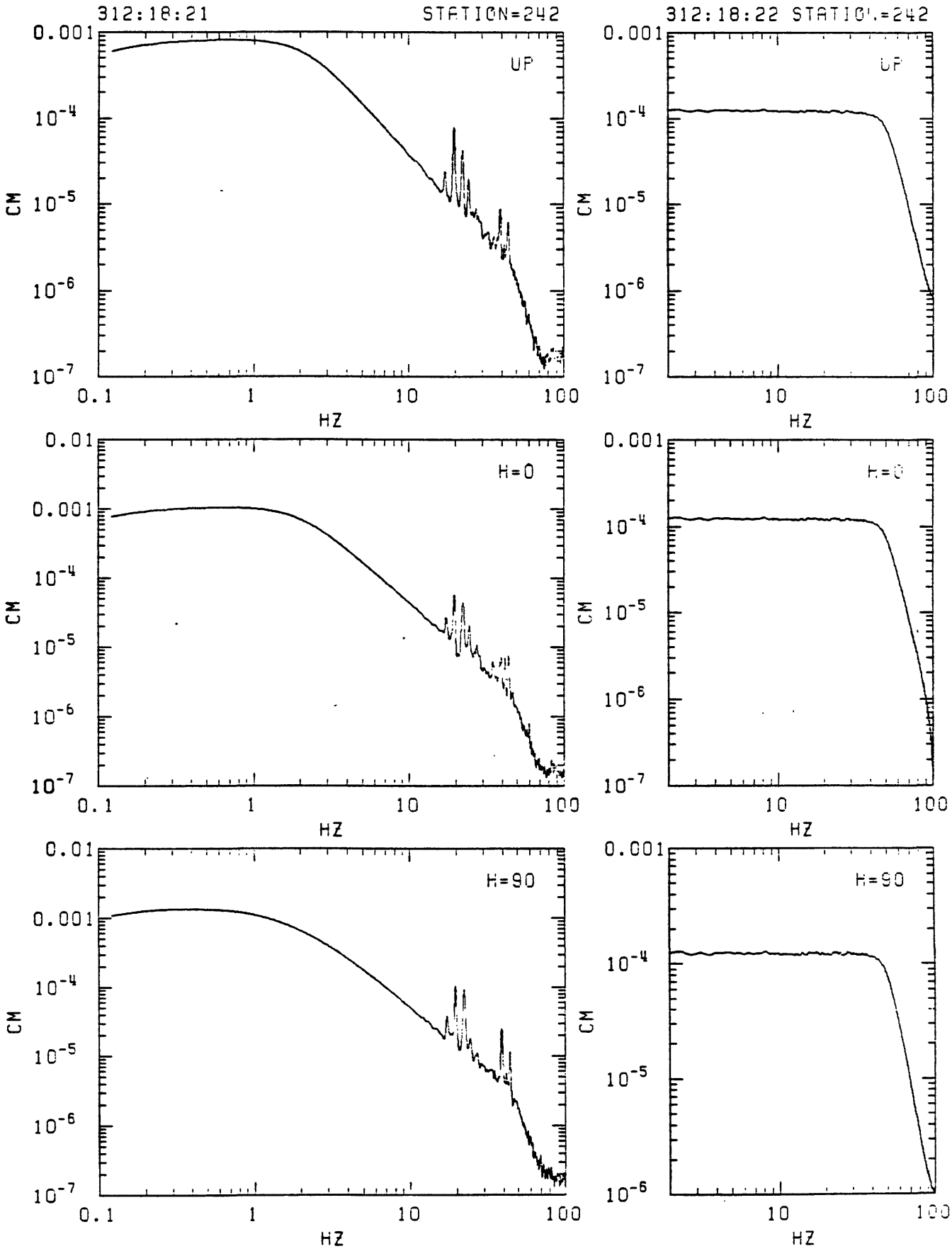

Figure C19. Station 242 in-situ velocity calibration spectra. Left: response to step in acceleration (seismometer mass released from rest at offset position). Right: response to delta function in velocity (voltage impulse applied to recorder input). From top: vertical, N20E and N110E.

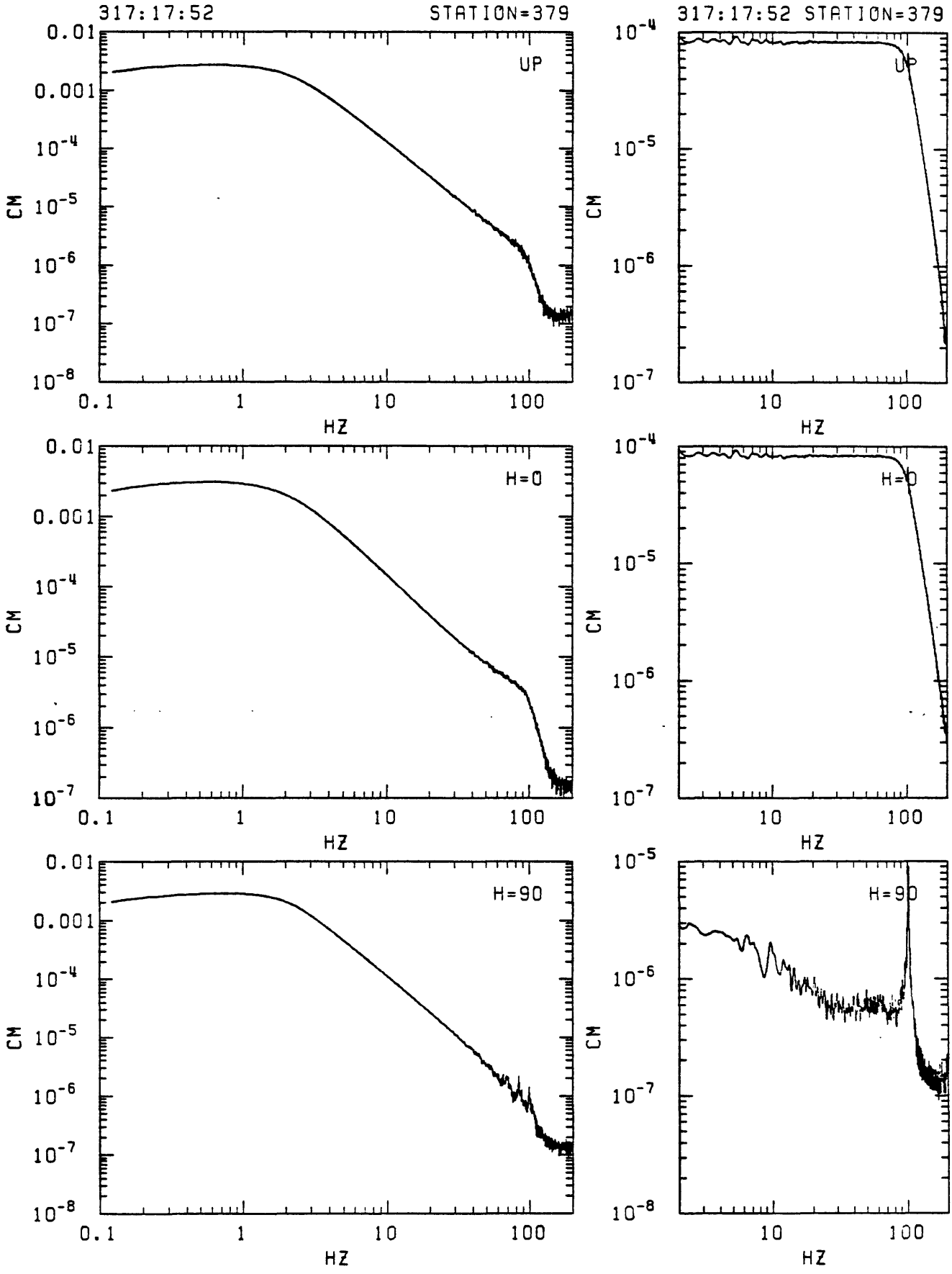

Figure C20. Station 379 in-situ velocity calibration spectra. Left: response to step in acceleration (seismometer mass released from rest at offset position). Right: response to delta function in velocity (voltage impulse applied to recorder input). From top: vertical, N25E and N115E.

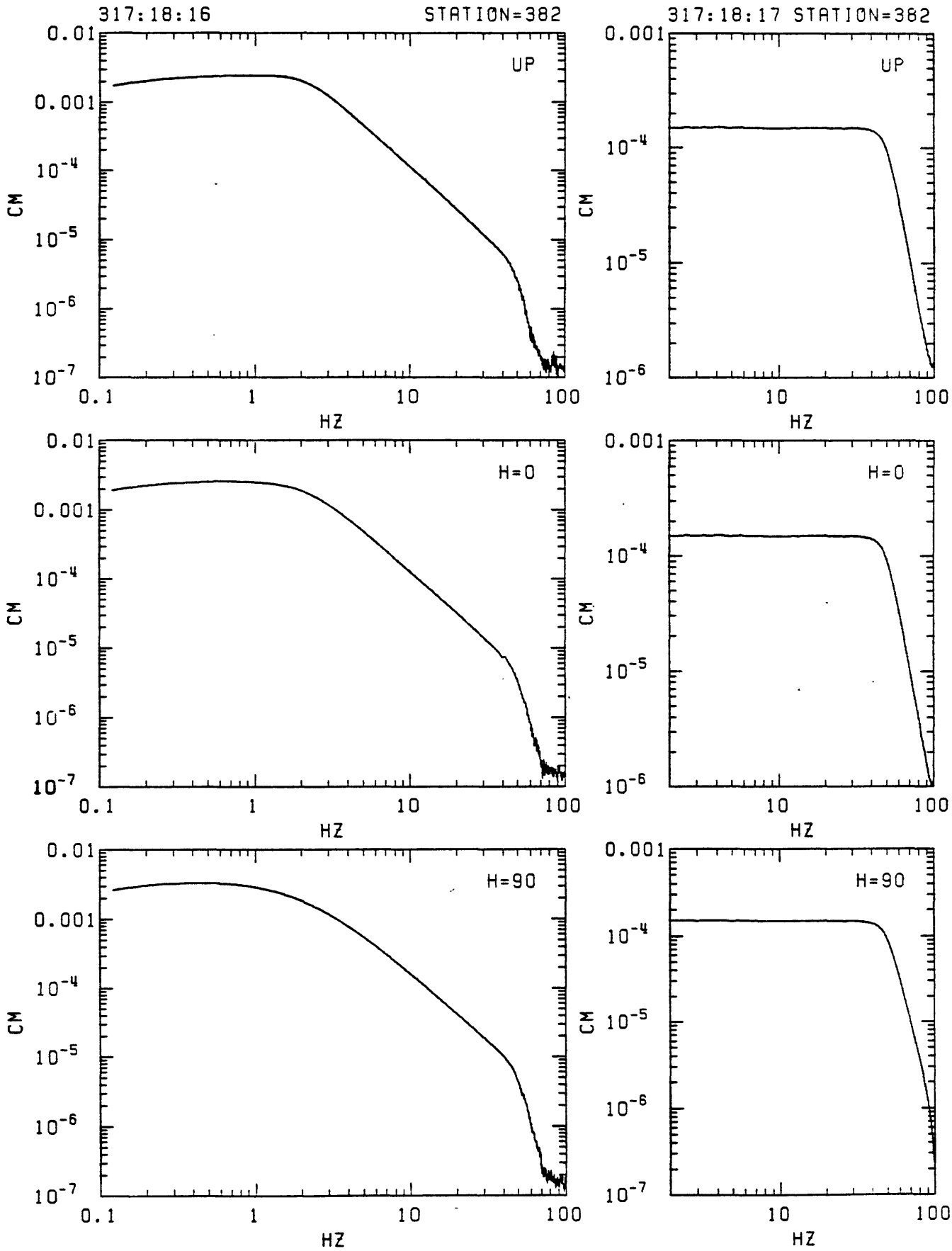

Figure C21. Station 382 in-situ velocity calibration spectra. Left: response to step in acceleration (seismometer mass released from rest at offset position). Right: response to delta function in velocity (voltage impulse applied to recorder input). From top: vertical, N25E and N115E.

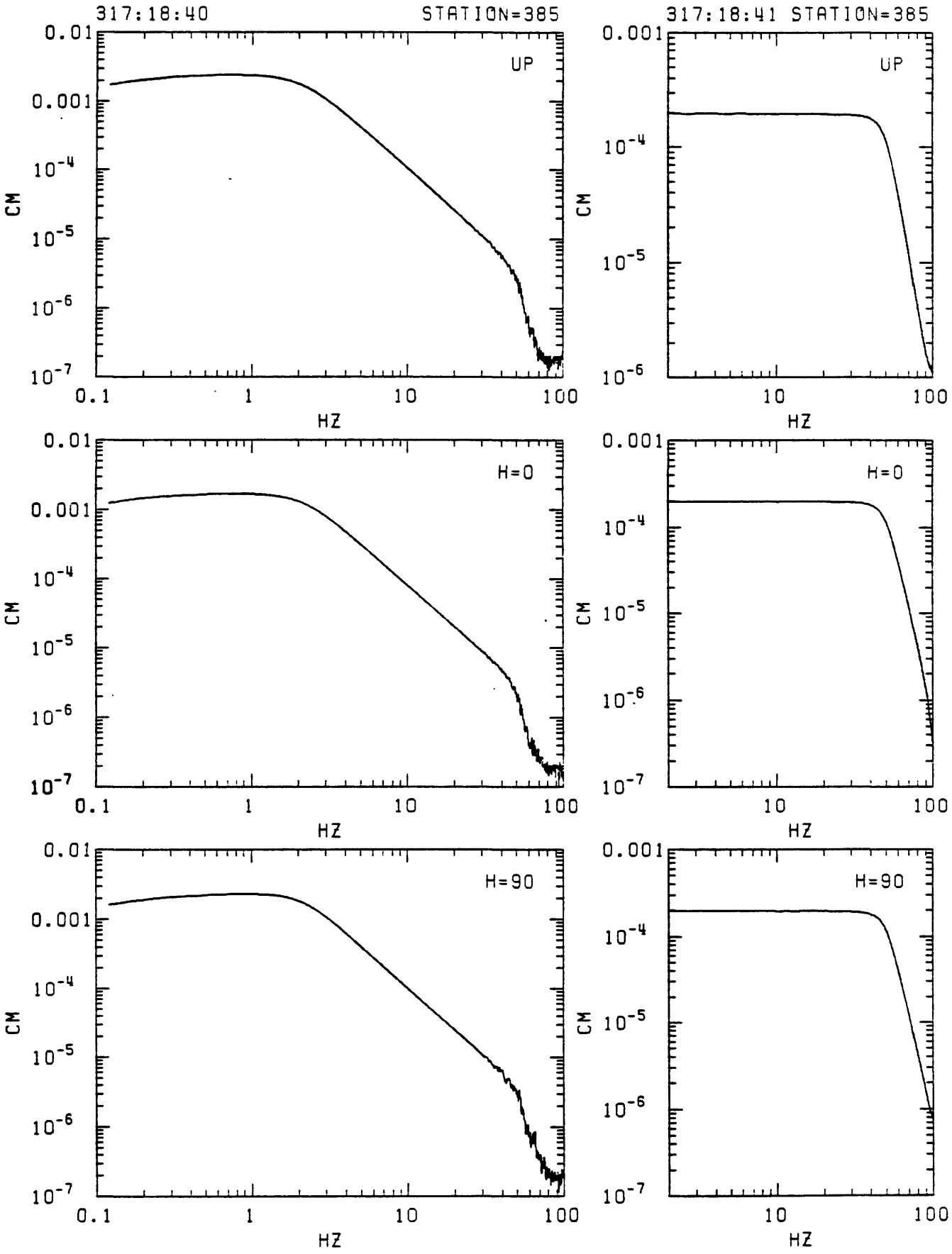

Figure C22. Station 385 in-situ velocity calibration spectra. Left: response to step in acceleration (seismometer mass released from rest at offset position). Right: response to delta function in velocity (voltage impulse applied to recorder input). From top: vertical, N25E and N115E.

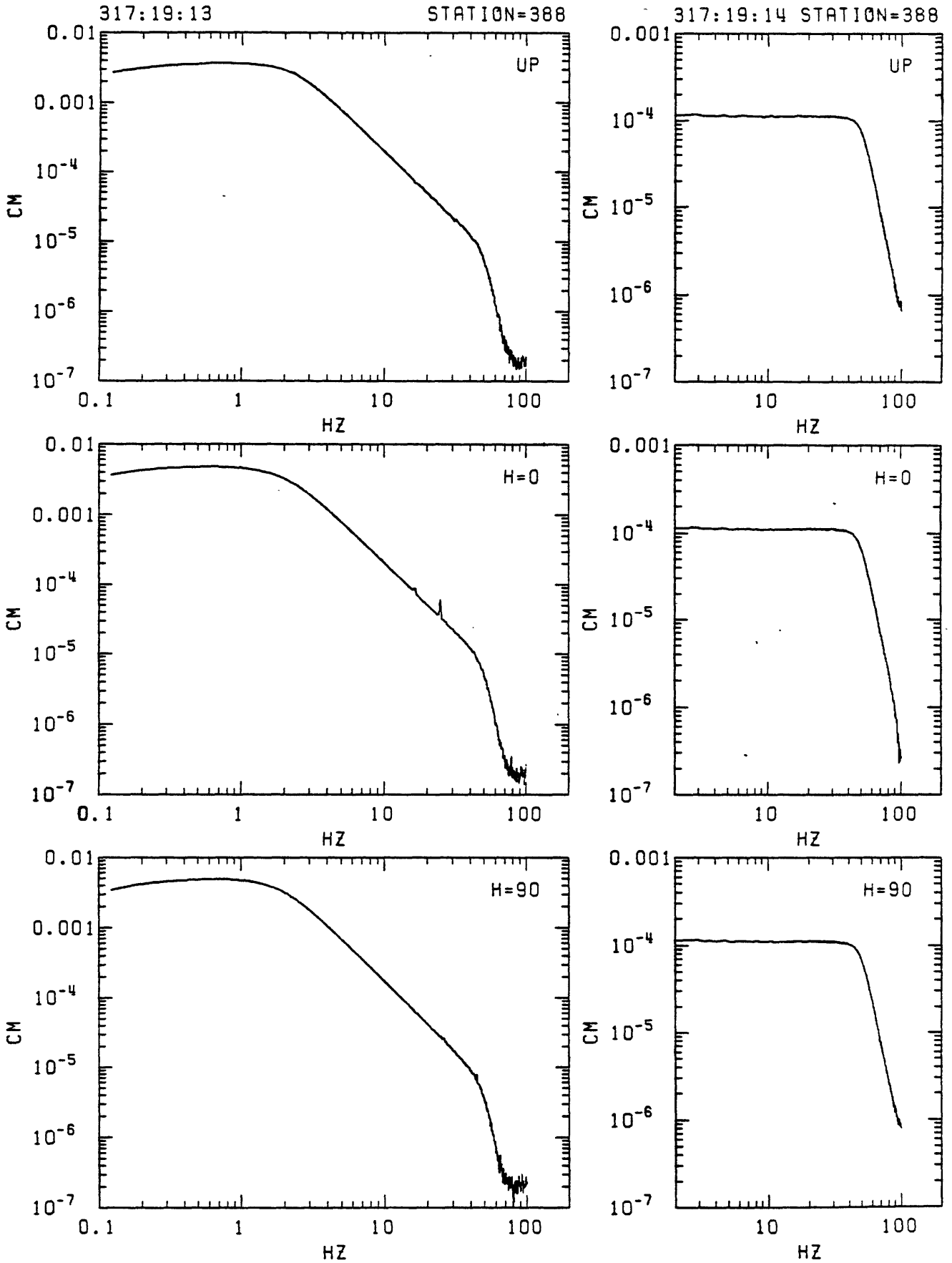

Figure C23. Station 388 in-situ velocity calibration spectra. Left: response to step in acceleration (seismometer mass released from rest at offset position). Right: response to delta function in velocity (voltage impulse applied to recorder input). From top: vertical, N25E and N115E.

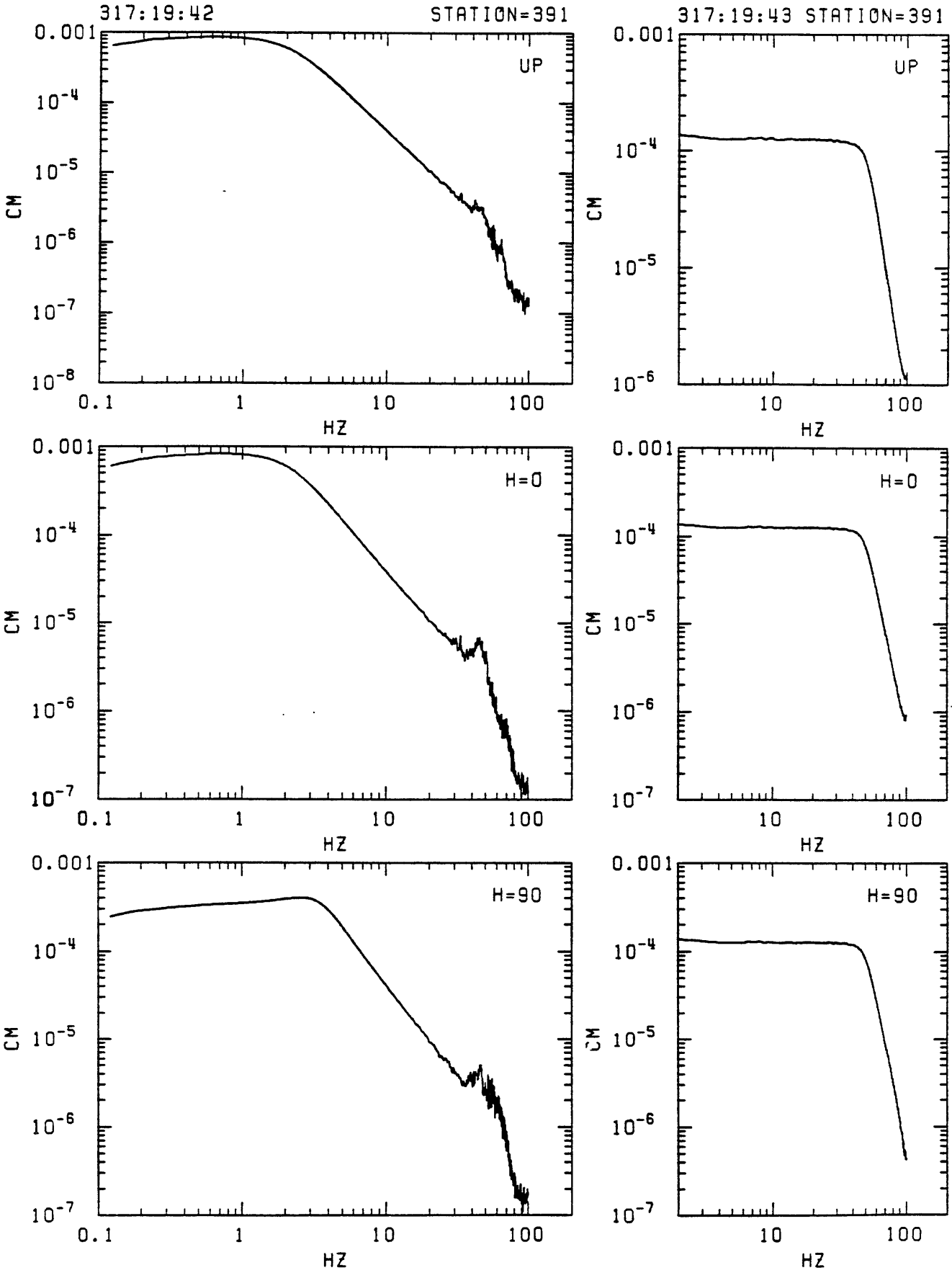

Figure C24. Station 391 in-situ velocity calibration spectra. Left: response to step in acceleration (seismometer mass released from rest at offset position). Right: response to delta function in velocity (voltage impulse applied to recorder input). From top: vertical, N25E and N115E.

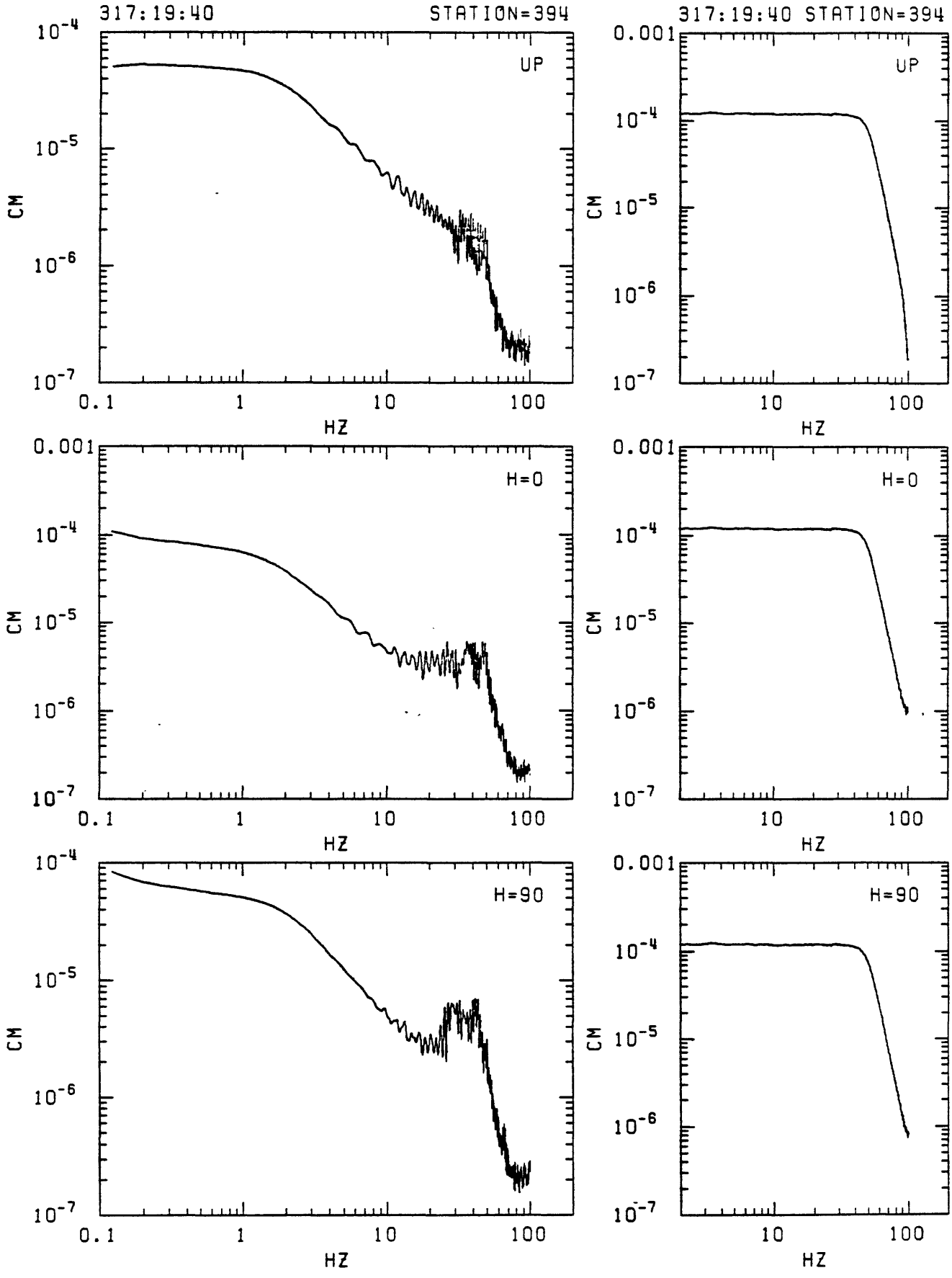

Figure C25. Station 394 in-situ velocity calibration spectra. Left: response to step in acceleration (seismometer mass released from rest at offset position). Right: response to delta function in velocity (voltage impulse applied to recorder input). From top: vertical, N25E and N115E.

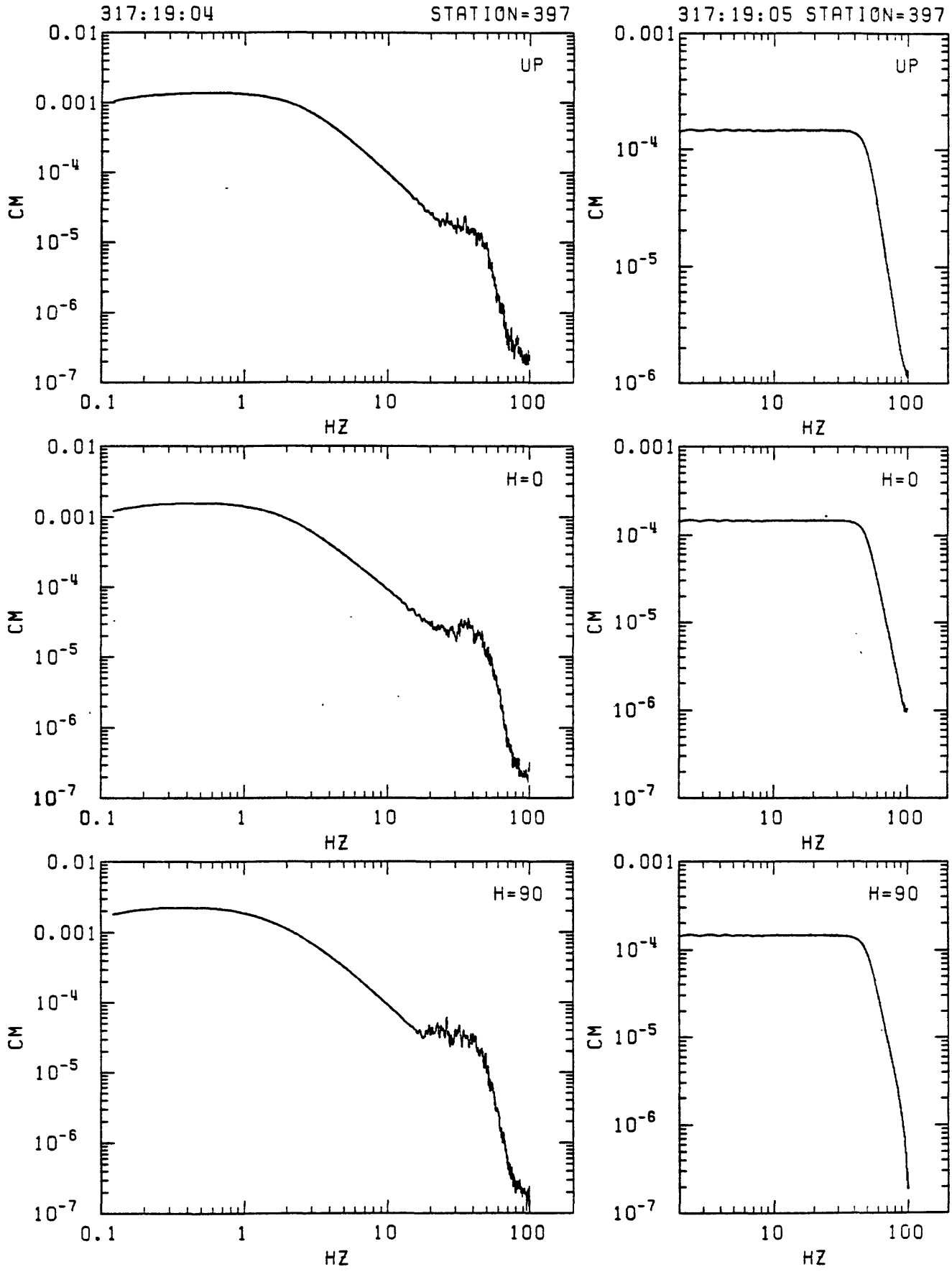

Figure C26. Station 397 in-situ velocity calibration spectra. Left: response to step in acceleration (seismometer mass released from rest at offset position). Right: response to delta function in velocity (voltage impulse applied to recorder input). From top: vertical, N25E and N115E.

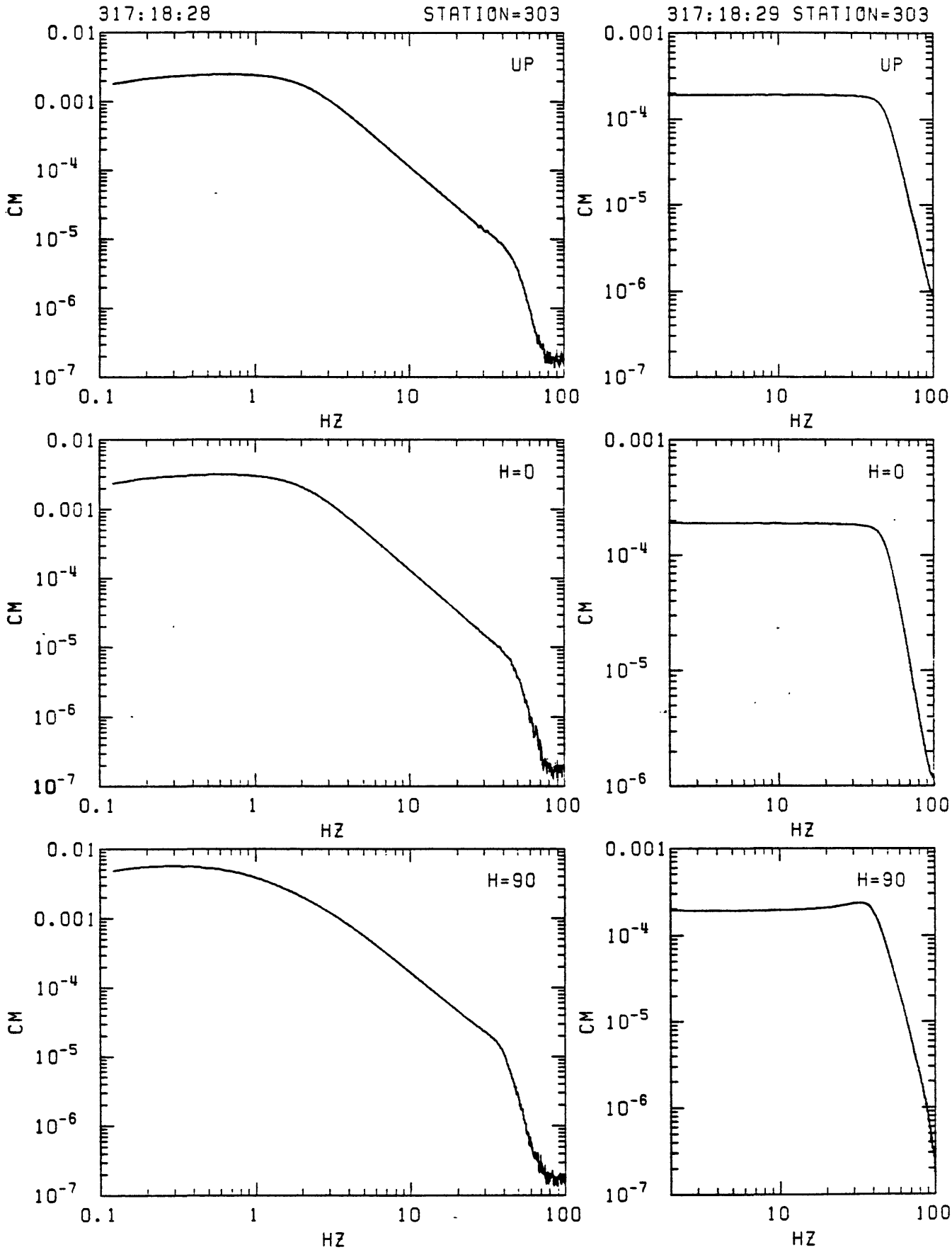

Figure C27. Station 303 in-situ velocity calibration spectra. Left: response to step in acceleration (seismometer mass released from rest at offset position). Right: response to delta function in velocity (voltage impulse applied to recorder input). From top: vertical, N25E and N115E.

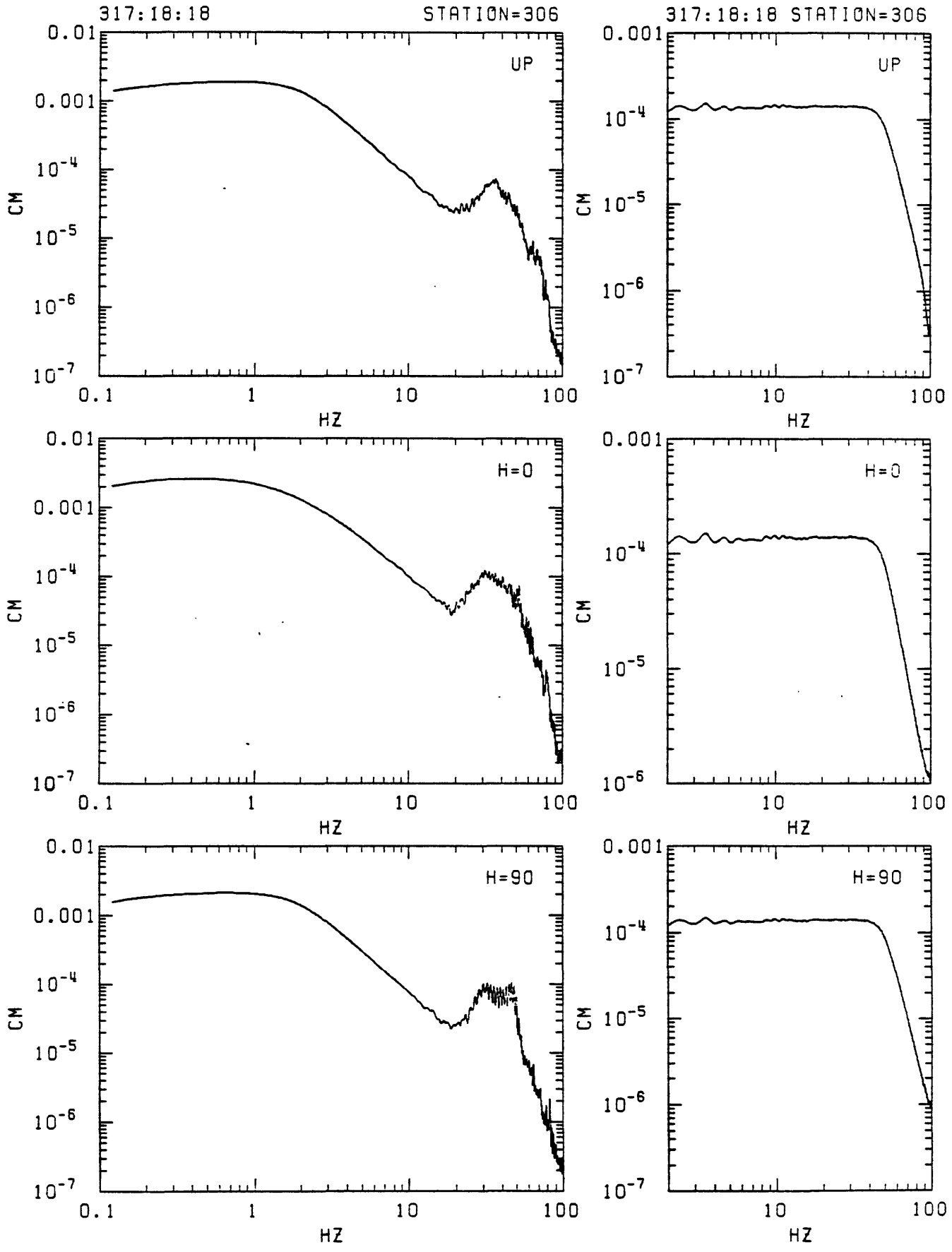

Figure C28. Station 306 in-situ velocity calibration spectra. Left: response to step in acceleration (seismometer mass released from rest at offset position). Right: response to delta function in velocity (voltage impulse applied to recorder input). From top: vertical, N25E and N115E.

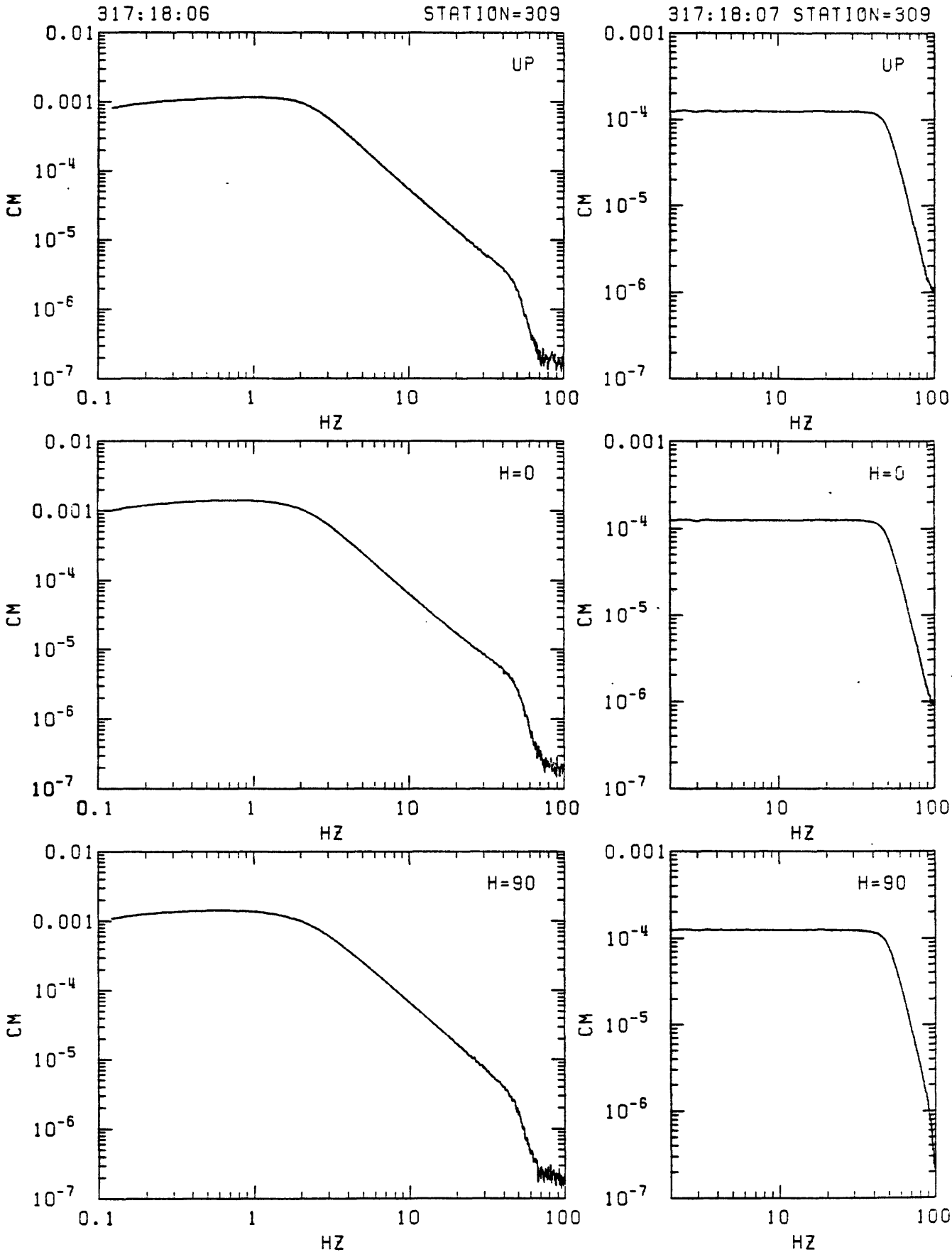

Figure C29. Station 309 in-situ velocity calibration spectra. Left: response to step in acceleration (seismometer mass released from rest at offset position). Right: response to delta function in velocity (voltage impulse applied to recorder input). From top: vertical, N25E and N115E.

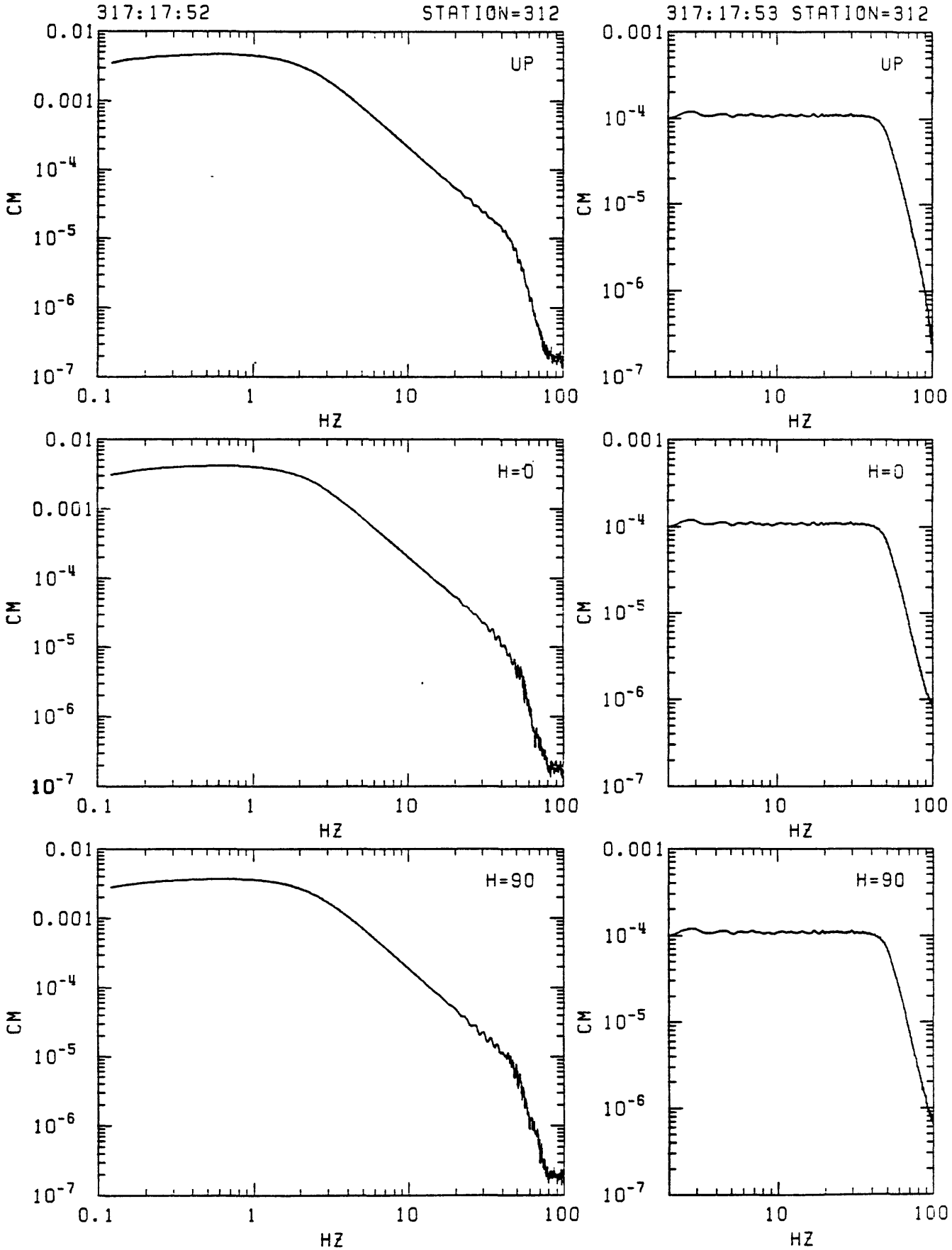

Figure C30. Station 312 in-situ velocity calibration spectra. Left: response to step in acceleration (seismometer mass released from rest at offset position). Right: response to delta function in velocity (voltage impulse applied to recorder input). From top: vertical, N25E and N115E.

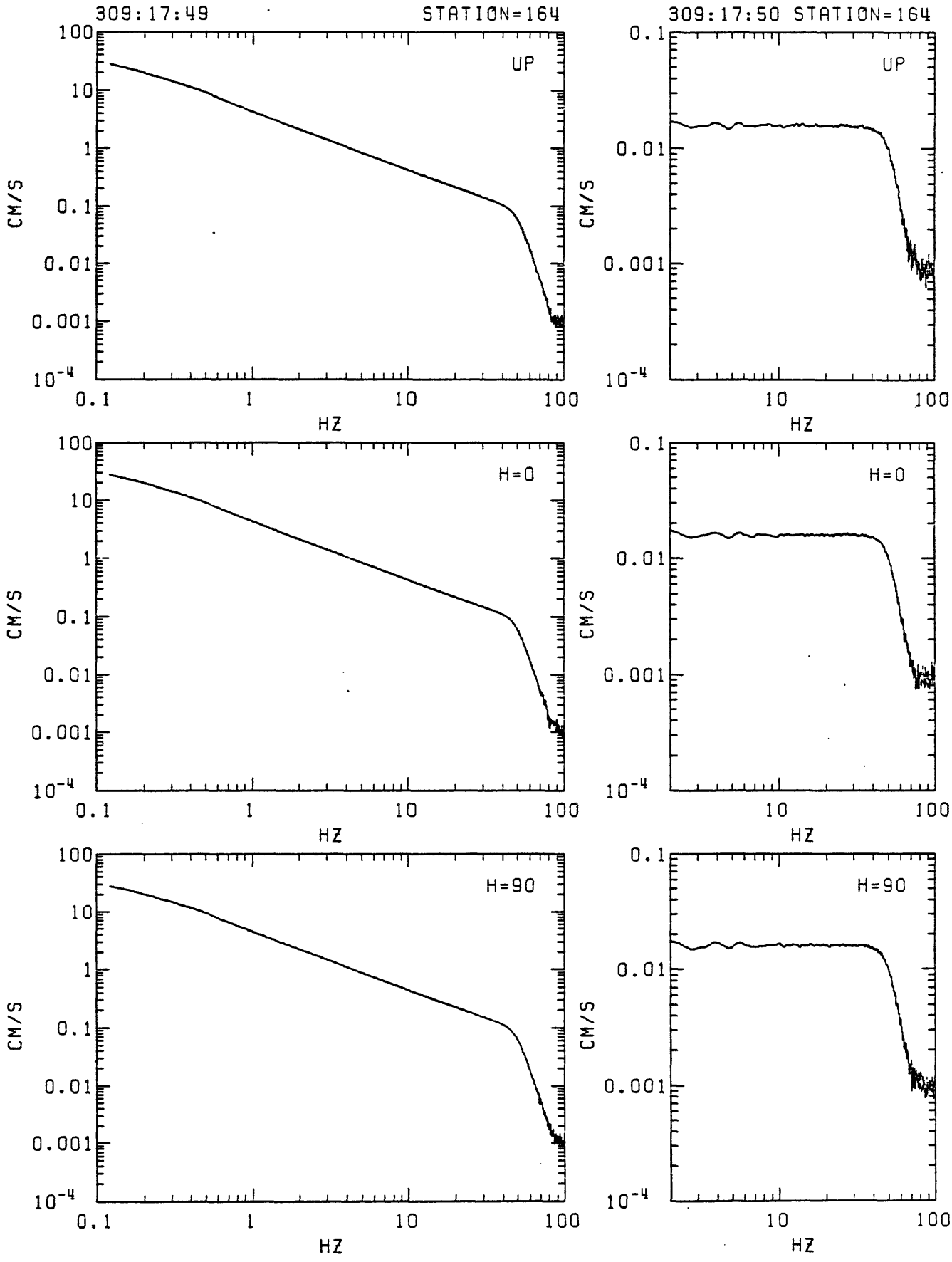

Figure D1. Station 164 in-situ 18db acceleration calibration spectra. Left: response to step in acceleration (reset FBA servo amplifier reference voltage from non-zero). Right: response to delta function in acceleration (voltage impulse applied to recorder input). From top: vertical, N33W and N57E.

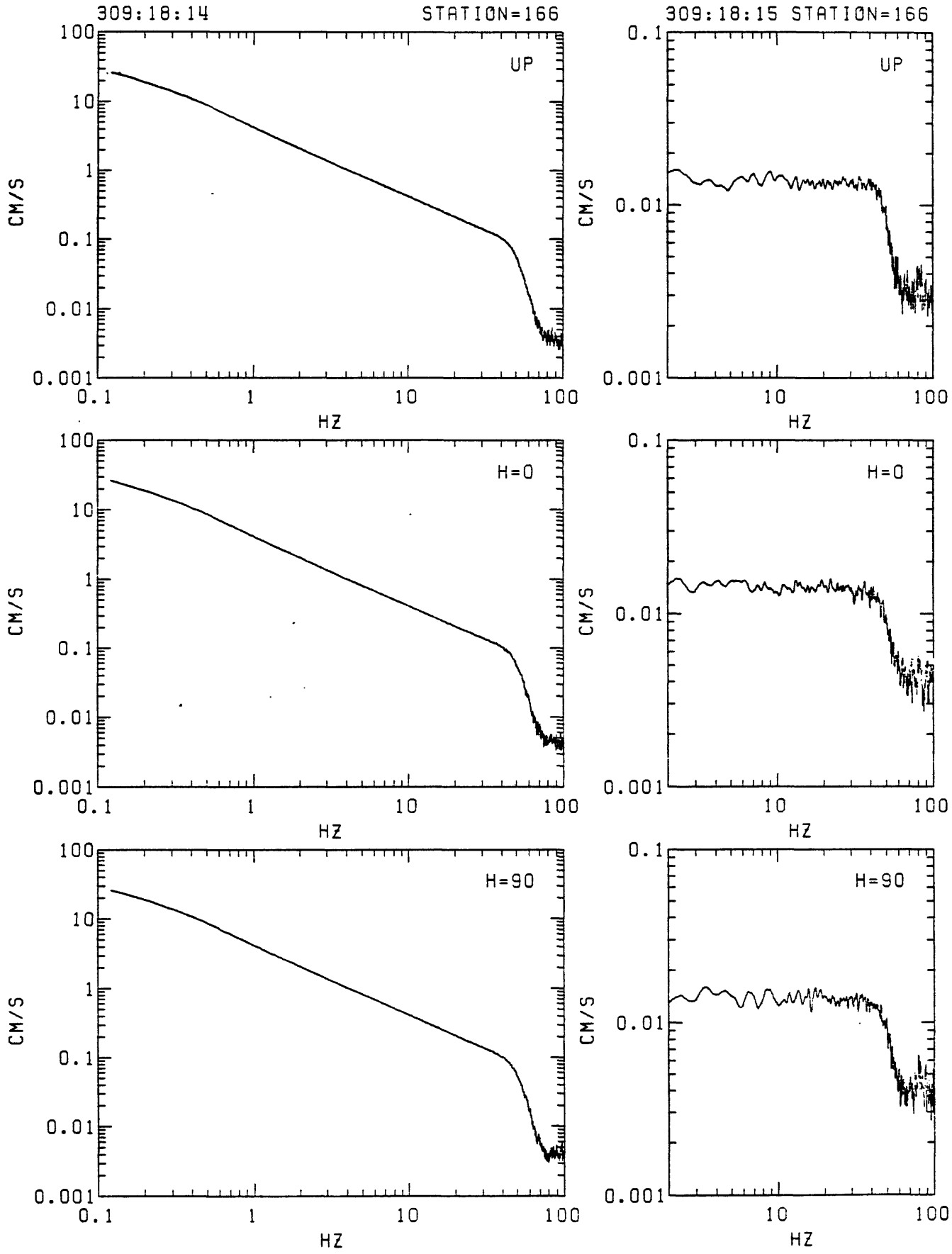

Figure D2. Station 166 in-situ 6db acceleration calibration spectra. Left: response to step in acceleration (reset FBA servo amplifier reference voltage from non-zero). Right: response to delta function in acceleration (voltage impulse applied to recorder input). From top: vertical, N33W and N57W.

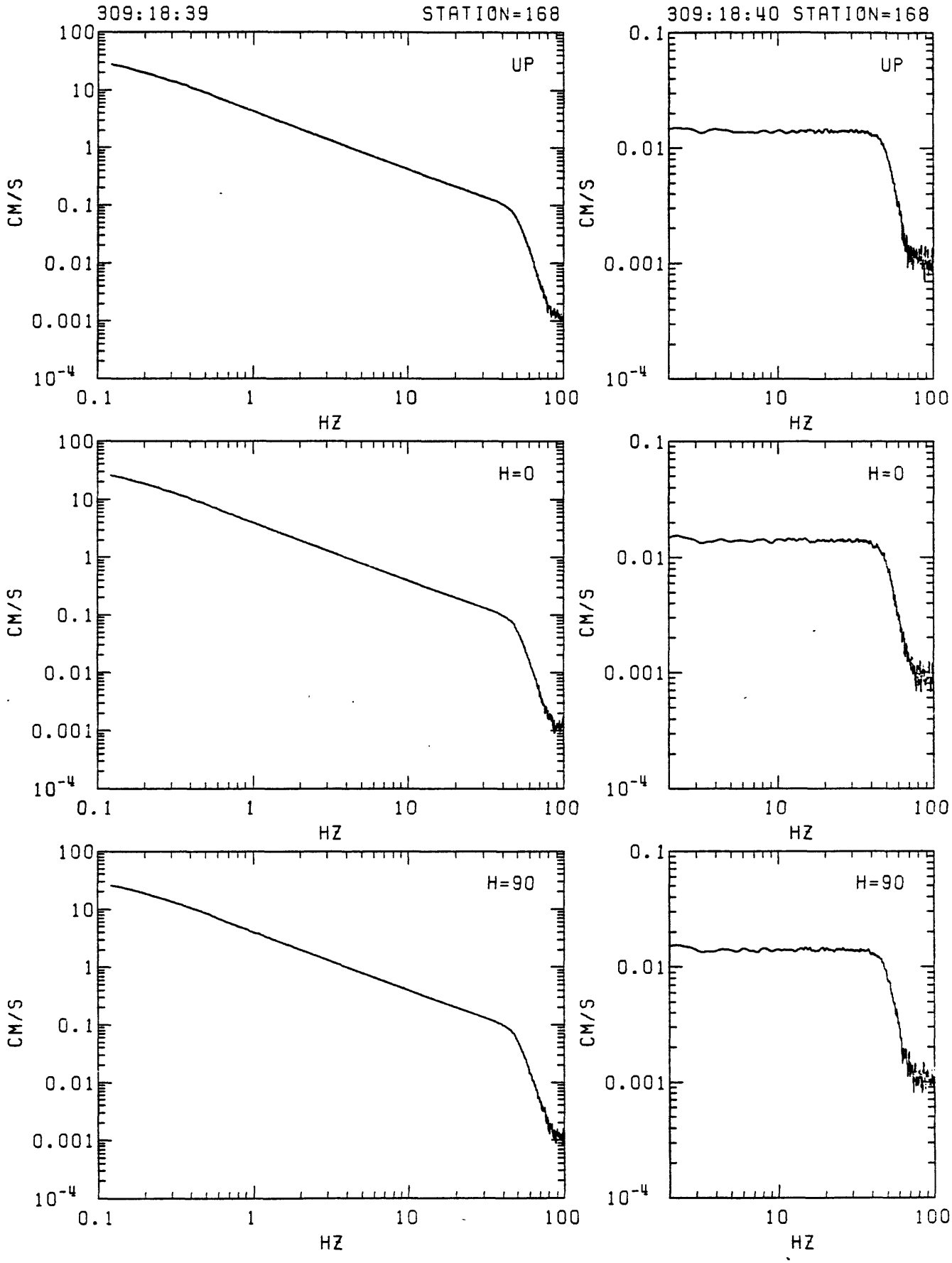

Figure D3. Station 168 in-situ 18db acceleration calibration spectra. Left: response to step in acceleration (reset FBA servo amplifier reference voltage from non-zero). Right: response to delta function in acceleration (voltage impulse applied to recorder input). From top: vertical, N33W and N57W.

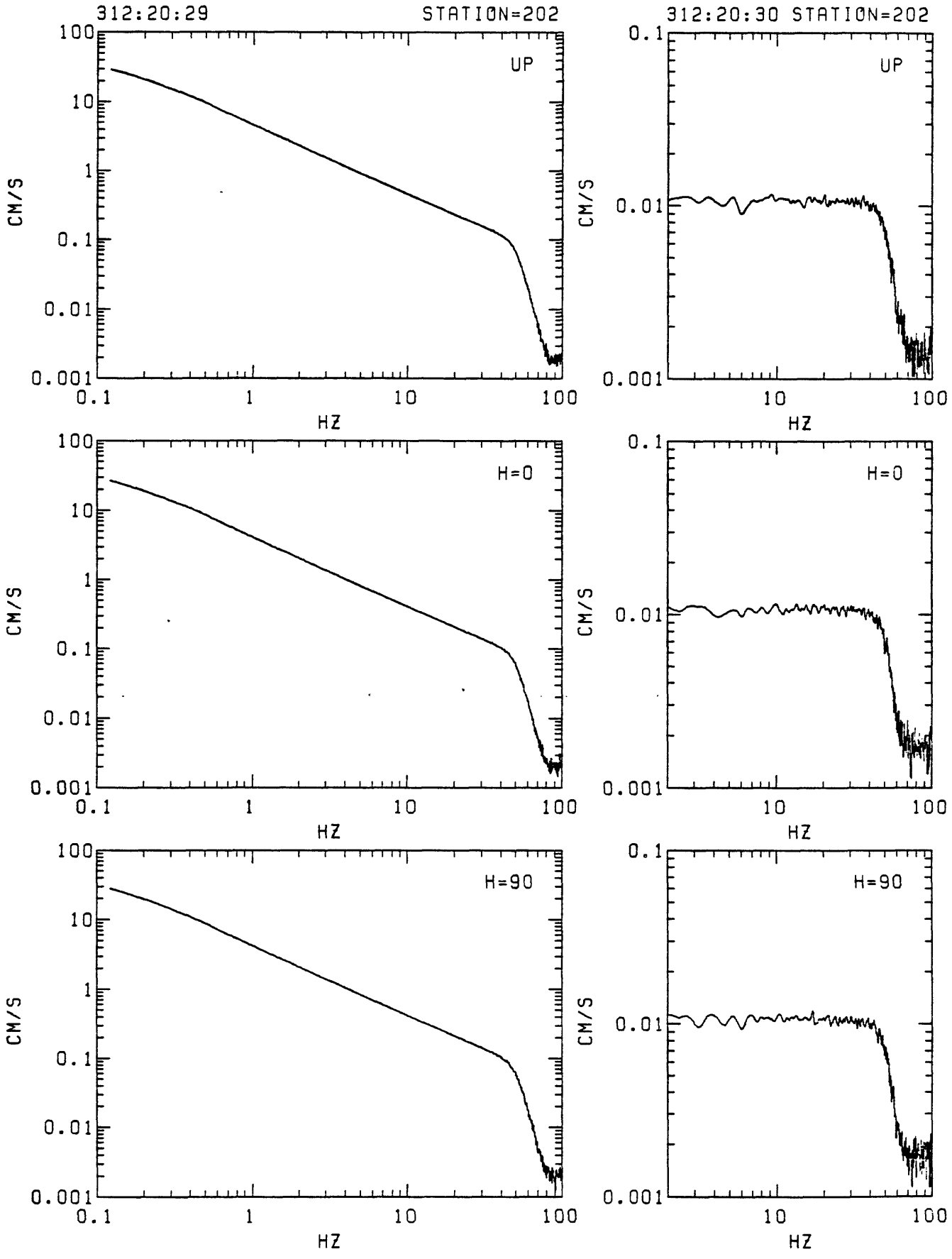

Figure D4. Station 202 in-situ 12db acceleration calibration spectra. Left: response to step in acceleration (reset FBA servo amplifier reference voltage from non-zero). Right: response to delta function in acceleration (voltage impulse applied to recorder input). From top: vertical, N20E and N110E.

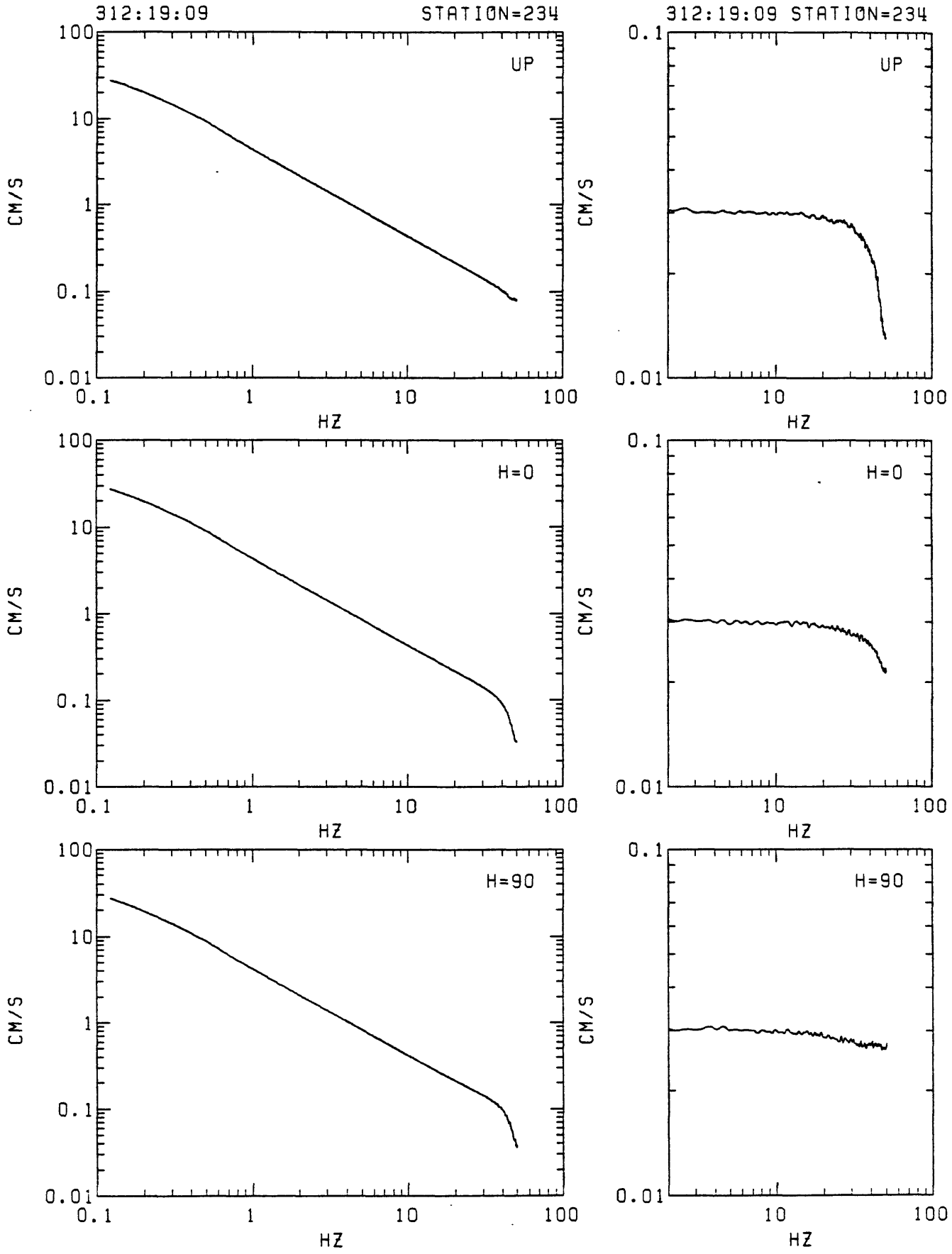

Figure D5. Station 234 in-situ 18db acceleration calibration spectra. Left: response to step in acceleration (reset FBA servo amplifier reference voltage from non-zero). Right: response to delta function in acceleration (voltage impulse applied to recorder input). From top: vertical, N20E and N110E.

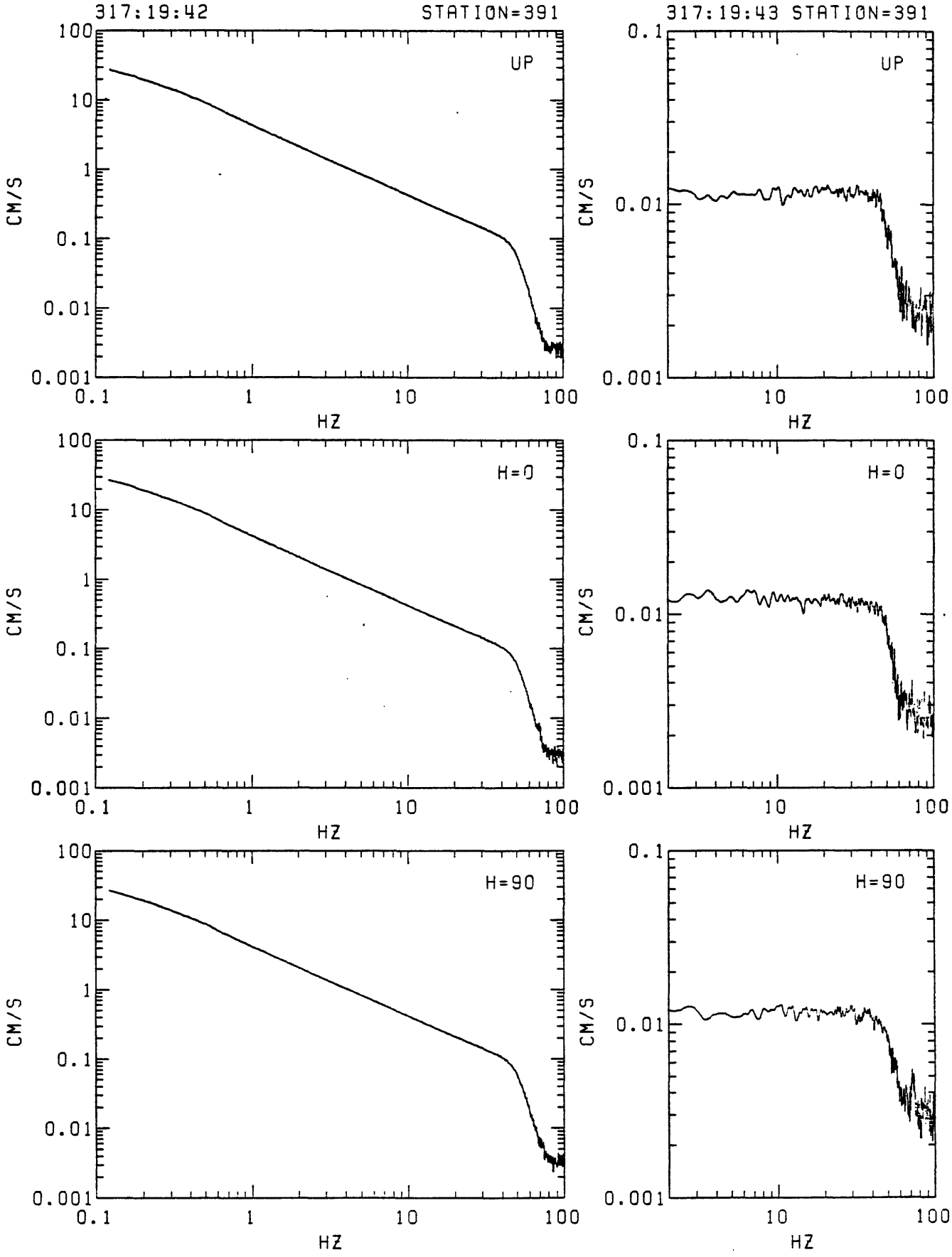

Figure D6. Station 391 in-situ 6db acceleration calibration spectra. Left: response to step in acceleration (reset FBA servo amplifier reference voltage from non-zero). Right: response to delta function in acceleration (voltage impulse applied to recorder input). From top: vertical, N25E and N115E.